PORT-WIDE GROUND MOTION STUDY
PORT OF LONG BEACH, CALIFORNIA
FINAL REPORT

Prepared For:

The Port of Long Beach
925 Harbor Plaza
Long Beach, CA 90801

Prepared By:

Earth Mechanics, Inc.
17660 Newhope Street, Suite E
Fountain Valley, CA 92708

EMI Project No. 01-143

August 7, 2006

Earth Mechanics, Inc.

Geotechnical & Earthquake Engineering

August 7, 2006
EMI Project No. 01-143

Mr. Doug Thiessen, P.E.
Chief Harbor Engineer
Port of Long Beach
925 Harbor Plaza
Long Beach, CA 90801

Attention: Mr. Cheng Lai, P.E., S.E.
Senior Structural Engineer

Subject: *Final Report on Port-Wide Ground Motion Study, Port of Long Beach, California*

Dear Mr. Lai:

Attached please find the Final Report of our port-wide ground motion study. This report contains the methodology and findings of our study and the resulting recommendations for design of port structures. The review comments received from the Port of Long Beach to date have been addressed into this report.

On behalf of the entire project team, we appreciate the opportunity to work with you on this project. If you have any questions or comments on this report, please do not hesitate to call us.

Sincerely,
EARTH MECHANICS, INC.

Bruce A. Schell, CEG 1434
Senior Engineering Geologist

(Arul) K. Arulmoli, GE 2090
Project Manager

Norman A. Abrahamson, Ph.D.
Consultant

Ignatius Po Lam, GE 2107
Principal

17660 Newhope Street, Suite E, Fountain Valley, California 92708   Tel: (714) 751-3826   Fax: (714) 751-3928

Copies:

(6) Port of Long Beach
(1) Dr. Tom Henyey, Technical Advisory Panel
(1) Dr. Geoffrey Martin, Technical Advisory Panel
(1) Dr. Nigel Priestley, Technical Advisory Panel

TABLE OF CONTENTS

TABLES

FIGURES

APPENDICES

EXECUTIVE SUMMARY

This report presents a port-wide ground motion study for the Port of Long Beach (POLB) performed by Earth Mechanics, Inc. (EMI) with an expert team review. The probabilistic seismic hazard analysis efforts were led by Dr. Norm Abrahamson, as a consultant to EMI, with EMI providing an independent check. The expert review team included Dr. Tom Henyey, Professor of Geological Sciences and Geophysics, University of Southern California (USC) and Director Emeritus of the Southern California Earthquake Center (SCEC); Dr. Geoffrey Martin, Professor, Department of Civil Engineering, USC; Dr. Nigel Priestley, Emeritus Professor of Structural Engineering, University of California, San Diego. The primary aim of the study was to develop consistent seismic ground motion recommendations for structures within the POLB area for operating-level earthquake (OLE) and contingency-level earthquake (CLE) design events.

Regional and site geology and seismicity were reviewed and summarized to establish the latest understanding on geological features and faults contributing to the seismic hazard at the POLB. Geotechnical ground conditions affecting site response were interpreted from review of available geotechnical data reports for numerous project sites located throughout the port area (no field investigations were undertaken for the purpose of the study). Four generalized site soil profiles representative of the POLB area were developed for site response assessment.

Probabilistic seismic hazard analysis was performed using the latest revisions of ground attenuation models commonly used in California, including the latest version of an attenuation model that is currently under development as part of the Pacific Earthquake Engineering Research (PEER)/ Lifelines Next Generation Attenuation (NGA) Project. Uncertainties in earthquake source and attenuation model parameters were addressed through the use of logic trees. Local site conditions were incorporated based on quantitative and qualitative assessment and supported by empirical strong motion data. The newly calculated Uniform Hazard Spectra (UHS) were compared to the history of prior spectra. A discussion is provided identifying the sensitivity of key parameters affecting ground motion criteria.

This report provides horizontal and vertical-component UHS for firm-ground conditions and design response spectra for OLE and CLE events that can be used by structural designers utilizing modal response spectrum analysis techniques. Damping values ranging from 1 to 25% were considered in the study. A total of 7 sets of horizontal and vertical spectrum-compatible acceleration-time histories are provided for firm-ground conditions and design ground conditions for each earthquake event. Simplified Newmark Sliding Block analyses were performed to develop the corresponding Newmark charts, providing estimates of ground displacement as a function of yield acceleration.

The report concludes with suggested guidelines for future design practice in site response analysis, including adjustments for deep-soil sites and near-fault rupturing effects. The report will require an update of the ground motion design criteria presented when changes in the state of practice in the seismological, geological, and geotechnical framework (such as the findings from the PEER NGA study) occur.

SECTION 1
INTRODUCTION

1.1　OUTLINE OF REPORT

Presented herein is a port-wide ground motion study for the Port of Long Beach (POLB) undertaken by Earth Mechanics, Inc. (EMI) with expert review. The site location is shown in Figure 1-1. The study was undertaken to address seismic recommendations corresponding to operating level earthquake (OLE) and contingency level earthquake (CLE) design events at the POLB. The primary aim of the study was to develop consistent seismic ground motion recommendations for design of POLB structures.

The report targets those parties involved with the seismic design of pile-supported container wharves and other structures within the POLB area. Key design inputs provided are uniform hazard spectra for OLE and CLE excitation levels. These are intended for direct use by structural designers utilizing modal response spectrum analysis techniques. Also provided are spectrum-compatible OLE and CLE acceleration-time histories for both design and firm-ground conditions.

1.2　BASIS OF STUDY

The ground motion study was performed by EMI under Contract No. HD-HD-6939 with the POLB. The study was performed using available data and office-based procedures. Geologic and seismicity information was reviewed on a regional and site-specific basis to establish the latest understanding on geological features contributing to the seismic hazard at the POLB. Ground conditions affecting site response within the POLB area were assessed from review of available geotechnical reports for project sites located throughout the POLB area. No field investigations were undertaken for the purpose of the study.

A probabilistic framework was adopted to account for seismic hazard, incorporating the latest revisions of four ground attenuation models commonly used in California. The probabilistic seismic hazard analysis efforts were led by Dr. Norm Abrahamson, as a consultant to EMI, with EMI providing an independent check. Treatment of the uncertainty in earthquake source and attenuation model parameters was provided through use of logic trees. Local site conditions were incorporated based on quantitative and qualitative assessment using proven methods and supported by empirical strong motion data.

In undertaking the ground motion study, a process of expert review was followed to promote consensus of opinion. The services of the following recognized experts were employed to solicit comments on seismic, geotechnical and structural matters: Dr. Tom Henyey, Professor of Geological Sciences and Geophysics, University of Southern California (USC) and Director Emeritus of the Southern California Earthquake Center (SCEC); Dr. Geoffrey Martin, Professor, Department of Civil Engineering, USC; Dr. Nigel Priestley, Emeritus Professor of Structural

Engineering, University of California, San Diego. Coordination with this group was maintained on a regular basis and their review comments incorporated into the study.

The following EMI and former EMI personnel are acknowledged for their efforts during coordination, analysis and preparation of this report: Andy Dodds, Ranjan Gunaranjan, Mike Kapuskar, Hubert Law, Raj Varatharaj, Chien-Tai Yang, and Amir Zand.

1.3   SCOPE

Tasks undertaken in accordance with the scope of work were as follows:

- Review past ground motion studies,
- Review and interpret pertinent geologic and fault information,
- Review and interpret available information on POLB ground conditions,
- Develop generalized site soil profiles representative of the POLB area for site response assessment,
- Perform probabilistic seismic hazard analysis addressing OLE and CLE performance levels,
- Perform sensitivity studies to identify key parameters affecting ground motion criteria,
- Perform Newmark displacement analyses, and
- Comment on needed update of the ground motion design criteria presented.

Deliverable items produced in accordance with the scope of work were as follows:

- Uniform hazard spectra (UHS) for design and firm-ground conditions for OLE and CLE events (horizontal and vertical spectra),
- Seven (7) sets of OLE and CLE spectrum-compatible acceleration-time histories (horizontal and vertical motions),
- Newmark displacement versus yield acceleration plots corresponding to the OLE and CLE acceleration-time histories, and
- Six (6) hard copies and one (1) electronic copy of this report ("pdf" format) presenting the study findings and design recommendations, and electronic ground motion files.

1.4   REPORT STATUS

Characterization of ground motion behavior is subject to periodic refinement and change given the uncertainty associated with earthquakes and the continued strong reliance on empirical observations to improve the understanding of their effects. Future earthquakes are expected to provide additional empirical data that will decrease the knowledge gap, but at the same time may require ongoing adjustment or changes to model parameterization and attenuation relations. A case in point is the major review of ground attenuation models being undertaken as part of a Pacific Earthquake Engineering Research (PEER) initiative, made possible due to empirical data that has increased significantly in size since 1997. This initiative will result in changes to current attenuation models, and are expected to be disseminated into practice within the next two years.

Given the ongoing activities involved with ground motion characterization, this report should be considered a "living" document that may require periodic revision. Elements of the report that may require particular attention in this respect include:

- Earthquake sources,
- Fault characterization (including developments of the Southern California Earthquake Community Fault Model), and
- Ground motion attenuation models.
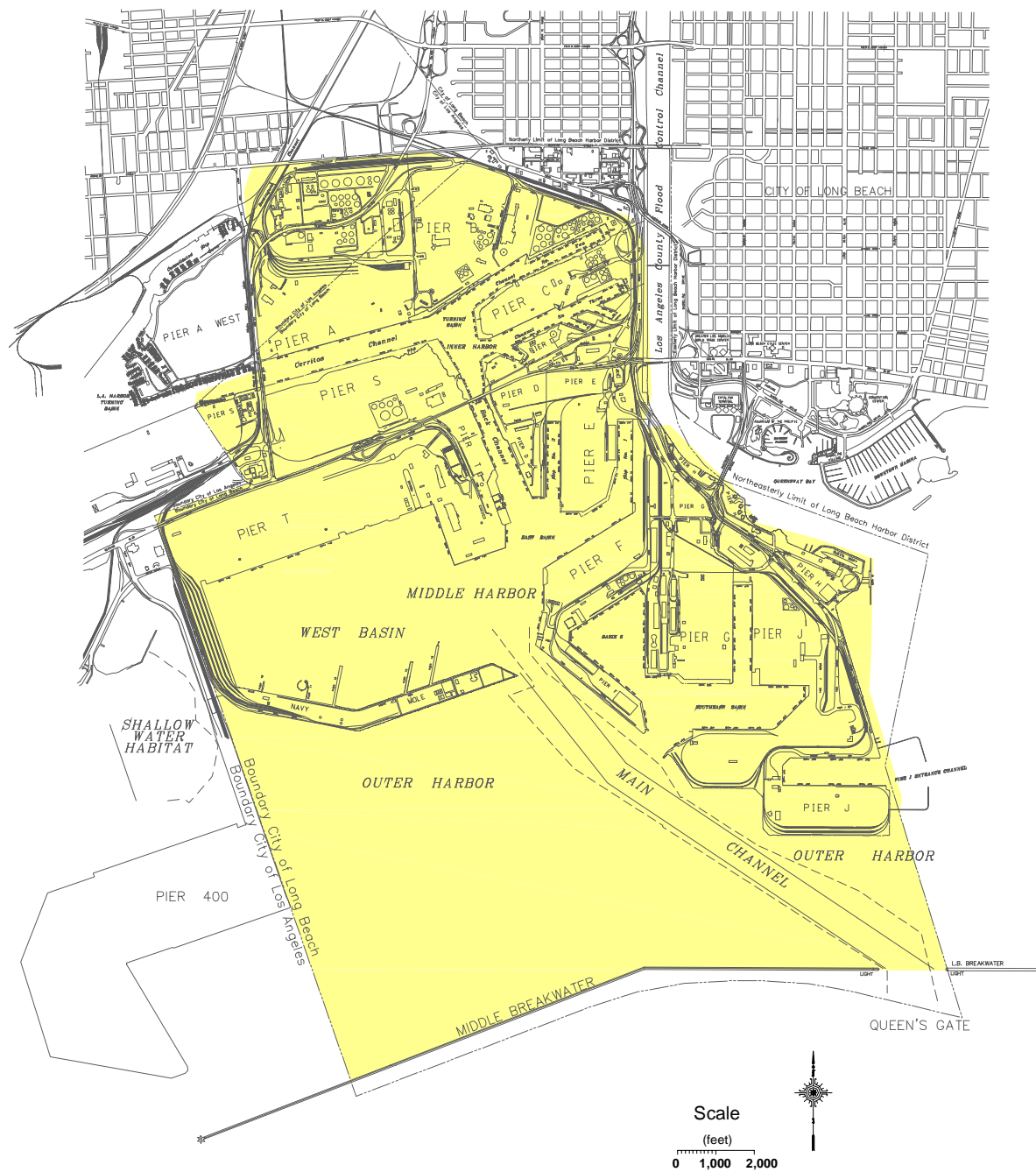
Figure 1-1.   Site Location Map

SECTION 2
GEOLOGICAL AND GEOTECHNICAL OVERVIEW

2.1   REGIONAL GEOLOGY AND SEISMICITY

A detailed description of the physiography, stratigraphy, geologic structure and seismicity for the region is provided in Appendix A. In summary, the POLB complex is located in the coastal area of the Los Angeles Basin, a low-lying plain that rises gently inland to the surrounding mountains including the Santa Monica Mountains to the north, the Repetto and Puente Hills to the northeast, the Santa Ana Mountains to the east, and the San Joaquin Hills to the southeast (see Figure 2-1).

The Los Angeles basin floor is characterized by unconsolidated Holocene-age sediments except for local exposures of the underlying Pleistocene-age formations in the small hills and mesas throughout the basin (for example, Signal Hill). Similar materials occur at the surface and subsurface within the POLB and the immediate offshore area. The Pleistocene materials consist of both non-marine and marine deposits referred to as the Lakewood and San Pedro formations. Both the Lakewood and San Pedro formations provide firm-ground conditions at the POLB.

The region is seismically active. Figure 2-2 shows the spatial distribution of earthquakes with larger, more notable events identified by name. On average, the greater Los Angeles area (i.e. the Los Angeles basin and the adjoining basins such as the San Fernando and San Gabriel valleys) is experiencing compression at rates of between 5 and 9 mm/yr as a result of north-northeasterly tectonic shortening. This compressional tectonic behavior results in a complex mixture of strike-slip and reverse (thrust) faulting and folding. Some of the reverse and thrust faults are poorly located and poorly understood, but earthquakes such as the 1987 Whittier Narrows and 1994 Northridge earthquakes are testimony to the existence of the subsurface reverse faults and for their importance to seismic design. Nevertheless, the bulk of tectonic activity in the Long Beach region during Quaternary time appears to have occurred along the nearby Palos Verdes fault and Newport-Inglewood Structural Zone (NISZ) (see Figure 2-1), both of which are primarily strike-slip faults and represent the most significant seismic potential for the POLB.

2.2   SITE GEOLOGY

2.2.1   Stratigraphy

A geologic structure map is shown in Figure 2-3 and characteristic geological cross sections in Figure 2-4 and Figure 2-5 that typify site stratigraphy and geologic structure in the POLB area. Surficial geology is characterized by Holocene-age, near-shore, marine and non-marine strata, including beach, estuary, tidal flat, lagoon, shallow-water bay sediments, and shoreline terrace deposits. Deposited as sea level rose during the Pleistocene age, these deposits have been significantly modified by dredging and filling operations for the numerous harbor facilities. The approximate location of the natural shoreline before harbor and urban development is partially

shown on Figure 2-3, indicating that most of the harbor facilities south of the coastal bluffs have been constructed on fill.

Figure 2-1. Regional Fault and Physiography Map
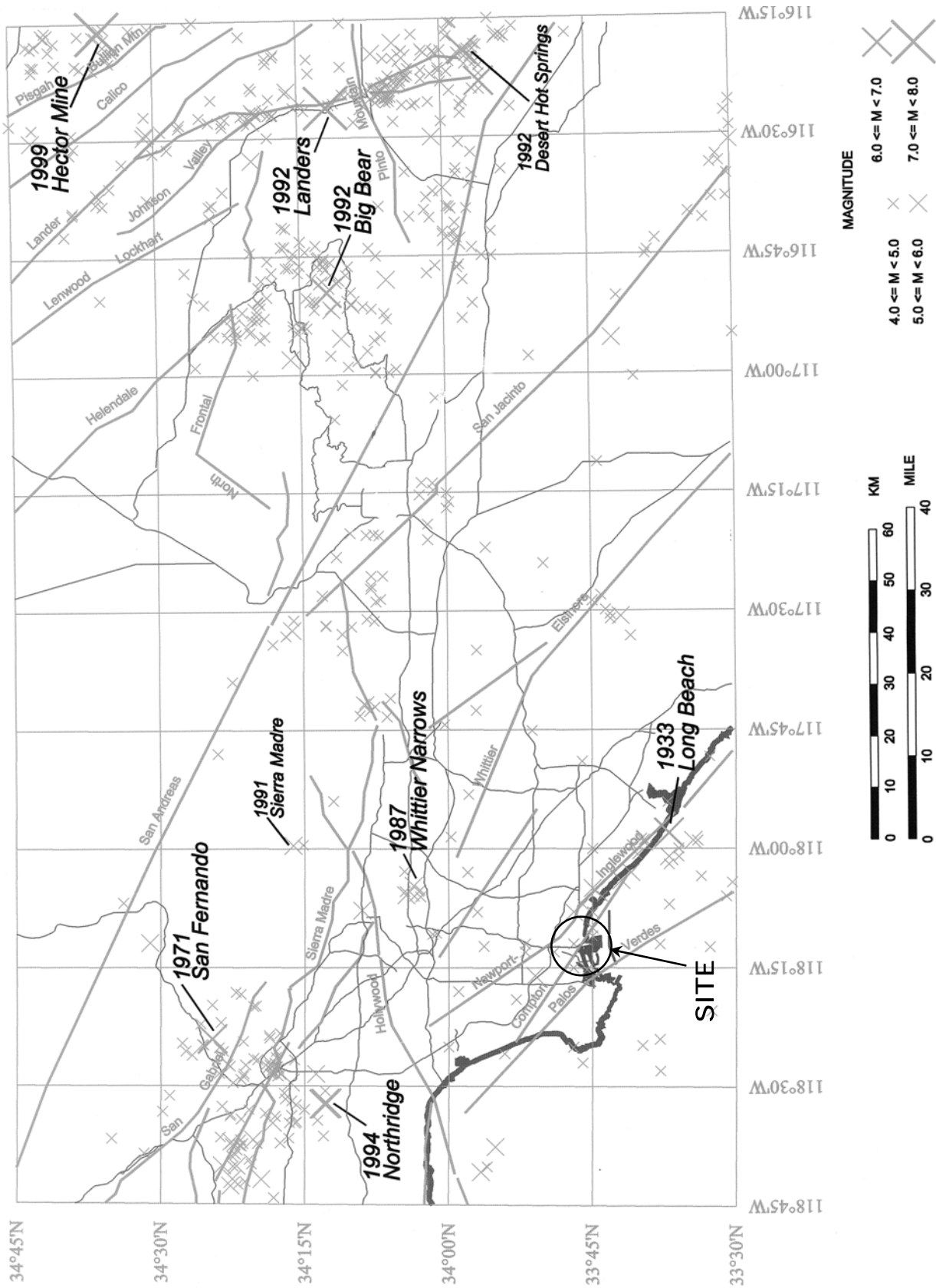
Figure 2-2. Seismicity Map
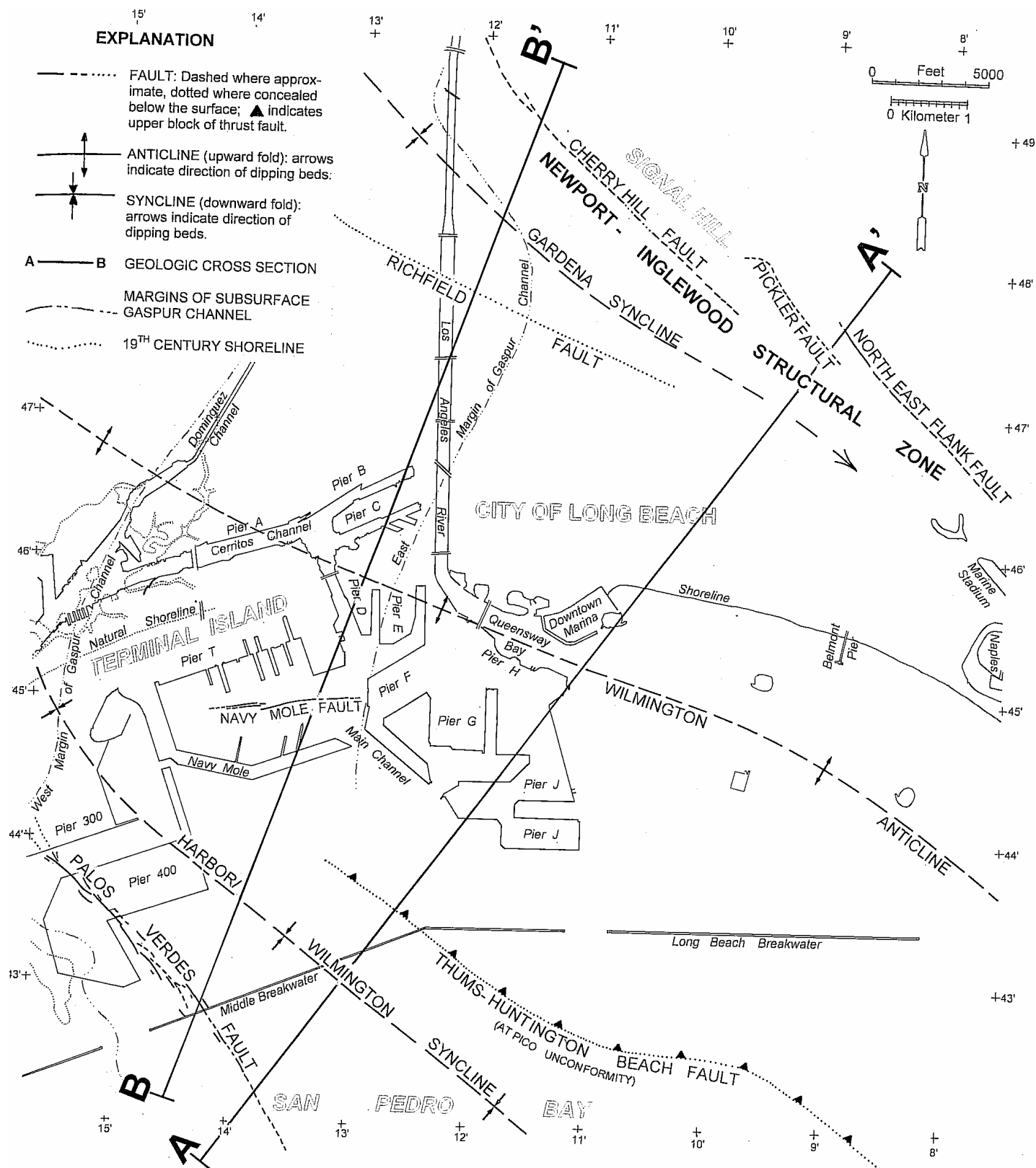
Figure 2-3.   Geologic Structure Map of the POLB Area
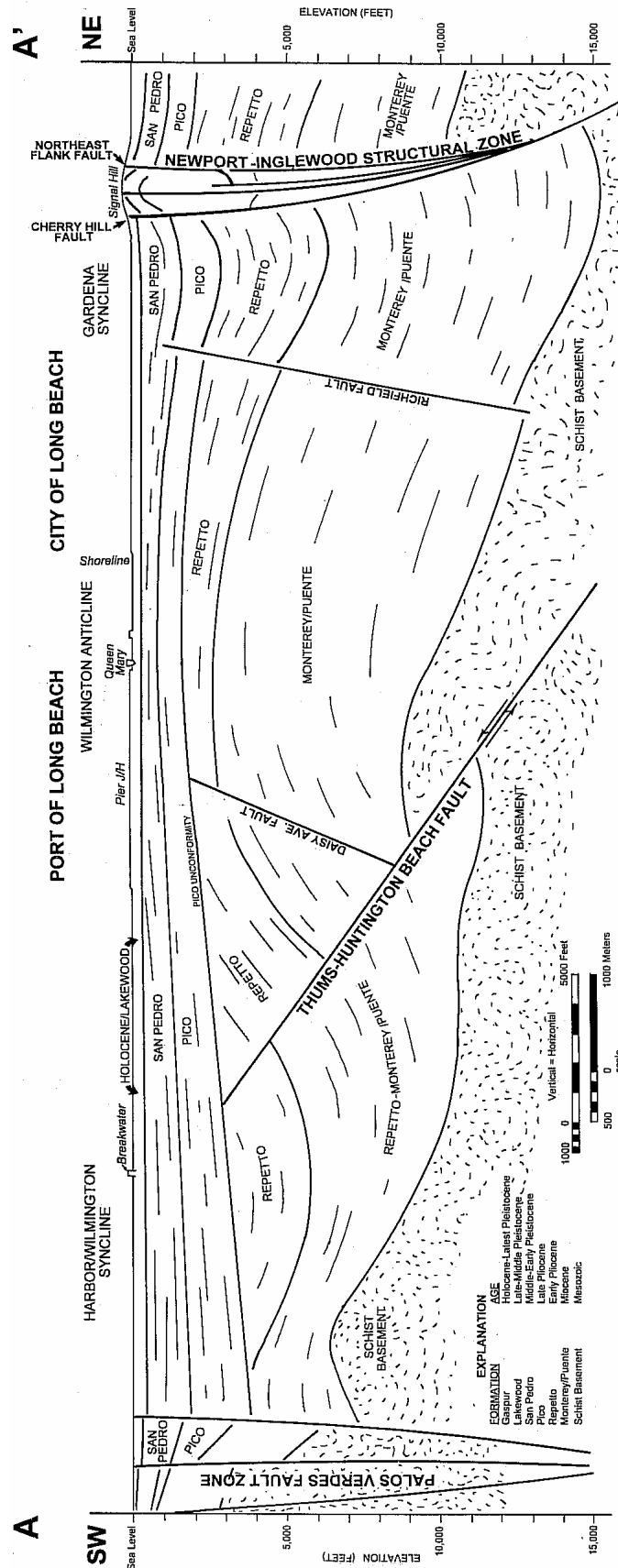
Figure 2-4. Geological Cross Section A-A'
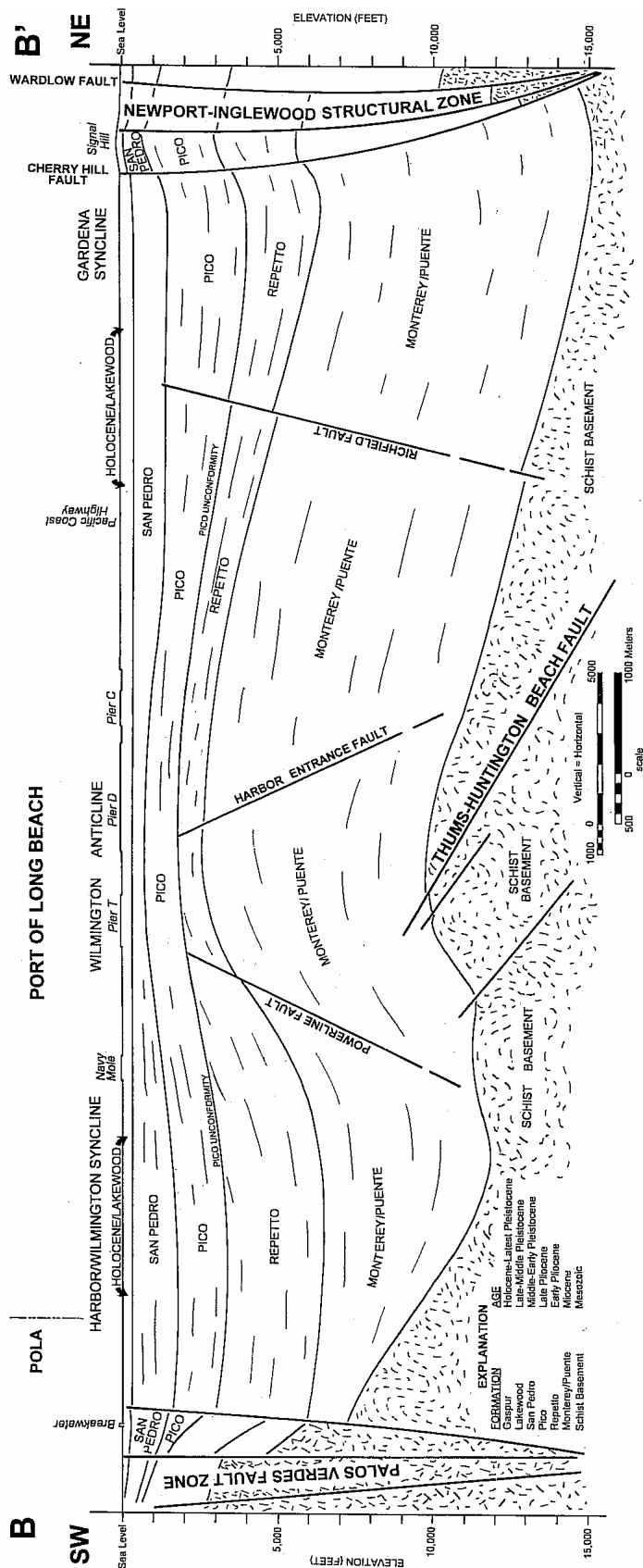
Figure 2-5. Geological Cross Section B-B'

Both the fill and the native near-shore sediments overlie similar older deposits of the late-Pleistocene-age Lakewood Formation, which in turn overlies the early Pleistocene San Pedro Formation (see Figure 2-4 and Figure 2-5). Differentiating the young sediments from the Lakewood or San Pedro formations is difficult in boreholes because of their similar origin and characteristics. Except for density, which is generally greater in the older Lakewood and San Pedro formations, the units can only be confidently differentiated by fossil analysis. Underlying strata comprise folded and faulted Pliocene- and Miocene-age formations, and the major angular Pico unconformity, separating the Quaternary and upper Pliocene sediments from lower Pliocene-Miocene deposits and Catalina Schist basement (see Figure 2-4 and Figure 2-5).

2.2.2 Geologic Structure

Several major folds and faults are apparent in the POLB area as shown on Figure 2-3, Figure 2-4, and Figure 2-5. The major folds are the Wilmington and Signal Hill anticlines, and the intervening Gardena and Harbor-Wilmington synclines. These folds are primarily the result of deformation along the Newport-Inglewood fault (NISZ), the THUMS-Huntington Beach (THB) fault, and the Palos Verdes fault. There are also numerous minor north-south trending cross-cutting faults in the region (see, for example, the Powerline, Harbor Entrance, and Daisy Avenue faults on Figure 2-4 and Figure 2-5), but these are largely secondary features and are inactive. Faults that contribute to the seismic hazard at the POLB, including the Newport-Inglewood and Palos Verdes faults, are discussed in Appendices A and B.

The Pico unconformity shown on Figure 2-4 and Figure 2-5 is a feature of tectonic significance. This unconformity indicates that the major folding of the Wilmington Anticline occurred prior to the Quaternary time. High-resolution, 3-dimensional, seismic-reflection data from the THUMS oil operations (Prior, 2004) clearly show that the THB fault is truncated at the Pico unconformity indicating that the fault has not been active since late Tertiary time. In contrast to the THB fault, the Palos Verdes and Newport-Inglewood faults extend to the surface and are associated with abundant Quaternary deformation and prominent surface uplifts such as the Palos Verdes Hills and Signal Hill. Increased activity on the NISZ in latest Tertiary and Quaternary time appears to coincide with the end of major activity on the THB fault.

A small amount of uplift has occurred in the area of the Wilmington Anticline since late Pliocene time, and some of this uplift appears to be Quaternary in age (Ponti, 2004; Edwards et al., 2002). This uplift is compatible with the regional compressional forces acting across the Los Angeles region. The compression can result in transpressional strike slip faulting, thrust faulting, and/or folding. Both the NISZ and the Palos Verdes faults are transpressional strike slip faults whereas the Wilmington anticline-syncline and Gardena syncline represent folding between the major faults. The documented uplift (Castle and Buchanan-Banks, 1989) in the Wilmington anticline area is associated with the 1933 Long Beach earthquake on the NISZ and represents evidence that at least some Quaternary-age folding of the Wilmington anticline is due to tectonics of the adjacent faults. Alternatively, thrusting on the subsurface Compton thrust ramp has been proposed as a cause of folding of the Wilmington anticline (Shaw, 1993).

2.3 GROUND CONDITIONS

Pier facilities at the POLB have been formed from natural coastal and man-made land masses, creating wide variations in ground conditions throughout the POLB area. Dredged fill materials have been used extensively in the construction of the man-made land masses. These materials generally are not considered representative of firm-ground conditions assumed in probabilistic hazard studies. An assessment of ground conditions was therefore undertaken to establish appropriate depths to firm-ground conditions and to assess appropriate site response behavior for design.

Firm-ground conditions were defined on the basis of average shear wave velocity. The average shear wave velocity $\overline{v}_s$ was calculated as follows:

$$\overline{v}_s = \frac{\sum_{i=1}^{n} d_i}{\sum_{i=1}^{n} \frac{d_i}{v_{si}}} \tag{2.1}$$

where

d_i = thickness of layer i (in ft), and
v_{si} = shear wave velocity in layer i (in ft/sec).

The depth to firm ground was defined at the top of a 100-ft (30-m) depth interval that has a minimum average shear wave velocity $\overline{v}_{s30}$ of approximately 1,000 ft/sec ($\approx$300 m/sec):

$$\overline{v}_{s30} = 1,000\ {}^{ft}\!/\!_{\sec} = \frac{100\,ft}{\sum_{i=1}^{n} \frac{d_i}{v_{si}}} \tag{2.2}$$

Information sources and the methodology for the development of these depths at various locations at the POLB are described below.

2.3.1 Information Sources

The primary source of information for ground conditions at the POLB was past project-specific reports made available by the POLB. These comprised mainly geotechnical reports undertaken at berths, piers and other structures as listed in the bibliography in Section 9. The ground information contained in these geotechnical reports was in the form of boring investigations with Standard Penetration Test (SPT) data generally provided at 5-foot intervals, and Cone Penetration Test (CPT) soundings. Depths investigated were typically on the order of 100 ft.

Other sources of ground investigation information included shear wave velocities obtained from the ROSRINE database (ROSRINE, 2001) and several of the projects listed in the bibliography where geophysical testing was also performed.

2.3.2   Soil Profiles for Seismic Response

Soil profiles were established through evaluation of the available information to determine appropriate response parameters (shear wave velocity and density) and to establish expected depths to firm-ground conditions. As boring investigations represented most of the available information, evaluation efforts were largely concerned with assimilation of the various soil descriptions, SPT blowcount, and density data indicated. CPT sounding and shear wave velocity data served to supplement and support this information. Findings suggested a demarcation of the POLB into four areas denoted as Zones I, II, III and IV in which similar soil profiles were apparent. The approximate extents of these zones are shown in Figure 2-6.

The four idealized soil profiles and shear wave velocity profiles corresponding to each zone are shown in Figure 2-7. Shear wave velocity profiles were established by reconciling SPT blowcount and density data with available shear wave measurements and drawing on experience with similar ground conditions in the area. Density values assigned varied between 115 pcf (harbor sediments), 120 pcf (alluvial fill) and 125 pcf (alluvial/Gaspur deposits). Depths to firm-ground conditions were based on $\bar{v}_s$ calculations using available shear wave velocity data and interpretation of SPT blowcounts in a similar manner. The profiles shown in Figure 2-7 end at depths corresponding to the defined firm-ground condition.

It should be noted that the available boring investigations, CPT soundings, and shear-wave velocity measurements provided data representative of ground conditions at specific locations only, and were not of sufficient extent to permit a comprehensive characterization. Therefore, the soil profiles presented are therefore only considered to be generally representative of local site conditions at the POLB. Specific ground investigations undertaken as part of a routine site investigation program are expected to establish which soil profile(s) are most appropriate on a site-by-site basis. This will also allow for the possibility of peculiar ground conditions that may require special attention.
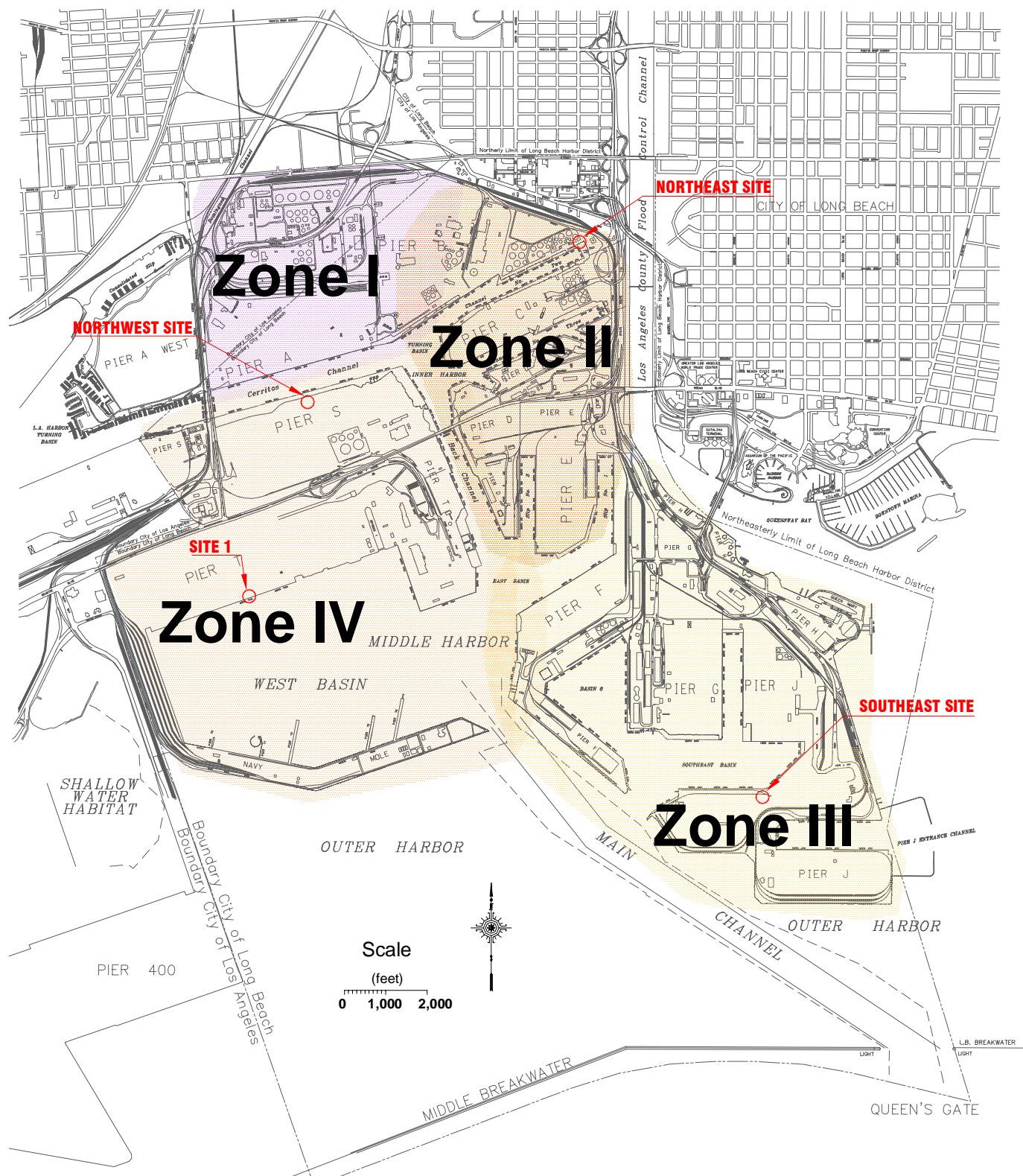
Figure 2-6.   Soil Zones Used for Seismic Response Analyses
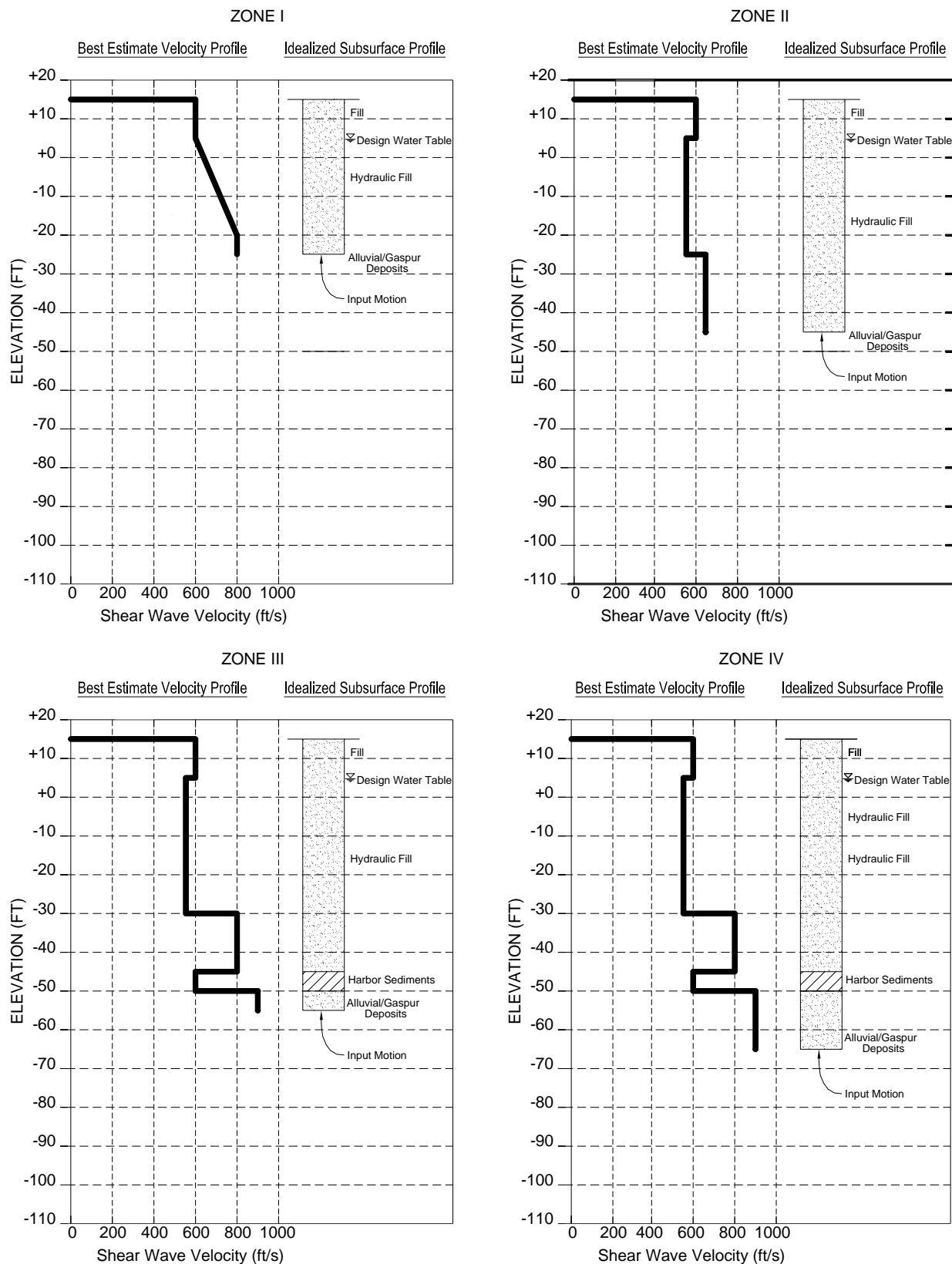
Figure 2-7.   Idealized Soil Profiles Used for Seismic Response Analyses

SECTION 3
PROBABILISTIC SEISMIC HAZARD ANALYSIS

3.1   GENERAL

3.1.1   PSHA Methodology

The probabilistic seismic hazard analysis (PSHA) follows the standard approach first developed by Cornell (1968). This approach has been expanded to more fully treat both the randomness (aleatory variability) and the scientific uncertainty (epistemic uncertainty). The mathematical formulation of the hazard analysis used in this study is described in Appendix C.1.

3.1.2   Earthquake Sources

Key seismic sources at the POLB are the Palos Verdes and Newport-Inglewood fault zones, as shown in Figure 3-1. Other nearby, but less active, seismic sources include the Compton Thrust, THUMS-Huntington Beach fault, Cabrillo fault, and Los Alamitos fault. A detailed discussion of these faults is given in Appendix A, and details on the source parameters used for the probabilistic seismic hazard analysis are given in Appendix B. Table 3-1 and Table 3-2 provide a summary of these parameters.

The segmentation of the offshore Palos Verdes and Newport-Inglewood faults is not well known. For faults with unknown segmentation, it is common to assume that the characteristic magnitude would correspond to 1/2 of the fault length. To address the uncertainty in the segmentation, two segmentation models were considered: (1) an "unsegmented model" in which the full length of the offshore Palos Verdes and Newport-Inglewood faults are assumed to rupture, and (2) a "segmented model" in which 1/2 of the length of the two offshore faults are assumed to rupture. The segmentation model reduces the mean characteristic magnitude of the Palos Verdes and Newport-Inglewood fault by 0.25 and 0.30 magnitude units, respectively. The reduction for the Palos Verdes fault is smaller because the Palos Verdes Hills segment is assumed to fully rupture for both the segmented and unsegmented model. Table 3-1 and Table 3-2 include the parameters used for both models. The segmented and unsegmented models were given equal logic-tree weightings. For the San Pedro Basin fault, a similar segmentation would apply; however, just the unsegmented model was used for simplicity as this is not a controlling fault.

The other active faults in the region, shown on Figure 2-1, were included in the source characterization for completeness. These are included in Table 3-3 which lists the faults in the region recognized by the U.S. Geological Survey (USGS). Since these faults do not contribute significantly to the hazards, they were simply modeled using USGS fault parameters.

Table 3-1.   Summary of Seismic Source Parameters for Local Faults

Fault (Map Abbreviation)	Depth to Top of Fault (km)	Depth to Bottom of Fault (km)	Dip (deg)	Slip Rate (mm/yr)	Mean Characteristic Earthquake, M_w	Style of Faulting[1]
Palos Verdes (PV-PVH, PV-SO)	0	11 to 18	90	2.0 to 4.0	6.65 to 7.2	Strike-Slip
Newport-Inglewood (NI)	0	13 to 16	90	0.5 to 1.5	6.7 to 7.2	Strike-Slip
Cabrillo (CAB)	0	15 to 18	70	0.1	6.25 to 6.5	Strike-Slip
San Pedro Basin (SPB)	0	15	90	0.5 to 1.0	7.1 to 7.2	Strike-Slip
Los Alamitos (LAL)	0	15	70	0.25 to 0.50	6.5	Strike-Slip
Compton Thrust (CT)	6	10	16	0.5 to 1.0	7.1 to 7.2	Reverse

Table 3-2.   Probabilistic Seismic Hazard Parameters and Logic-Tree Weightings

Fault (Map Abbreviation)		Activity (Weighting)	Length in km	Width in km (Weighting)	Slip-Rate in mm/yr (Weighting)	Characteristic Earthquake Magnitude, M_w (Weighting)
Palos Verdes Fault[1] (PV)	Palos Verdes Hill Segment (PVH)	Active (1.0)	12 (0.5)	15 (0.5) 18 (0.5)	2.0 (0.4) 3.0 (0.5) 4.0 (0.1)	$6.9^u/6.65^s$ (0.225) $7.0^u/6.75^s$ (0.390) $7.1^u/6.85^s$ (0.275) $7.2^u/6.95^s$ (0.110)
	Southern Offshore Segment (SO)		$50^u/25^s$ (0.5)	11 (0.2) 13 (0.6) 15 (0.2)		
Newport-Inglewood (NI)		Active (1.0)	$65^u/33^s$ (0.5)	13 (0.5) 16 (0.5)	0.5 (0.2) 1.0 (0.6) 1.5 (0.2)	$7.0^u/6.7^s$ (0.33) $7.1^u/6.8^s$ (0.50) $7.2^u/6.9^s$ (0.17)
Cabrillo (CAB)		Active (1.0)	18 (0.5)	15 (0.5) 18 (0.5)	0.1 (1.0)	6.4 (0.25) 6.5 (0.75)
San Pedro Basin (LAL)		Active (1.0)	70 (0.5)	15 (1.0)	0.5 (0.6) 1.0 (0.4)	7.1 (0.50) 7.2 (0.50)
Los Alamitos (LAL)		Active (1.0)	35 (0.5)	15 (1.0)	0.25 (0.5) 0.5 (0.5)	6.5 (1.0)
Compton (CT) - Los Alamitos Fault Zone/Thrust Ramp[2]		Active (0.2) Inactive (0.8)	70 (0.5)	20 (1.0)	0.5 (0.5) 1.0 (0.5)	7.1 (0.67) 7.2 (0.33)

Notes: Logic-tree weightings are given in parentheses.

1) The Santa Monica Bay segment of the Palos Verdes fault is modeled as a separate, inactive segment with zero slip rate (see discussion in Appendix B).

2) If THUMS-Huntington Beach fault is active, it is included as part of Compton-Los Alamitos fault (see discussion in Appendix B).

u) Unsegmented model

s) Segmented model

Table 3-3.   **Seismic Source Parameters for Other Faults Based on Best-Estimate Values from USGS**

Fault (*Map Abbreviation*)	Depth to Top of Fault (km)	Depth to Bottom of Fault (km)	Dip (deg)	Slip Rate (mm/yr)	Mean Characteristic Earthquake Magnitude, M_w	Style of Faulting[1]
Whittier (*WH*)	0	15	75 NE	2.5	6.8	R/O
Santa Monica (*SN*)	0	13	75 N	1.0	6.6	R/O
Hollywood (*HY*)	0	13	70 N	1.0	6.4	R/O
Malibu Coast (*MC*)	0	13	75 N	1.0	6.7	R/O
Sierra Madre (San Fernando) (*SM-SF*)	0	13	45 N	2.0	6.7	R
Sierra Madre (*SM*)	0	13	45 N	2.0	7.2	R
Cucamonga (*CM*)	0	13	45 N	5.0	6.9	R
Santa Susana (*SS*)	0	13	55 N	5.0	6.7	R
Raymond (*RY*)	0	13	75 N	1.5	6.5	R/O
Chino (*CH*)	0	18	90	1.3	6.7	O
Verdugo (*VD*)	0	13	45 NE	0.5	6.9	R
San Jose (*SJS*)	0	13	75 NW	0.5	6.4	R/O (?)
San Gabriel (*SG*)	0	13	90	1.0	7.2	SS
San Andreas – Carrizo (*SA-C*)	0	12	90	34.0	7.4	SS
San Andreas – Mojave (*SA-M*)	0	12	90	30.0	7.4	SS
San Andreas – San Bernardino Mountains (*SA-SBM*)	0	18	90	24.0	7.5	SS
San Jacinto (San Jacinto Valley & San Bernardino) (*SJ-SJV+SB*)	0	15	90	12.0	7.0	SS
San Jacinto (Anza) (*SJ-A*)	0	15	90	12.0	7.0	SS
Elsinore (*EL*)	0	15	90	15.0	7.0	SS
Northridge (*NR*)	5	20	42 S	1.5	7.0	R
Upper Elysian Park (*EP*)	3	13	50 NE	1.3	6.4	R
Puente Hills	5	13	25 N	0.7	7.1	R
San Joaquin Hills (*SJH*)	2	8	23 S	0.5	6.6	R
Notes: 1) R = Reverse; O = Oblique; SS = Strike-Slip						
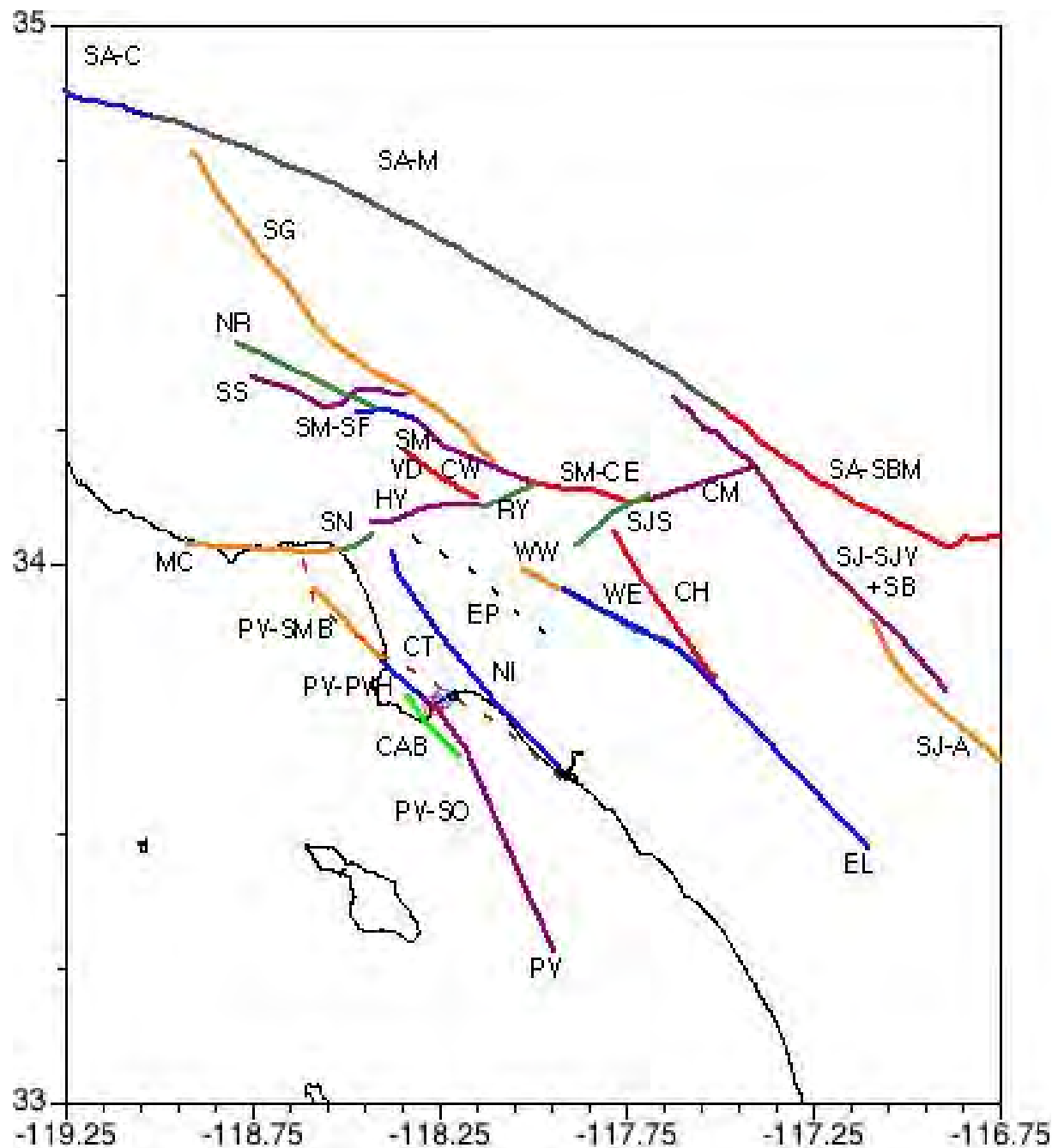
Figure 3-1.　　Map of Principal Fault Sources Used in PSHA

3.1.3　Earthquake Rupture Dimensions

Earthquake rupture dimensions were established using three magnitude-area relations reported by Wells and Coppersmith (1994), USGS, and Hanks and Bakun (2002), as given below by Equations (3.1), (3.2) and (3.3), respectively.

$$M = 3.98 + 1.02 \log A \tag{3.1}$$

$$M = 4.2 + \log A \tag{3.2}$$

$$M = 3.98 + \log A \qquad \text{for } A \leq 468 \text{ km}^2, \text{ and}$$

$$M = 3.09 + \frac{4}{3} \log A \qquad \text{for } A > 468 \text{ km}^2 \tag{3.3}$$

where

M = magnitude, and
A = rupture area in km.

The latter two models are used in the USGS source models. The Wells and Coppersmith (1994) model is included because there is support for this model from numerical modeling (Somerville et al., 1999).

3.1.4   Earthquake Recurrence Models

The approach used to derive the magnitude recurrence is to balance the long-term moment-rate on the faults. Given this approach, the Youngs and Coppersmith (1985) characteristic earthquake model is used for the magnitude probability density function (pdf). The standard truncated exponential model is not considered because it tends to overestimate the rate of moderate magnitude earthquakes when moment-rate is balanced. The Youngs and Coppersmith model is a combination of a pure characteristic model and an exponential model. The key aspect of the Youngs and Coppersmith model is that about 94% of the moment-rate is accommodated in characteristic earthquakes and only about 6% of the total moment-rate is accommodated by the exponential tail.

3.2   ATTENUATION MODELS

3.2.1   Site Classification for Ground Motion

The site classification for *firm ground* was characterized with average shear wave velocities of 300 m/sec ($\approx$1,000 ft/sec) over a depth of 30 m ($\approx$100 ft). This site classification is best correlated with typical "soil" site classifications of published empirical attenuation relationships.

3.2.2   Standard Attenuation Models

A total of three standard empirical attenuation relationships for soil site conditions were used: Sadigh et al. (1997), Abrahamson and Silva (1997) and Campbell (1997). The depth to basement bedrock for the Campbell (1997) attenuation relationship was set to 4.0 km for soil site conditions. All three empirical attenuation relationships were for a spectral damping of 5%. These models were given equal weight.

3.2.3   Updated Attenuation Models

The suite of ground motion attenuation relationships commonly used in California for shallow crustal earthquakes are currently being revised as part of the PEER/Lifelines Next Generation Attenuation (NGA) project. These new models are based on a greatly expanded and improved empirical database. In particular, there is a great increase in the number of recordings from large magnitude earthquakes resulting from the 1999 Kocaeli (M7.5), 1999 Chi-Chi (M7.6), 1999 Duzce (M7.1), 2000 Hector Mine (M7.1), and 2002 Denali (M7.9) events. The ground motions from these large-magnitude events are smaller than predicted by the existing attenuation relations. Three preliminary NGA models were presented at the December 3, 2004 PEER/ Lifelines workshop. Two of these models (Abrahamson and Silva, and Campbell and Bozorgnia) showed a significant reduction in the median ground motion for large magnitudes (M>7) as compared to the existing models. There is also an increase in the standard deviation for large magnitudes for all three models.

To represent these new models, the Abrahamson and Silva (2005) preliminary model (which was the only model available to the EMI team at the time of this study) was used. The formulation of this model is provided in Appendix C.2. A weight of 1/3 was given to the new preliminary Abrahamson and Silva model and the standard models were given a total weight of 2/3.

3.2.4   Directivity Effects

A major component in the subject port-wide seismic hazard study was to update the attenuation relationships in order to better model rupture directivity effects observed account for lessons learned from strong motion recordings from recent major seismic events around the world. Those recordings provided information relevant to POLB and POLA design conditions resulting from the fact that the port is located relatively close to major faults. Lessons from recent earthquakes led to the observation that there is a tendency for much stronger ground shaking at sites near an earthquake fault for a scenario when the fault rupturing process is propagating toward the project site as opposed to fault rupturing away from the site. For such forward-rupturing events, the long-period motion ground shaking would have larger amplitude in the fault-normal direction (i.e. in the direction perpendicular to the fault) as compared to the fault-parallel direction.

In the course of the project, we have incorporated information from the latest attenuation models in available literature (including research data developed from the recent San Francisco-Oakland Bay Bridge East Span Seismic Safety project on which Earth Mechanics served as the geotechnical consultant) into our port-wide seismic hazard study with regards to near-fault directivity aspects.

The (average) horizontal motion attenuation relations (average of the two horizontal components of ground motion) available in the literature were adjusted to account for near-fault directivity effects using a modified form of the Somerville et al. (1997) fault-rupture directivity model developed in the course of the Bay Bridge East Span project. Somerville et al. (1997) developed an empirically-based model quantifying the effects of rupture directivity on horizontal response spectra that can be used to scale the average horizontal component computed from attenuation relations. The Somerville et al. (1997) model comprises two period-dependent scaling factors that may be applied to any ground motion attenuation relationship. The first factor accounts for

the increase in shaking intensity in the average horizontal component of motion due to near-fault rupture directivity effects. The second factor reflects the directional nature of the shaking intensity (i.e., response spectrum amplitude) using two ratios: fault normal (FN) and fault parallel (FP) versus the average (FA) component ratios. The fault-normal component is taken as the major principal axis resulting in an FN/FA ratio larger than 1, and the fault parallel component is taken as the minor principal axis with an FP/FA ratio smaller than 1. The two scaling factors depend on whether fault rupture is acting in the forward or backward direction, and also the length of fault rupturing toward the site. The degree of ground shaking increase for near-fault forward rupturing and the FN/FA ratios was accounted for by an additional rupture directivity parameter in the probabilistic hazard analysis. Directivity effects become stronger as the return period increases. For directivity effects to be strong, the return period of the ground motion must be at least twice the recurrence interval of characteristic size earthquakes. For shorter return periods, such as the 72-year return period OLE, there is no effect from rupture directivity. For longer return periods, (e.g., the 475-year CLE), the effects of rupture directivity is non-zero, but is still small.

The ground motions are developed for the fault normal component. At long spectral periods, the ground motions on the fault normal component will be larger than on the fault parallel component due to directivity effects.

3.3 PROBABILITY COMPUTATION

The OLE and CLE events were identified by the POLB as having a 50% and 10% probability of exceedance in 50 years (72 and 475-year return period), respectively. The hazard is computed for a site at the western end of the Port within Pier T (118.2367^{o}W, 33.7533^{o}N). This site (hereafter referred to as "Site 1") was selected because it is in the area of the Port that is closest to the Palos Verdes fault and is expected to experience larger ground motions than at other locations in the port area, particularly for the CLE event. A comparison of the hazard at other locations given in Section 3.3.3 shows that for the CLE, the hazard at Site 1 is slightly higher than other locations, while the hazard for the OLE is generally unchanged (less than 5% difference between the highest and lowest values) within the POLB area.

3.3.1 Seismic Hazard Results

The seismic hazard is computed at 12 spectral periods from 0 to 4 sec for the fault normal and fault parallel components. The mean hazard by seismic source for peak ground acceleration (PGA) is shown in Figure 3-2 and spectral acceleration (Sa) for T = 1.0 sec in Figure 3-3. These plots show that the hazard at the Port is dominated by the Palos Verdes fault for return periods greater than about 200 years (approximate annual probability of exceedance 1/200=0.005).

The epistemic uncertainty in the hazard due to the alternative models considered in the logic tree is shown in Figure 3-4 for PGA. The uncertainty in the source models and ground motion models leads to 10-15% uncertainty in the PGA for return periods of 200-1,000 years. This is a typical uncertainty range for sites close to well-characterized seismic sources. The sensitivity of the mean hazard to the selection of the attenuation relation is shown in Figure 3-5 for PGA. The new Abrahamson & Silva (2005) model falls within the range of the previous models for return periods of 200-500 years. At longer return periods, the increase in the standard deviation for

larger earthquakes relative to the 1997 Abrahamson and Silva attenuation model leads to higher ground motions.

3.3.2   Deaggregation

The deaggregation for PGA for the 72-yr and 475-yr return periods is shown in Figure 3-6 and Figure 3-8, respectively. For the 72-yr return period, there is a wide range of events that contribute to the hazard. The dominant sources are M6.5–7.5 earthquakes for distances of 0 to 100 km. For the 475-yr return period, the hazard is dominated by the same magnitude range, but short distances (0 to 5 km). Similar deaggregation for T = 1 sec spectral acceleration is shown in Figure 3-7 and Figure 3-9 for the OLE and CLE, respectively. The controlling events based on the deaggregation at T = 1 sec are similar to the controlling events for PGA.
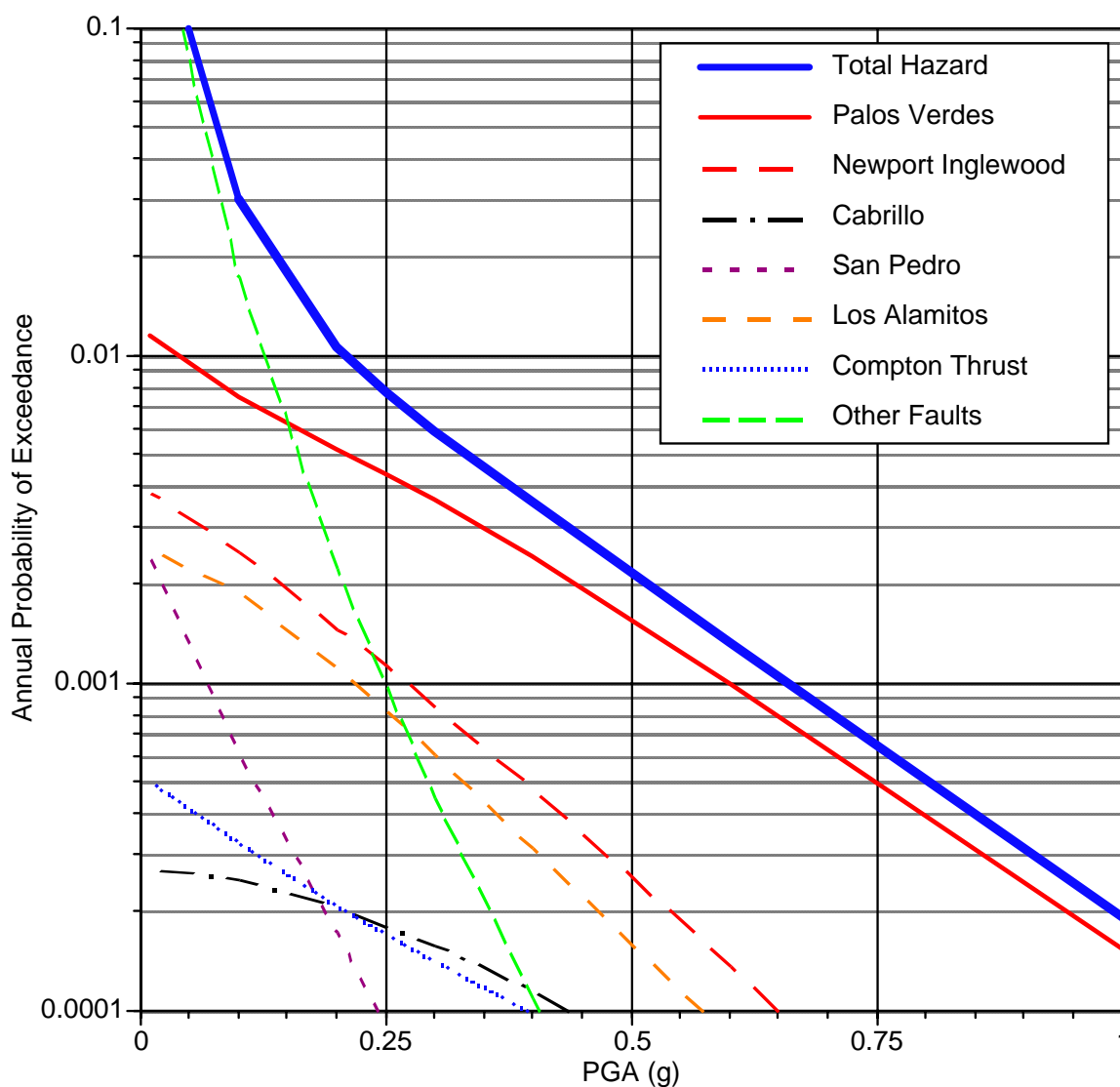
Figure 3-2.   Peak Ground Acceleration (PGA) Hazard by Source
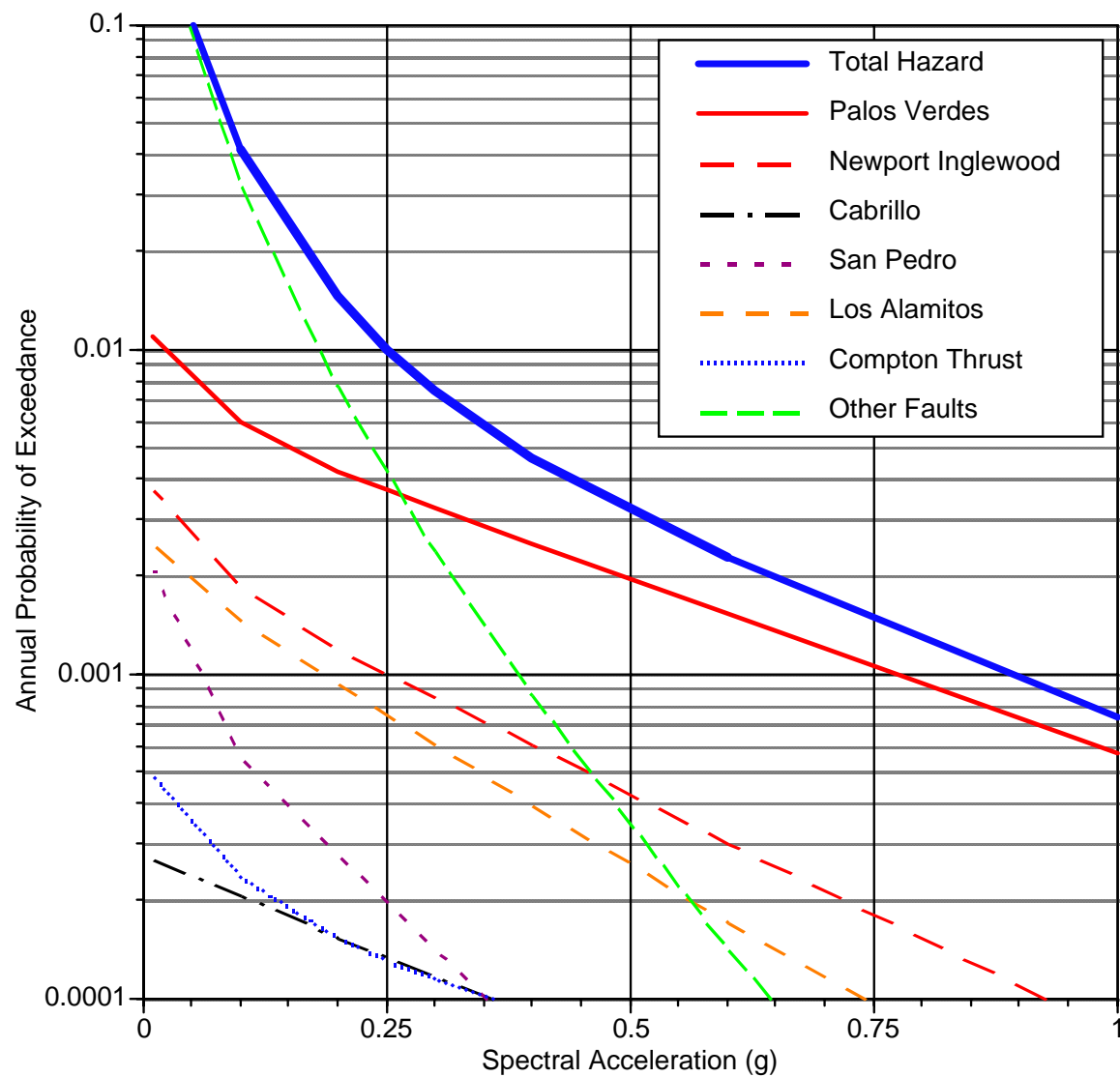
Figure 3-3.   T = 1.0 sec Spectral Acceleration Hazard by Source
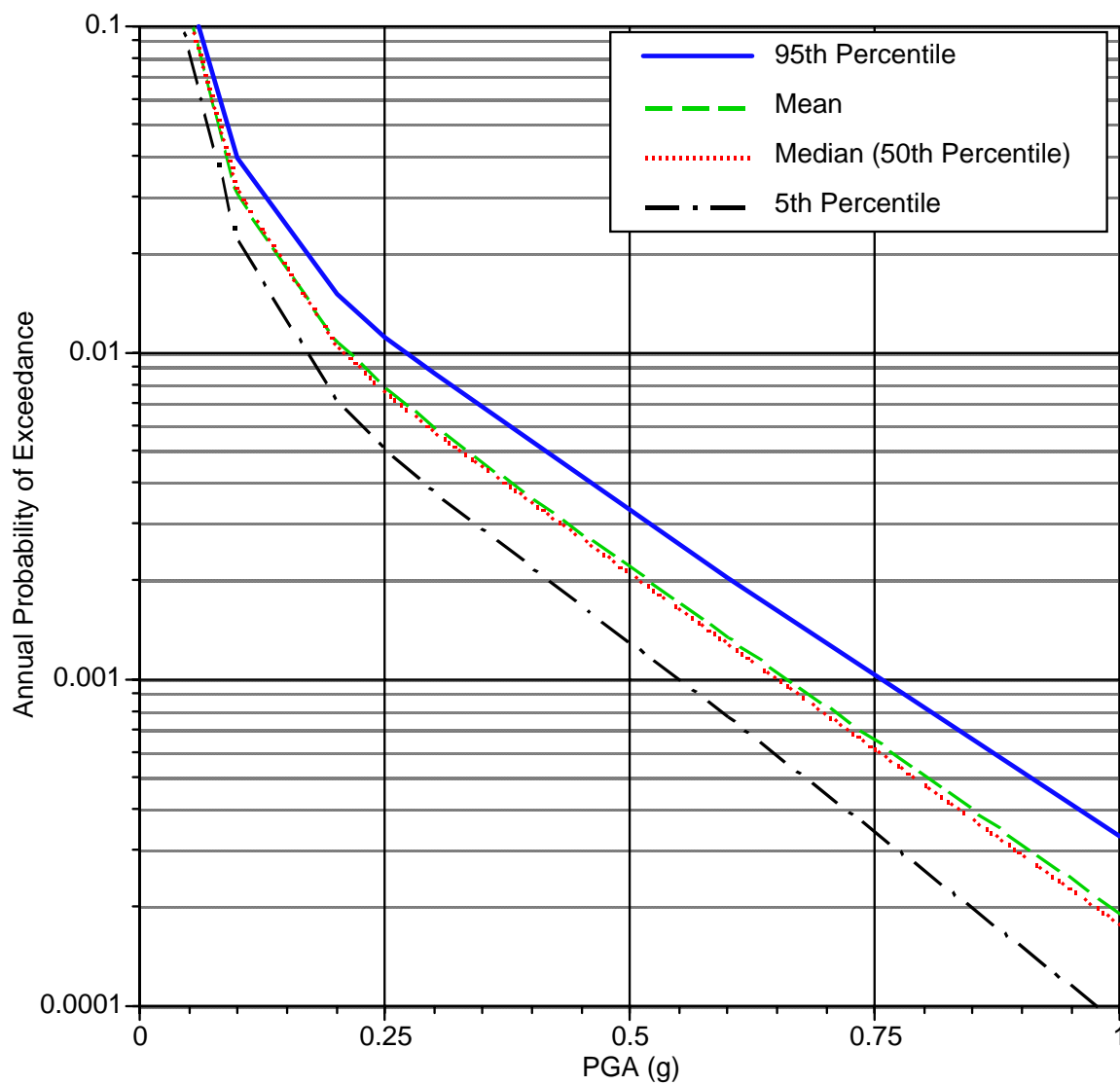
Figure 3-4.   Fractiles of the PGA Hazard Due to the Logic Tree
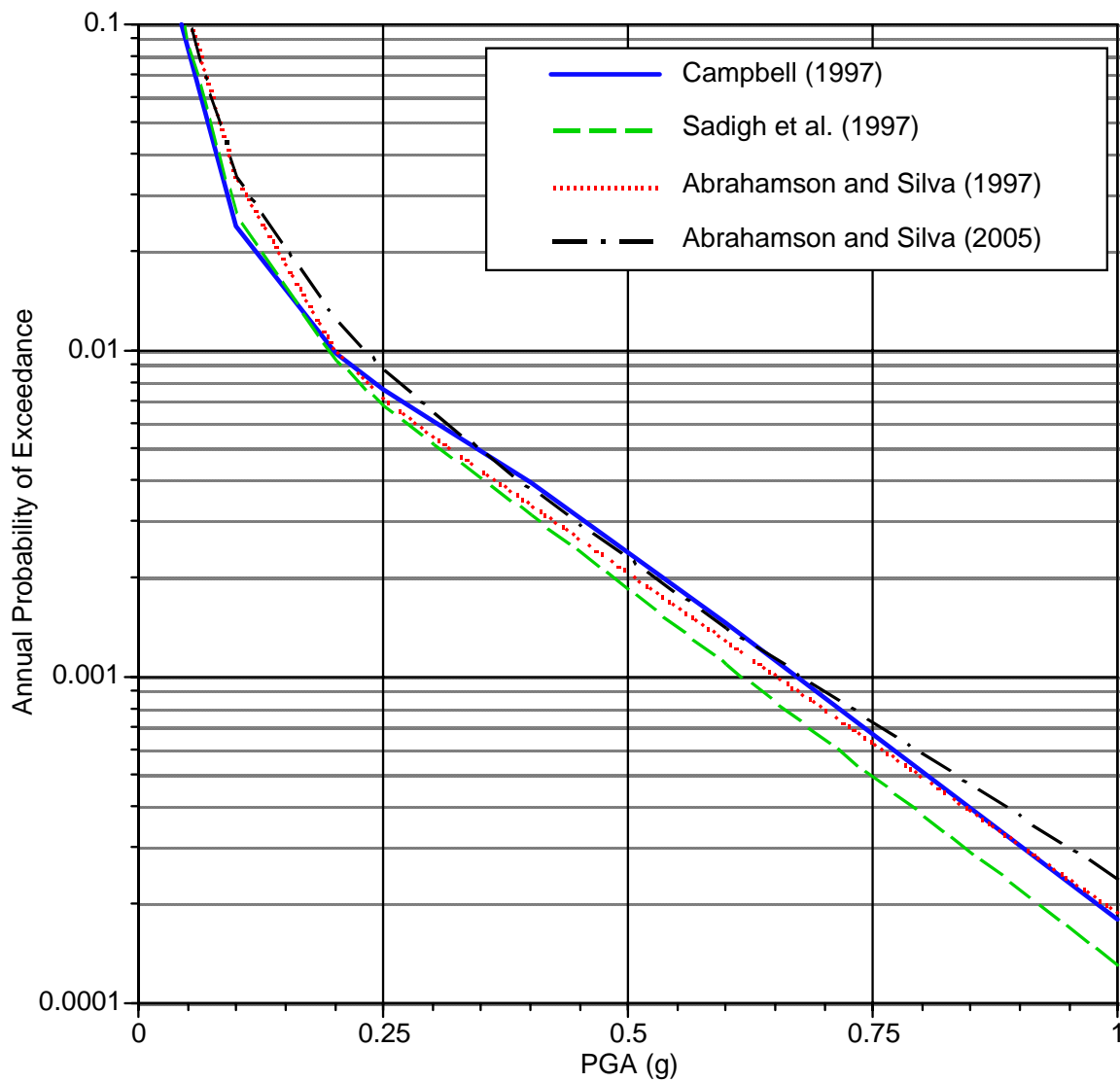
Figure 3-5.   Sensitivity of PGA Hazard to the Attenuation Relation
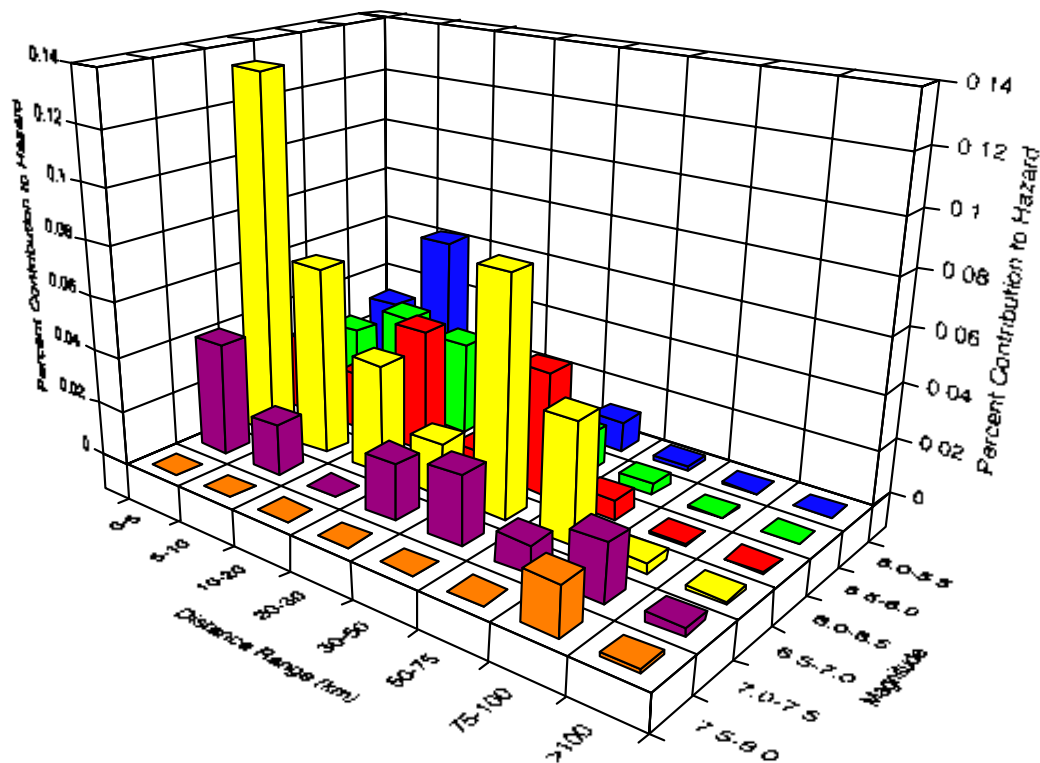
Figure 3-6.　　Deaggregation for PGA for 72-yr Return Period (OLE)
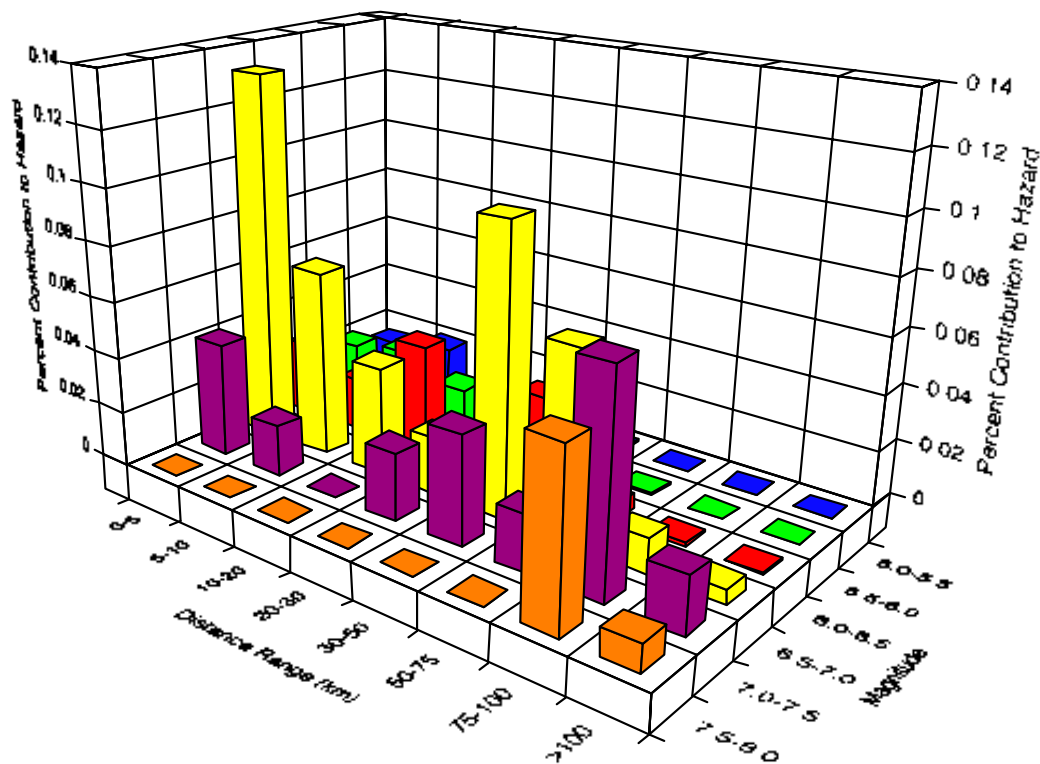
Figure 3-7.　　Deaggregation for T = 1.0 sec for 72-yr Return Period (OLE)
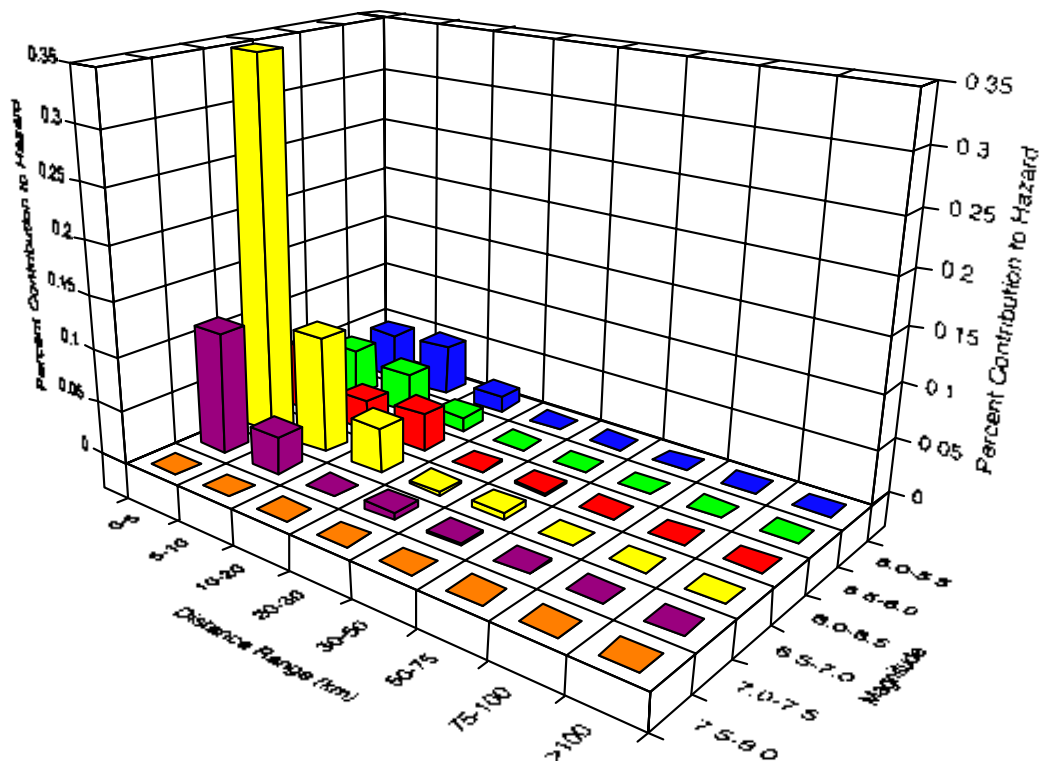
Figure 3-8.　Deaggregation for PGA for 475-yr Return Period (CLE)
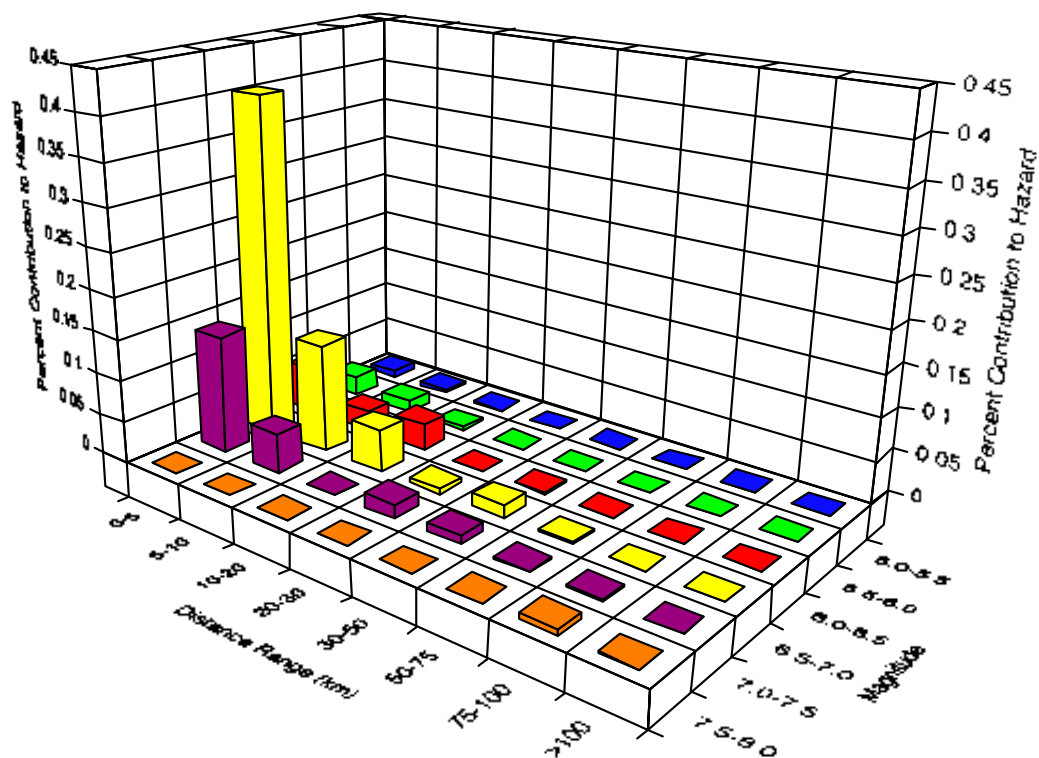
Figure 3-9.　Deaggregation for T = 1.0 sec for 475-yr Return Period (CLE)

3.3.3 Uniform Hazard Spectra for Firm Ground

The horizontal (FN and FP) and vertical (FV) components of the uniform hazard spectra for firm ground and return periods of 72 and 475 years are shown in Figure 3-10 and Figure 3-11, respectively. The spectral coordinates are listed in Table 3-4. These spectra are for Site 1 within Pier T at the western end of the Port which is located closest to the Palos Verdes fault zone. The spectra were extrapolated to a period of 10 sec based on empirical spectral shapes (normalized at T = 2 sec) of empirical ground motions that are reliable out to T = 10 sec.

The vertical spectrum is computed using the horizontal UHS with a V/H ratio. The V/H ratio is computed for the 72-yr (OLE) and 475-year (CLE) return periods using the Abrahamson and Silva (1997) model for the dominant source (M, R) identified in the deaggregation. For the OLE, the dominant source is a M6.5± earthquake at a distance of about 20 km. For the CLE, the dominant source is a M7.0± earthquake at a distance of about 4 km. The V/H ratios for these two hazard levels are shown in Figure 3-12. Note that the V/H ratio is not the commonly assumed value of 2/3. At short periods, the V/H ratio is greater than 2/3 and at moderate and long periods, the V/H ratio is less than 2/3.

Table 3-5 shows the average horizontal spectral acceleration and pseudo relative displacement values for various damping levels (1%, 2%, 5%, 10%, 20%, and 25%) for the OLE event. Table 3-6 shows the spectral values for the CLE event.

The firm-ground UHS in Table 3-4 is for Site 1 which is located at Pier T (118.2367°W, 33.7533°N) at the western end of the Port closest to the Palos Verdes fault zone. To evaluate the variability of the UHS across the Port, the UHS for both return periods was computed for three alternative locations:

- Southeast Site/Pier J (118.1958°W, 33.7400°N),
- Northeast Site/Pier C (118.2103°W, 33.7771°N), and
- Northwest Site/Pier S (118.2319°W, 33.7664°N).

The site locations are shown on the map of Figure 2-6. The average horizontal UHS at these sites are shown in Figure 3-13 for the 72-yr return period (OLE) and Figure 3-14 for the 475-yr period. The figures show that the UHS are similar among all sites (within 5%). The hazard is slightly higher at the Site 1 for the CLE.

Figure 3-15 shows the average horizontal FN and FP components of the firm-ground UHS for return periods of 72 (OLE), 100, 300, 475 (CLE), 1000, 1500, 2000 and 2500 years for Site 1 and 5% damping. Table 3-7 tabulates the corresponding firm-ground UHS acceleration values.

Table 3-4. **Spectral Acceleration Values of UHS for Firm Ground at Site 1**
(5% Damping)

Period (sec)	72-yr Return Period			475-yr Return Period		
	Horizontal Fault Normal	Horizontal Fault Parallel	Vertical	Horizontal Fault Normal	Horizontal Fault Parallel	Vertical
0.010	0.173	0.173	0.129	0.496	0.496	0.515
0.020	0.173	0.173	0.129	0.496	0.496	0.515
0.030	0.173	0.173	0.157	0.496	0.496	0.687
0.050	0.214	0.214	0.247	0.614	0.614	1.229
0.075	0.266	0.266	0.287	0.762	0.762	1.456
0.100	0.317	0.317	0.289	0.910	0.910	1.386
0.120	0.335	0.335	0.276	0.954	0.954	1.231
0.150	0.361	0.361	0.268	1.021	1.021	1.032
0.170	0.379	0.379	0.255	1.066	1.066	0.928
0.200	0.405	0.405	0.235	1.132	1.132	0.800
0.300	0.399	0.399	0.179	1.121	1.121	0.540
0.400	0.360	0.360	0.144	1.029	1.029	0.418
0.500	0.329	0.329	0.122	0.958	0.958	0.340
0.750	0.257	0.257	0.091	0.735	0.733	0.231
1.000	0.212	0.212	0.074	0.620	0.616	0.186
1.500	0.152	0.152	0.053	0.449	0.444	0.131
2.000	0.114	0.115	0.043	0.331	0.327	0.108
3.000	0.063	0.063	0.027	0.196	0.190	0.073
4.000	0.039	0.039	0.020	0.129	0.125	0.056
5.000	0.026	0.026	0.014	0.092	0.089	0.045
6.000	0.019	0.019	0.012	0.068	0.066	0.036
8.000	0.011	0.011	0.008	0.041	0.040	0.027
10.000	0.007	0.007	0.005	0.026	0.026	0.017

Table 3-5. Spectral Acceleration and Relative Displacement Values for Firm-Ground UHS at Site 1 for OLE at Various Damping Levels

Period (sec)	Damping											
	1%		2%		5%		10%		20%		25%	
	Acc. (g)	Disp. (in)	Acc. (g)	Disp. (in)	Acc. (g)	Disp. (in)	Acc. (g)	Disp. (in)	Acc. (g)	Disp. (in)	Acc. (g)	Disp. (in)
0.01	0.173	0.000	0.173	0.000	0.173	0.000	0.173	0.000	0.173	0.000	0.173	0.000
0.03	0.186	0.002	0.181	0.002	0.173	0.002	0.165	0.001	0.156	0.001	0.154	0.001
0.10	0.430	0.04	0.385	0.04	0.317	0.03	0.264	0.03	0.211	0.02	0.195	0.02
0.20	0.590	0.23	0.514	0.20	0.405	0.16	0.322	0.13	0.244	0.10	0.222	0.09
0.30	0.582	0.51	0.507	0.45	0.399	0.35	0.318	0.28	0.241	0.21	0.219	0.19
0.40	0.524	0.82	0.456	0.71	0.360	0.56	0.286	0.45	0.217	0.34	0.197	0.31
0.50	0.479	1.17	0.417	1.02	0.329	0.81	0.262	0.64	0.198	0.49	0.180	0.44
0.75	0.375	2.06	0.326	1.80	0.257	1.42	0.205	1.13	0.155	0.85	0.141	0.78
1.00	0.305	2.98	0.267	2.61	0.212	2.07	0.170	1.66	0.130	1.27	0.118	1.16
1.50	0.215	4.72	0.189	4.17	0.152	3.36	0.124	2.73	0.096	2.12	0.088	1.95
2.00	0.158	6.18	0.140	5.50	0.115	4.49	0.094	3.69	0.074	2.91	0.069	2.69
3.00	0.084	7.40	0.076	6.67	0.063	5.58	0.053	4.69	0.043	3.81	0.040	3.54
4.00	0.050	7.90	0.046	7.20	0.039	6.14	0.034	5.27	0.028	4.37	0.026	4.10
5.00	0.032	7.91	0.030	7.29	0.026	6.32	0.023	5.52	0.019	4.67	0.018	4.42
6.00	0.024	8.48	0.022	7.81	0.019	6.78	0.017	5.91	0.014	5.01	0.013	4.74
8.00	0.014	9.05	0.013	8.34	0.012	7.23	0.010	6.31	0.009	5.35	0.008	5.05
10.00	0.009	9.05	0.009	8.34	0.007	7.23	0.006	6.31	0.005	5.35	0.005	5.05

Table 3-6. Spectral Acceleration and Relative Displacement Values for Firm-Ground UHS at Site 1 for CLE at Various Damping Levels

Period (sec)	Damping											
	1%		2%		5%		10%		20%		25%	
	Acc. (g)	Disp. (in)	Acc. (g)	Disp. (in)	Acc. (g)	Disp. (in)	Acc. (g)	Disp. (in)	Acc. (g)	Disp. (in)	Acc. (g)	Disp. (in)
0.01	0.496	0.000	0.496	0.000	0.496	0.000	0.496	0.000	0.496	0.000	0.496	0.000
0.03	0.534	0.005	0.520	0.005	0.496	0.004	0.475	0.004	0.450	0.004	0.442	0.004
0.10	1.232	0.12	1.102	0.11	0.910	0.09	0.756	0.07	0.604	0.06	0.560	0.05
0.20	1.649	0.65	1.437	0.56	1.132	0.44	0.900	0.35	0.682	0.27	0.621	0.24
0.30	1.633	1.44	1.422	1.25	1.121	0.99	0.891	0.79	0.675	0.59	0.615	0.54
0.40	1.499	2.35	1.305	2.04	1.029	1.61	0.818	1.28	0.620	0.97	0.564	0.88
0.50	1.394	3.41	1.215	2.97	0.958	2.34	0.761	1.86	0.577	1.41	0.525	1.28
0.75	1.069	5.88	0.931	5.13	0.734	4.04	0.584	3.21	0.442	2.43	0.402	2.21
1.00	0.896	8.77	0.782	7.65	0.618	6.05	0.493	4.83	0.375	3.67	0.342	3.34
1.50	0.638	14.06	0.560	12.32	0.446	9.83	0.359	7.90	0.275	6.06	0.252	5.54
2.00	0.464	18.18	0.409	16.02	0.329	12.89	0.267	10.45	0.207	8.10	0.190	7.43
3.00	0.265	23.31	0.236	20.75	0.193	16.98	0.159	13.99	0.126	11.07	0.116	10.23
4.00	0.170	26.69	0.153	23.97	0.127	19.92	0.106	16.67	0.086	13.43	0.080	12.48
5.00	0.119	29.04	0.107	26.30	0.091	22.17	0.077	18.80	0.063	15.40	0.059	14.39
6.00	0.088	31.14	0.080	28.20	0.067	23.77	0.057	20.16	0.047	16.51	0.044	15.43
8.00	0.053	33.21	0.048	30.08	0.040	25.35	0.034	21.50	0.028	17.61	0.026	16.46
10.00	0.034	33.21	0.031	30.08	0.026	25.35	0.022	21.50	0.018	17.61	0.017	16.46
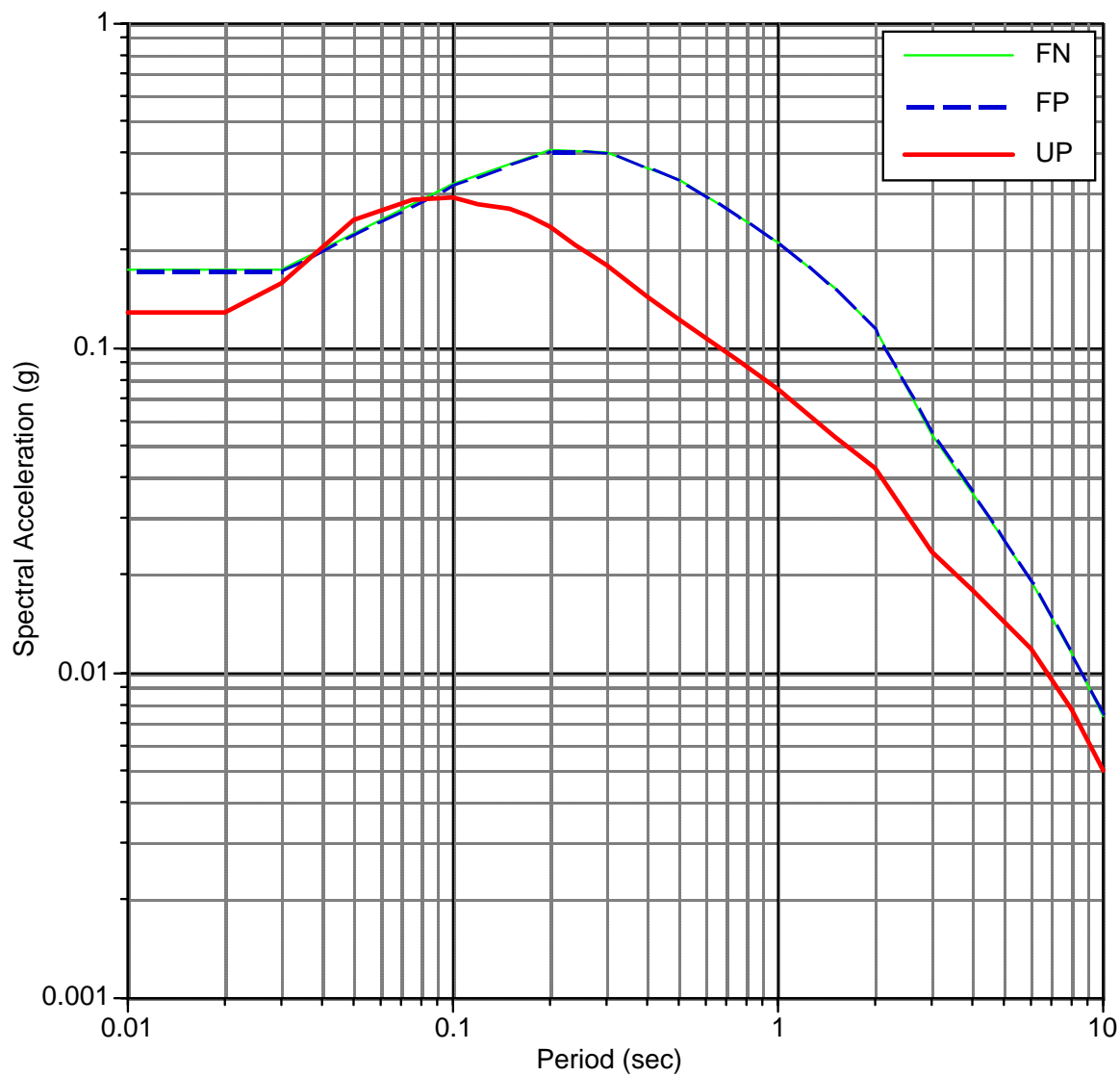
Figure 3-10.   Firm-Ground Uniform Hazard Spectra for 72-yr Return Period (OLE)
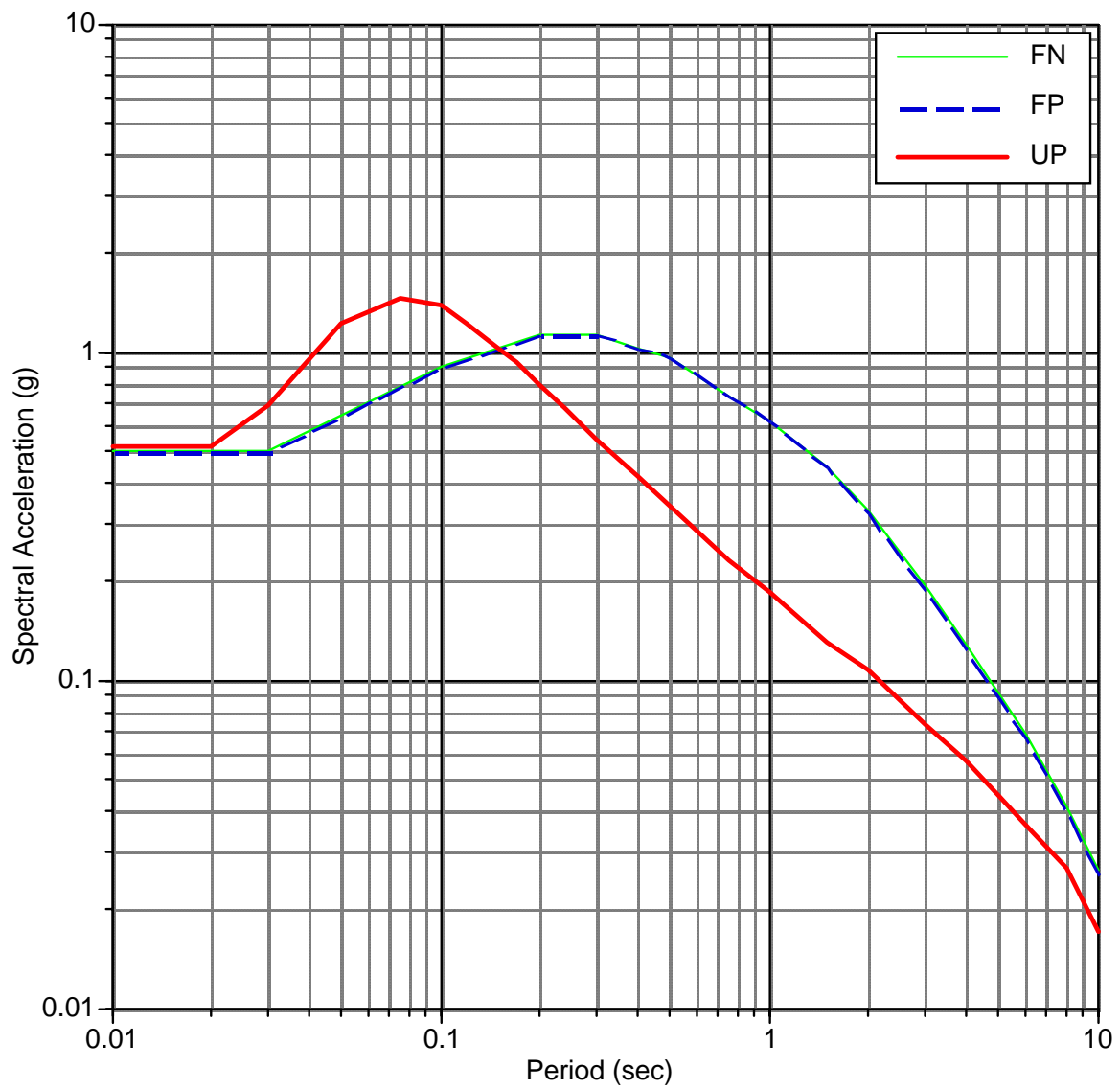
Figure 3-11. Firm-Ground Uniform Hazard Spectra for 475-yr Return Period (CLE)
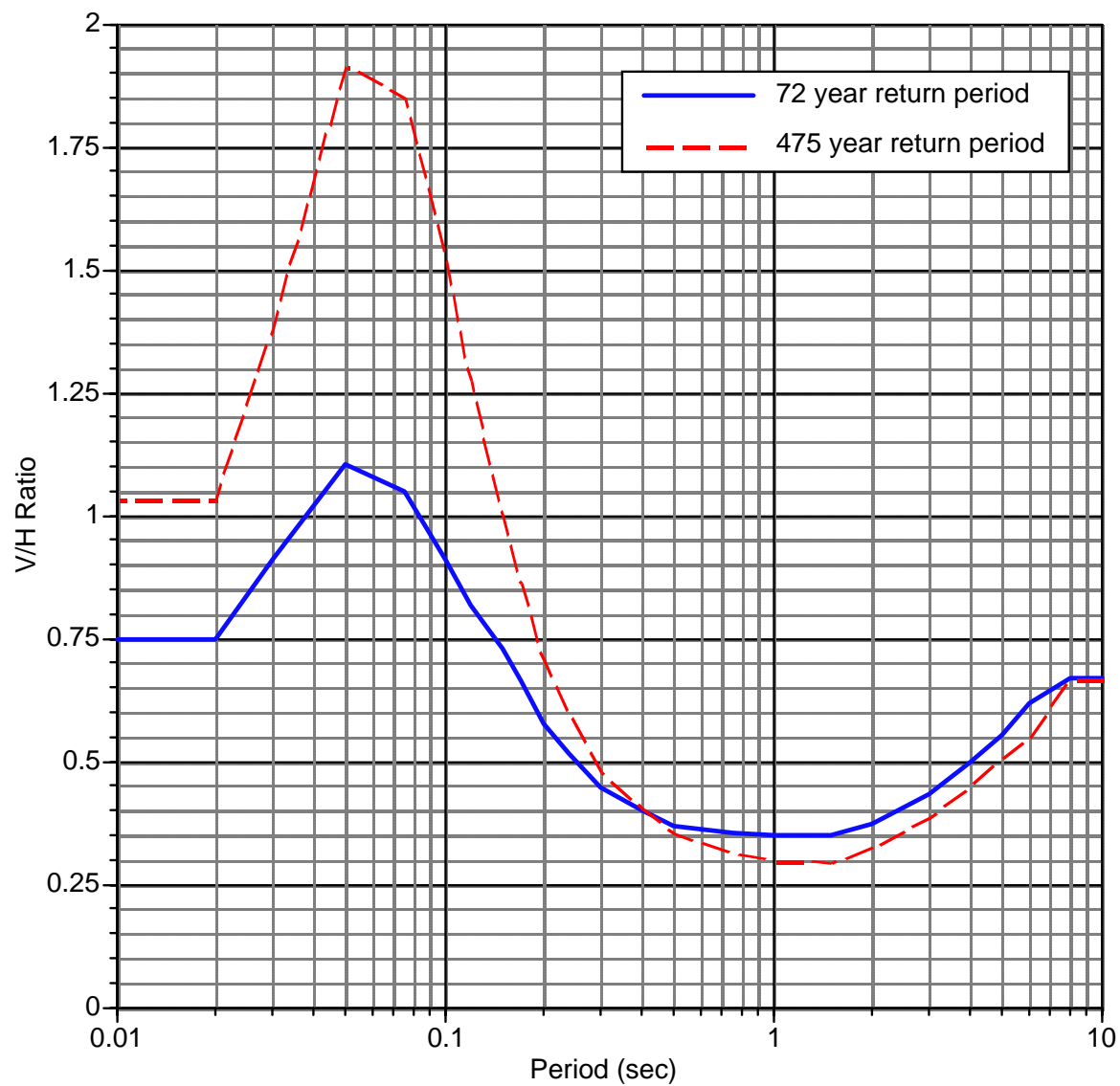
Figure 3-12.   V/H Ratio Based on Controlling Source for 72-yr and 475-yr Return Periods
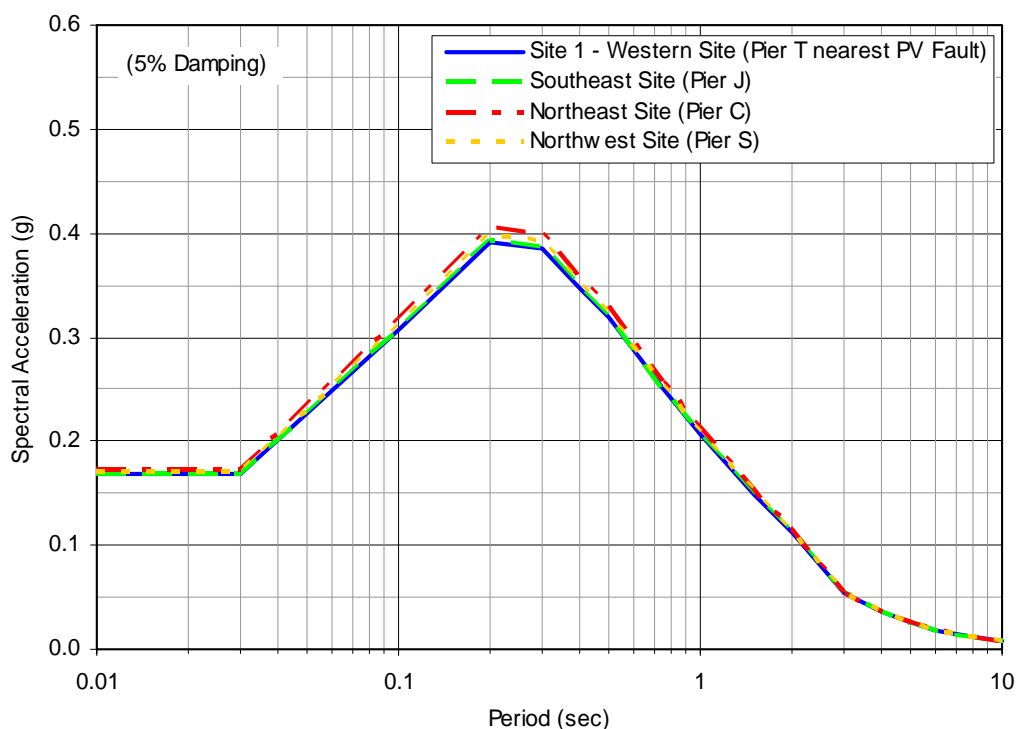
Figure 3-13.   Comparison of Firm-Ground UHS for 72-yr Return Period (OLE) at Four Sites
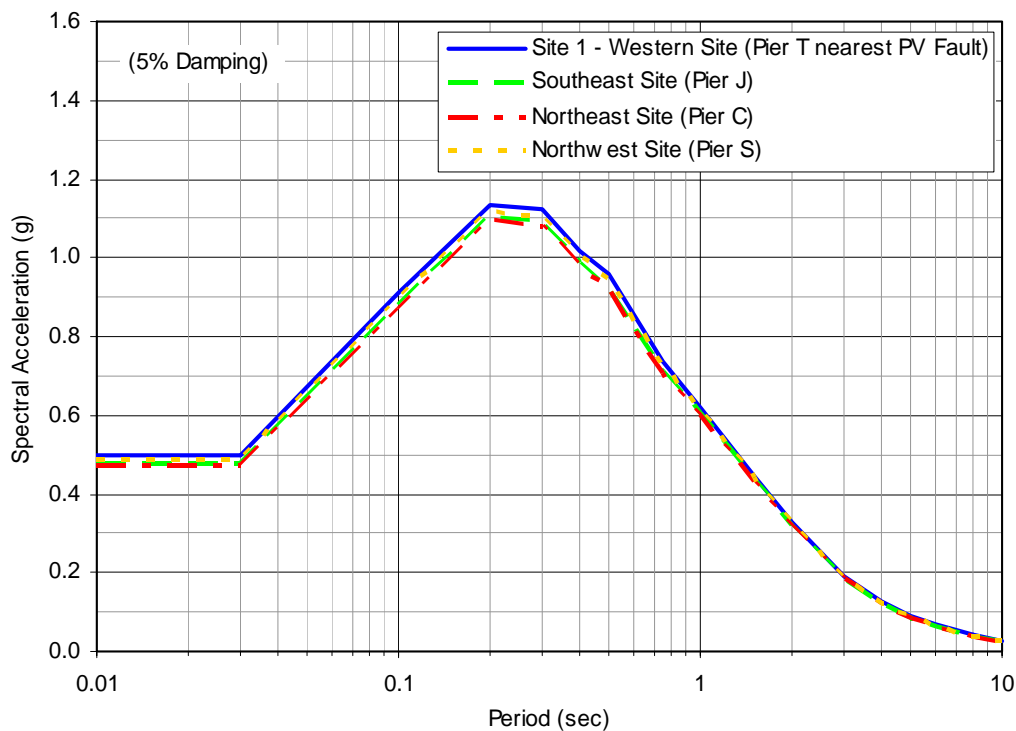
Figure 3-14.   Comparison of Firm-Ground UHS for 475-yr Return Period (CLE) at Four Sites

3-20
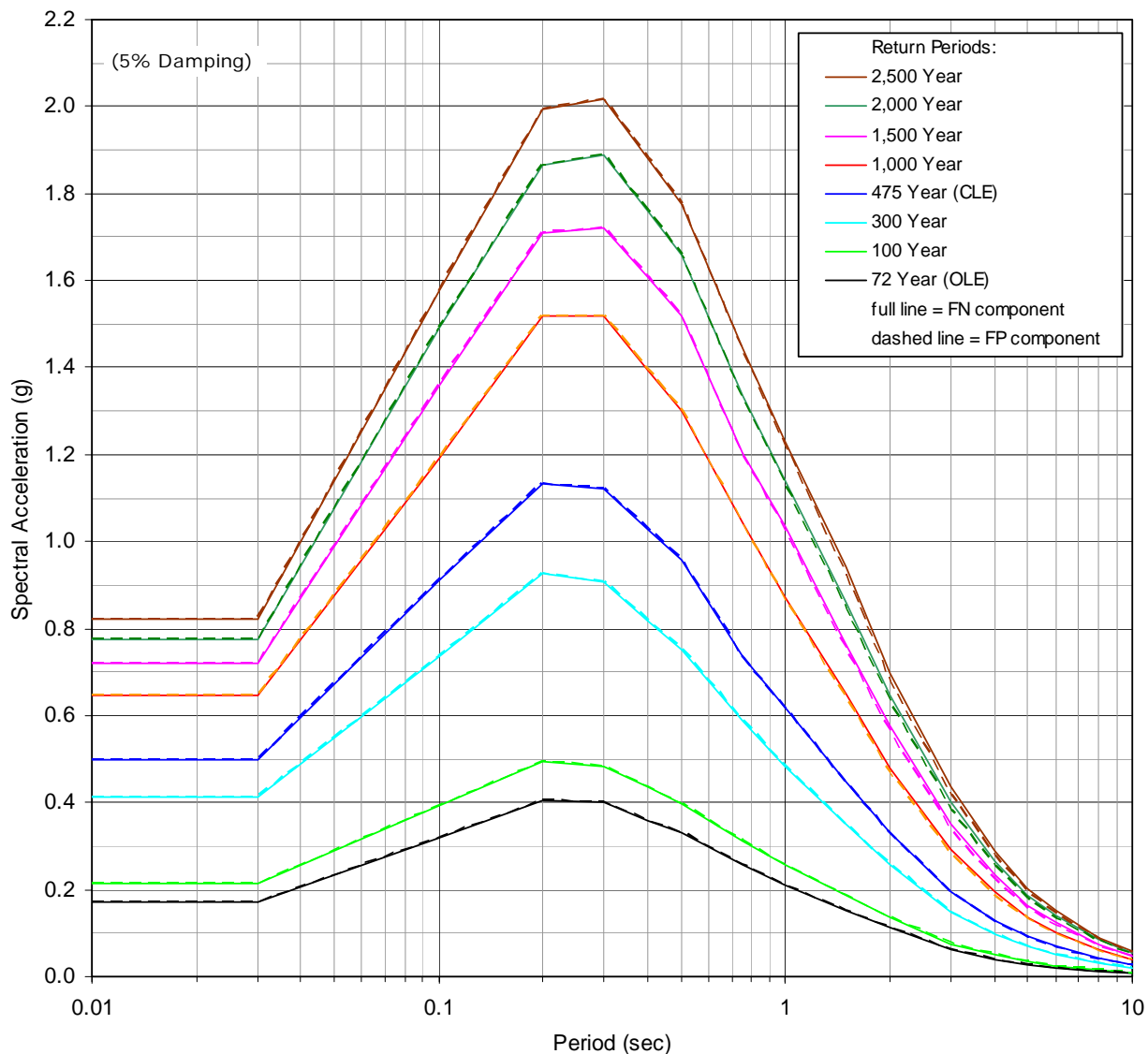
Figure 3-15.   Comparison of Firm-Ground UHS for Various Return Periods

Table 3-7. **Spectral Acceleration Values of Firm Ground UHS for Various Return Periods (5% Damping)**

Period (sec)	Spectral Acceleration (g) for Return Period of							
	72 Years (OLE)		100 Years		300 Years		475 Years (CLE)	
	FN	FP	FN	FP	FN	FP	FN	FP
0.01	0.173	0.173	0.213	0.213	0.413	0.413	0.496	0.496
0.03	0.173	0.173	0.213	0.213	0.413	0.413	0.496	0.496
0.10	0.317	0.317	0.393	0.393	0.734	0.734	0.910	0.910
0.20	0.405	0.405	0.494	0.494	0.926	0.926	1.132	1.132
0.30	0.399	0.399	0.484	0.484	0.908	0.908	1.121	1.121
0.40	0.360	0.360	0.436	0.436	0.819	0.819	1.029	1.029
0.50	0.329	0.329	0.398	0.398	0.750	0.750	0.958	0.958
0.75	0.257	0.257	0.310	0.310	0.588	0.587	0.735	0.733
1.00	0.212	0.212	0.256	0.256	0.483	0.481	0.620	0.616
1.50	0.152	0.152	0.185	0.185	0.350	0.347	0.449	0.444
2.00	0.114	0.115	0.137	0.138	0.258	0.256	0.331	0.327
3.00	0.063	0.063	0.076	0.076	0.149	0.147	0.196	0.190
4.00	0.039	0.039	0.049	0.049	0.098	0.097	0.129	0.125
5.00	0.026	0.026	0.034	0.034	0.070	0.069	0.092	0.089
6.00	0.019	0.019	0.025	0.025	0.052	0.051	0.068	0.066
8.00	0.011	0.011	0.015	0.015	0.031	0.031	0.041	0.040
10.00	0.007	0.007	0.010	0.010	0.020	0.020	0.026	0.026
Period (sec)	Spectral Acceleration (g) for Return Period of							
	1,000 Years		1,500 Years		2,000 Years		2,500 Years	
	FN	FP	FN	FP	FN	FP	FN	FP
0.01	0.647	0.647	0.719	0.719	0.776	0.776	0.823	0.823
0.03	0.647	0.647	0.719	0.719	0.776	0.776	0.823	0.823
0.10	1.193	1.193	1.358	1.358	1.493	1.493	1.577	1.577
0.20	1.519	1.519	1.711	1.711	1.866	1.866	1.994	1.994
0.30	1.519	1.519	1.722	1.722	1.887	1.887	2.017	2.017
0.40	1.396	1.396	1.607	1.607	1.758	1.758	1.881	1.881
0.50	1.300	1.300	1.517	1.517	1.659	1.659	1.775	1.775
0.75	1.042	1.038	1.203	1.197	1.335	1.328	1.446	1.438
1.00	0.872	0.863	1.034	1.026	1.142	1.131	1.231	1.219
1.50	0.648	0.639	0.764	0.750	0.861	0.844	0.943	0.923
2.00	0.480	0.469	0.576	0.560	0.644	0.629	0.697	0.679
3.00	0.293	0.280	0.352	0.335	0.401	0.381	0.434	0.416
4.00	0.193	0.185	0.232	0.221	0.264	0.251	0.287	0.275
5.00	0.138	0.131	0.165	0.158	0.188	0.179	0.204	0.196
6.00	0.103	0.098	0.123	0.117	0.140	0.133	0.152	0.146
8.00	0.062	0.059	0.074	0.070	0.084	0.080	0.091	0.087
10.00	0.039	0.038	0.047	0.045	0.054	0.051	0.058	0.056

3.3.4 Spectrum-Compatible Time Histories for CLE

Based on the deaggregation, the controlling earthquake for the 475-yr return period is of magnitude 6.5 to 7.5 occurring at a distance of 0 to 5 km with forward directivity.

The PEER NGA data set (version 5), consisting of over 3,500 recordings, was searched for ground motions from magnitudes 6.5 to 7.5 and stations with distances of 0 to 10 km, resulting in 68 candidate recordings. From this subset, the spectral shape of the empirical ground motion was compared to the spectral shape of the firm-ground UHS for the CLE for the average horizontal component. The 7 sets of candidate time histories which were used in the spectral matching procedure were selected from the resulting 68 records based on the similarity between the recorded spectral shape and the target spectral shape, forward directivity recording, and selection of several earthquakes. The seven selected sets of time histories are listed in Table 3-8. For each recording, the directivity parameter $x \cdot \cos \theta$ is given. This parameter is defined between values of 0 and 1, with larger values indicating a forward directivity case.

These ground motions were modified to match the UHS using the program RSPMATCH which uses the time-domain approach. The goal of this approach is to preserve the general non-stationary character of the ground motion in acceleration, velocity, and displacement while modifying the spectral response to match a given target response spectrum.

The initial 3-component time histories, modified time histories, and comparison of the matched spectra with the firm-ground UHS for the CLE are shown in Appendices D.1.

3.3.5 Spectrum-Compatible Time Histories for OLE

Based on the deaggregations, the controlling earthquake for the 72-yr return period is of Magnitude 6.0 to 7.0 occurring at about 20 km distance with neutral directivity. The startup time history records used for the OLE spectrum-compatible motions as well as firm-ground and design motions are discussed in Section 5.3.1.5.

Table 3-8.   Time Histories Selected for CLE Spectral Matching

Set	Earthquake	Magnitude	Station	Distance (km)	Directivity Parameter $x \cdot \cos \theta$
1	1999 Hector Mine	7.1	Hector	12	0.57
2	1989 Loma Prieta	6.9	Gilroy 03	13	0.45
3	1979 Imperial Valley	6.5	Brawley	10	0.75
4	1999 Duzce	7.1	Lamont 1059	4	0.36
5	1992 Erzikan	6.7	Erzikan	4	0.31
6	1940 Imperial Valley	7.0	El Centro	6	0.14
7	1995 Kobe	6.9	Kobe University	1	0.42

SECTION 4
EARTHQUAKE SITE RESPONSE

4.1   METHODOLOGY

Incorporation of earthquake site response was based on one-dimensional response theory with adjustments applied to address modeling and physical issues. One-dimensional response calculations were undertaken using the computer program SHAKE91 (Idriss and Sun, 1992), a proven and widely used numerical analysis method. However, the program assumes horizontally layered soil deposits subjected to vertically propagating shear wave and only recognizes nonlinear stress-strain behavior of soil in the form of shear-strain-dependent equivalent-linear shear modulus and damping values.

4.2   RESULTS

Site response analyses were conducted using SHAKE91 for the four representative soil columns for Zones I, II, III and IV shown in Figure 2-7. The effect of site response modification is expressed in terms of a period-dependent transfer function defined by the ratio of the resultant ground surface spectral amplitude to the firm-ground spectral amplitude for each period. For each soil column, site response analyses were conducted for a best-estimate shear wave velocity profile as well as for a stiffer and a softer shear wave velocity profile to account for basic uncertainties in site soil properties. For each of the three shear wave velocity models, site response analyses were conducted using 6 horizontal component input motions for each of the OLE and the CLE ground shaking levels. This resulted in 18 site response solutions for each of the 4 soil columns for the OLE and CLE. The 18 solutions were then averaged to develop the site response transfer function for each soil profile as shown in Figure 4-1 and Figure 4-2 for OLE and CLE, respectively.

It can be observed from both figures that the shapes of transfer functions for Zones II, III and IV are similar in the entire period range. For these three zones, the transfer functions for OLE in Figure 4-1 are less than 1 at periods below 0.5 sec and greater than 1 at higher periods. The transfer function for the CLE in Figure 4-2 is less than 1 at periods below 0.2 sec, and greater than 1 at higher periods for the three zones. In contrast, Zone I reflects the stiffest shear wave velocity profile analyzed (see Figure 2-7) and the transfer functions for OLE and CLE are closer to 1 throughout the entire period range than for the other three zones. At the fundamental site response period for the four soil profiles (periods above 0.5 sec), the transfer function of Zones III has the highest values compared to the other zones for both OLE and CLE. For periods below 0.5 sec, the transfer function of Zone I has the highest values for both OLE and CLE.

The OLE and CLE firm-ground spectra for Site 1 representative for the port-wide UHS were shown in Figure 3-10 and Figure 3-11, respectively. The spectral ordinates of these spectra were listed in Table 3-5 and Table 3-6, respectively. As a result of the above observations, the transfer functions for Zones I and III were applied to the OLE and CLE port-wide firm-ground UHS (respectively) by direct scaling to conservatively account for site-response effects port-wide.

For the OLE, all four site effect-adjusted UHS and the firm-ground UHS were then enveloped to obtain the resultant port-wide theoretical site effect-adjusted UHS shown in Figure 4-3. The spectral values are given in Table 4-1.

For the CLE, a similar approach but with additional adjustments was used. Experienced geotechnical engineers have long recognized that there are some inherent problems in the site response analysis procedure using SHAKE91. Generally, the equivalent-linear site response analysis procedure tends to overdamp the ground motion at short-period range and over-exaggerate the site response effect at the fundamental frequency of the soil column. Also, it is common knowledge that the equivalent-linear site response method yields more reasonable site response solutions at lower ground shaking levels (with PGA below 0.3g range), whereas at higher levels, the equivalent-linear site response solutions begin to break down due to stronger nonlinear stress-strain behavior of the soil. As a result, the site effect-adjusted spectra for the CLE were modified to compensate for these limitations in the equivalent-linear site response analysis. The port-wide theoretical site effect-adjusted spectrum was obtained by enveloping the four site effect-adjusted and the firm-ground spectra at the short-period range up to 0.5 sec and by softening the site effect-adjusted UHS over the 0.5 to 2.0-sec period range. The resulting port-wide theoretical site effect-adjusted spectrum is shown in Figure 4-4 and the spectral values are given in Table 4-1. The difference between this spectrum and the firm-ground spectrum is consistent with the site soil adjustment factors recommended by NEHRP (Table 3.3-2 in FEMA, 2003) for spectral accelerations at 1 sec period.

Table 4-1.   Spectral Values for Theoretical Site-Effect Adjusted UHS (5% Damping)

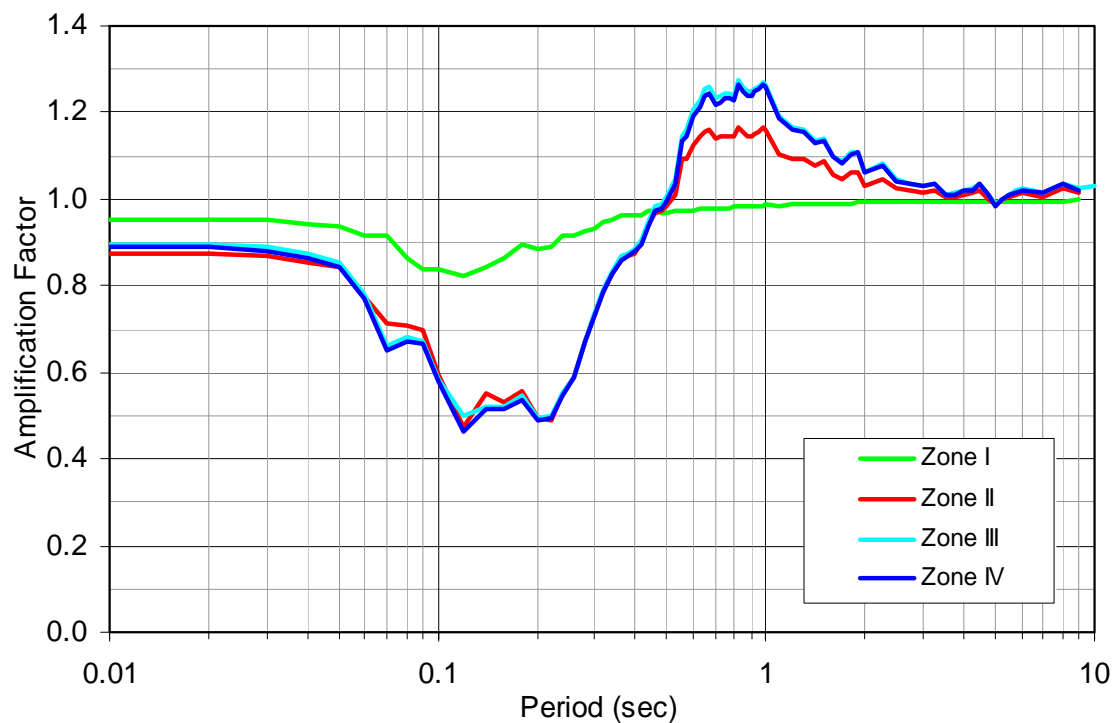| Period (sec)	Average Horizontal Spectral Acceleration (g)	
	OLE (see Figure 4-3)	CLE (see Figure 4-4)
0.01	0.173	0.497
0.03	0.173	0.497
0.10	0.317	0.910
0.20	0.405	1.138
0.30	0.400	1.210
0.40	0.382	1.133
0.50	0.365	1.028
0.75	0.320	0.840
1.00	0.268	0.717
1.50	0.174	0.515
2.00	0.122	0.362
3.00	0.065	0.199
4.00	0.040	0.128
5.00	0.026	0.091
6.00	0.020	0.068
8.00	0.012	0.041
10.00	0.008	0.026

Figure 4-1. **Transfer Functions for 72-yr Return Period (OLE)**
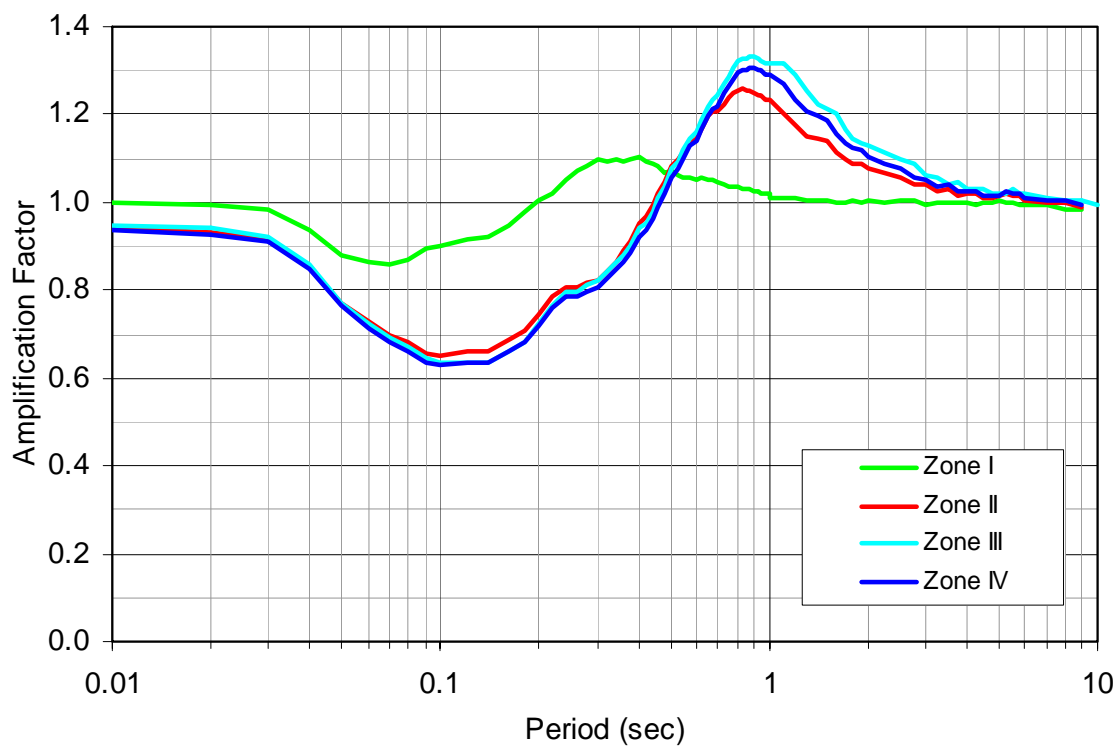

Figure 4-2. **Transfer Functions for 475-yr Return Period (CLE)**
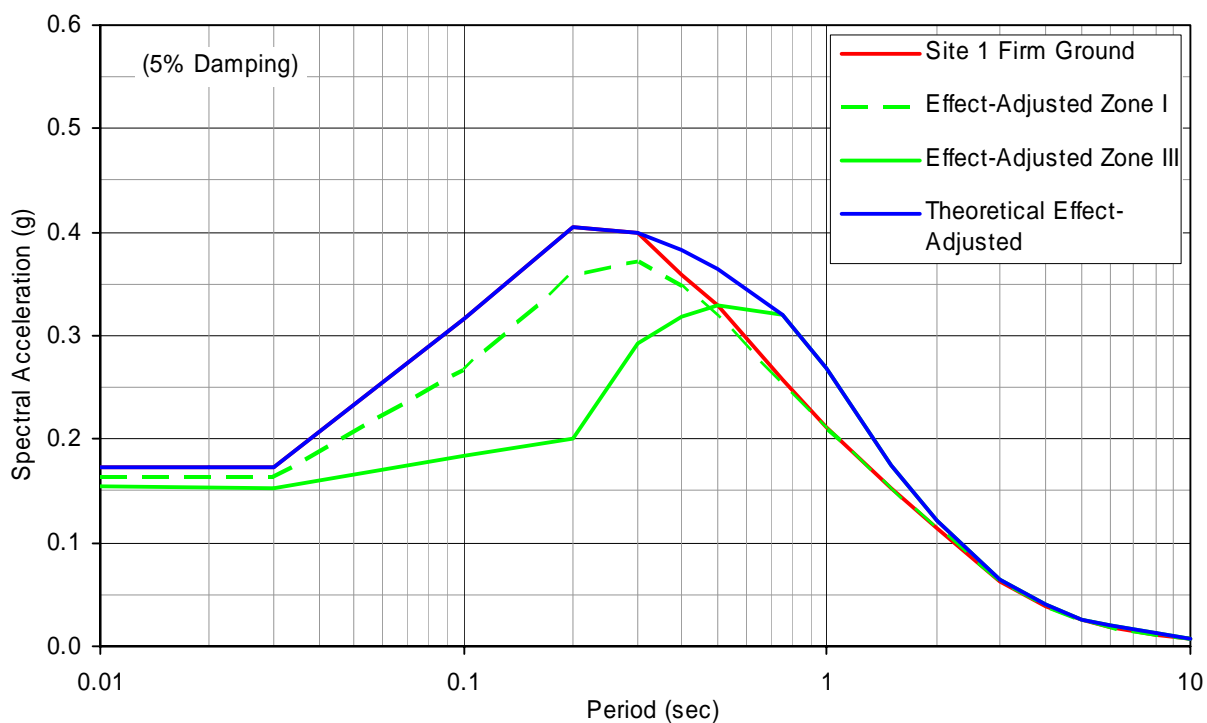
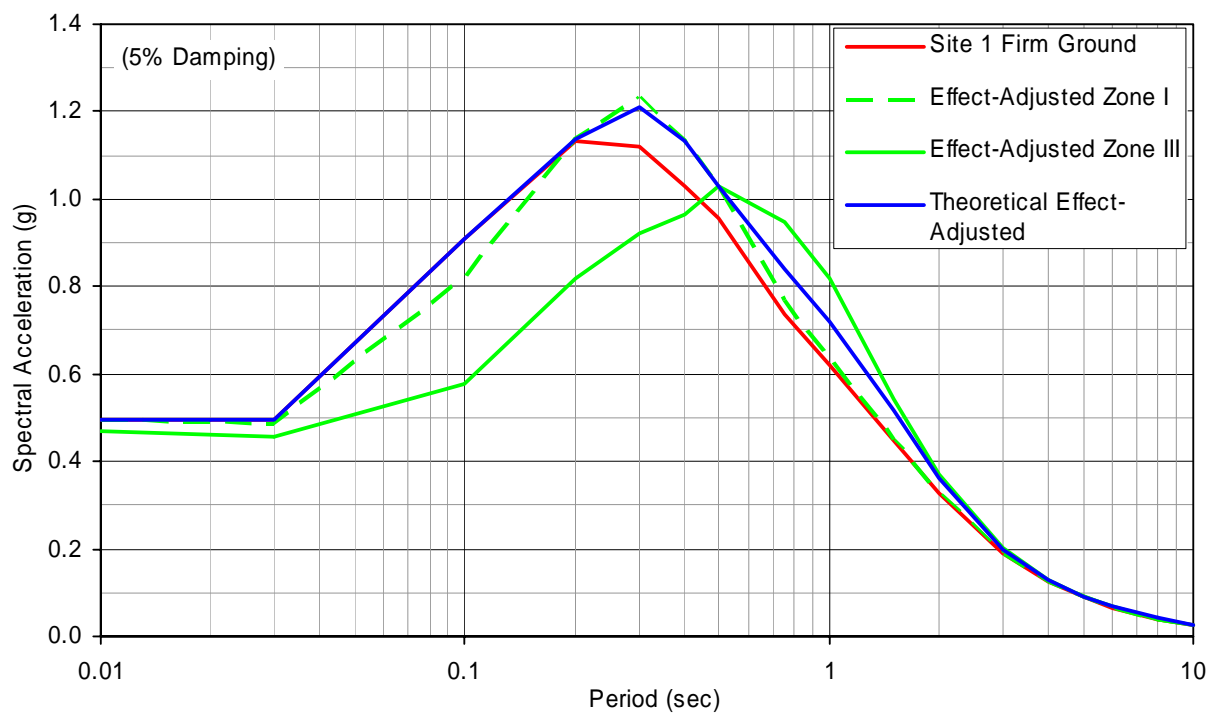**Figure 4-3.** **Theoretical Site Effects for OLE**

Figure 4-4. **Theoretical Site Effects for CLE**

SECTION 5
SUMMARY, CONCLUSIONS,
AND DESIGN RECOMMENDATIONS

5.1   OVERVIEW

The Port's past practice toward the development of ground motion criteria for design has been to conduct site-specific studies for each project by the design teams selected for these projects. This approach has the benefit of site-specific data being utilized for each project. However, over the years, there have often been significant discrepancies among various recommendations among various consultants.

EMI's scope of work includes conducting a port-wide ground motion study to resolve some of the inherent issues contributing to inconsistent design criteria experienced among past POLB projects and to develop a consistent set of ground motion recommendations that can be used on future container wharf projects and other types of structures. The scope of work included:

- Assemble an expert advisory panel representing the academic community and practicing professionals to review past ground motion studies sponsored by the POLB, and to determine reasons contributing to discrepancies in prior studies.

- Together with the expert panel, review developments in the seismological, geological and geotechnical communities to select the most up-to-date and appropriate basis for conducting a ground motion study for the POLB.

- Using the most appropriate models and technical approaches, conduct sensitivity studies to clarify the key parameters affecting ground motion design criteria for the POLB structures.

- Propose appropriate ground motion design criteria to be used for future design of conventional container wharves and other types of structures within the POLB.

- Identify potential future developments that would require updates of the ground motion recommendations developed in this study.

5.2   MAJOR FINDINGS

As the first task in our scope of work, we compiled OLE (72-year return period) and CLE (475-year return period) design response spectra recommended in several past consultants' reports to the POLB in order to appreciate the range of variations in the recommended spectra.

Figure 5-1 and Figure 5-2 summarizes the comparisons for OLE and CLE spectra from the various POLB ground motion criteria studies, respectively. It can be observed that there is a wide range of variation in the recommended design spectra proposed to the POLB. For the OLE, the ratio of highest to lowest shaking values were on the order of 2.1 at 0.5 sec, 2.4 at 0.7 sec, 2.5 at 1 sec, and over 2.0 at periods longer than 2 sec. For the CLE, the highest versus the lowest shaking values were observed to be approximately 1.3 at 0.5 sec, 1.4 at 0.7 sec, 1.6 at 1 sec, and 1.8 at periods longer than 2 sec. The reasons for the large variation cannot be easily explained, especially from the structural designer's point of view. The following are possible reasons for the observed variations:

- Differences in the modeling approach for the seismic sources.

- Differences in the assumed recurrence relationships. This issue could contribute to significant variations in the various recommended OLE spectra (see Section 5.3.1).

- Differences in treatment of attenuation relationships, especially for long-period motion adjustments to account for near-fault directivity effects. We believe that this issue may account for the observed variation of the CLE spectra, especially at longer-period range above 2 sec.

- Differences in the approach to resolve site response issues also contributed to significant variations in the recommended design spectra.

We also reviewed the ground motion recommendations provided to the POLB from other consultants, and conducted a number of sensitivity studies. The results and findings summarized below speculate on some of the reasons for the wide range of recommendations among different consultants and provide some key conclusions on which our recommendations to the POLB were based:

- The Palos Verdes fault dominates the ground motion at various locations at the POLB, especially for the CLE scenario. The Newport Inglewood fault also contributes to the ground motion shaking hazard at POLB to some minor extent. Other more distant faults can generally be ignored for ground shaking issues associated with the CLE event.

- Variation in expected shaking levels due to differing distances among POLB locations to the Palos Verdes fault is small (less than 12% for the CLE and less than 4% for the OLE). This would justify adopting one set of port-wide design spectra for all future port projects.

- As discussed in Section 4, unlike other ports, such as the Port of Oakland or the Port of Los Angeles (POLA), anomalous soil conditions such as underconsolidated to normally consolidated soft clay sites that are the cause for extremely large site amplification effects do not seem prevalent in the predominately alluvial deposit geologic environment at the POLB. Based on our findings from the site response analyses, it would be easy to exaggerate site amplification effects due to defining input motions at large depths, or by creating artificial impedance contrasts in the site response model such as at the transmitting boundary for the SHAKE91 profile. From our experience, if a site response

analysis is properly conducted, site amplification effects tend to be no higher than about 35% for alluvial sites such as those present at the POLB. Undoubtedly, there are other issues such as basin effects or topography effect of the slope configuration which can contribute to arguments for changes to the ground motion design criteria. However, we believe that much of these variations have been implicitly accounted for in a probabilistic seismic hazard solution by the large standard deviation used in the attenuation relationship. Also, from what we have observed as presented by comparisons of past consultant recommendations on ground motion criteria to the POLB, there is a great danger for projecting unsubstantiated variations in the design criteria which largely led to delays and inconsistencies in the resulting design.

We believe that there is significant merit in adopting the ground motion criteria for port-wide design applications provided in Section 5.3. However, it should be recognized that this report is a living document that needs to be updated periodically to incorporate future advances in the seismological, geological, and geotechnical communities. Section 7 discusses some potential developments that could trigger the need for such updates.
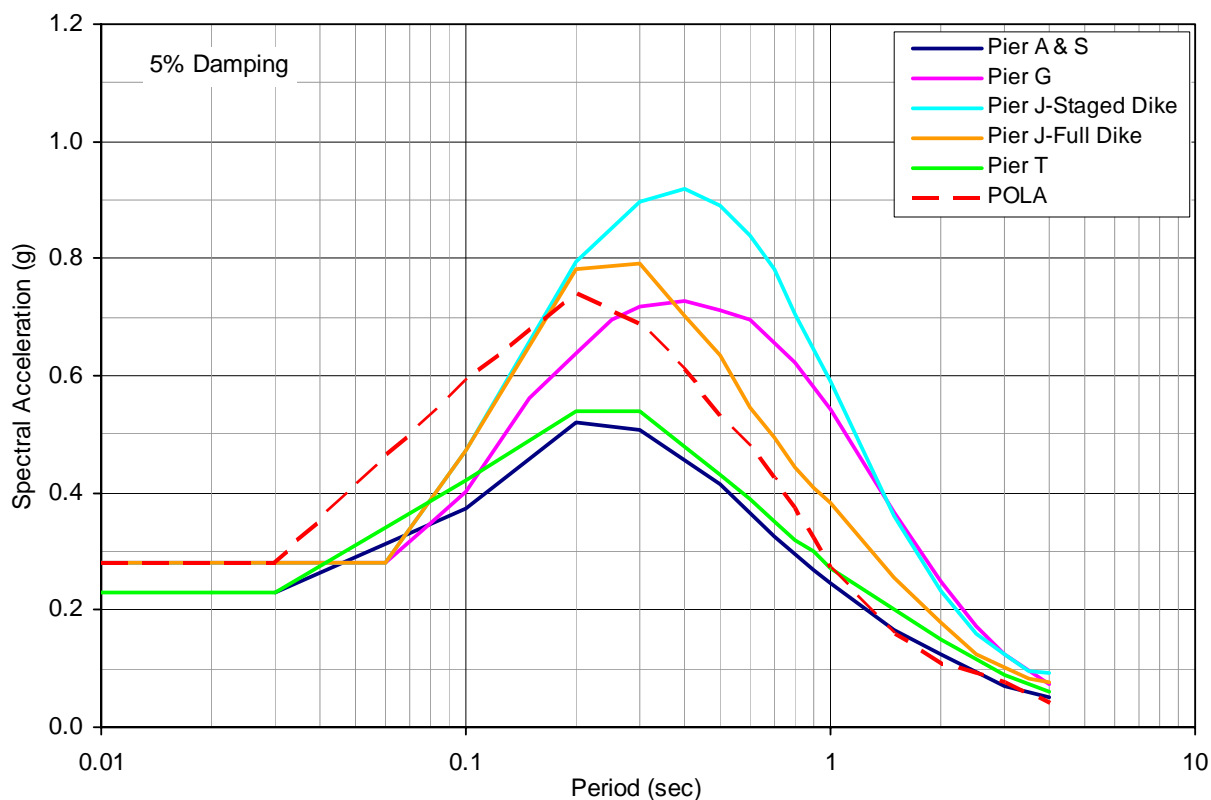
Figure 5-1.　　Comparison of OLE Spectra from Past Projects
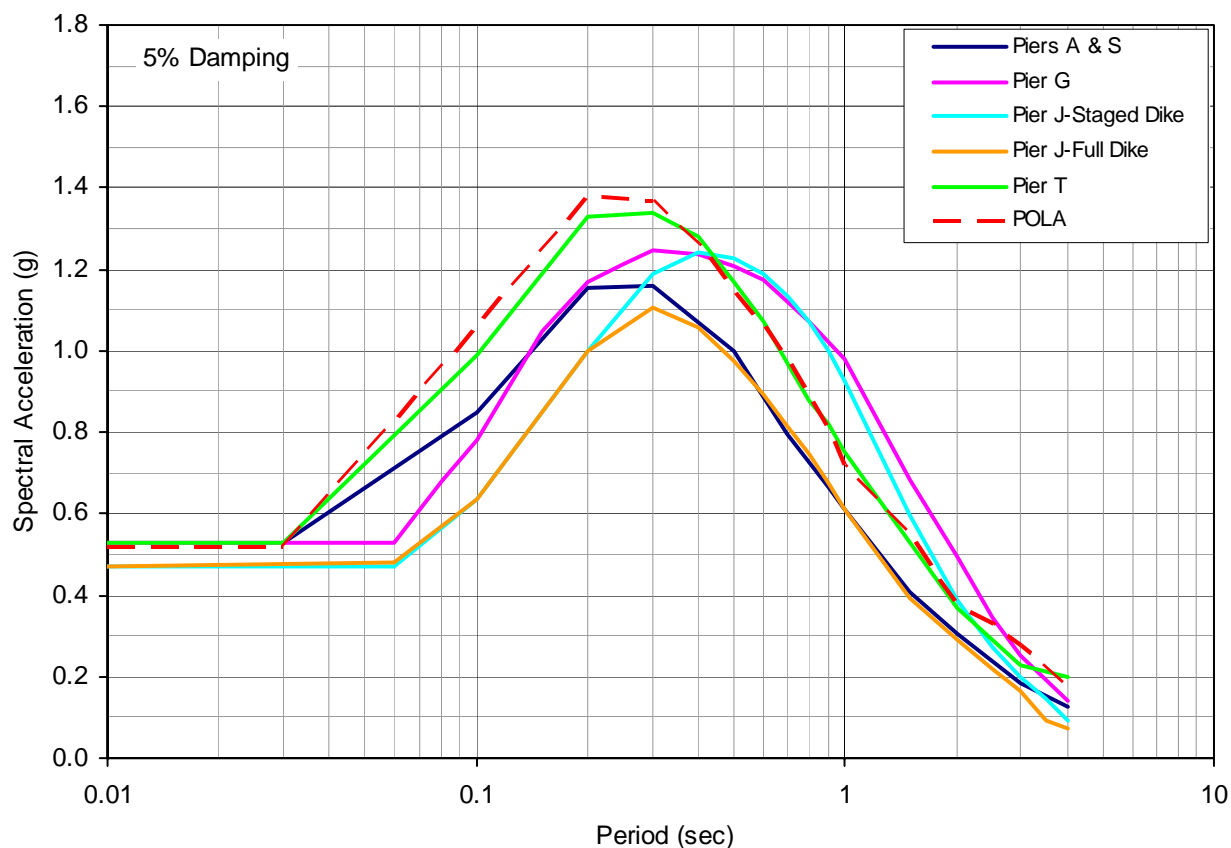
Figure 5-2.   Comparison of CLE Spectra from Past Projects

5.3   GROUND MOTION RECOMMENDATIONS

5.3.1   OLE Spectra Recommendations

5.3.1.1   General

The port-wide theoretical site effect-adjusted UHS for OLE (72-yr return period) developed in Section 4.2 (see Figure 4-3 and Table 4-1) is compared in Figure 5-3 with a range of OLE design spectra recommended for past projects by other consultants. It can be seen that the OLE spectrum from this current study is below or near the lower bound of the range of prior spectra in the entire period range. The following sections provide justification for the development of the OLE spectrum recommended for design of future structures.
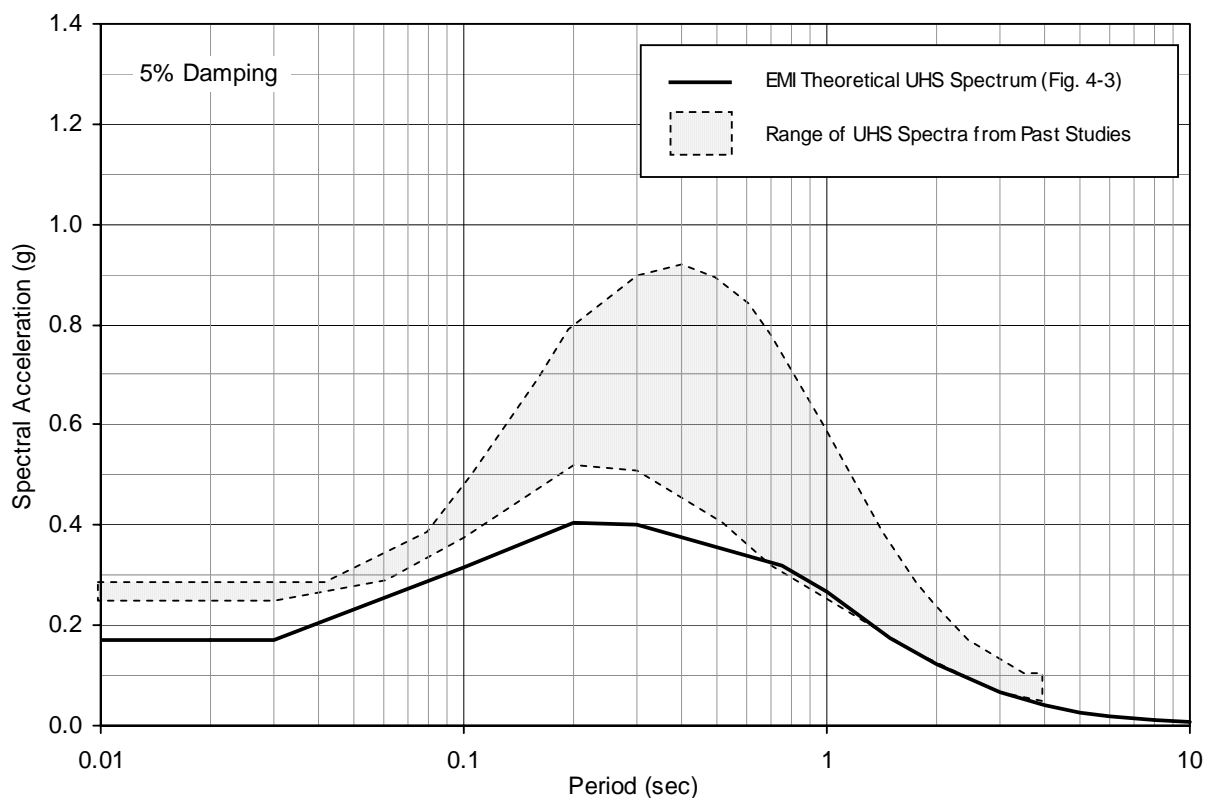
Figure 5-3.   Comparison of Theoretical Design UHS for 72-yr Return Period for OLE with Past OLE Spectra

5.3.1.2   Independent Check

EMI performed a probabilistic seismic hazard analysis (PSHA) as an independent check of the validity of Dr. Abrahamson's probabilistic hazard analyses and studies to clarify the cause of the observed differences in solutions. The check was performed for Site 1 for the OLE using the computer program FRISKSP 4.00 (Blake, 2000). This program first solves for the annual probability of exceeding a ground motion level for each earthquake source. The built-in standard California Geological Survey fault model with the characteristic earthquake recurrence relationship and a model without the characteristic relationship were used. The probability values for each fault are then integrated to obtain the total probability of exceedance curve. Three different firm-ground attenuation relationships were used to ascertain a possible spread of the probability analysis results: (1) Abrahamson and Silva (1997), (2) Campbell (1997), and (3) Sadigh et al. (1997). The log-average of the three results was then computed to obtain the final curve shown in Figure 5-4. From this figure, it can be seen that the resulting UHS for OLE using FRISKSP and the characteristic relationship compares well with the UHS for Site 1 from PSHA analysis presented in Figure 3-13.
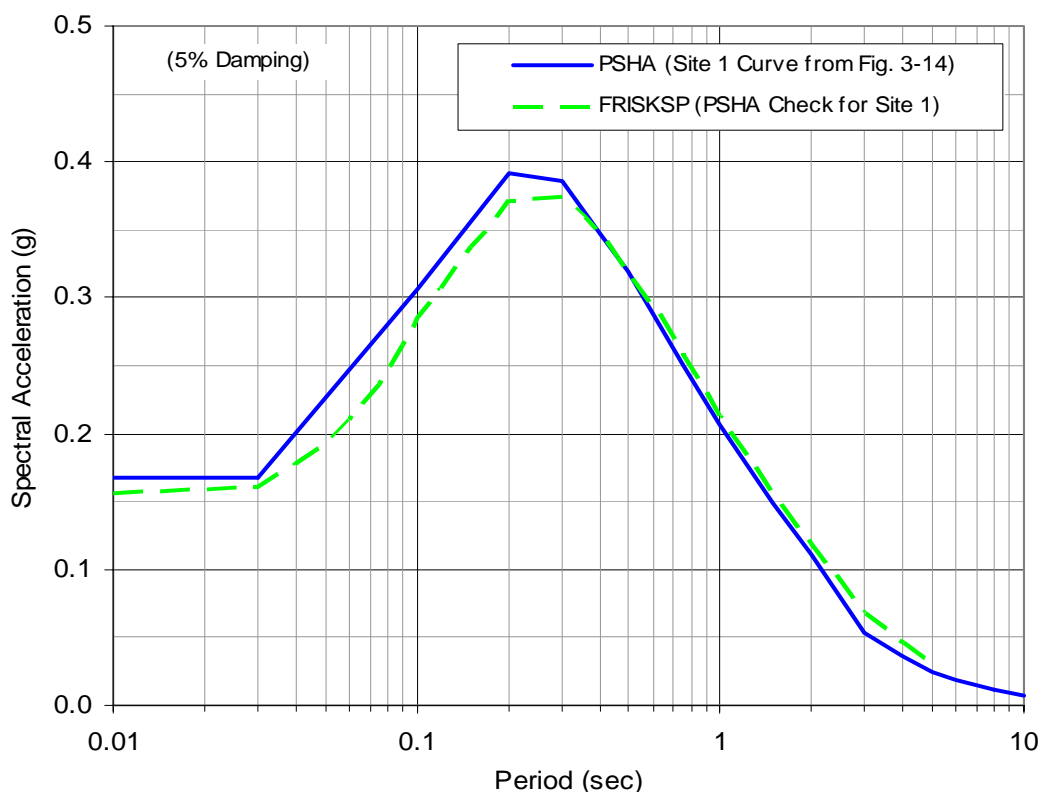
Figure 5-4. **Comparison of UHS for 72-Yr Return Period from PSHA and FRISKSP (Firm-Ground Site Attenuation Solutions)**

5.3.1.3 Comparison of Gutenberg-Richter and Characteristic Earthquake Recurrence Relationships

A careful review of this current PSHA model as compared to the prior PSHA model by EMI (2001) adopted by POLA showed that the primary cause for the difference in the OLE spectra is due to differences in the recurrence relationship. In this study, the characteristic model was adopted whereas the Gutenberg and Richter truncated exponential recurrence model was used for the EMI's PSHA (2001). The following discussion is presented to clarify this aspect.

Gutenberg and Richter (1954) noted that earthquake magnitude and frequency appeared to have a systematic exponential relationship whereby earthquakes of one magnitude unit were about ten times as frequent as those of a larger magnitude unit. This was expressed as the equation

$$log_{10} N = a - b M \tag{5.1}$$

where

N = annual rate of the number of earthquakes of a given magnitude M or greater,
a = constant representing the level of seismic activity, and
b = ratio of small to larger events.

In seismic hazard analyses where the relationship is truncated at some maximum magnitude, the semi-log plot of linear log_{10} N versus magnitude is referred as the "truncated exponential" model. When earthquakes are evaluated on a large regional basis, the b value turns out to be close to about 1.0. Historically, seismologists such as Gutenberg and Richter (hereafter referred to as "GR") made use of recorded activities of smaller earthquakes (say in the M = 3 to 5 range) to anchor the recurrence relationship (such as the truncated exponential model) and then extrapolated the curve to the larger-magnitude, less frequent earthquakes. Such a practice was nearly universal for seismic hazard analyses conducted for older studies (in the 1970's).

However, toward the late 1980s, geologists such as Schwartz and Coppersmith (1984) observed that this practice of extrapolating activity rates of smaller earthquakes tends to underpredict larger earthquakes along major prominent active faults. Figure 5-5 shows a graph from Schwartz and Coppersmith (1984) that illustrates this issue. They pointed out that geologic processes are often long-term processes, much longer than the 50 years or so of instrumental seismicity data experience. Hence, it might be more valid to base the recurrence rate of the larger magnitude earthquakes on prominent faults using geologic information (including trenching studies and historical accounts of past large earthquakes) which reflects experience from a much longer duration of geologic history and therefore be more representative (especially to account for the more destructive larger magnitude earthquakes) of design interest for a life-safety design goal.

Geologic evaluation of faults by Schwartz and Coppersmith (1984) suggested that some faults showed repeated displacement amounts indicating recurring large magnitude events, but few if any smaller displacements as would be expected if smaller earthquakes occurred. From this, they concluded that individual faults have a tendency to produce repeated larger earthquakes within a specific or narrow range, i.e. a characteristic size. Probabilistic seismic hazard analyses in the past decade or so have increasingly favored the characteristic model over the GR model. The characteristic earthquake model has become more accepted in developing recurrence relationships for major faults based on balancing long-term release of seismic energy (seismic moment) in terms of the observed long-term accumulation of seismic moment due to the slip-rate on the fault. Also, it has become more popular to assume that most of the accumulated energy (about 90%) is released by large-magnitude characteristic earthquakes. Such characteristic earthquake models lead to the more complex type of recurrence relationship as depicted by Schwartz and Coppersmith.

Previous probabilistic seismic hazard analyses performed by EMI in early 1990's for the POLA to characterize the Palos Verdes fault utilized the GR relationship truncated at magnitude 7 (EMI, 1993). Figure 5-6 presents the EMI's 1993 recurrence relationship for the Port of Los Angeles and compares it to the four characteristic-earthquake-model recurrence curves adopted for this current port-wide seismic hazard model. The four recurrence relationships are the Maximum, Median, Mean, and Minimum characteristic curves. These four relationships have been implemented in the current PSHA solution using a logic-tree approach that considers multiple hypotheses. It can be noted that both the GR and the Mean/Median characteristic curves approximate similar large-magnitude events (M 7) at recurrence intervals of about 1,000 years. The similarity of the large-magnitude recurrence results in similar CLE design events regardless of which recurrence model is used. However, when the smaller earthquakes are considered, the

GR relationship suggests that an M 5 earthquake could be expected approximately every 20 years whereas the characteristic relationship for the Median/Mean curve indicates an M 5 event every 100 to 120 years. Because the OLE design event is controlled by the smaller events that recur within the shorter time period, design values will be substantially lower when using the characteristic relationship rather than the GR relationship.

These differences between the GR and characteristic magnitude-frequency relationships are the principal reason the CLE values of the previous analyses are similar to the present recommendation while the previous OLE values are considerably larger.

5.3.1.4   Recommended Spectra for OLE

Horizontal Design Spectrum. Figure 5-3 compares the port-wide theoretical site effect-adjusted UHS for OLE (72-yr return period) developed in Section 4.2 with the range of OLE design spectra recommended for past projects by other consultants. It can be seen that the OLE spectrum from this current study is below or near the lower bound of the range of prior spectra in the entire period range.

For the period range significant for wharf design (approximately 0.5 to 1.0 sec), the present theoretical UHS spectral value at 0.5 sec is about 10% below the lower bound of the range of the other past spectra, and is about the same as the lower bound at about 1.0 sec period. The reason for the differences was discussed in Section 5.3.1.3. The present study uses the most up-to-date geologic and seismic understanding, but updates will be needed when changes in this knowledge occur in the future. As a result, future changes in spectral values cannot be ruled out. From a practical standpoint, it is therefore prudent to incorporate some conservatism in the port-wide design spectrum to allow for possible future increases in spectral values. To address this issue, and following discussion with the Port, the design spectrum was obtained by increasing the spectral values of the theoretical site effect-adjusted spectrum by 20% in the short-period range (from 0 to 0.5 sec), by 10% at 0.75 sec and using the theoretical spectrum for the periods of 1.0 sec or larger. Minor adjustments to smooth acceleration and relative displacement spectra were then applied. The recommended PGA value for geotechnical evaluations is 0.21g (the corresponding dominant source is recommended as an M 6.5 earthquake at a distance of 20 km).

The resultant acceleration and pseudo relative displacement spectra (for 5% damping) recommended for port-wide design of structures are given in Figure 5-7 and Figure 5-8 respectively. Spectral values for a range of damping values are given in Table 5-2.

Horizontal Firm-Ground Spectrum. The firm-ground target spectrum compatible with the design spectrum at the ground surface was generated by dividing the recommended design spectra of Figure 5-7 by the transfer function between firm-ground and ground surface motions. The transfer function was obtained by ratio of the theoretical site-effect adjusted spectra and the firm-ground horizontal UHS shown in Figure 4-3. Appendix D.2 provides details of the methodology, and includes the resulting target firm-ground spectrum.

Vertical Firm-Ground and Design Spectrum. The firm-ground vertical spectrum was derived from the firm-ground spectrum (Figure 3-10) and the V/H ratios (Figure 3-12). The

recommended spectrum is shown in Figure 5-9. This spectrum may be used for both firm-ground conditions and design.

5.3.1.5 Spectrum-Compatible Time Histories

Compatible to Design Spectra. Seven (7) sets of startup firm-ground time histories (see Table 5-1) were selected for an Operating-Level Earthquake reflecting earthquakes ranging from Magnitude 6 to 7 with distances extending from near-fault to moderate distance events. These 3-component time histories were modified to be spectrum-compatible to the design response spectra of Figure 5-7 and Figure 5-9 adjusted for the site-specific soil conditions for the OLE.

The spectrum-matched three-component acceleration, velocity and displacement time histories, and comparisons of the corresponding spectra with the target design spectrum are provided in Appendix D.4.

Compatible to Firm-Ground Spectra. The startup time histories shown in Table 5-1 were modified to match the horizontal firm-ground target design spectrum adjusted for the site-specific soil conditions as described above. Appendix D.2 provides further details on the selection of records and the methodology of analysis.

Appendix D.2 also provides the resulting spectrum-matched 2-component horizontal acceleration, velocity and displacement time histories, and comparisons of the corresponding spectra with the target firm-ground spectrum. The vertical-component time histories for the design spectrum can be used for firm-ground conditions as well.

Table 5-1.   Time Histories Selected for OLE Spectral Matching

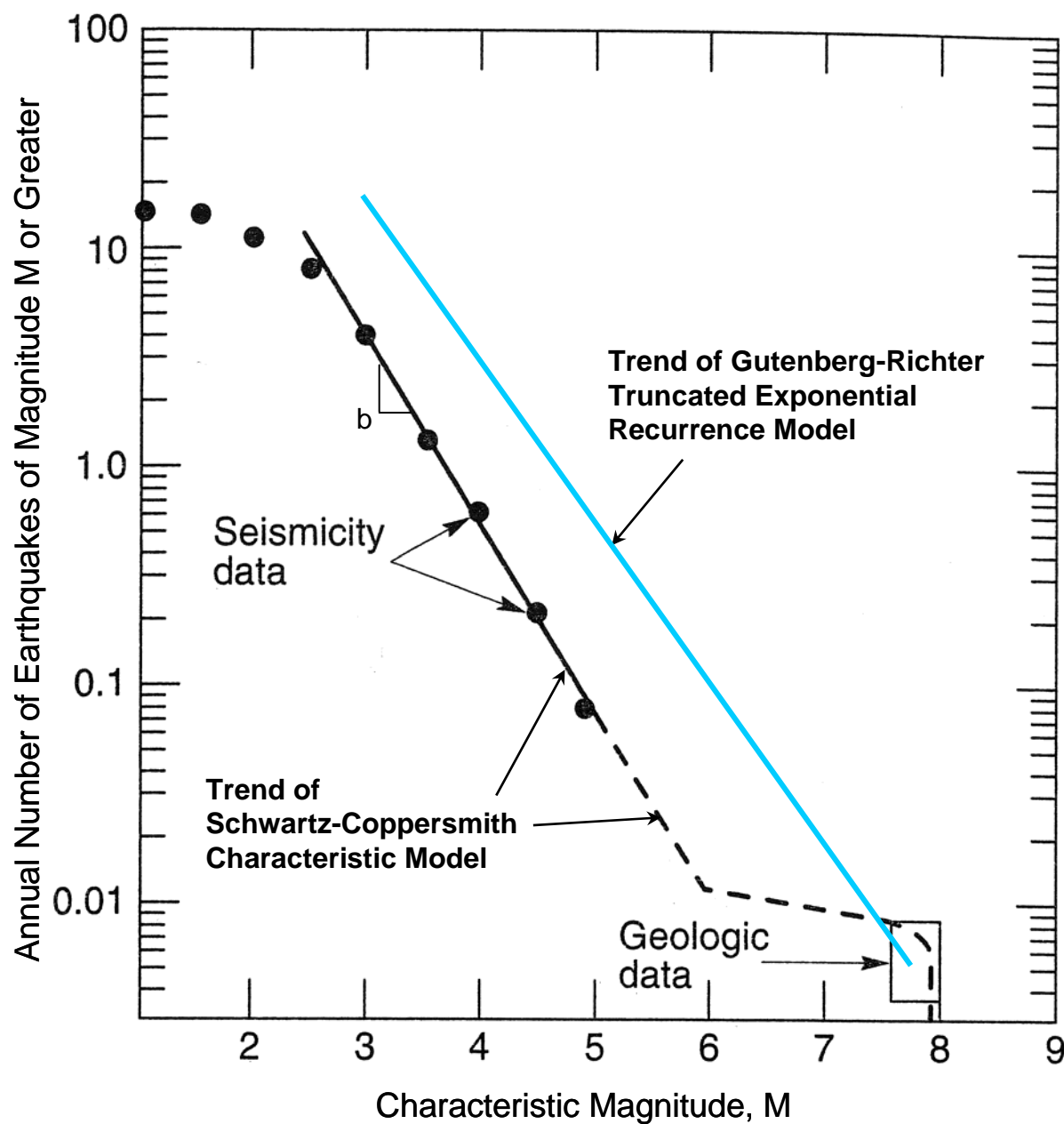| Set	Earthquake	Magnitude	Station	Distance (km)
1	1989 Loma Prieta	6.9	Saratoga – Aloha Ave.	13.0
2	1987 Superstition Hill	6.3	Wildlife Liquefaction Array	24.7
3	1987 Whittier	6.0	Northridge-Saticoy St.	39.8
4	1979 Imperial Valley	6.5	EC CO Center FF	7.6
5	1979 Imperial Valley	6.5	Calexico Fire Station	10.6
6	1992 Erzikan	6.9	Erzikan	2.0
7	1994 Northridge	6.7	Century City, LACC	25.7

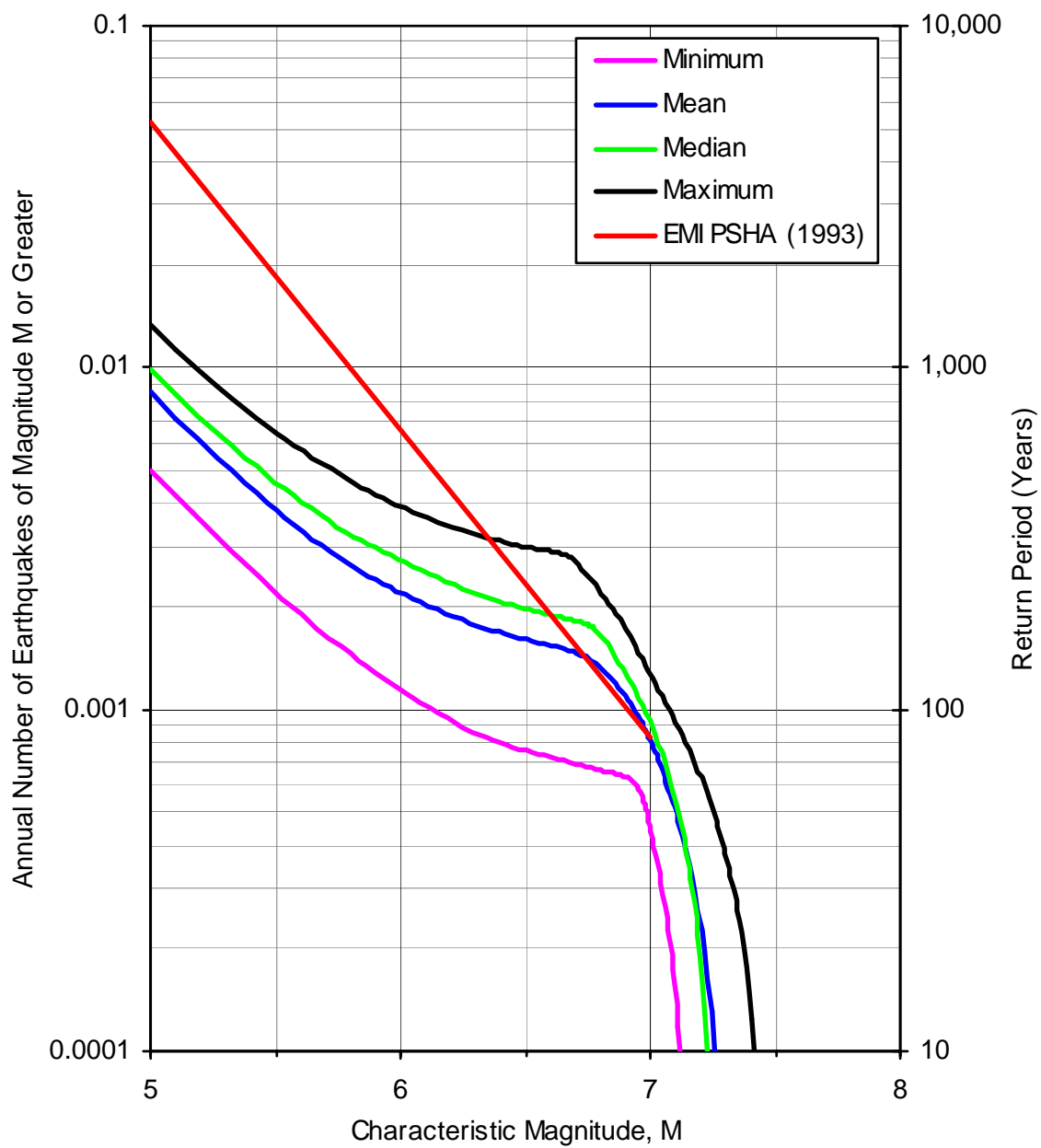**Figure 5-5.   Historical Development of Recurrence Relationships**

Figure 5-6.   Various Assumed Recurrence Rates of the Palos Verdes Fault
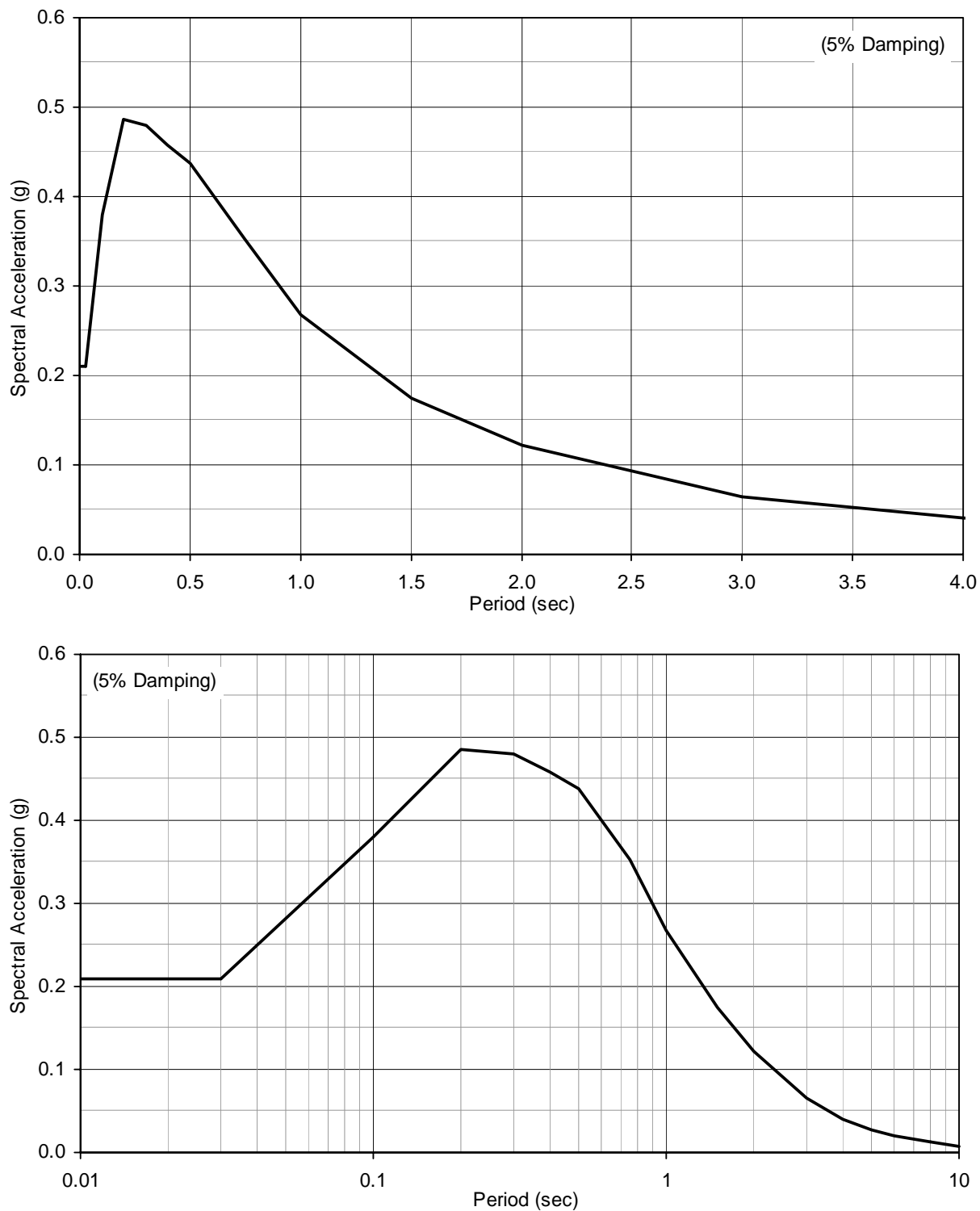
Figure 5-7. **Recommended Design Spectrum (Horizontal Acceleration) for 72-yr Return Period (OLE)**
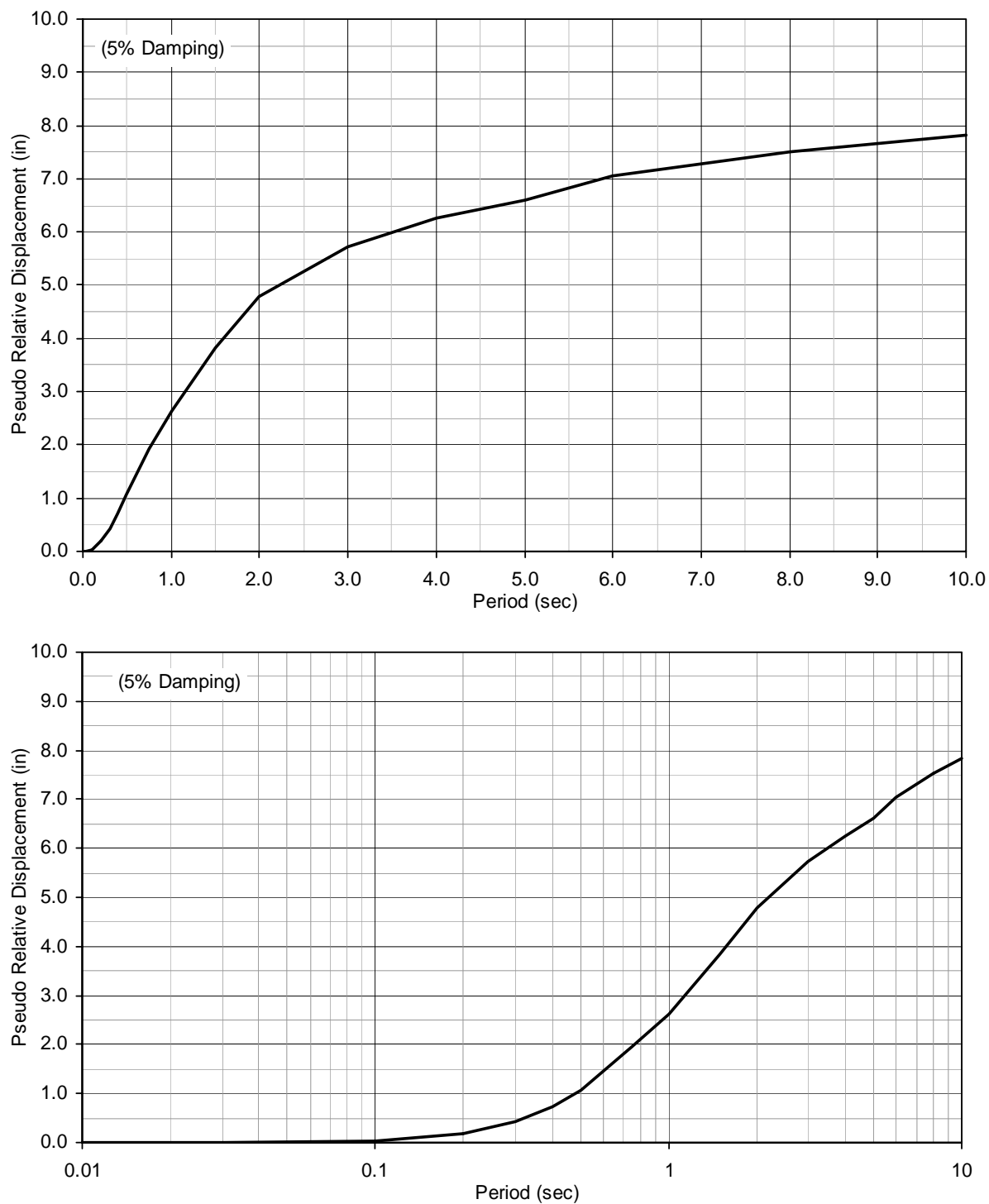
Figure 5-8. Recommended Design Spectrum (Horizontal Relative Displacement) for 72-yr Return Period (OLE)
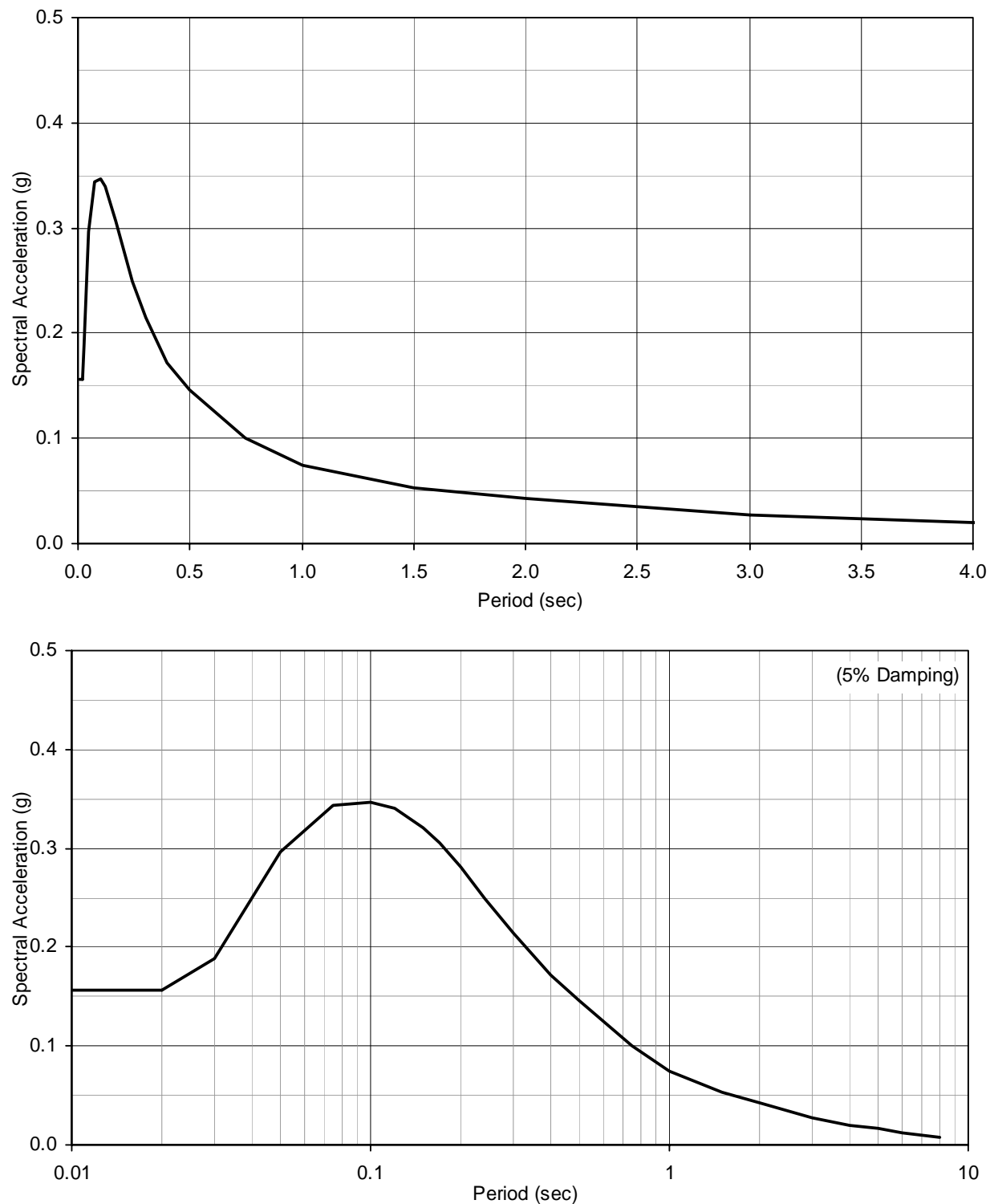
Figure 5-9. Recommended Firm-Ground and Design Spectrum (Vertical Acceleration) for 72-yr Return Period (OLE)

Table 5-2.　　**Spectral Values (Horizontal) for Recommended Design for 72-yr Return Period (OLE)**

Period (sec)	Damping											
	1%		2%		5%		10%		20%		25%	
	PSA (g)	Disp. (in)	PSA (g)	Disp. (in)	PSA (g)	Disp. (in)	PSA (g)	Disp. (in)	PSA (g)	Disp. (in)	PSA (g)	Disp. (in)
0.01	0.210	0.000	0.210	0.000	0.210	0.000	0.210	0.000	0.210	0.000	0.210	0.000
0.03	0.226	0.002	0.220	0.002	0.210	0.002	0.201	0.002	0.190	0.002	0.187	0.002
0.10	0.515	0.05	0.461	0.05	0.380	0.04	0.316	0.03	0.252	0.02	0.234	0.02
0.20	0.708	0.28	0.617	0.24	0.486	0.19	0.386	0.15	0.293	0.11	0.266	0.10
0.30	0.699	0.62	0.609	0.54	0.480	0.42	0.382	0.34	0.289	0.25	0.263	0.23
0.40	0.667	1.04	0.581	0.91	0.458	0.72	0.364	0.57	0.276	0.43	0.251	0.39
0.50	0.638	1.56	0.556	1.36	0.438	1.07	0.348	0.85	0.264	0.65	0.240	0.59
0.75	0.513	2.82	0.447	2.46	0.352	1.94	0.280	1.54	0.212	1.17	0.193	1.06
1.00	0.386	3.77	0.337	3.30	0.268	2.62	0.215	2.10	0.164	1.61	0.150	1.47
1.50	0.245	5.39	0.216	4.76	0.174	3.83	0.141	3.11	0.110	2.42	0.101	2.22
2.00	0.168	6.58	0.149	5.85	0.122	4.78	0.100	3.93	0.079	3.10	0.073	2.86
3.00	0.086	7.60	0.078	6.85	0.065	5.73	0.055	4.82	0.044	3.91	0.041	3.64
4.00	0.051	8.06	0.047	7.35	0.040	6.26	0.034	5.37	0.028	4.46	0.027	4.19
5.00	0.034	8.27	0.031	7.61	0.027	6.61	0.024	5.76	0.020	4.88	0.019	4.62
6.00	0.025	8.82	0.023	8.12	0.020	7.05	0.017	6.15	0.015	5.21	0.014	4.92
8.00	0.015	9.40	0.014	8.66	0.012	7.52	0.010	6.56	0.009	5.56	0.008	5.25
10.00	0.010	9.80	0.009	9.02	0.008	7.83	0.007	6.83	0.006	5.79	0.006	5.47

5.3.2　CLE Design Recommendations

5.3.2.1　Design Spectra

Horizontal Design Spectrum. Figure 5-10 compares the port-wide theoretical site effect-adjusted UHS for CLE (475-yr return period) developed in Section 4.2 with a range of design CLE spectra recommended by other consultants. It can be seen from this figure that the current recommended spectrum is within the range of past historical CLE design spectra. The reason for this is the recurrence rates for large-magnitude (approximately M7) events assumed in this study are consistent with prior studies (see Figure 5-6) where the large magnitude recurrence rates are anchored to the geologic slip rate of the Palos Verdes and the Newport-Inglewood faults, which have remained largely unchanged in the past ten years.
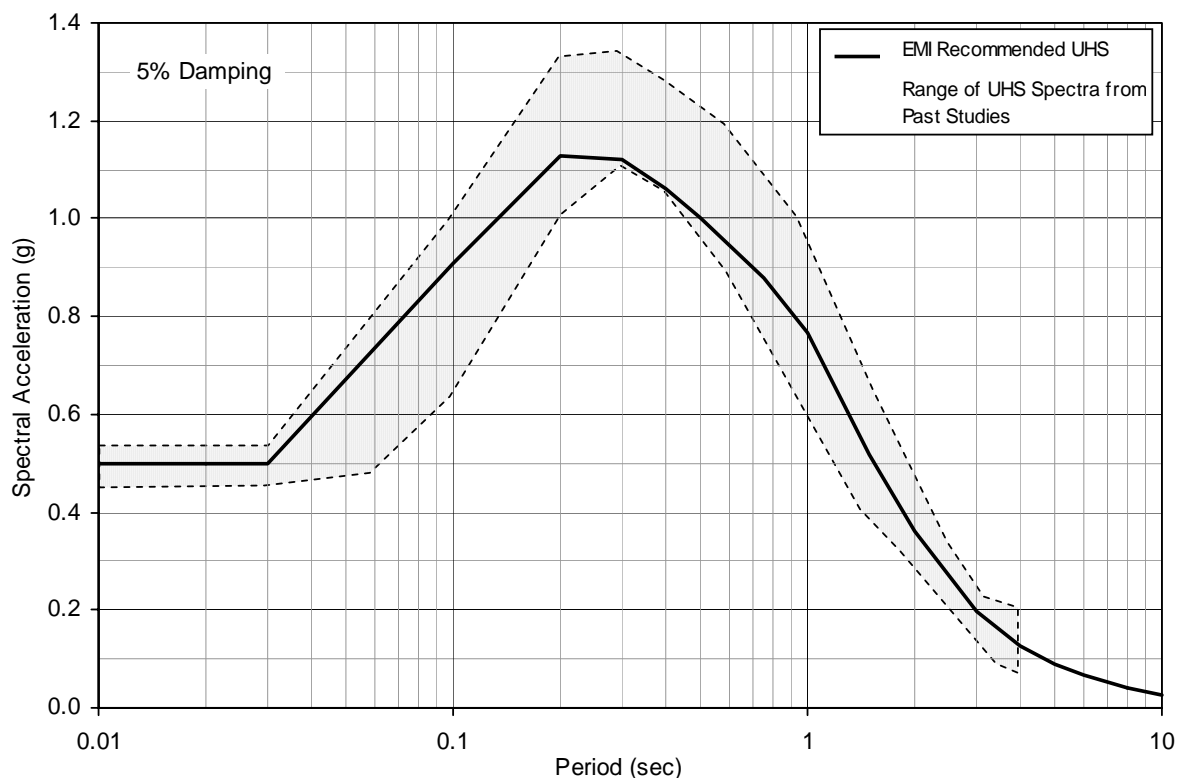
Figure 5-10. Comparison of Design UHS for 475-yr Return Period for CLE with Past CLE Spectra

As a result, the port-wide theoretical site effect-adjusted UHS shown is recommended for port-wide design of structures, with a recommended PGA value for the CLE of 0.50g (with the corresponding dominant source of M 7.0 at a distance of 4 km) and minor adjustments to smooth acceleration and relative displacement spectra.

The resultant acceleration and pseudo relative displacement design spectra for 5% damping are given in Figure 5-11 and Figure 5-12, respectively. The spectral coordinates for a range of damping values are listed in Table 5-3.

Vertical Design Spectrum. The firm-ground vertical spectrum was derived from the firm-ground spectrum (Figure 3-11) and the V/H ratios (Figure 3-12). The recommended spectrum is shown in Figure 5-13. This spectrum may be used for both firm-ground conditions and design.
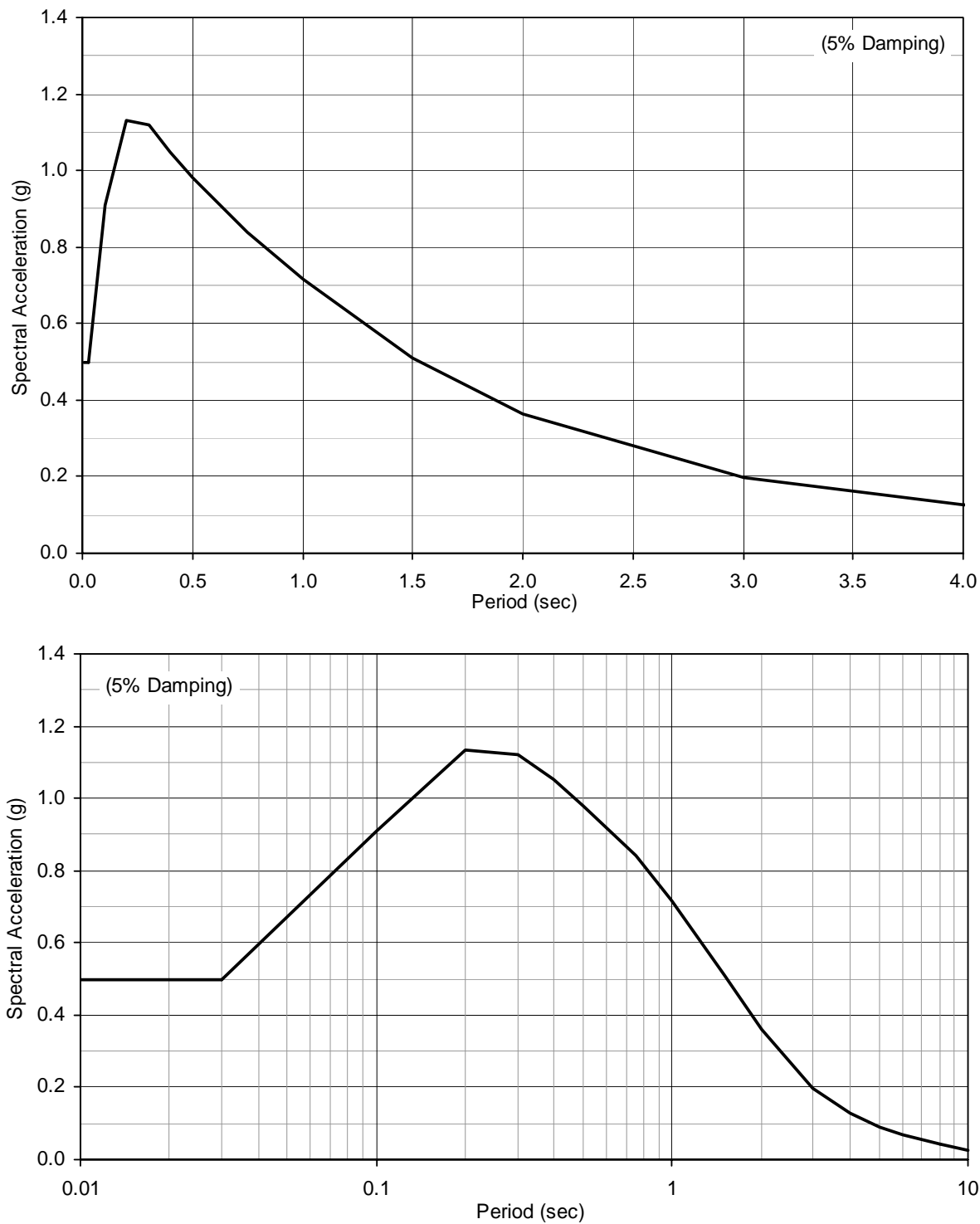
Figure 5-11. Recommended Design Spectrum (Horizontal Acceleration) for 475-yr Return Period (CLE)
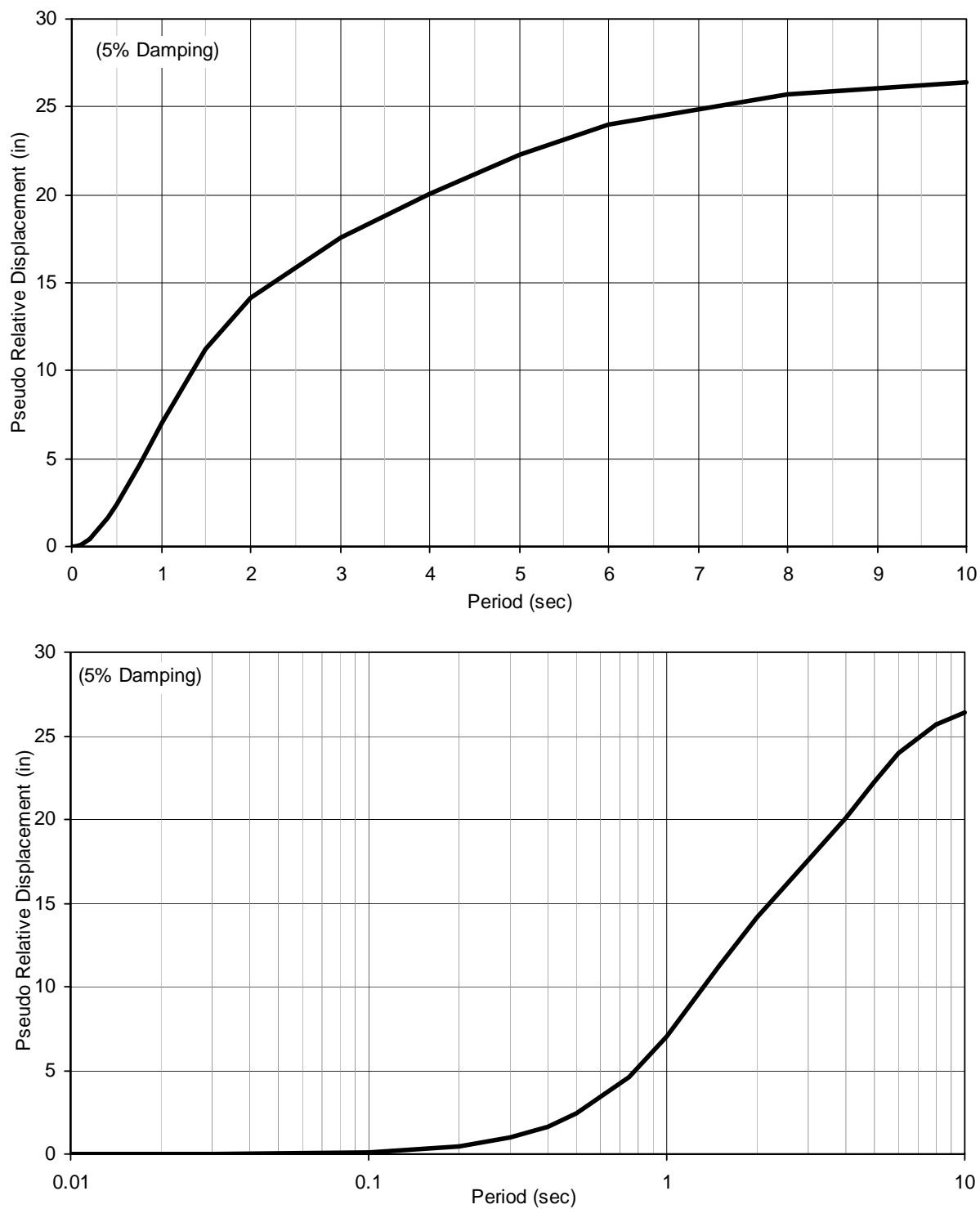
Figure 5-12. Recommended Design Spectrum (Horizontal Relative Displacement) for 475-yr Return Period (CLE)
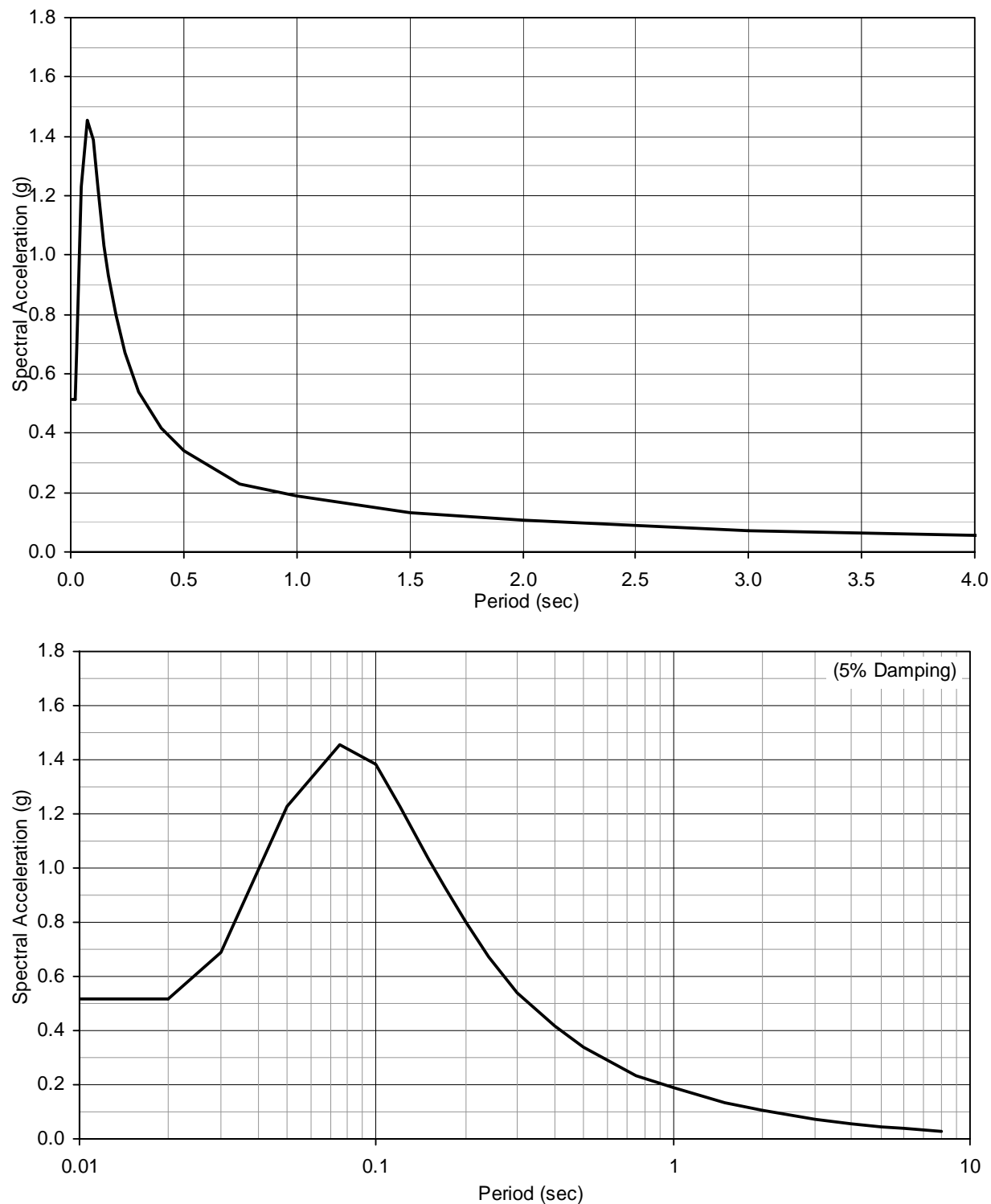
Figure 5-13.   Recommended Firm-Ground and Design Spectrum (Vertical Acceleration) for 475-yr Return Period (CLE)

Table 5-3. Spectral Values for Recommended Design for 475-yr Return Period (CLE)

Period (sec)	Damping											
	1%		2%		5%		10%		20%		25%	
	PSA (g)	Disp. (in)	PSA (g)	Disp. (in)	PSA (g)	Disp. (in)	PSA (g)	Disp. (in)	PSA (g)	Disp. (in)	PSA (g)	Disp. (in)
0.01	0.500	0.000	0.500	0.000	0.500	0.000	0.500	0.000	0.500	0.000	0.500	0.000
0.03	0.538	0.005	0.524	0.005	0.500	0.004	0.478	0.004	0.453	0.004	0.445	0.004
0.10	1.233	0.12	1.103	0.11	0.910	0.09	0.756	0.07	0.604	0.06	0.560	0.05
0.20	1.649	0.65	1.436	0.56	1.132	0.44	0.900	0.35	0.682	0.27	0.621	0.24
0.30	1.633	1.44	1.422	1.25	1.121	0.99	0.891	0.79	0.675	0.59	0.615	0.54
0.40	1.529	2.39	1.332	2.09	1.050	1.64	0.835	1.31	0.632	0.99	0.576	0.90
0.50	1.427	3.49	1.243	3.04	0.980	2.40	0.779	1.91	0.590	1.44	0.537	1.31
0.75	1.223	6.73	1.066	5.87	0.840	4.62	0.668	3.68	0.506	2.79	0.460	2.54
1.00	1.039	10.17	0.907	8.87	0.717	7.02	0.572	5.60	0.435	4.26	0.396	3.88
1.50	0.729	16.07	0.640	14.09	0.510	11.23	0.410	9.03	0.315	6.93	0.288	6.34
2.00	0.511	19.99	0.450	17.62	0.362	14.17	0.294	11.49	0.228	8.91	0.209	8.17
3.00	0.273	24.07	0.243	21.43	0.199	17.53	0.164	14.45	0.130	11.43	0.120	10.56
4.00	0.172	26.86	0.154	24.12	0.128	20.05	0.107	16.77	0.086	13.51	0.080	12.56
5.00	0.119	29.17	0.108	26.42	0.091	22.27	0.077	18.89	0.063	15.47	0.059	14.46
6.00	0.089	31.39	0.081	28.43	0.068	23.96	0.058	20.32	0.047	16.65	0.044	15.55
8.00	0.054	33.65	0.049	30.47	0.041	25.68	0.035	21.78	0.028	17.84	0.027	16.67
10.00	0.035	34.62	0.032	31.36	0.027	26.43	0.023	22.41	0.019	18.36	0.018	17.16

5.3.2.2 Spectrum-Compatible Time Histories

The seven (7) sets of 3-component startup firm-ground time histories (see Table 3-8) selected for CLE were modified to be spectrum-compatible to the design response spectra of Figure 5-11 and Figure 5-13 adjusted for the site-specific soil conditions. The spectrum-matched three-component acceleration, velocity and displacement time histories, and comparisons of the corresponding spectra with the target design spectrum are provided in Appendix D.3. The vertical-component time histories developed for firm-ground conditions are applicable for design evaluations as well.

5.3.3 Firm-Ground Sites

It should be noted that for sites where the top of stiff soil as described in Section 3.2.1, is encountered (either in their existing condition or due to ground improvement to mitigate soil liquefaction concerns) at or above El. -10 ft MLLW and the soil thickness above it is no more than 25 ft, the firm-ground UHS may be used for design.

5.4 NEWMARK DISPLACEMENTS

Simplified Newmark sliding block-type analyses were conducted to estimate lateral ground displacements due to the CLE and OLE firm-ground motions. The methodology of analysis and the resulting ground displacements are provided in Appendix E. Figure 6-7 and Table 6-5

provide the recommended lateral ground displacement versus yield acceleration curves for both events.

Because these analyses are based on the firm-ground outcropping motions, the recommended curves are considered conservative and may be used as a screening tool to determine if a particular project requires further evaluations such as site-specific site response analysis and/or soil-structure interaction analysis. The benefits of such analyses to the project should be clearly demonstrated and approval should be obtained from the Port before performing these analyses.

SECTION 6
DESIGN RECOMMENDATIONS

Based on the port-wide ground motion study completed by EMI as described in this report, the following recommendations are made:

(1)   The horizontal and vertical firm-ground uniform hazard spectra (UHS) for 5% damping for the operating level earthquake (OLE), which correspond to a 72-yr return period, are provided in Figure 6-1 and Table 6-1. The horizontal and vertical firm-ground spectra for the contingency level earthquake (CLE), which correspond to a 475-yr return period, are provided in Figure 6-2 and Table 6-2. A total of seven (7) sets of spectrum-compatible 3-component time histories for firm-ground spectra for both CLE and OLE are provided in Appendix D.1 and D.2, respectively.

(2)   The horizontal acceleration and pseudo relative displacement spectra for port structure design (for 5% damping, including site response effects) are shown in Figure 6-3 and Figure 6-4 for OLE, and in Figure 6-5 and Figure 6-6 for the CLE, respectively. The acceleration and relative displacement values for a range of damping ratios are provided in Table 6-3 for the OLE and Table 6-4 for CLE. A total of seven (7) sets of spectrum-compatible time histories for port design for both CLE and OLE are provided in Appendix D.3 and D.4, respectively.

(3)   For vertical UHS for port design, the firm-ground UHS (Figure 6-1 and Table 6-1 for OLE, Figure 6-2 and Table 6-2 for CLE) may be used.

(4)   For sites where soil with an average shear wave velocity (as defined in Section 2.3) of about 1,000 ft/sec is encountered at a maximum depth of 25 ft below ground surface and at or above El. -10 ft MLLW, the firm-ground UHS (Figure 6-1 and Table 6-1 for OLE, and Figure 6-2 and Table 6-2 for CLE) may be used for structure design.

(5)   The recommended peak ground acceleration (PGA) value corresponding to the OLE for geotechnical evaluations is 0.21g. The corresponding dominant source is recommended as a M 6.5 earthquake at a distance of 20 km. The recommended PGA value corresponding to the CLE is 0.50g with the corresponding dominant source of M 7.0 at a distance of 4 km.

(6)   The appropriateness of the recommended design spectra for sites with unique subsurface conditions that are significantly outside the range of soil profiles covered in this study should be determined on a project-specific basis.

(7)   The recommended Newmark displacement estimates curves shown in Figure 6-7 and Table 6-5 may be used as a screening tool to determine if more detailed analyses such as site-specific site response analysis and/or soil-structure interaction analysis are

needed for a particular project. The benefits of such analyses to the project should be clearly demonstrated and approval by the Port should be obtained before conducting these analyses.

(8)   Recommendations for future design practice are provided in Section 7.

(9)   It is suggested that the recommendations provided in this report be reviewed and revised as necessary on a regular basis to include the latest developments in the seismological, geological, and geotechnical communities. Specifically, it is recommended that the first review be performed in about two to three years from the date of this report to incorporate the findings from the on-going PEER NGA study. Subsequent reviews may be performed every five years or as necessary based on further developments in the state of practice.

Table 6-1.   Firm-Ground Spectra for OLE (5% Damping)

Period (sec)	Average Horizontal Acceleration (g)	Vertical Acceleration (g)
0.010	0.208	0.156
0.020	0.208	0.156
0.030	0.208	0.189
0.050	0.281	0.296
0.075	0.339	0.344
0.100	0.380	0.346
0.120	0.408	0.340
0.150	0.442	0.321
0.170	0.461	0.306
0.200	0.486	0.281
0.240	0.483	0.250
0.300	0.479	0.215
0.400	0.431	0.172
0.500	0.395	0.146
0.750	0.283	0.100
1.000	0.212	0.074
1.500	0.152	0.053
2.000	0.115	0.043
3.000	0.063	0.027
4.000	0.039	0.020
5.000	0.027	0.016
6.000	0.020	0.012
8.000	0.012	0.008
10.000	0.008	0.005
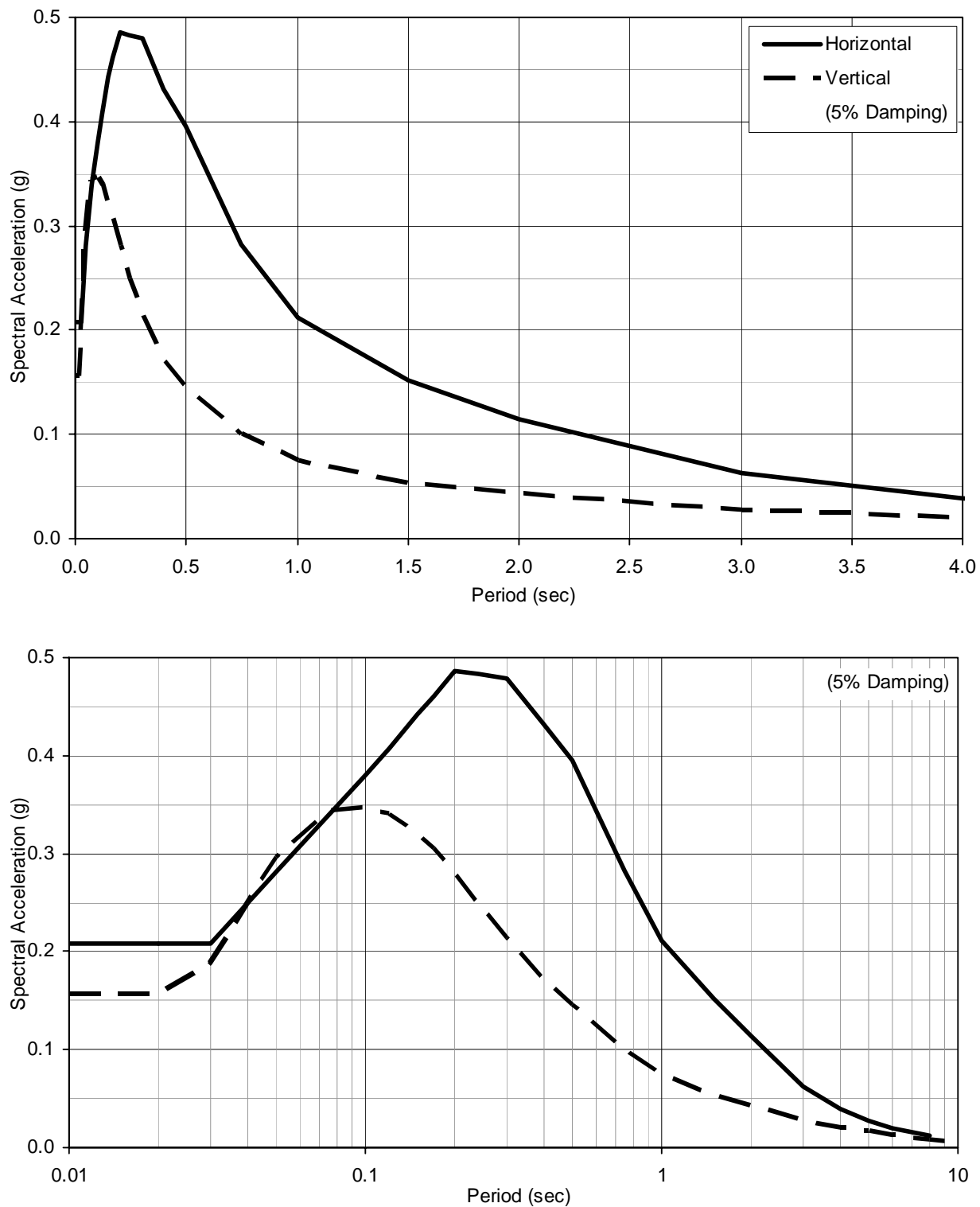
Figure 6-1.   Recommended Firm-Ground Spectra for OLE (5% Damping)

Table 6-2. **Firm-Ground Spectra for CLE (5% Damping)**

Period (sec)	Average Horizontal Acceleration (g)	Vertical Acceleration (g)
0.010	0.496	0.515
0.020	0.496	0.515
0.030	0.496	0.687
0.050	0.672	1.229
0.075	0.811	1.456
0.100	0.910	1.386
0.120	0.968	1.231
0.150	1.040	1.032
0.170	1.080	0.928
0.200	1.132	0.800
0.240	1.127	0.672
0.300	1.121	0.540
0.400	1.029	0.418
0.500	0.958	0.340
0.750	0.734	0.231
1.000	0.618	0.186
1.500	0.446	0.131
2.000	0.329	0.108
3.000	0.193	0.073
4.000	0.127	0.056
5.000	0.091	0.045
6.000	0.067	0.036
8.000	0.040	0.027
10.000	0.026	0.017
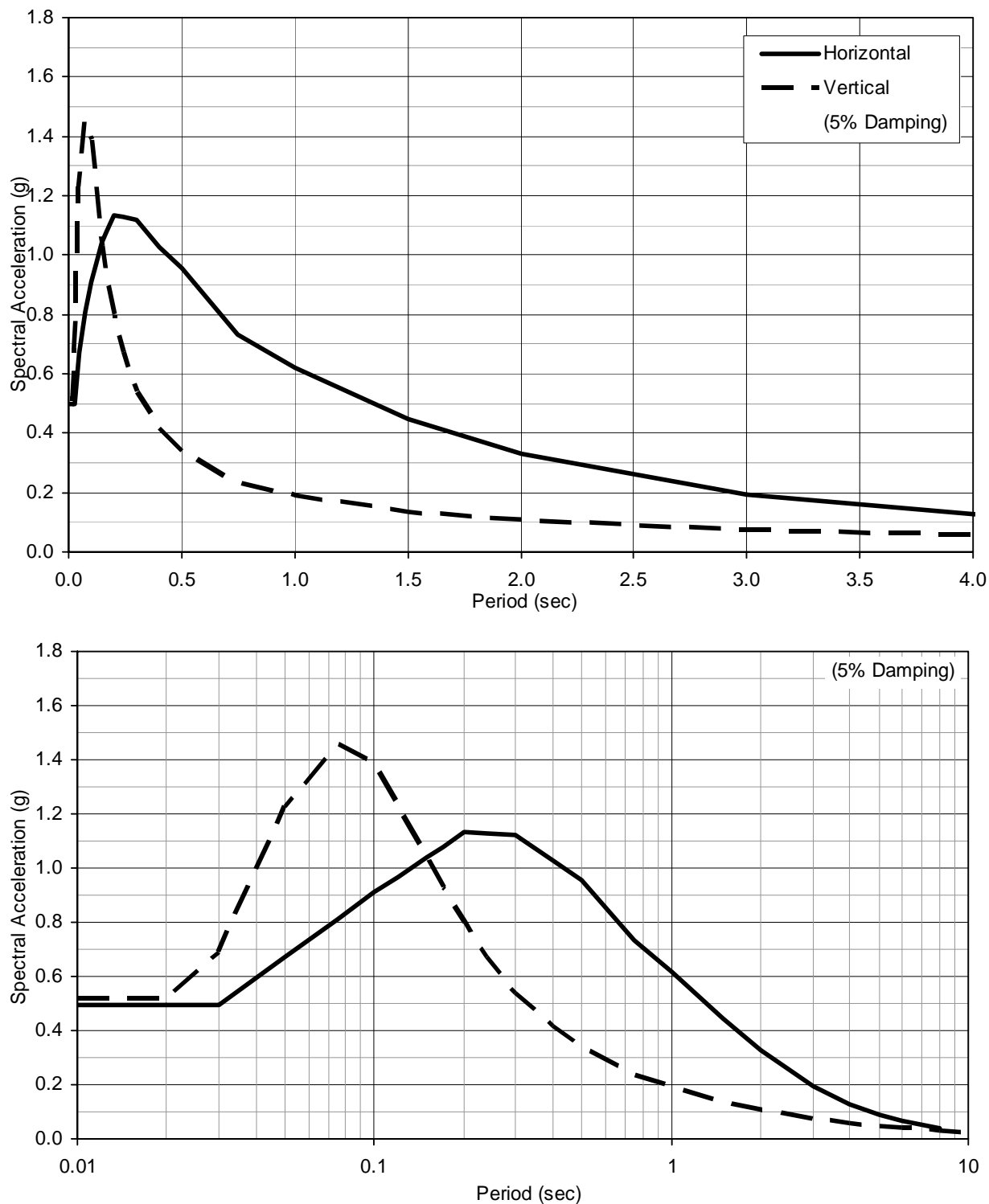
Figure 6-2.   Recommended Firm-Ground Spectra for CLE (5% Damping)

Table 6-3. **Recommended Horizontal Design Spectra for OLE**

| Period (sec)	Damping											
	1%		2%		5%		10%		20%		25%	
	Acc. (g)	Displ. (in)	Acc. (g)	Displ. (in)	Acc. (g)	Displ. (in)	Acc. (g)	Displ. (in)	Acc. (g)	Displ. (in)	Acc. (g)	Displ. (in)
0.01	0.210	0.000	0.210	0.000	0.210	0.000	0.210	0.000	0.210	0.000	0.210	0.000
0.03	0.226	0.002	0.220	0.002	0.210	0.002	0.201	0.002	0.190	0.002	0.187	0.002
0.10	0.515	0.05	0.461	0.05	0.380	0.04	0.316	0.03	0.252	0.02	0.234	0.02
0.20	0.708	0.28	0.617	0.24	0.486	0.19	0.386	0.15	0.293	0.11	0.266	0.10
0.30	0.699	0.62	0.609	0.54	0.480	0.42	0.382	0.34	0.289	0.25	0.263	0.23
0.40	0.667	1.04	0.581	0.91	0.458	0.72	0.364	0.57	0.276	0.43	0.251	0.39
0.50	0.638	1.56	0.556	1.36	0.438	1.07	0.348	0.85	0.264	0.65	0.240	0.59
0.75	0.513	2.82	0.447	2.46	0.352	1.94	0.280	1.54	0.212	1.17	0.193	1.06
1.00	0.386	3.77	0.337	3.30	0.268	2.62	0.215	2.10	0.164	1.61	0.150	1.47
1.50	0.245	5.39	0.216	4.76	0.174	3.83	0.141	3.11	0.110	2.42	0.101	2.22
2.00	0.168	6.58	0.149	5.85	0.122	4.78	0.100	3.93	0.079	3.10	0.073	2.86
3.00	0.086	7.60	0.078	6.85	0.065	5.73	0.055	4.82	0.044	3.91	0.041	3.64
4.00	0.051	8.06	0.047	7.35	0.040	6.26	0.034	5.37	0.028	4.46	0.027	4.19
5.00	0.034	8.27	0.031	7.61	0.027	6.61	0.024	5.76	0.020	4.88	0.019	4.62
6.00	0.025	8.82	0.023	8.12	0.020	7.05	0.017	6.15	0.015	5.21	0.014	4.92
8.00	0.015	9.40	0.014	8.66	0.012	7.52	0.010	6.56	0.009	5.56	0.008	5.25
10.0	0.010	9.80	0.009	9.02	0.008	7.83	0.007	6.83	0.006	5.79	0.006	5.47
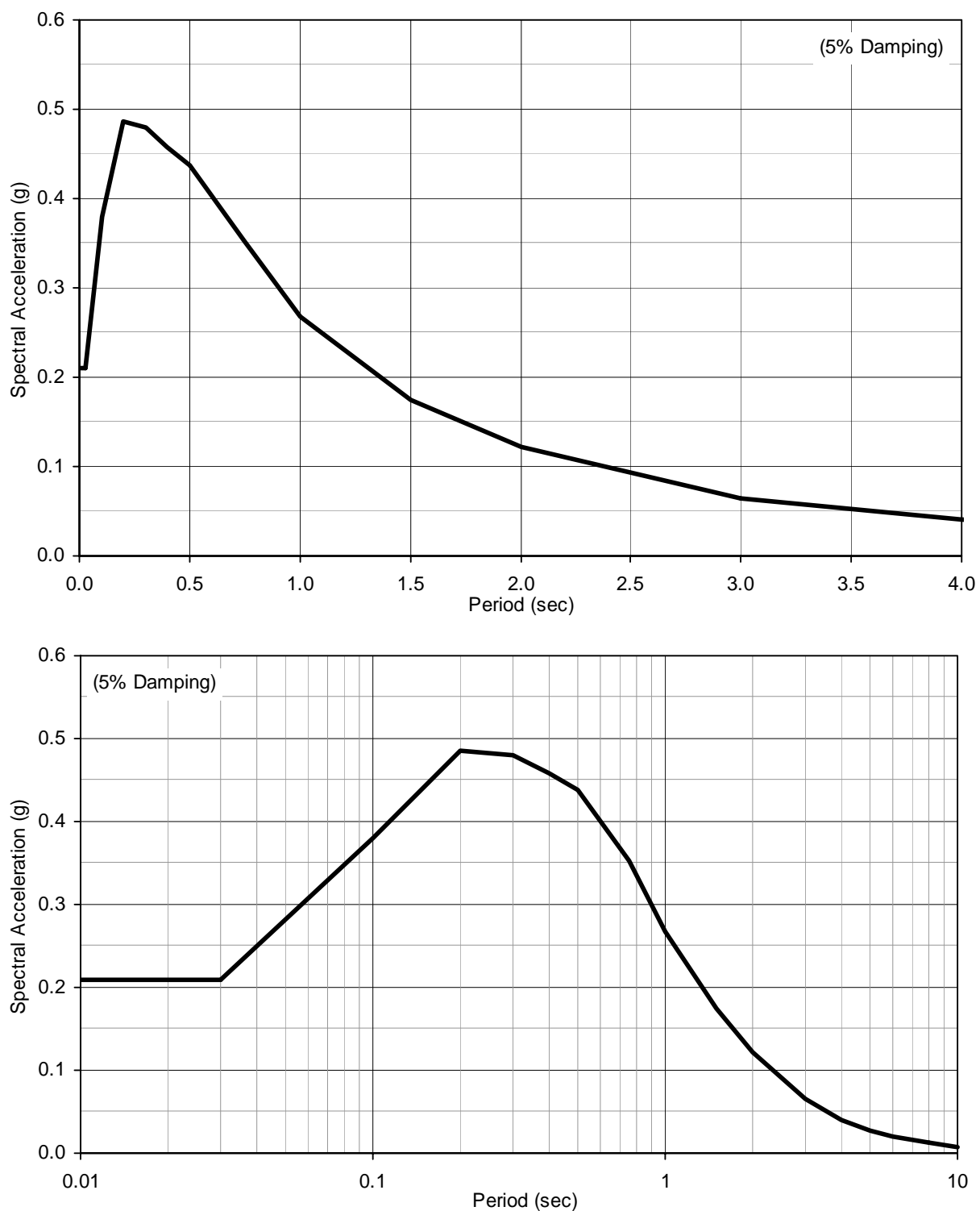
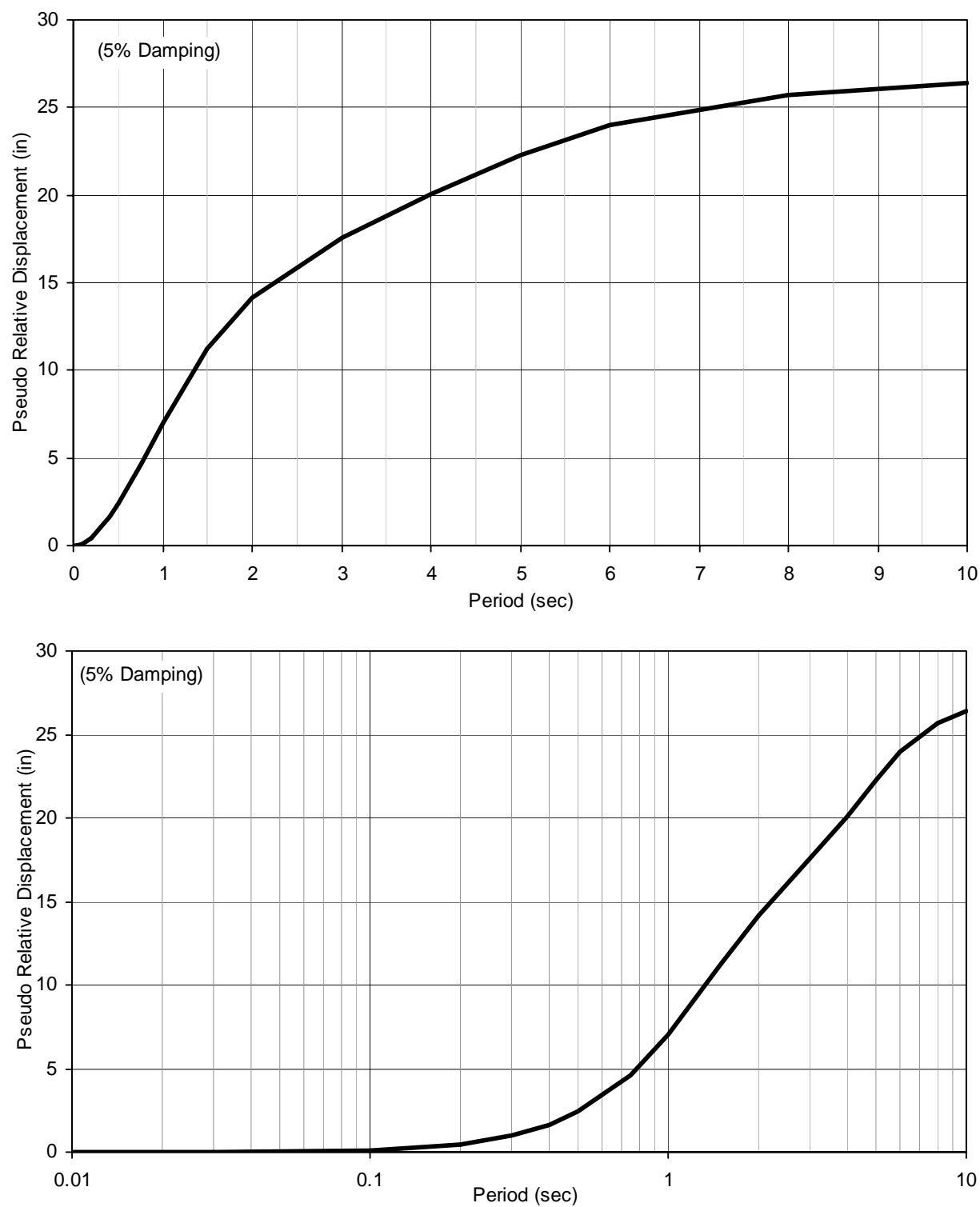**Figure 6-3.　Recommended Design Spectrum (Horizontal Acceleration) for OLE (5% Damping)**
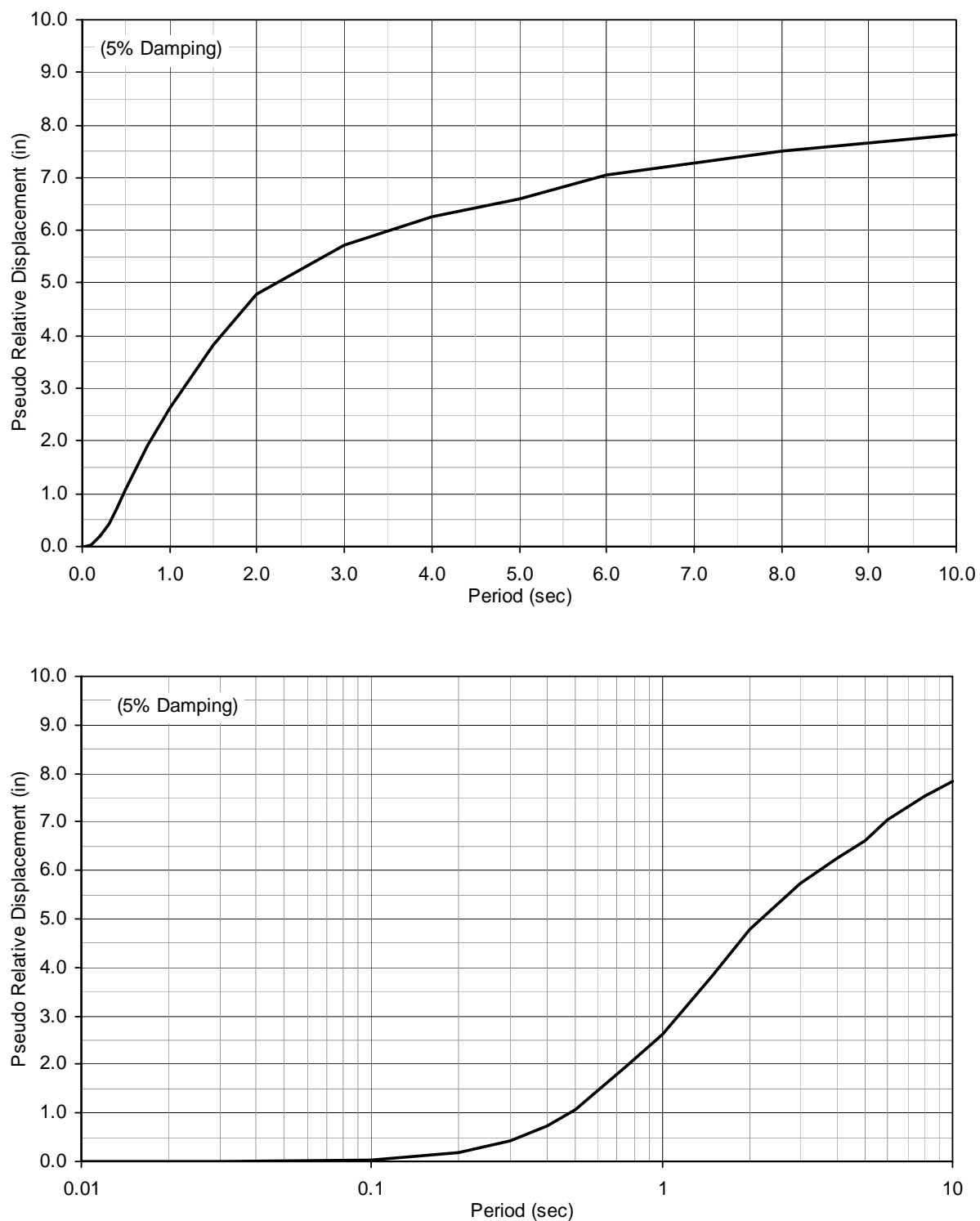
Figure 6-4.   Recommended Design Spectrum (Horizontal Relative Displacement) for OLE (5% Damping)

Table 6-4. **Recommended Horizontal Design Spectra for CLE**

Period (sec)	Damping											
	1%		2%		5%		10%		20%		25%	
	Acc. (g)	Displ. (in)	Acc. (g)	Displ. (in)	Acc. (g)	Displ. (in)	Acc. (g)	Displ. (in)	Acc. (g)	Displ. (in)	Acc. (g)	Displ. (in)
0.01	0.500	0.000	0.500	0.000	0.500	0.000	0.500	0.000	0.500	0.000	0.500	0.000
0.03	0.538	0.005	0.524	0.005	0.500	0.004	0.478	0.004	0.453	0.004	0.445	0.004
0.10	1.233	0.12	1.103	0.11	0.910	0.09	0.756	0.07	0.604	0.06	0.560	0.05
0.20	1.649	0.65	1.436	0.56	1.132	0.44	0.900	0.35	0.682	0.27	0.621	0.24
0.30	1.633	1.44	1.422	1.25	1.121	0.99	0.891	0.79	0.675	0.59	0.615	0.54
0.40	1.529	2.39	1.332	2.09	1.050	1.64	0.835	1.31	0.632	0.99	0.576	0.90
0.50	1.427	3.49	1.243	3.04	0.980	2.40	0.779	1.91	0.590	1.44	0.537	1.31
0.75	1.223	6.73	1.066	5.87	0.840	4.62	0.668	3.68	0.506	2.79	0.460	2.54
1.00	1.039	10.17	0.907	8.87	0.717	7.02	0.572	5.60	0.435	4.26	0.396	3.88
1.50	0.729	16.07	0.640	14.09	0.510	11.23	0.410	9.03	0.315	6.93	0.288	6.34
2.00	0.511	19.99	0.450	17.62	0.362	14.17	0.294	11.49	0.228	8.91	0.209	8.17
3.00	0.273	24.07	0.243	21.43	0.199	17.53	0.164	14.45	0.130	11.43	0.120	10.56
4.00	0.172	26.86	0.154	24.12	0.128	20.05	0.107	16.77	0.086	13.51	0.080	12.56
5.00	0.119	29.17	0.108	26.42	0.091	22.27	0.077	18.89	0.063	15.47	0.059	14.46
6.00	0.089	31.39	0.081	28.43	0.068	23.96	0.058	20.32	0.047	16.65	0.044	15.55
8.00	0.054	33.65	0.049	30.47	0.041	25.68	0.035	21.78	0.028	17.84	0.027	16.67
10.0	0.035	34.62	0.032	31.36	0.027	26.43	0.023	22.41	0.019	18.36	0.018	17.16
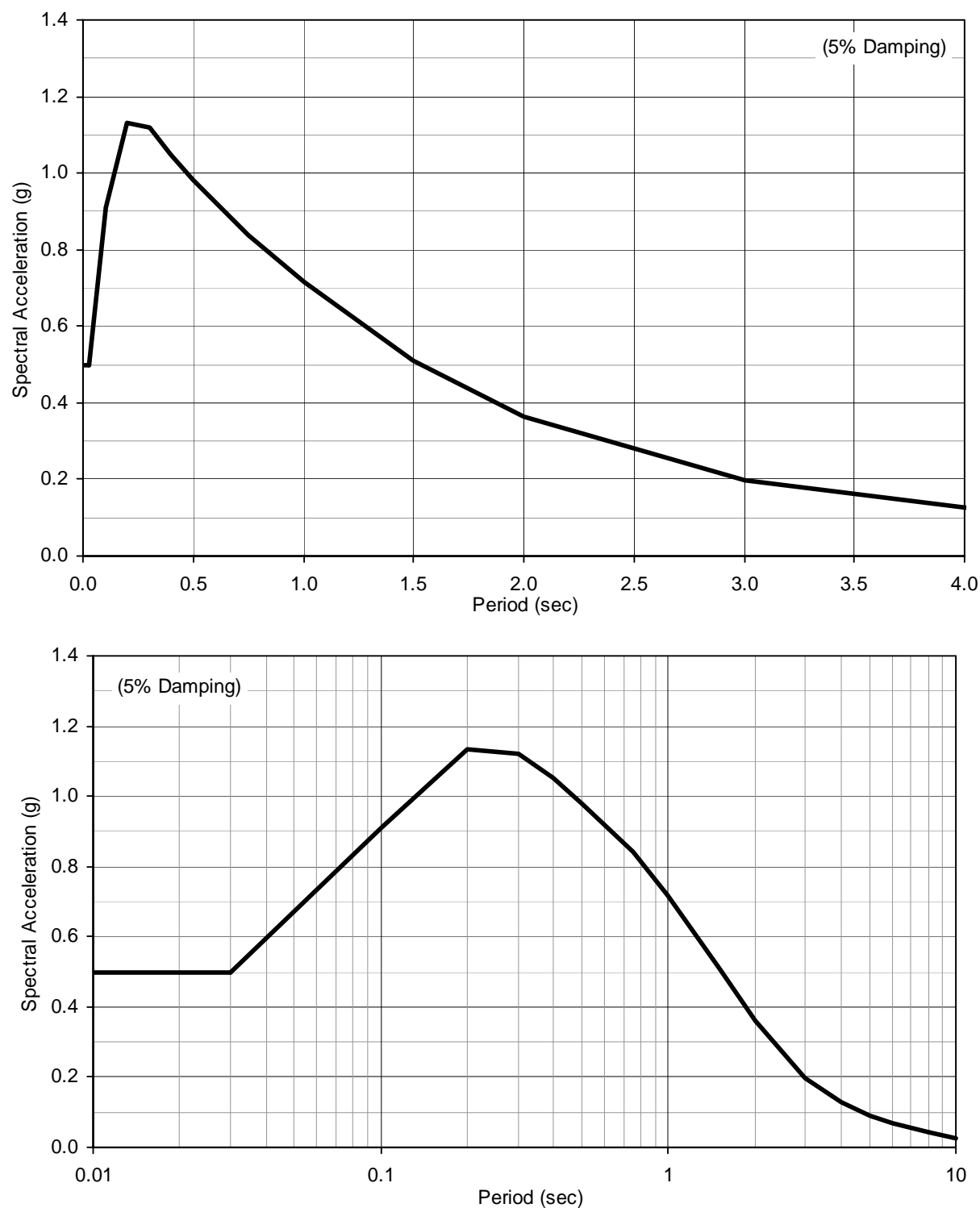
Figure 6-5.   Recommended Design Spectrum (Horizontal Acceleration) for CLE (5% Damping)

Figure 6-6. **Recommended Design Spectrum (Horizontal Relative Displacement) for CLE (5% Damping)**

Table 6-5.   Recommended Newmark Displacement Estimates for Site Screening

Yield Acceleration (g)	Slope Displacement due to OLE (in)	Slope Displacement due to CLE (in)
0.03	10.0	58
0.05	4.0	32
0.075	1.5	18
0.10	1.0	11
0.15	0.5	4.0
0.20	< 0.5	2.0
0.25	< 0.5	1.0
0.30	< 0.5	< 0.5

Figure 6-7.   Recommended Newmark Displacement Curves for Site Screening

SECTION 7
FUTURE DESIGN PRACTICE GUIDELINES

The following guidelines are offered to help minimize unintended variations in future ground motion studies for the Port.

7.1   ADJUSTMENT FOR NEAR-FAULT RUPTURING EFFECTS

In addition to the issues that contributed to unintended variations and inconsistencies in ground motion criteria discussed in previous sections, and based on our past experience on several past seismic design projects (including past Caltrans seismic retrofit and bridge replacement projects, the San Francisco International Airport Expansion Project, and other major projects), we have found that large differences in the UHS (especially for the CLE spectrum) are often due to different assumptions and treatments in the so-called near-fault forward-rupturing effects on the ground motion hazard. Figure 7-1 shows the potential period-dependent adjustment factors for the most adverse assumption for near-fault fault rupturing effects. As can be observed in the figure, the effect can be very significant and would have a profound influence in the result of the UHS solution, especially for longer return periods.

Technical development in this area is in a state of flux. For example, during the San Francisco-Oakland Bay Bridge East Span Project, critical review on this issue led to the need to change the Somerville et al. (1997) near-fault directivity fault-rupturing model, which had a profound influence on the resultant recommended ground motion criteria. For some time, such updates were only documented in a draft EMI Bay Bridge Report (EMI, 1998) that was not accessible to other consultants. Since then, the modified directivity model has been documented in the Abrahamson (2000) publication. This modification might not be widely known by all consultants. Also, there is a great deal of undocumented details regarding how to develop the degree of near fault rupture directivity adjustment (i.e. the x·cos θ parameter) for various return periods. All these issues have not been well documented and potentially contribute to variations among different probabilistic analyses conducted by various consultants. It is conceivable that mistakes are made in the course of implementation of this near fault directivity effect in a probabilistic hazard analysis. This is the reason why it is important to involve experts such as Dr. Abrahamson (a well-known expert in probabilistic hazard analysis theories and also a key co-author in the near-fault directivity attenuation model) in conducting the probabilistic hazard analyses.

7.2   SITE RESPONSE PROCEDURES

We have outlined our site response analysis procedure suggested for future site evaluations. Major issues include the following as discussed previously:

- The need to input the generated firm-ground motion appropriately and avoid to model an overly deep soil column that has a tendency to exaggerate site response effects. In

conducting site response analyses, one should first recognize the benchmark site soil condition compatible to the basis of the attenuation model used for the probabilistic seismic hazard analyses. The firm-ground attenuation models (e.g. the Abrahamson and Silva (1997), Campbell (1997), Sadigh et al. (1997), and Boore et al. (1997) attenuation models) commonly used by consultants supporting POLB's projects are all based on regression analysis of ground surface strong motion records at typical alluvial sites within the Los Angeles Basin.

Based on shear wave velocity profiles collected following the Northridge earthquake at various strong motion stations at California (ROSRINE, 2001), the common opinion among seismologists appears to be that typical firm-ground sites have an average shear wave velocity $\bar{v}_{s30}$ over the upper 100-ft depth of about 1,000 ft/sec. Based on our review of available shear wave velocity profiles at POLB sites, we established four generalized soil profiles as shown in Figure 2-7 representing ranges of soil conditions typical for the POLB. Following a rigorous interpretation of a $\bar{v}_{s30}$ of 1,000 ft/sec definition, input time history records scaled to the reference firm-ground conditions should be used as input at a depth no deeper than about 80 ft. Typical soil profiles at POLB sites have an average shear wave velocity value exceeding about 700 ft/sec within 80-ft depth, increasing to over about 1,200 ft/sec in the next 100-ft depth with a $\bar{v}_{s30}$ approximating the reference 1,000 ft/sec value. In the past, it appears that consultants typically would input the firm-ground input motions from PSHA solutions at the Gaspur formation below 120-ft depth. Based on a more rigorous review of site response solutions, we concluded that such past practice might have resulted in an exaggeration of the site response amplification effect for the long-period range above 0.7 sec.

- In the course of conducting our site response analyses, we also observed that the conventional site response procedure in treating the elastic halfspace beneath the soil column needs to be modified for the deep soil condition typically encountered at the Port. The site response analysis procedure, originally developed by researchers at the University of California at Berkeley, was originally intended to address soil conditions found in the San Francisco Bay Area where bedrock with a shear wave velocity of about 2,500 ft/sec is typically found at 200 to 300-ft depth. Therefore, it is common to conduct probabilistic seismic hazard analysis using bedrock attenuation models to establish the reference target design spectrum that is then used for generating input time histories for site response analyses. As a result, a typical site response analysis conducted for a Bay Area site would have two objectives: (1) to account for the site-specific soil condition such as for a Bay Mud site, and (2) to account for the impedance contrast at the soil-rock interface.

  Typically, the classical site response analysis involves conducting analysis of a soil column to bedrock that has a significant stiffness (impedance) contrast. The soil column is characterized by the measured shear wave velocity profile which will be modified in an iterative equivalent-linear soil modulus adjustment ratio for each layer to account for the nonlinear behavior of soils. Beneath the soil column, a transmitting boundary concept is used in modeling an infinite elastic halfspace at the interface between the soil column and the underlying elastic halfspace. The impedance contrast (the change in soil and bedrock

stiffness) at this transmitting boundary is taken into account implicitly in the conventional site response analysis.

However, soil conditions in the POLB area and many other Los Angeles Basin sites differ from those around the Bay Area in regards to the impedance contrast issue. First, bedrock is typically encountered at large depths. In most cases, the depth to bedrock is not known or cannot be verified by conventional boring programs by geotechnical consultants. For example, during the Vincent Thomas Bridge seismic retrofit design project in the Port of Los Angeles, Caltrans drilled two very deep boreholes, at a great expense, to locate the depth to bedrock. However, that effort had to be abandoned by terminating the boreholes at about 600 ft due to budget and equipment limitations. At the termination depth, the measured shear wave velocity was only about 1,500 ft/sec, well below the 2,500 ft/sec value considered appropriate for bedrock. Difficulty in locating the depth to bedrock and also concern over conducting site response analyses using overly deep soil columns for the Los Angeles Basin sites led to most consultants in Southern California to conduct probabilistic seismic hazard analyses based on firm-ground attenuations rather than based on bedrock attenuations.

In summary, the soil conditions at the POLB should be characterized as a deep soil site where there is no apparent boundary of significant soil stiffness (impedance) contrast between two adjacent soil layers such as the soil-rock interface typically encountered in the San Francisco Bay Area. Hence, the key objective for a site response analysis at the POLB would be to reconcile the somewhat softer surficial soil condition as compared to those typical firm-ground sites found within the Los Angeles Basin. We concluded that a slight change in the procedure in modeling the elastic halfspace beneath the soil column model would give better site response solutions to the deep soil condition at the POLB. We also found that for site response analysis of modeling a relatively short soil column (less than about 80 ft in depth), the cyclic shear strain at the base of the soil column model would remain relatively high (say larger than 0.2% cyclic strain, or 0.5% peak strain). The resultant iterated equivalent-linear shear modulus ratio to adjust the low-strain shear wave velocity profile implicit in a site response solution would degrade the soil layer at the column base to less than 0.5 of the initial low-strain shear modulus basis. This would cause a significant artificial impedance contrast in the site response model at the boundary of base of soil column-underlying halfspace beneath the transmitting boundary of stiffness ratio of larger than at least 2.0.

Naturally, such an impedance contrast is only introduced artificially in the site response model unintentionally whereas there is no true impedance contrast dictated by the site soil condition at the POLB. We found that such an artificial impedance contrast introduces appreciable artificial site amplification at the important structure period range between 0.5 and 1.0 sec. To avoid such an artificial impedance contrast associated with the deep alluvial deposit condition at the POLB, we found that the halfspace shear wave velocity value beneath the transmitting boundary needs to be adjusted manually in an iterative manner. We recommend that after a site response run, the equivalent-linear shear modulus ratio must be extracted at the base of the soil column and then this ratio applied

to soften the shear modulus (velocity) value of the underlying elastic halfspace to avoid the undesirable effect from an impedance contrast on the site response solution.
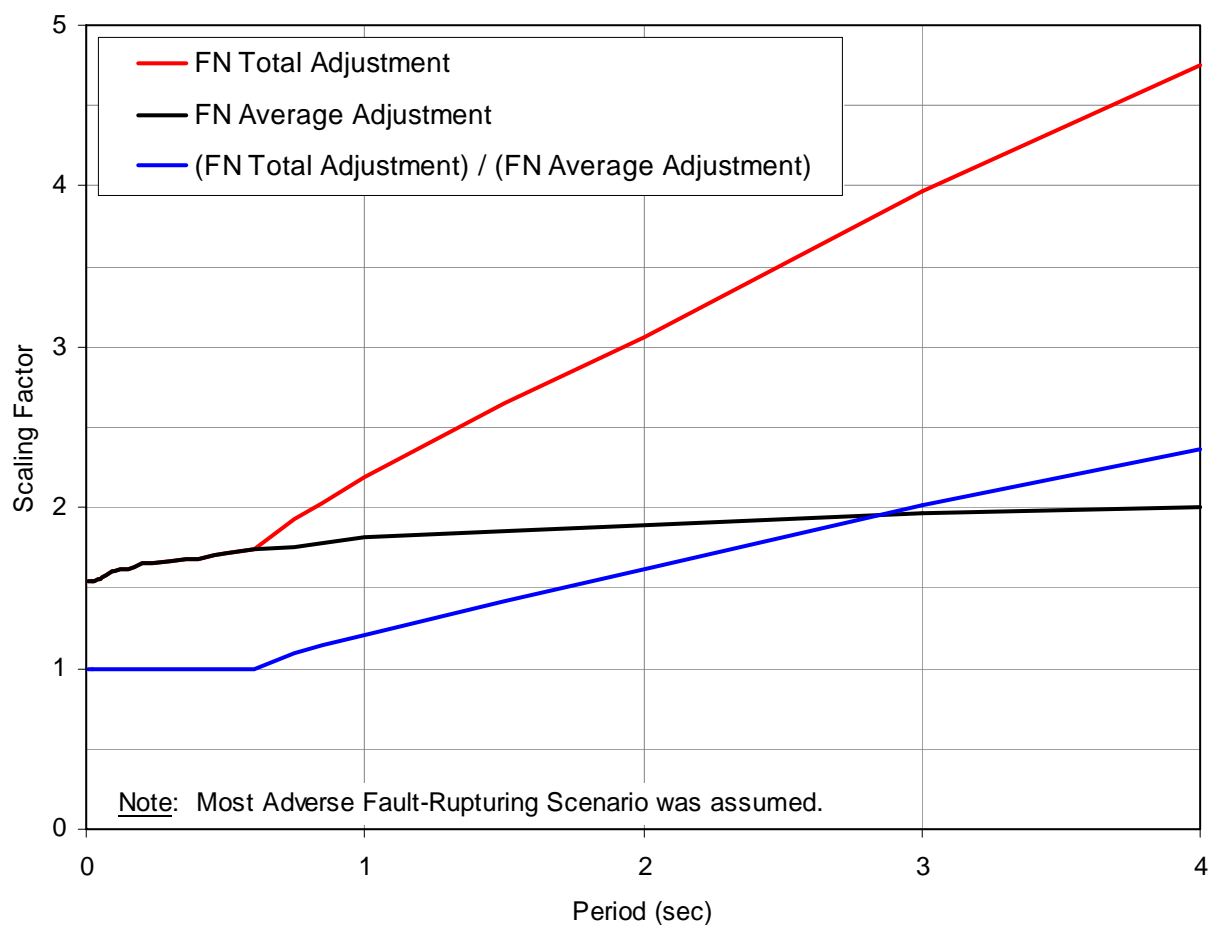
Figure 7-1.   Period-Dependent Adjustment Factors for Near-Fault Fault-Rupturing Effects

SECTION 8
REFERENCES

Abrahamson, N. A., 2000, "Effects of rupture directivity on probabilistic seismic hazard analysis," Proceedings of 6th International Conference on Seismic Zonation, November 12-15, Palm Springs, California, Earthquake Research Institute, Oakland, California.

Abrahamson, N. A., and Silva, W., 1997, "Empirical response spectral attenuation relations for shallow crustal earthquakes," Seismological Research Letters, Vol. 68, No. 1, January/ February.

Abrahamson, N. A., and Silva, W., 2005. Attenuation Model A *(see Appendix C.2 of this report).*

American Association of Petroleum Geologists, 1988, "Correlation section across Los Angeles Basin from Palos Verdes to San Gabriel Mountains," Pacific Section, CS3R.

Atwater, T., and Stock, J., 1998, "Neogene plate tectonic history of southwestern United States: an update," New Zealand Geophysical Society, Joint Annual Conference, Programme and Abstracts, Geological Society of New Zealand Miscellaneous Publication 101A.

Benioff, H., 1938, "The determination of the extent of faulting with application to the Long Beach earthquake," Bulletin of the Seismological Society of America, Vol. 28, p. 77-84.

Bird, P., and Rosenstock, R.W., 1984, "Kinematics of present crust and mantle flow in southern California," Geological Society of America Bulletin, Vol. 95, p. 946-957.

Blake, F., 2000, "FRISKSP User's Manual - 4.00 Update," Documentation, April.

Bommer, J.J., Acevedo, A.B., Douglas, J., 2003, "The selection and scaling of real earthquake accelerograms for use in seismic design and assessment," ACI International Conference on Seismic Design and Retrofit for Earthquake Resistance, San Diego, California, December.

Bonilla, , M.G., 1973, "Trench exposures across surface fault ruptures associated with the San Fernando earthquake," *in* "San Fernando, California, earthquake of February 9, 1971, Vol. 3: Geological and Geophysical Studies," Murphy L.M., ed., Washington, D.C., National Oceanic and Atmospheric Administration, p. 173-182.

Boore, D.M., Joyner, W.B., and Fumal, T.E., 1997, "Equations for estimating horizontal response spectra and peak acceleration from western north American earthquakes: a summary a recent work," Seismological Research Letters, Vol. 68, No. 1, January/February.

Bullard, T.F., and Lettis, W.R., 1993, "Quaternary fold deformation associated with blind thrust faulting, Los Angeles basin, California," Journal of Geophysical Research, Vol. 98, p. 8349-8369.

California Building Code (CBC), 2001, "Chapter 31F [for SLC], Marine Oil Terminals," Supplement, January 31.

California Department of Water Resources, 1961, "Planned utilization of the ground water basins of the Coastal Pain of Los Angeles County, Appendix A, Ground Water Geology," Department of Water Resources Bulletin No. 104.

California Geological Survey, 2003, "The revised 2002 California probabilistic seismic hazard maps," California Geological Survey website by Cao, T., Bryant, W.A., Rowshandel, B., Branum, D., and Wills, C.J., June 2003.

Campbell, K. W., 1997, "Empirical near-source attenuation relationships for horizontal and vertical components of peak ground acceleration, peak ground velocity, and pseudo-absolute acceleration response spectra," Seismological Research Letters, Vol. 68, No. 1, pp.154-179.

Castle, R.O., and Buchanan-Banks, J.M., 1989, "Vertical surface displacements along a part of the Newport-Inglewood zone of folds and faults, Los Angeles and Orange counties, California," U.S. Geological Survey Miscellaneous Field Studies Map MF 2088.

Clark, B.R., Zeiser, F.L., and Gath, E.M., 1986, "Evidence for determining activity level of the Pelican Hill fault, coastal Orange County, California." Association of Engineering Geologists, Annual Meeting, Abstracts with Program, p. 146.

Clarke, S.H., Greene, H.G., Kennedy, M.P. and Vedder, J.G., 1987, "Geological map of the inner-southern continental margin, California Continental Margin Geologic Map series: California," California Division of Mines and Geology.

Clarke, S.H., and Kennedy, M.P., 1998, "Analysis of Late Quaternary faulting in the Los Angeles harbor area and hazard to the Vincent Thomas bridge," California Department of Conservation, Division of Mines and Geology, Open-File Report 98-01.

Clarke, D., 2004, Geologist for the City of Long Beach, personal communication.

Cornell, C.A., 1968, "Engineering seismic risk analysis," Seismological Society of America Bulletin, v. 58, p. 1583-1606.

Crook, R., Jr., Allen, C.R., Kamb, B., Payne, C.M., and Proctor, R.J., 1987, "Quaternary geology and seismic hazard of the Sierra Madre and associated faults, western San Gabriel Mountains," *in* "Recent reverse faulting in the Transverse Ranges, California," U.S. Geological Survey, Professional Paper 1339, p. 27-64.

Crook R.C. Jr., and Proctor, R.J., 1992, "The Santa Monica and Hollywood faults and the southern boundary of the Transverse Ranges province," *in* "Engineering geology practice in southern California," Association of Engineering Geologists, Southern California Section, Special Publication 4, p. 233-246.

Crouch, J.K., and Suppe, J., 1993, "Late Cenozoic tectonic evolution of the Los Angeles basin and inner California borderland: a model for core complex-like crustal extension," Geological Society of America Bulletin, Vol. 105, p. 1415-1434.

Davis, T.L., and Namson, J., and Yerkes, 1989, "A cross section of the Los Angeles area: seismically active fold and thrust belt, the 1987 Whittier Narrows earthquake and earthquake hazard," Journal of Geophysical Research, Vol. 94, p. 9644-9664.

Dibblee, T.W., Jr., 1999, "Geologic Map of the Palos Verdes Peninsula and Vicinity, Redondo Beach, Torrance and San Pedro quadrangles," Dibblee Geological Foundation Map DF 70.

Dolan, J.F., Sieh, K., Rockwell, T.K., Yeats, R.S., Shaw, J., Suppe, J., Huftile, G.J., and Gath, E.M., 1995, "Prospect for larger or more frequent earthquakes in the Los Angeles metropolitan region, California," Science, Vol. 267, p. 199-205.

Dolan, J.F., Sieh, K., Rockwell, T.K., Guptill, P. and Miller, G., 1997, "Active Tectonics, Paleoseismology, and Seismic Hazards of the Hollywood Fault, Northern Los Angeles Basin, California," Geological Society of America Bulletin, Vol. 109, p. 1595-1616.

Dolan, J.F., Stevens, D., Rockwell, T.K., 2000a, "Paleoseismologic evidence for an early- to mid-Holocene age of the most recent surface rupture on the Hollywood fault, Los Angeles, California," Bulletin of the Geological Society of America, Vol. 90, p. 334-344.

Dolan, J.F., Sieh, K., Rockwell, T.K., 2000b, "Late Quaternary activity and seismic potential of the Santa Monica fault system, Los Angeles, California," Geological Society of America Bulletin, Vol. 112, p. 1559-1581.

Dolan, J.F., Christofferson, S.A., and Shaw, J.H., 2003, "Recognition of paleoearthquakes on the Puente Hills blind thrust fault, California," science, Vol. 300, p. 115-118.

Drumm, P.L., 1992, Holocene displacement of the central splay of the Malibu Coast fault zone, Latigo Canyon, Malibu, *in* Engineering geology practice in southern California: Association of Engineering Geologists, Southern California Section, Special Publication 4, p. 247-254.

Earth Mechanics, Inc, 1993, "Probabilistic seismic-hazard assessment and free-field site Response, Port of Los Angeles, Pier 400," Report for Pier 400 Design Consultants, Carson, CA, EMI project No. 92-204.

Earth Mechanics, Inc, 1995, "Interim design response spectrum, Vincent Thomas bridge retrofit," Report for Moffatt & Nichol and Caltrans Translab, EMI project No. 95-126, August 14.

Earth Mechanics, Inc. 1998, "Seismic ground motion report for the San Francisco-Oakland Bay Bridge East Span Seismic Safety Project, Bridge No. 34-006, Contract No. 59A0053," Draft Report submitted to Caltrans, December 24.

Earth Mechanics, Inc, 2001, "Final ground motion and fault study report, West Basin, Port of Los Angeles, San Pedro, California," Report for Port of Los Angeles, San Pedro, CA, EMI project No. 00-115-8, April 27.

Edwards, B.D., Catchings, R.D., Hildebrand, T.G., Miller, M.S., Ponti, D.J., and Wolfe, S.C., 2001, "Quaternary sedimentary structure of the southwestern Los Angeles basin region," Geological Society of America Abstracts with Program, Vol. 33, PA-41.

Edwards, B.D., Ponti, D.J., Ehmann, K.D., Tinsley, J.C., III, and Reicherdt, E.G., 2002, "Offshore stratigraphic controls on saltwater intrusion in Los Angeles area coastal aquifers," American Geophysical Union Fall Meeting, San Francisco, CA, EOS, Vol. 83, p. F567.

Edwards, B.D., Ehmann, K.D., Ponti, D.J., Tinsley, J.C., III, and Reicherdt, E.G., 2003, "Offshore stratigraphic controls on saltwater intrusion in Los Angeles area coastal aquifers," *in* "LA Basin 2003, Original Urban Oil Field Legends, Conference Program and Abstracts," American Association of Petroleum Geologists, Pacific Section and Western Region Society of Petroleum Engineers, Abstract, p. 62.

Fall, E.W., Rzonca, G.F., Spellman, H.A., 1987, "Late Quaternary faulting, Malibu Coast fault zone, Malibu, California," Association of Engineering Geologists, Annual Meeting Abstracts with Program, p. 38.

Federal Emergency Management Agency (FEMA), 2003, NEHRP Recommended Provisions for Seismic Regulations for New Buildings and Other Structures (FEMA 450), Part 1–Provisions, 2003 Edition, Building Seismic Safety Council of the National Institute of Building Sciences, Washington, D.C.

Fischer, P.J., Rudat, J.H., Patterson, R.H., and Simila, G., 1987, "The Palos Verdes fault zone: onshore and offshore," *in* "Geology of the Palos Verdes Peninsula and San Pedro Bay," Society of Economic Paleontologists and Mineralogists, Pacific Coast Section, Guidebook 55, p. 91-133.

Fisher, M.A., Normark, W.R., Bohannon, R.G., Sliter, R.W., and Calvert, A.J., 2003, "Geology of the continental margin beneath Santa Monica Bay, Southern California, from seismic-reflection data," Bulletin of the Seismological Society of America, Vol. 93, p. 1955-1983.

Fisher, M.A., Normark, W.R., Langenheim, V.E., and Calvert, A.J., 2004, "The offshore Palos Verdes Fault zone near San Pedro, Southern California," Bulletin of the Seismological Society of America, Vol. 94, p. 506-530.

Freeman, S.T., Heath, E.G, Guptill, P.D., and Waggoner J.T., 1992, "Seismic hazard assessment, Newport-Inglewood Fault Zone," *in* "Engineering geology practice in Southern California," Association of Engineering Geologists, Southern California Section, Special Publication 4, p. 211-231.

Geomatrix Consultants, 1992, "Seismic Ground Motion Study for West Span San Francisco Bay Bridge," Report to California Department of Transportation, Contract No. 59N772.

Geomatrix Consultants, 1995, "Adjustments to rock spectra for Caltrans toll bridges in Northern California," Report prepared for Caltrans Division of Structures, Sacramento, California.

Grant, L.B., Waggoner, J.T., Rockwell, T.K., and Von Stein, C., 1997, "Paleoseismicity of the north branch of the Newport-Inglewood fault zone in Huntington Beach, California, from cone penetrometer test data," Bulletin of the Seismological Society of America, Vol. 87, p 277-293

Greene, H.G., and Kennedy, M.P., 1986, "Geology of the mid-southern California continental margin," California Division of Mines and Geology, California Continental Margin Geologic Map Series, Area 2 of 7.

Gutenberg, B., and Richter, C.F., 1954, "Seismicity of the Earth and associated phenomena," Princeton University Press, Princeton, N.J.

Hanks, T.C., and Bakum, W.H., 2002, "A bilinear source-scaling model for M-log A observations of continental earthquakes," Bulletin of the Seismological Society of America, Vol. 92, p.1841-1846.

Harding Lawson Associates, 1989, "Seismic and Geotechnical Overview, 2020 Project, Ports of Los Angeles and Long Beach, San Pedro Bay, California," Report to Vickerman/Zachary/Miller, Oakland, HLA Job. No. 13134,015.11.

Harding, T.P. and Tuminas, A.C., 1988, "Interpretation of footwall (lowside) fault traps sealed by reverse faults and convergent wrench faults," American Association of Petroleum Geologists Bulletin, Vol. 72, p. 738-757.

Hauksson, E., 1987, "Seismotectonics of the Newport-Inglewood fault zone in the Los Angeles Basin, southern California." Bulletin of the Seismological Society of America, v. 77, p. 539-561.

Hauksson, E., 1990, "Earthquakes, faulting, and stress in the Los Angeles basin," Journal of Geophysical Research, Vol. 95, p. 15,365-15,394.

Hauksson, E., 1995, "Seismological overview of the 1994 Northridge earthquake sequence in California," *in* "The Northridge California earthquake of 17 January 1994," Woods, M.C., and Seiple, W.R., editors, California Department of Conservation, Division of Mines and Geology, Special Publication 116, p. 17-38.

Hauksson, E. and Gross, S., 1991, "Source parameters of the 1933 Long Beach earthquake," Bulletin of the Seismological Society of American, Vol. 81, p. 81-98.

Hummon, C., Schneider, C.L., Yeats, R.S., Dolan, J.F., Sieh, K.E., and Huftile, G.J., 1994, "Wilshire fault: earthquakes in Hollywood?," Geology, Vol. 22, p. 291-294.

Idriss, I.M, and Sun, J.I.,1992, "User's Manual for SHAKE91: A computer program for conducting equivalent linear seismic response analyses of horizontally layered soil deposits," User's Manual, Center for Geotechnical Modeling, Dept. of Civil & Environmental Engineering, University of California, Davis, CA, November.

Jennings, C.W., 1994, "Fault activity map of California and adjacent areas with locations and ages of recent volcanic eruptions," Department of Conservation, Division of Mines and Geology, California Geologic Data Map Series, Map No. 6.

Lindvall S.C., and Rockwell, T.K., 1995, "The Rose Canyon fault and earthquake hazards of San Diego," Association of Engineering Geologists, Annual Meeting, Abstract, p. 58.

Los Angeles County Seismic Safety Element, 1990, "Technical appendix to the safety element of the Los Angeles County general plan, hazard reduction in Los Angeles County," Prepared for Department of Regional Planning by Leighton and Associates and Sedway Cooke Associates.

Luyendyk, B.P., Kamerling, M.J., and Terres, R.R., 1980, "Geometric model for Neogene crustal rotations in Southern California," Geological Society of America Bulletin, Vol. 91, p. 211-217.

McMurdie, D.S., 1973, "Geology and general history of the Dominguez oil field in an urban environment -Los Angeles County, California," Pacific Sections, American Society of Petroleum Geologists- Society of Exploration Paleontologists and Mineralogists-Society of Exploration Geophysicists, Guidebook, Trip 1, p. 25-31.

McNeilan, T.W., Rockwell, T.K., and Resnick, G.S., 1996, "Style and rate of Holocene slip, Palos Verdes fault, Southern California," Journal of Geophysical Research, Vol. 101, p. 8317-8334.

Mualchin, L., 1996, "California seismic hazard map, 1996," California Department of Transportation, Revision 1, July 1996.

Mueller, K.J., 1997, "Recency of folding along the Compton-Los Alamitos trend: implications for seismic risk in the Los Angeles basin," EOS Transactions of the American Geophysical Union, Vol. 78, p. F702.

Nardin, T.R., and Henyey, T.L., 1978, "Pliocene-Pleistocene diastrophism of Santa Monica and San Pedro shelves, California continental borderland," American Association of Petroleum Geologists Bulletin, Vol. 62, p.247-272.

Oskin, M., and Sieh, K.E., 1998, "The Elysian Park anticlinorium; surficial evidence of an active blind reverse fault beneath downtown Los Angeles," Geological Society of America, Abstracts with Programs, Cordilleran Section, n. 6471, p. 57.

Oskin M., Sieh, K., Rockwell, T., Miller, G., Guiptill, P., Curtis M., McArdle, S. and Elliot, P., 2000, "Active parasitic folds on the Elysian Park anticline: implications for seismic hazard in central Los Angeles, California," Geological Society of America Bulletin, Vol. 113, p. 693-707.

Ponti, D. J., 1989, "Aminostratigraphy and chronostratigraphy of Pleistocene marine sediments, southwestern Los Angeles Basin, California," Ph. D. dissertation, Boulder, Co., University of Colorado.

Ponti, D.J., 2004, U.S. Geological Survey, Principal Investigator for Coastal Groundwater Investigation, personal communication.

Ponti, D.J., and LaJoie, K.R., 1992, "Chronostratigraphic implications for tectonic deformation of Palos Verdes and Signal Hills, Los Angeles Basin, California," Association of Engineering Geologists, 35th Annual Meeting, Proceedings, p. 617-620.

Prior, S., 2004, THUMS Senior Geologist, personal communication.

Rivero, C., Shaw, J.H., and Mueller, K.L., 2000, "Oceanside and Thirtymile Bank blind thrusts: implications for earthquake hazards in coastal Southern California," Geology, Vol. 28, p. 891-894.

Rockwell, T.K., Hatch, M.E., and Schug, D.L., 1987, "Late Quaternary rates of Agua Blanca and Borderland faults," U.S. Geological Survey, Final Technical Report 14-08-0001-22012.

ROSRINE, 2001, "Resolution of site response from the Northridge Earthquake," Website: http://geoinfo.usc.edu/rosrine/

Rubin, C.M., Lindvall, S.C., and Rockwell, T.K., 1998, "Evidence for large earthquakes in metropolitan Los Angeles," Science, Vol. 281, p. 398-402.

Sadigh, K., Chang K.-Y., Egan, J.A., Makdisi, F., and Youngs, R.R., 1997, "Attenuation relationships for shallow crustal earthquakes based on California strong motion data," Seismological Research Letters, Vol. 68, No. 1, January/February.

Schell, B.A., 1991, "Seismotectonic zonation and seismic hazard analyses in Southern California," Fourth International Conference on Seismic Zonation, Proceedings, Vol. 2, p. 19-26.

Schell, B.A., 1997, "Seismotectonics of the Los Angeles Basin and seismic hazards associated with the Norwalk, Peralta Hills, El Modeno, and Los Alamitos faults, Southern California," Association of Engineering Geologists Annual Meeting, Portland, Oregon, Abstracts with Program, p. 145.

Schwartz, H.B., and Coppersmith, K.L., 1984, "Fault behavior and characteristic earthquakes; examples from the Wasatch and San Andreas fault zones," Journal of Geophysical Research, v. 89, p. 5681-5698.

Shaw, J.H., 1993, "Active blind-thrust faulting and strike-slip fault-bend folding in California," Princeton University (Ph.D. Thesis), Princeton, New Jersey, 216 p.

Shaw, J.H., 2004, personal communication.

Shaw, J.H., Plesch, A., Dolan, J.F., Pratt, T.L., and Fiore, P., 2002, "Puente Hills blind-thrust system, Los Angeles, California," Bulletin of the Seismological Society of America, Vol. 92, p. 2946-2960.

Shaw, J.H., and Shearer, P.M., 1999, "An elusive blind-thrust fault beneath metropolitan Los Angeles," Science, Vol. 283, p.1516 (5 March)

Shaw, J.H., and Suppe, J., 1996, "Earthquake hazards of active blind thrust faults under the central Los Angeles basin, California," Journal of Geophysical Research, Vol. 101, p. 8623-8642.

Shlemon, R.J., Elliott, P., and Franzen, S., 1995, "Holocene displacement history of the Newport-Inglewood, North Branch fault splays, Santa Ana River floodplain, Huntington Beach, California," Geological Society of America, Abstracts with Programs, Vol. 27, p. A-375.

Somerville, P.G., Irikura, K., Graves, R.W., Sawasa, S., Wald, D., Abrahamson, N.A., Iwasaki, Y., Kagawa, T., Smith, N., and Kowada, A., 1999, "Characterizing crustal earthquake slip models for prediction of strong ground motion," Seismological Research Letters, Vol. 70, No. 59-80.

Somerville, P.G., Smith, N.F., Graves, R.W., and Abrahamson, N.A., 1997, "Modification of empirical strong ground motion attenuation relations to include the amplitude and duration effects of rupture directivity," Seismological Research Letters, Vol. 68, No. 1, January/February.

Truex, J.N., 1974, "Structural evolution of Wilmington, California anticline," American Association of Petroleum Geologists Bulletin, Vol. 58, p. 2398-2410

Tsutsumi, H., Yeats, R.S., and Huftile, G.J., 2001, "Late Cenozoic tectonics of the northern Los Angeles fault system, California," Geological Society of America Bulletin, Vol. 113, p. 454-468.

Tucker, A.Z., and Dolan, J.F., 2001, "Paleoseismologic evidence for a >8ka age of the most recent surface rupture on the eastern Sierra Madre fault, northern Los Angeles metropolitan region, California," Bulletin of the Seismological Society of America, Vol. 91, p. 232-249.

Vedder, J.G., Greene, H.G., Clarke, S.H., and Kennedy, M.P., 1986, "Geologic map of the mid-Southern California continental margin," California Division of Mines and Geology, California Continental Margin Geologic Map Series, Map No. 2A.

Ward, S.N., 1994, "A multidisciplinary approach to seismic hazard in Southern California," Bulletin of the Seismological Society of America, Vol. 84, p. 1293-1309.

Ward, S.N., and Valensise, G., 1994, "The Palos Verdes terraces, California: bathtub rings from a buried reverse fault," Journal of Geophysical Research, Vol. 99, p. 4485-4494.

Wells, D. and K. Coppersmith, 1994, "Updated empirical relationships among magnitude, rupture length, rupture area, and surface displacement," Bull Seism. Soc. Am., Vol. 84, 974-1002.

Woodring, W.P., Bramlette, M.N., and Kew, W.S.W., 1946, "Geology and Paleontology of Palos Verdes Hills, California," U.S. Geological Survey, Professional Paper 207.

Woodward Clyde Consultants, 1976, "Geotechnical Investigation, Los Angeles Outer Harbor, Port of Los Angeles, California," Report to POLA, Project No. A653I.

Wright, T.L., 1991, "Structural geology and tectonic evolution of the Los Angeles Basin, California," *in* "Active basin margins," Biddle, K.T., ed., American Association of Petroleum Geologists Memoir 52.

Yerkes, R.F., McColloch, T.H., Schoellhamer, J.E., and Vedder, J.G., 1965, "Geology of the Los Angeles Basin, California - an introduction," U.S. Geological Survey, Professional Paper 420-A.

Youngs, R. R. and K. Coppersmith, 1985, "Implications for fault slip rates and earthquake recurrence models to probabilistic seismic hazard estimates," Bull. Seism. Soc. Am., Vol. 75, 939-964.

Zielbauer, E.J., Kues, H.A., Burnham, W.L., and Keene, A.G., 1962, "Dominguez Gap Barrier Project Geologic Investigation," Los Angeles County Flood Control District, March 1962.

SECTION 9
BIBLIOGRAPHY

Brown & Caldwell, 1996, "Results of Ocean Boulevard Widening Project Soil Sampling," Prepared for Port of Long Beach, July 12.

Dames & Moore, 1981, "Report Geotechnical Engineering and Environmental Services, Proposed Marine Tanker Terminal and Crude Oil Transfer Facility Berth 121, Pier E, Long Beach, California," Prepared for Port of Long Beach, February 26.

Dames & Moore, 1989, "Geotechnical Investigation, West Seventh Street Development, Port of Long Beach, California," Report to Port of Long Beach, May 25.

Dames & Moore, 1990, "Seismic Stability Evaluation, Proposed North Wharf, Pier J Expansion Project for the Port of Long Beach," Report to Port of Long Beach, October 17.

Dames & Moore, 1993, "Report Geotechnical Investigation Proposed Scrap Metal Handling Facility Berths T-118 and T-119 Port of Long Beach," for Port of Long Beach, August 31.

Dames & Moore, 1994, "Geotechnical Investigation Proposed Landfill and Wharf Construction, Slip No. 2, Port of Long Beach," for the Port of Long Beach, December 23.

Dames & Moore, 1999, "Report, Phase I Geotechnical Investigation for Pier S Backland Development Port of Long Beach," for Port of Long Beach, January 20.

Diaz Yourman & Associates, 1997, "Geotechnical Investigation, Data Report, Naval Station Container Terminal, Long Beach, California", Report Prepared for KPFF Consulting Engineers, January 20.

Diaz Yourman & Associates, 1999, "Geotechnical Investigation, The Waterfront at the Queen Mary – Phase I, Long Beach, California", Report Prepared for Queen's SeaPort Development Inc, May 28.

Diaz Yourman & Associates, 2002, "Geotechnical Investigation Dredging and Wharf Extension Phase II Pier T Marine Terminal," Report Prepared for KPFF Consulting Engineers, July 22.

Diaz Yourman & Associates, 2002, "Geotechnical Investigation Filling of Drydock No. 1 and Surrounding Area Pier T Marine Terminal, Port of Long Beach," Report Prepared for KPFF Consulting Engineers, June 27.

Diaz Yourman & Associates, 2003, "Geotechnical Data Report, Gerald Desmond Bridge Replacement Project, Long Beach, California," Report to Parsons/HNTB Joint Venture, September 29.

Diaz Yourman & Associates, 2004, "Geotechnical Investigation, Liquefied Natural Gas and Liquid Bulk Terminals, Long Beach, California," Prepared for KPFF Consulting Engineers, Seattle, WA, August 5.

Diaz Yourman & Associates, 2005, "Geotechnical Investigation, POLB Security Command and Control Center, Long Beach, California," Prepared for POLB, June 6.

Earth Mechanics, Inc., 1991, "Port of Long Beach Feasibility Study for Deepening of Pier C, Seismic Response Analysis", Prepared for Port of Long Beach, September 20.

Earth Mechanics, Inc., 1996, "Foundation Report for Pier J Grade Separation, Port of Long Beach, California," Prepared for MK-Centennial.

Earth Mechanics, Inc., 1997, Final Geotechnical Investigation Report, Ocean Boulevard Storm Pump station, Long Beach, California, Port of Long Beach, November 19.

Earth Mechanics, Inc., 2005, "Preliminary Ground Motion Criteria for Gerald Desmond Bridge for Caltrans Interim Review," Prepared for Caltrans, February 4.

Earth Mechanics, Inc., 2006, "Geotechnical Report for Pier T, Berth T121 BP Cold Ironing Project, Port of Long Beach," Prepared for DMJM HARRIS, February 8.

Earth Mechanics, Inc. & Diaz Yourman Associates, 2005, "Preliminary Geotechnical Report for Gerald Desmond Bridge Replacement Project, Long Beach, California, Draft Report Prepared For PTG/HNTB Joint Venture, July.

Ertec Western, Inc., 1982, "Report (Draft) Geotechnical Investigation Proposed Long Beach International Coal Project Long Beach, California", for The Port of Long Beach, April 23.

Fugro-McClelland, 1992, "Post-Improvement Geotechnical Study, 122-Acre Hydraulic Landfill Ground Improvement Project, Contract B - Phase III Areas, Terminal Island, Port of Los Angeles, San Pedro, CA."

Fugro West, Inc., 1978, "Geotechnical Investigation, Proposed Sohio Terminal, Long Beach, California," Report Prepared for Port of Long Beach, July 11.

Fugro West, Inc., 2002, "Dike Design, Pier 300 Extension, Port of Los Angeles, California," Report to U.S. Army Corps of Engineers.

Fugro West, Inc., 2004, "Preliminary Geotechnical Engineering Study California United Terminal, Port of Long Beach, California," Prepared for Moffatt & Nichol Engineers, February 26.

Fugro West, Inc., 2006, "Geotechnical Site Characterization, Pier E Redevelopment Project, Port of Long Beach, California," Revised Draft Report for Moffatt & Nichol Engineers, March.

Geofon, Inc., 1986, "Geotechnical Investigation, Pier J Expansion Project, Port of Long Beach, Long Beach, California," Prepared for the Port of Long Beach, October 29.

Geofon, Inc., 1987, "Geotechnical Data Collection, Pier J Expansion Project Port of Long Beach," Submitted to Port of Long Beach, August 26.

Geofon, Inc., 1991a, "Geotechnical Investigation, 100-Acre Surcharge Area, Pier J Expansion Project – Phase II, Port of Long Beach, California," Final Report to Port of Long Beach, April 11.

Geofon, Inc., 1991b, "Final Report Geotechnical Investigation, Pier J Expansion Project - Phase 2 Lagoon Area Port of Long Beach," Prepared for The Port of Long Beach, December 30.

Geofon, Inc., 1994, "Geotechnical Report, Anaheim Street Grade Separation, Port of Long Beach," Prepared for De Lew Cather, Inc., November 21.

Geotechnical Professionals, Inc., 2002, "Draft Report Geotechnical Investigation for Pier S Wharf, Port of Long Beach," Prepared for Port of Long Beach, September 16.

Geotechnical Professionals, Inc., 2003a, "Draft Marine Geotechnical Investigation for Pier S Wharf Dredging Port of Long Beach," Prepared for Port of Long Beach, March 5.

Geotechnical Professionals, Inc., 2003b, "Geotechnical Studies for Pier S Wharf, Port of Long Beach," Report to Port of Long Beach, July 21.

Group Delta Consultants, Inc., 2001, "Draft Structure Foundation Report, Pier S/Pier T connector UC (Br. No. 53-2940), Pier S/Pier T W/B Connector Ramp UC (Br. No. 53-2941), Pier S/Pier T E/B Connector Ramp UC (Br. No. 53-2942), Terminal Island/Ocean Blvd. Interchange Project, Port of Long Beach, California," Prepared for Port of Long Beach, March 8.

Group Delta Consultants, Inc., 2001, "Geotechnical Investigation, Wharf Design and Construction Pier S, Berths S102-S108, Port of Long Beach," Prepared for the Port of Long Beach, May 17.

Group Delta Consultants, Inc., 2001, "Final Structure Foundation Report, Terminal Island Freeway Separation Terminal Island/Ocean Blvd. Interchange Project, Port of Long Beach, California," Prepared for Port of Long Beach, August 17.

Group Delta Consultants, Inc., 2001, "Final Structure Foundation Report, Henry Ford Avenue Undercrossing Terminal Island/Ocean Blvd. Interchange Project, Port of Long Beach," Prepared for Port of Long Beach, August 17.

Group Delta Consultants, Inc., 2002, "Geotechnical Design Report, Ocean Boulevard/ Terminal Island Freeway Interchange Project, Port of Long Beach, Long Beach, California," Prepared for Port of Long Beach, October 22.

Harding Lawson Associates, 1990, "Field and Laboratory Data, Pier J Expansion Project, North Wharf, Port of Long Beach, California," Report to Port of Long Beach, January 31.

Kleinfelder, 1996, "Report of Geotechnical Investigation for the Proposed New Container Wharf at Pier J, Berths J235 and J236, Port of Long Beach, California," Report to Port of Long Beach, Long Beach, California, Project No. 58-5337-01, March 29.

Kleinfelder, 2000a, "Geotechnical Investigation, Volume 1 – Soil Data Report, Port of Long Beach, Pier G Terminal Development Project," Prepared for Port of Long Beach, Long Beach, California, June.

Kleinfelder, 2000b, "Geotechnical Investigation, Volume 2 – Geotechnical Design Guidelines, Port of Long Beach, Pier G Terminal Development Project," Prepared for Port of Long Beach, July.

Kleinfelder, 2003, "Report of Geotechnical Feasibility Investigation, Proposed New Port of Long Beach Administration and Maintenance Buildings, 669 Harbor Plaza, Long Beach, California," Prepared for POLB, Contract No. HD-6642, Work Order No. HA-1234, August.

Law/Crandall, Inc., 1994a, "Final Report of Geotechnical Investigation Proposed Railroad Bridge and Railway Improvements Portion of the Anaheim Street Viaduct Widening Project Los Angeles, CA," Report to the Port of Los Angeles, September 1.

Law/Crandall, Inc., 1994b, "Revised Final Report of Geotechnical Investigation Proposed Anaheim Street Viaduct Widening Project Los Angeles, CA," Report to the Port of Los Angeles, October 31.

Leighton and Associates, Inc., 1990, "Geotechnical Investigation, Berth 95-97 Development Project, Port of Long Beach," Prepared for Port of Long Beach, May 4.

Leighton and Associates, Inc., 1995, "Draft Report of Geotechnical investigation for Berths A88-A98 Development Project, Port of Long Beach, Volume I," Prepared for Port of Long Beach, September 29.

Leighton and Associates, Inc., 1995, "Draft Report of Geotechnical investigation for Berths A88-A98 Development Project, Port of Long Beach, Volume II," Prepared for Port of Long Beach, September 29.

Leighton and Associates, Inc., 1996, "Geotechnical Investigation for Wharf Design and Construction at Pier A, Berths A88-A96, Port of Long Beach," Report to Port of Long Beach, January 19.

MAA Engineering Consultants, Inc., 1992, "42-Acre Site, Phase I Post-Surcharge Investigation, Port of Los Angeles." Prepared for Port of Los Angeles.

Woodward Clyde Consultants, 1996, "Ground motion evaluation, Long Beach Naval Station Container Terminal, Long Beach, California," Report to Diaz-Yourman & Associates, Tustin, California, Project No. 964G076, June 11.

APPENDIX A

Geology, Seismicity and Fault Details

APPENDIX A
GEOLOGY, SEISMOLOGY, AND FAULT DETAILS

TABLE OF CONTENTS

FIGURES

APPENDIX A
GEOLOGY, SEISMICITY AND FAULT DETAILS

A.1   REGIONAL GEOLOGY AND SEISMICITY DETAILS

A.1.1   Regional Physiography

The POLB area is in the Los Angeles Basin near the juncture of two major physiographic/ geologic provinces, the Peninsular Ranges to the south and the Western Transverse Ranges to the north. In very simple terms the Peninsular Ranges comprise a series of northwest-southeast trending ranges and valleys whereas the Transverse Ranges comprise east-west trending ranges and valleys. Both of these provinces extend into the offshore area and include the Santa Barbara Basin and the Continental Borderland. In both of the provinces the valleys and ranges are separated by major fault zones; these faults trend subparallel to the ranges, that is, northwest-southeast within the Peninsular Ranges and east-west in the Transverse Ranges. The area between the two provinces comprises the Santa Monica Bay, Los Angeles, San Gabriel, and Upper Santa Ana River Valley basins which contain a complex mixture of faults and folds with orientations typical of both provinces.

The POLB is within the coastal area of the Los Angeles Basin which is a large low-lying coastal plain bordered by the Santa Monica Mountains on the north, the Repetto and Puente Hills on the northeast, the Santa Ana Mountains on the east, and the San Joaquin Hills on the south (refer to Figure 2-1). The southwestern margin of the basin is open to the Pacific Ocean except for one prominent hill, the Palos Verdes Hills or Peninsula. The offshore area to the southwest is characterized by a broad, relatively shallow, shelf or bench that extends about 5 to 15 km where it drops off steeply to deep ocean basins, the Santa Monica Basin north of the Palos Verdes Hills and the San Pedro Basin south of the hills. The offshore area is characterized by a series of islands and submarine shoal areas, or banks, separated by deep basins, and commonly referred to as the Southern California Continental Borderland.

The floor of the Los Angeles Basin is a relatively flat surface rising gently from sea level along the coastline to the surrounding mountains which then rise abruptly to a few thousand feet above the plain. The flat basin floor is interrupted in a few localities by small hills such as the northwesterly alignment of hills and mesas extending from the Newport Beach area on the south to the Beverly Hills area on the north. This northwest-trending alignment of hills divides the basin floor into two major plains, the Downey-Tustin Plain northeast of the hills and the Torrance Plain on the southwest.

The inland margins of the Los Angeles Basin are commonly elevated somewhat above the general level of the basin floor within an apron of higher elevation surfaces such as the Santa Monica Plain, La Brea Plain, Montebello Plain, Santa Fe Springs Plain, and the Coyote Hills (see Figure 2-1). These elevated plains generally comprise slightly dissected older alluvial surfaces.

The major drainages in the Los Angeles Basin enter the basin through narrow passes or gaps in the hills and then flow southerly to the ocean. The major drainages are the Los Angeles River, the San Gabriel River, and the Santa Ana River. Other local significant drainages are Rio Hondo, Coyote Creek, Ballona Creek, Compton Creek, and San Diego Creek. The Port of Long Beach lies within the coastal delta of the Los Angeles and San Gabriel rivers, but this drainage system has been highly modified by channelization of the streams within a network of concrete and rip-rap lined aqueducts.

A.1.2 Regional Stratigraphy

The floor of the Los Angeles Basin, the marginal plains, and the adjacent submarine shelf are directly underlain by Quaternary-age sandy sediments with local silts, clays, and gravels. These generally can be subdivided into nonindurated, loose Holocene-age sediments that cover the bulk of the basin and shelf, and Pleistocene-age materials which are exposed only locally within some of the uplifts within the Newport-Inglewood Structural Zone and the marginal plains.

Onshore, the uppermost Pleistocene materials are generally non-marine deposits referred to as the Lakewood Formation which is on the order of 125,000 to 500,000 years old (California Department of Water Resources, 1961). These late- to middle-Pleistocene sediments overlie older early Pleistocene marine sediments referred to as the San Pedro Formation which is more than 500,000 years old. The San Pedro Formation overlies marine Tertiary-age (> 2 million years) sediments and sedimentary rocks. These include the Pico, Repetto, Fernando, Puente, and Monterey formations. The Tertiary-age sediments and rocks, in turn, overlie Mesozoic-age (~100 million years) crystalline basement rocks at depths ranging from about 1,500 to 3,000 m west of the Newport-Inglewood Structural Zone (NISZ) to as much as 10,000 m in the deepest part of the central basin east of the NISZ (Yerkes et al., 1965). The basement west of the NISZ is primarily metamorphic rock (schist) whereas the basement to the east includes both metamorphic and igneous rocks.

A.1.3 Regional Geologic Structure

The present-day tectonic stress field is one of north-northeasterly compression. This is seen in the geologic structure, and is indicated by earthquake focal-mechanism solutions and by geodetic measurements. These data suggest compression rates of between 5 and 9 mm/yr across the greater Los Angeles area.

Except for a few marginal zones, the geologic structure of the Los Angeles basin is characterized by relatively flat-lying, late-Quaternary strata overlying slightly folded early-Pleistocene strata, which in turn overlie gently to moderately dipping Pliocene strata of the Fernando, Pico, and Repetto formations and the Miocene Puente/Monterey Formation.

The central part of the basin is a deep trough that rises rather abruptly due to faulting and folding. The principal zones faulting are the NISZ-Los Alamitos system on the west and the Puente Hills fault system (Los Angeles-Santa Fe Springs-Coyote Hills-Peralta Hills faults) on the east.

Except for the Newport-Inglewood Structural Zone, most surface geological faults such as the Santa Monica, Hollywood, and Whittier faults occur along the basin margins. In addition to

these known surface faults, the Los Angeles region is underlain by subsurface thrust and reverse faults (commonly referred to as "blind" faults and shown on Figure 2-1 as dotted lines). These are poorly understood features with poorly known locations and orientations. Most of the known subsurface faults underlie the higher-standing plains along the inland margin of the basin, but others have been proposed (for example, the San Joaquin Hills thrust fault). Most large earthquakes associated with these subsurface features are most likely to originate at depths between 10 and 15 km. The 1987 Whittier earthquake occurred on one of these buried faults that dips northerly under the Repetto Hills and San Gabriel Basin northeast of the site.

The Los Angeles region has a complicated history. Within much of the area, the basement is buried beneath sedimentary and volcanic rocks no older than Miocene. Apparently, basement rocks in the region were unroofed and exposed across wide areas when the ancient Farallon oceanic plate, which was being subducted from the west, stopped subducting below the area (Atwater and Stock, 1998). Upon cessation of subduction, regional rifting and strike-slip faulting occurred oblique to the continental margin leading to clockwise rotation of the Transverse Ranges (Luyendyk et al., 1980) involving the existing faults. In late Pliocene and Quaternary time (the past 4 million years), faults that previously formed by extension were involved in regional crustal compression (Wright 1991; Crouch and Suppe, 1993). During the transition from extension to compression, some middle Miocene normal faults were reactivated as reverse and strike-slip faults (Rivero et al., 2000). Blind thrust faults and folds may have begun to form about this time. In the project area, evidence for the Pliocene onset of the compressive deformation comes from the large Wilmington anticline which deforms rocks deposited since lower Pliocene time. The folding and faulting that formed this anticline apparently was largely completed before the end of the late Pliocene (Truex, 1974).

The present tectonic regime appears to have been in place since middle Pleistocene time and the present-day configuration of the Los Angeles basin would have been recognizable about 200,000 to 300,000 years ago, although the sea may have still occasionally migrated into some low-lying coastal channels (Ponti, 1989). The bulk of tectonic activity in the Long Beach region during Quaternary time appears to have occurred along the Palos Verdes fault and the NISZ, both of which form the most prominent uplifts in the Los Angeles Basin. The Signal Hill uplift within the NISZ, for example, formed in the past couple hundred thousand years (Ponti and Lajoie, 1992). If these deformation characteristics can be applied basin wide, the greatest tectonic activity within late Pleistocene time has occurred primarily in proximity to the major surface faults such as the Palos Verdes, Malibu-Santa Monica-Hollywood, Newport-Inglewood, Whittier, and Sierra Madre faults. The subsurface thrust faults within the region have not been active enough to create similar prominent uplifts and only a few (e.g. Santa Fe Springs) even have subtle recognizable surface expression.

A.1.4 Regional Seismicity

The southern California area is seismically active as the seismicity map shown in Figure 2-2 would suggest. Additional seismicity information is provided in Figure A-1 and Figure A-2, indicating some of the notable earthquakes in the Los Angeles Basin and their focal mechanisms, respectively. Seismicity in the Los Angeles Basin does not clearly correlate to surface faults. There is no concentration or clustering of earthquakes in the site region except perhaps along the

NISZ where a series of aftershocks from the 1933 event are located. Ward (1994) suggested that as much as 40% of the tectonic strain in southern California is not released on known faults.
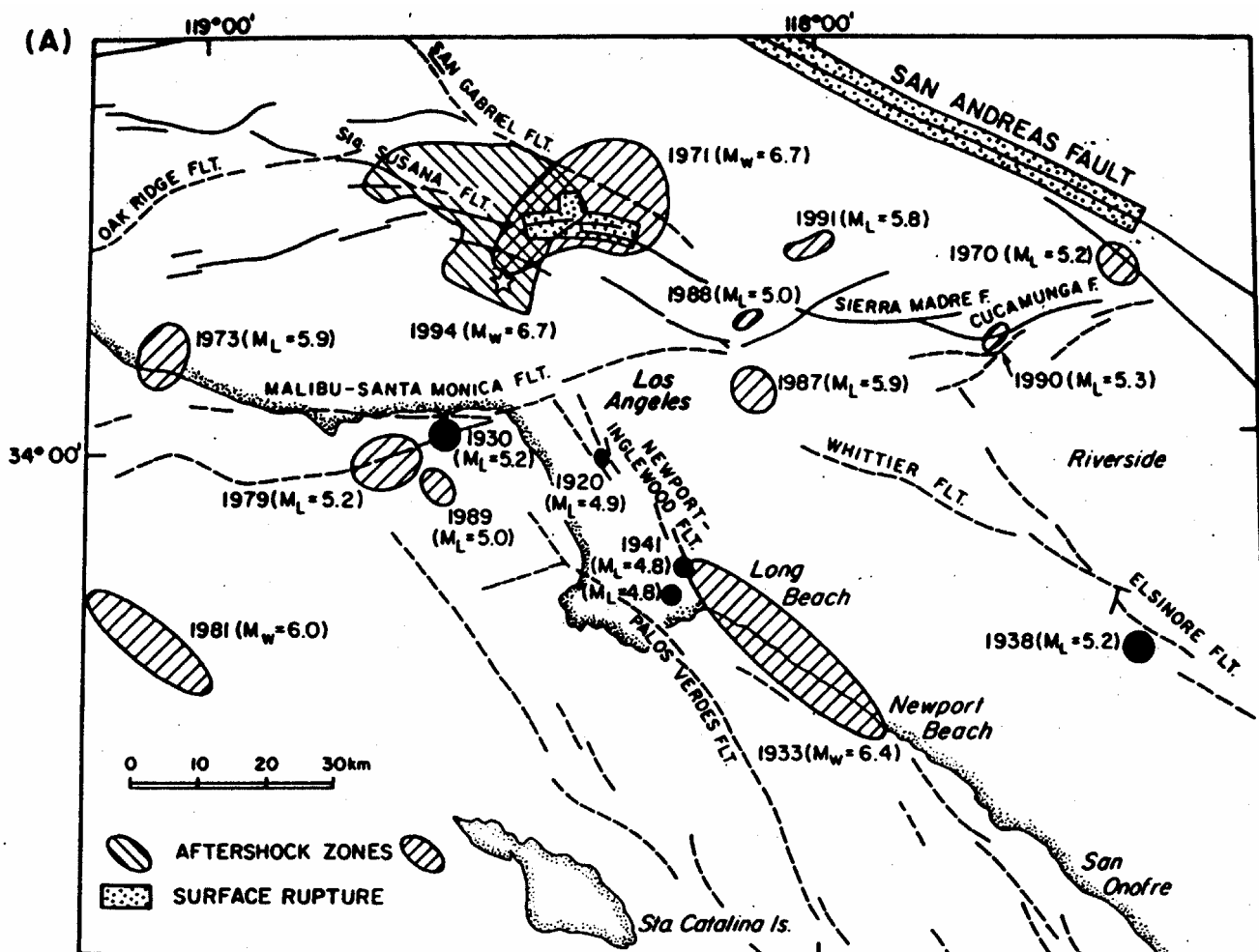
Note: Cross-hatched areas indicate aftershock zones (after Hauksson, 1995)

Figure A-1.   Significant Earthquakes in the Los Angeles Area
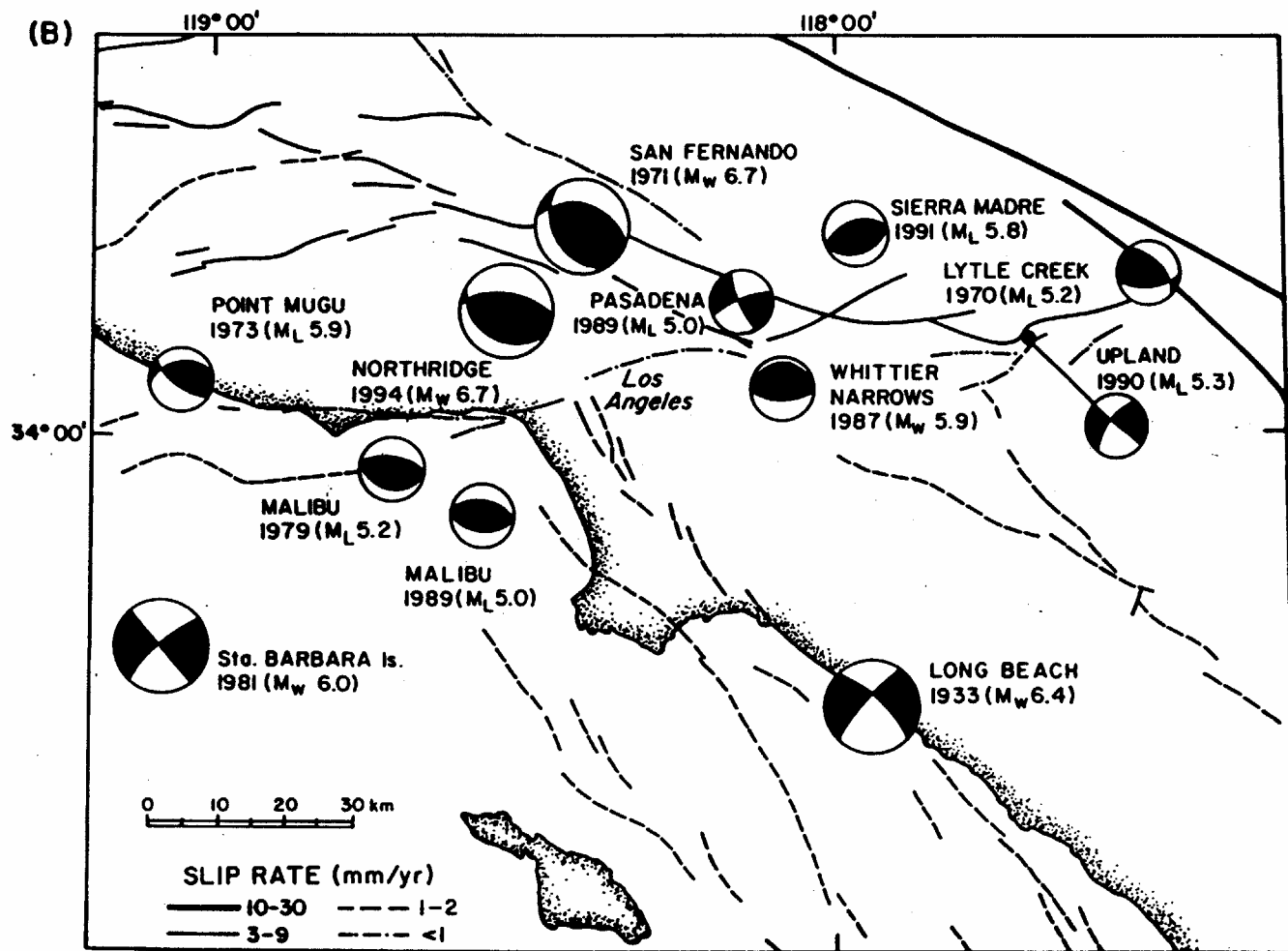
(after Hauksson, 1995)

Figure A-2.   Focal Mechanisms for Significant Earthquakes Since 1993

The largest historical earthquake within the Los Angeles Basin was the 1933 Long Beach earthquake of Moment Magnitude M_W 6.4 (Local Magnitude M_L 6.3). The 1971 San Fernando (M_L 6.4, M_W 6.7) earthquake occurred outside of the basin along the northern margin of the San Fernando Valley within a zone of mapped surface faults. The more-recent 1987 Whittier earthquake (M_L 5.9, M_W 5.9) and the 1994 Northridge (M_L 6.4, M_W 6.7) earthquakes occurred under the San Gabriel Valley and the San Fernando Valley, respectively, but were not associated with surface faults.

The Long Beach earthquake is generally believed to have been associated with the Newport-Inglewood Structural Zone (Benioff, 1938). This association was based on abundant ground failures along the trend but no unequivocal surface rupture was identified. Hauksson and Gross (1991) reevaluated the seismic history and relocated the 1933 earthquake to a depth of about 10 km below the Huntington Beach-Newport Beach city boundary.

Hauksson (1987, 1990) analyzed the historical seismicity of the Los Angeles Basin. Although several older events were included, the principal time frame of the earthquake record studied was from 1977 to 1989, only about 12 years. This is a short time relative to the geologic time scales that control crustal tectonic activity, and thus the results of the study must be used cautiously. Also, there were few moderate and no large events in this record. History has shown repeatedly that small earthquakes are not necessarily indicative of large events and/or of the principal tectonic regime. Of 244 earthquake focal mechanisms, 59% were predominantly strike-slip, 32% were reverse, and the rest were normal-fault mechanisms. All of the events were widely distributed and intermixed, and patterns are ambiguous. A large proportion of the strike-slip events occurred along the NISZ but the distribution is generally loosely scattered. More of the reverse mechanisms occurred north of the latitude of Palos Verdes Hills than to the south but like the strike-slip events the pattern is loose and typified by widely scattered events. Most of the normal-fault mechanisms occurred in the offshore area, but several also occur along the NISZ.

The average stress field indicated by the data is compression with a north-northeast orientation. Combined with the limited time span of the record, the weak patterns are not very revealing other than that earthquakes are quite intermixed, i.e. there are few areas where one type of mechanism clearly dominates. However, this in itself is an important result because it illustrates the complexity of local tectonics. All in all, the focal mechanisms are very compatible with the geologic data which indicate a mixture of predominantly strike-slip and reverse fault structures. Considering the nature of faulting one should not be surprised to see strike-slip and reverse mechanisms in close proximity. The NISZ, for example, comprises numerous branches which form upward branching configurations referred to as flower structures. Lateral slip in a transpressional tectonic environment along the main central shear zone of the NISZ can be accompanied by small reverse displacements along flank faults. The NI faults are commonly en echelon, suggesting variable slip orientations. Like the mixture of strike-slip and reverse events along the NISZ, the complex intersection of the northwest-trending folds and faults within the Santa Monica-Hollywood fault system along the northern margin of the Basin should yield both strike-slip and reverse focal mechanisms. Also, it should be pointed out that many of the focal mechanisms are not pure strike-slip or reverse; many of them have significant vertical components.

In overview, both the earthquakes and the geologic structures in the Los Angeles Basin appear to characterize tectonic environments whereby the northernmost part of the Basin, adjacent to and including the Santa Monica Mountains, is primarily a contractional tectonic regime (thrust and reverse faulting); the middle part of the Basin (to about a line connecting the north side of the Palos Verdes Hills-Signal Hill-Peralta Hills is a mixture of contractional and transcurrent (transpressional) structures, and the southern part of the Basin is primarily a transcurrent regime (strike-slip faulting).

Without a history of repeated large earthquakes within the basin, it is difficult to characterize the maximum earthquake potential. Neither the 1971 San Fernando, the 1987 Whittier, nor the 1994 Northridge earthquakes occurred within the Los Angeles Basin. However, they occurred within the same basic compressional tectonic regime and thus are probably representative of the size of earthquakes likely to occur on the larger subsurface faults within the basin.

A.2   FAULT DETAILS

The following sections describe the principal active faults in the Los Angeles region that might contribute to ground shaking in the POLB area. Locations of these faults are shown on Figure 2-1. This information is given from a regional perspective for understanding the nature of the faults, and provides the basis for the parameters used in the probabilistic seismic hazard analysis as discussed in Appendix B and summarized in Section 3.

A.2.1   Palos Verdes Fault

The Palos Verdes fault extends through the Port of Los Angeles from the east side of the Palos Verdes Peninsula southeasterly to the Lasuen Knoll area offshore and northwesterly into the Santa Monica Bay, for a total length of about 100 km (Figure 2-1).

The southern part of the Palos Verdes fault is well defined by seismic-reflection data which documents seafloor and shallow subsurface disruption of young sediments. The Palos Verdes fault extends southeasterly (about S33^{o}E) from the Los Angeles harbor area, across the San Pedro shelf, to the Lasuen Knoll area (Vedder et al, 1986; Fisher et al, 2004). The nature of the fault changes markedly along strike southeastward across the San Pedro shelf and slope (Fisher et al, 2004). Under the north part of the San Pedro shelf, the fault zone includes several strands, with the main strand dipping west. To the southeast, under the slope, the main fault strand exhibits normal separation and mostly dips east. Farther to the southeast near Lasuen Knoll, the fault zone locally dips at a low angle, but elsewhere near this knoll, the fault dips steeply. Fisher et al. (2004) explain the observed structural variations as the result of changes in strike and fault geometry along a master right-lateral strike-slip fault at depth.

Vertical fault separation of the schist basement rocks is about 350 m in the area south of the offshore Beta oil field (Fischer et al., 1987) and about 600 m in the Beta field (Wright, 1991). This basement complex is buried beneath sedimentary rocks no older than Miocene age (Fisher et al, 2004).

The Palos Verdes fault is difficult to trace southeast of Lasuen Knoll. This is partly due to poor geophysical coverage but also may be because motion is transferred onto several fault splays southeast of the knoll (Fisher, et al., 2004); based on the sharp escarpment along the west side of Lasuen Knoll, the main fault appears to be west of Lasuen Knoll. Lasuen Knoll, like the Palos Verdes Hills and most of the other islands and submarine banks in the Southern California Continental Borderland, is composed of Tertiary-age rocks which have been uplifted by faulting and folding. The extension of faulting south of Lasuen Knoll trends toward the Coronado Banks fault zone (Vedder et al., 1986) which has led some (e.g. Rockwell et al., 1987) to conclude that the faults are interconnected. However faults to the south of Lasuen Knoll are discontinuous, and the sense of separation is opposite of that on the Palos Verdes fault north of Lasuen Knoll; if they are interconnected, the connection is indirect.

The Palos Verdes fault trends through Los Angeles Harbor to the east side of the Palos Verdes Peninsula. Onshore, the Palos Verdes fault has a northwesterly trend along the northeast margin of the peninsula forming a restraining bend in the region just north of the POLA. Although there are no unequivocal surface exposures of the Palos Verdes fault, it is recognized in oil wells at

shallow depths as sheared zones, steeply dipping discordant beds, and old-over-younger rocks. The fault appears to dip southwesterly under the Palos Verdes Hills at a relatively steep angle. Woodring et al. (1946) and Zielbauer et al. (1962) show the Palos Verdes fault to be generally coincident with the topographic break along the northern and northeast margin of the Palos Verdes Hills but there are many interpretations that suggest locations upslope within the Palos Verdes Hills. Synthesis of oil-well, geomorphic, fault trenches, and seismic-reflection data indicate that the fault dips about 65° to 70° to the southwest under the Palos Verdes Hills. Recent trenching (2003-2004) of upslope lineaments in the Chandler quarry and adjacent golf course area did not reveal any significant faulting supporting the interpretation that the fault lies near the topographic base of the hills. Other oil wells, geomorphology, and surface geological mapping to the northwest indicate that the Palos Verdes fault continues northwesterly along the northeast margin of the Palos Verdes Hills toward the Redondo Beach area.

In Santa Monica Bay to the north of Palos Verdes, the Palos Verdes fault is difficult to locate; a fan-shaped array of subsurface, northwesterly trending faults is generally considered to represent a continuation of the Palos Verdes fault (Figure 2-1). These features have a much lesser rate of activity than the southern Palos Verdes fault. Nardin and Henyey (1978), Clark et al. (1987), and Fisher et al. (2004) found little evidence of faults displacing strata any younger than Pliocene, and thus Quaternary activity on the northern Palos Verdes fault is doubtful. Seismic-reflection profiles by Fisher et al. (2003) across the area revealed undeformed sediment across the projected location of the fault. There are several other faults in Santa Monica Bay, (for example, the Dume, San Pedro Basin, San Pedro Escarpment faults), which by comparison exhibit more-abundant and more-prominent evidence of youthful fault activity indicating that they may be more active than the Palos Verdes fault. Nardin and Henyey (1978) proposed that the east-west trending Redondo Canyon represents a fault zone that may separate the southern active Palos Verdes fault from the Santa Monica Bay part of the fault.

The Palos Verdes fault is predominantly a strike-slip fault but has a small vertical component (about 10% to 15%). The slip rate of the Palos Verdes fault is based primarily on the geophysical and geological studies in the outer harbor of the Port of Los Angeles by McNeilan et al. (1996). McNeilan et al. estimated a long term horizontal slip rate of between 2.0 and 3.5 mm/yr with a range of about 2.3 to 3.0 mm/yr for the middle- to late- Holocene time period. The rate preferred by the geological community has, by default, conservatively been assumed to be the 3.0 mm/yr rate. Such a slip rate makes the Palos Verdes fault one of the most active faults in the Los Angeles region. However, other geophysical surveys in the Los Angeles Harbor area (e.g. Clarke and Kennedy, 1998) could not verify this slip rate so it is uncertain whether the rate is valid for the entire fault zone or whether it is a local rate due to some local slip enhancement. A slip rate of 3.0 mm/yr (±1mm) is the rate used by the California Geological Survey and the U.S. Geological Survey and therefore is the preferred rate for the current study.

There are virtually no direct data to constrain the recurrence interval for large earthquakes on the Palos Verdes fault. There have been no significant earthquakes on the fault since arrival of the Franciscan missionaries in the 1700s. Using the empirical data of Wells and Coppersmith (1994) to indirectly make judgments on how long it would take to store up enough strain to generate a magnitude 6.8 to 7.4 earthquake, it appears that recurrence intervals for such earthquakes on the Palos Verdes fault would range from a few hundred to a few thousand years. For example, fault

rupture scenarios evaluated by McNeilan et al. ranged from 180 to 630 years for a M6.8 event, 400 to 440 years for a M7.1 event, 1,000-1,100 years for a M7.2 event, and 830 to 1,820 years for a M7.4 event (these numbers are quoted from McNeilan et al., 1996). Other scenarios may be just as likely and would yield similar ranges. Previous seismic hazard analyses for the Port of Los Angeles and the Vincent Thomas bridge (Earth Mechanics, Inc., 1993, 1995, 2001) used recurrence intervals in the middle of the range (800-900 years).

The maximum earthquake is also highly uncertain for the reasons discussed above. Because the segment in Santa Monica Bay does not show any evidence of Quaternary faulting it is not likely to be involved in faulting with the southern part. Therefore, the maximum earthquake should be based on a fault length of about 60 to 70 km or on Palos Verdes Peninsula segment and the offshore San Pedro Shelf segment. The magnitudes evaluated for the current study are presented in see Appendix B).

A.2.2 Newport-Inglewood Structural Zone

The Newport-Inglewood Structural Zone (NISZ) consists of the northwest-southeast trending series of faults and folds forming an alignment of hills in the western Los Angeles Basin extending from the Baldwin Hills on the north to Newport Mesa on the south (Figure 2-1). The fault seems to have originated in about late Miocene time but based on relative stratigraphic thickness of bedding across the zone, the greatest activity seems to have been post Pliocene indicating the fault is quite young.

The NISZ comprises several individual faults and branch faults (refer to Figure 2-1, Figure 2-3, Figure 2-4, and Figure 2-5), few of which have good surface expression as actual fault scarps. A few somewhat linear "scarps" and lineaments can be seen on old aerial photographs but urban development has essentially obscured most natural surface evidence except for the series of young hills and mesas along the alignment. The faults are best known primarily from oil-well data. Faulting is relatively linear and narrow along the central part of the zone in the Long Beach-Seal Beach area. To the north of Dominguez Hill, the faults are shorter, less continuous, and exhibit a left-stepping en echelon arrangement with several folds between fault branches. In the south near Costa Mesa and Newport Beach, the NISZ widens to about 5 or 6 kilometers where it includes several subparallel faults such as the Bolsa, Fairview, and Pelican Hill faults. How all of these subparallel faults are related is not clear. The main fault is believed to be the South Branch (Freeman et al., 1992).

The NISZ extends offshore to about the Dana Point area. Farther offshore to the south, the fault is believed to connect via the Offshore Zone of Deformation near San Onofre to the Rose Canyon fault in the San Diego region forming a major structural trend commonly referred to as the Santa Monica-Baja Zone of Deformation (SMB).

The maximum earthquake used for the NISZ in local geotechnical investigations has generally been magnitude 7.0. This may be relatively small for a feature as long as the SMB zone but the magnitude is based on the concept that the zone consists of shorter discontinuous faults, or segments, that behave independently. The fault was the source of the 1993 Long Beach earthquake of magnitude 6.3, but as with the Palos Verdes fault, the history of earthquakes on the NISZ is incomplete so it is difficult to estimate a maximum earthquake. Empirical fault-

length/earthquake-magnitude relations (Wells and Coppersmith, 1994) suggest an MCE of about M 7.0. The range of magnitudes used in this evaluation is discussed in Appendix B.

The recurrence interval for the maximum earthquake on the NISZ is very long, on the order of a thousand years or more (Schell, 1991; Freeman et al., 1992; Shlemon et al., 1995; Grant et al., 1997). Grant et al. (1997) conducted a detailed cone-penetrometer investigation on the fault in the Huntington Beach area and postulated three to five surface ruptures in Holocene time. In the Newport area, Shlemon et al. (1995) interpreted five surface ruptures in Holocene time. These interpretations suggest average recurrence intervals of about 2,000 to 3,500 years per event; Grant et al. estimated that at least two of the events they interpreted occurred about 1200 years apart indicating irregular inter-event time intervals.

The rate of fault slip is poorly known but seems to be very slow. Although there is quite a wide range of slip rates proposed by various published sources, most of them are of uncertain validity because they are based on short-term, local, vertical components rather than regional horizontal slip. Grant et al. (1997) inferred a minimum rate of 0.34 to 0.55 mm/yr but suspected the actual rate might be higher. Shlemon et al. estimated a rate of 1.5 to 2.5 mm/yr. The southern segment of the SMB system comprising the Rose Canyon fault in the San Diego area has a slip rate of about 1.1 to 1.5 mm/yr (Lindvall and Rockwell, 1995). The northern part of the NISZ is commonly considered to have a much lower rate, on the order of 0.1 mm/yr but good data to support such a rate is lacking. Most seismic hazard studies have used a long-term rate of 0.5 mm/yr based on offset of Pliocene fold structures and strata (Schell, 1991; Freeman et al., 1992). However, most of the deformation within the NISZ seems to have occurred within Quaternary time so the rate during more-recent times may differ from the long-term rate. Recent seismic hazard models by the California Geological Survey (2003) use a slip rate of about 1.0 mm/yr. The current study considered a range of slip rates from 0.5 to 1.5 mm/yr, with 1.0 mm/yr being the preferred estimate (see Appendix B).

A.2.3 Cabrillo Fault

The Cabrillo fault forms a prominent northeast facing scarp in the 100,000 year-old terrace in the San Pedro-Point Fermin area (refer to Figure 2-1). The fault dips about 50° to 70^oeasterly with a vertical displacement of about 100-200 ft (Woodring et al., 1946). The fault trends northwesterly inland for about 7 km (Woodring et al., 1946; Dibblee, 1999). Southerly from Cabrillo Beach, the fault extends offshore for a distance of about 11 km where it appears to merge with the Palos Verdes fault (Vedder et al., 1986; Fischer et al., 1987). The offshore fault is shown as a zone of disruption up to 500 m wide.

Offshore activity along the fault appears to be of Holocene age as indicated by south-facing scarps 1.2 m high, and two or possibly three positive topographic sea-floor anomalies along its trend (Fischer et al., 1987). These topographic anomalies are within sediments estimated to be about 5,000-6,000 years old.

The maximum magnitude and slip rate are difficult to estimate due to lack of data. The fault is considered to be predominantly a strike-slip fault due to its association with the Palos Verdes fault, but may also have a normal component of displacement. Based on empirical fault-length/earthquake-magnitude relationships (Wells and Coppersmith, 1994) the fault could be

capable of about an M ~ 6.25 to 6.5 earthquake. Fischer et al. (1987) estimated a vertical slip rate of 0.4 to 0.7 mm/yr which is greater than the Palos Verdes fault estimates and therefore is questionable as a long-term rate. Most studies suggest that the Cabrillo fault is a minor feature and Ward and Valensise (1994) estimated a slip rate of 0.1 mm/yr which seems to be a more-realistic estimate.

A.2.4 Sierra Madre Fault

The Sierra Madre fault is one of the major faults in the Los Angeles region and lies along the southern margin of the San Gabriel Mountains forming one of the most impressive geomorphic features in the Los Angeles area. The fault is recognized by juxtaposition of rock types, shearing and crushing along the fault trace, and by linear land forms (geomorphology). The fault is primarily a thrust fault that has thrust the ancient igneous and metamorphic rocks of the San Gabriel Mountains up and over young Quaternary-age alluvial deposits. The fault zone is very complex and over much of its length comprises several subparallel branches along the northern edge of the San Fernando and San Gabriel valleys. The fault may also be divided into segments along length, each with somewhat different rupture characteristics and histories.

The poor documentation of Quaternary faulting on the Sierra Madre fault makes it difficult to assess its earthquake capability. Based on worldwide empirical fault-length/earthquake-magnitude relationships (Wells and Coppersmith, 1994), the Sierra Madre fault is capable of producing earthquakes in the 7.0 to 7.5 magnitude range (Dolan et al., 1995). If the fault ruptures one of the segments independently, earthquakes of M 7.0 are more likely; if more than one segment ruptures together, larger earthquakes are possible.

About 20 km of the westernmost part of the Sierra Madre fault ruptured the ground surface during the 1971 San Fernando earthquake (M_w 6.7). The 1971 event was characterized by reverse faulting along a fault dipping about 45° to 50° northerly. Geological studies (trenching) of the 1971 rupture (Bonilla, 1973) suggested that a previous rupture had occurred on this fault within the prior few hundred years. In 1991, a M 5.8 earthquake occurred below the San Gabriel Mountains at a depth of about 16 km and is generally believed to have occurred on a branch of the Sierra Madre fault zone. The best available information indicates that large earthquakes on the Sierra Madre fault occur sometime between a few hundred years to a few thousand years (~5,000 years according to Crook et al, 1987). Geological and paleoseismological studies by Rubin et al. (1998) suggest that two prehistoric ruptures within the past 15,000 years had large displacements typical of earthquakes in the M 7.0-7.5 range. For the current study, M 7.2 is preferred.

Reliable geological information on the slip rate of the Sierra Madre fault is scarce and the average time between large ground rupturing earthquakes is poorly known. Some geological studies have indicated that the average rate of displacement for the Sierra Madre fault may be as high as about 3 to 4 mm/year (Southern California Earthquake Center). However, recent paleoseismological studies (Rubin et al., 1998) suggested an average slip rate of only 0.6 mm/yr. This lower rate is based on only one locality within a very long and complex branching fault system, and therefore this rate may not be representative of the entire fault zone. Paleoseismological studies by Tucker and Dolan (2001) on the eastern part of the fault near Azusa revealed a similar minimum slip rate of 0.6 to 0.9 mm/yr and an elapsed time interval

since the most recent surface rupture of 8,000 years or more, but their investigation was also on one of several subparallel faults so the slip rate may be faster if all branches are considered. The California Geological Survey used a slip rate of 2.0 mm/yr (±1.0 mm). In the current study a rate of 2.0 mm/yr is preferred.

A.2.5 Malibu Coast, Santa Monica, Hollywood Fault System (Southern Frontal Fault System)

One of the major fault systems in the Los Angeles Basin is the along the southern edge of the Santa Monica Mountains separating Mesozoic plutonic rocks from Tertiary and Quaternary sedimentary rocks. The fault system consists of the Santa Monica and Hollywood faults and smaller segments such as the Malibu Coast and Potrero faults (refer to Figure 2-1). Continuation of the fault to the west of Santa Monica is uncertain and the fault system may be related to the Dume-Anacapa fault zone in the offshore area south of Malibu. Together, these faults form the southern boundary fault of the Santa Monica Mountains.

The Santa Monica Mountains rise abruptly to 500-600 m above the Los Angeles Basin floor and are indicative of a large vertical component of faulting. Earthquake focal mechanisms and local geologic relationships suggest reverse faulting with a subordinate left-lateral component. Traditionally, the Santa Monica and Hollywood faults have been considered to comprise the surface expression of the major thrust fault that is responsible for uplift of the Santa Monica Mountains, but investigations in the past decade or so (e.g. Davis et al., 1989; Dolan et al., 1995) postulate that the Santa Monica and Hollywood fault are predominantly strike-slip features and that the mountains are underlain by a separate, but related, blind thrust fault. These interpretations are driven by theoretical stratigraphic models and are based on little specific structural data. Investigations for the Metro Rail Red Line subway drove a tunnel through the Hollywood segment of the fault system and found a major shear zone with the plutonic rocks of the Santa Monica Mountains uplifted over Quaternary alluvium and colluvium. The fault zone consists of a northerly dipping fault with about a 100-m-wide sheared gouge zone.

There have been no large earthquakes associated with Western Transverse Ranges southern boundary fault zone in historical time, but geological studies (e.g. Crook and Proctor, 1992; Drumm, 1992; Fall et al., 1987; Dolan et al., 1997, 2000a, 2000b) have documented Holocene faulting. Although it seems certain that the fault system is one of the major features in the Los Angeles Basin, success at determining slip rates and recurrence intervals has been elusive and the feature remains somewhat of an enigma.

Documented slip rates are less than 1.0 mm/yr but this estimate suffers from lack of data on the lateral slip (Dolan et al., 1997). The California Geological Survey (2003) assumes a slip rate up to about 1.0 mm/yr (± 0.5 mm).

The great length of the fault system suggests that it is capable of generating a large earthquake (M~7.5) but the discontinuous nature of faulting suggests that faults may behave independently and perhaps a smaller maximum earthquake (M~6.5 to 7.0) is more appropriate. Dolan et al (1997) postulated a M_w 6.6 event for the Hollywood fault. The earthquake recurrence interval is very long and could be on the order of a few thousand years (Dolan et al., 1997).

A.2.6   San Pedro Basin Fault

The San Pedro Basin fault is one of the major faults within the nearby deep seafloor (see Figure 2-1). The fault trends southeasterly from near the base of the Malibu-Santa Monica shelf, past the subsea Redondo Knoll, to about Avalon Knoll east of Catalina Island, a distance of about 70 to 80 km. The fault is expressed as a complicated association of folds, flower structures, and tensional (normal) structures. The fault dips steeply to nearly vertical, which along with the structural expression, indicates it is a strike slip fault (Fisher et al., 2003). Southeast of the Palos Verdes Peninsula, this fault coincides with the western limit of a dense distribution of small-magnitude (M_w 3 to 5) earthquakes.

The fault has several lines of evidence indicating it is an active feature; these include prominent sea floor scarps and deformed young sediments, including flower structures. The San Pedro Basin fault zone lies along or near the contact between basement rocks on the west and basin sedimentary fill to the east. The nature of fault separation across the fault varies considerably within short distances. The sense of displacement changes in closely spaced (a couple kilometers) seismic-reflection profiles from reverse to normal faulting. Such changes are typical of strike-slip faults.

The slip rate is unknown but the similarity of geomorphology, structures, and length to the NISZ suggest that they are similar features and therefore could have similar slip rates of about 1 mm/yr and similar maximum earthquakes. Fault-length/earthquake-magnitude relationships (Wells and Coppersmith, 1994) indicate a maximum earthquake of about M 7.0 to 7.2 but the feature is highly segmented indicating smaller magnitudes (M~ 6.5-7.0) may be more likely.

A.2.7   Elysian Park Fold and Thrust Belt

The Elysian Park Fold and Thrust Belt (EPFT) was initially a product of Davis et al. (1989) who postulated that the Los Angeles area is underlain by a deep master detachment fault and that most of the folds and faults in the region result from slip along the detachment causing folding and blind thrust faulting at bends and kinks in the detachment fault. Shaw and Suppe (1996) further developed and refined the detachment/blind thrust model. They proposed several zones of subsurface faulting and folding consisting of the Elysian Park trend, the Compton-Los Alamitos trend, and the Torrance-Wilmington trend. Few of these thrust ramps have actually been seen in well data or seismic-reflection surveys because the features are generally postulated at depths beyond the capability of drilling or seismic reflection methods (e.g. 10 to 15+ km). Geophysical methods that can reach the necessary depths do not have the capability to resolve the features so these structures remain problematic.

The detachment/blind thrust model was initially embraced primarily because the 1987 Whittier Narrows earthquake occurred in proximity to one of the postulated thrust ramps beneath the Elysian Park fold belt. Subsequent work (e.g. Shaw and Suppe, 1996; Oskin and Sieh, 1998; Bullard and Lettis, 1993; Shaw and Shearer, 1999; Shaw et al., 2002) has highly modified the original model and at present most seismic hazard analyses recognize only the Upper Elysian Park Thrust (see Figure 2-1).

Shaw and Suppe (1996) postulated a slip rate of 1.7±0.4 mm/yr for the Elysian Park thrust. Estimates of earthquake magnitudes associated with these thrust faults range from 6.6 to 7.3

depending on the size (area) of the individual segments and whether they rupture independently or together. Recurrence interval estimates range from 340 to 1,000 years. Oskin et al. (2000) model the Upper Elysian Park thrust as extending from the Hollywood fault to the Alhambra Wash fault with a slip rate of 0.8 to 2.2 mm/yr and magnitude 6.2 to 6.7 earthquakes with recurrence interval in the range of 500 to 1300 years. The California Geological Survey, following the lead of Oskin et al. (2000), models the Upper Elysian Park thrust as a feature about 18 km long and dipping 50° northeasterly with a slip rate estimate of about 1.3±0.4 mm/yr. The current study preferred a mean characteristic earthquake of 6.4, and utilized the 1.3 mm/yr slip rate.

A.2.8 Puente Hills Fault System

The Puente Hills Thrust fault system (PHT) is the name currently given to a series of northerly dipping subsurface thrust faults (blind thrusts) extending about 40-45 km along the eastern margin of the Los Angeles Basin. Shaw and Shearer (1999) synthesized oil-company data and seismicity to interpret three discrete thrust faults underlying the LaBrea/Montebello Plain, Santa Fe Springs Plain, and Coyote Hills. These faults are similar to faults previously named the Las Cienegas and Norwalk faults (see for example, Wright, 1991; Harding and Tuminas, 1988; Schell, 1997). These faults form an en echelon arrangement from the northern Los Angeles Basin to the southern part of the Puente Hills (refer to Figure 2-1). Although not included in the Puente Hills fault system as presently conceived, similar en echelon, north-dipping thrust faults continue southeasterly along the entire northeastern Los Angeles Basin margin into the Santa Ana Mountains; these other faults occur below the Richfield oil field and the Peralta Hills (see Figure 2-1). The Whittier Narrows earthquake is now believed to have occurred on this structure (Shaw and Shearer, 1999).

Down-dip projection of the Santa Fe Springs segment of the Puente Hills faults extends to the approximate depth of the 1987 Whittier Narrows earthquake which Shaw and Shearer (1999) relocated to about 15 km depth. The close association of seismicity to the fault projections indicates that the fault is seismically active. Shaw and Shearer proposed that the Puente Hills fault system was capable of generating about magnitude 6.5 to 7.0 earthquakes and had a slip rate of between 0.5 to 2.0 mm/yr. The 0.5 mm/yr rate was derived by dividing the postulated slip by the age of strata (i.e. Quaternary ~1.6 million years), whereas the 2.0 mm/yr slip rate was derived by assuming that all of the unaccounted-for, geodetically determined, crustal shortening across the Los Angeles Basin (~ 8 to 9.5 mm/yr) is occurring on the Puente Hills fault system. Depending upon ones interpretation, there may be much less than 2.0 mm/yr of slip unaccounted for by known faults, and there may be other yet-undiscovered subsurface faults so the 2.0 mm/yr rate for the Puente Hills fault seems too high for just one fault. It should be noted that this rate is twice that of the Newport-Inglewood structural zone, a prominent active fault of about the same age with abundant surface manifestations such as surface faulting and uplifted hills and mesas as well as abundant historical earthquake activity.

Subsequent work on the fault system (Shaw et al., 2002) infers that the en echelon segments of the Puente Hills Thrust are related and displacements are gradually transferred from one segment to the next. These later studies resulted in estimates of slip between 0.44 to 1.7 mm/yr with the preferred rate between 0.62 and 1.28 mm/yr. Using empirical data on rupture area, magnitude, and coseismic displacement, Shaw et al. (2002) estimated earthquakes of M_W 6.5-6.6 and multi-

segment rupture of M_W 7.1. The recurrence intervals for these events are on the order of 400 to 1,320 years for single events and 780-2600 years for M 7.1 events.

Paleoseismological studies using trenching and borings in the Santa Fe Springs area (Dolan et al., 2003) identified four buried folds which they interpreted to be a result of M_W 7.0± earthquakes within the past 11,000 years.

The most recent seismic hazard model by the California Geological Survey (2003) used a slip rate of 0.7 ± 0.4 mm/yr. This rate was adopted in the current study, and a mean characteristic earthquake of 7.1 considered appropriate.

A.2.9   THUMS-Huntington Beach Fault

The THUMS-Huntington Beach (THB) fault has been interpreted in many different ways and there is disagreement on many aspects and at many different levels. The THB has been interpreted as both a high-angle normal fault and an oblique right-lateral normal fault (Truex, 1974; Clarke et al., 1987; Wright, 1991). Davis et al. (1989) interpreted the THB fault to be a high-angle (80°) reverse fault in the upper plate of a 45° northeast-dipping Torrance-Wilmington blind thrust fault. Wright (1991) and Truex (1974) described the fault as a southeast-trending fault extending offshore from the Palos Verdes fault in the Los Angeles Harbor area along the southwest flank of the Wilmington Anticline, past the Huntington Beach oil field to the Newport Beach area where it converges with the Newport-Inglewood Structural Zone. This alignment is about 35 to 40 km long but is discontinuous, poorly expressed, and was based on very limited and spotty data (Wright, 1991). In the area between Long Beach and Huntington Beach, several offshore geophysical (seismic-reflection) investigations for numerous oil and engineering projects (e.g. pipelines, offshore power plant, drilling islands, etc) have documented several near-surface faults but these are short, small displacement, discontinuous, random features that do not appear to align such that they could be considered representative of a major regional active fault.

Recent, detailed, high-resolution, 3-dimensional seismic-reflection data in the Long Beach-Los Angeles harbor area reveals it as a low-angle easterly dipping thrust fault (D. Clarke, Long Beach City Geologist, 2004; and S. Prior, THUMS Senior Geologist, 2004). This fault revealed by the geophysical data is shown on the cross sections A-A' (see Figure 2-4) and B-B' (see Figure 2-5). The fault generally dips about 25° to 35° easterly, displacing schist basement over Miocene-age marine sedimentary rocks. Displacement decreases northwesterly and the fault dies out near the cross-section B-B' (see Figure 2-5) located in the western area of the Long Beach Harbor, where the basement offset decreases to zero (compare cross sections A-A' and B-B').

The 3-dimensional seismic data show the fault terminating at a prominent angular unconformity at the base of the Pico Formation which is of late Pliocene age (~2 to 3 million years old). The termination is abrupt and represents a cessation of principal activity on the THB fault, and a long period of submarine erosion. The strata directly overlying the unconformity are concordant with the unconformity and do not exhibit any onlap or offlap that might indicate continuing displacement on the fault during deposition of the younger sediments. This indicates a long period of inactivity for the fault.

However, the overlying strata do exhibit a gentle dip of about 6°, on both the northeast and southwest flanks of the anticline, indicating that some uplift occurred in the region during Pleistocene or later time. The source of this warping is undoubtedly tectonic but the implications are poorly understood. At least some of the uplift is related to regional tectonics as indicated by documented uplift in the area of the anticline associated with the 1933 Long Beach earthquake (Castle and Buchanan-Banks, 1989). Recent interpretations by Edwards et al. (2001, 2002, 2003) have interpreted the warped unconformity as indicating that the THB fault has been active in Quaternary time (i.e. the past 400,000 to 600,000 years) and that the fault is capable of generating large-magnitude earthquakes with recurrence intervals on the order of a thousand to several thousand years (Ponti, 2004).

If the THB fault is projected dipping downward to the east, it would intersect the NISZ at about 8 to 9 km depth raising the issue of whether it cuts off the NISZ or whether the NISZ cuts off the THB (Figure B-8). The high degree of young deformation on the NISZ and its historical seismic activity indicate that the NISZ is much more active and therefore favors the latter interpretation. If so, the warping in the Wilmington anticline area could be related to regional tectonic compression between the more-active Palos Verdes and Newport-Inglewood faults, both of which have prominent surface expression and abundant evidence of much-more-recent seismotectonic activity. The THB structure, like many other contractile structures in the Los Angeles Basin (Tsutsumi et al., 2001), appears to have become largely inactive beginning in Pliocene time with younger deformation occurring on structures such as the Palos Verdes and NISZ.

A.2.10 Compton-Los Alamitos Thrust Ramp

As discussed above under the Elysian Park Thrust, several geoscientists have proposed that the Los Angeles region is underlain by a network of low-angle to horizontal thrust faults and detachment faults. None of these structures have been imaged on seismic reflection data or encountered in boreholes. One of the major features in these models is the Compton-Los Alamitos (CLA) trend is hypothesized to dip easterly under the central Los Angeles basin. The trend is several kilometers wide and dips downward at low angles to the northeast and extends from the Central Basin detachment (decollement) to the Torrance-Wilmington trend where it becomes a horizontal detachment fault. Included within the wide swath are the Los Alamitos fault, the Newport-Inglewood Structural Zone, and the Palos Verdes fault which are discussed independently above as discrete features unrelated to the detachment/blind thrust models.

The CLA thrust model was developed by Shaw and Suppe (1996) following the lead of Davis et al. (1989). The feature comprises a thrust ramp and several overlying folds which are postulated to result from slip on the deep detachment and interconnected thrust ramps. Folded Pliocene and Quaternary strata indicate slip rates of 1.4 mm/yr. Assuming that slip is released in large earthquakes, Shaw and Suppe (1996) estimate earthquake magnitudes of 6.3 to 6.8 on individual ramp segments, and magnitude 6.9 to 7.3 if segments rupture together. Recurrence intervals are estimated from empirical earthquake-magnitude/fault-displacement relationships (Wells and Coppersmith, 1994). Estimates of earthquake recurrence intervals range from 380 years for single segments to 1300 years for multiple segment ruptures. As mentioned in the description of the Elysian Park Thrust, these rates and events are commonly greater than estimates for the more-prominent surface faults within the region.

Because these postulated blind fault/detachment faults extend below the major active surface faults in the Los Angeles region, the models must incorporate and accommodate these faults. Generally the models involve some type of transecting relationship whereby the major faults like the Palos Verdes, NISZ, and Whittier faults are cut off at depth. Generally this relegates the most prominent and active features in the Los Angeles region to secondary roles. This has resulted in these models being rejected by most seismic hazard analyses, or given only secondary importance. The California Geological Survey removed the Compton blind thrust from their seismic-hazard model based on investigations by Rockwell and Mueller (Mueller, 1997) who excavated a trench and placed cone penetrometer borings across the axial trace of the feature and found that peat deposits dated at 1,900 years and the Gaspur aquifer dated at 15,000-20,000 years are not deformed. However, there are still unresolved issues so the Compton Thrust is included in the current study for the sake of conservatism.

A.2.11 Los Alamitos Fault

The Los Alamitos fault is a northwest-southeast trending subsurface fault along the northeast side of the NISZ (see Figure 2-1). The fault is not well known because it is not exposed at the surface. The fault extends upward from the basement rocks to an elevation of about -300 ft (MSL), and is subparallel to the NISZ from at least Seal Beach to Rosecrans. The American Association of Petroleum Geologists (1988) regional cross section shows the feature dipping about 70° to the southwest. The fault is shown as a dotted feature (i.e. buried fault) on the state fault map of Jennings (1994) who assigned it an age of late Quaternary. The Los Angeles County Seismic Safety Element (1990) shows it as potentially active. The fault is shown on the Caltrans seismic hazard map (Mualchin 1996) with a maximum earthquake magnitude of 6.0.

The existence of the feature is known from oil-field data in the Dominguez Oil field that shows faulted and steeply dipping strata (McMurdie, 1973), and from gravity data (Yerkes et al., 1965). Earthquake activity along the northeast side of the NISZ suggests the presence of a seismically active fault. Analysis of historical seismicity by Hauksson (1987) showed a relatively large number of earthquakes 3 to 5 km northeast of the NISZ. The northeastern limit of these events is quite linear, and earthquake focal mechanisms indicate both normal and right-lateral strike-slip motions. Wright (1991) suggests that the feature represents the eastern edge of uplifted basement of the western Los Angeles Basin and that the fault is a zone of en echelon tension joints or gash fractures along the edge of the basement block. Wright considered that the feature may extend from about the San Joaquin Hills to the Baldwin Hills and that it represents a right-oblique reverse fault along which the northeast flank of the NISZ has overthrust the axial portion of the Los Angeles Basin central trough.

The youngest displaced sediments are the middle-Pleistocene-age (~650,000-800,000 years old) San Pedro formation. Although there is no documented surface faulting or even late-Quaternary displacement, the fault should be considered as a potential source of small- or moderate-magnitude earthquakes, similar to other buried faults in the Los Angeles Basin. For seismic design purposes, a M 6.0-6.5 earthquake is appropriate for the maximum earthquake based on the fault's length according to the empirical fault-length/earthquake-magnitude relationships of Wells and Coppersmith (1994). A slip rate of 0.5 mm/yr is assumed in the current study.

A.2.12 Other Faults

There are several minor unnamed faults on the offshore San Pedro shelf. These features were detected by various geophysical surveys for local pipelines. These features are too small and discontinuous to represent a seismic hazard and therefore are not significant for seismic design. An example of this type of feature is the Navy Mole Fault as shown on Figure 2-3.

APPENDIX B

Details on Seismic Source Parameters

APPENDIX B
DETAILS ON SEISMIC SOURCE PARAMETERS

TABLE OF CONTENTS

FIGURES

APPENDIX B
DETAILS ON SEISMIC SOURCE PARAMETERS

This appendix provides a more-detailed discussion of the various aspects of the faults that were used in the seismic hazard analysis for the POLB. All faults which might have a potential impact on the site are described in detail in Appendix A and are summarized in Sections 2 and 3 (see Tables 3-1, 3-2 and 3-3) of the main text.

B.1 PALOS VERDES FAULT

The Palos Verdes fault extends from the east side of the Palos Verdes Peninsula offshore southeasterly to the Lasuen Knoll area and northwesterly into the Santa Monica Bay, for a total length of about 100 km. However, as described Appendix A, the northern part in Santa Monica Bay is not considered to be active so the hazard model is based on the southern segment from the Redondo Canyon fault to Lasuen Knoll, a total length of 62 km. The location of the Palos Verdes fault in the Port of Long Beach region is shown in Figure 2-3.

B.1.1 Segmentation

Three segments of the Palos Verdes fault are considered: the Southern Offshore segment (SO), Palos Verdes Hills segment (PVH), and the Santa Monica Bay segment (SMB). The approximate lengths of the segments are 36 km for the SMB segment, 12 km for the PVH segment, and 50 km for the SO segment.

The 2003 USGS fault model does not include a segmentation point along the Palos Verdes fault. Since the SMB segment does not displace strata younger than Pliocene, this segment is not considered to be active in our model. Therefore, unlike the USGS model, the SMB segment is modeled as a separate segment (with zero slip-rate).

The segmentation of the SO segment is not well known. For faults with unknown segmentation, common practice is to assume that the characteristic magnitude would correspond to rupture at 1/2 of the mapped fault length. To address the segmentation uncertainty, two segmentation models were considered: (1) an "unsegmented model" in which the full length of the SO segment is assumed to rupture, and (2) a "segmented model" in which 1/2 of the length of the SO segment is assumed to rupture. The PVH segment is assumed to fully rupture for both the segmented and unsegmented model. The segmented and unsegmented models were given equal logic-tree weightings.

In the USGS model, the dip of the fault is 90° and the down-dip fault width is 13 ± 2 km. As discussed in Appendix A.2.1, the dip of the Palos Verdes fault changes along the strike. This variation in dip can be seen in the Southern California Earthquake Center (SCEC) community

fault (CF) model (refer to Figure B-1). In the SCEC CF Model, the crustal thickness is 18 km for the PVH and SMB segments, thinning for the SO segment (Shaw, 2004).
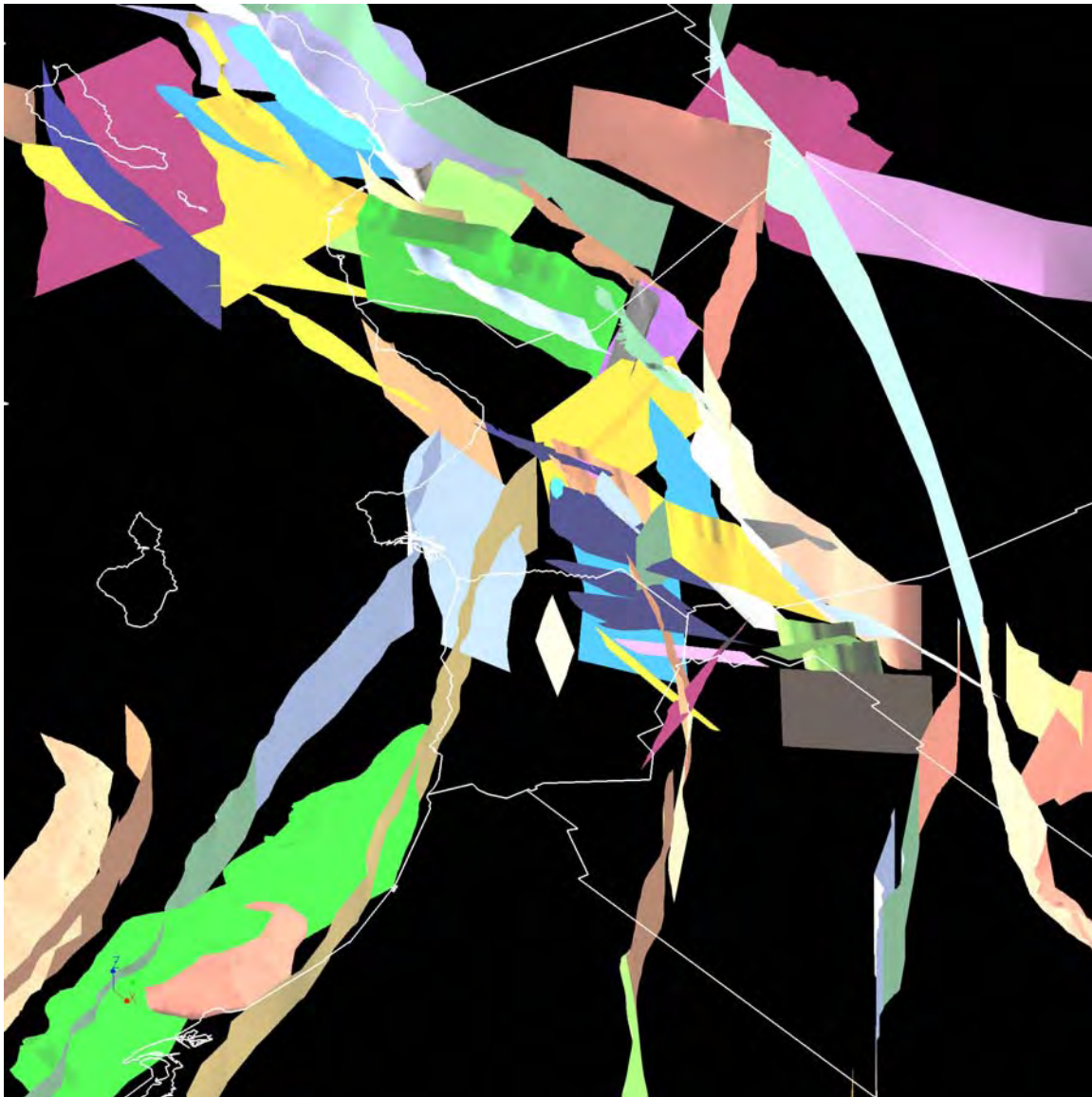
Figure B-1.   Faults from the Southern California Earthquake Center (SCEC) Community Fault (CF) Model

For the hazard analysis, a single dip and fault width is used for each segment. A dip of 90° is used for all three segments. For the PVH segment, widths of 15 and 18 km are used with equal weights, corresponding to the SCEC CF Model width and the thicker end of the USGS model. For the SO segment, widths of 11, 13, and 15 km are used with weights of 0.2, 0.6 and 0.2, respectively, based on the USGS model.

B.1.2 Slip-Rate

As discussed in detail in Appendix A.2.1, the Palos Verdes fault has a range of slip rates of about 2.0 to 4.0 mm/yr. The favored rate most commonly used by the geological community is the 3.0 mm rate and this rate is considered conservative because it is based on the maximum slip/ displacement data. A slip-rate of 2 mm/yr is considered more likely than a slip-rate of 4 mm/yr because the 3.0 mm/yr rate was based on maximum parameters. Therefore, the following slip-rates and weights are used for the slip-rate on the PVH and SO segments: 2.0 mm/yr (weight=0.4); 3.0 mm/yr (weight=0.5); 4.0 mm/yr (weight=0.1).

B.1.3 Style of Faulting

The Palos Verdes fault was modeled as a strike-slip fault for ground motion calculations. Geological data discussed in Appendix A indicate a horizontal to vertical slip ratio of 6 or 7 (H) to 1(V) with up to about 10 % of the slip comprising the vertical slip component.

B.1.4 Characteristic Earthquake Magnitude

The mean magnitude of the characteristic earthquake is computed using the three magnitude-area relations given in Section 3 of the main text for the range of segment lengths and widths given above. The segmentation model described in Section B.1.1 reduces the mean characteristic magnitude of the fault by 0.25 magnitude units. Mean magnitudes range from 6.9 to 7.2 for the unsegmented model, and 6.65 to 6.95 for the segmented model. The alternative values of the mean characteristic magnitudes and their associated weights are shown in Figure B-2. The segmented and unsegmented models were given equal logic-tree weightings.
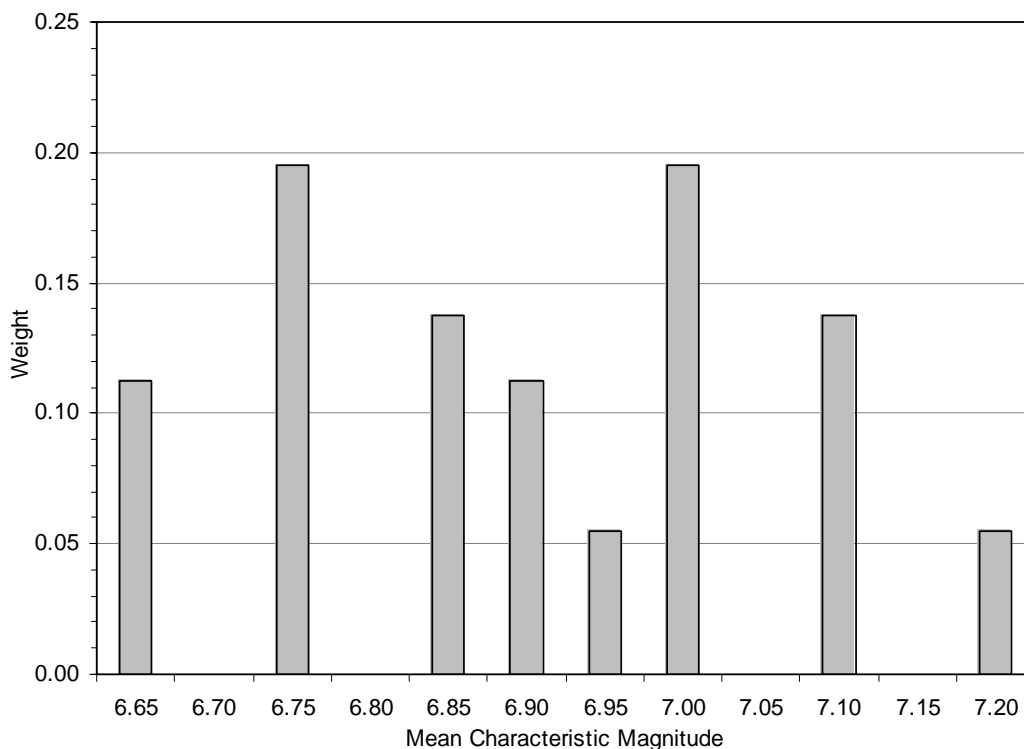
Figure B-2.   Mean Characteristic Magnitudes for the Palos Verdes Fault

B.1.5   Recurrence

The recurrence models that result using the slip-rates and characteristic magnitudes given above with the Youngs and Coppersmith (1985) magnitude probability density function are shown in Figure B-3. Using the mean model, the recurrence interval of magnitude≥7 earthquakes is about 1,000 years.
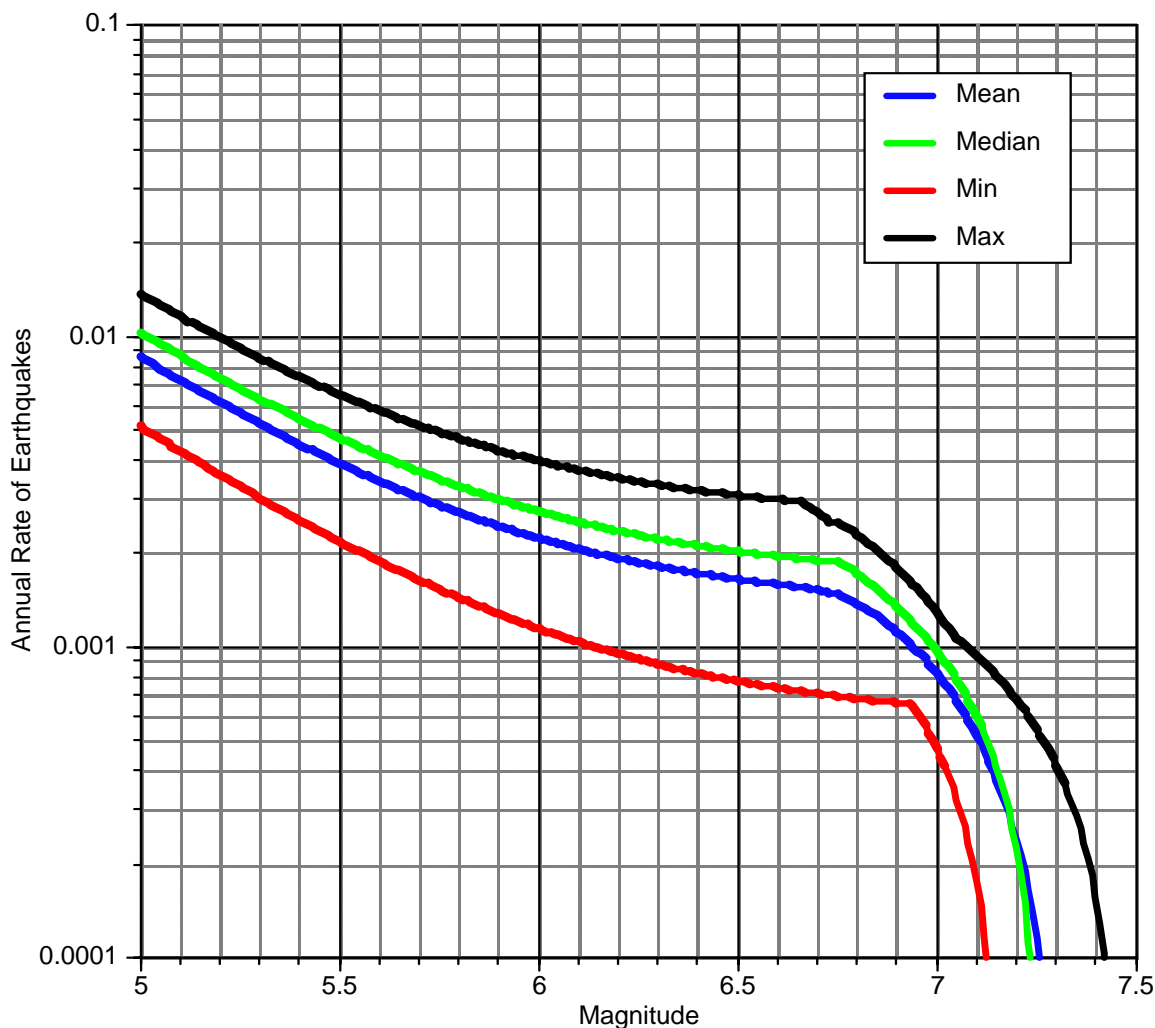
Figure B-3.   Recurrence for the Palos Verdes Fault

B.2   NEWPORT-INGLEWOOD STRUCTURAL ZONE

The Newport-Inglewood Structural Zone (NISZ) comprises a northwest-southeast trending series of faults and folds underlying the alignment of hills in the western Los Angeles Basin, between the Baldwin Hills and the area offshore of Newport Mesa. A detailed discussion of the NISZ is provided in Appendix A.

B.2.1 Segmentation

The total length of the NI fault is 65 km. The Newport-Inglewood (NI) fault lacks clear-cut segment boundaries. The USGS (2003) uses a down-dip width of 13 ± 2 km. The SCEC CF Model uses a width of about 18 km along the northern part of the NI fault, with a thinning fault in the south. The average width is about 16 km. Widths of 13 and 16 km were used with equal weights.

The segmentation of the offshore NI fault is not well known. For faults with unknown segmentation, common practice is to assume that the characteristic magnitude would correspond to 1/2 of the fault length. To address the segmentation uncertainty, two segmentation models were considered (analogous to the model described in Section B.1.1 for the PV fault): (1) an "unsegmented model" in which the full length of the offshore fault is assumed to rupture, and (2) a "segmented model" in which 1/2 of the length of the fault is assumed to rupture. The unsegmented and segmented models were given equal weights.

B.2.2 Slip-Rate

The rate of fault slip is poorly known but seems to be very low. Although quite a wide range of slip rates are proposed by various published sources, most of them are of uncertain validity because they are based on short-term, local, vertical components rather than regional horizontal slip. Most seismic hazard studies have used a long-term rate of 0.5 mm/yr based on offset of Pliocene structures and strata (Freeman et al., 1992). However, most of the deformation within the NISZ seems to have occurred within Quaternary time so the rate during more recent times may be greater. Recent seismic hazard studies (e.g. California Geological Survey, 2003) commonly use a slip rate of about 1.0 mm/yr.

Following the USGS model, the slip-rate is 1.0 ± 0.5 mm/yr. The following values are used in the logic tree: 0.5 mm/yr (weight=0.2), 1.0 mm/yr (weight=0.6), and 1.5 mm/yr (weight=0.2).

B.2.3 Characteristic Earthquake Magnitude

The mean magnitude of the characteristic earthquake is computed using the three magnitude-area relations described in Section 3.1. The segmentation model described in Section B.1.1 reduces the mean characteristic magnitude of the fault by 0.30 magnitude units. The estimates of the mean characteristic magnitudes range from 7.0 to 7.2 for the unsegmented model, and 6.7 to 6.9 for the segmented model. The maximum historical earthquake was a magnitude 6.3 event in 1933. The resulting alternative values of the mean characteristic magnitude and their associated weights are shown on Figure B-4. The unsegmented and segmented models were given equal weights.
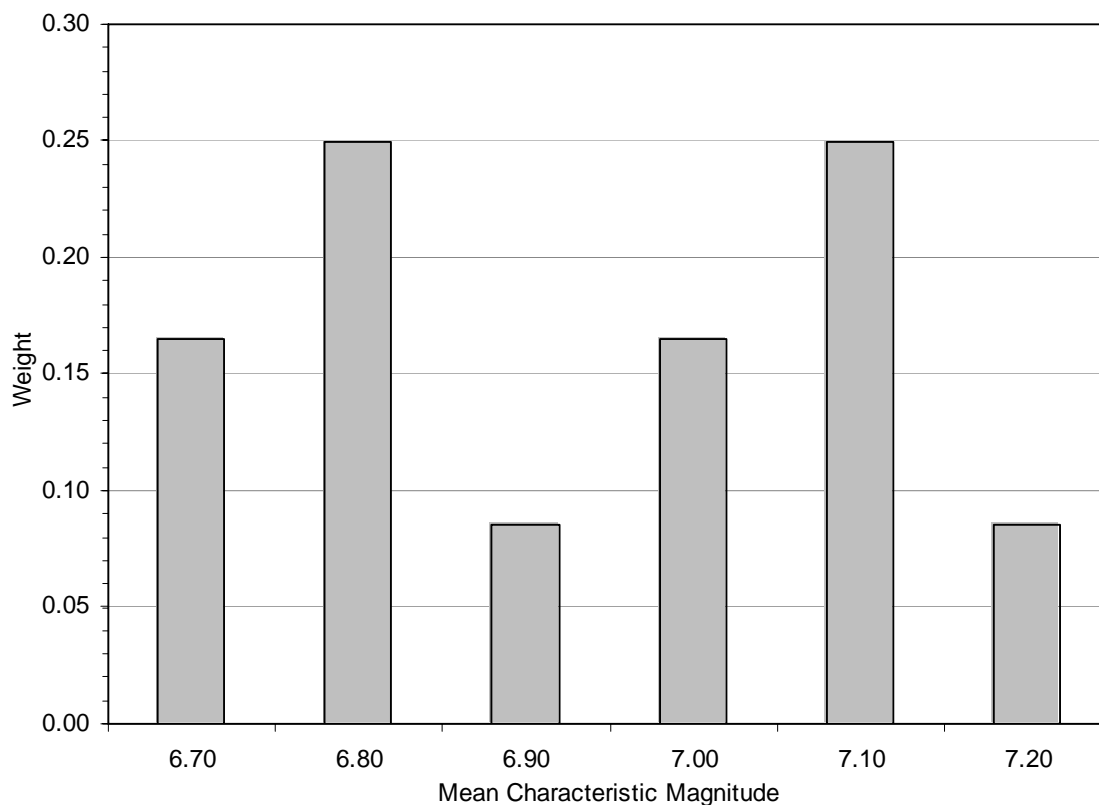
Figure B-4.   Mean Characteristic Magnitudes for the Newport-Inglewood Structural Zone Fault

B.2.4   Recurrence

The recurrence intervals for large earthquakes on the NISZ are poorly known but all estimates are long, generally in the thousand-year range. Geological data indicate that the fault has had 3 to 5 surface ruptures in Holocene time (refer to Appendix A.2.2) suggesting average recurrence intervals of a couple thousand years. The recurrence relations used in this model are shown on Figure B-5.
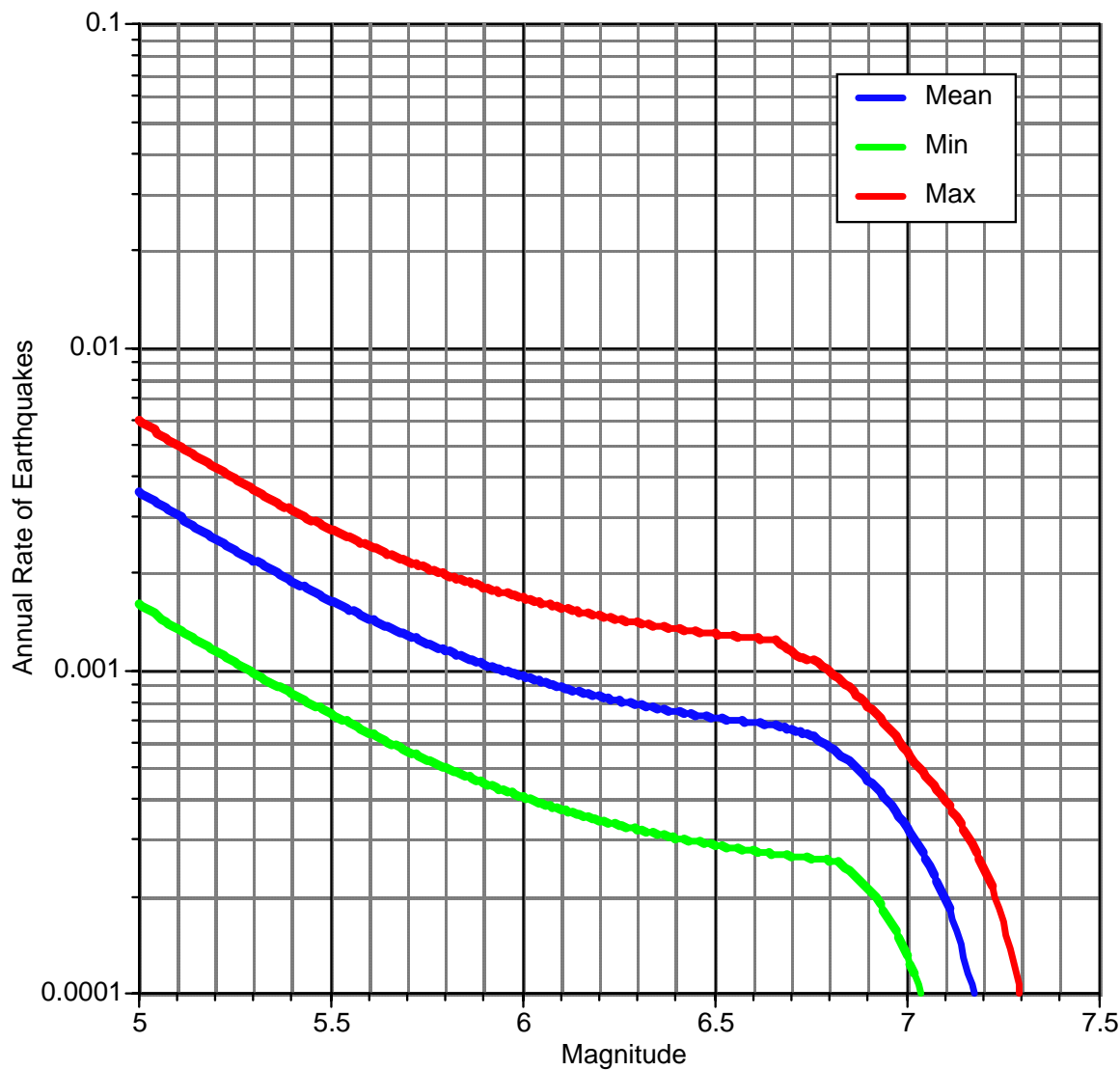
Figure B-5.   Recurrence for the Newport-Inglewood Structural Zone Fault

B.3   CABRILLO FAULT

The Cabrillo fault extends from the Palos Verdes Hills into the offshore area where it appears to deform the seafloor and to merge southeasterly with the Palos Verdes fault (refer to Figure 2-1). The length is 18 km and the fault dips 50° to 70°. The width of the fault plane is assumed to be the similar to the Palos Verdes fault, i.e. 15 or 18 km with equal weight. The fault is described in detail in Appendix A.2.3. The Cabrillo fault is commonly not considered in most seismic hazard analyses but it was included here because of its proximity to the POLB.

B.3.1 Slip-Rate

The slip rate is difficult to estimate due to lack of data. Most geoscientists feel that the Cabrillo fault is a minor feature, and Ward and Valensise (1994) estimated a slip rate of 0.1 mm/yr which seems to be a realistic estimate for such a minor feature.

B.3.2 Style of Faulting

Although the Cabrillo fault may have a small component of normal displacement, it is assumed to be strike-slip primarily because of its close association with the strike-slip Palos Verdes and Newport-Inglewood faults, as well as other faults in the Southern California Continental Borderland, such as the San Pedro Basin fault, which are primarily strike-slip faults.

B.3.3 Characteristic Earthquake Magnitude

The mean magnitude of the characteristic earthquake is computed using the Wells and Coppersmith (1994) model and Hanks and Bakun (2002) model. The Ellsworth model (described in Chapter 4 in USGS, 2003) is only applicable for areas greater than 500 km^2, so it has not been used here. Using these models, the mean characteristic magnitudes are 6.4 and 6.5 for widths of 15 and 18 km, respectively.

B.3.4 Recurrence Relation

The alternative recurrence relations for the Cabrillo fault are shown in Figure B-6.
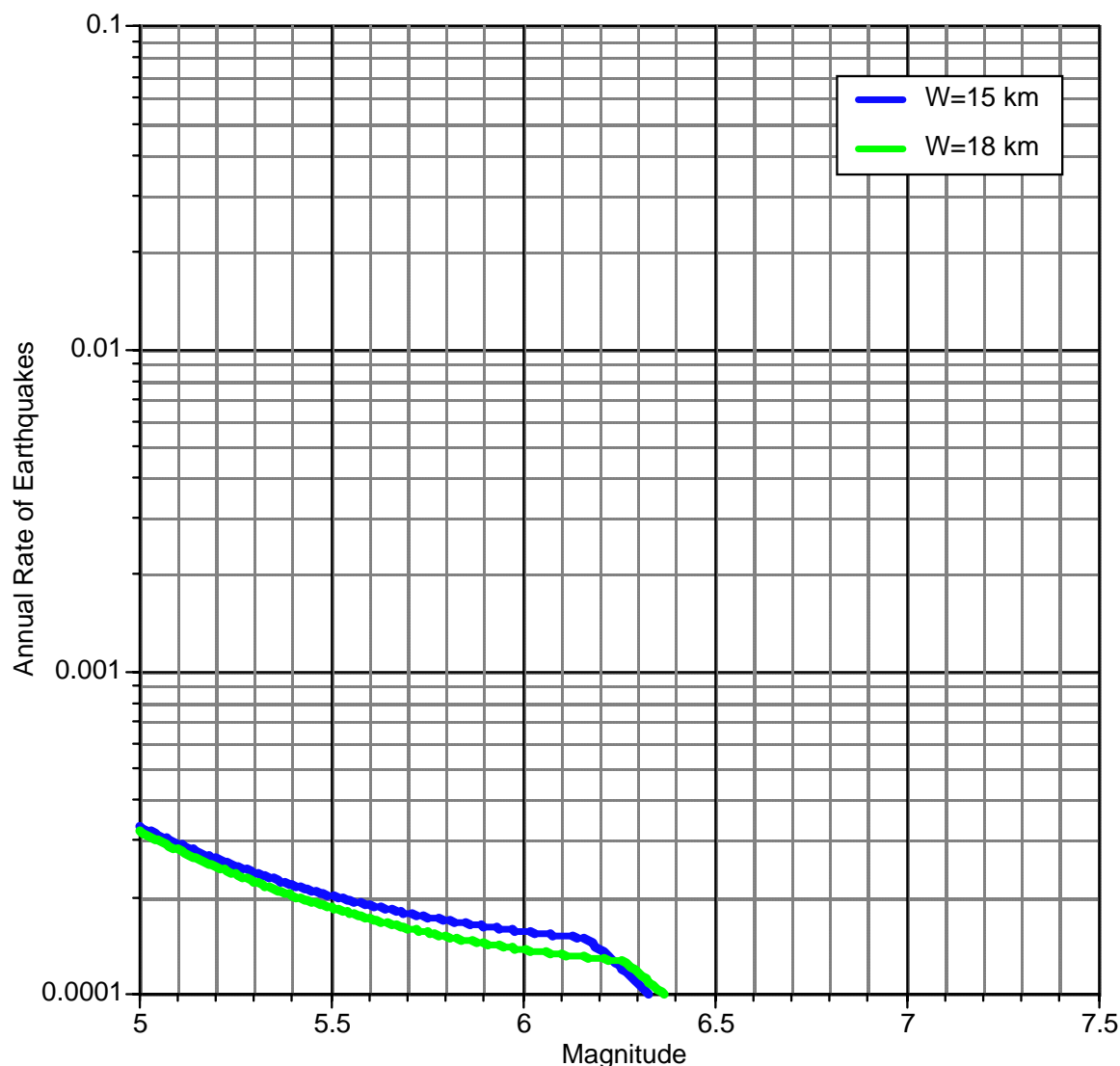
Figure B-6.   Recurrence for the Cabrillo Fault

B.4   SAN PEDRO BASIN FAULT

The San Pedro Basin fault is one of the major faults within the nearby seafloor. Described in detail in Appendix A, the fault zone comprises a zone of faults and folds that trend southeasterly from near the base of the Malibu-Santa Monica shelf to the vicinity of Avalon Knoll, a distance of about 70 km. Although the faults in the zone have many variances, at depth the fault dips nearly vertical, indicating that it is probably a strike slip fault (Fisher et al., 2003). The fault has abundant evidence indicating that it is an active feature including a coincidence with small-magnitude earthquakes near its southeastern end. The width of the San Pedro Basin fault was assumed to be 15 km.

B.4.1   Segmentation

The segmentation of this fault is not well known. Rather than applying a segmentation model similar to that described in Section B.1.1 for the PV fault, this fault was assumed to be unsegmented for simplicity and because it is not a controlling fault.

B.4.2   Slip-Rate

There are no specific data on the rate of slip for the San Pedro Basin fault. The length of the fault and the prominent seafloor geomorphic expression, both of which are similar to the NISZ, suggest that the fault is a major feature. The slip-rates assumed for the San Pedro Basin fault are 0.5 and 1.0 with weights of 0.6 and 0.4, respectively.

B.4.3   Style of Faulting

The San Pedro Basin fault is thought to be a strike-slip slip fault because of its structural character (e.g. vertical-dip flower structures) and its association with other strike-slip faults in the southern California region.

B.4.4   Characteristic Earthquake Magnitude

The mean magnitude of the characteristic earthquake is computed using the Wells and Coppersmith (1994) model and Hanks and Bakun (2002) model. The Ellsworth model (described in Chapter 4 in USGS, 2003) is only applicable for areas greater than 500 km^2 so it has not been used here. Using these models, the mean characteristic magnitudes are 7.1 and 7.2 with equal weights.

B.4.5   Recurrence

The alternative recurrence relations for the San Pedro Basin fault are shown in Figure B-7.
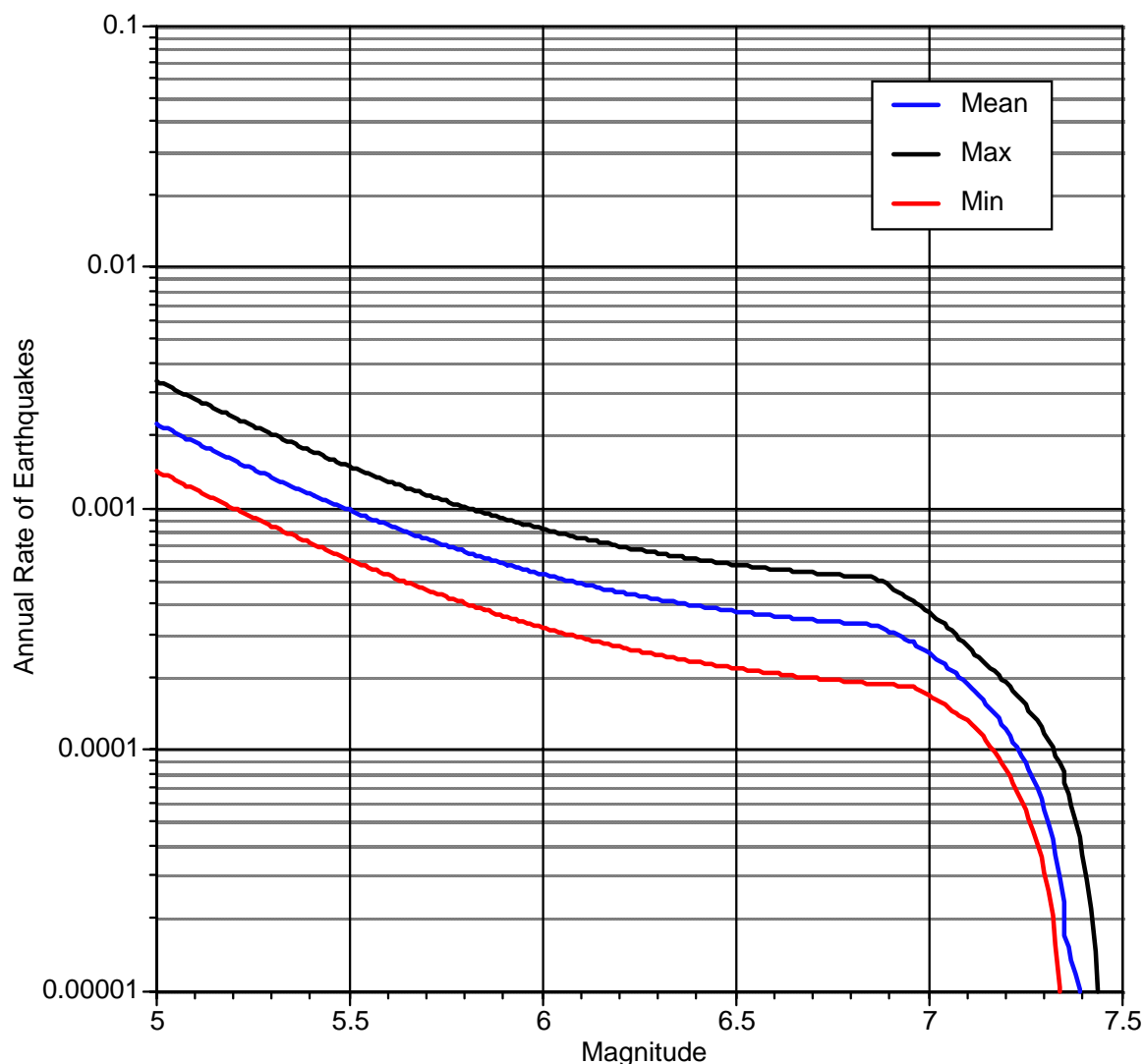
Figure B-7.   Recurrence for the San Pedro Basin Fault

B.5   THUMS-HUNTINGTON BEACH FAULT

Shaw (2004) considers the THB fault to be the updip extension of the Compton Thrust (refer to Figure B-8). Therefore, the THB is not modeled as a separate source. The inclusion of the THB fault does not affect the characteristic magnitude of the Compton Thrust because it makes only a very small change to the total fault area. The main impact of considering the THB fault active is that the closest distance from the Compton Thrust fault is reduced from 6 km to <1 km. While it is considered unlikely that the THB is an active fault (refer to Appendix A), the Shaw (2004) model was included with a weight of 0.1. The weight for the THB fault being inactive is 0.9.
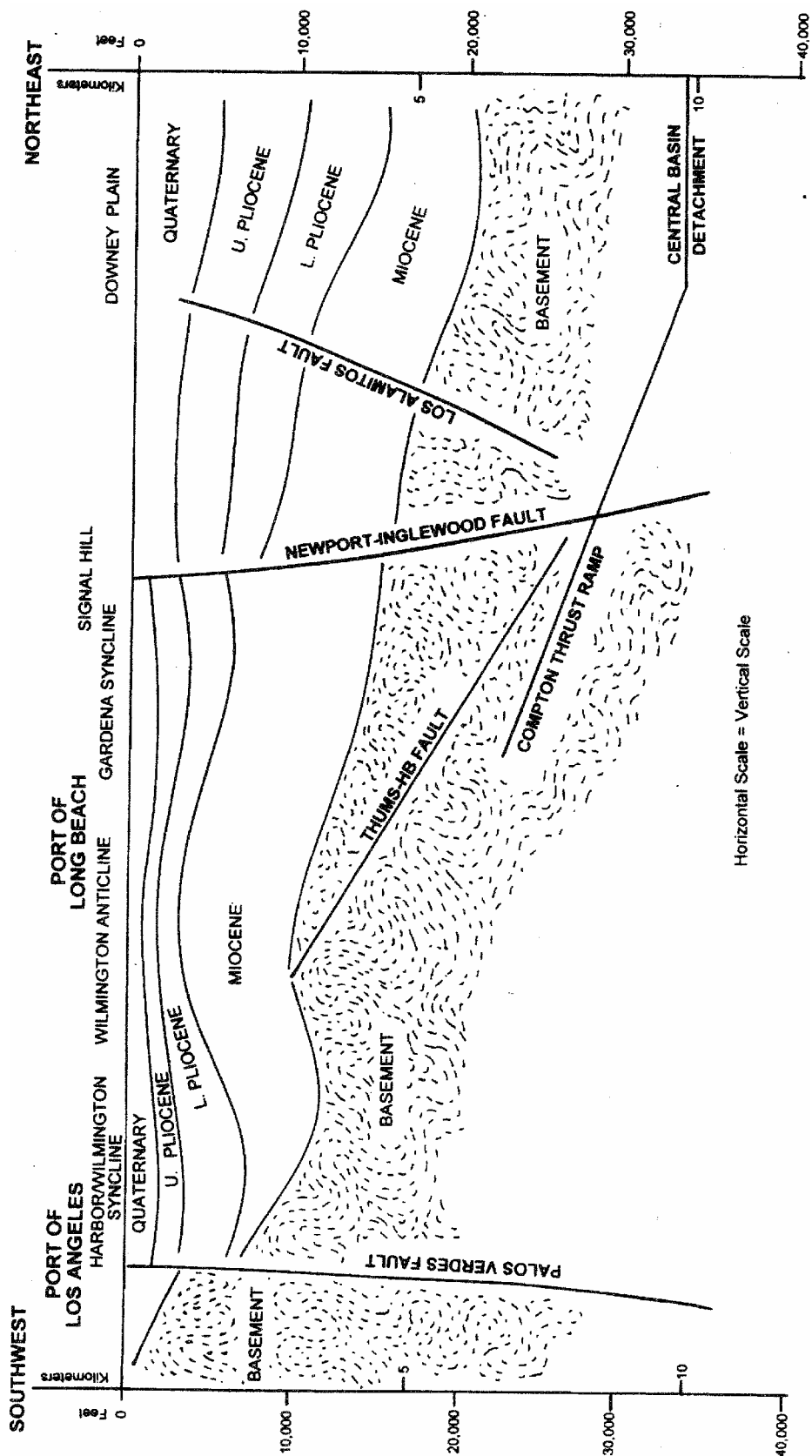
Figure B-8. Structural relations of postulated Compton Thrust Ramp and known faults

B.6   COMPTON-LOS ALAMITOS FAULT ZONE/THRUST RAMP

In the SCEC CF Model (refer to Figure B-1), the Compton thrust is no longer interpreted to cut off the Palos Verdes fault, except for the Santa Monica Bay segment which is modeled as an inactive fault. Shaw (2004) proposes that the Newport-Inglewood Structural Zone is offset at depth (10-11 km) by the Compton Ramp (refer to Figure B-8); however, this offset is not considered to prevent rupture of either the shallow (<10 km) or the deep (10 to 18 km) segments of the Newport-Inglewood fault. Because these blind fault/detachment fault models extend below the major active surface faults but largely fail to provide mechanisms by which they all could be active within a very limited strain budget, these models have been rejected by most seismic-hazard analyses or given only secondary importance. While considered unlikely that the Compton thrust is an active fault, it was considered as an alternative in the logic tree. The weight given to the fault being an active source is 0.2.

B.6.1   Slip-Rate

Shaw (2004) recommended using a slip-rate on the Compton ramp of 0.5 – 1.0 mm/yr, and for this study slip-rates of 0.5 and 1.0 mm/yr were therefore used with equal weights.

B.6.2   Style-of-faulting

The style-of-faulting is assumed to be reverse.

B.6.3   Characteristic Earthquake Magnitude

Using the SCEC CF model, the length of the Compton Thrust is about 70 km. The width of the Compton Thrust varies along its strike. The average downdip width is 15 km. Using the three magnitude-area relations discussed in section 3.1 results in characteristic magnitudes of 7.1 to 7.2 with weights of 0.67 and 0.33, respectively.

B.6.4   Recurrence

Figure B-9 shows the recurrence relationships for the Compton Thrust.

B.7   LOS ALAMITOS FAULT

The Los Alamitos fault is a northwest-southeast trending subsurface fault along the northeast side of the NISZ (refer to Figures 2-1 and 3-1). The fault offsets Quaternary-age strata which combined with the seismicity in the area indicates an active fault. The length of the fault is about 40 km.

B.7.1   Slip-rate

The slip rate is unknown as is the earthquake recurrence interval. Because the Los Alamitos fault is a much smaller feature that the main NISZ fault, the slip-rate was assumed to be less. The slip-rate is assumed to be 0.25 mm/yr to 0.5 mm/yr with equal weights, based on the fault's association with the NISZ which has a minimum slip-rate of about 0.5 mm/yr.

B.7.2 Style-of-faulting

The style-of-faulting is assumed to be strike-slip.
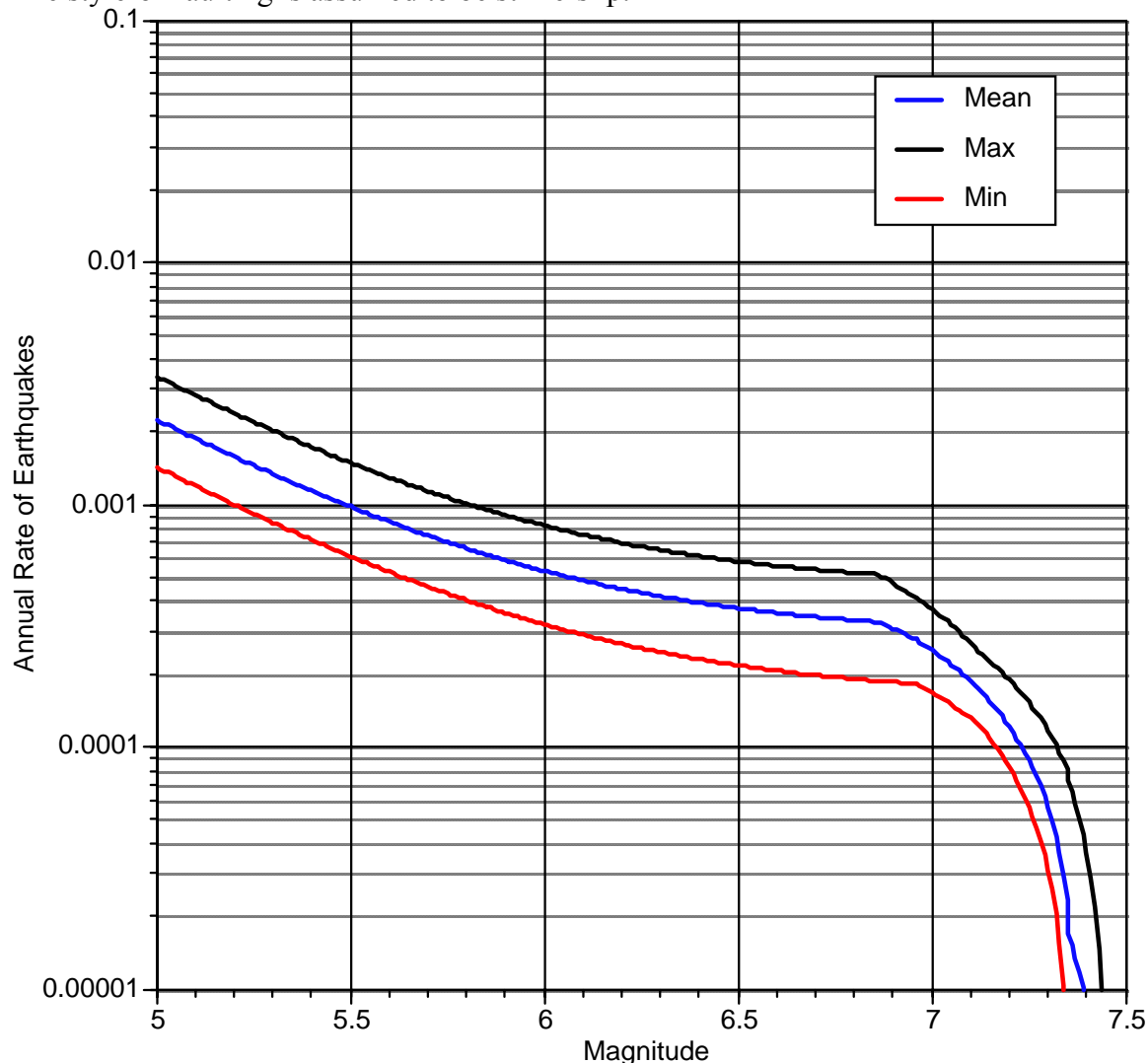
Figure B-9.　**Recurrence for the Compton Thrust (Assuming that it is Active)**

B.7.3 Characteristic Magnitude

If the fault width of the Los Alamitos fault is assumed to be the same as the Newport-Inglewood fault, the mean characteristic earthquake magnitude based on the magnitude-area scaling relations would be 6.7 to 7.0; however, earthquake of this size would likely occur on the more active Newport-Inglewood fault. Therefore, the mean characteristic magnitude for the Los Alamitos fault is assumed to be 6.5.

B.7.4 Recurrence

Figure B-10 shows the recurrence relationship for the Los Alamitos fault.
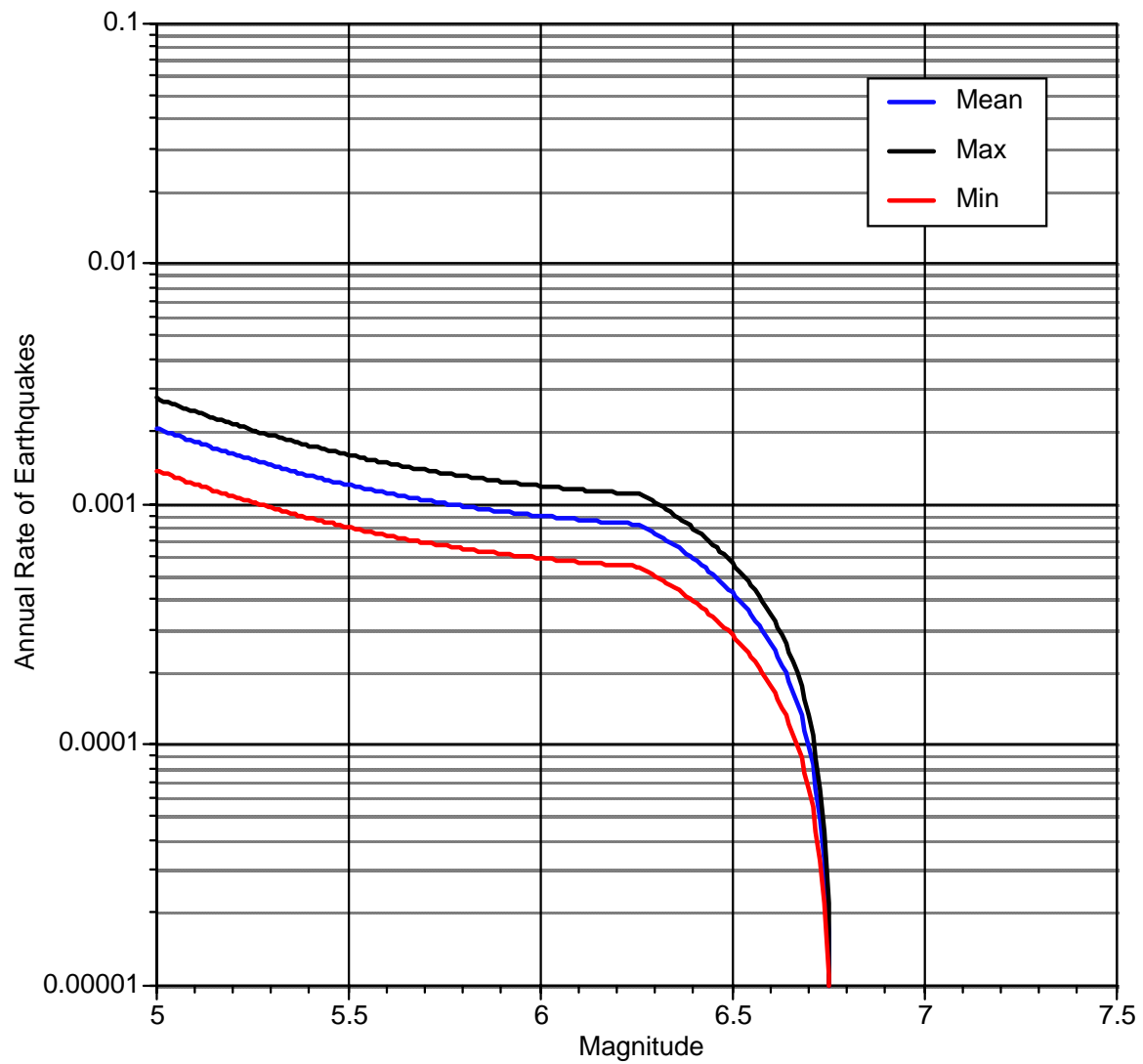
Figure B-10. Recurrence for the Los Alamitos Fault

APPENDIX C

Details on Probabilistic Seismic Hazard Assessment

APPENDIX C
DETAILS ON PROBABILISTIC SEISMIC HAZARD ASSESSMENT

TABLE OF CONTENTS

FIGURES

TABLES

APPENDIX C
DETAILS ON PROBABILISTIC SEISMIC HAZARD ASSESSMENT

C.1 MATHEMATICAL FORMULATION

The probabilistic seismic hazard analysis follows the standard approach first developed by Cornell (1968). The main change from the original work is that more parameters are randomized (a more complete description of the aleatory variables) and epistemic uncertainty is considered. In particular, the aleatory variability in the ground motion was not considered in the original work. The ground motion aleatory variability has a large effect on the hazard and can not be ignored.

The basic methodology involves computing how often a specified level of ground motion will be exceeded at the site. The hazard analysis computes the annual number of events that produce a ground motion parameter A that exceeds a specified level "a". This number of events per year ν is also called the "annual frequency of exceedance". The inverse of ν is called the "return period".

The calculation of the annual frequency of exceedance ν involves the rate of earthquakes of various magnitudes, the rupture dimension of the earthquakes, the location of the earthquakes relative to the site, and the attenuation of the ground motion from the earthquake rupture to the site.

The annual rate of events from the ith source that produce ground motions that exceed "a" at the site is the product of the probability that the ground motion exceeds the test value given that an earthquake has occurred on the ith source and the annual rate of events with magnitude greater than m_{min} on the ith source.

$$\nu_i(A > a) = N_i(m_{min})P_i(A > a \mid E_i(m > m_{min})) \tag{C-1}$$

where $N_i(m_{min})$ is the annual number of events with magnitude greater than m_{min} on the ith source and $E_i(m_{min})$ indicates that an event with magnitude $\geq m_{min}$ has occurred on the ith source.

For multiple seismic sources, the total annual rate of events with ground motions that exceed z at the site is just the sum of the annual rate of events from the individual sources (assuming that the sources are independent).

$$\nu(A > a) = \int_{i=1}^{N_{source}} \nu_i(A > a) \tag{C-2}$$

C.1.1   Hazard for Fault Sources

Fault sources are modeled by multiple-planes, which allows changing the strike of the fault. For planar sources (e.g. known faults), we need to consider the finite dimension and location of the rupture in order to compute the closest distance. Specifically, we need to randomize the rupture length, rupture width, rupture location along strike, rupture location down dip, and hypocenter location along the rupture length (for strike-slip faults). Since rupture width and length are correlated, it is easier to consider the rupture area and rupture width and then back calculate the rupture length.

The general form of the conditional probability for the ith fault is given by

$$P_i(A > a \mid E_i(m \geq m_{min})) = \begin{cases} \int\limits_{RA=0}^{\infty} \int\limits_{RW=0}^{\infty} \int\limits_{Ex=0}^{1} \int\limits_{Ey=0}^{1} \int\limits_{x=0}^{1} \int\limits_{m=M_{min}}^{M_{max_i}} f_{m_i}(m) f_{RA_i}(m) f_{RW_i}(m) f_{Ex_i}(Ex) f_{Ey_i}(Ey) f_{x_i}(x)... \\ \\ ...P_i(A > a \mid m, r(Ex, Ey, RA, RW), x) \, dm \, dx \, dEy \, dEx \, dRW \, dRA) \end{cases} \tag{C-3}$$

where $f_{RW}(m)$, $f_{RA}(m)$, $f_{Ex}(Ex)$, $f_{Ey}(Ey)$, $f_x(x)$, and $f_m(m)$ are probability density functions for the rupture width, rupture area, rupture location along strike, rupture location down dip, hypocenter location in the rupture plane, and magnitude, respectively. The models used for these probability density functions are described later.

For the fault normal component (FN), the probability of exceeding the ground motion "*a*" for a given magnitude, *m*, and closest distance, *r*, and hypocenter location, *x,* is given by

$$P(A > a \mid m, r, x) \;=\; 1 - \Phi\left(\frac{\ln(a) - \ln(Sa_{FN}(m, r, x))}{\sigma(m)}\right) \tag{C-4}$$

where *Sa(m,r,x)* and *σ(m)* are the median and standard deviation of the ground motion from the attenuation relations for the fault normal component as described later in Section C.1.8, and $\Phi()$ is the normal probability integral given by

$$\Phi(z) = \int_{-\infty}^{z} \frac{1}{\sqrt{2\pi}} e^{-u^2/2} \, du \tag{C-5}$$

C.1.1.1   Probability of Exceedance

The annual rate of events given in Eq. (C-2) is not probability; it can exceed 1. To convert the annual rate of events to a probability, we consider the probability that the ground motion exceeds test level "*a*" at least once during a specified time interval.

At this step, a common assumption is that the occurrence of earthquakes is a Poisson process. That is, there is no memory of past earthquakes, so the chance of an earthquake occurring in a

given year does not depend on how long it has been since the last earthquake (non-Poisson models are discussed later). If the occurrence of earthquakes is a Poisson process then the occurrence of peak ground motions is also a Poisson process. For a Poisson process, the probability of an event (e.g. ground motion exceeding a level z) occurring n times in time interval t is given by

$$p_n(t) = \exp(-vt)\,(vt)^n/n! \tag{C-6}$$

The probability that at least one event occurs (e.g. $n{\geq}1$) is 1 minus the probability that no events occur:

$$P(n{\geq}1,t) = 1 - p_o(t) = 1 - \exp(-vt) \tag{C-7}$$

So the probability of at least one occurrence of ground motion level z in t years is given by

$$P(A{>}a,t) = 1 - \exp(-v(A{>}a)t) \tag{C-8}$$

For t=1 year, this probability is the annual hazard.

C.1.2 Aleatory and Epistemic Uncertainty

The basic part of the hazard calculation is computing the integrals in Eq. (C-3). All of the aleatory variables are inside of the hazard integral. The randomness of the seismic source variables is characterized by the probability density functions which are discussed below. The randomness of the attenuation relation is accounted for in the probability of exceeding the ground motion "a", for a given magnitude and closest distance.

Epistemic (scientific) uncertainty is considered by using alternative models and/or parameter values for the probability density functions, attenuation relation, and activity rate. For each alternative model, we recalculate the hazard and compute alternative hazard curves. Epistemic uncertainty is typically handled using a logic tree approach for specifying the alternative models for the density function, attenuation relation, and activity rates.

C.1.3 Activity Rate

There are two approaches to estimating the fault activity rate: historical seismicity and geologic (and geodetic) information.

If historical seismicity catalogs are used to estimate the activity rate, then the estimate of $N(m^L)$ is usually based on fitting the truncated exponential model (discussed below) to the historical data. Maximum likelihood procedures are generally preferred over least-squares for estimating the activity rate and the b-value.

When using geologic information on slip-rates of faults, the activity rate is computed by balancing the energy build-up estimated from geologic evidence with the total energy release of earthquakes. Knowing the dimension of the fault, the slip-rate, and the rigidity of the fault, we

can balance the long term seismic moment so that the fault is in equilibrium (e.g., Youngs and Coppersmith, 1985).

The seismic energy release is balanced by requiring the build up of seismic moment to be equal to the release of seismic moment in earthquakes. The build up of seismic moment is computed from the long term slip-rate. The seismic moment, M_o (in dyne cm), is given by

$$M_o = \mu\, A\, D \tag{C-9}$$

where μ is the rigidity of the crust, A is the area of the fault (in cm^2), and D is the average displacement (slip) on the fault surface (in cm).

The annual rate of build up of seismic moment is given by

$$M_o = \mu\, A\, S \tag{C-10}$$

where S is the slip-rate in cm/year.

The seismic moment released during an earthquake is given by

$$\log_{10} M_o = 1.5\, m + 16.05 \tag{C-11}$$

where m is the moment magnitude of the earthquake.

To balance the moment build up and the moment release, the annual moment rate from the slip-rate is set equal to the sum of the moment released in all of the earthquakes that are expected to occur each year:

$$\mu AS = N(m^L) \int_{m=M^L}^{m^U} f_m(m)\, 10^{(1.5m + 16.05)}\, dm \tag{C-12}$$

Given the slip-rate, fault area, and magnitude density function, the activity rate, $N(m^L)$ is given by:

$$N(m^L) = \frac{\mu AS}{\displaystyle\int_{m=m^L}^{m^U} f_m(m) 10^{(1.5m+16.05)}\, dm} \tag{C-13}$$

C.1.4 Magnitude Density Distribution

The magnitude density distribution describes the relative number of large magnitude and moderate magnitude events that occur on the seismic source. Two alternative magnitude density functions are considered: the truncated exponential model and the characteristic model.

The truncated exponential model is the standard Gutenberg-Richter model that is truncated at the minimum and maximum magnitudes and renormalized so that it integrates to unity. The density function for the truncated exponential model is given by

$$f_m(m) = \frac{\beta \exp(-\beta(m-m^L))}{1-\beta \exp(-\beta(m^U-m^L))}$$

(C-14)

where β is ln(10) times the *b*-value. Regional estimates of the b-value are usually used with this model.

The characteristic model assumes that more of the seismic energy is released in large magnitude events than for the truncated exponential model. That is, there are fewer small magnitude events for every large magnitude event for the characteristic model than for the truncated exponential model. There are different models for the characteristic model. Two commonly used models are the "characteristic model" as defined by Youngs and Coppersmith (1985) and the "maximum magnitude" characteristic model.

The density function for the generalized form of the Youngs and Coppersmith characteristic model is given by

$$f_m(m) = \begin{cases} \dfrac{\beta \exp(-\beta(m-m^L))}{1-\beta \exp(-\beta(m^U-\Delta m_2-m^L))} \dfrac{1}{1+c} & \dots for\ m < m^U - \Delta m_2 \\ \dfrac{\beta \exp(-\beta(m^U-\Delta m_1-\Delta m_2-m^L))}{1-\beta \exp(-\beta(m^U-\Delta m_2-m^L))} \dfrac{1}{1+c} & \dots for\ m \geq m^U - \Delta m_2 \end{cases}$$

(C-15)

where

$$c = \frac{\beta \exp(-\beta(m^U-\Delta m_1-\Delta m_2-m^L))}{1-\beta \exp(-\beta(m^U-\Delta m_2-m^L))} \Delta m_2$$

(C-16)

The density function for this model is shown in Figure C-1. In the Youngs and Coppersmith model, $\Delta m_1 = 1.0$ and $\Delta m_2 = 0.5$.

Comparing the examples of the truncated exponential and characteristic density functions shown in Figure C-1, we see that the density functions themselves are similar at small magnitudes. However, when the geologic moment-rate is used to set the annual rate of events, $N(m^L)$, then there is a large impact on $N(m^L)$ depending on the selection of the magnitude density function. Figure C-2 shows the comparison of the magnitude recurrence relation for the truncated exponential and characteristic models (using the Youngs and Coppersmith value for Δm_1 and Δm_2) when they are constrained to have the same total moment rate. The characteristic model has many fewer moderate magnitude events than the truncated exponential model (about a factor of 10 difference).

Recent studies have found that the characteristic model does a better job of matching observed seismicity than the truncated exponential (Geomatrix, 1992; Woodward-Clyde, 1994) when the total moment rate is constrained by the geologic slip-rate.

C.1.5 Rupture Dimension Density Functions

For the rupture area and rupture width, the density functions are determined from regression models which give the rupture area and rupture width as a function of magnitude. For this project, the Wells and Coppersmith (1994) empirical models for rupture area and rupture width are used:

$$\log_{10}(RA) = -3.49 + 0.91 \, m \pm 0.24 \tag{C-17}$$

$$\log_{10}(W) = -1.01 + 0.32 \, m \pm 0.15 \tag{C-18}$$

where m is the magnitude. The density functions, $f_{RA}(m)$ and $f_{RW}(m)$ are log-normal distributions centered about the median values given by Eq. (C-15) and (C-16). These distributions are truncated at $\pm 2\sigma$ in the hazard calculations.

C.1.6 Rupture Location Density Functions

The center of the rupture location is parameterized in terms of the normalized fault length and fault width. *Ex* is the fraction of the fault length (measure along strike) and *Ey* is the fraction of the fault width (measured down dip). The location of the center of the rupture plane is assumed to be uniformly distributed over the fault plane. The resulting density functions for $f_{Ex}(Ex)$ and $f_{Ey}(Ey)$ are unity.

C.1.7 Hypocenter Location Density Function

For a given rupture dimension (length and width) and rupture location, the location of the hypocenter along strike is parameterized in terms of the normalized rupture length. The location of the hypocenter is assumed to be uniformly distributed over the rupture plane. The resulting density function for $f_x(x)$ is unity. In the hazard analysis, a total of 10 hypocenter locations evenly spaced along the rupture length are used for each magnitude, rupture location, and rupture dimension.

C.1.8 Directivity Effects Model

The empirical attenuation relations were developed for the average horizontal component without regard to the direction of rupture. Somerville et al. (1997) developed an empirically based model quantifying the effects of rupture directivity on horizontal response spectra that can be used to scale the average horizontal component from attenuation relations. There are two effects of rupture directivity on long period response spectral values that are modeled by Somerville. First, there is an increase in the average horizontal component for cases of rupture coming toward the site and there is a decrease in the average horizontal motion for rupture running away from the site. Second, there is a systematic difference in the two horizontal components of motion when they are oriented parallel and perpendicular to the strike of the fault. At long periods, the fault normal component is larger than the fault parallel component. This increase in the fault normal component has also been studied by Geomatrix (1995).

In this project, a modified form of the Somerville et al. (1997) model has been used to characterize the two parts of the directivity effect.

C.1.8.1 Somerville et al. (1997) Model

Somerville et al. (1997) provides scale factors to account for directivity effects for the horizontal components. The Somerville et al. model for the difference in the two horizontal components (fault normal and fault parallel) for strike-slip earthquakes is given by

$$\ln\left(\frac{FN}{Ave\,H}\right) = \begin{cases} \cos(2\phi)\left[C_1 + C_2 \ln(r+1\,km) + C_3(m-6)\right] & for\ m > 6\ and\ \phi < 45^o \\ 0 & otherwise \end{cases} \tag{C-19}$$

where *Ave H* is the average horizontal component, ϕ is the azimuth angle from the epicenter to the station, and *r* is the rupture distance. The coefficients C_1, C_2 and C_3 are listed in Table C-1. This model is used without modification in this study.

Somerville et al. also provides a model for the effect of rupture direction on the average horizontal component. This model was modified for use on this project as described below.

C.1.8.2 Modifications of the Somerville et al. (1997) Model

There are several aspects of the empirical model for the average horizontal component scale factors developed by Somerville et al. that needed to be modified to make the model applicable to a probabilistic hazard analysis.

(A) Distance Dependence

As published, the model is independent of distance. The data set used in the analysis includes recordings at distances of 0 to 50 km. A distance-dependent taper function was applied to the model that reduces the effect to zero for distances greater than 60 km:

$$T_d(r) = \begin{cases} 1 & for\ r < 30\,km \\ 1 - \frac{r-30}{30} & for\ 30\,km < r < 60\,km \\ 0 & for\ r > 60\,km \end{cases} \tag{C-20}$$

(B) Magnitude Dependence

As published, the model is applicable to magnitudes greater than 6.5. A magnitude taper was applied that reduces the effect to zero for magnitudes less than 6.0:

$$T_m(m) = \begin{cases} 1 & for\ m < 6.5 \\ 1 - \frac{m-6.5}{0.5} & for\ 6 < m < 6.5 \\ 0 & for\ m < 6 \end{cases} \tag{C-21}$$

(C) Saturation of Directivity with x·cos θ

The empirical model uses a form that increases a constant rate as x increases from 0 to 1. There is little empirical data with *x·cos* θ values greater than 0.6, particularly for rupture distances less than 20 km. The short-distance data suggest that there may be a saturation of the directivity effect as a function of *x·cos* θ. The extrapolation of the model to larger *x·cos* θ values is not well constrained. To evaluate this extrapolation, three separate groups applied their seismological numerical modeling methods to generate synthetic time histories for a range of *x·cos* θ values. The numerical modeling results indicated that the directivity effect saturates for *x·cos* θ > 0.4. As a result, the functional form of the directivity model was changed to include saturation with *x·cos* θ. The coefficients of the model were based on the empirical data, and not on the synthetics.

Based on the trends in the numerical simulations, the form of the directivity function is modified to reach a maximum at *x·cos* θ = 0.4. The model was developed for a spectral period of 3 sec. The slope is greater than the Somerville et al. model, but it flattens out at a lower level. The hazard calculation is sensitive to the model values at large *x·cos* θ) (say greater than 0.9) so this change results in a reduction of the ground motion.

The T = 3 sec value is used to guide the adjustment of the model at all periods. The resulting model is given by

$$y_{Dir}(x,\theta,T) = \begin{cases} C_1(T) + 1.88\,C_2(T)\cdot x\cdot\cos\theta & \textit{for } x\cdot\cos\theta = 0.4 \\ C_1(T) + 0.75\,C_2(T) & \textit{for } x\cdot\cos\theta > 0.4 \end{cases} \tag{C-22}$$

where $C_1(T)$ and $C_2(T)$ are the coefficients from Somerville et al. and are listed in Table C-2.

C.1.8.3 Reduction of the Standard Deviation

Including the directivity effect should result in a reduction of the standard deviation of the attenuation relation. The standard deviation of the data within 20 km of distance including the directivity was compared to the standard deviation of the published model. At T = 3 sec, there is a reduction of about 0.05 natural log units. The period dependence of the reduction is approximated by the period dependence of the slope of the directivity effect. To account for the reduction in the standard deviation due to including the directivity effect as part of the model, the standard deviations for the published attenuation relations were modified for use in the hazard analysis using the following relation:

$$\sigma'(m,T) = \sigma(m,T) - 0.05\,C_2(T)/1.333 \tag{C-23}$$

where $C_2(T)$ is given in Table C-1.

C.1.8.4 Final Directivity Model

The following model is used for the average horizontal component for strike-slip faults

$$\ln Sa_{dir} (m,r,x,\theta,T) = \ln Sa(m,r) + y_{Dir}(x,\theta,T) \, T_d(r) \, T_m (m) \qquad \text{(C-24)}$$

where *Sa(m,r)* is an empirical attenuation relation without directivity.

Table C-1. Coefficients for Somerville et al. (1997) Model

Period (sec)	C_1	C_2	C_3
0.60	0.000	0.0000	0.000
0.75	0.061	-0.0155	0.000
1.00	0.104	-0.0255	0.000
1.50	0.164	-0.0490	0.034
2.00	0.207	-0.0613	0.059
3.00	0.353	-0.1007	0.093
4.00	0.456	-0.1282	0.118
5.00	0.450	-0.1269	0.137

Table C-2. Period-Dependent Coefficients for Modified Somerville et al. (1997) Model

Period (sec)	Strike-Slip		Dip-Slip	
	$C_1(T)$	$C_2(T)$	$C_1(T)$	$C_2(T)$
0.60	0.000	0.000	0.000	0.000
0.75	-0.084	0.185	-0.045	0.008
1.00	-0.192	0.423	-0.104	0.178
1.50	-0.344	0.759	-0.186	0.318
2.00	-0.452	0.998	-0.245	0.418
3.00	-0.605	1.333	-0.327	0.559
4.00	-0.713	1.571	-0.386	0.659
5.00	-0.797	1.757	-0.431	0.737
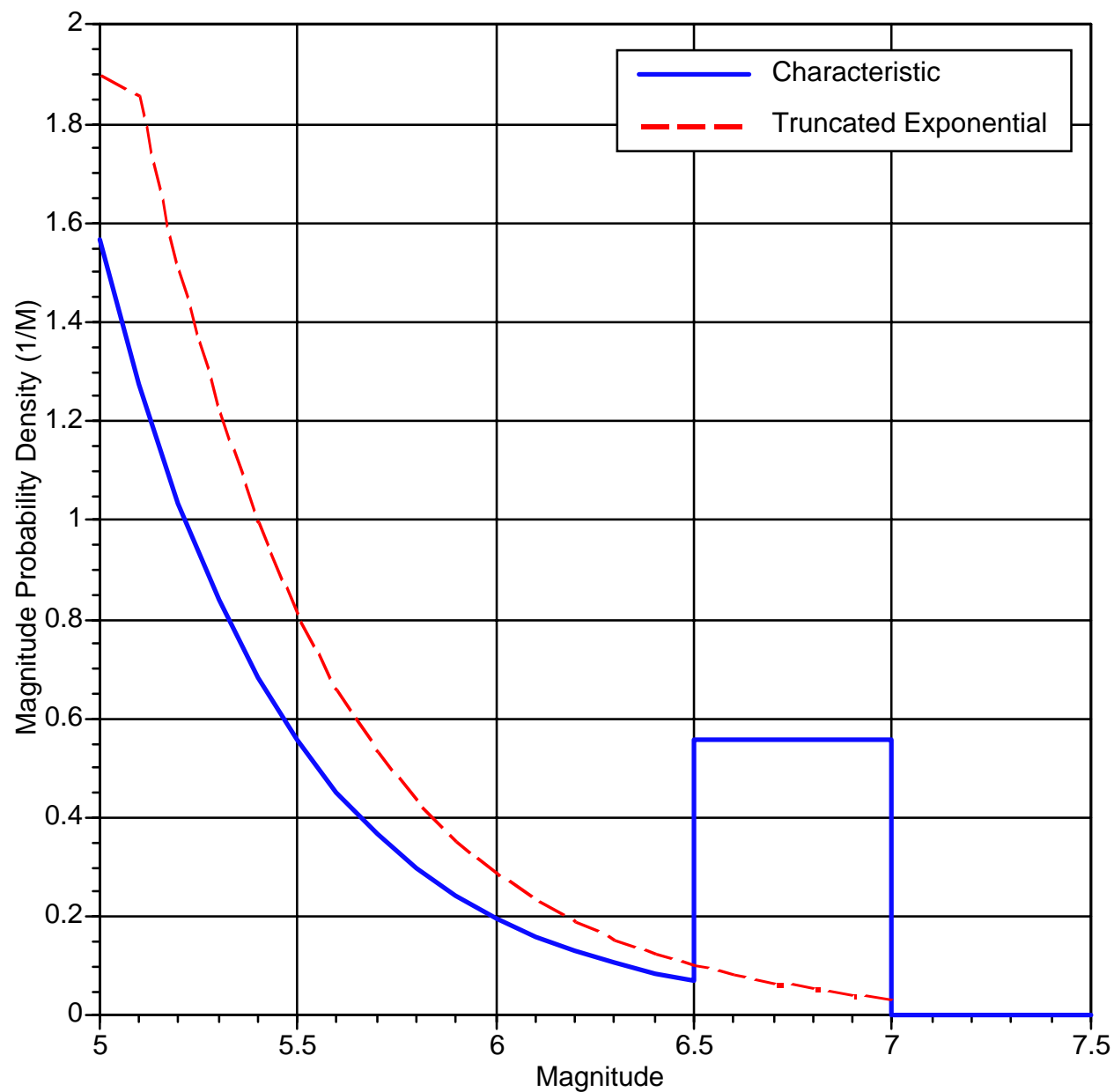
Figure C-1. **Density Function for Truncated Exponential and Characteristic Models**
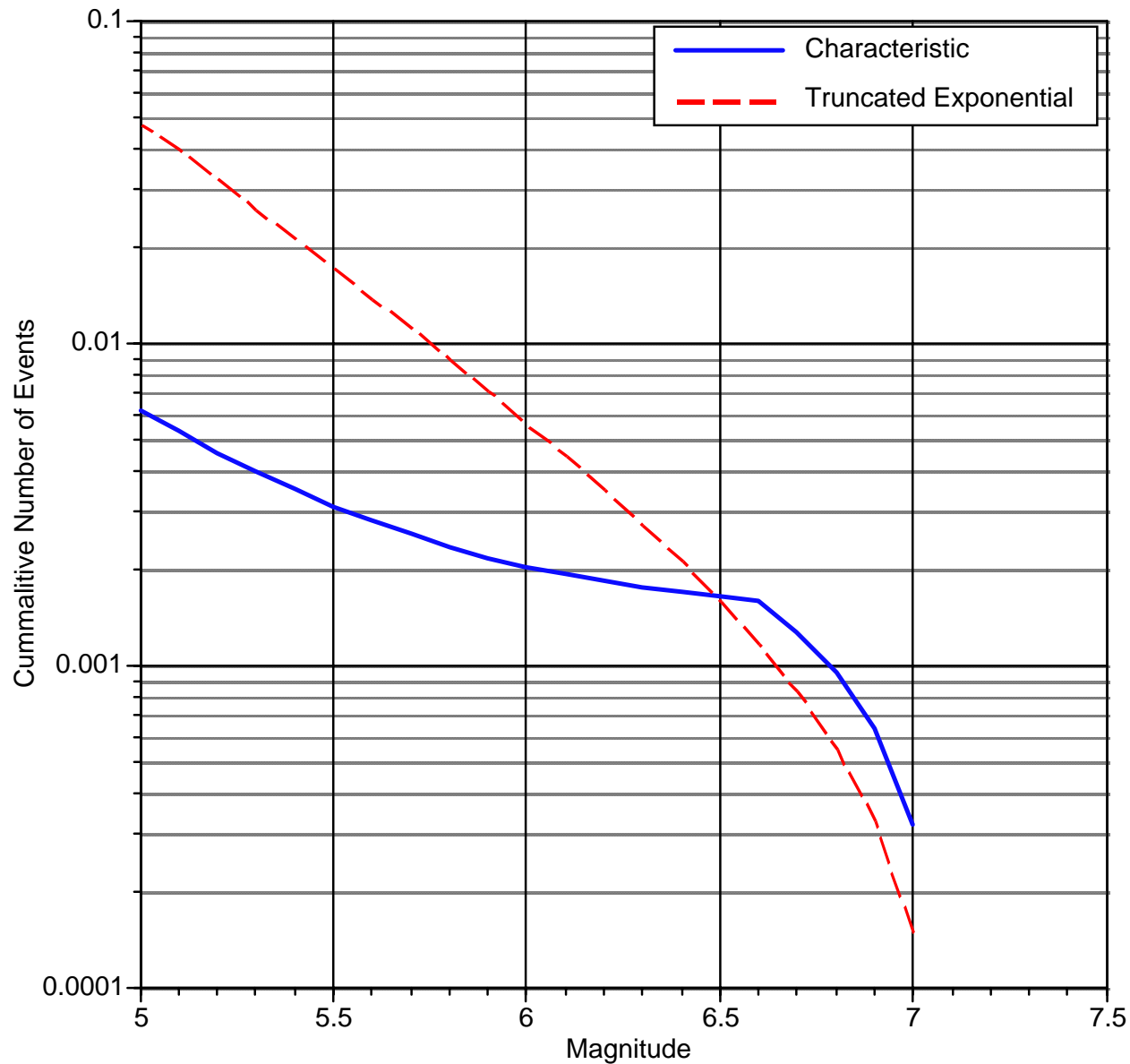
Figure C-2. **Density Function for Truncated Exponential (GR) and Characteristic Models (Youngs and Coppersmith)**

C.2 ABRAHAMSON AND SILVA (2005) ATTENUATION MODEL A

As part of the current revision of empirical ground motion attenuation models for shallow crustal earthquakes being performed for the PEER/Lifelines Next Generation Attenuation project, the Abrahamson and Silva (1997) attenuation model is being updated. This update is based upon the inclusion of more recently recorded strong ground motion data, especially for larger magnitude events such as: 1999 Kocaeli (M7.5), 1999 Chi-Chi (M7.6), 1999 Duzce (M7.1), 2000 Hector Mine (M7.1), and 2002 Denali (M7.9) earthquakes.

The updated version of the Abrahamson and Silva attenuation model, identified as Model A, that was used in the PSHA is described as follows:

$$
\begin{aligned}
Ln(Sa) = {} & C_1(T) + (C_2(T) + C_3(T) \cdot (7.5 - M)) \cdot Ln(R) + C_9(T) \cdot (8.5 - M)^2 + b_5(T) \cdot M \\
& + C_6(T) \cdot (Ln(AR) - Ln(1.5)) \cdot Taper(M) \\
& + HW(T, M, r_{jb}) \\
& + C_5(T) \cdot F \\
& + SoilAmp(T, PGA_{rock}, V_{s30m}) \\
& + Sigma(T, PGA_{rock}, V_{s30m})
\end{aligned}
\tag{C-25}
$$

where

Sa = soil amplitude,
T = period,
C_i = regression coefficients listed in Table C-3,
M = moment magnitude,
AR = aspect ratio (i.e., fault length divided by fault width)
r_{jb} = Joyner-Boore distance,
$Taper()$ = taper function (see below),
$HW()$ = hanging wall/foot wall effect (see below),
F = fault mechanism (see below),
$SoilAmp()$ = soil amplification function (see below), and
$Sigma()$ = standard deviation in natural log units (see below).

The R parameter is defined as

$$
R = \sqrt{r_{rup}^2 + h(T)^2}
\tag{C-26}
$$

where

r_{rup} = rupture distance, and
$h(T)$ = fictitious depth term.

The *Taper* function is defined as

$$Taper(M) = \begin{cases} 1.0 & \text{for } M \geq 7.0 \\ (M - 6.5)^2 & \text{for } 7.0 > M > 6.5 \\ 0.0 & \text{for } M \leq 6.5 \end{cases}$$

(C-27)

The *HW* hanging wall/foot wall function is defined by

$$HW(T, M, r_{jb}) = \frac{C_7(T)(30.0 - r_{jb})}{30.0} \cdot \frac{(90.0 - Dip)}{45.0} \cdot Taper2(M)$$

(C-28)

where *Dip* is the dip angle of the fault and *Taper2(M)* is defined as

$$Taper2(M) = \begin{cases} 1.0 & \text{for } M \geq 6.5 \\ (M - 6.0)^2 & \text{for } 6.0 > M > 6.5 \\ 0.0 & \text{for } M \leq 6.0 \end{cases}$$

(C-29)

The mechanism term, *F*, is defined as follows based on the *Rake* angle of the fault:

$$F = \begin{cases} 1.0 & \text{for } 157.5 > Rake > 22.5 \\ 0.0 & \text{otherwise} \end{cases}$$

(C-30)

The *SoilAmp* function is defined as

$$SoilAmp(T, PGA_{rock}, V_{s30m}) = \begin{cases} \begin{aligned} & C_8(T) * Ln\left(\frac{V_{s30m}}{V_{sref}(T)}\right) - b_{soil}(T) * Ln(1.0 + PGA_{rock}) \\ & \qquad + b_{soil}(T) * Ln\left(PGA_{rock} + \frac{V_{s30m}}{V_{sref}(T)}\right) \quad \text{if } V_{s30m} < V_{sref}(T) \end{aligned} \\ \\ \begin{aligned} & C_8(T) * Ln\left(\frac{V_{s30m}}{V_{sref}(T)}\right) \\ & \qquad + b_{soil}(T) * Ln\left(PGA_{rock} + \frac{V_{s30m}}{V_{sref}(T)}\right) \quad \text{if } V_{s30m} \geq V_{sref}(T) \end{aligned} \end{cases}$$

(C-31)

The standard deviation *Sigma* is defined as

$$Sigma(T, PGA_{rock}, V_{s30m}) = \sqrt{Sigma_0^2(T) + tau^2(T, PGA_{rock}, V_{s30m})} \tag{C-32}$$

where the function *tau* is defined as

$$tau(T, PGA_{rock}, V_{s30m}) = \sqrt{\begin{array}{l} tau_0^2(T) + \left(\dfrac{\partial Amp}{\partial PGA_{rock}} tau_0(PGA) \right)^2 \\ + 2.0 \dfrac{\partial Amp}{\partial PGA_{rock}} tau_0(PGA) \cdot tau_0(T) \cdot tauCorr(T) \end{array}} \tag{C-33}$$

and $\dfrac{\partial Amp}{\partial PGA_{rock}}$ is the partial derivative of the natural log of the soil amplitude function with respect to the natural log of the rock PGA:

$$\frac{\partial Amp}{\partial PGA_{rock}} = \begin{cases} b_{soil}(T) \cdot PGA_{rock} \cdot \left(\dfrac{-1.0}{PGA_{rock} + 1.0} + \dfrac{1.0}{PGA_{rock} + \dfrac{V_{s30m}}{V_{sref}(T)}} \right) & for\ V_{s30m} \geq V_{sref} \\ \\ 0.0 & otherwise \end{cases} \tag{C-34}$$

Figure C-1 compares the PGA attenuation from the Abrahamson and Silva (1997) model and the Abrahamson and Silva (2005) Model A for various magnitudes for soil site conditions. Figure C-4 compares the PGA standard deviation for the two models.

Table C-3.   Regression Coefficients for Abrahamson and Silva (2005) Model A Attenuation Relationship

Period (sec)	C_1	C_2	C_3	C_5	C_6	C_7	C_8	C_9
0.00	3.53968	-0.95816	-0.26582	-0.33482	0.23408	-0.11054	0.28921	1.10778
0.02	3.61720	-0.97279	-0.25914	-0.32791	0.22547	-0.11688	0.29881	1.11124
0.05	3.94594	-1.05038	-0.26528	-0.34222	0.20355	-0.13165	0.45107	0.96458
0.10	4.65586	-1.15893	-0.26847	-0.35539	0.18006	-0.09028	0.23222	1.07856
0.15	5.02847	-1.17720	-0.25380	-0.33600	0.18351	-0.10018	0.12074	1.33755
0.20	5.03419	-1.13190	-0.22514	-0.30182	0.18910	-0.10696	0.08913	1.52918
0.30	4.57992	-0.99576	-0.22129	-0.27420	0.21559	-0.12811	0.21979	1.72303
0.40	4.38899	-0.94736	-0.21967	-0.24511	0.16301	-0.12282	0.21393	1.77987
0.50	4.25542	-0.91351	-0.22353	-0.24806	0.14975	-0.16275	0.27339	1.75103
0.75	3.47103	-0.76506	-0.24911	-0.26812	0.13947	-0.17326	0.29806	1.57877
1.00	3.37820	-0.75555	-0.25551	-0.26037	0.12270	-0.17149	0.30612	1.30057
1.50	3.12468	-0.75604	-0.20759	-0.16908	0.04234	-0.10429	-0.01350	0.73224
2.00	2.73061	-0.74427	-0.18515	-0.11108	0.02164	-0.07017	0.27184	0.29305
3.00	2.62683	-0.80779	-0.20086	-0.09146	0.00814	-0.11400	0.13396	-0.38835
4.00	2.46375	-0.83260	-0.14711	-0.03425	-0.07395	-0.02066	0.16311	-1.03567

Table C-3 (Cont.)

Period (sec)	h	b_{soil}	$Sigma_0$	tau_0	V_{sref}	b_5	$tauCorr$
0.00	5.4	-1.65	0.506	0.349	855	-0.31	1.00
0.02	5.4	-1.65	0.506	0.351	855	-0.31	0.99
0.05	5.3	-1.49	0.521	0.411	1150	-0.31	0.95
0.10	6.4	-1.61	0.545	0.451	1265	-0.31	0.92
0.15	6.9	-1.88	0.540	0.443	1140	-0.31	0.92
0.20	6.8	-2.10	0.537	0.391	990	-0.31	0.92
0.30	5.4	-2.35	0.545	0.328	786	-0.31	0.89
0.40	5.2	-2.44	0.547	0.348	674	-0.31	0.85
0.50	5.2	-2.44	0.562	0.349	601	-0.31	0.82
0.75	4.0	-2.28	0.586	0.333	515	-0.31	0.68
1.00	4.4	-2.06	0.604	0.344	445	-0.31	0.57
1.50	3.9	-1.60	0.618	0.340	400	-0.31	0.45
2.00	3.8	-1.21	0.616	0.369	400	-0.31	0.28
3.00	5.2	-0.50	0.569	0.378	400	-0.31	0.28
4.00	6.4	0.20	0.577	0.354	400	-0.31	0.17

Note: For the Abrahamson and Silva (2005) Model A:
V_{s30m}=300m/sec, Aspect Ratio=1.5, Dip=90°, Strike-slip fault.

Figure C-3.   **Comparison of PGA Attenuation Models for M=5, 6, 7, and 8 for Abrahamson and Silva (1997) and Abrahamson and Silva (2005) Model A for Soil Site Conditions**
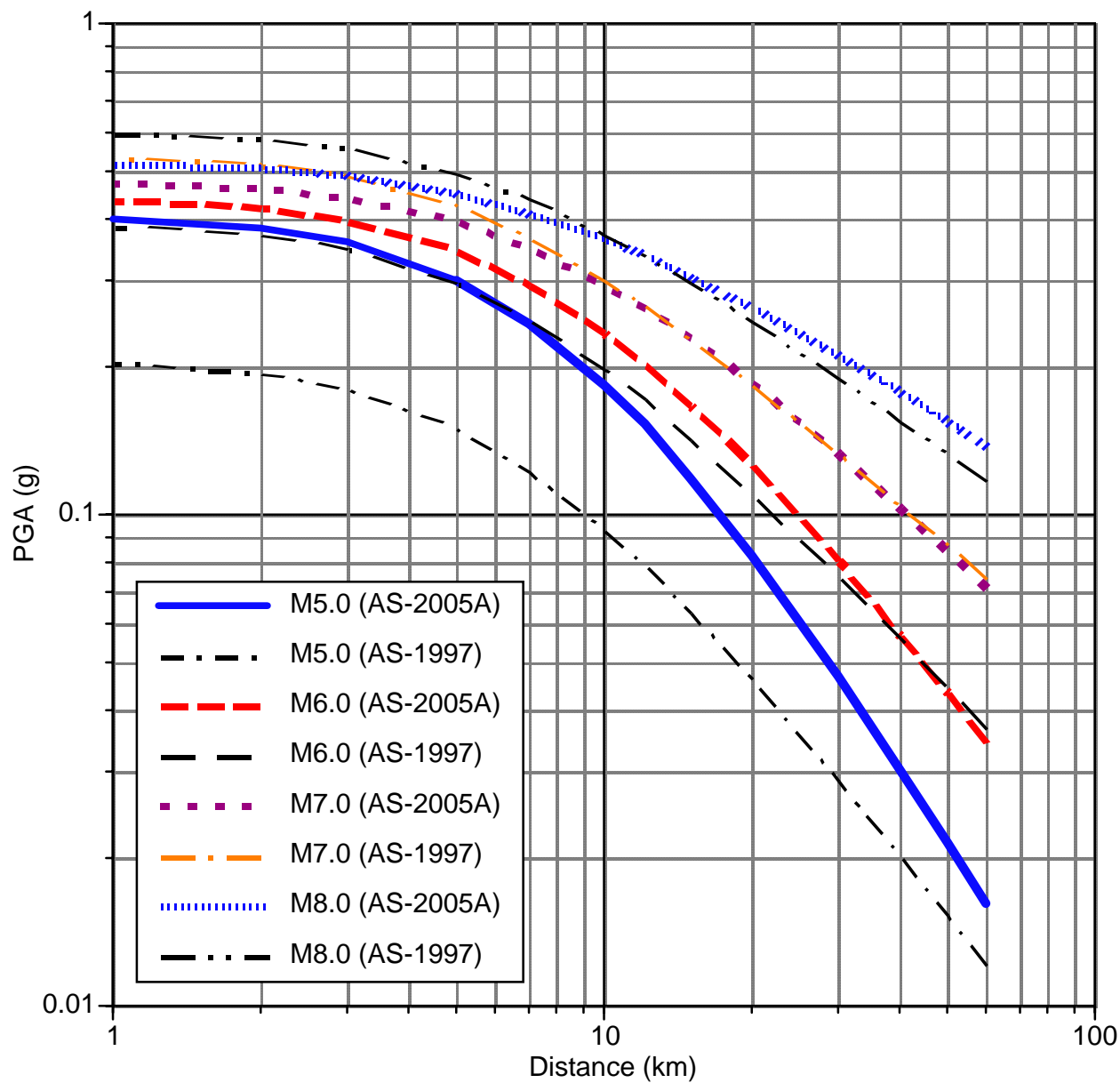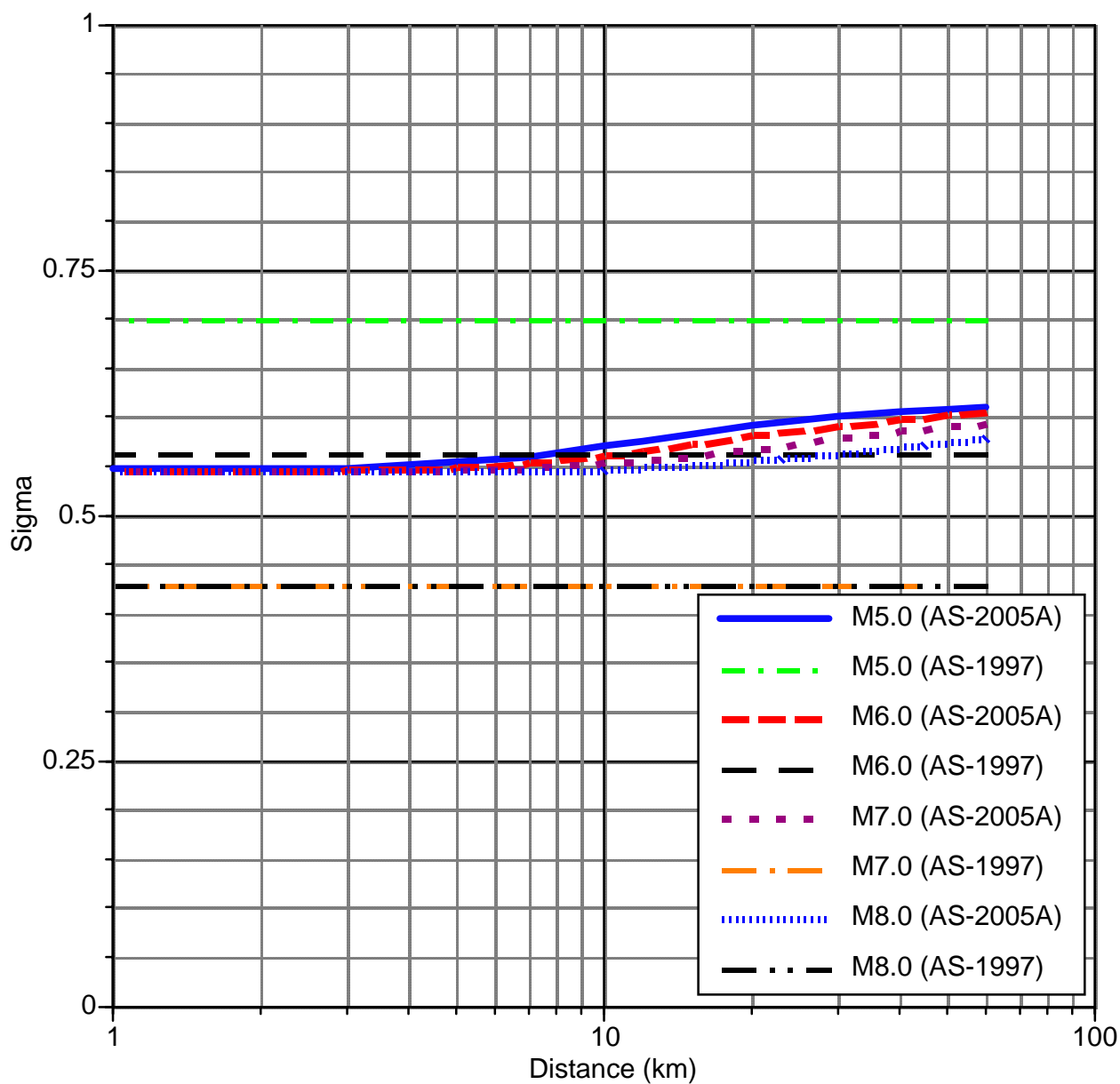
Note: For the Abrahamson and Silva (2005) Model A:
V_{s30m}=300m/sec, Aspect Ratio=1.5, Dip=90°, Strike-slip fault.

Figure C-4. **Comparison of PGA Sigma Models for M=5, 6, 7, and 8 for Abrahamson and Silva (1997) and Abrahamson and Silva (2005) Model A for Soil Site Conditions**

APPENDIX D

Spectrum-Compatible Time Histories

_____

APPENDIX D
SPECTRUM-COMPATIBLE TIME HISTORIES

TABLE OF CONTENTS

TABLES

FIGURES

APPENDIX D
SPECTRUM-COMPATIBLE TIME HISTORIES

D.1 FIRM-GROUND TIME HISTORIES COMPATIBLE TO CLE FIRM-GROUND SPECTRA

The seven (7) sets of 3-component time histories discussed in Section 3.3 and listed below in Table D-1 are modified to match the CLE firm-ground spectra using the time-domain approach. Each set has three (3) components (FN, FP and FV), resulting in a total of 21 time histories. For each time history, the following is plotted:

- Initial acceleration, velocity and displacement time histories scaled to PGA,

- Modified (spectral-matched) acceleration, velocity and displacement time histories, and

- Comparison of the target CLE spectrum with the spectra of the initial scaled and the modified time histories.

These plots are shown in Figure D-1 through Figure D-7 for the CLE time history set number 1 through set number 7, respectively.

Table D-1.   Ground Motion Sets Selected for CLE Spectral Matching

Set	Earthquake	Station	Magnitude	Distance (km)	Directivity Parameter X cos(θ)
1	1999 Hector mine	Hector	7.1	12	0.57
2	1989 Loma Prieta	Gilroy 03	6.9	13	0.45
3	1979 Imperial Valley	Brawley	6.5	10	0.75
4	1999 Duzce	Lamont 1059	7.1	4	0.36
5	1992 Erzikan	Erzikan	6.7	4	0.31
6	1940 Imperial Valley	El Centro	7.0	6	0.14
7	1995 Kobe	Kobe University	6.9	1	0.42
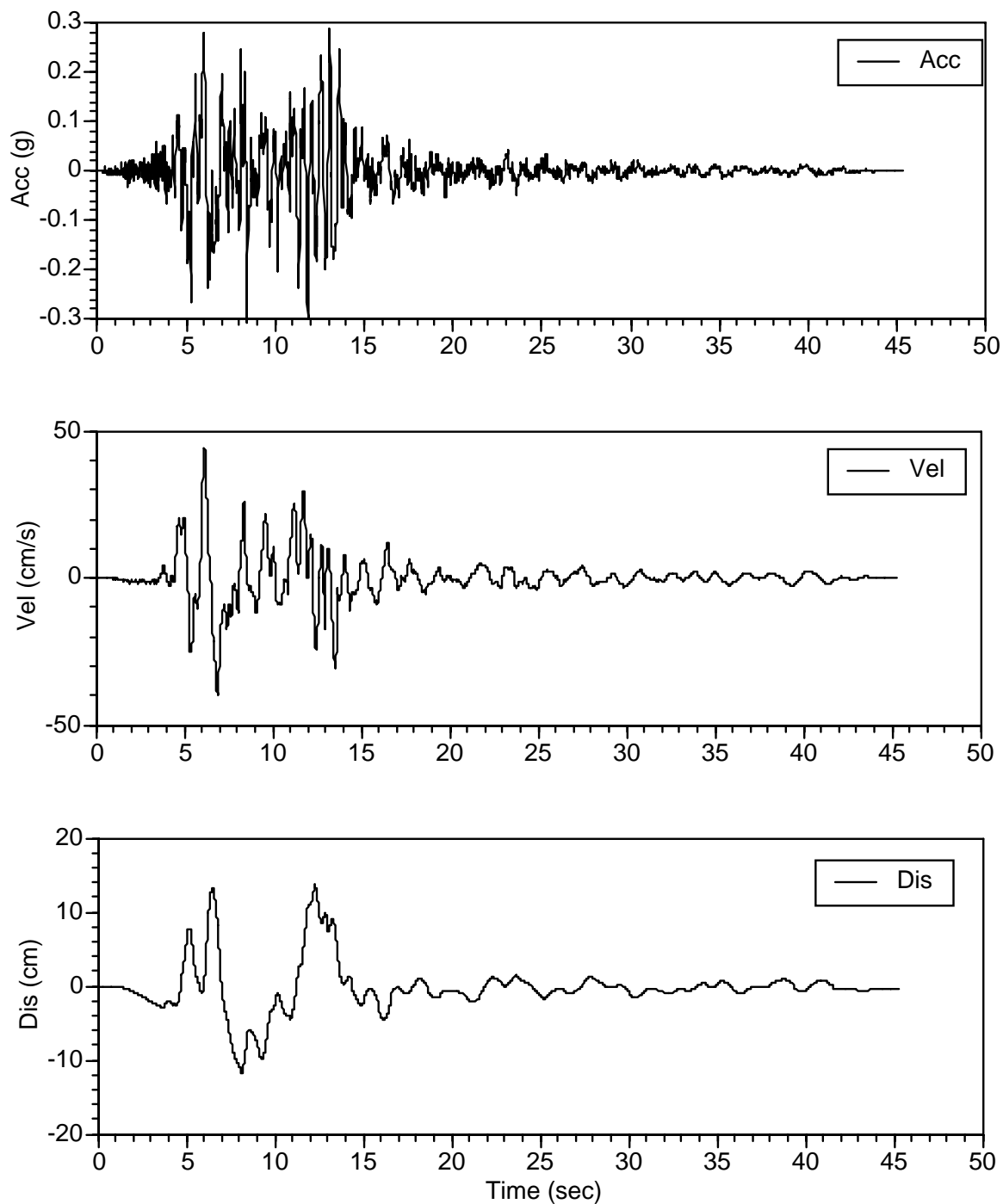
Figure D-1. **Firm-Ground Time Histories Compatible to CLE Firm-Ground Spectra, Set 1**
    (a) Initial Time History for FN Component
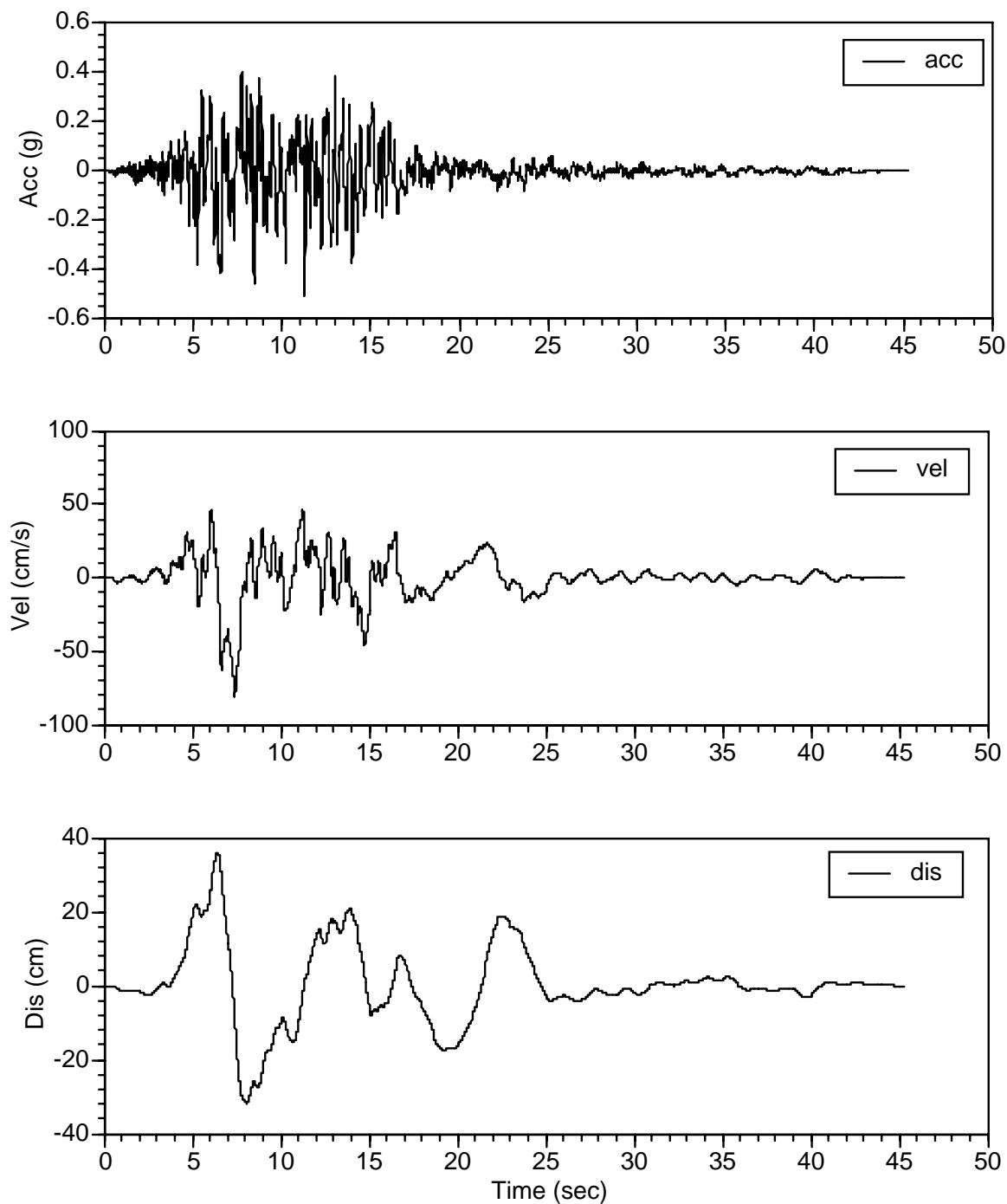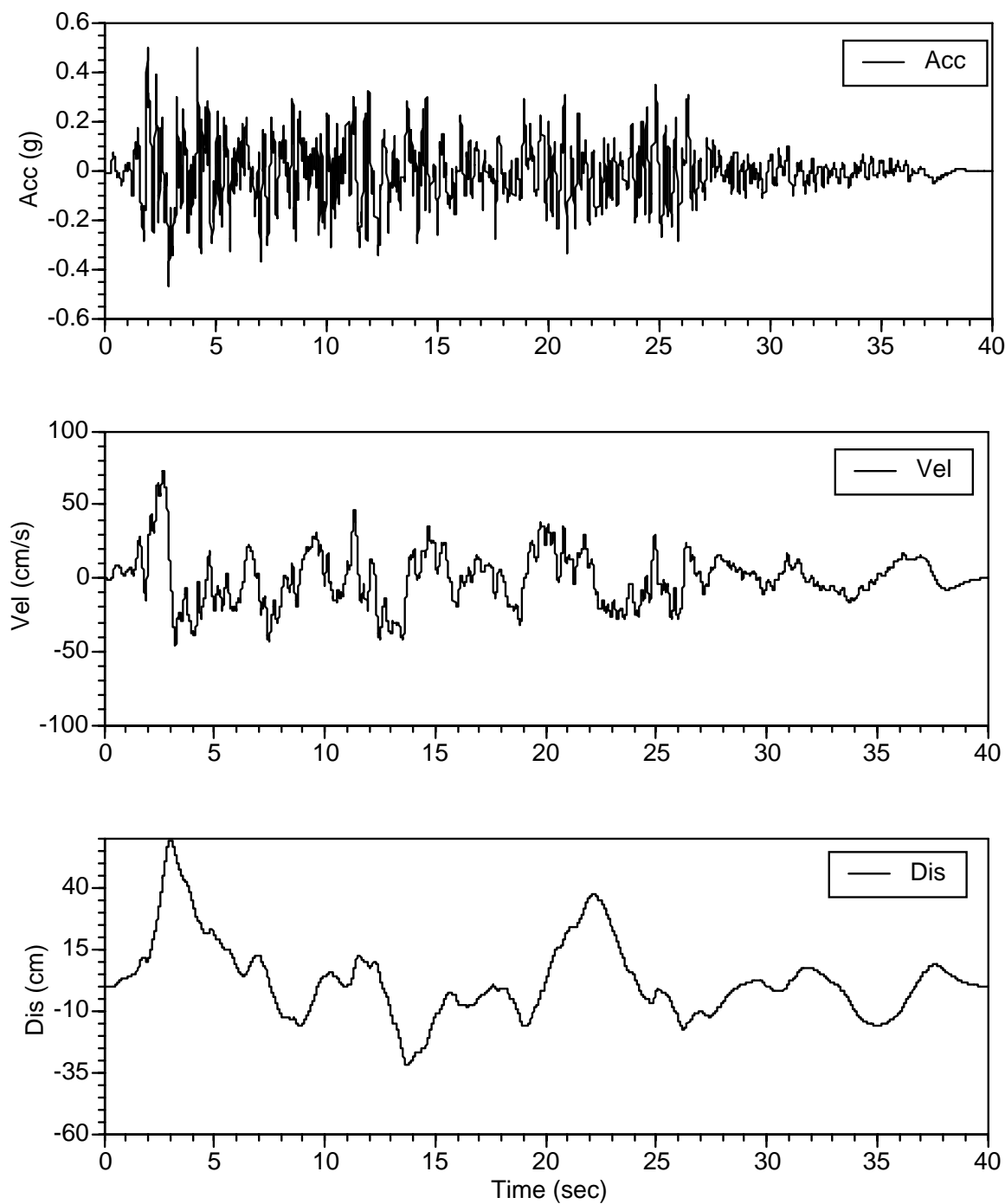
Figure D-1.   Firm-Ground Time Histories Compatible to CLE Firm-Ground Spectra, Set 1
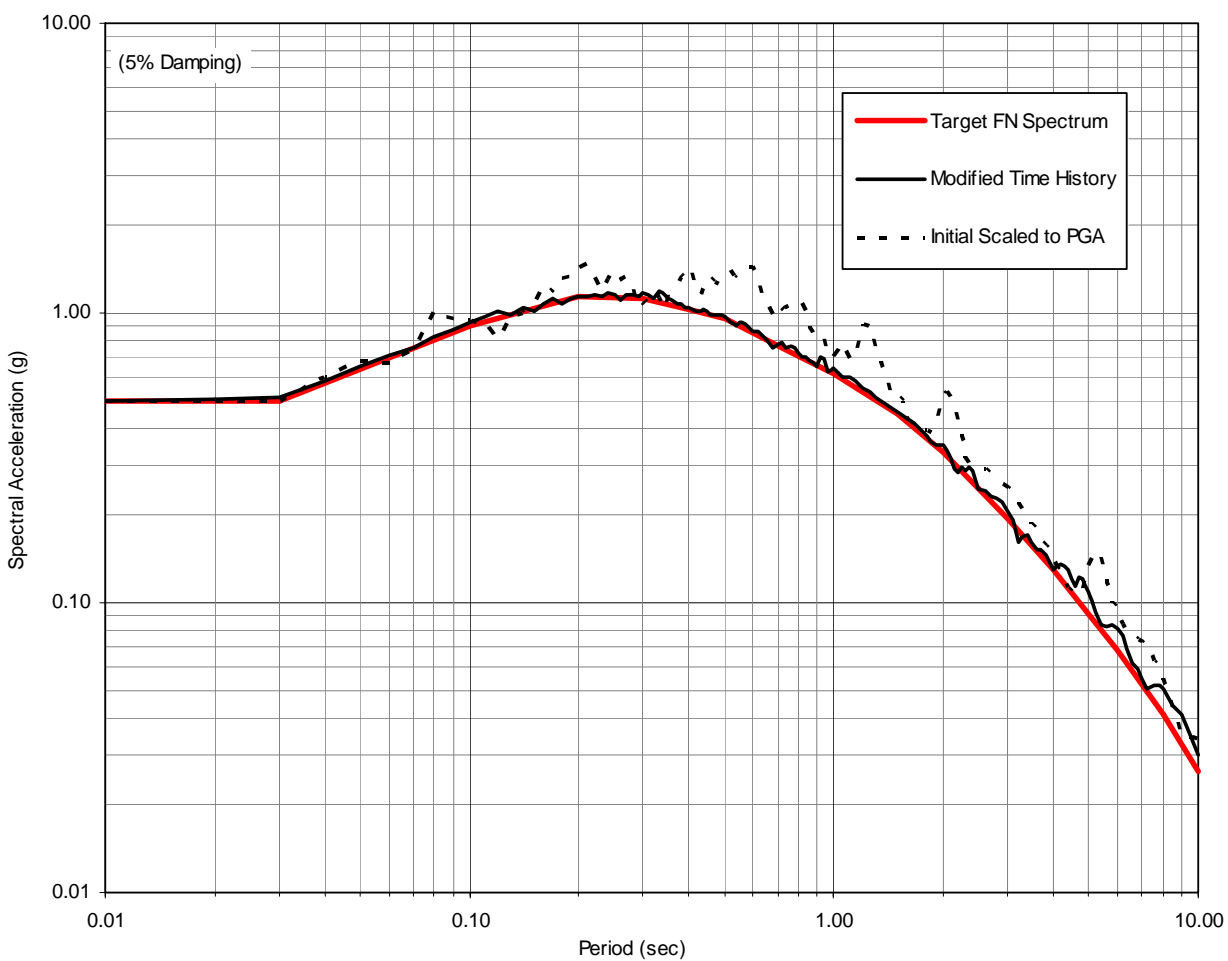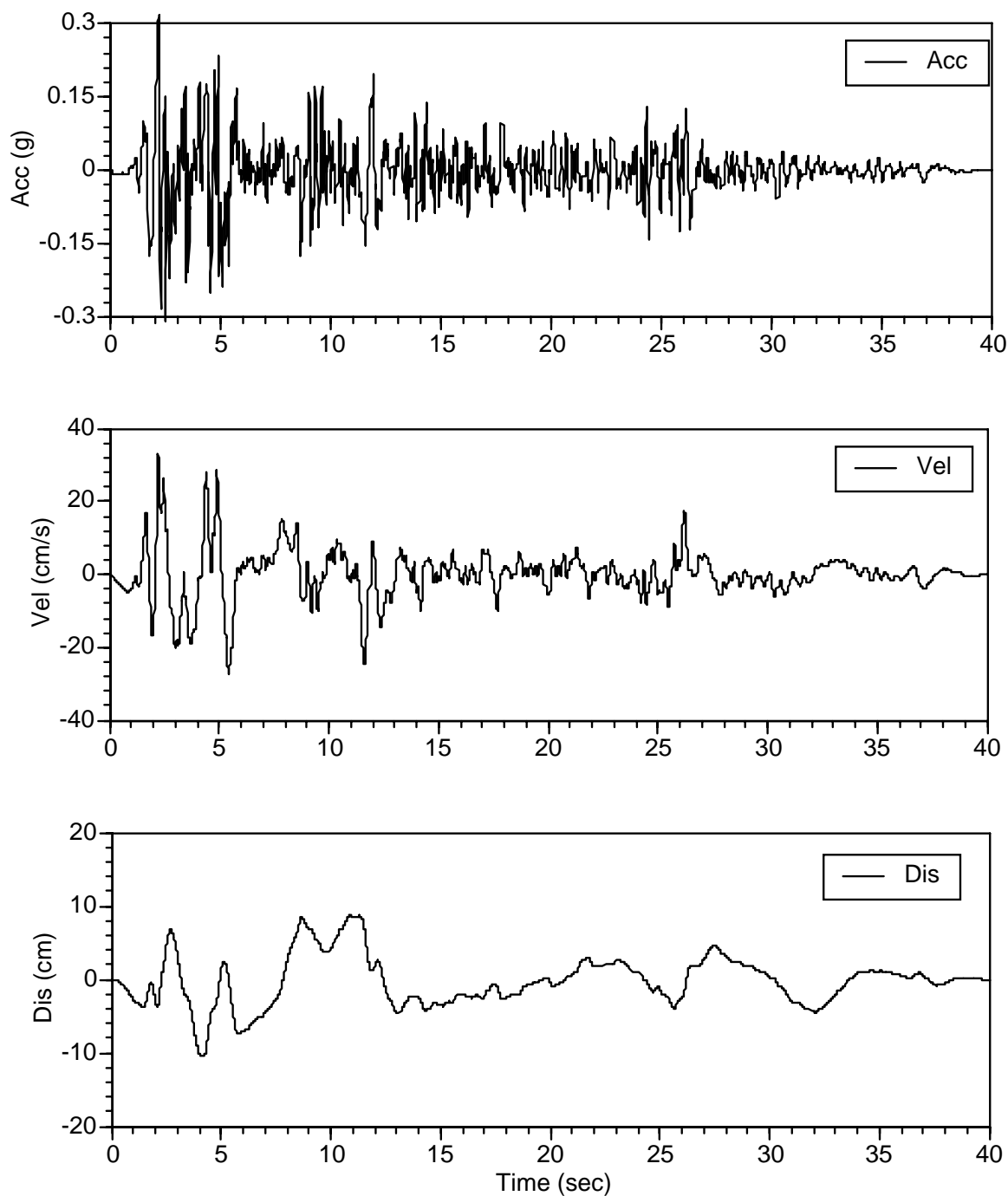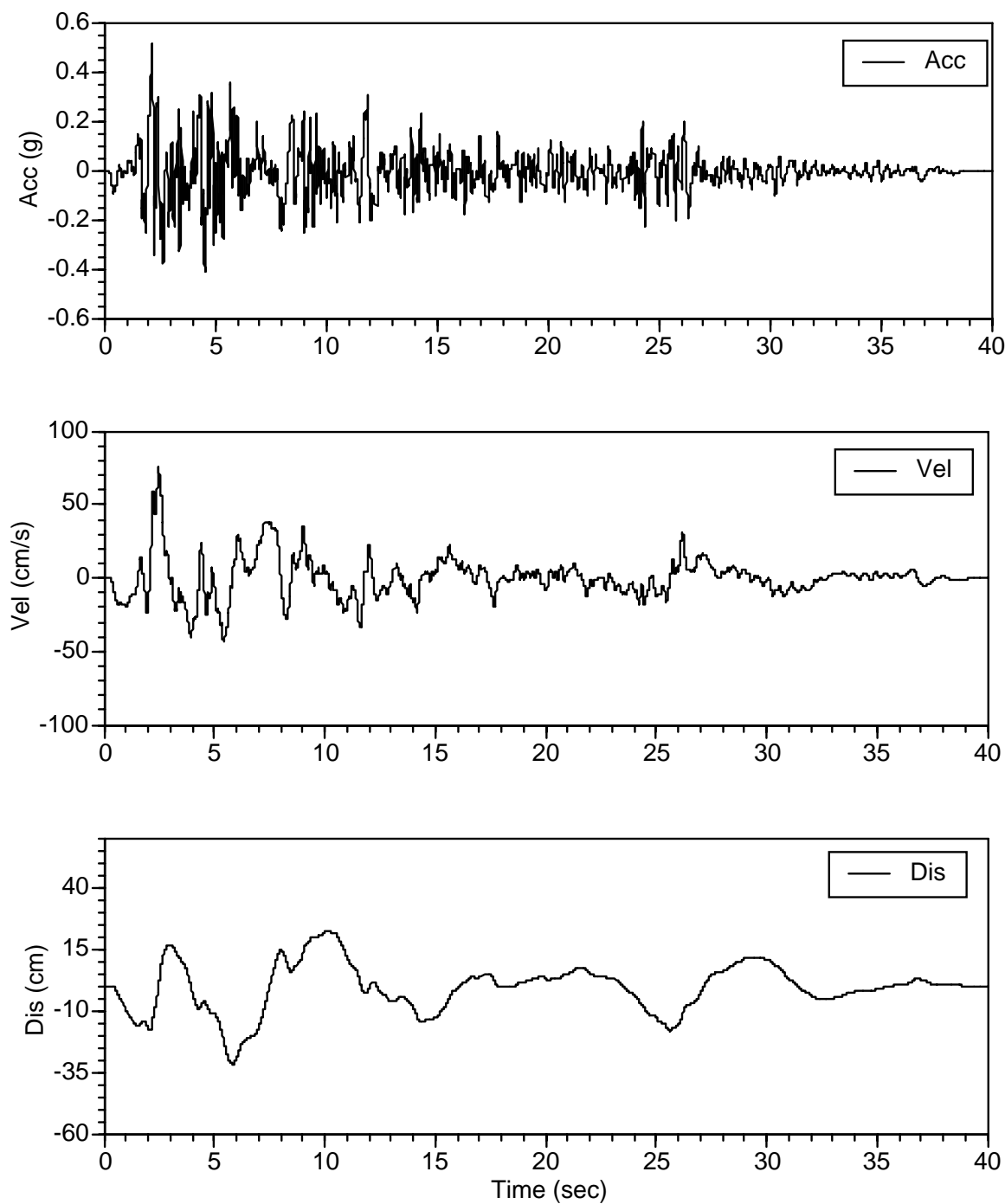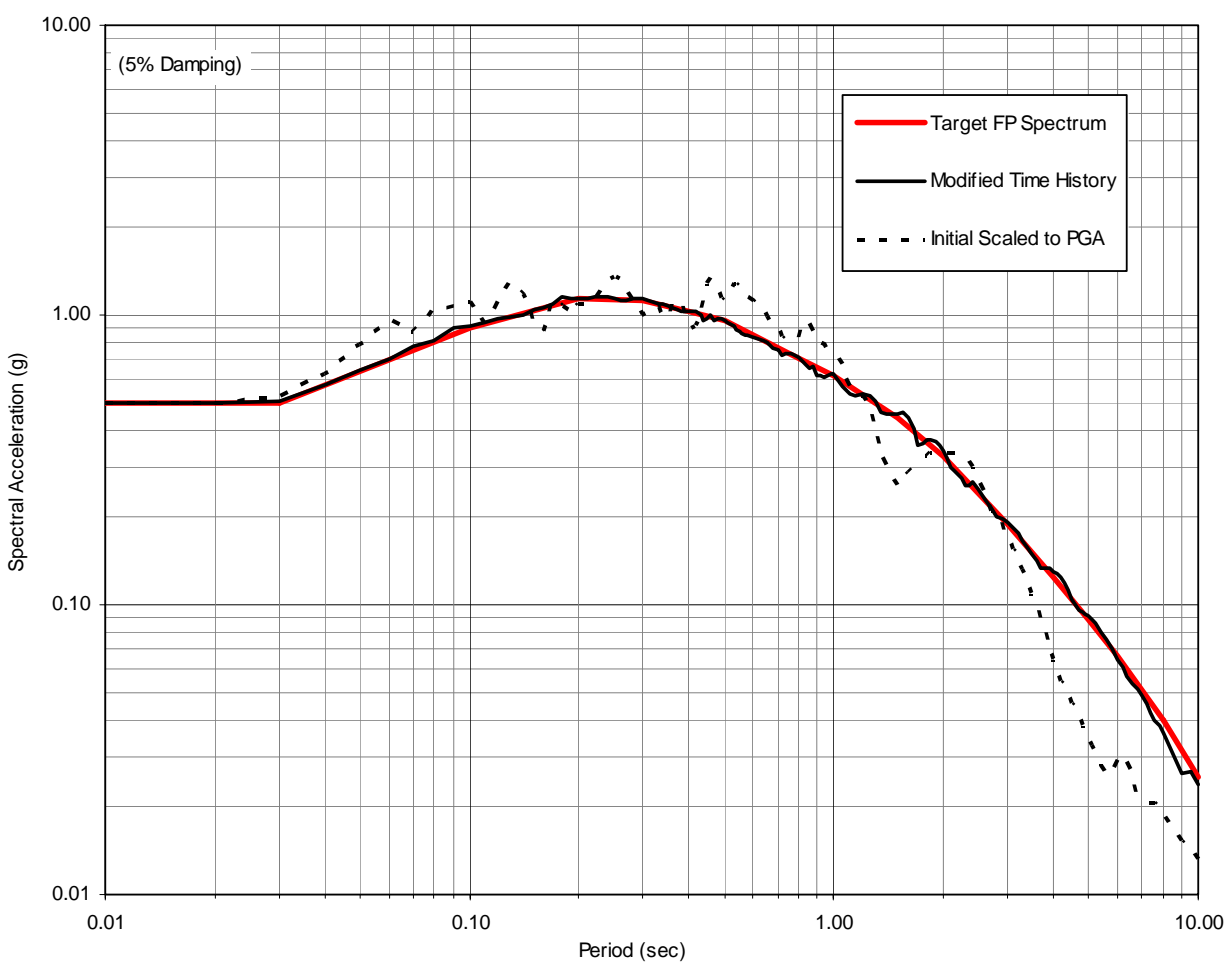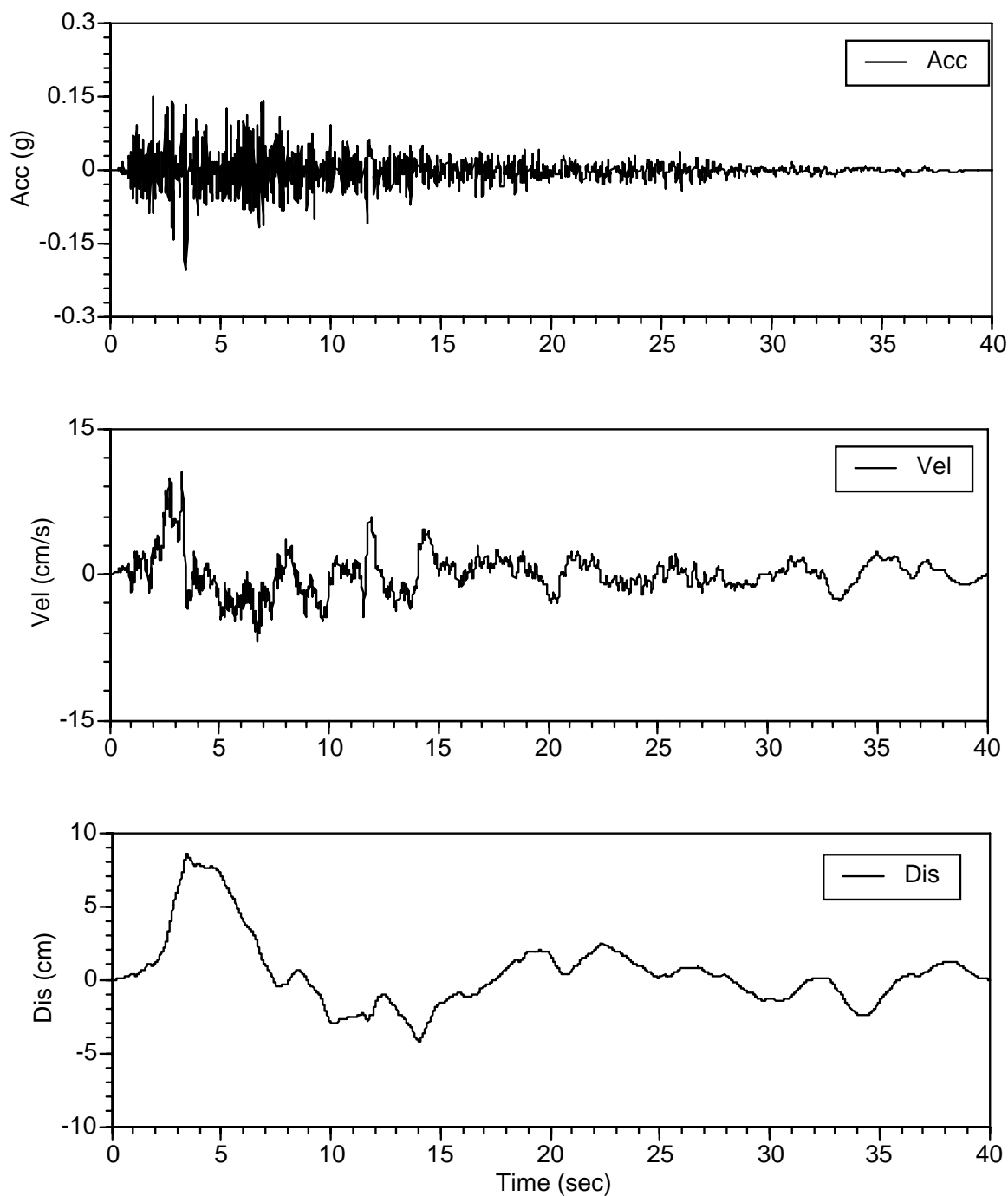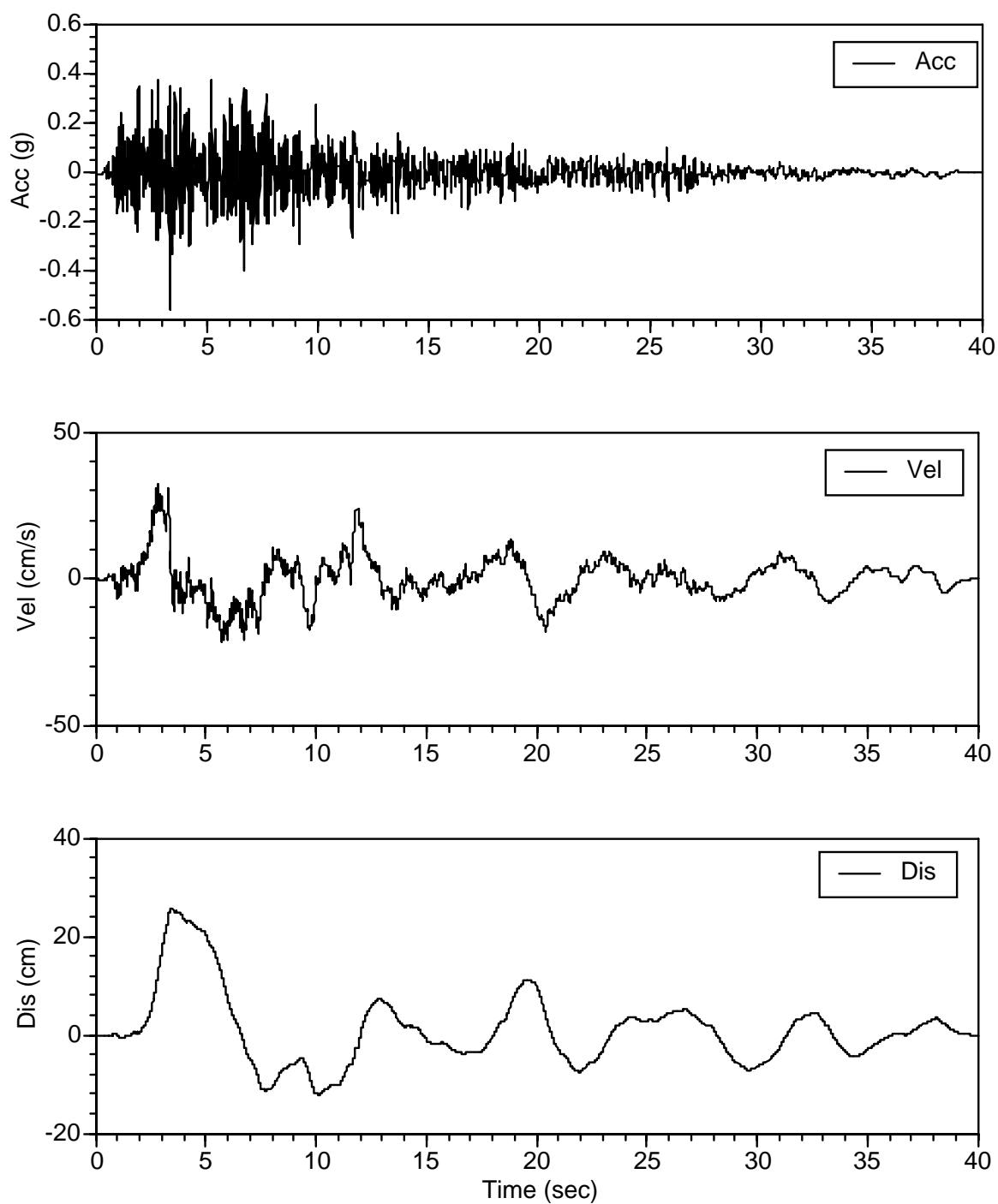**   (b) Modified Time History for FN Component**
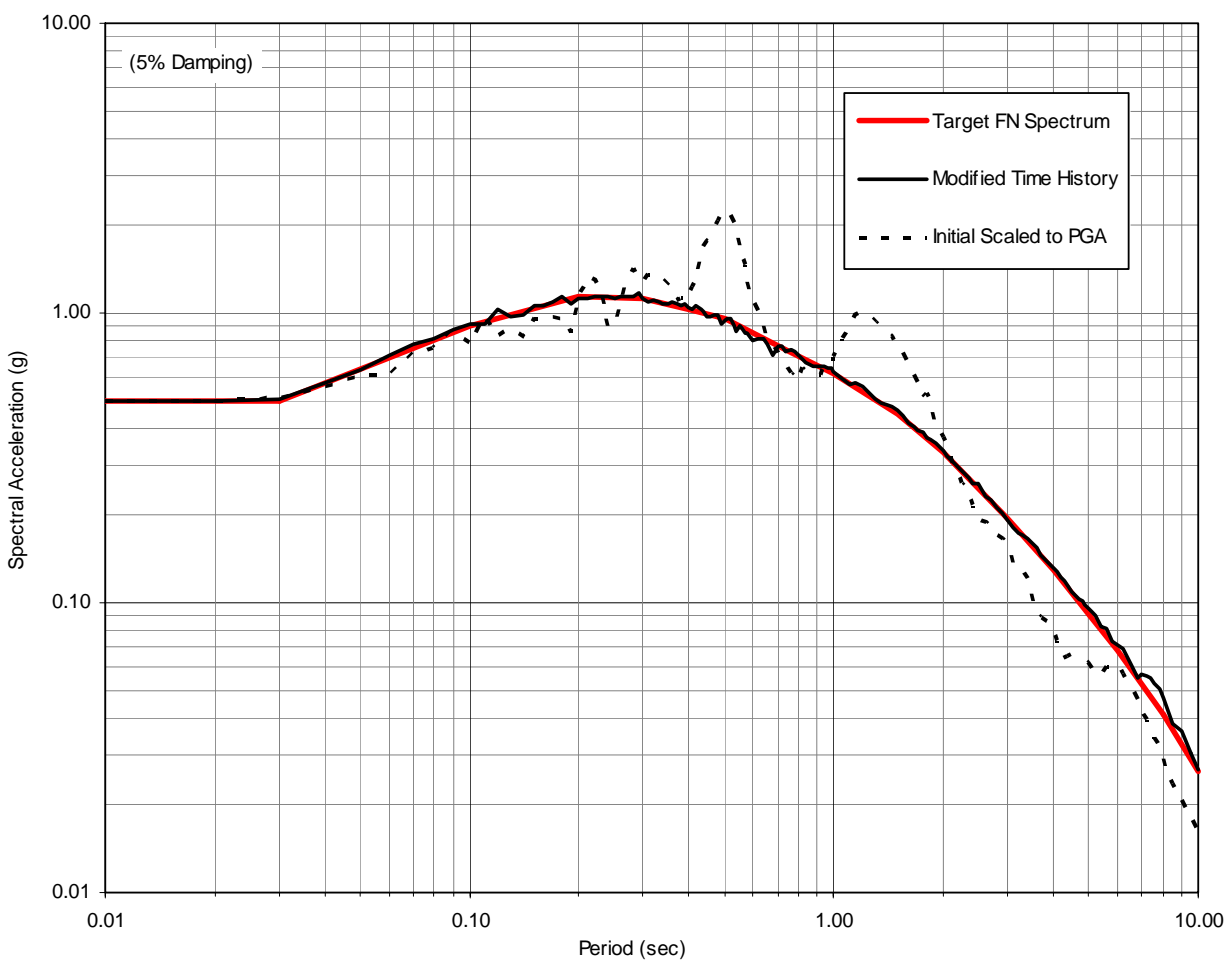
Figure D-1.   Firm-Ground Motions Compatible to CLE Firm-Ground Spectra, Set 1
(c) Comparison of Target Spectrum with Spectra of Scaled and Modified Time
Histories, FN Component
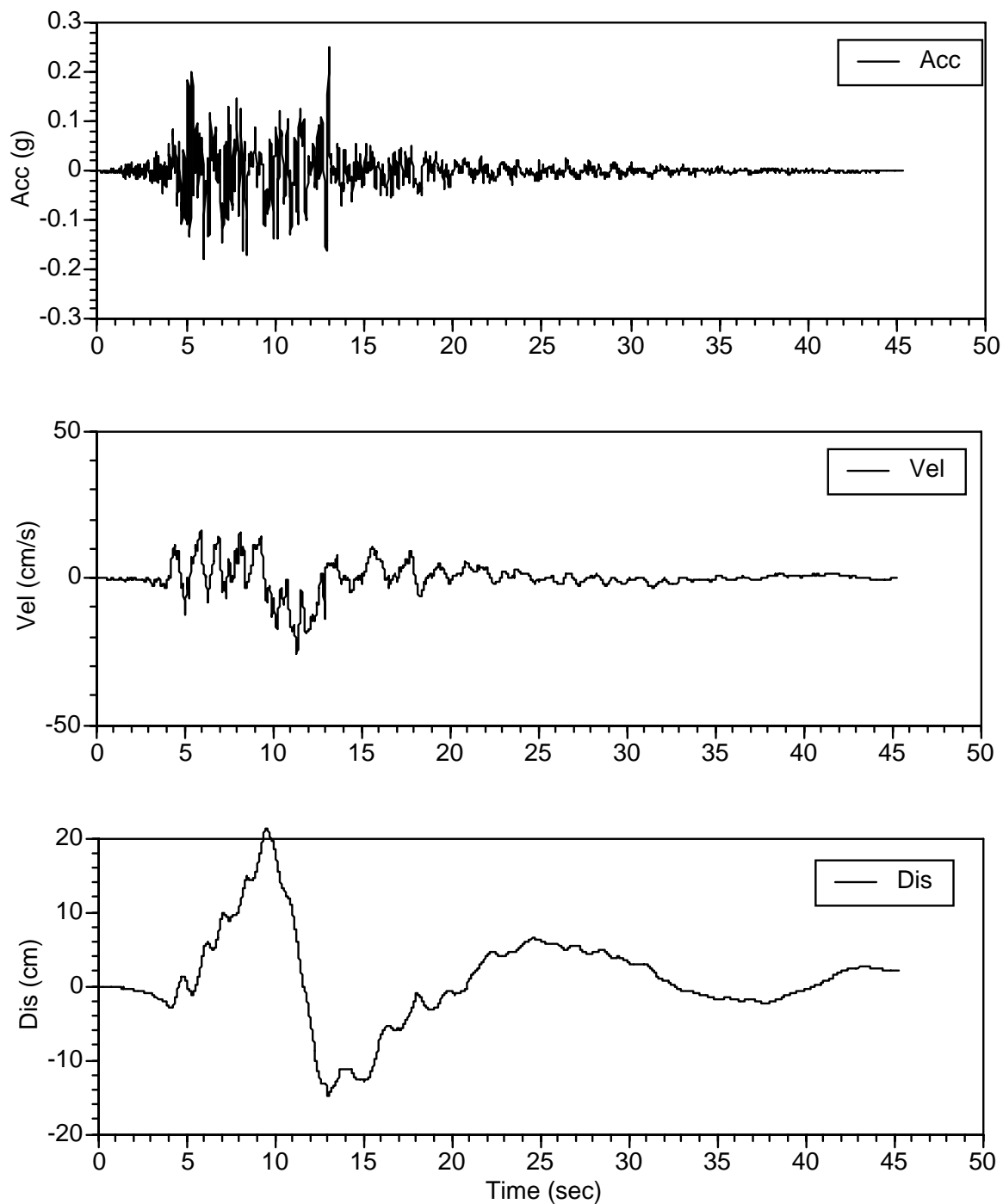
**Figure D-1.   Firm-Ground Time Histories Compatible to CLE Firm-Ground Spectra, Set 1
          (d) Initial Time History for FP Component**
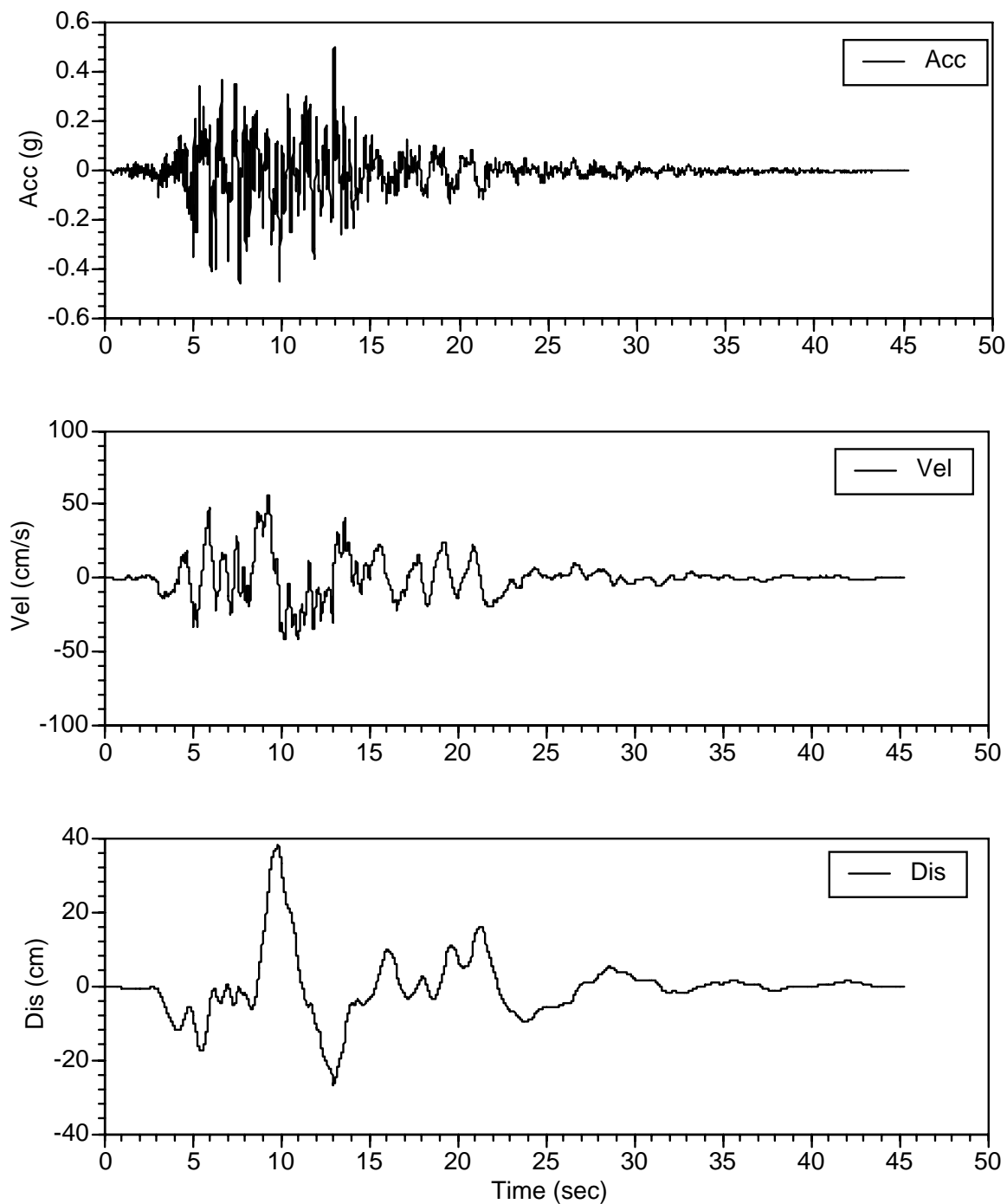
**Figure D-1.   Firm-Ground Time Histories Compatible to CLE Firm-Ground Spectra, Set 1
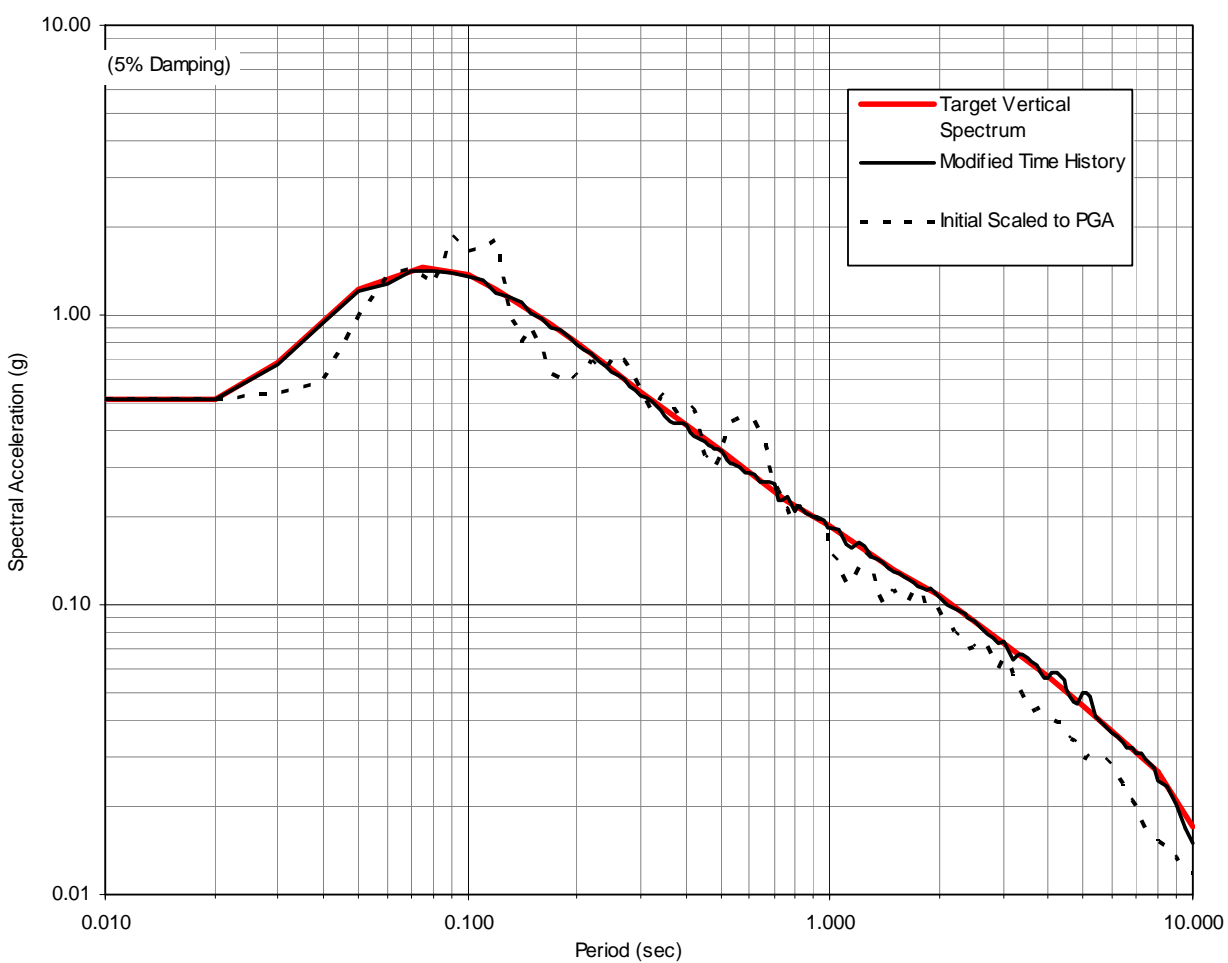   (e) Modified Time History for FP Component**
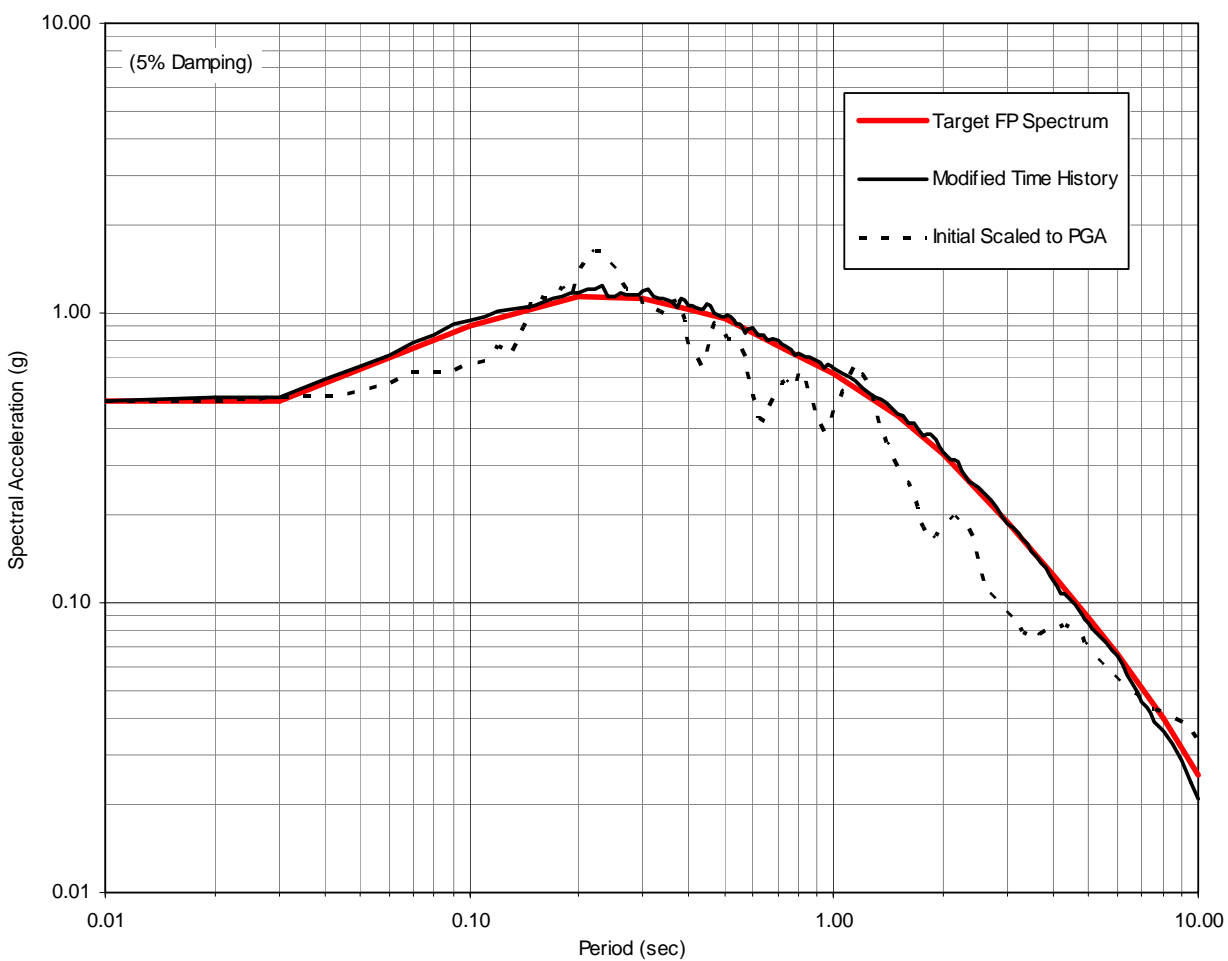
Figure D-1.   Firm-Ground Motions Compatible to CLE Firm-Ground Spectra, Set 1
(f) Comparison of Target Spectrum with Spectra of Scaled and Modified Time
Histories, FP Component
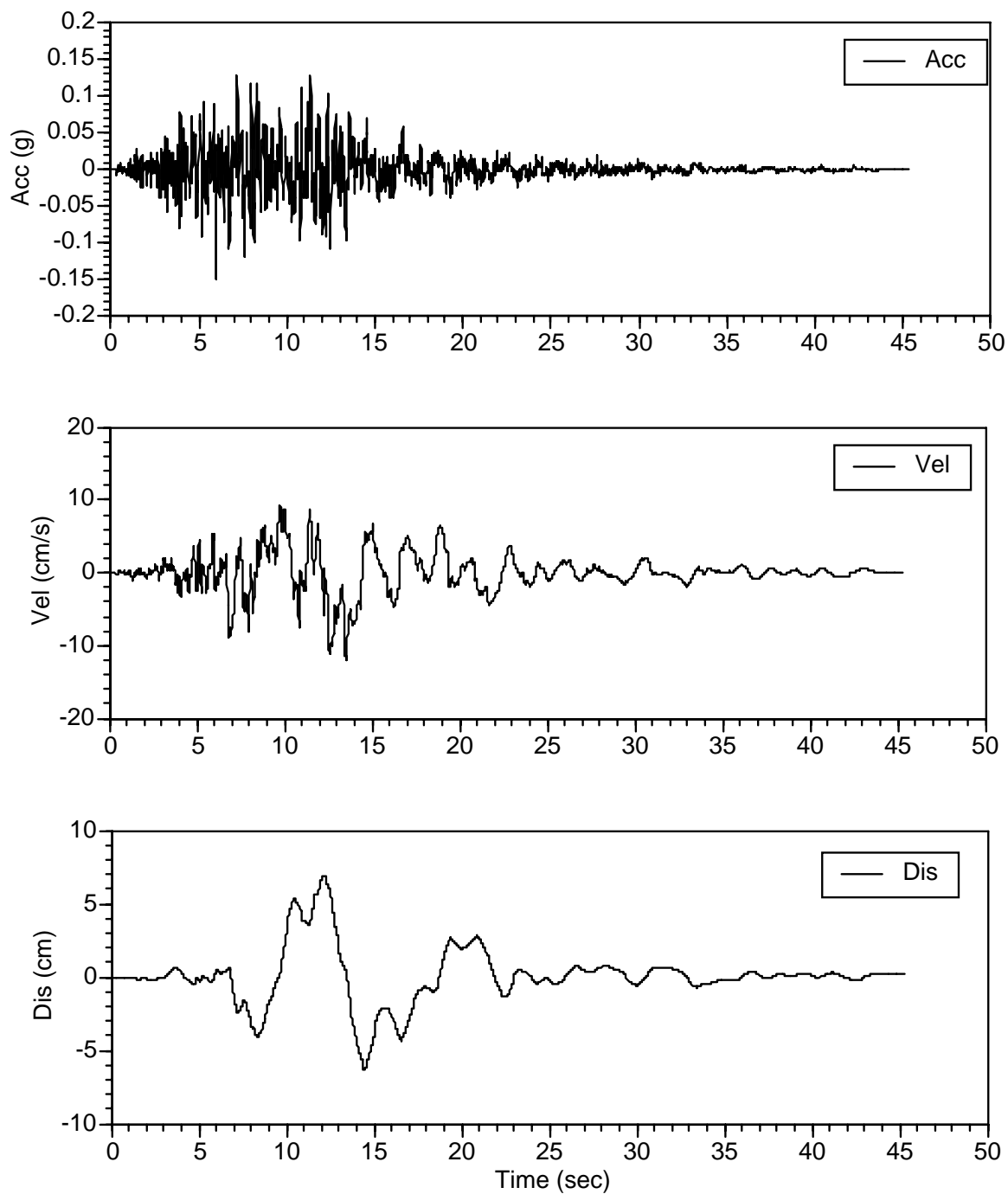
Figure D-1.   Firm-Ground Time Histories Compatible to CLE Firm-Ground Spectra, Set 1
**   (g) Initial Time History for FV Component**
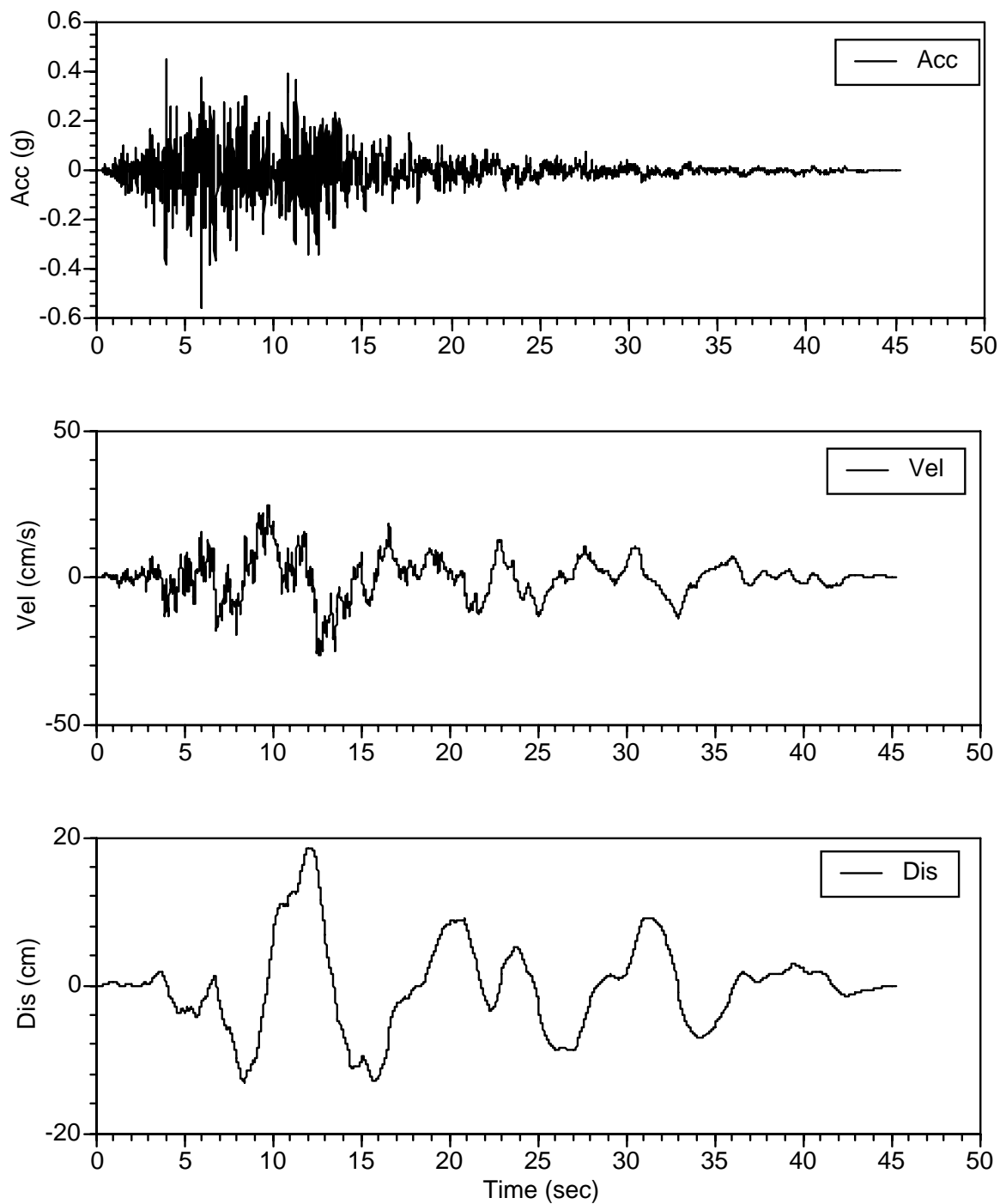
**Figure D-1. Firm-Ground Time Histories Compatible to CLE Firm-Ground Spectra, Set 1
(h) Modified Time History for FV Component**
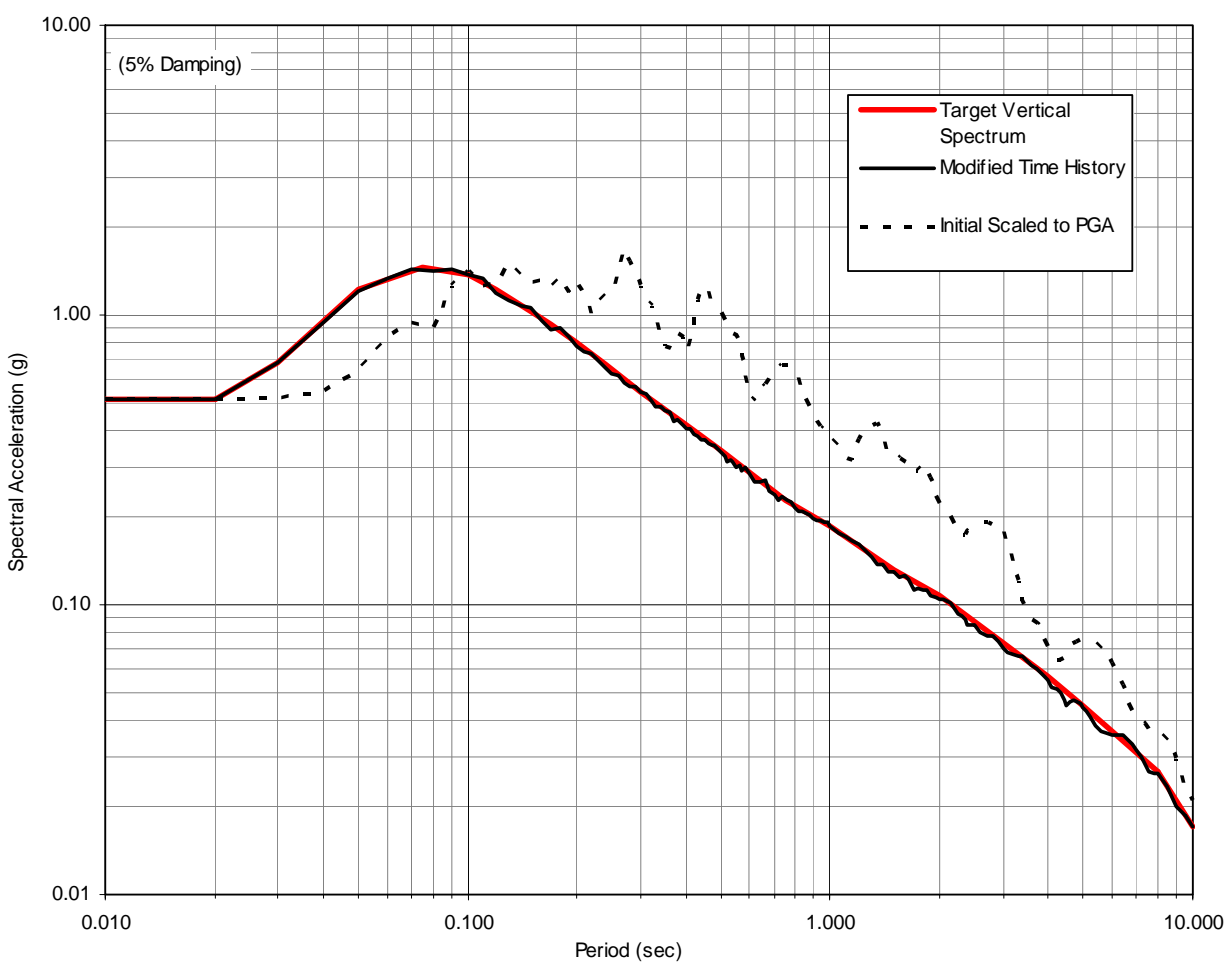
**Figure D-1.   Firm-Ground Motions Compatible to CLE Firm-Ground Spectra, Set 1
(i) Comparison of Target Spectrum with Spectra of Scaled and Modified Time
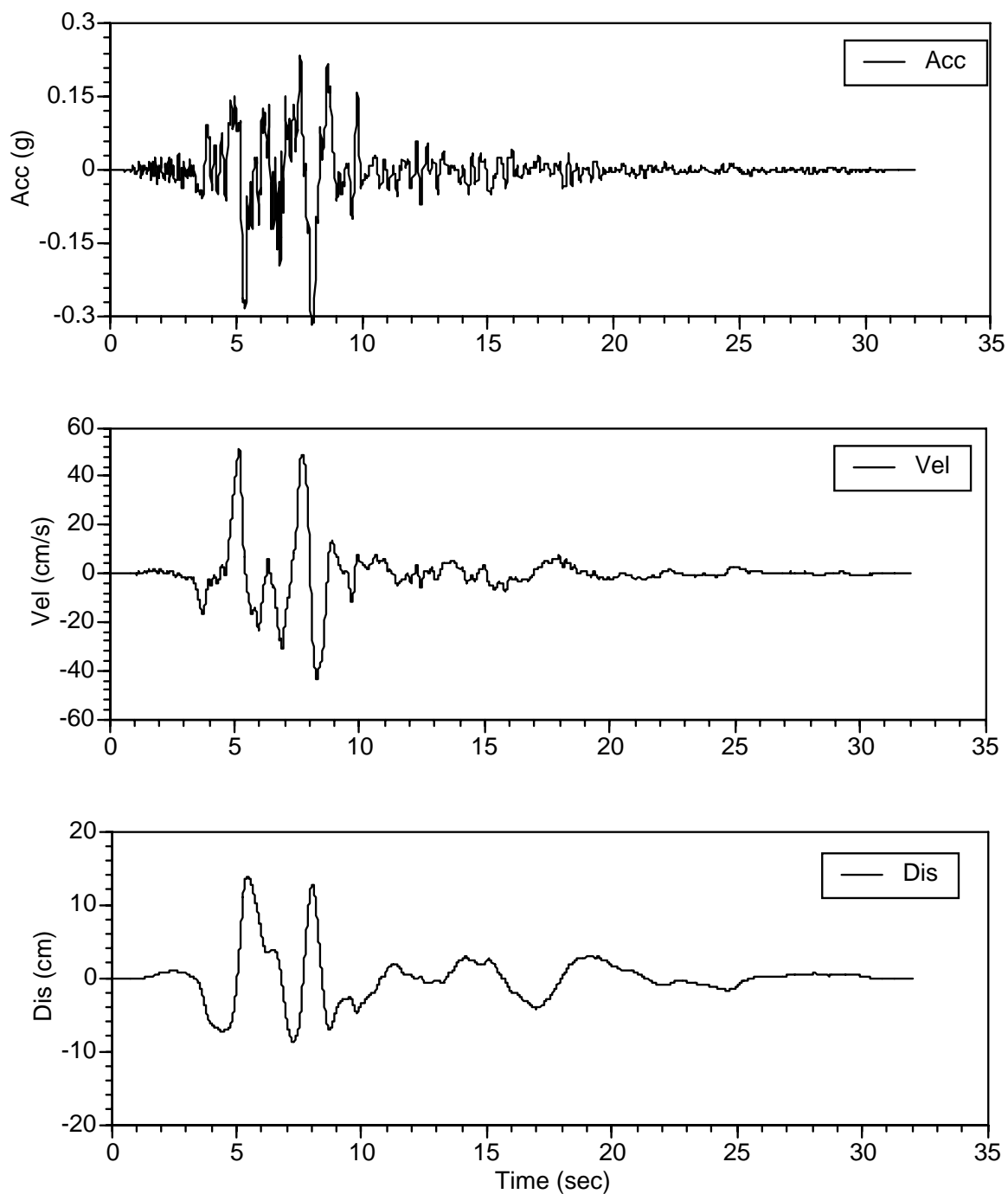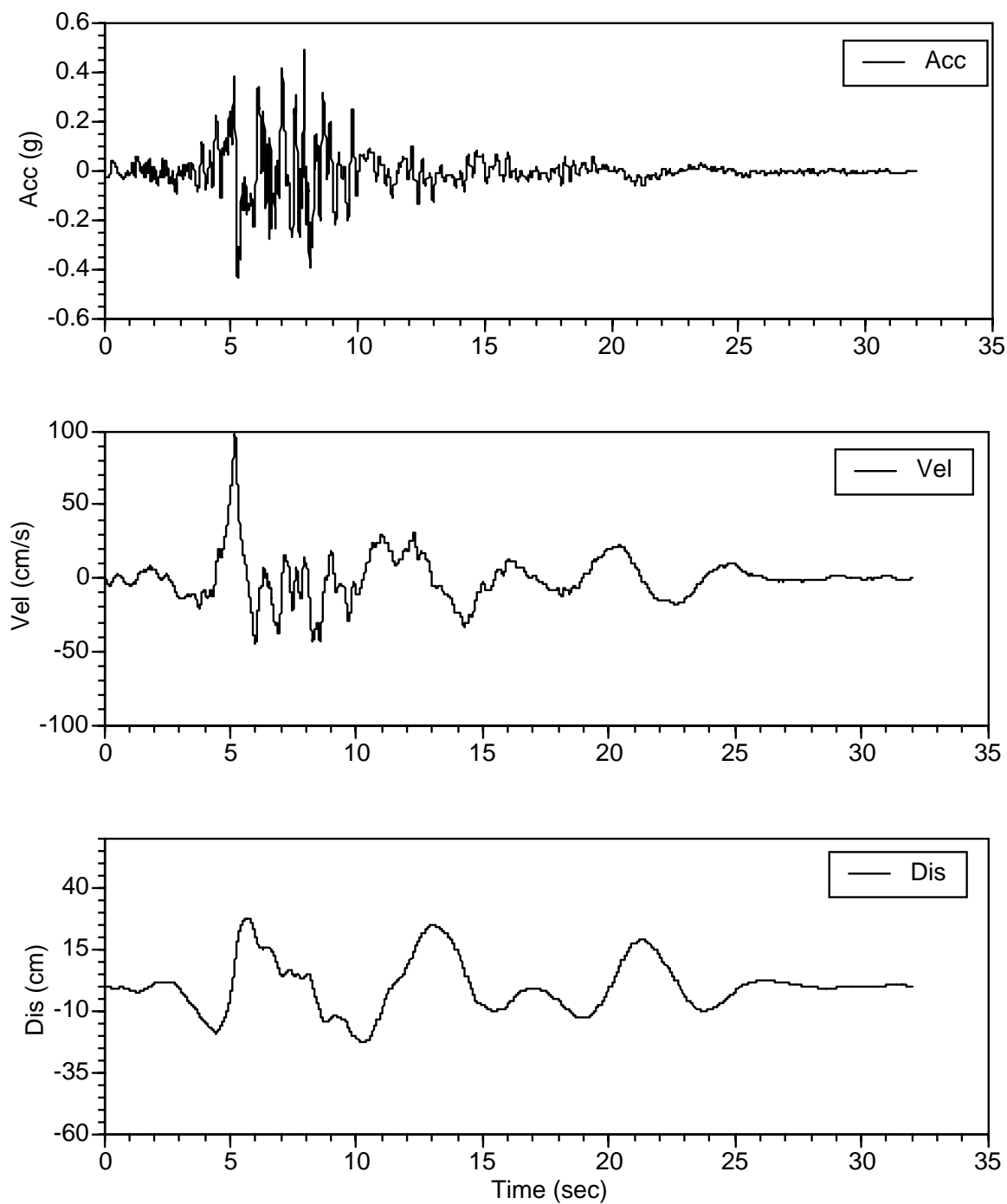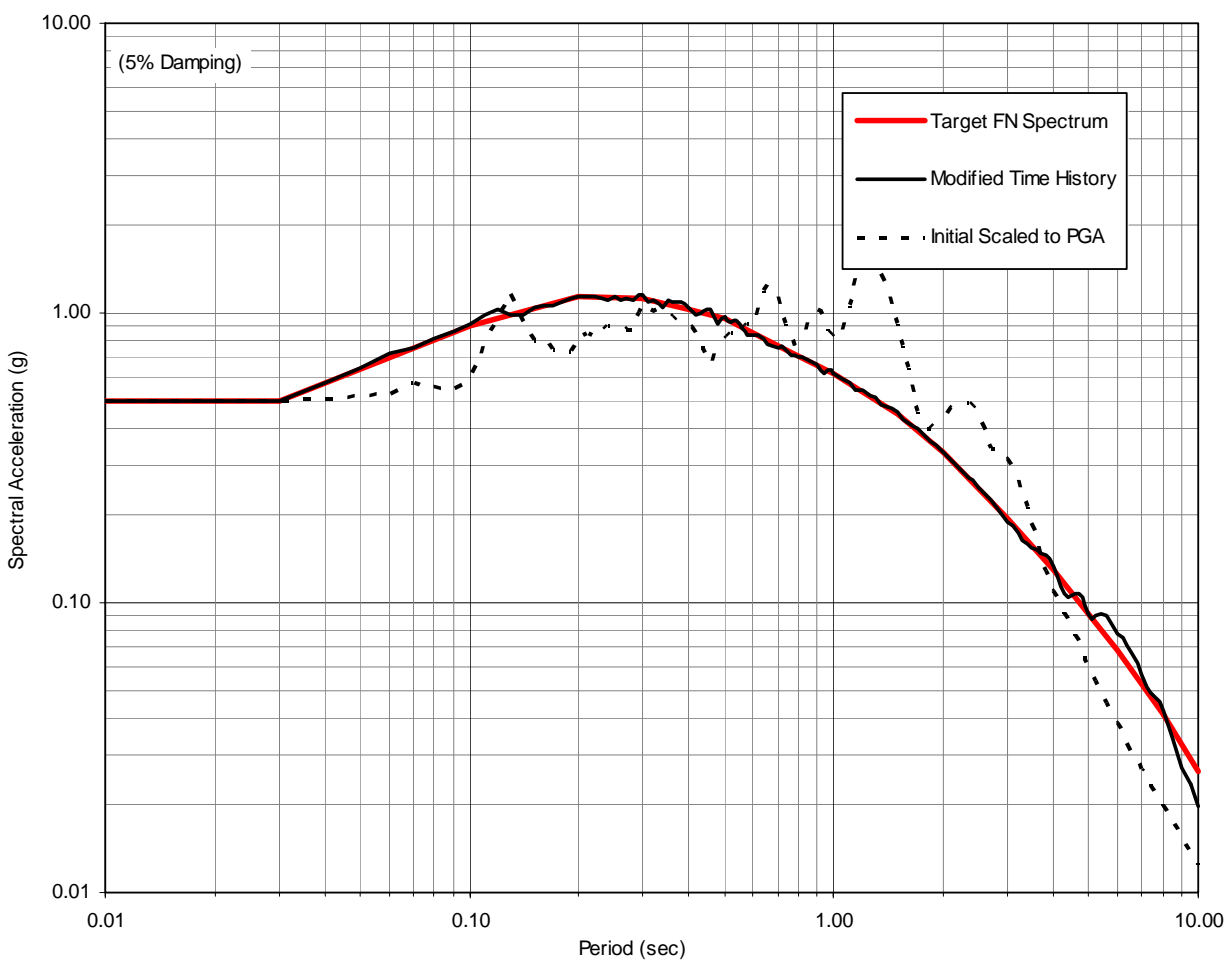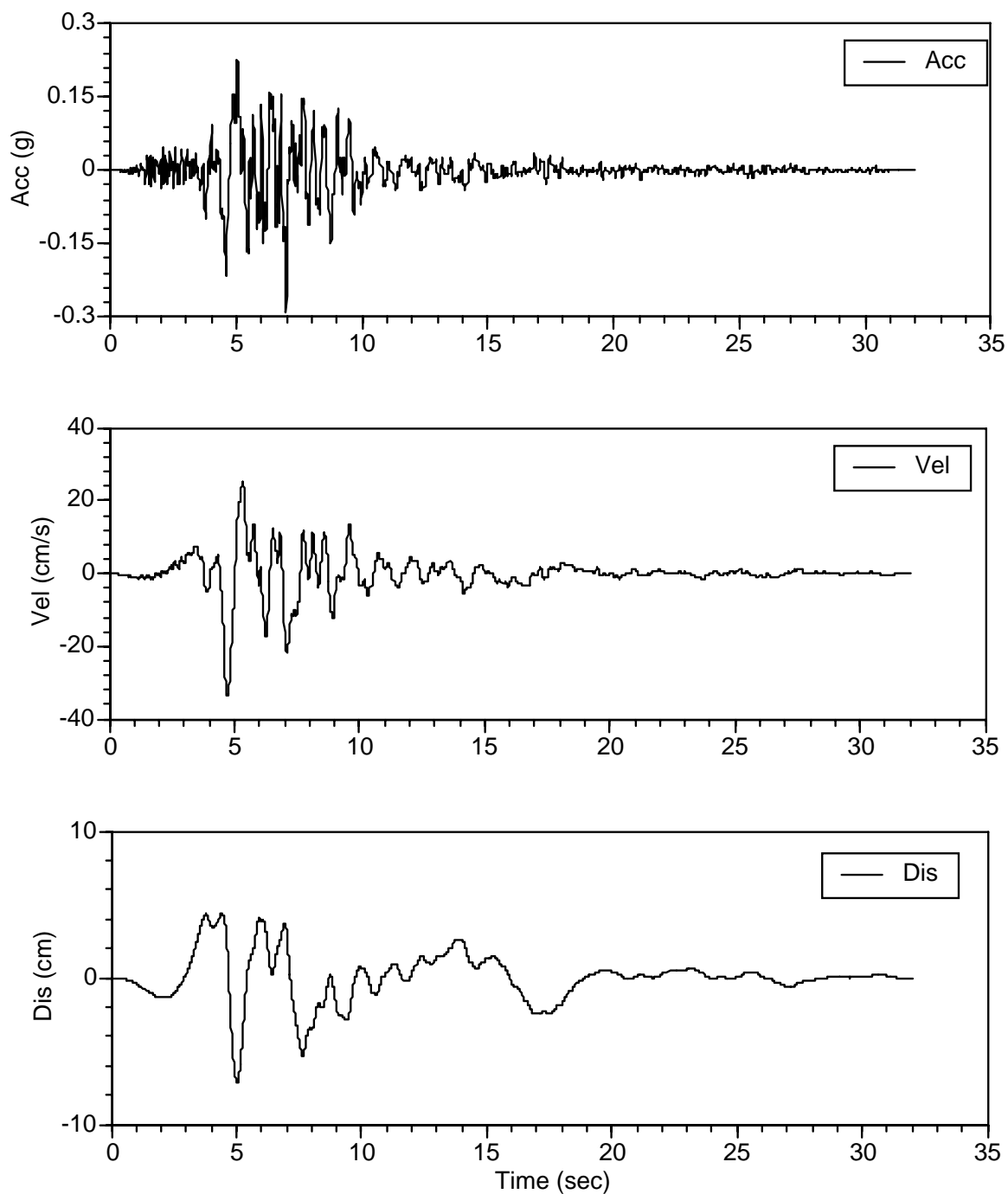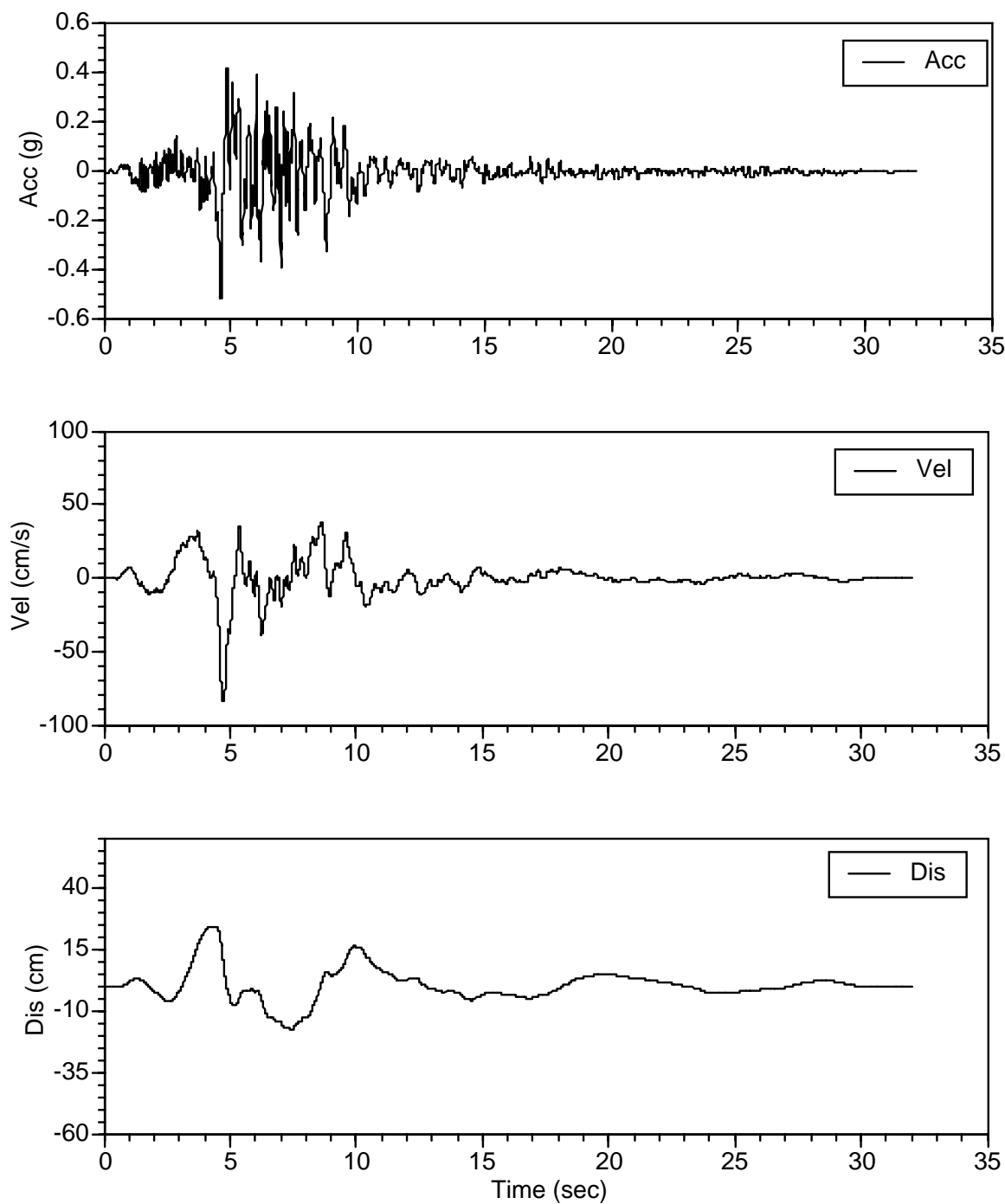Histories, FV Component**
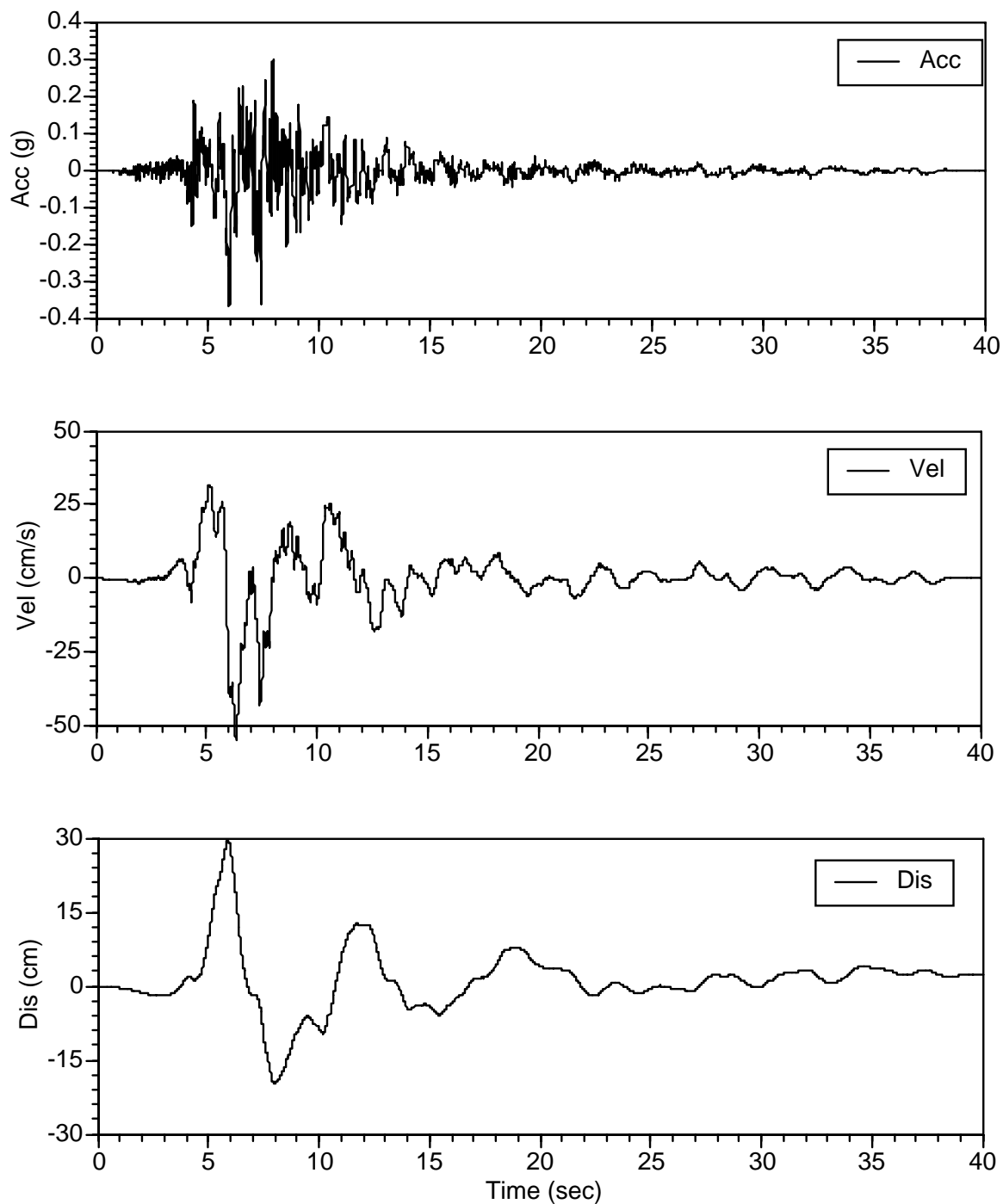
Figure D-2.   **Firm-Ground Time Histories Compatible to CLE Firm-Ground Spectra, Set 2**
            (a) Initial Time History for FN Component
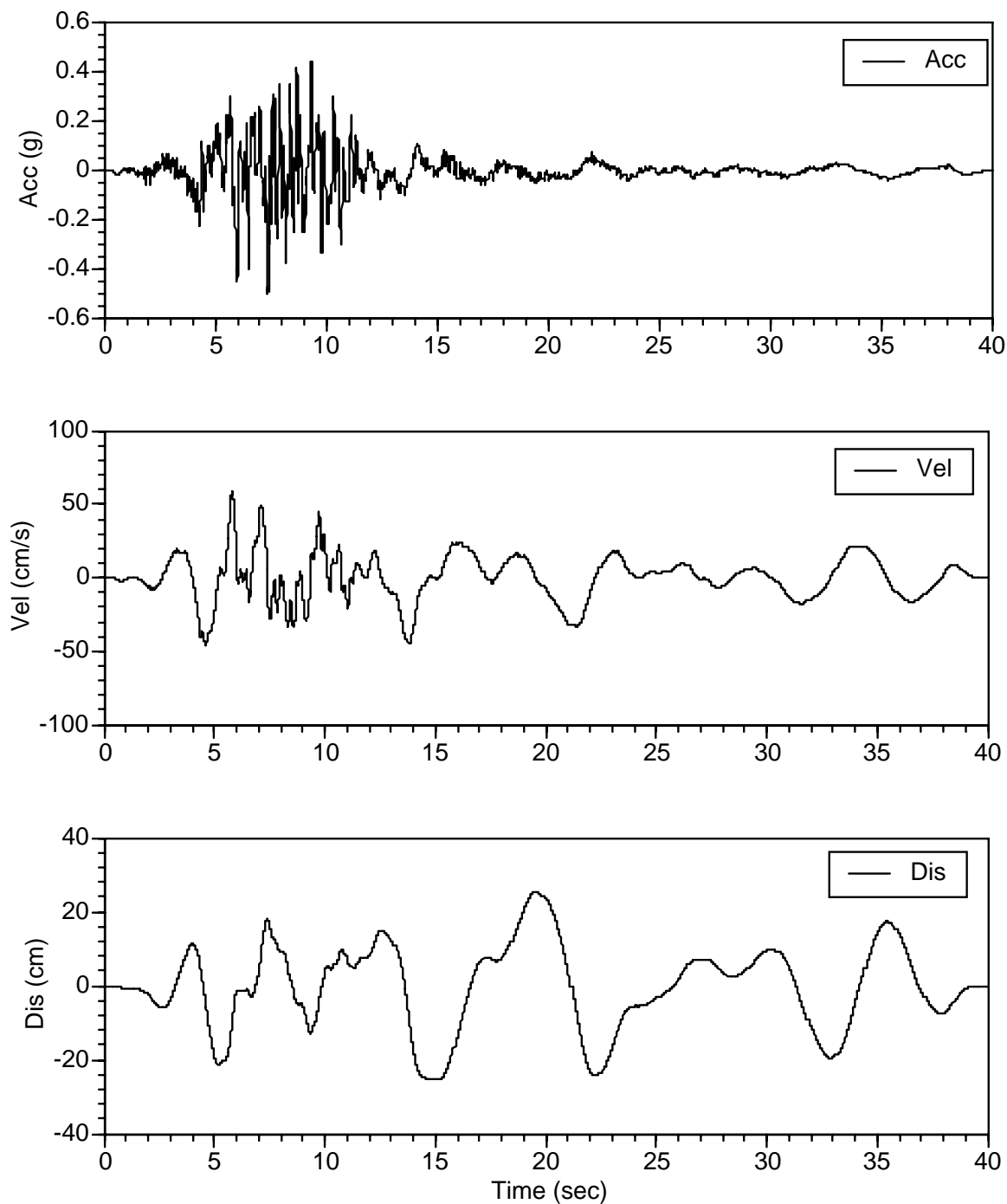
Figure D-2. **Firm-Ground Time Histories Compatible to CLE Firm-Ground Spectra, Set 2**
(b) Modified Time History for FN Component
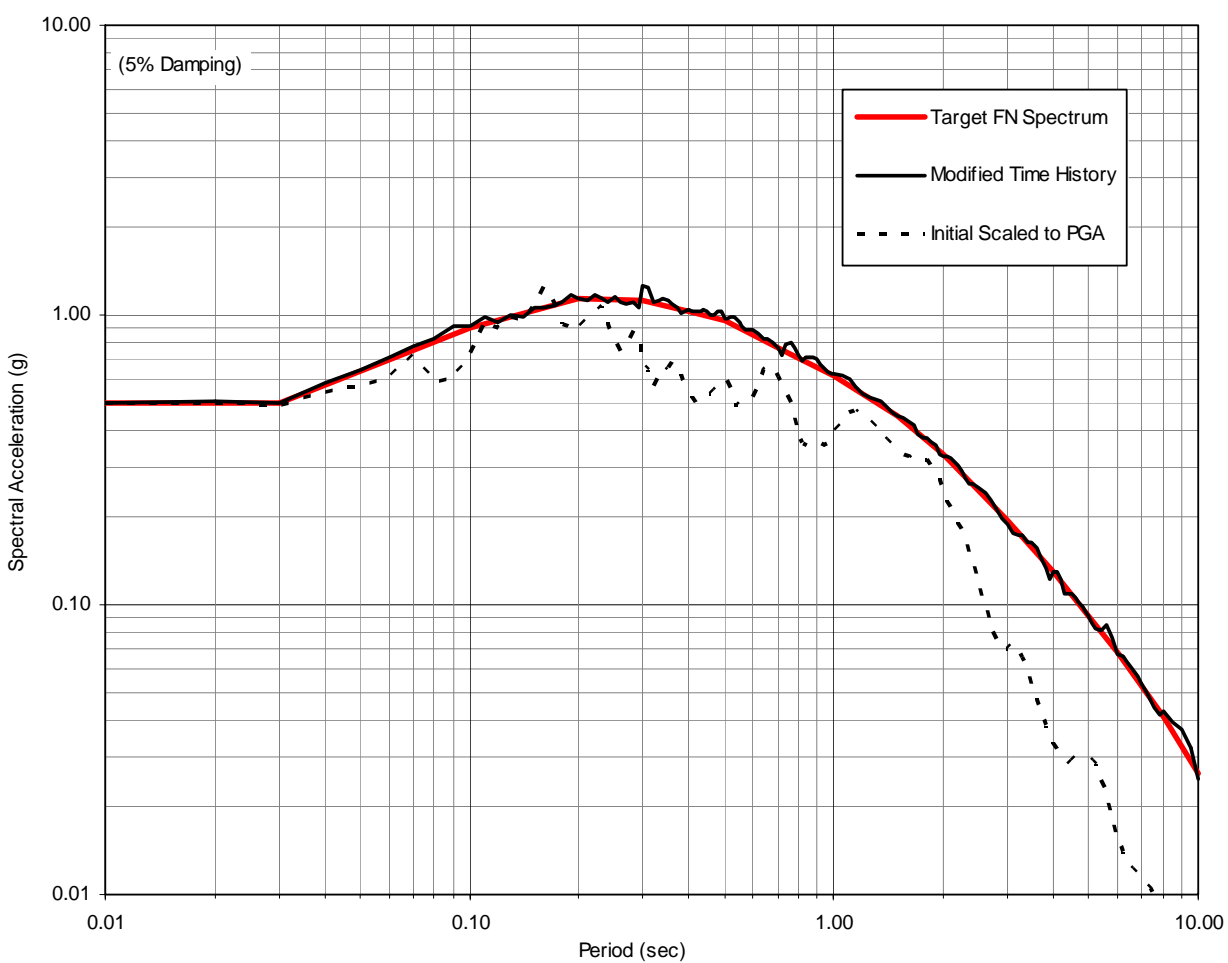
Figure D-2.　**Firm-Ground Motions Compatible to CLE Firm-Ground Spectra, Set 2**
　　　　　　　(c) Comparison of Target Spectrum with Spectra of Scaled and Modified Time
　　　　　　　Histories, FN Component
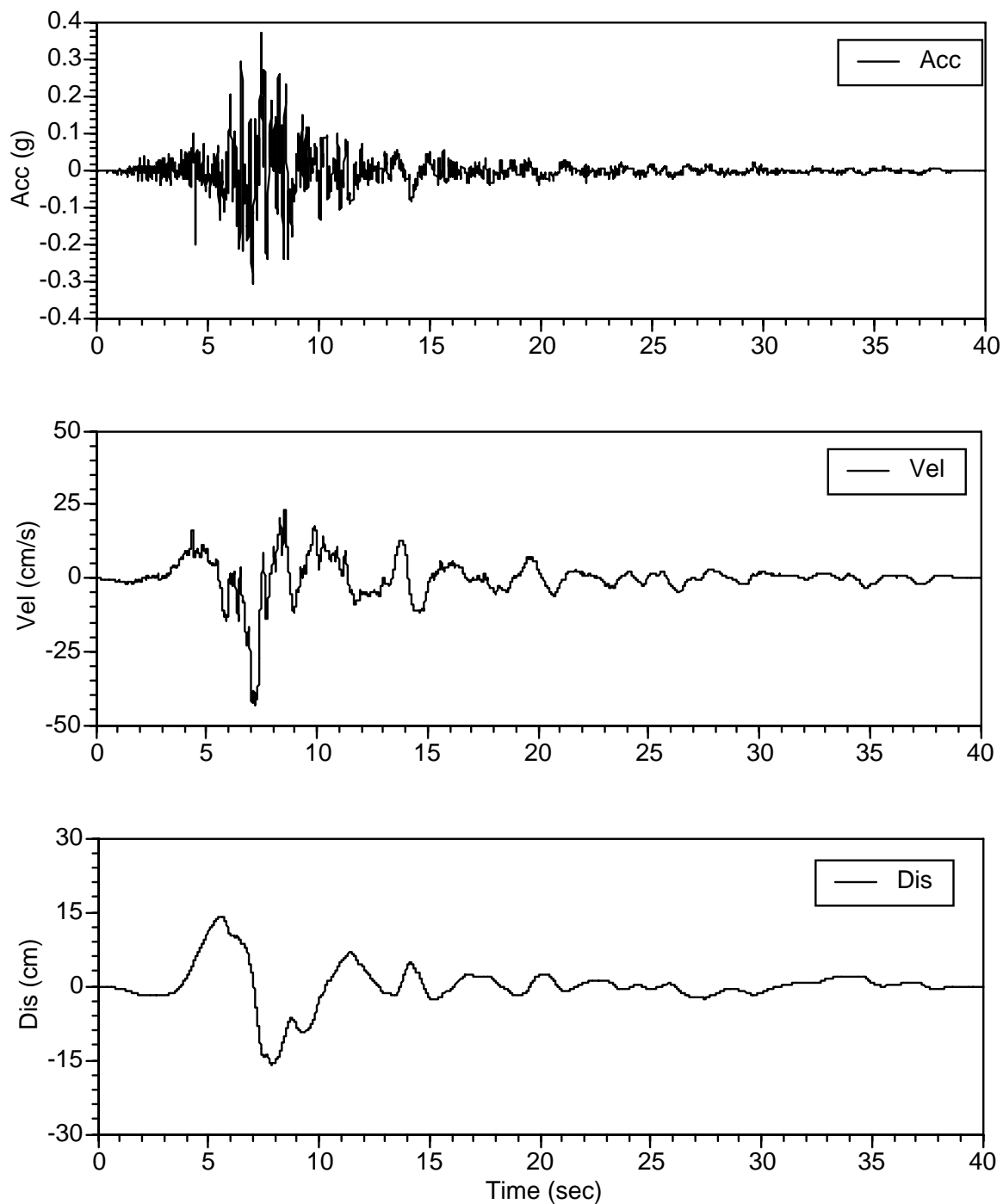
Figure D-2. **Firm-Ground Time Histories Compatible to CLE Firm-Ground Spectra, Set 1**
(d) Initial Time History for FP Component
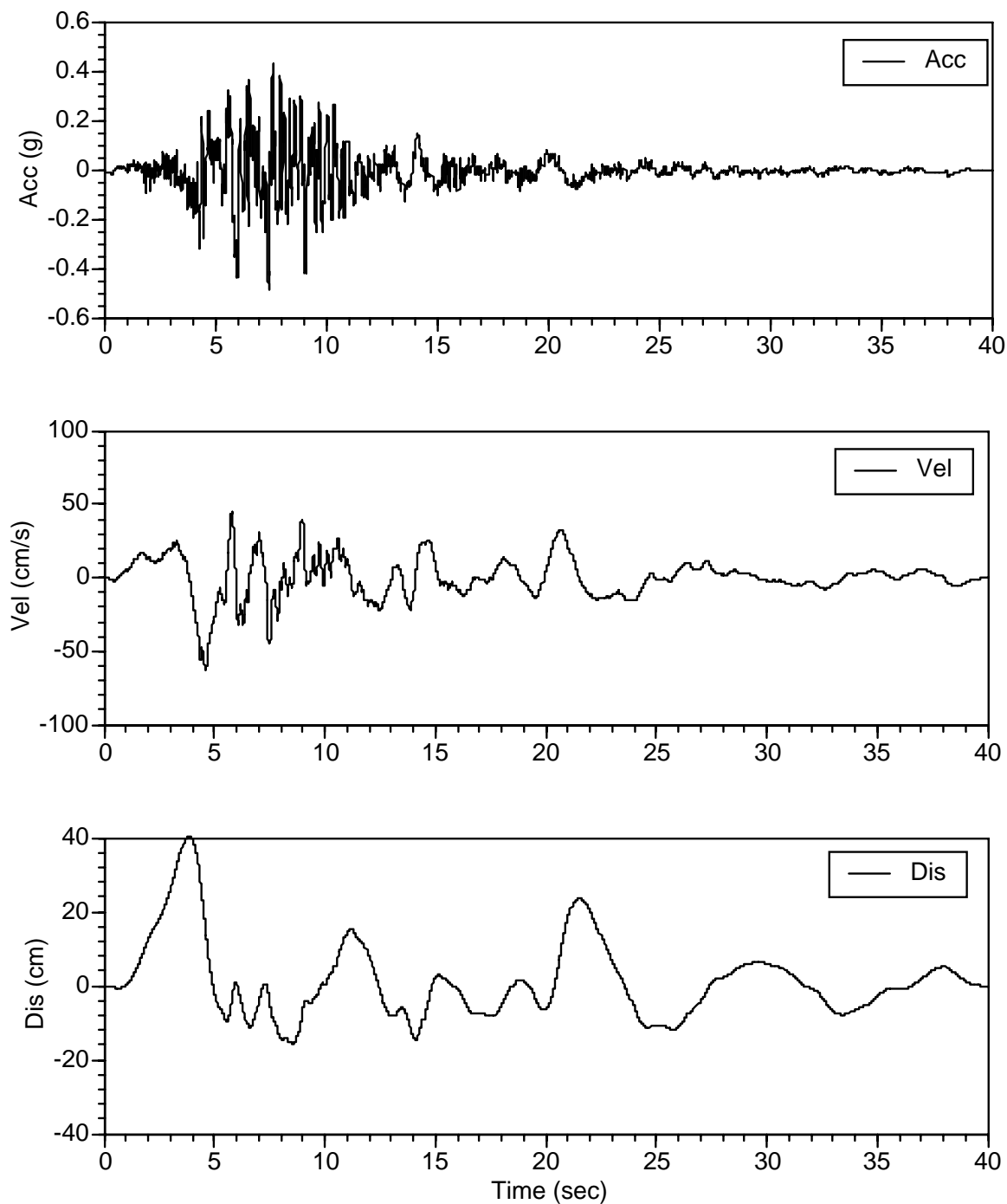
**Figure D-2. Firm-Ground Time Histories Compatible to CLE Firm-Ground Spectra, Set 2
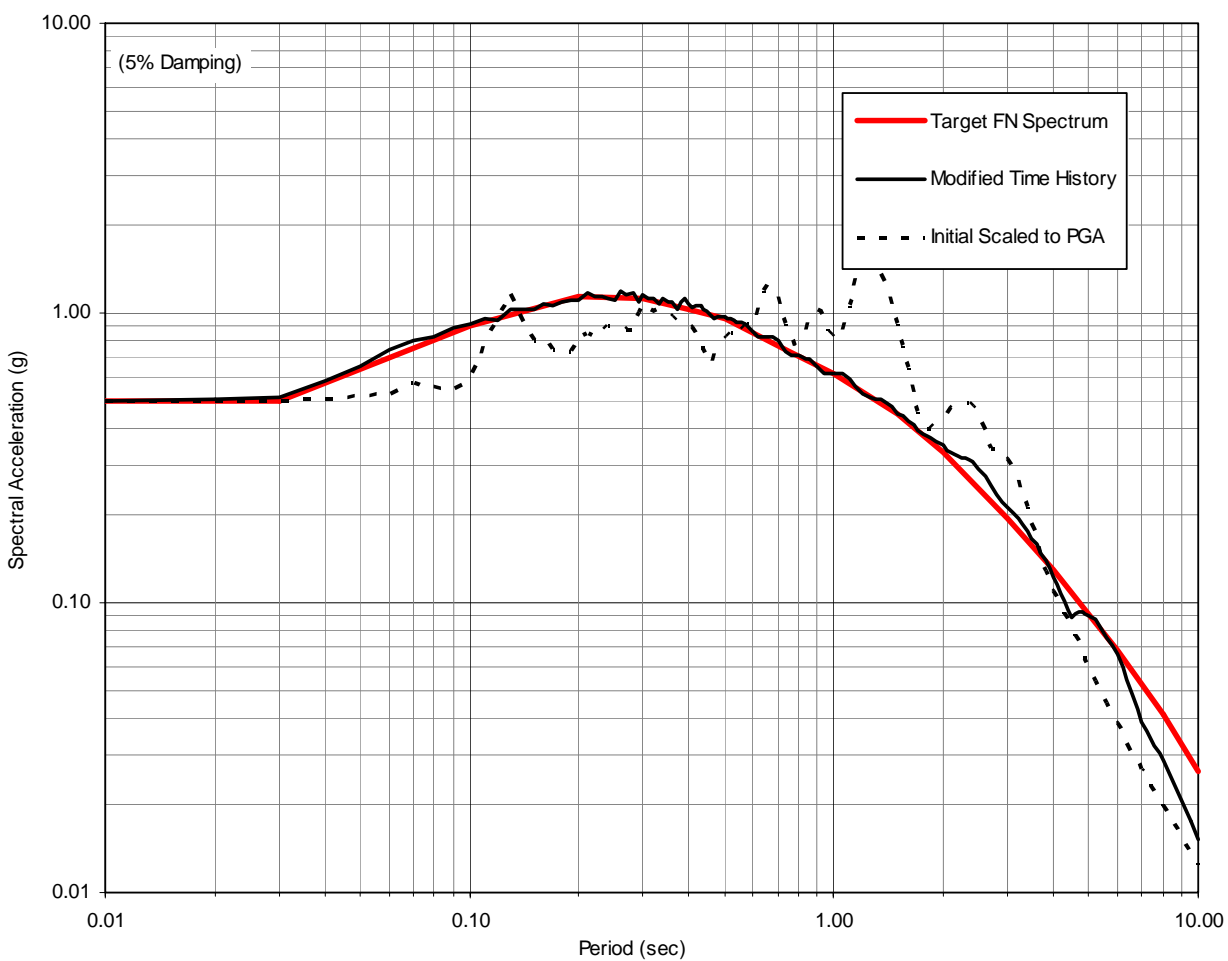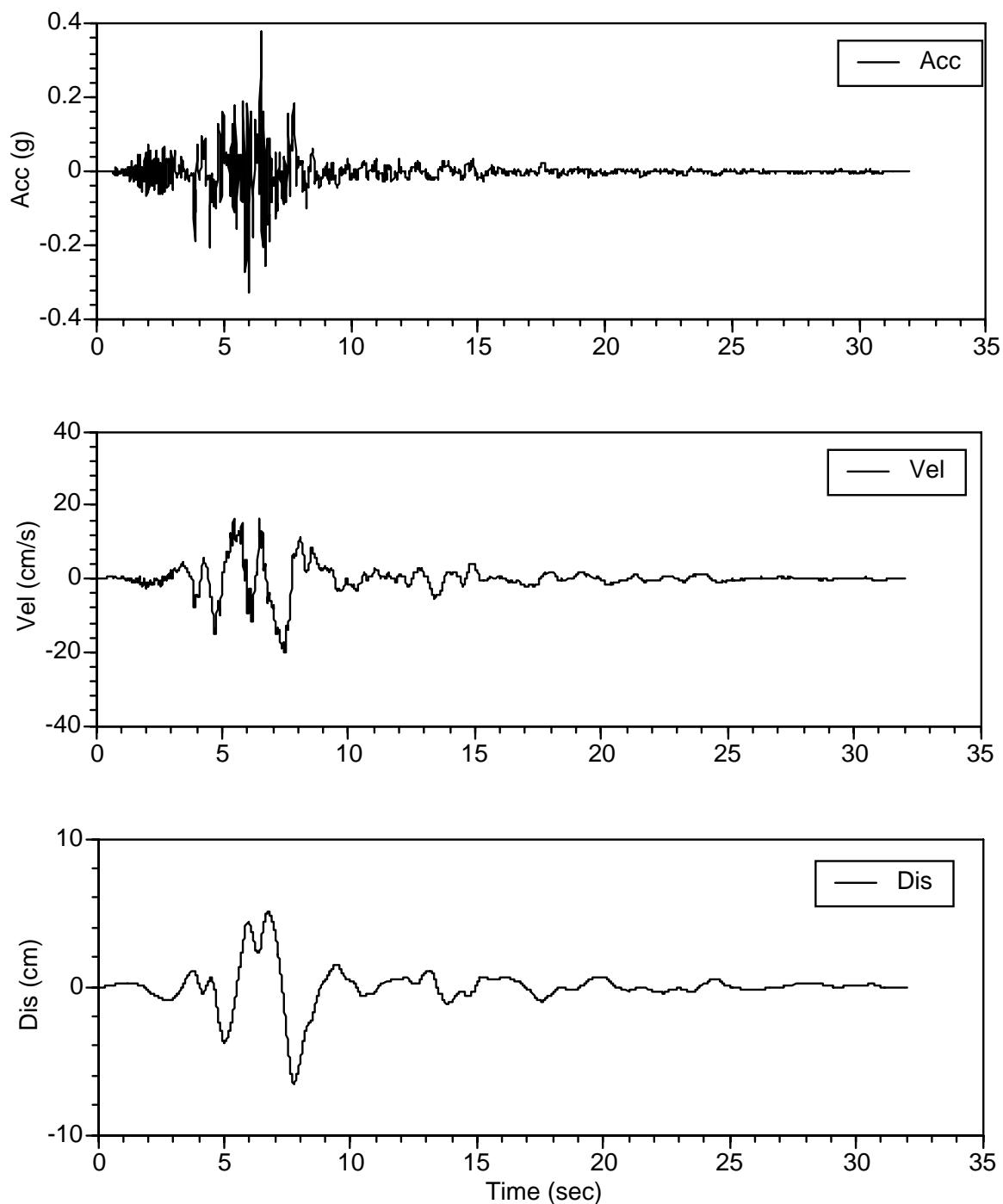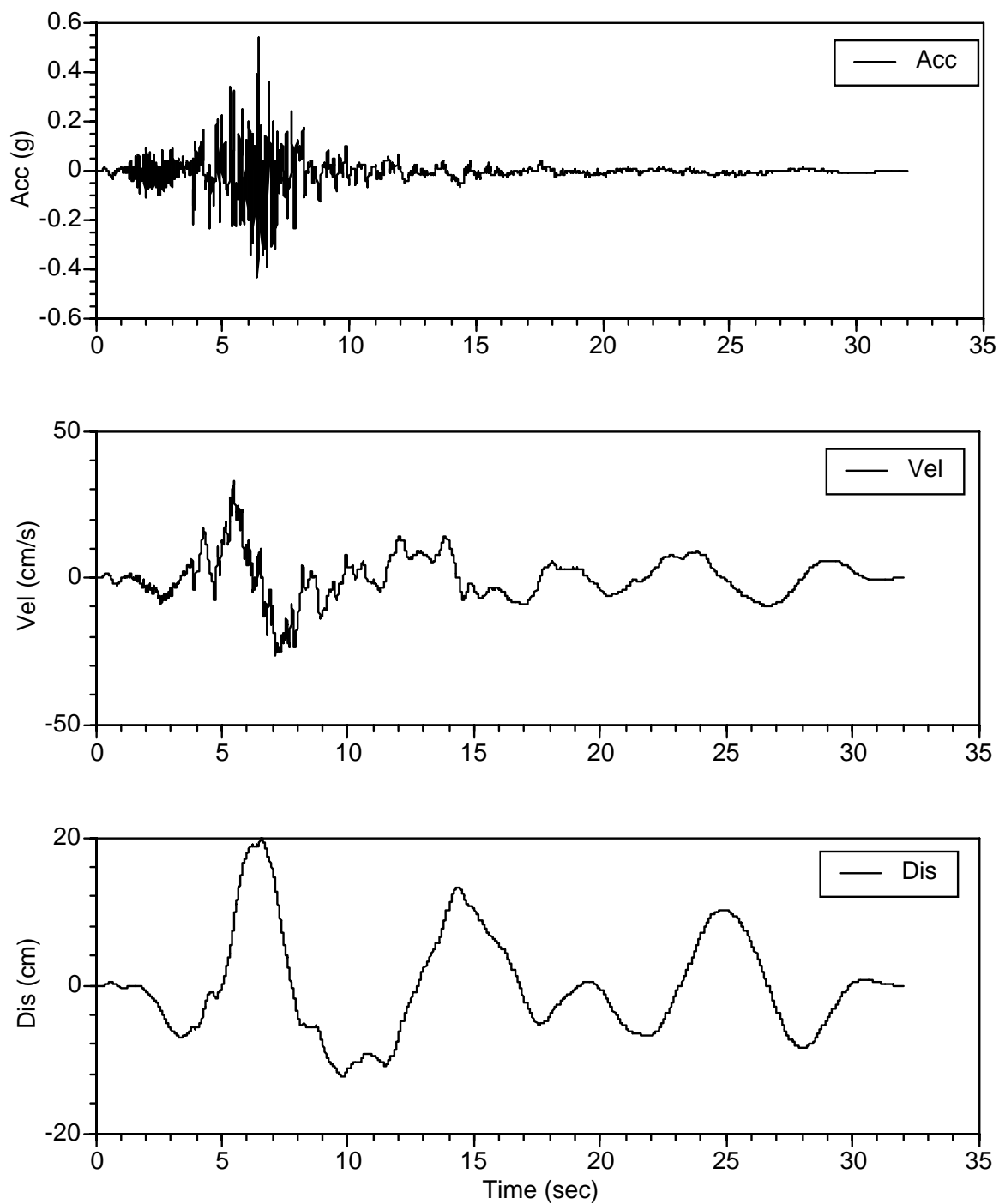(e) Modified Time History for FP Component**
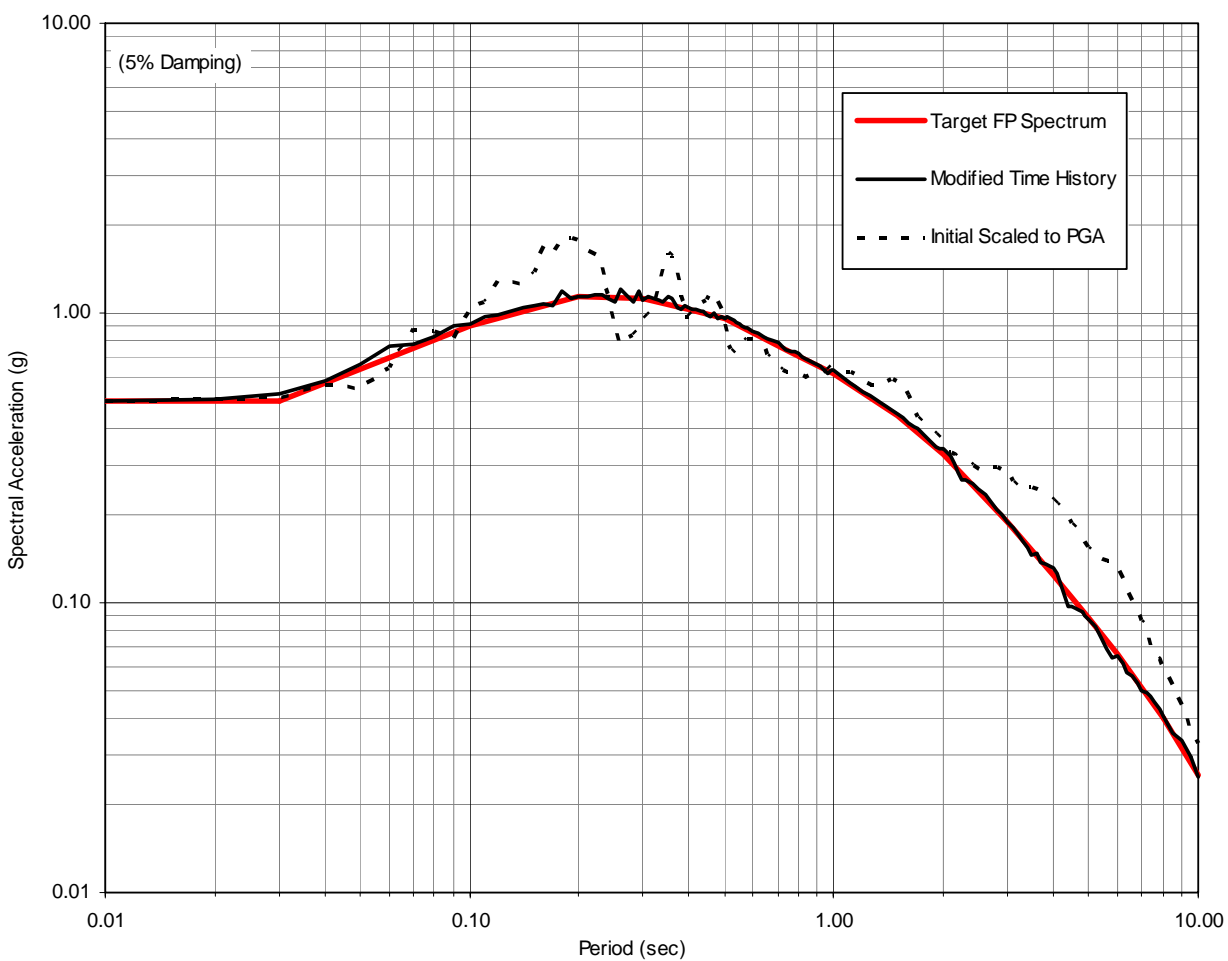
Figure D-2. **Firm-Ground Motions Compatible to CLE Firm-Ground Spectra, Set 2**
(f) Comparison of Target Spectrum with Spectra of Scaled and Modified Time
Histories, FP Component
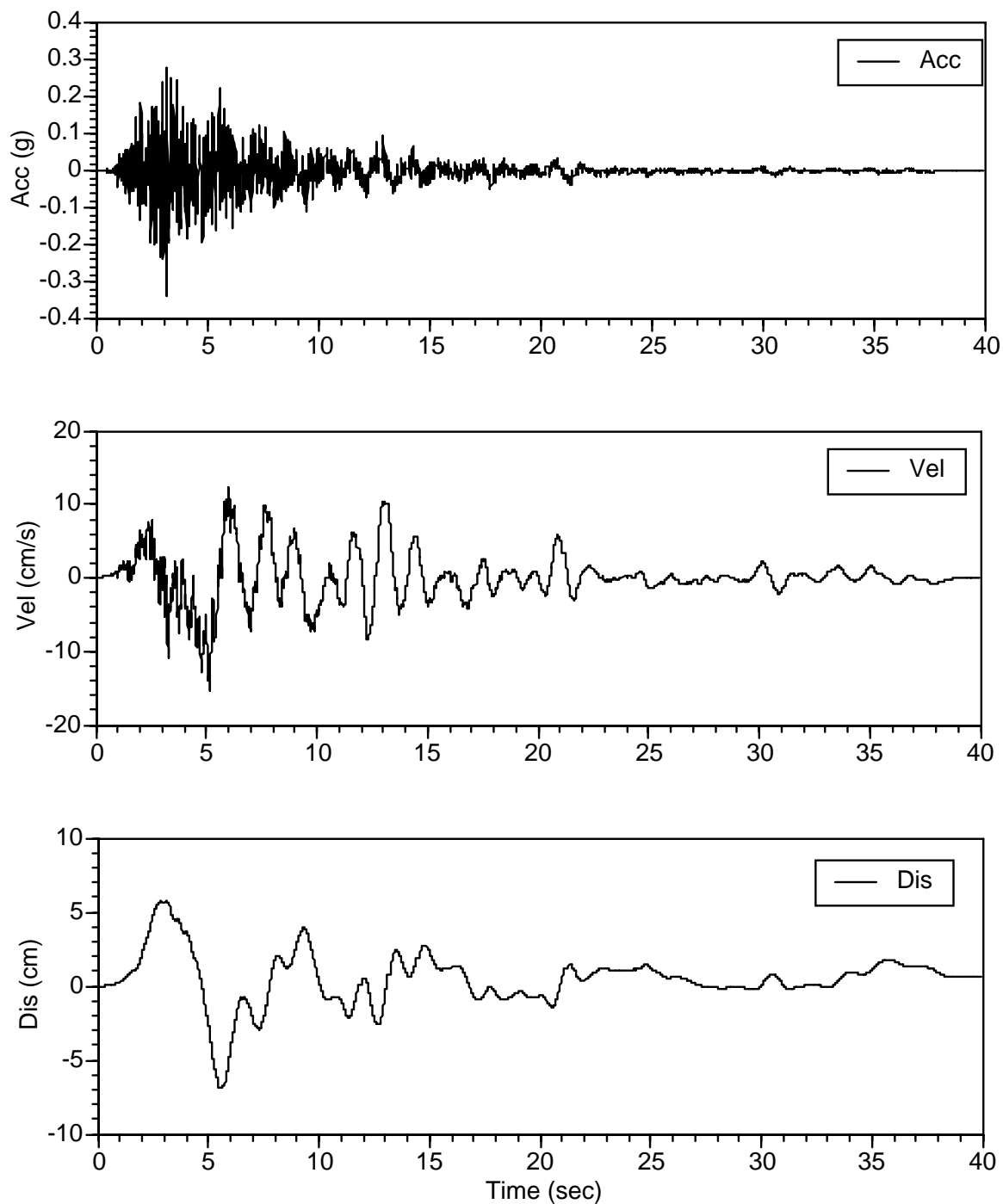
**Figure D-2.   Firm-Ground Time Histories Compatible to CLE Firm-Ground Spectra, Set 2
(g) Initial Time History for FV Component**
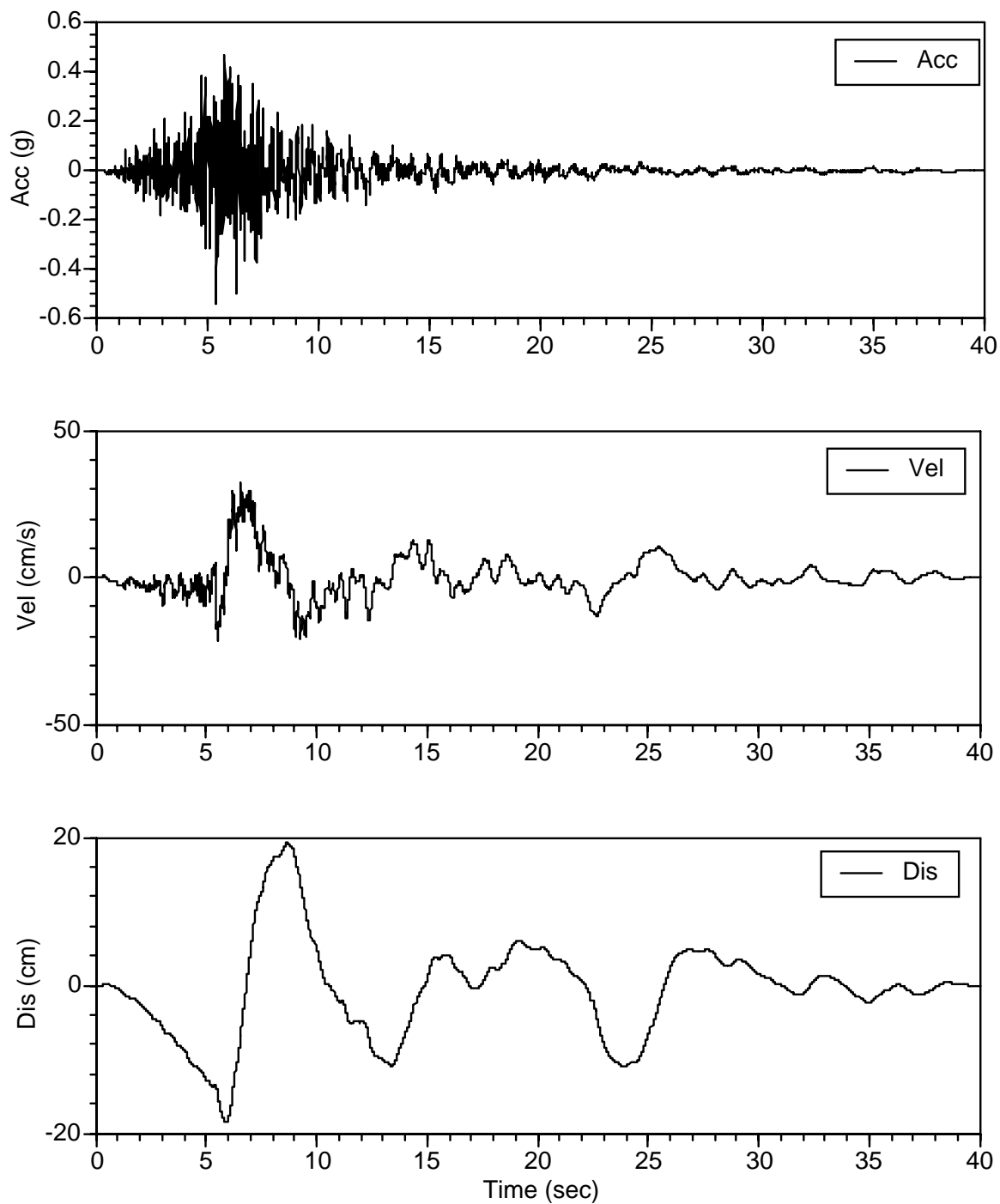
Figure D-2.   Firm-Ground Time Histories Compatible to CLE Firm-Ground Spectra, Set 2
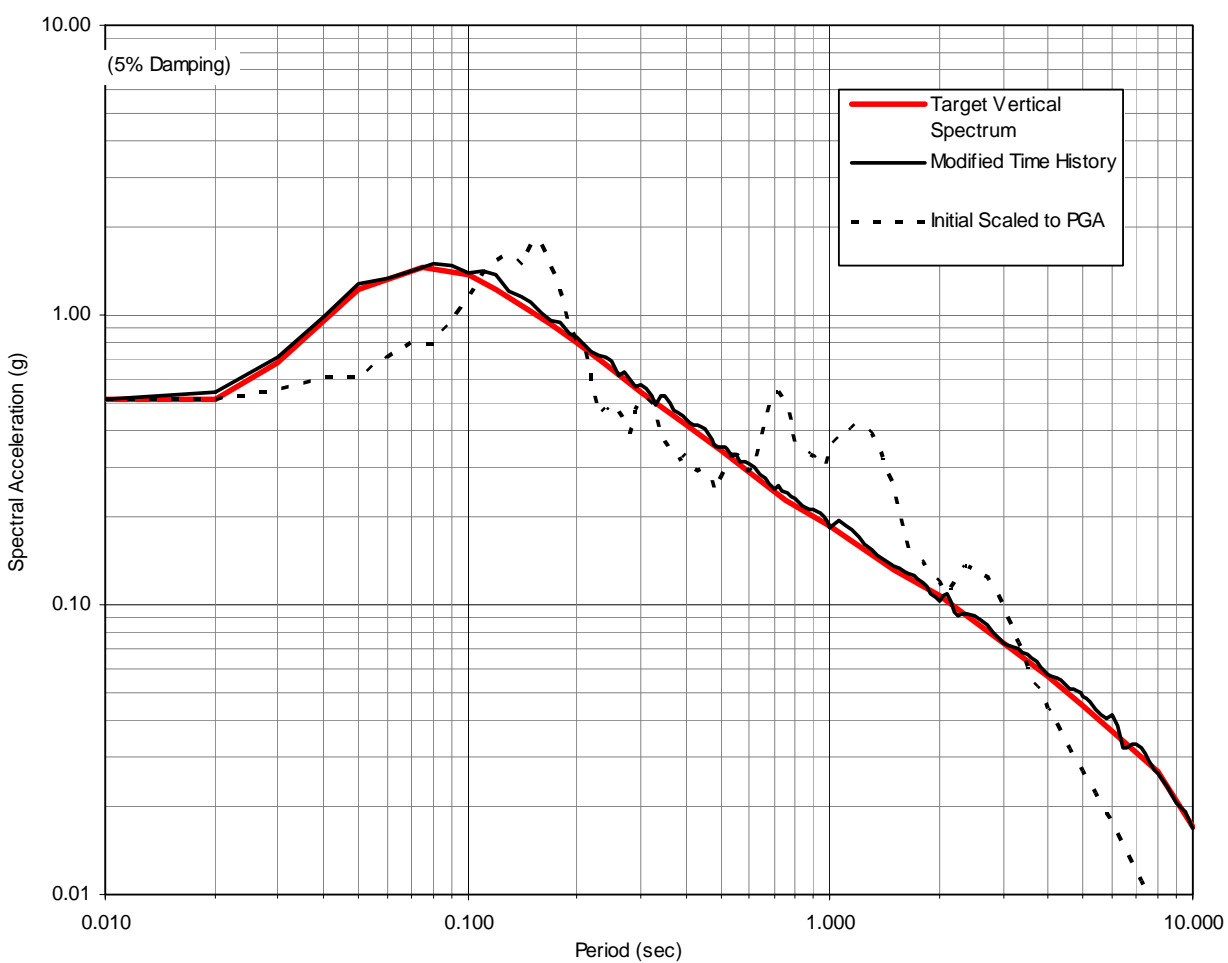**(h) Modified Time History for FV Component**
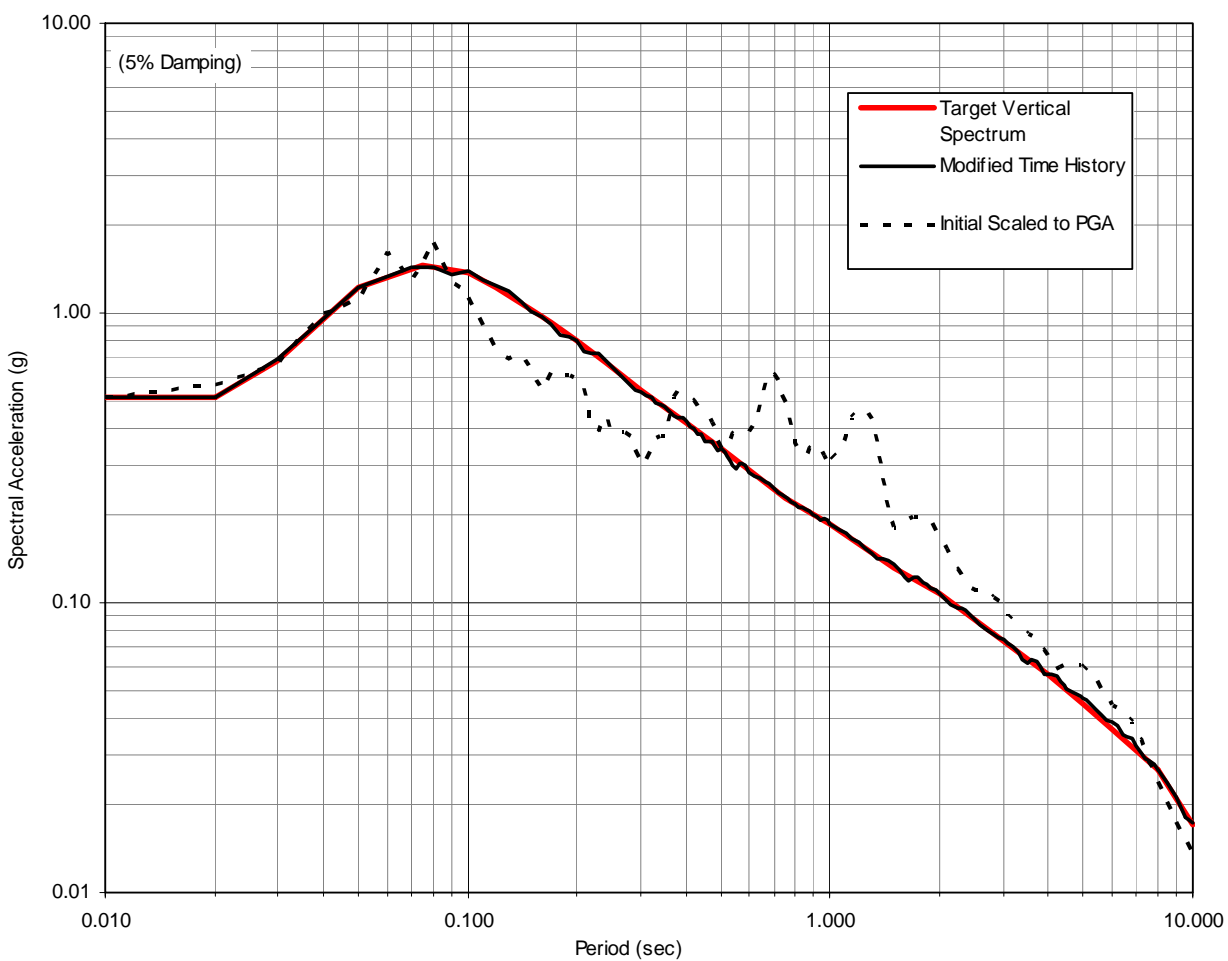
Figure D-2. **Firm-Ground Motions Compatible to CLE Firm-Ground Spectra, Set 2 (i) Comparison of Target Spectrum with Spectra of Scaled and Modified Time Histories, FV Component**
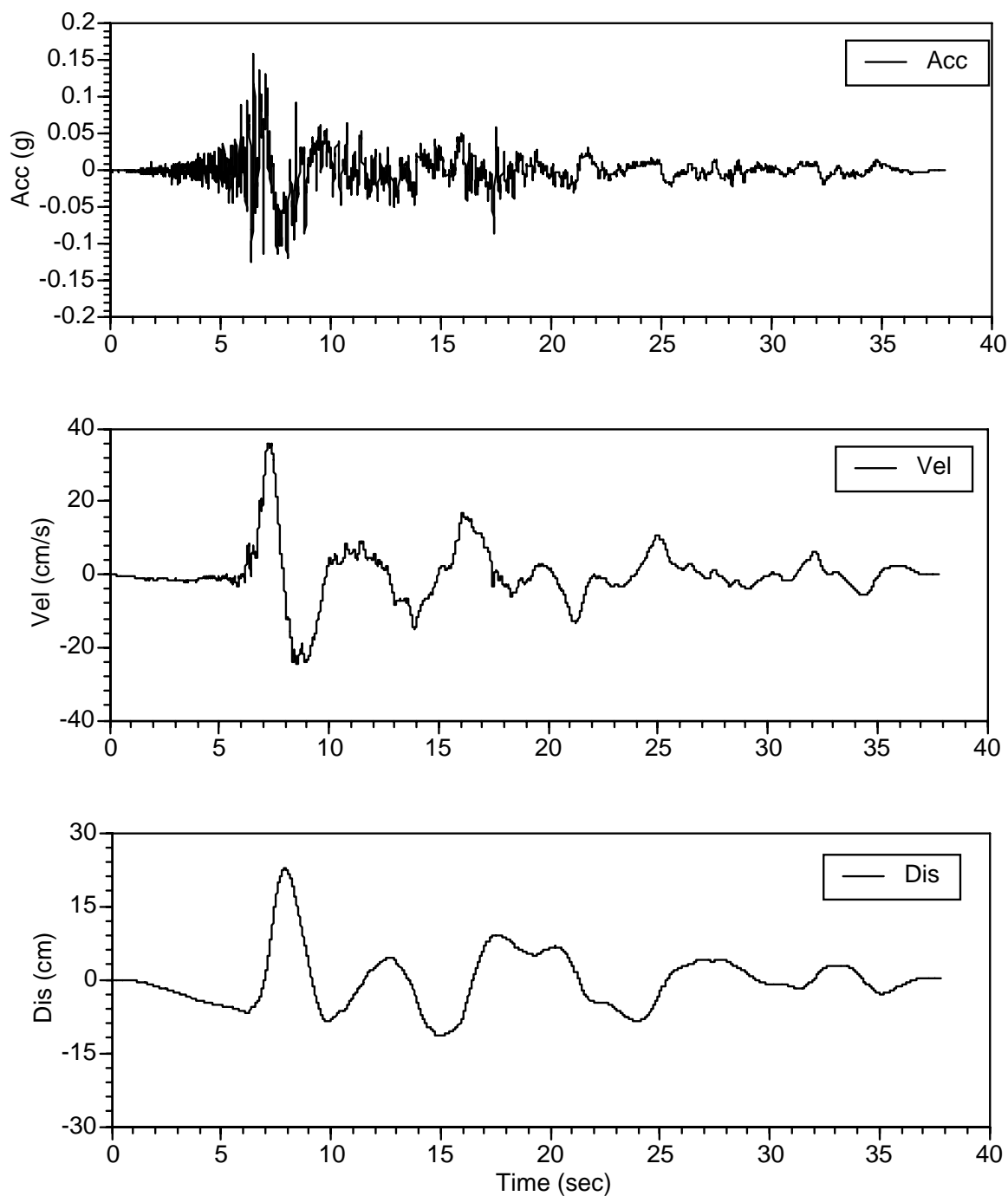
Figure D-3. **Firm-Ground Time Histories Compatible to CLE Firm-Ground Spectra, Set 3**
(a) Initial Time History for FN Component
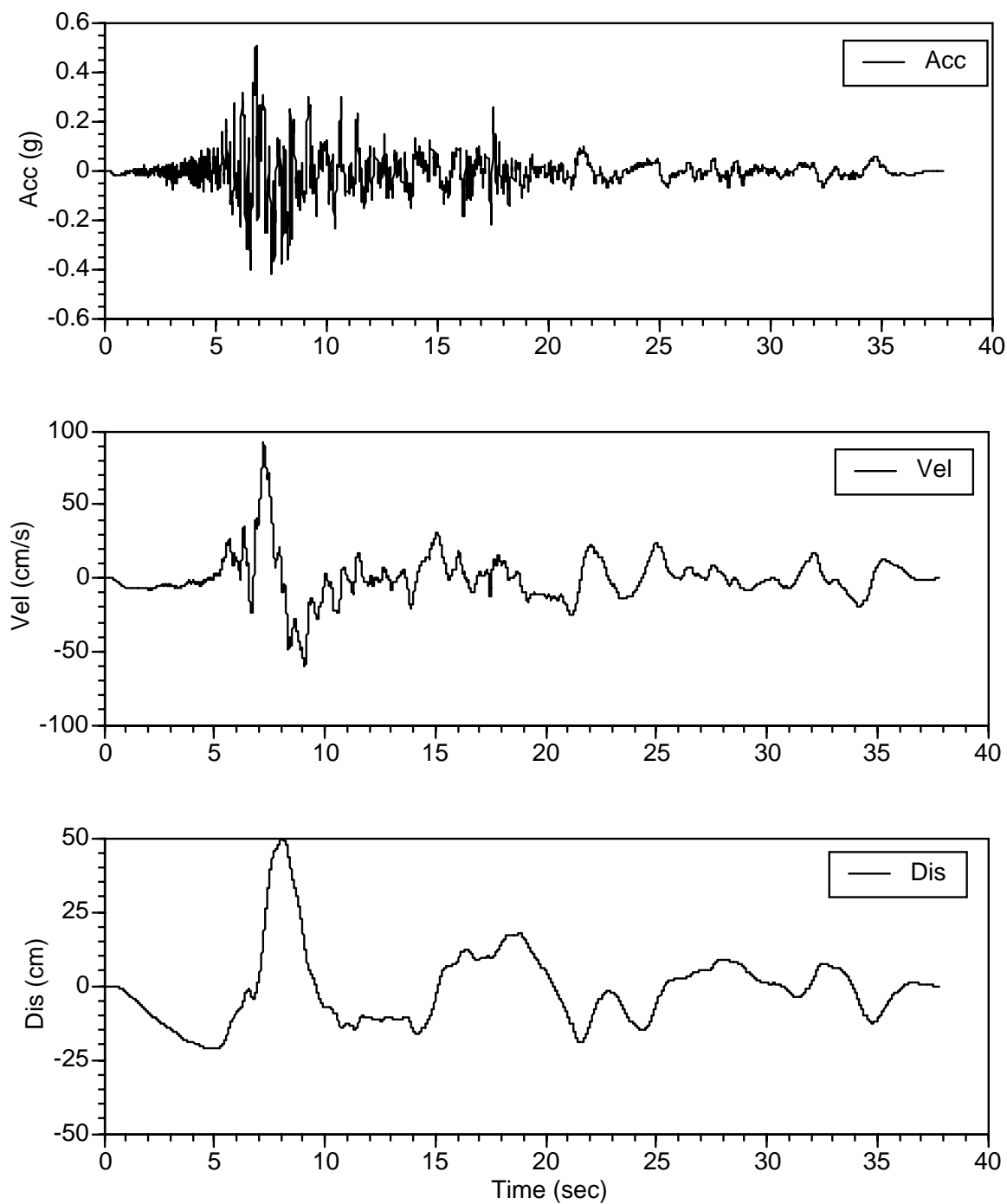
Figure D-3. **Firm-Ground Time Histories Compatible to CLE Firm-Ground Spectra, Set 3**
(b) Modified Time History for FN Component
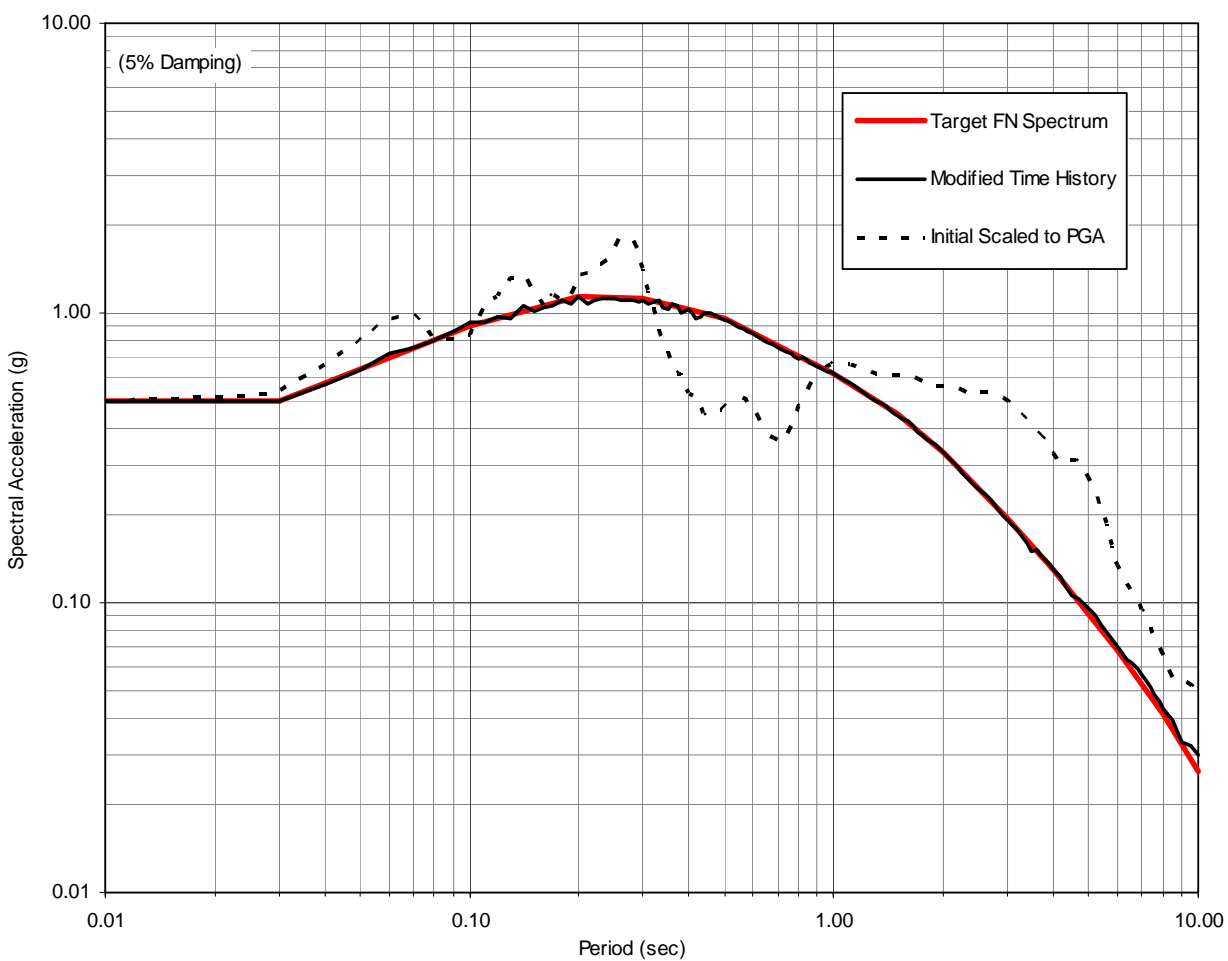
Figure D-3.   Firm-Ground Motions Compatible to CLE Firm-Ground Spectra, Set 3
(c) Comparison of Target Spectrum with Spectra of Scaled and Modified Time
Histories, FN Component
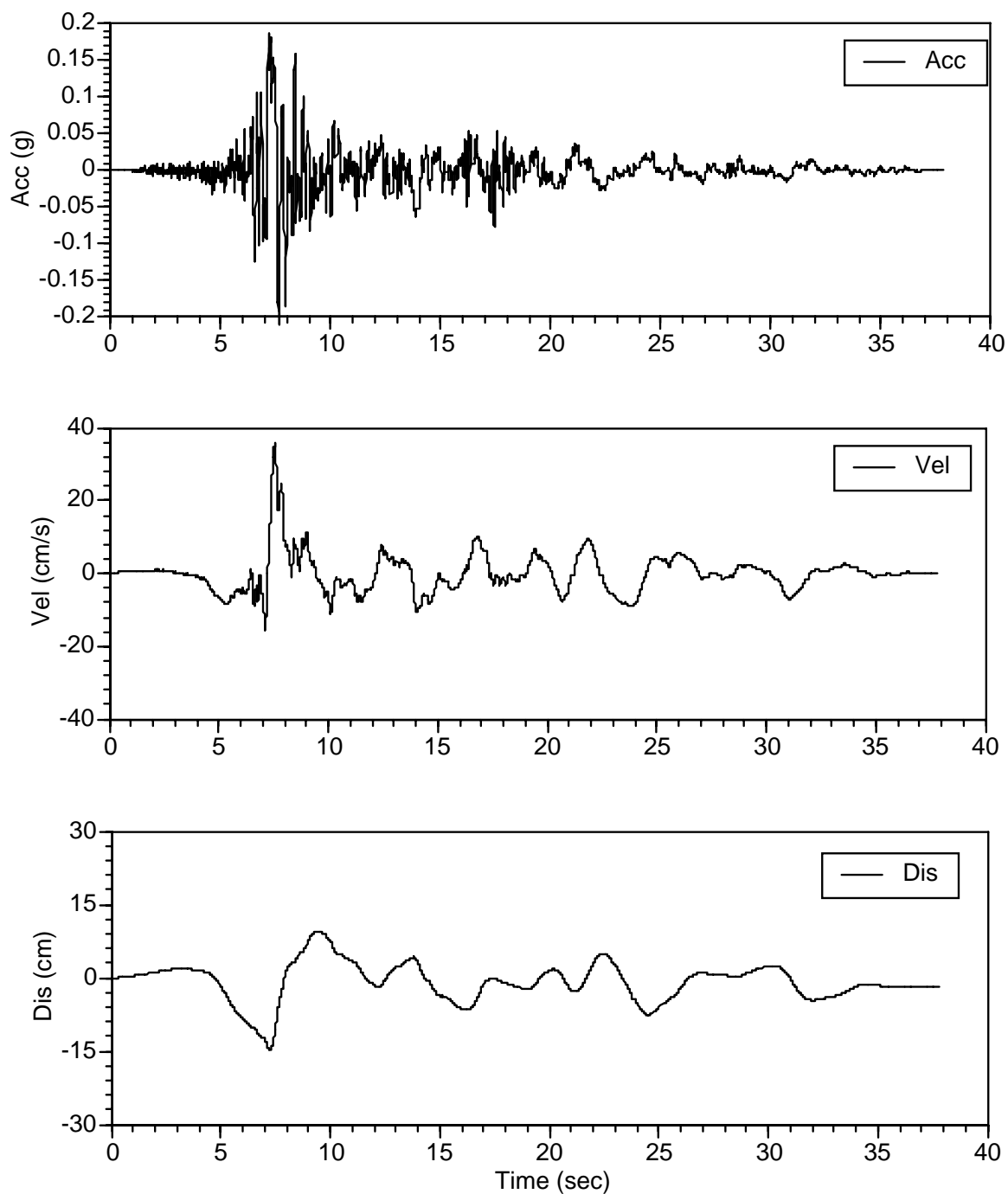
**Figure D-3.   Firm-Ground Time Histories Compatible to CLE Firm-Ground Spectra, Set 3
(d) Initial Time History for FP Component**
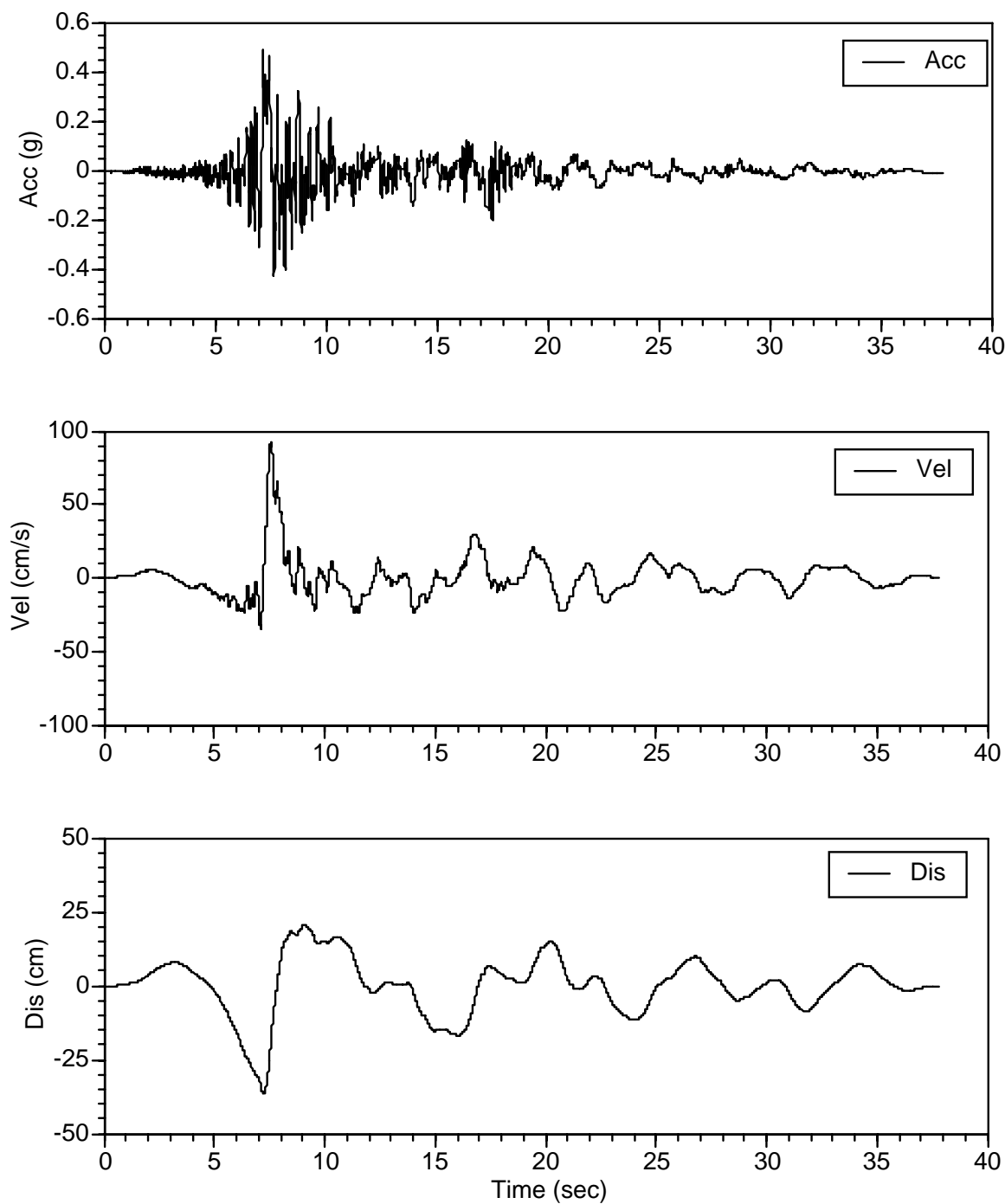
Figure D-3. **Firm-Ground Time Histories Compatible to CLE Firm-Ground Spectra, Set 3**
(e) Modified Time History for FP Component
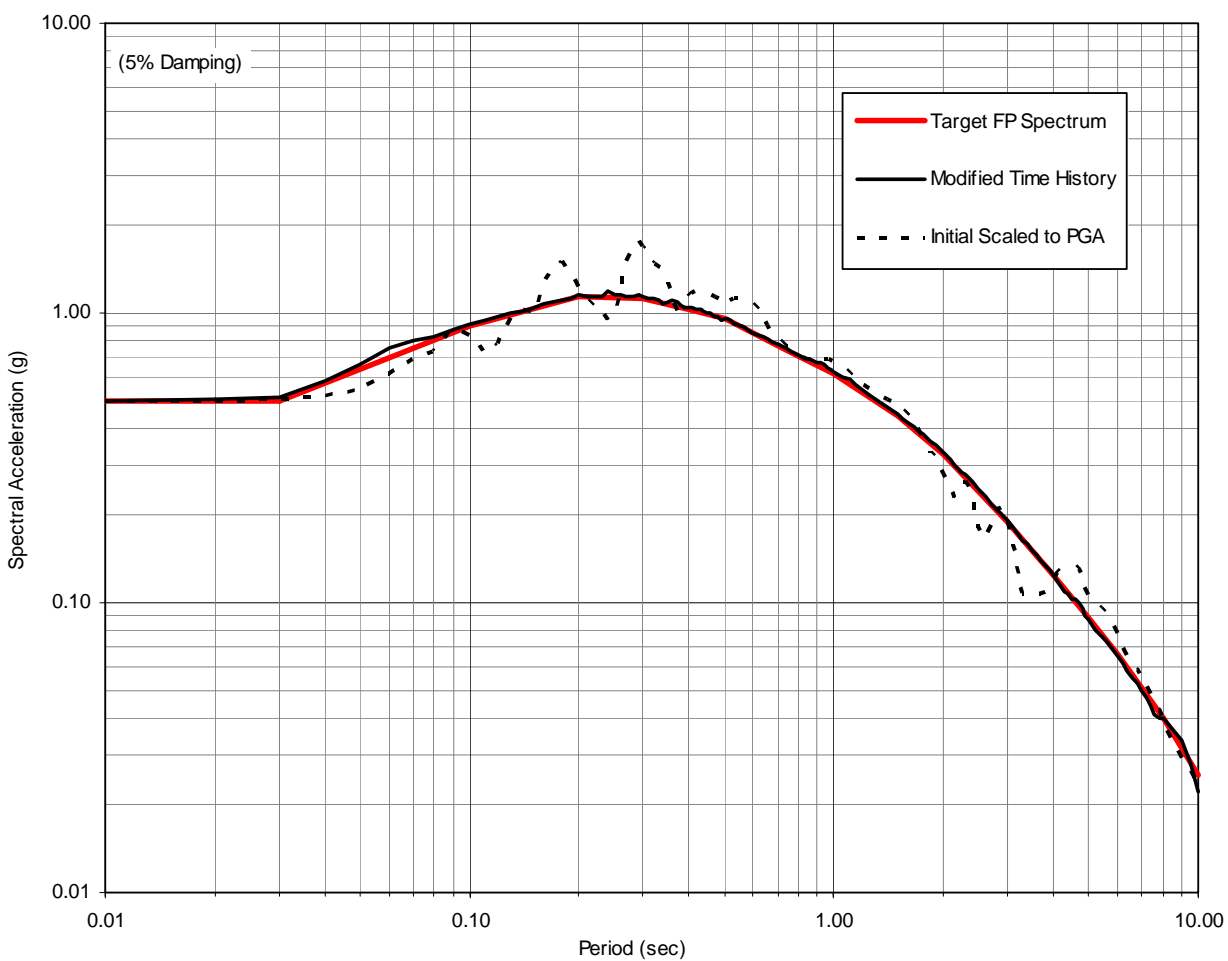
Figure D-3.   Firm-Ground Motions Compatible to CLE Firm-Ground Spectra, Set 3
(f) Comparison of Target Spectrum with Spectra of Scaled and Modified Time
Histories, FP Component
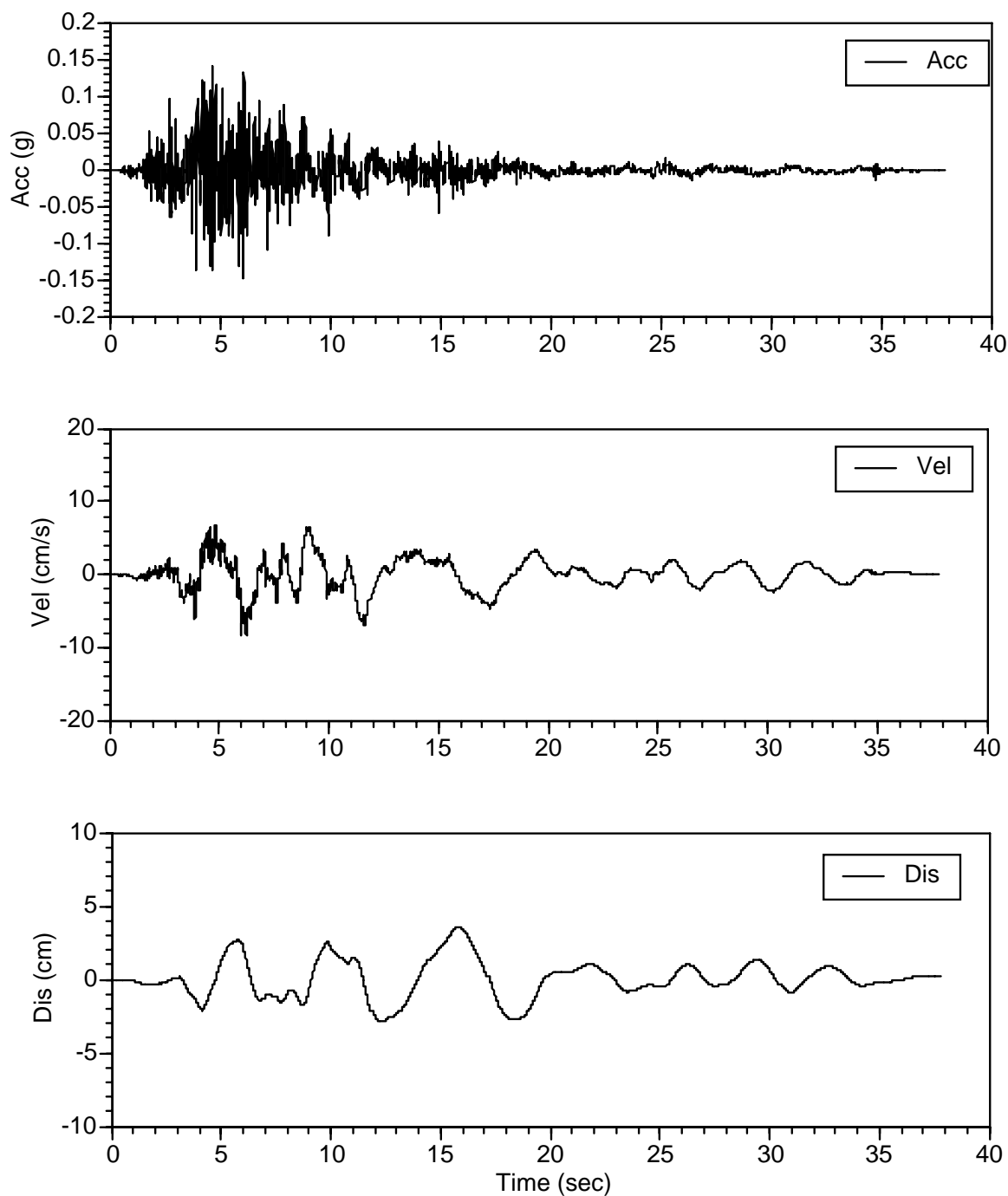
Figure D-3. Firm-Ground Time Histories Compatible to CLE Firm-Ground Spectra, Set 3 (g) Initial Time History for FV Component
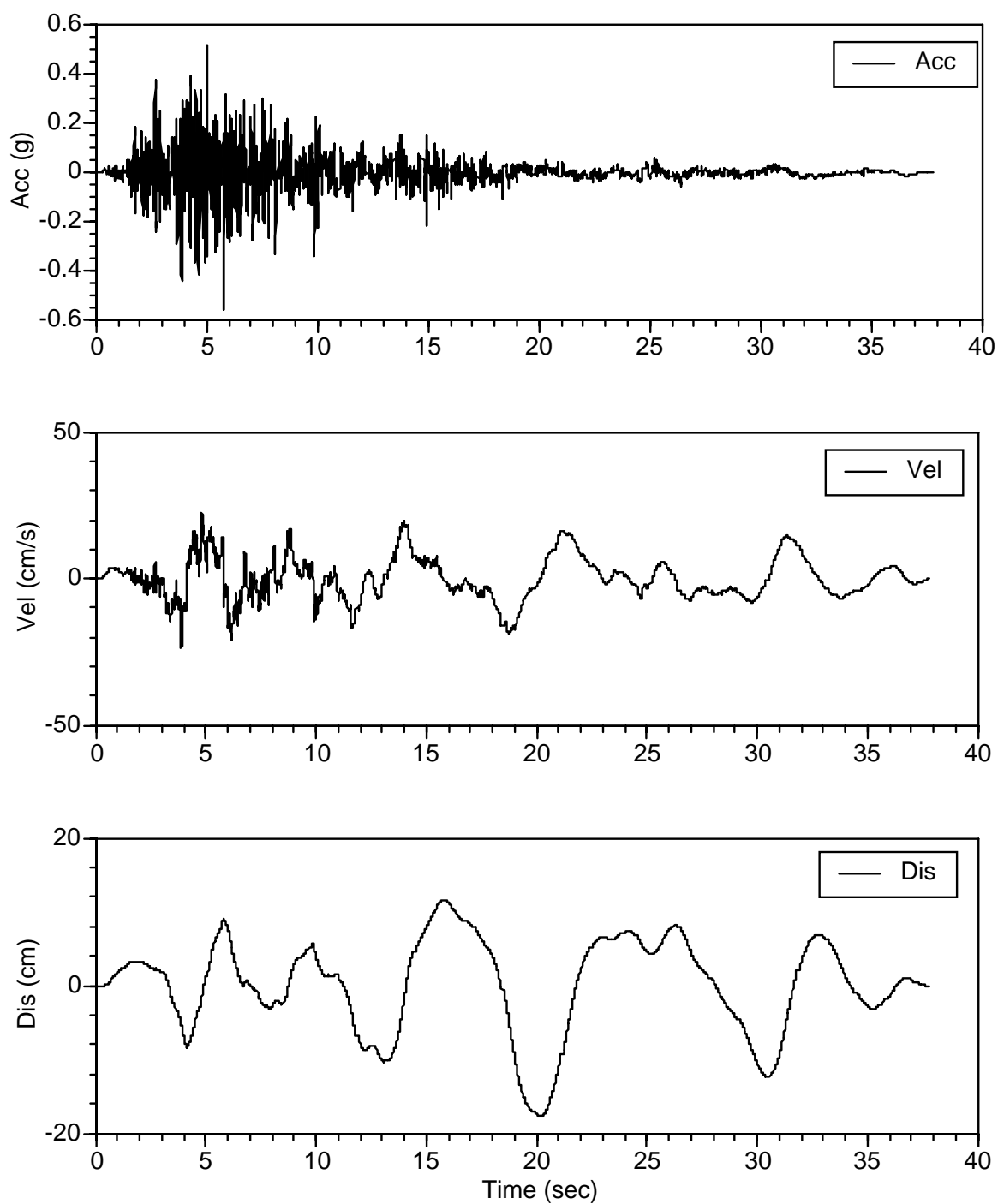
Figure D-3. **Firm-Ground Time Histories Compatible to CLE Firm-Ground Spectra, Set 3**
        (h) Modified Time History for FV Component
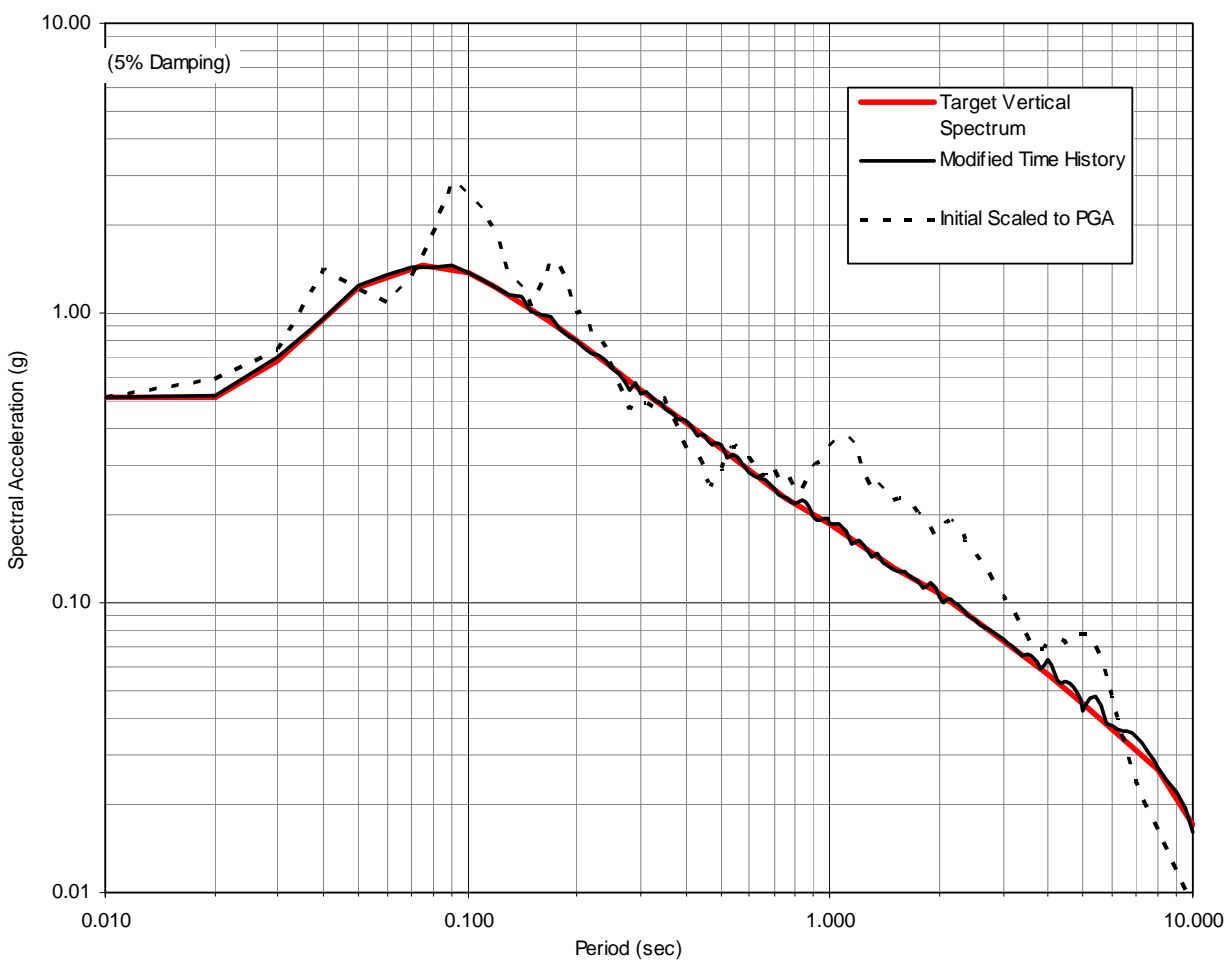
Figure D-3.   Firm-Ground Motions Compatible to CLE Firm-Ground Spectra, Set 3
(i) Comparison of Target Spectrum with Spectra of Scaled and Modified Time
Histories, FV Component
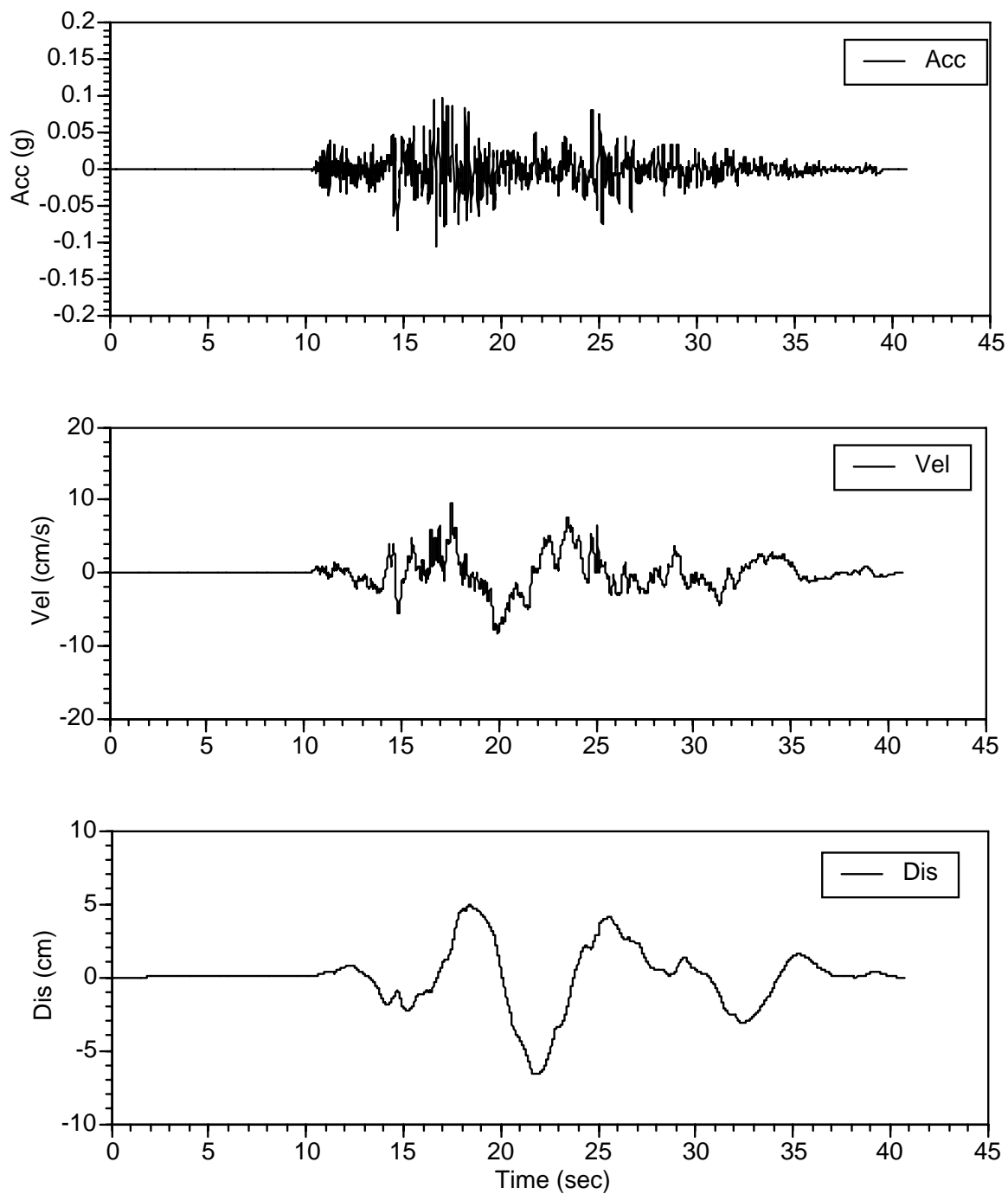
Figure D-4.   Firm-Ground Time Histories Compatible to CLE Firm-Ground Spectra, Set 4
(a) Initial Time History for FN Component
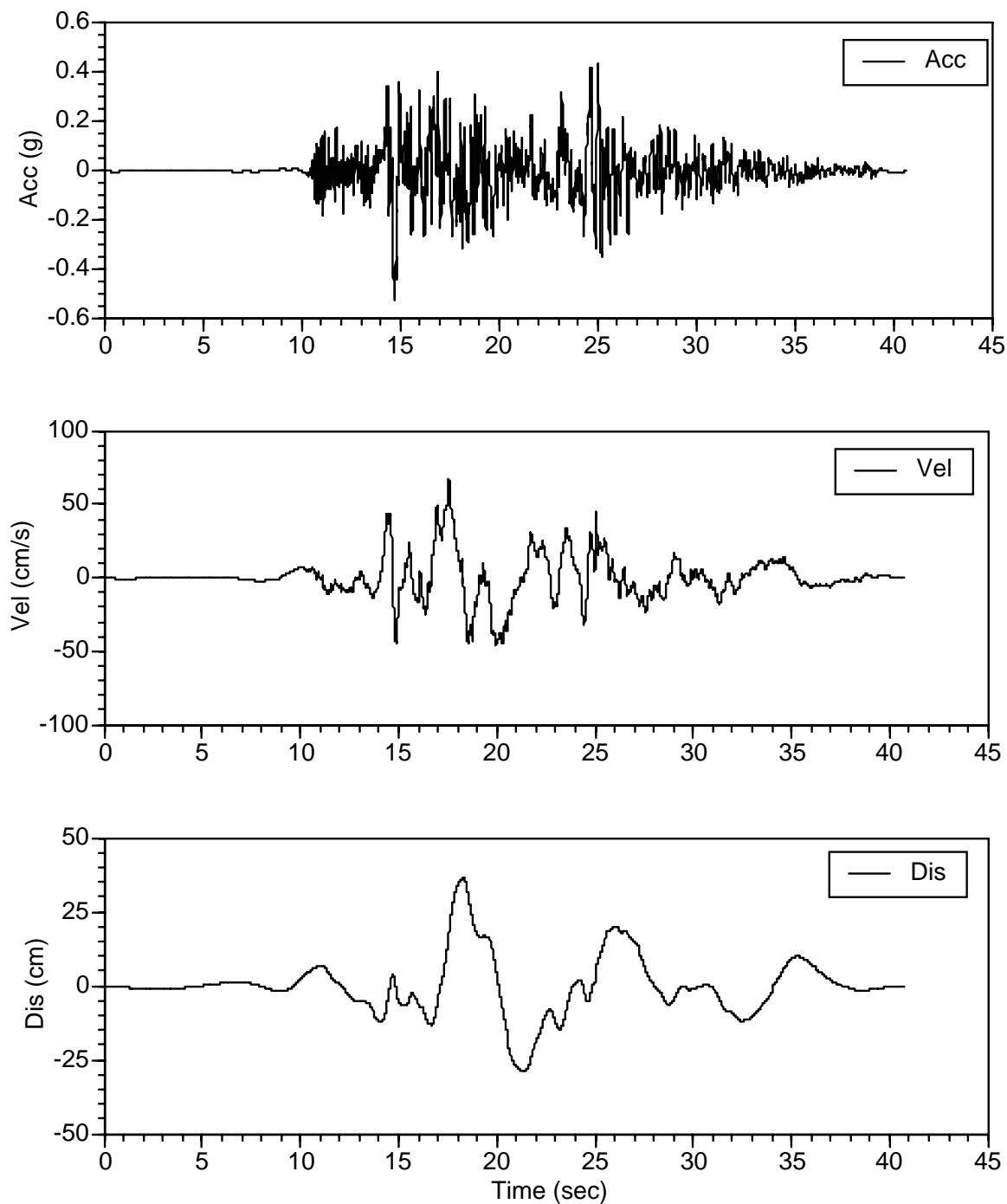
Figure D-4.   Firm-Ground Time Histories Compatible to CLE Firm-Ground Spectra, Set 4
(b) Modified Time History for FN Component
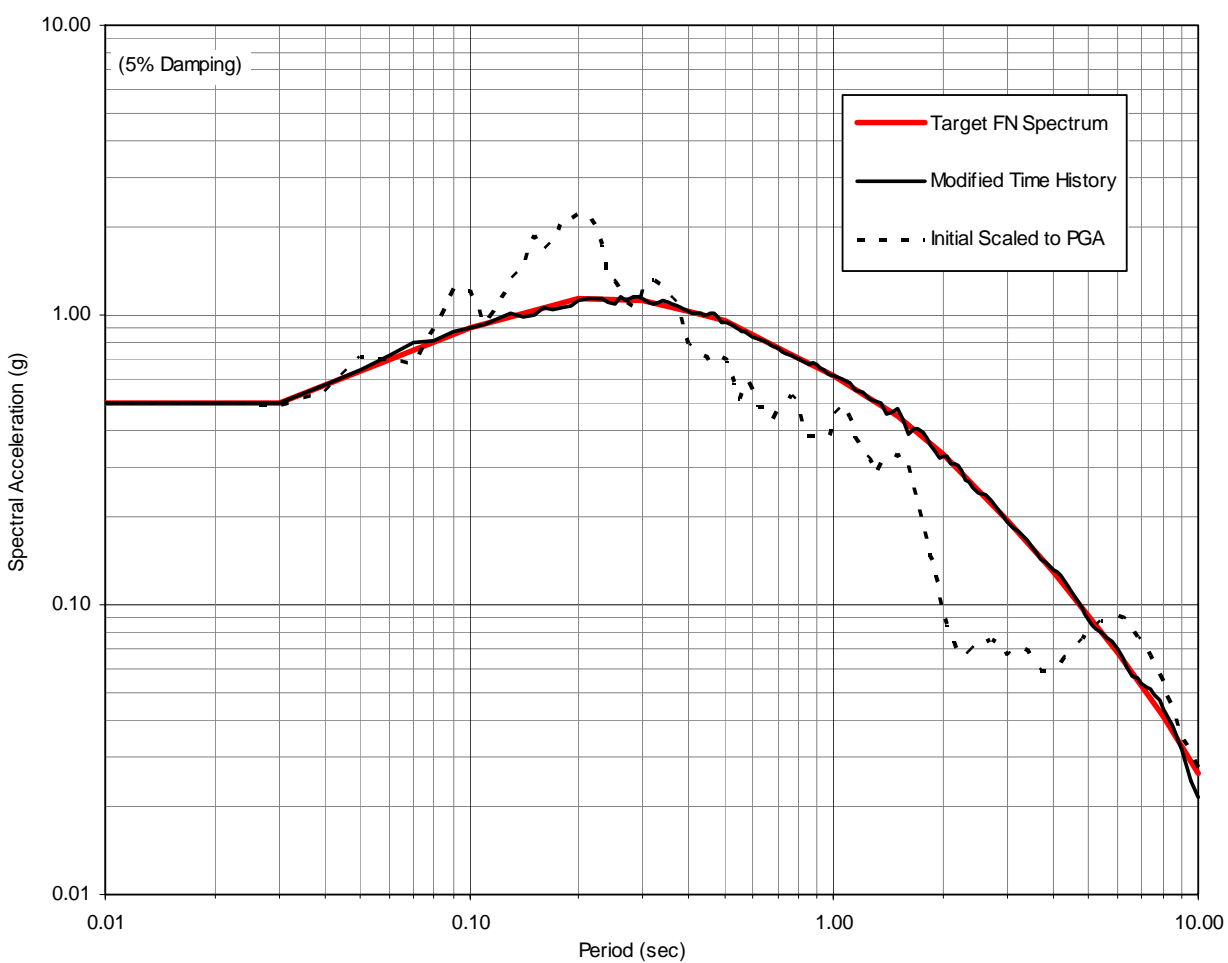
**Figure D-4.   Firm-Ground Motions Compatible to CLE Firm-Ground Spectra, Set 4
(c) Comparison of Target Spectrum with Spectra of Scaled and Modified Time
Histories, FN Component**
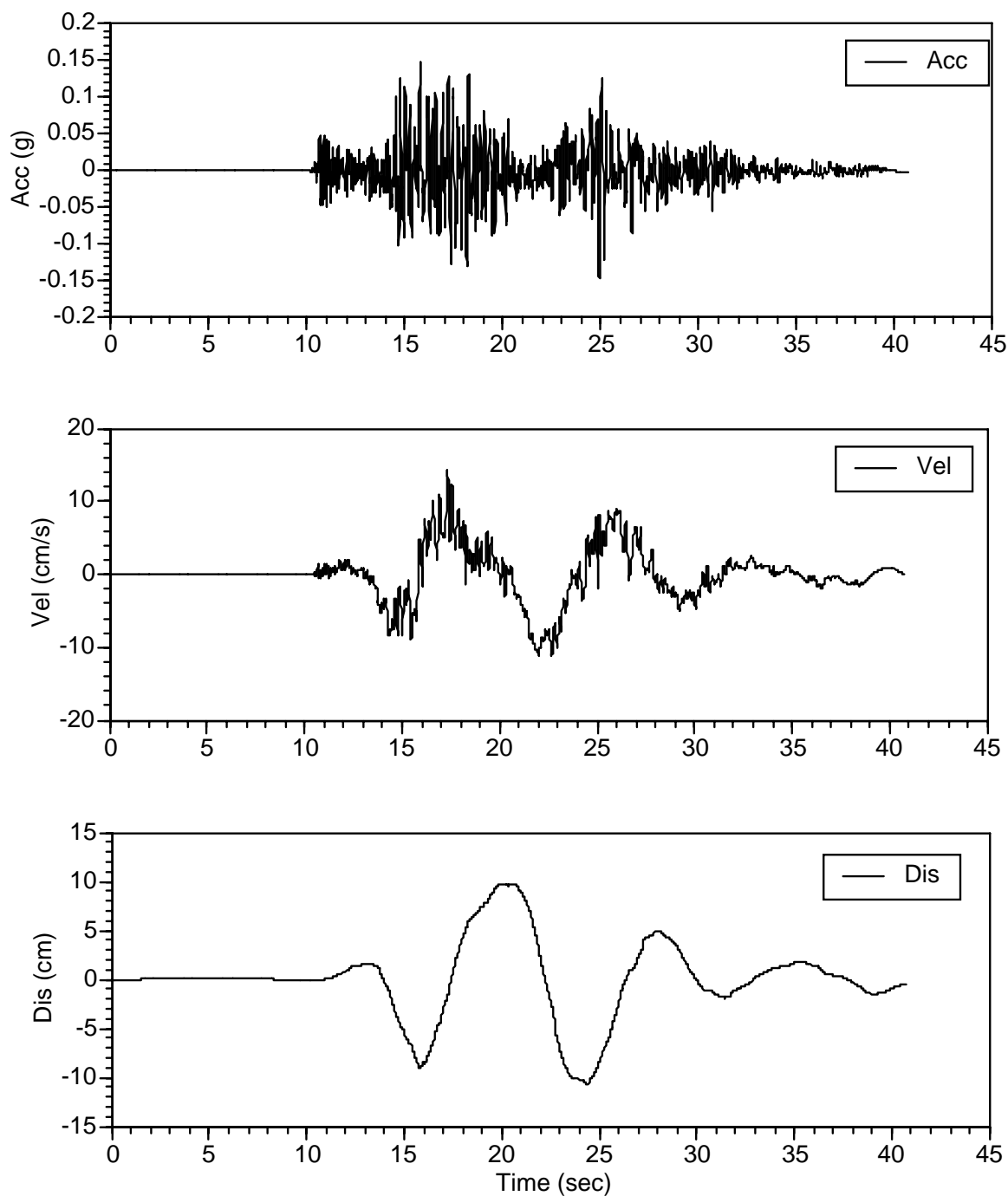
Figure D-4. **Firm-Ground Time Histories Compatible to CLE Firm-Ground Spectra, Set 4**
(d) Initial Time History for FP Component
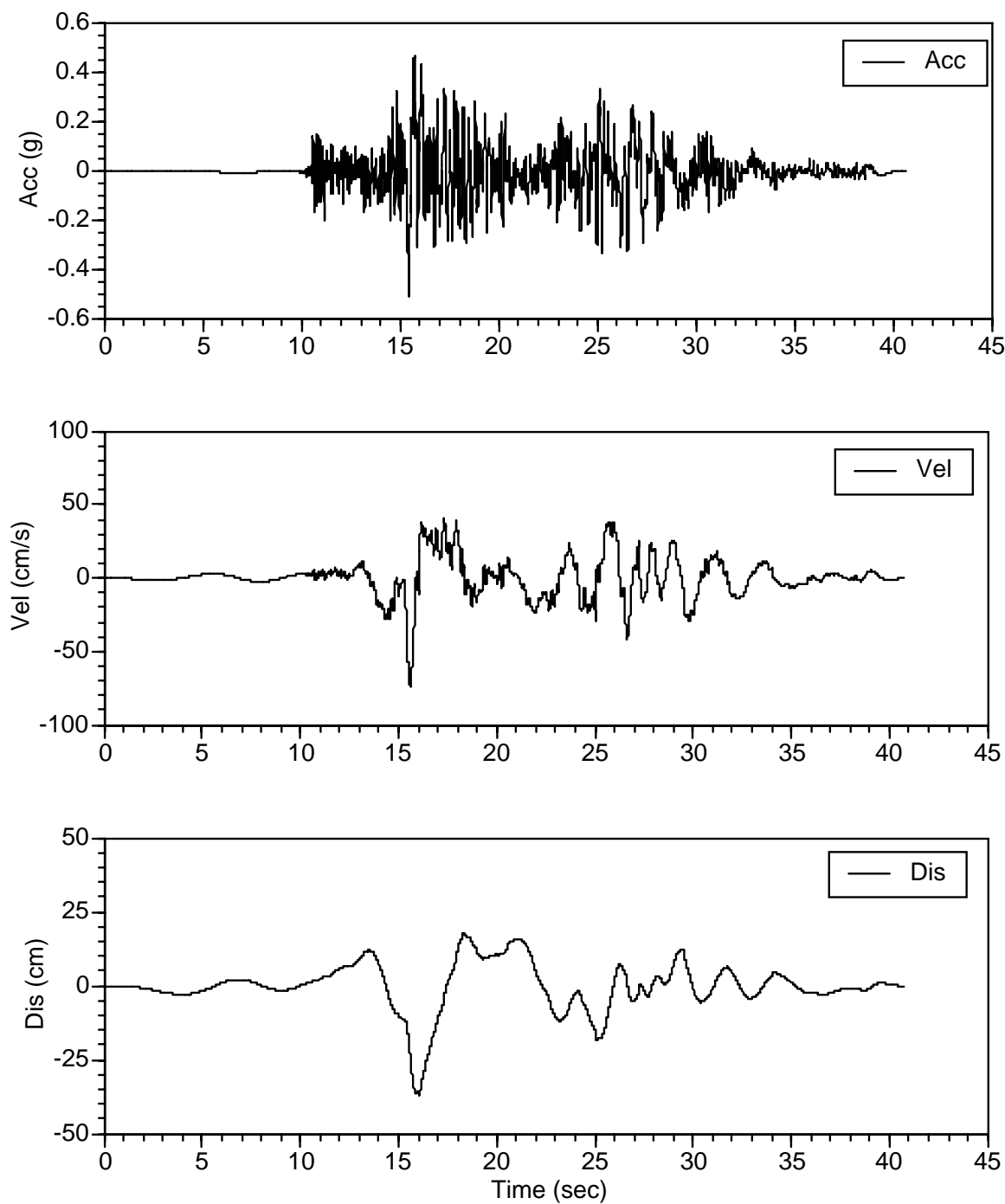
Figure D-4. **Firm-Ground Time Histories Compatible to CLE Firm-Ground Spectra, Set 4**
(e) Modified Time History for FP Component
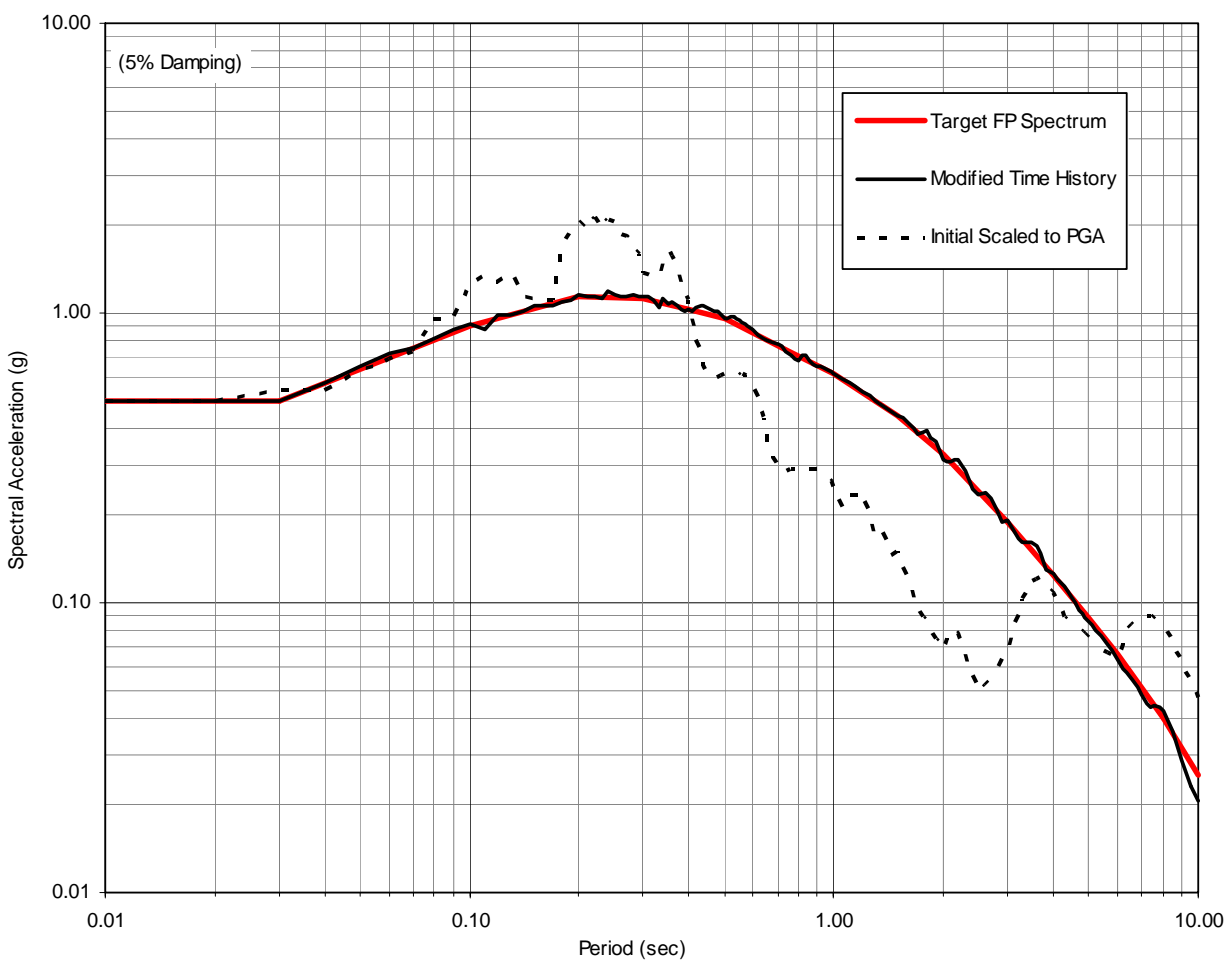
Figure D-4.   Firm-Ground Motions Compatible to CLE Firm-Ground Spectra, Set 4
(f) Comparison of Target Spectrum with Spectra of Scaled and Modified Time
Histories, FP Component
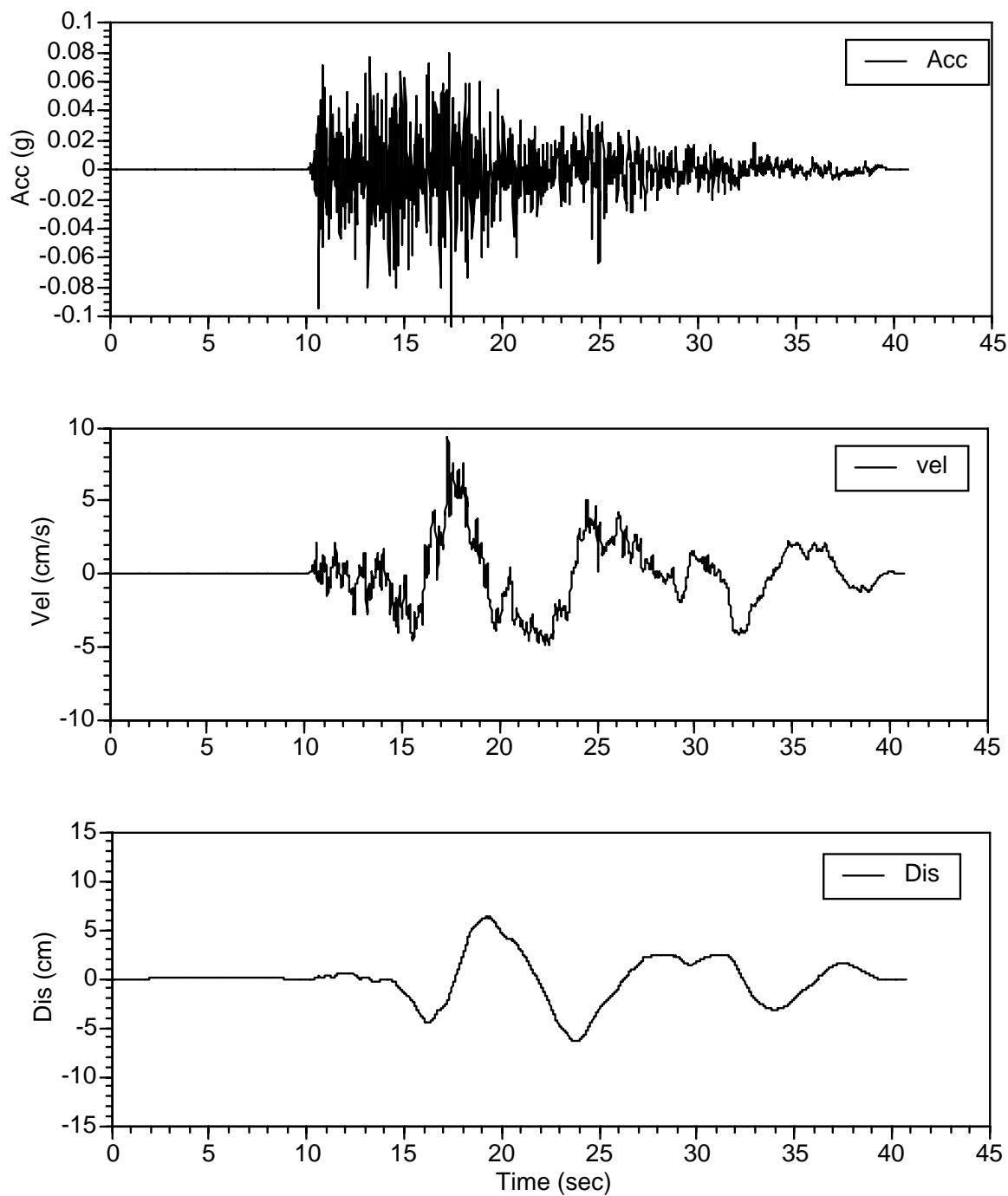
**Figure D-4.   Firm-Ground Time Histories Compatible to CLE Firm-Ground Spectra, Set 4
(g) Initial Time History for FV Component**
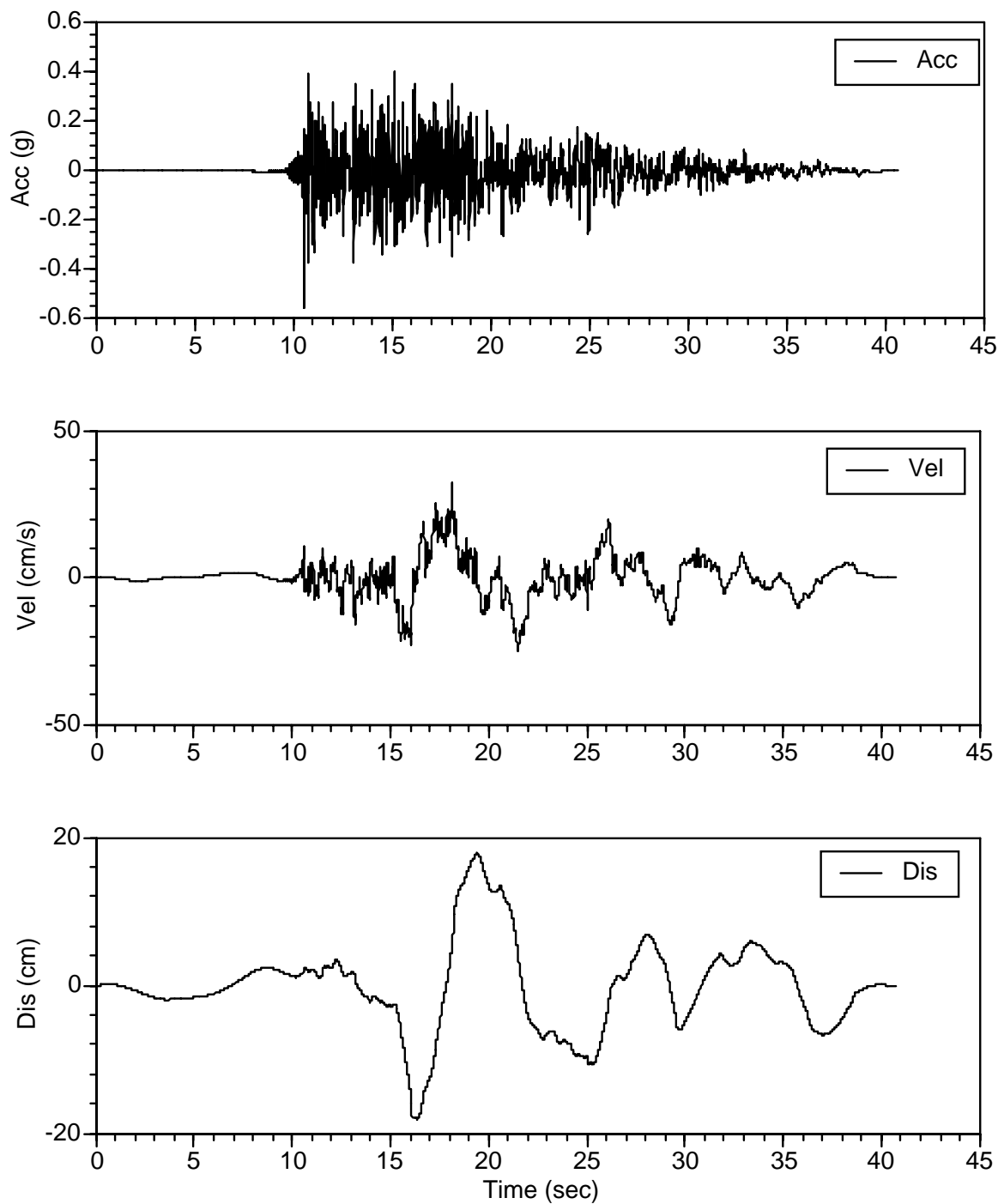
Figure D-4. **Firm-Ground Time Histories Compatible to CLE Firm-Ground Spectra, Set 4**
(h) Modified Time History for FV Component
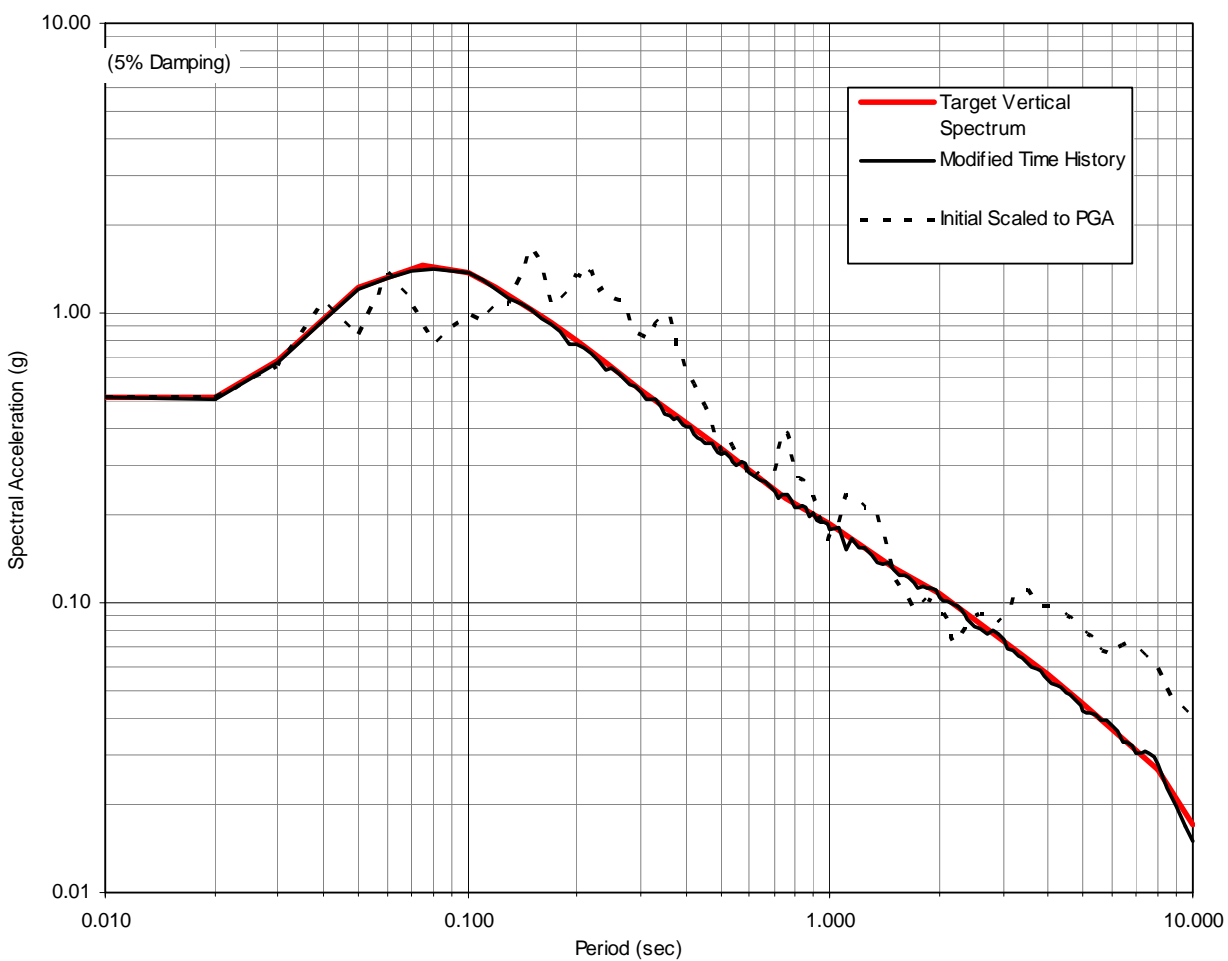
**Figure D-4.   Firm-Ground Motions Compatible to CLE Firm-Ground Spectra, Set 4
(i) Comparison of Target Spectrum with Spectra of Scaled and Modified Time
Histories, FV Component**
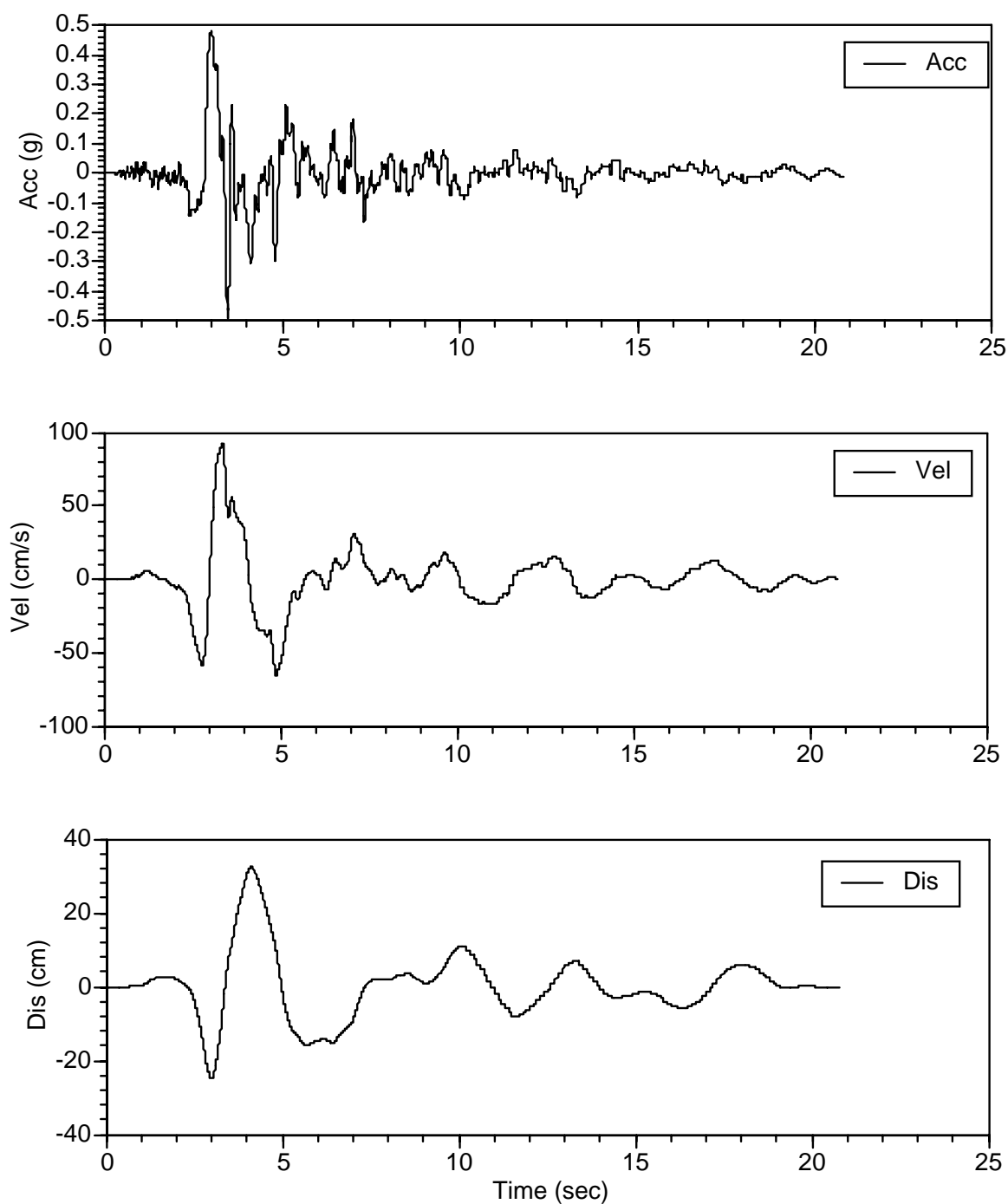
Figure D-5.   Firm-Ground Time Histories Compatible to CLE Firm-Ground Spectra, Set 5
(a) Initial Time History for FN Component
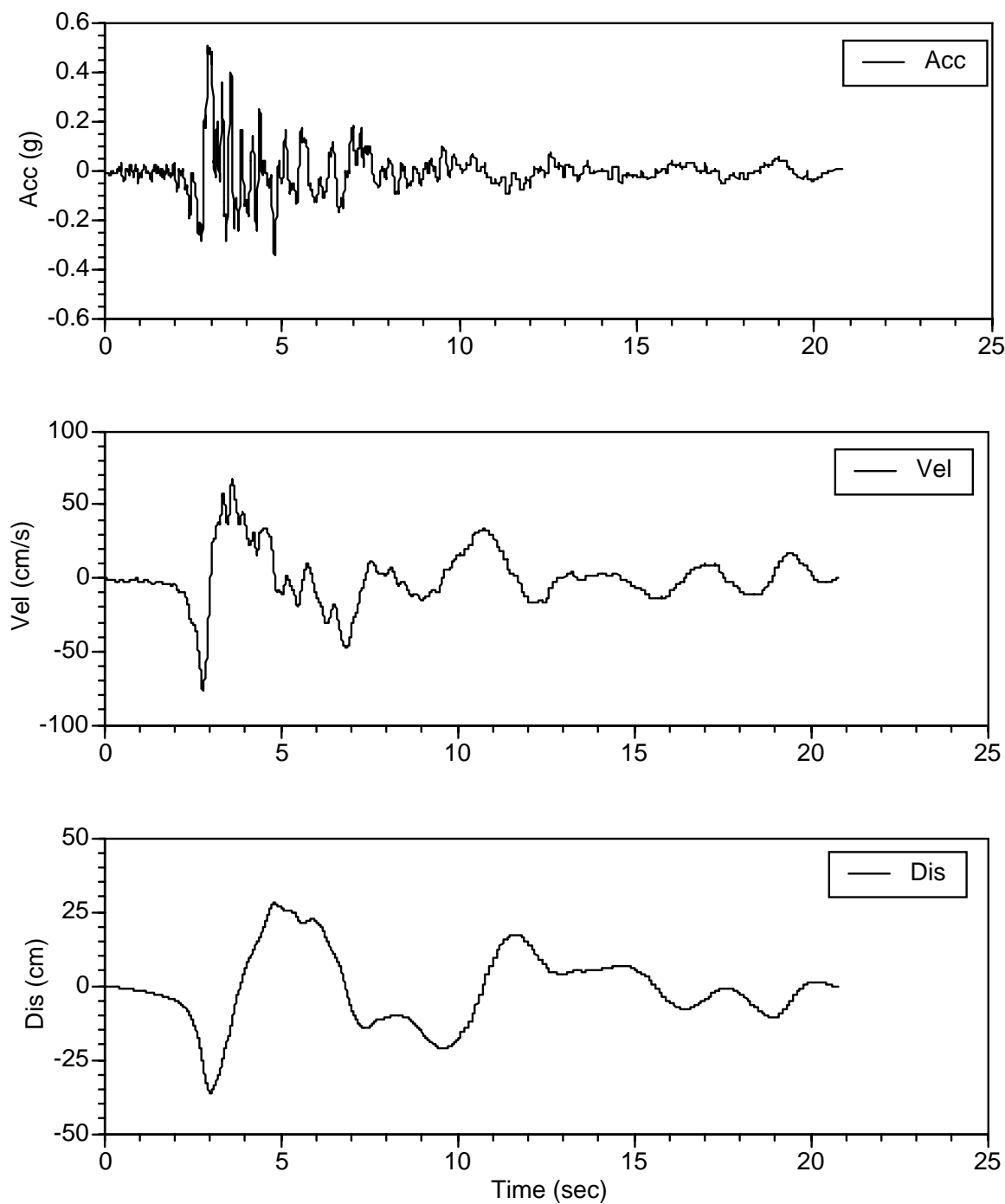
Figure D-5. **Firm-Ground Time Histories Compatible to CLE Firm-Ground Spectra, Set 5**
(b) Modified Time History for FN Component
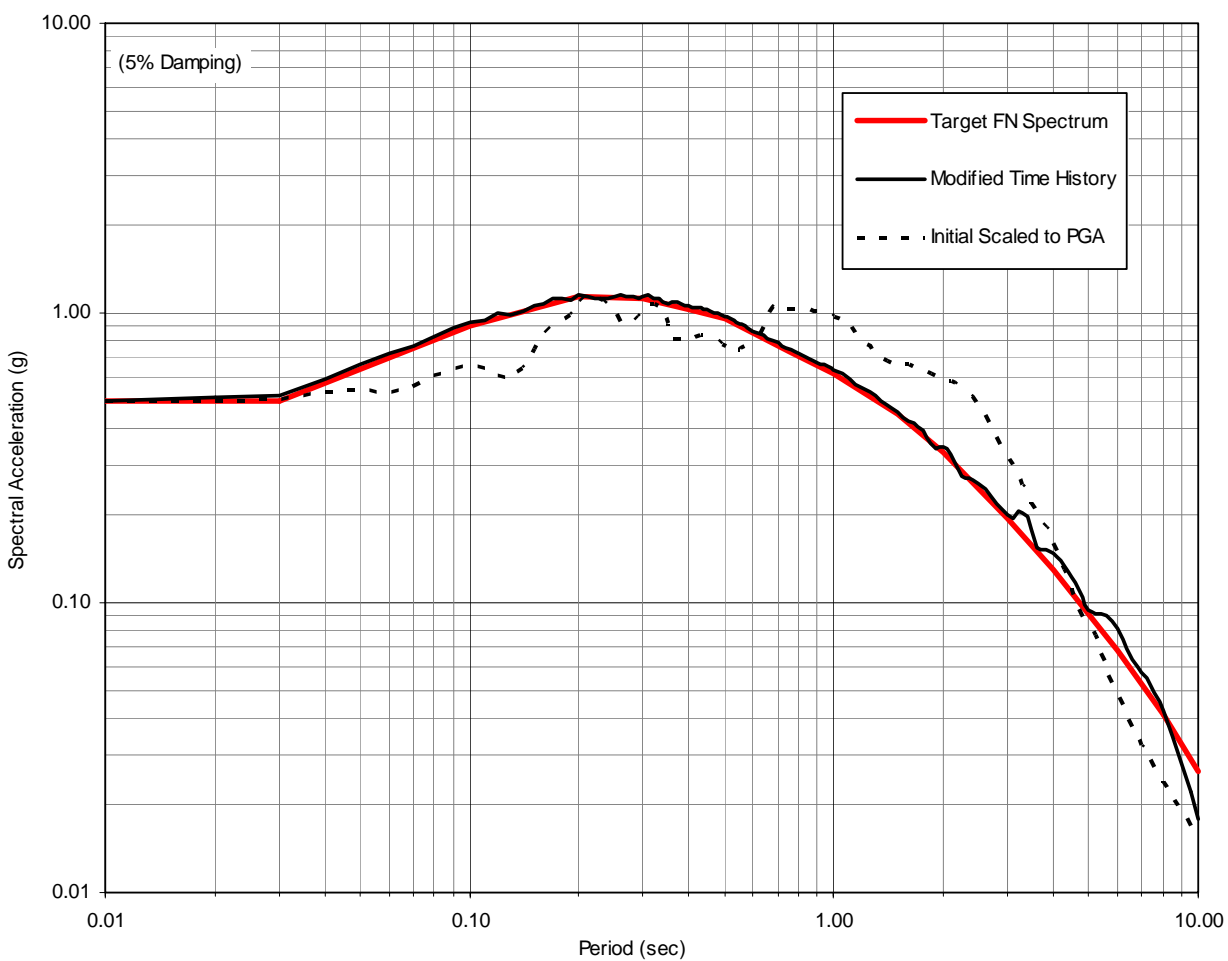
Figure D-5. **Firm-Ground Motions Compatible to CLE Firm-Ground Spectra, Set 5**
(c) Comparison of Target Spectrum with Spectra of Scaled and Modified Time Histories, FN Component
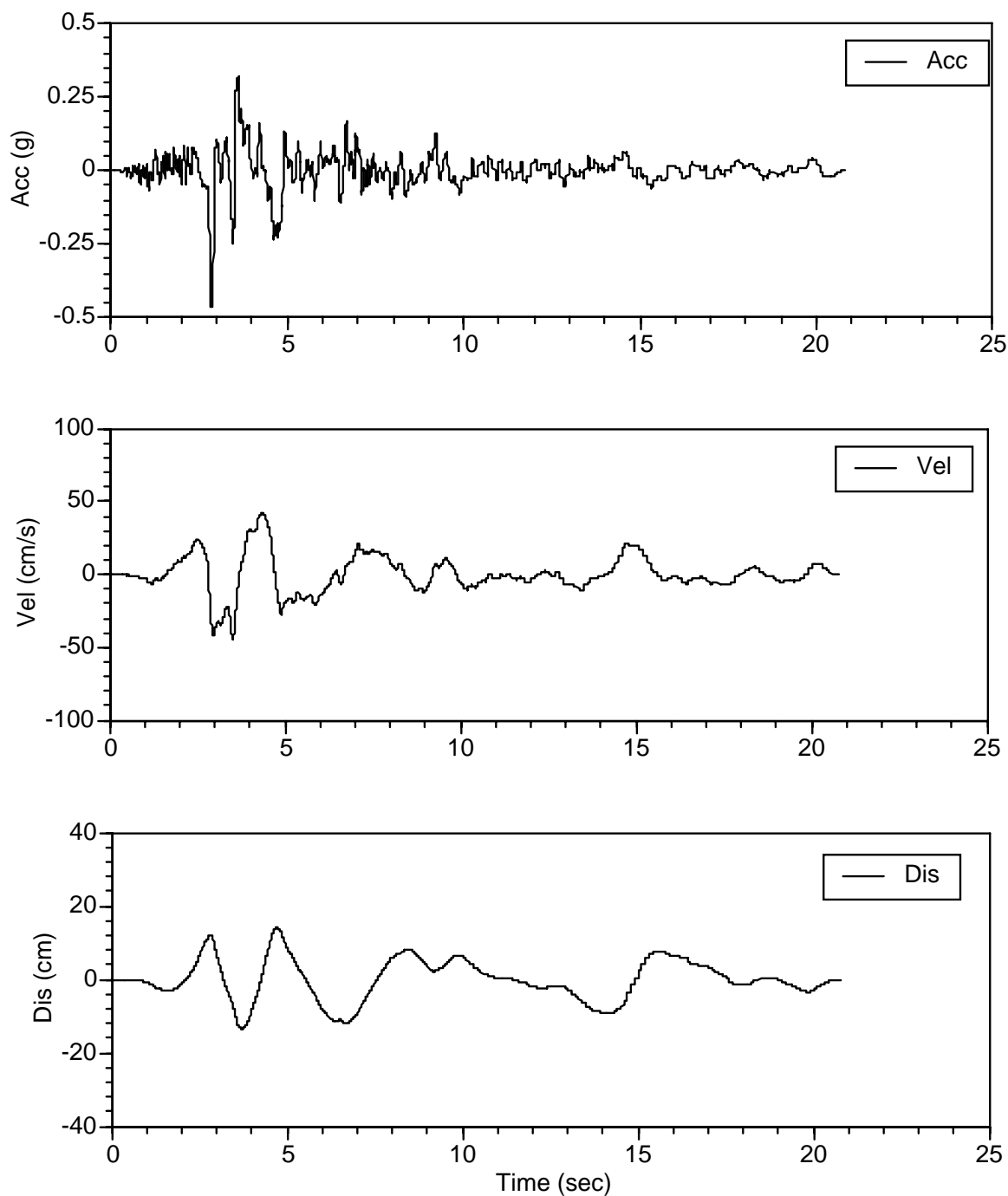
Figure D-5. **Firm-Ground Time Histories Compatible to CLE Firm-Ground Spectra, Set 5**
(d) Initial Time History for FP Component
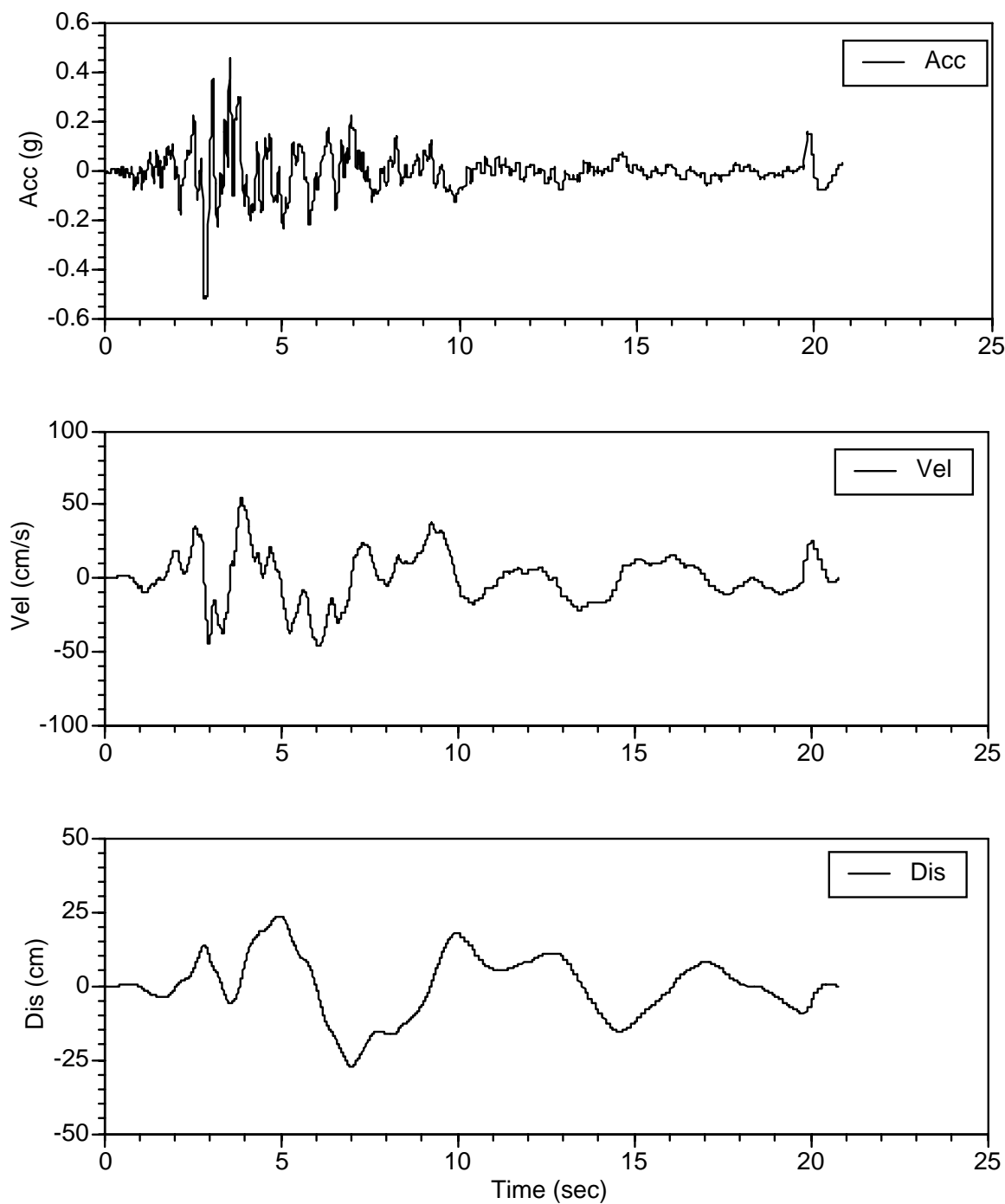
Figure D-5.   Firm-Ground Time Histories Compatible to CLE Firm-Ground Spectra, Set 5
(e) Modified Time History for FP Component
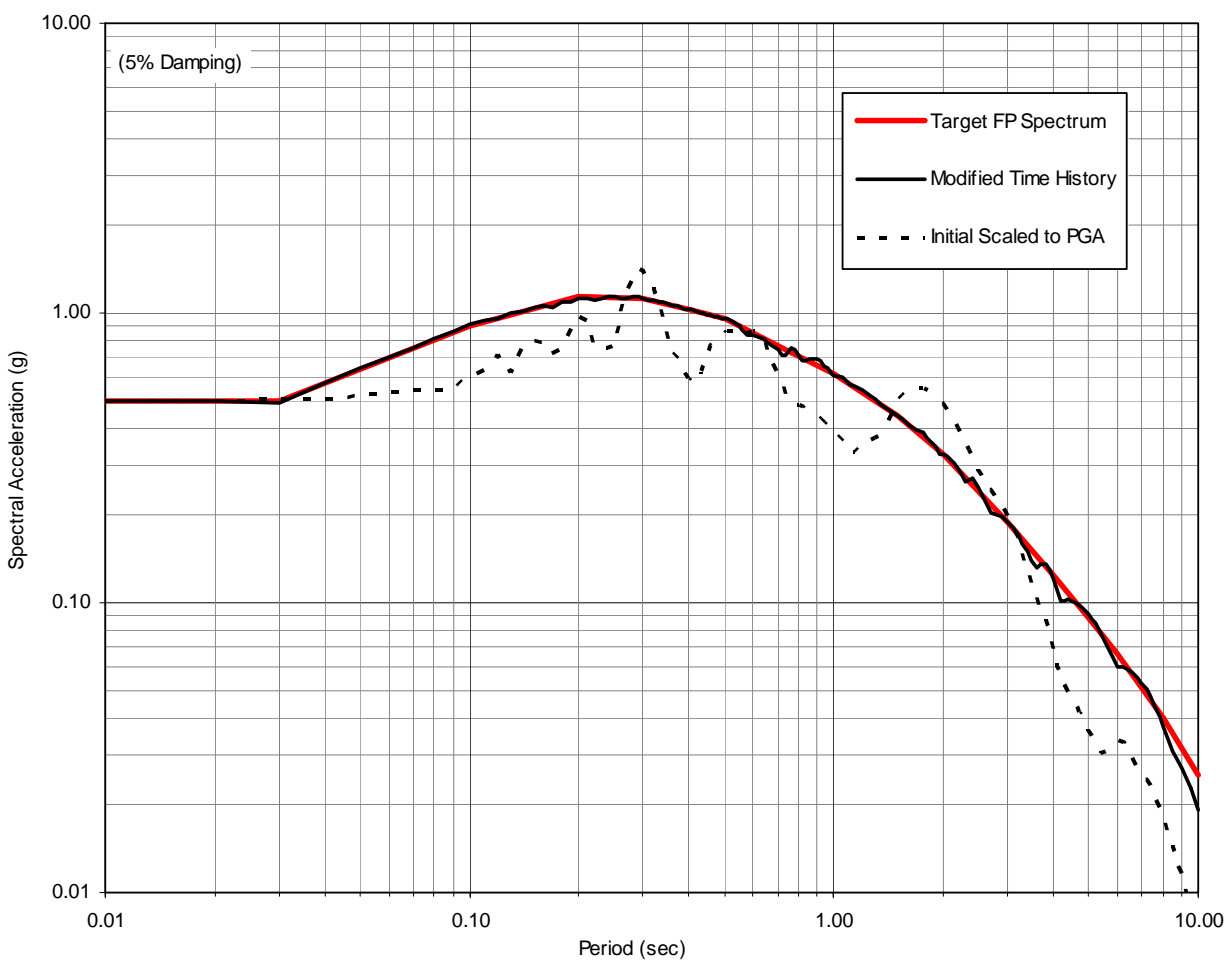
Figure D-5.   Firm-Ground Motions Compatible to CLE Firm-Ground Spectra, Set 5
(f) Comparison of Target Spectrum with Spectra of Scaled and Modified Time
Histories, FP Component
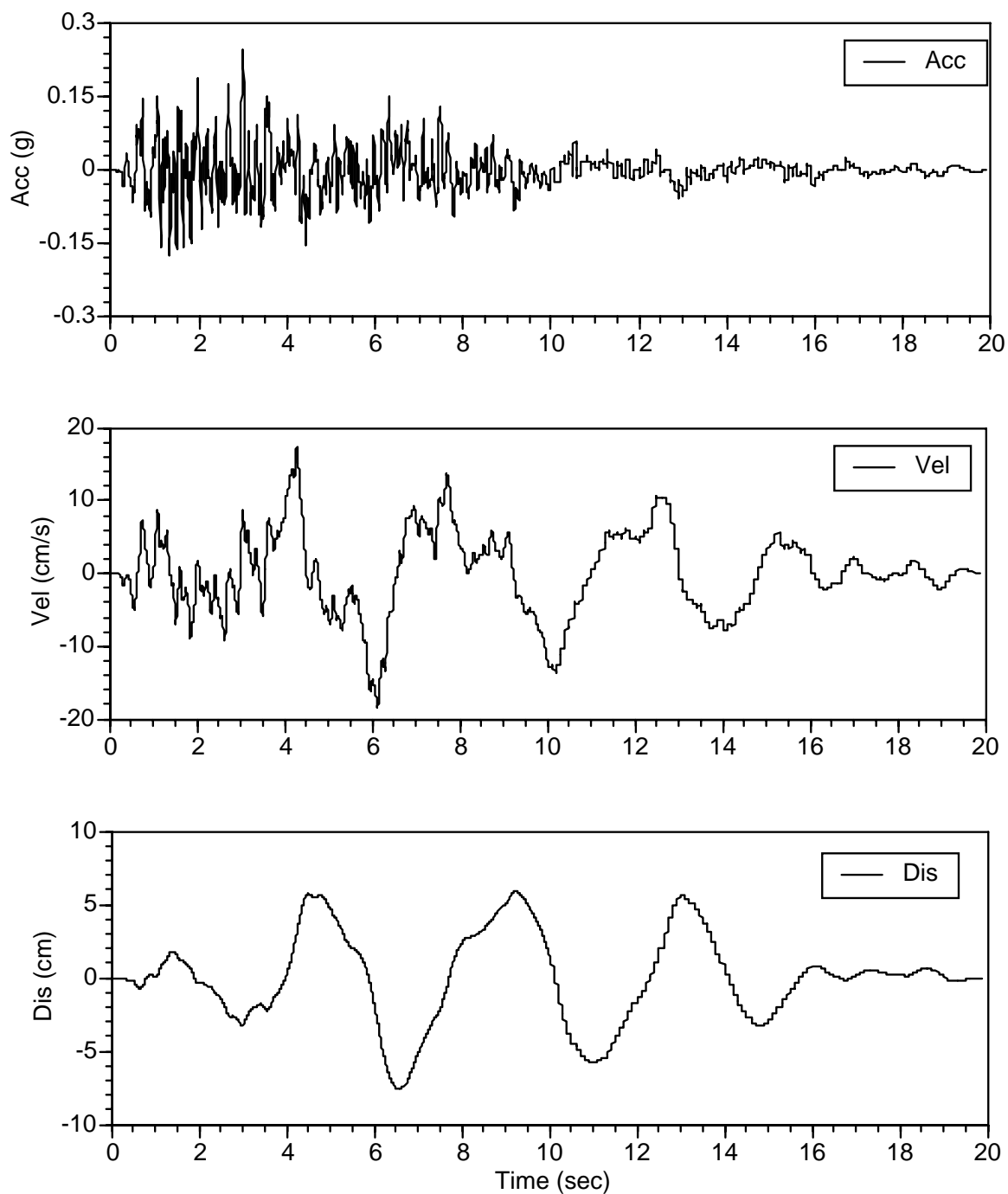
**Figure D-5. Firm-Ground Time Histories Compatible to CLE Firm-Ground Spectra, Set 5
(g) Initial Time History for FV Component**
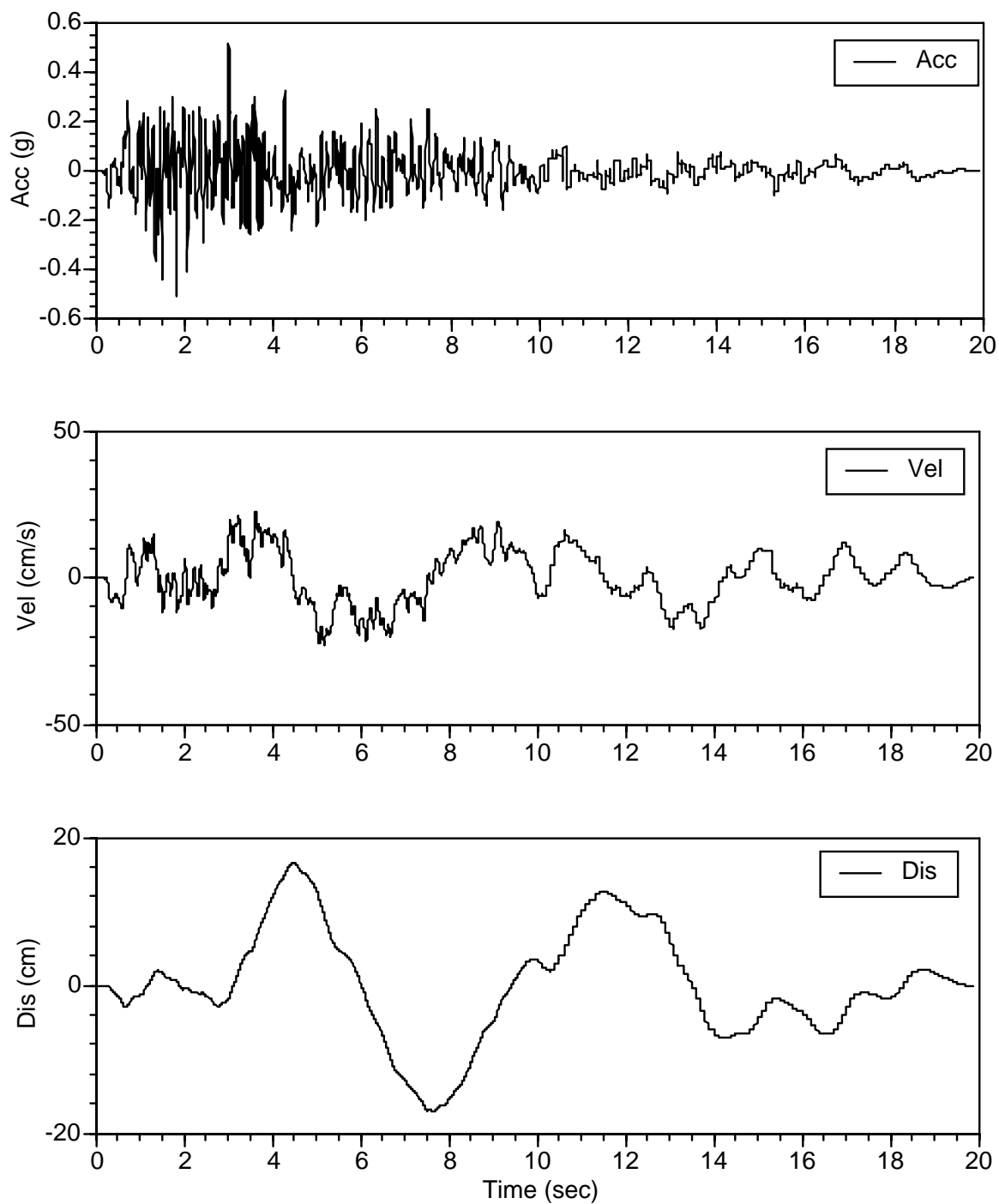
Figure D-5.   Firm-Ground Time Histories Compatible to CLE Firm-Ground Spectra, Set 5
(h) Modified Time History for FV Component
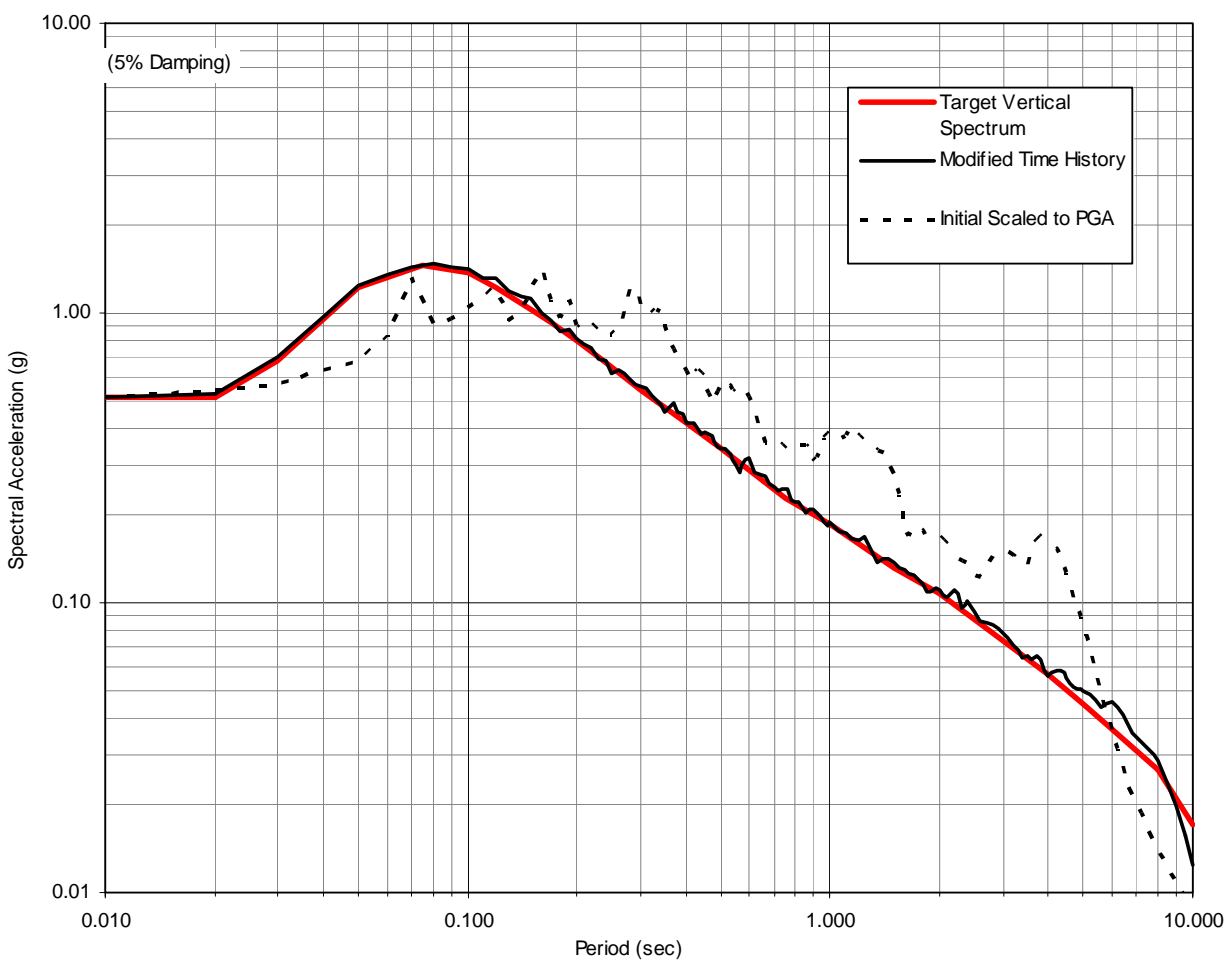
Figure D-5. **Firm-Ground Motions Compatible to CLE Firm-Ground Spectra, Set 5**
(i) Comparison of Target Spectrum with Spectra of Scaled and Modified Time
Histories, FV Component
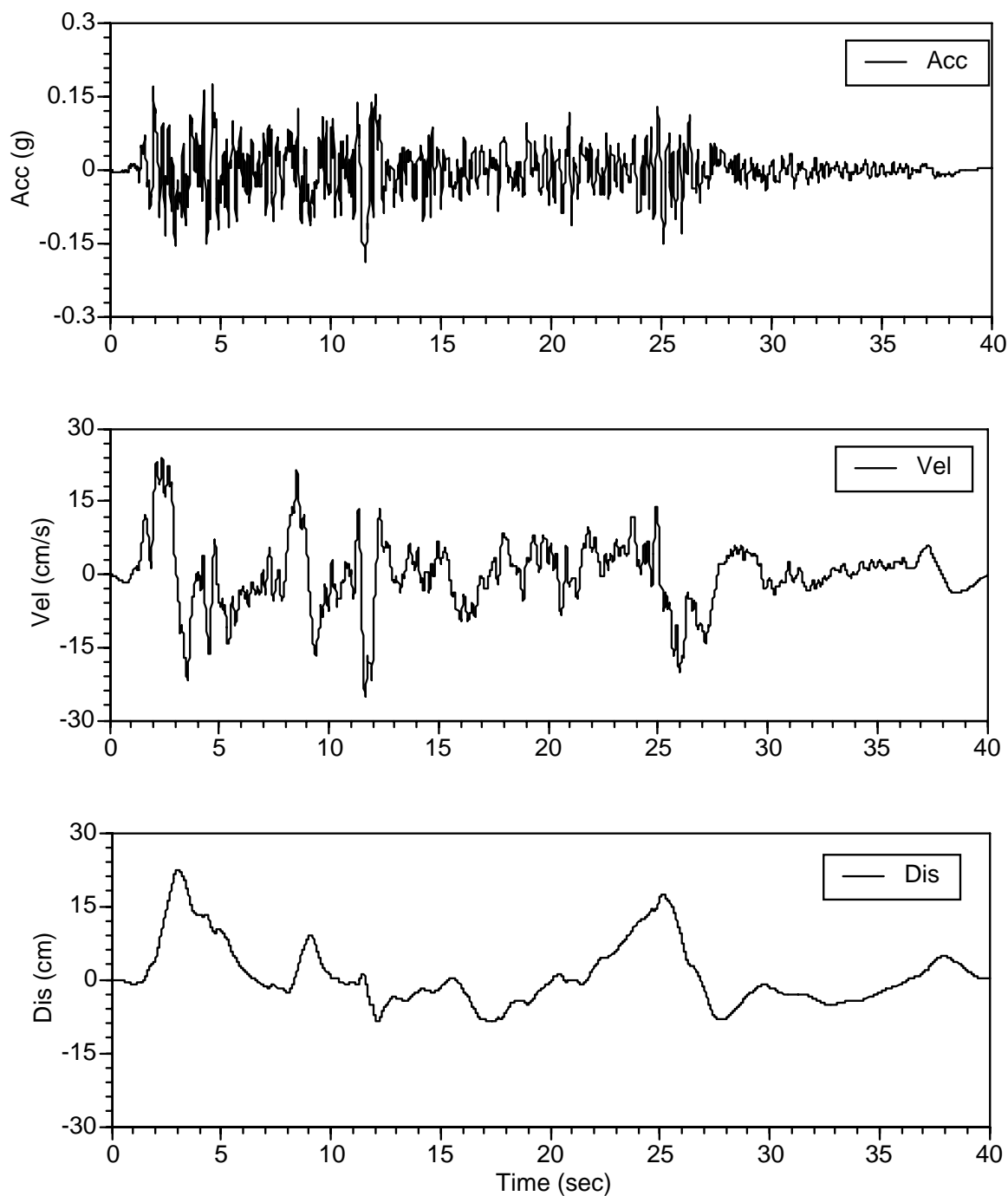
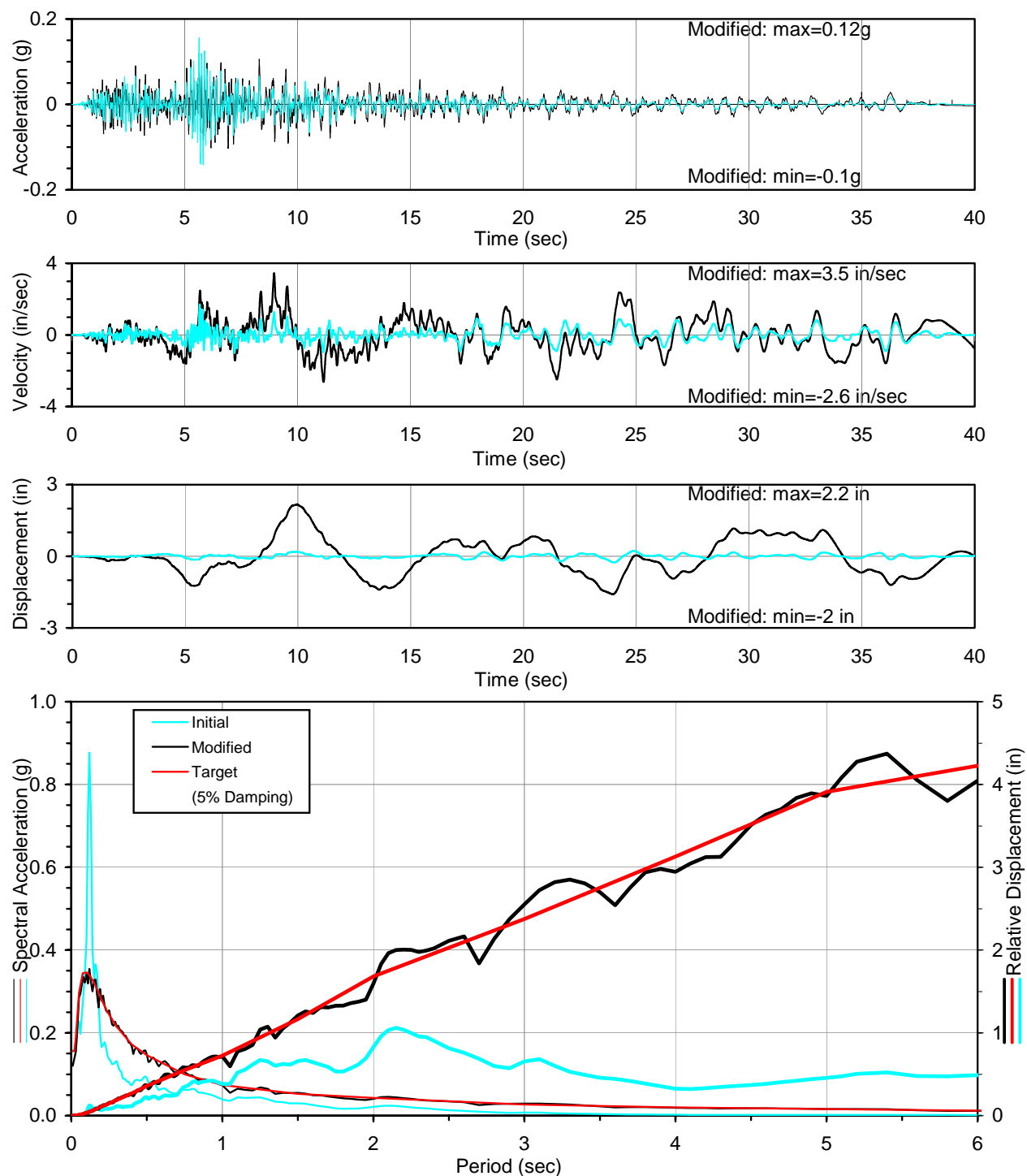**Figure D-6.   Firm-Ground Time Histories Compatible to CLE Firm-Ground Spectra, Set 6
(a) Initial Time History for FN Component**

Figure D-6. Firm-Ground Time Histories Compatible to CLE Firm-Ground Spectra, Set 6
(b) Modified Time History for FN Component

Figure D-6. **Firm-Ground Motions Compatible to CLE Firm-Ground Spectra, Set 6**
(c) Comparison of Target Spectrum with Spectra of Scaled and Modified Time
Histories, FN Component

Figure D-6. **Firm-Ground Time Histories Compatible to CLE Firm-Ground Spectra, Set 6**
(d) Initial Time History for FP Component

**Figure D-6.   Firm-Ground Time Histories Compatible to CLE Firm-Ground Spectra, Set 6
   (e) Modified Time History for FP Component**

**Figure D-6.   Firm-Ground Motions Compatible to CLE Firm-Ground Spectra, Set 6
(f) Comparison of Target Spectrum with Spectra of Scaled and Modified Time
Histories, FP Component**

**Figure D-6.   Firm-Ground Time Histories Compatible to CLE Firm-Ground Spectra, Set 6
(g) Initial Time History for FV Component**

Figure D-6. **Firm-Ground Time Histories Compatible to CLE Firm-Ground Spectra, Set 6**
(h) Modified Time History for FV Component

Figure D-6. **Firm-Ground Motions Compatible to CLE Firm-Ground Spectra, Set 6**
(i) Comparison of Target Spectrum with Spectra of Scaled and Modified Time
Histories, FV Component

Figure D-7.   Firm-Ground Time Histories Compatible to CLE Firm-Ground Spectra, Set 7
(a) Initial Time History for FN Component

Figure D-7. **Firm-Ground Time Histories Compatible to CLE Firm-Ground Spectra, Set 7**
(b) Modified Time History for FN Component

**Figure D-7.   Firm-Ground Motions Compatible to CLE Firm-Ground Spectra, Set 7
(c) Comparison of Target Spectrum with Spectra of Scaled and Modified Time
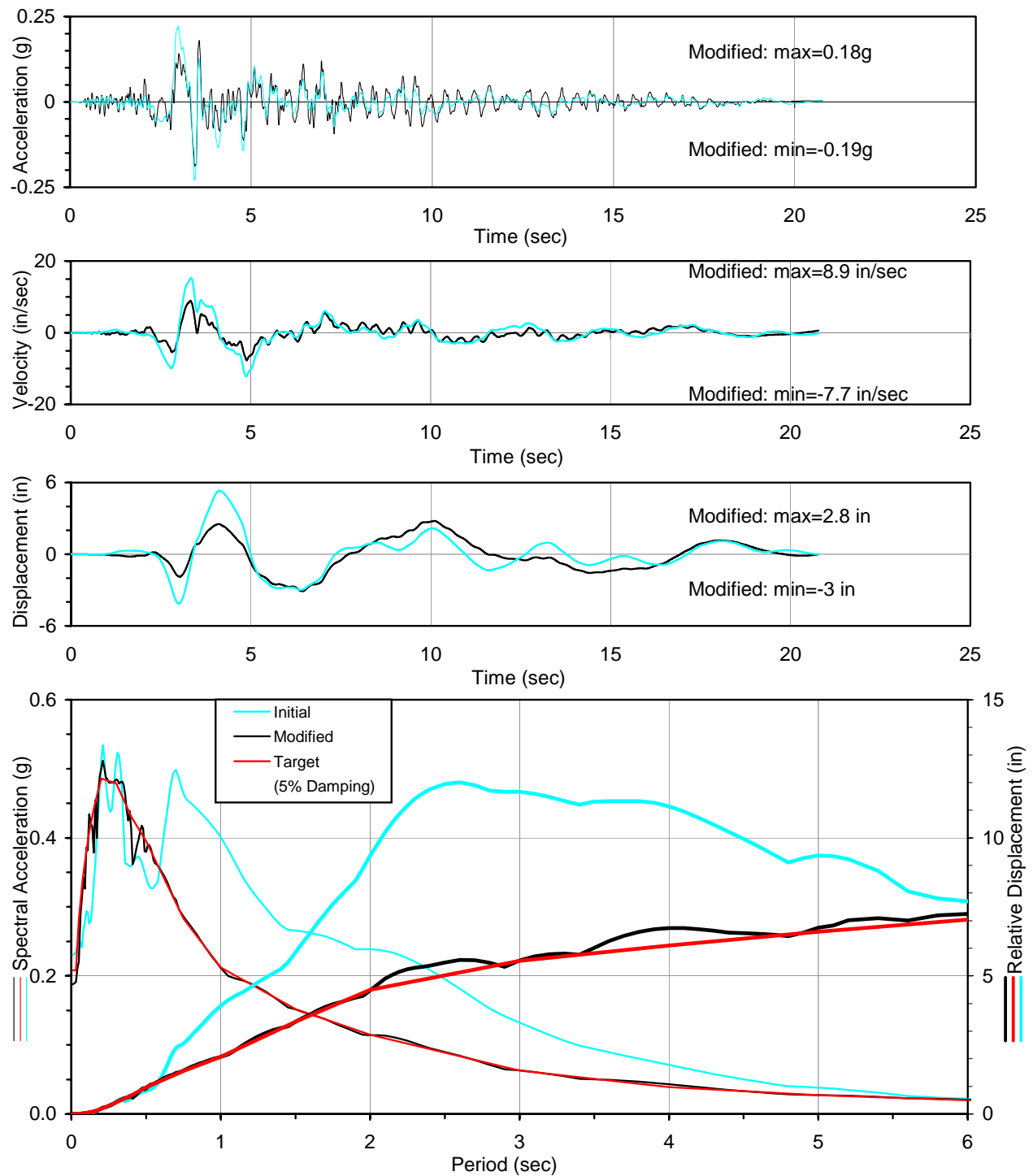Histories, FN Component**

Figure D-7. **Firm-Ground Time Histories Compatible to CLE Firm-Ground Spectra, Set 7**
(d) Initial Time History for FP Component

Figure D-7. **Firm-Ground Time Histories Compatible to CLE Firm-Ground Spectra, Set 7**
(e) Modified Time History for FP Component

**Figure D-7.   Firm-Ground Motions Compatible to CLE Firm-Ground Spectra, Set 7
(f) Comparison of Target Spectrum with Spectra of Scaled and Modified Time
Histories, FP Component**

**Figure D-7.　Firm-Ground Time Histories Compatible to CLE Firm-Ground Spectra, Set 7
　　　(g) Initial Time History for FV Component**
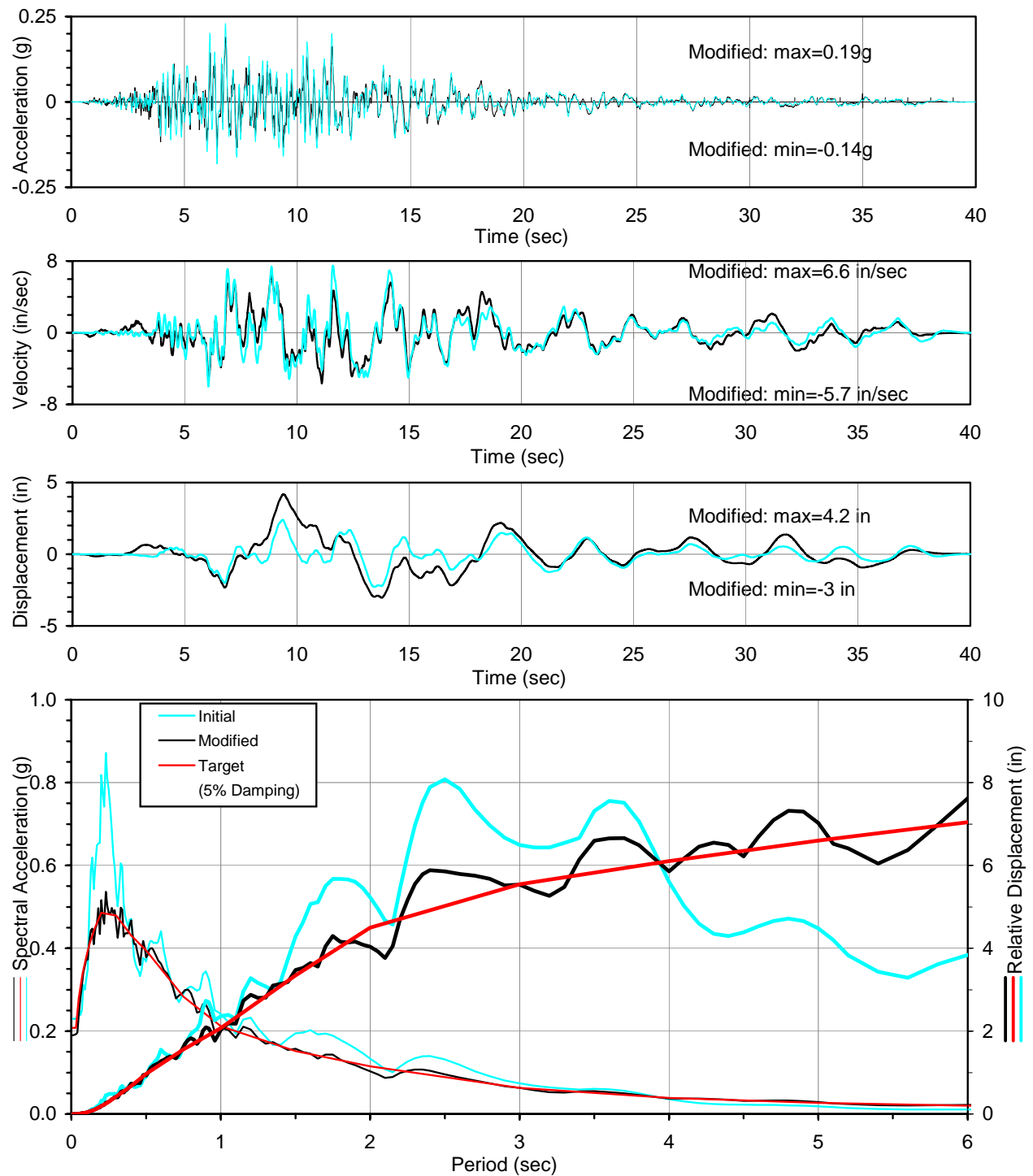
Figure D-7. **Firm-Ground Time Histories Compatible to CLE Firm-Ground Spectra, Set 7**
(h) Modified Time History for FV Component

Figure D-7. **Firm-Ground Motions Compatible to CLE Firm-Ground Spectra, Set 7 (i) Comparison of Target Spectrum with Spectra of Scaled and Modified Time Histories, FV Component**

D.2   FIRM-GROUND TIME HISTORIES COMPATIBLE TO OLE FIRM-GROUND SPECTRA

The seven (7) sets of 3-component startup time histories for an Operating-Level Earthquake are listed in Table D-2. These time histories were modified to match the target design spectrum adjusted for the site-specific soil conditions. The seven sets of time histories were chosen based on the 72-year deaggregation hazard solutions which show that the hazards at the 72-year return period could be associated with many possible events, including Magnitude 6.5-7.0 earthquakes from nearby faults (0-10 km) including the Palos Verdes fault, but also could be associated with other larger magnitude (say M7.5) from more distance faults (30-100 km). Therefore, the seven startup motions reflect earthquakes ranging from Magnitude 6.5-7.0, and from distances extending from near-fault to moderate distance events. To obtain a firm-ground target spectrum compatible with the design spectrum at the ground surface, the recommended horizontal design spectrum (Figure 5-7) was divided by the transfer function between firm-ground and ground surface motions. The transfer function is the ratio of the theoretical site-effect adjusted spectrum and the horizontal firm-ground UHS (Figures 3-11 and 3-13) and (Figure 4-3).

Each motion set has three (FN, FP and FV) Components, resulting in a total of 21 time histories. For each time history, the following is plotted:

- Initial acceleration, velocity and displacement time histories scaled to PGA,

- Spectrum-matched acceleration, velocity and displacement time histories, and

- Comparison of the corresponding spectra of spectrum-matched time histories with the target firm-ground OLE spectrum that is compatible to the design spectrum.

These plots are shown in Figure D-8 through Figure D-14 for the OLE time history set number 1 through set number 7, respectively.

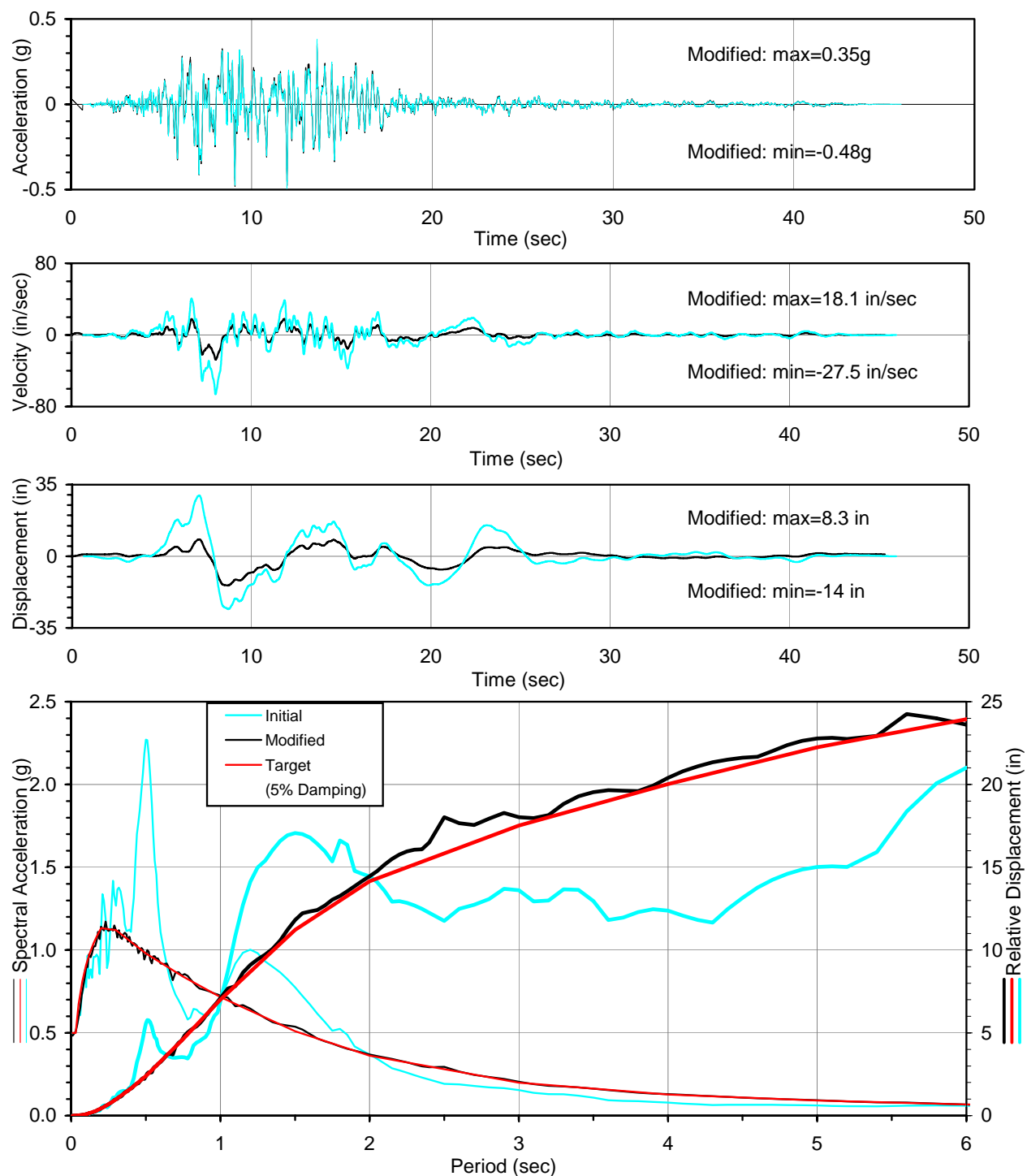**Table D-2.   Ground Motion Sets Selected for OLE Spectral Matching**

Set	Earthquake	Mag.	Station	Distance (km)
1	1989 Loma Prieta	6.9	Saratoga – Aloha Ave.	13.0
2	1987 Superstition Hill	6.3	Wildlife Liquefaction Array	24.7
3	1987 Whittier	6.0	Northridge-Saticoy St.	39.8
4	1979 Imperial Valley	6.5	EC CO Center FF	7.6
5	1979 Imperial Valley	6.5	Calexico Fire Station	10.6
6	1992 Erzikan	6.9	Erzikan	2.0
7	1994 Northridge	6.7	Century City, LACC	25.7

Figure D-8.   Firm-Ground Time Histories Compatible to OLE Firm-Ground Spectra, Set 1
(a) FN Component
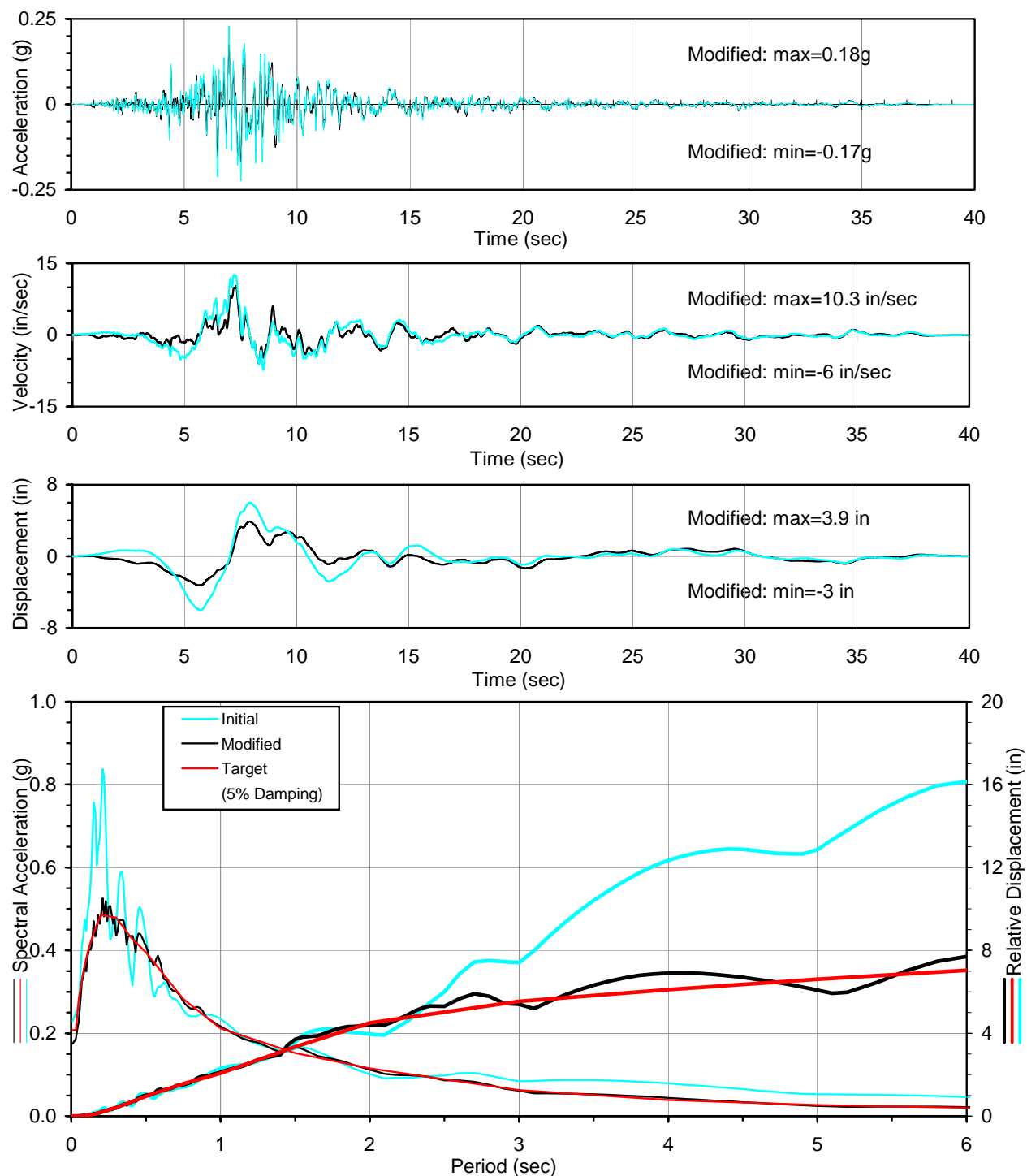
**Figure D-8.   Firm-Ground Time Histories Compatible to OLE Firm-Ground Spectra, Set 1
(b) FP Component**
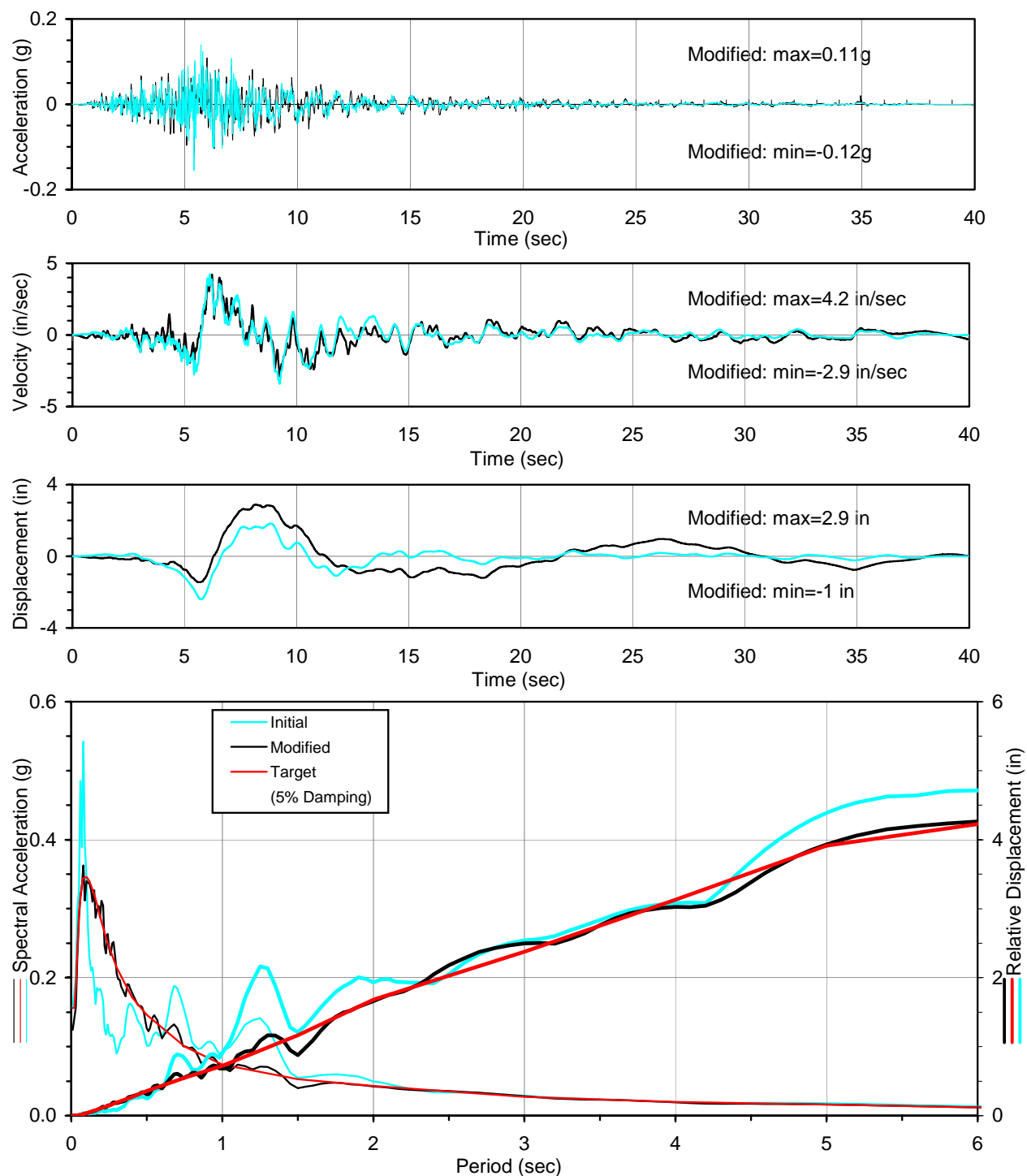
Figure D-8. **Firm-Ground Time Histories Compatible to OLE Firm-Ground Spectra, Set 1 (c) FV Component**
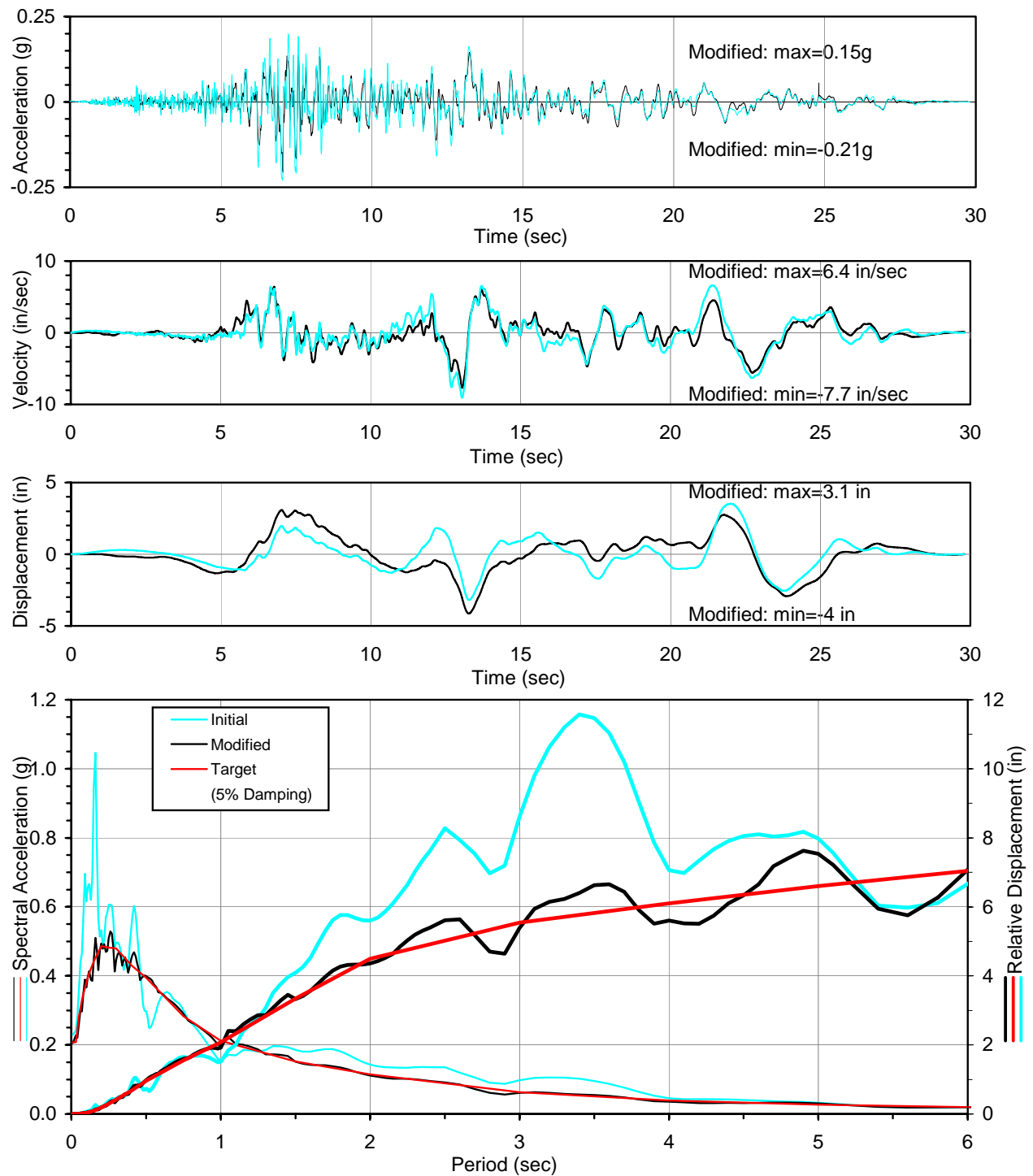
Figure D-9.   Firm-Ground Time Histories Compatible to OLE Firm-Ground Spectra, Set 2
(a) FN Component
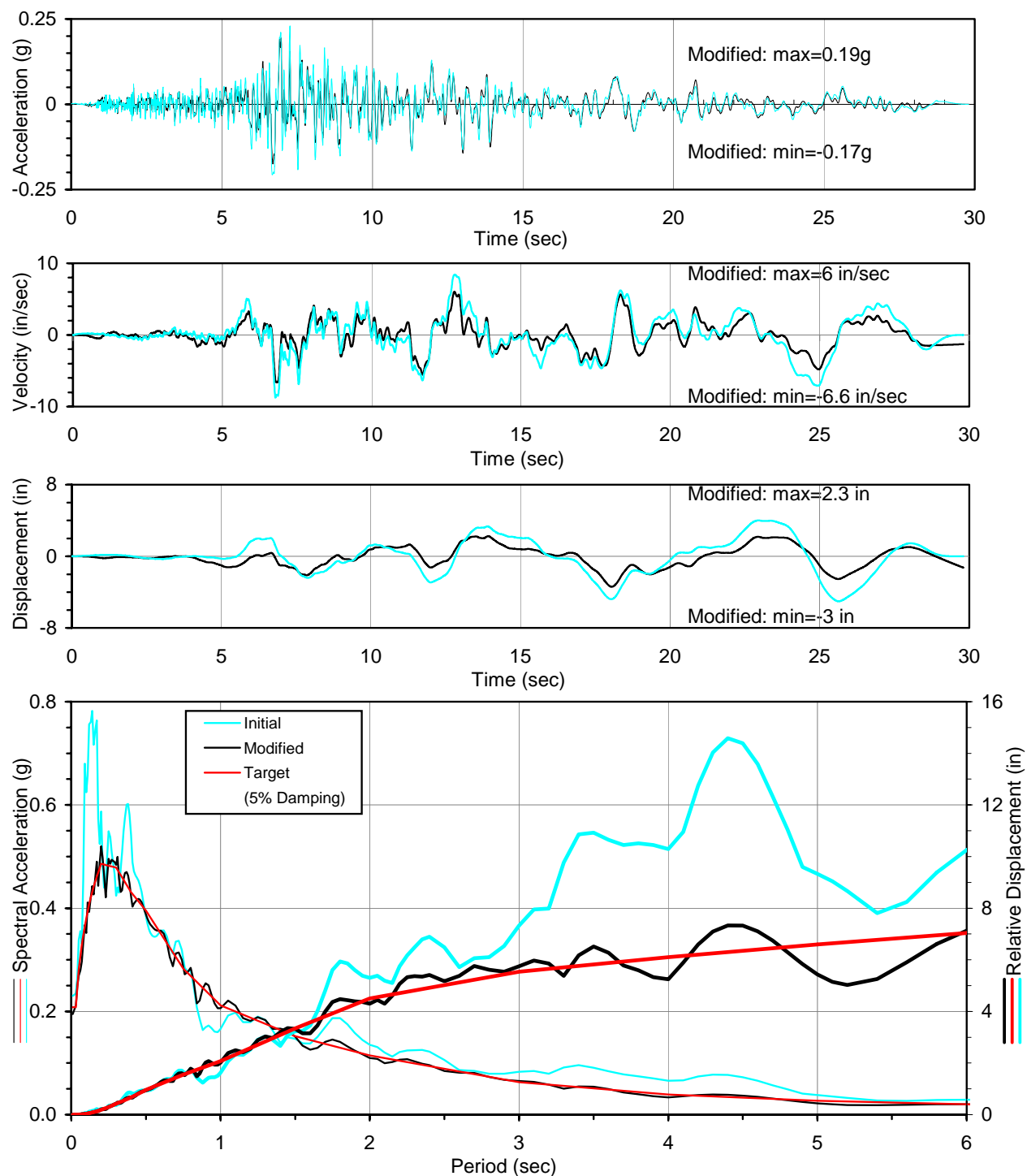
**Figure D-9. Firm-Ground Time Histories Compatible to OLE Firm-Ground Spectra, Set 2
(b) FP Component**
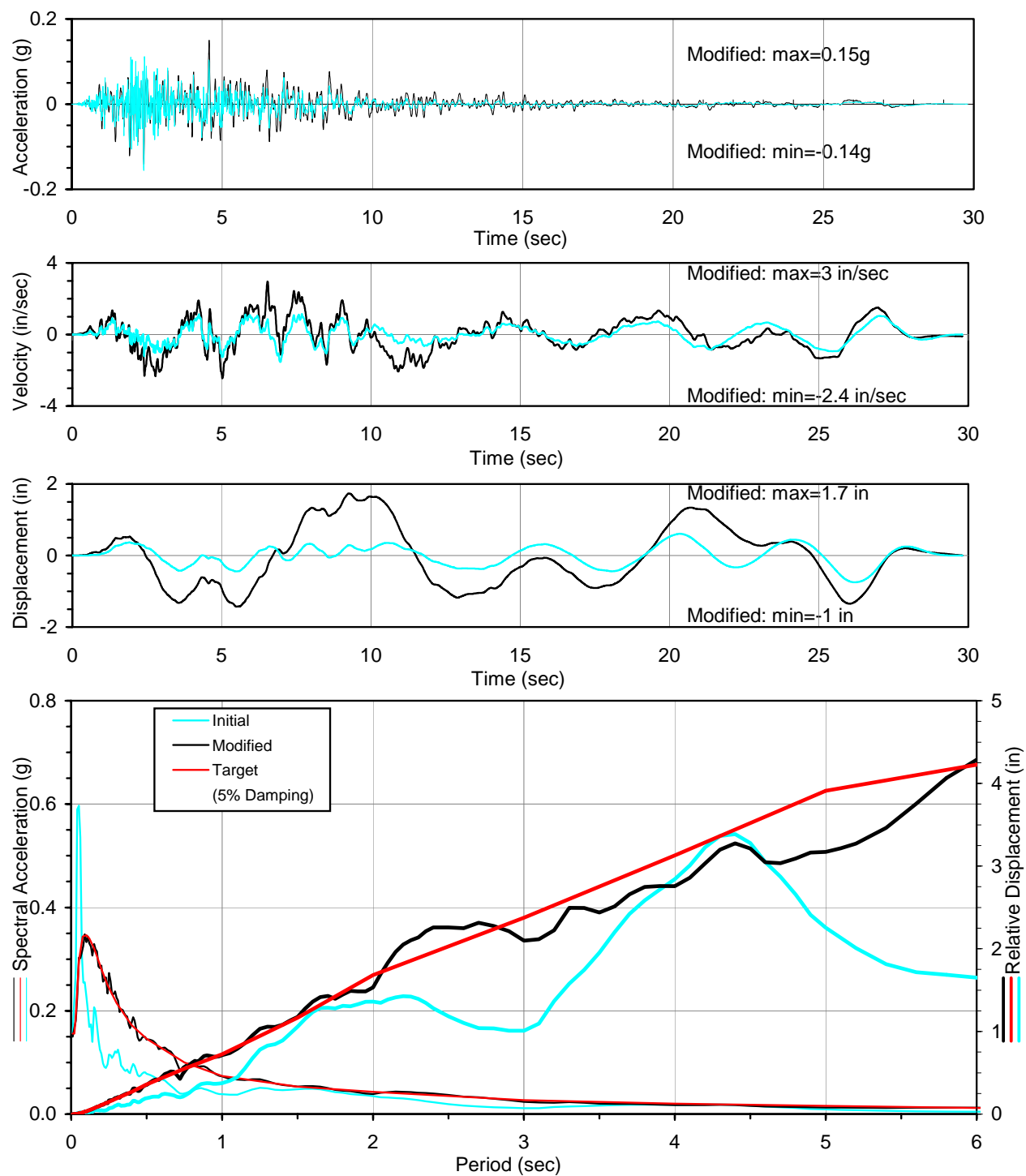
**Figure D-9.   Firm-Ground Time Histories Compatible to OLE Firm-Ground Spectra, Set 2
(c) FV Component**
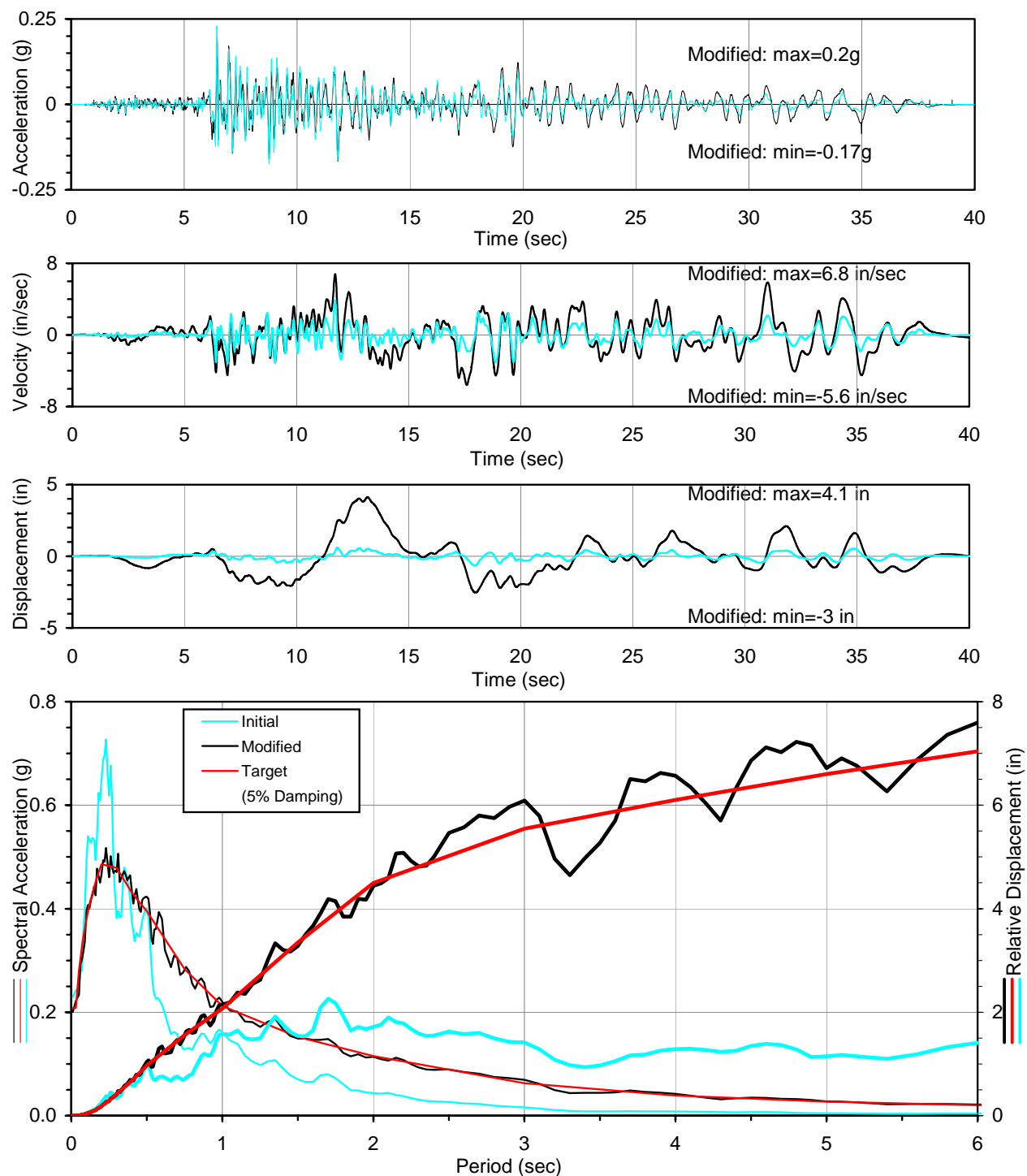
Figure D-10. Firm-Ground Time Histories Compatible to OLE Firm-Ground Spectra, Set 3
(a) FN Component
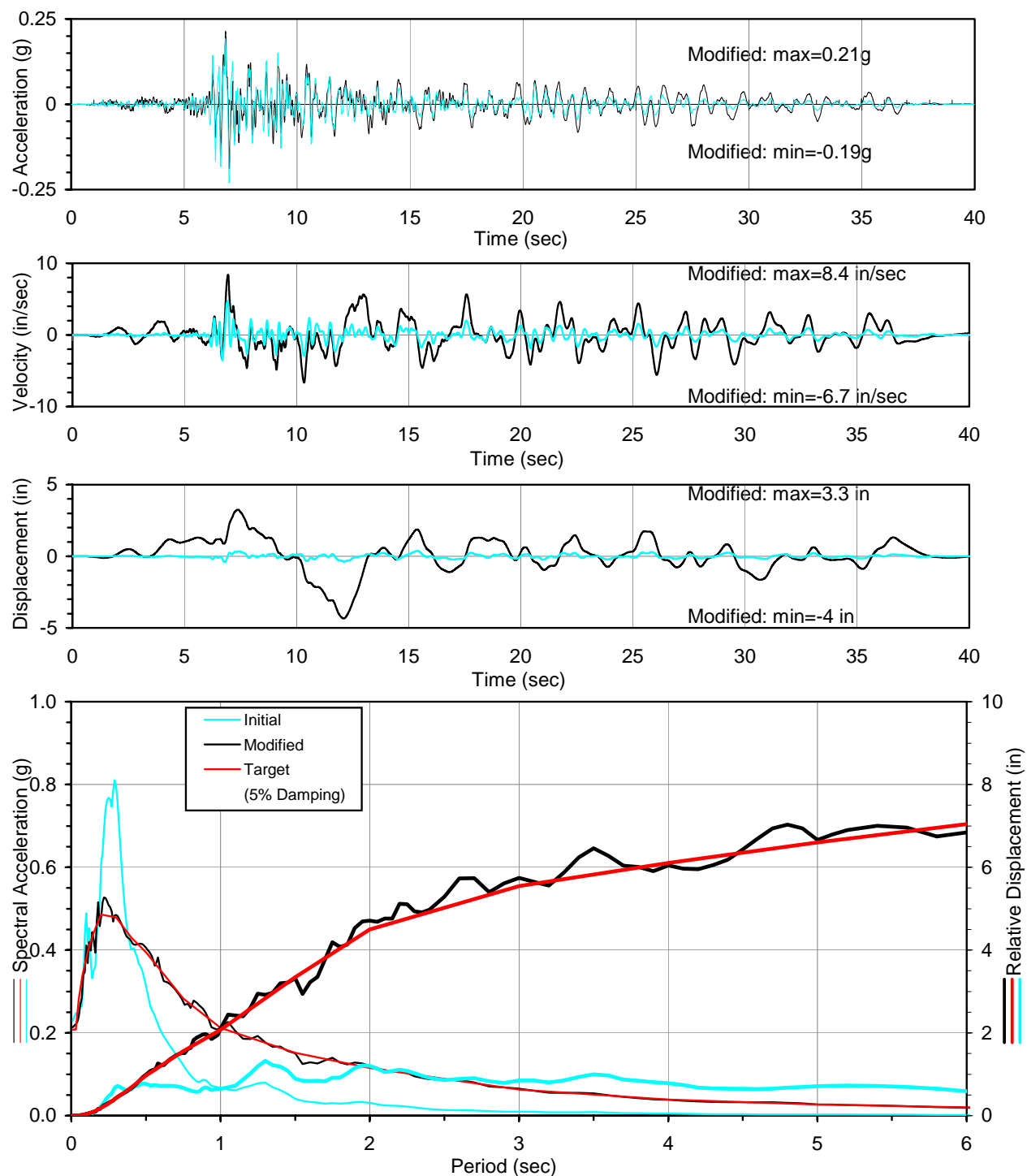
Figure D-10. Firm-Ground Time Histories Compatible to OLE Firm-Ground Spectra, Set 3 (b) FP Component

**Figure D-10. Firm-Ground Time Histories Compatible to OLE Firm-Ground Spectra, Set 3
(c) FV Component**
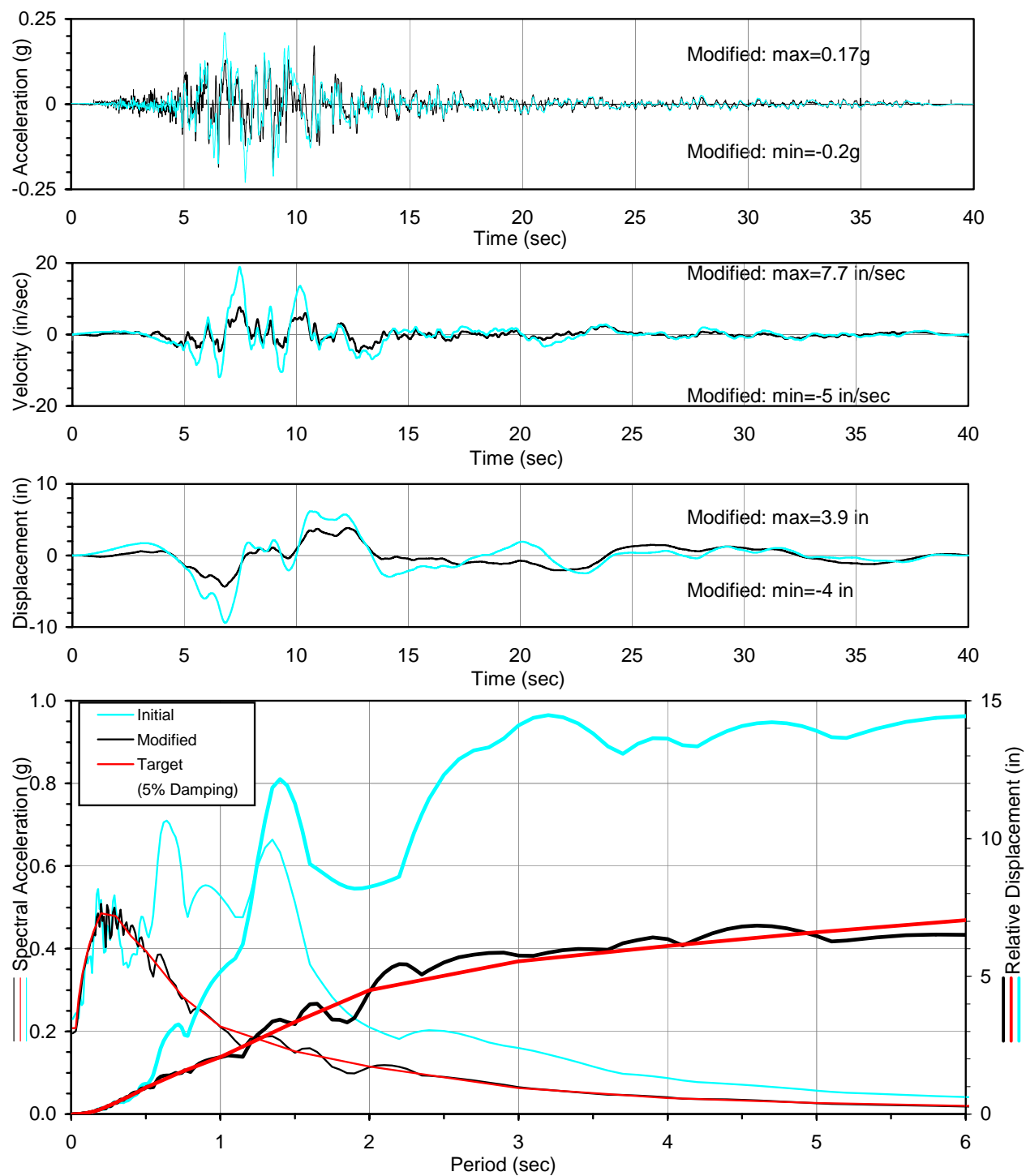
Figure D-11. Firm-Ground Time Histories Compatible to OLE Firm-Ground Spectra, Set 4
(a) FN Component
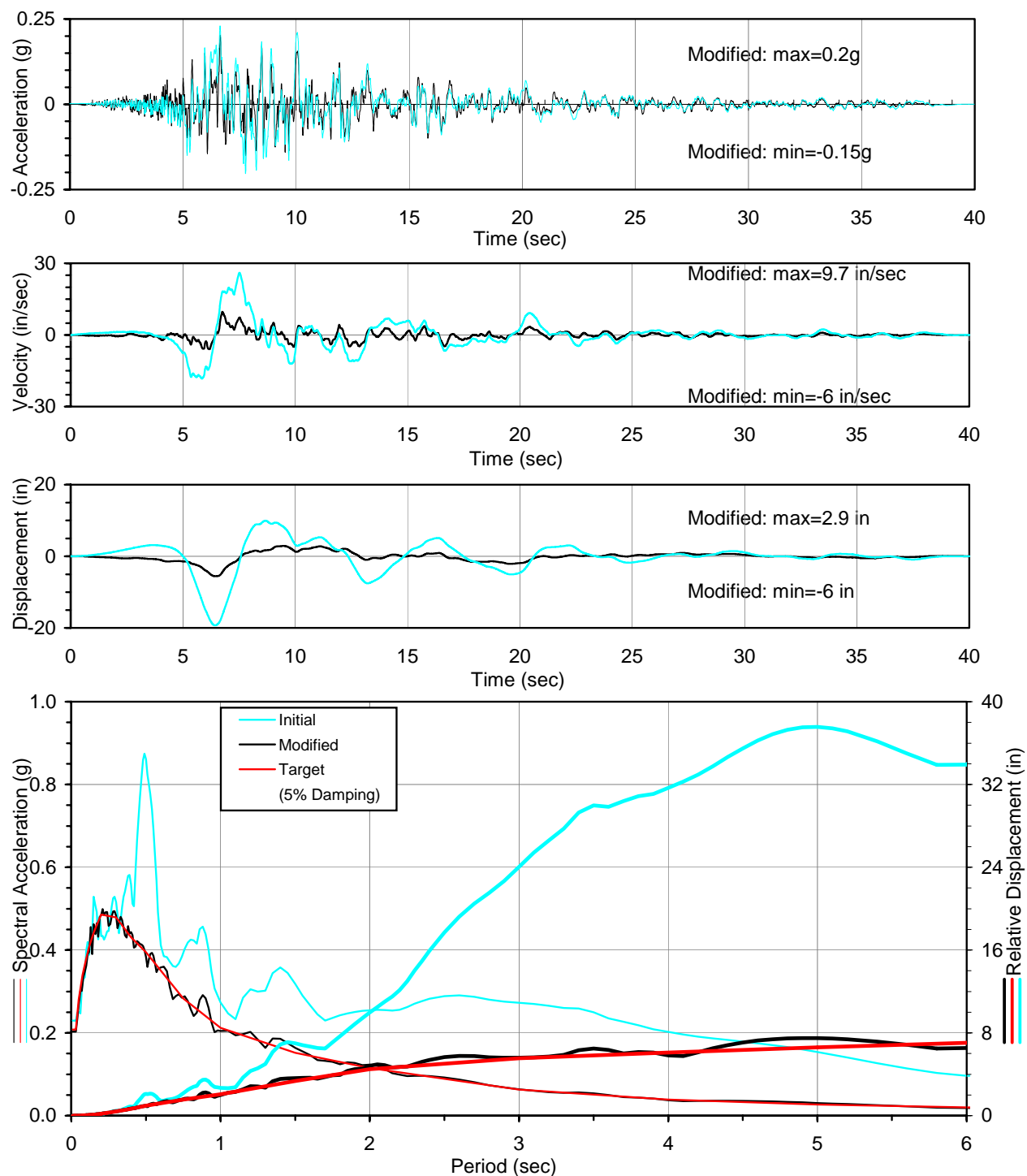
Figure D-11. Firm-Ground Time Histories Compatible to OLE Firm-Ground Spectra, Set 4
(b) FP Component
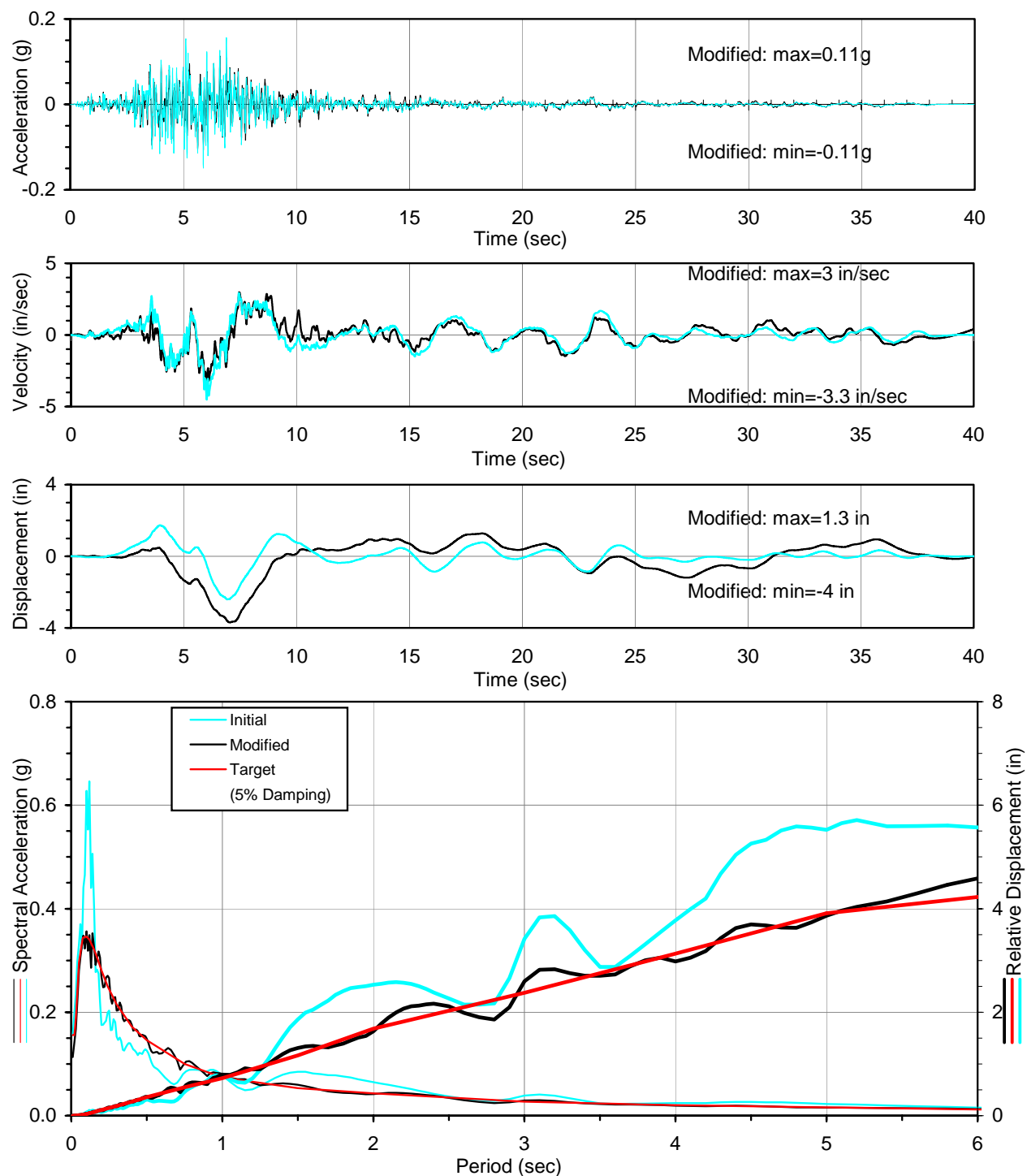
**Figure D-11. Firm-Ground Time Histories Compatible to OLE Firm-Ground Spectra, Set 4
(c) FV Component**
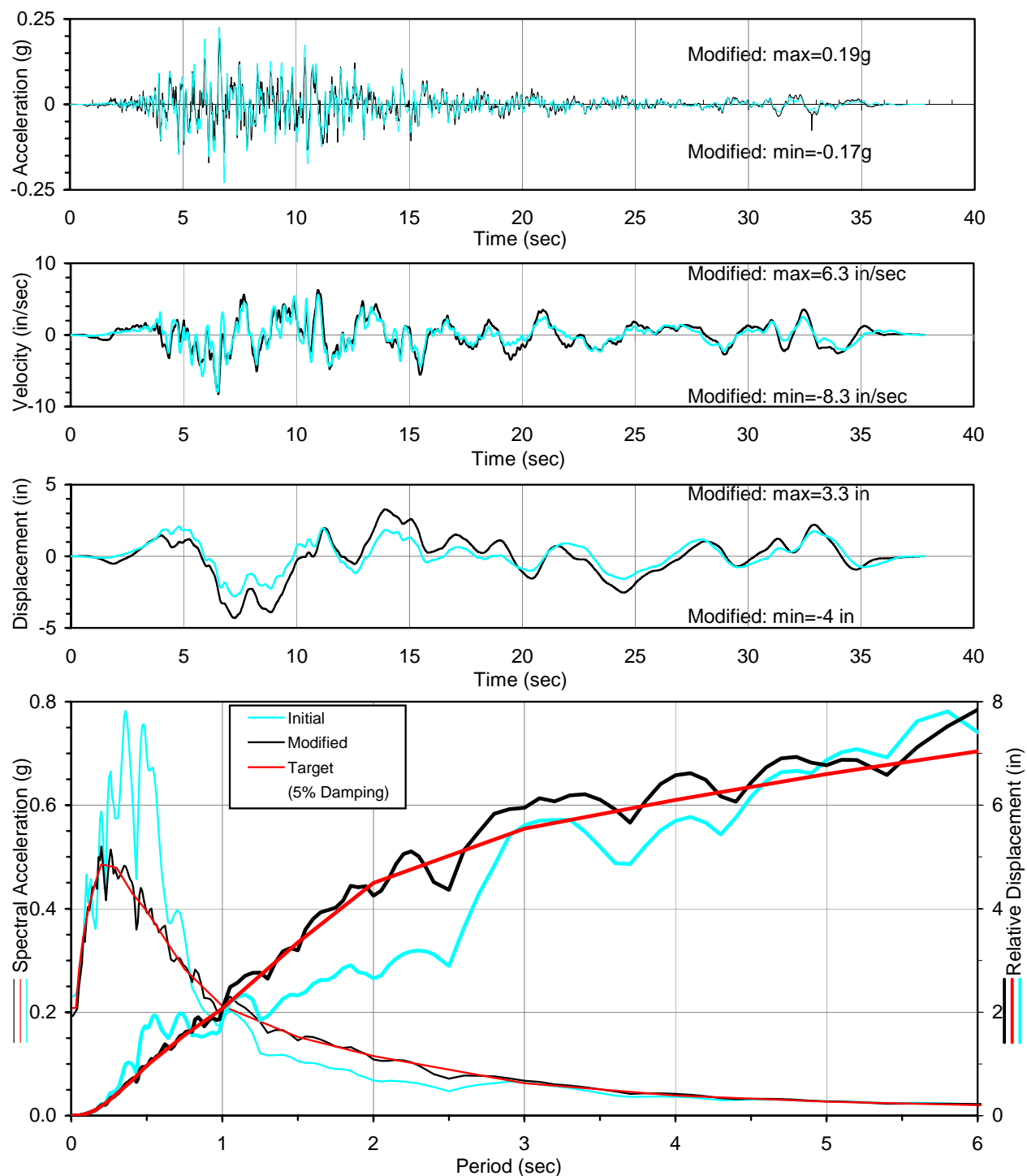
Figure D-12. Firm-Ground Time Histories Compatible to OLE Firm-Ground Spectra, Set 5
(a) FN Component
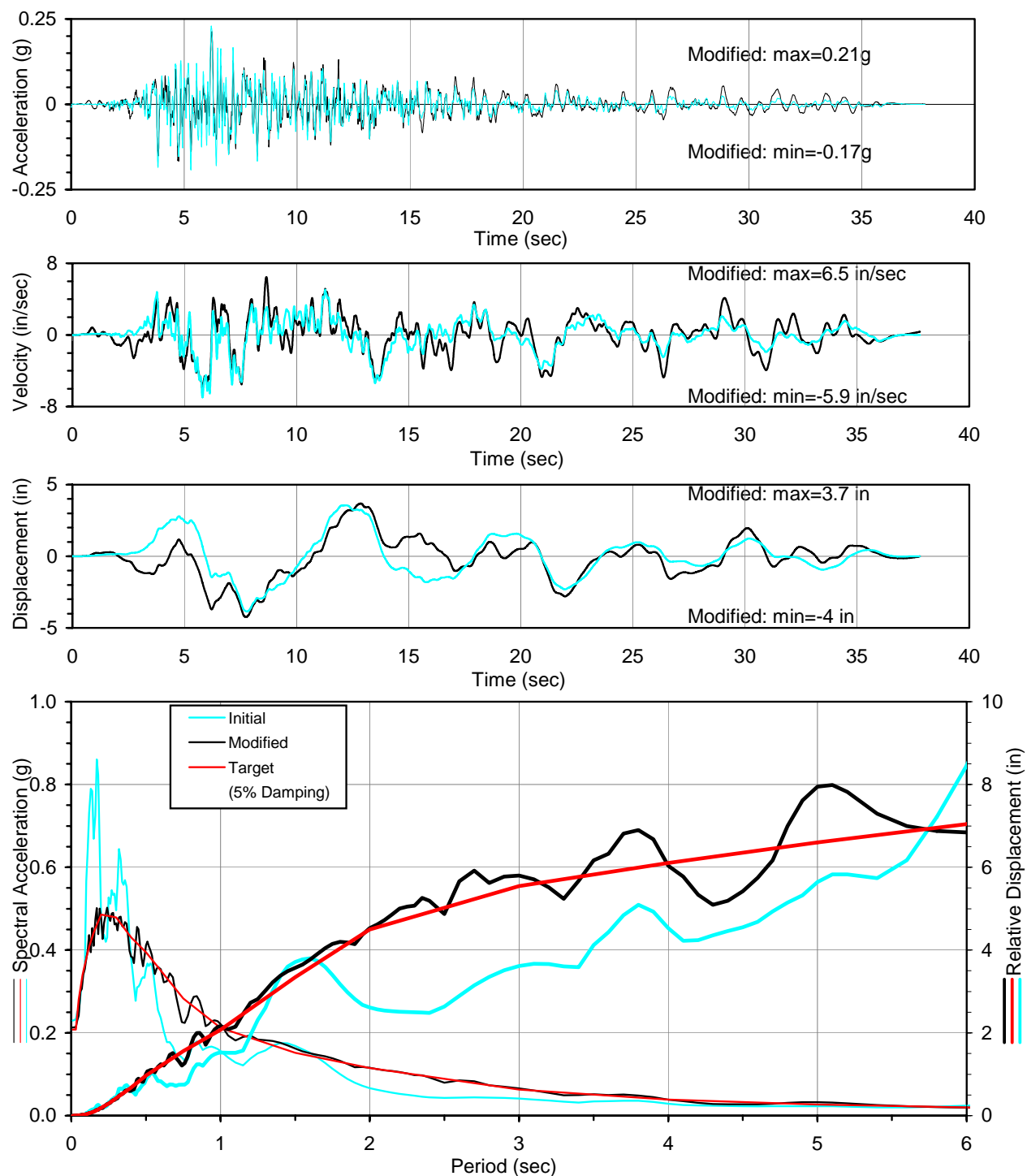
**Figure D-12. Firm-Ground Time Histories Compatible to OLE Firm-Ground Spectra, Set 5
(b) FP Component**
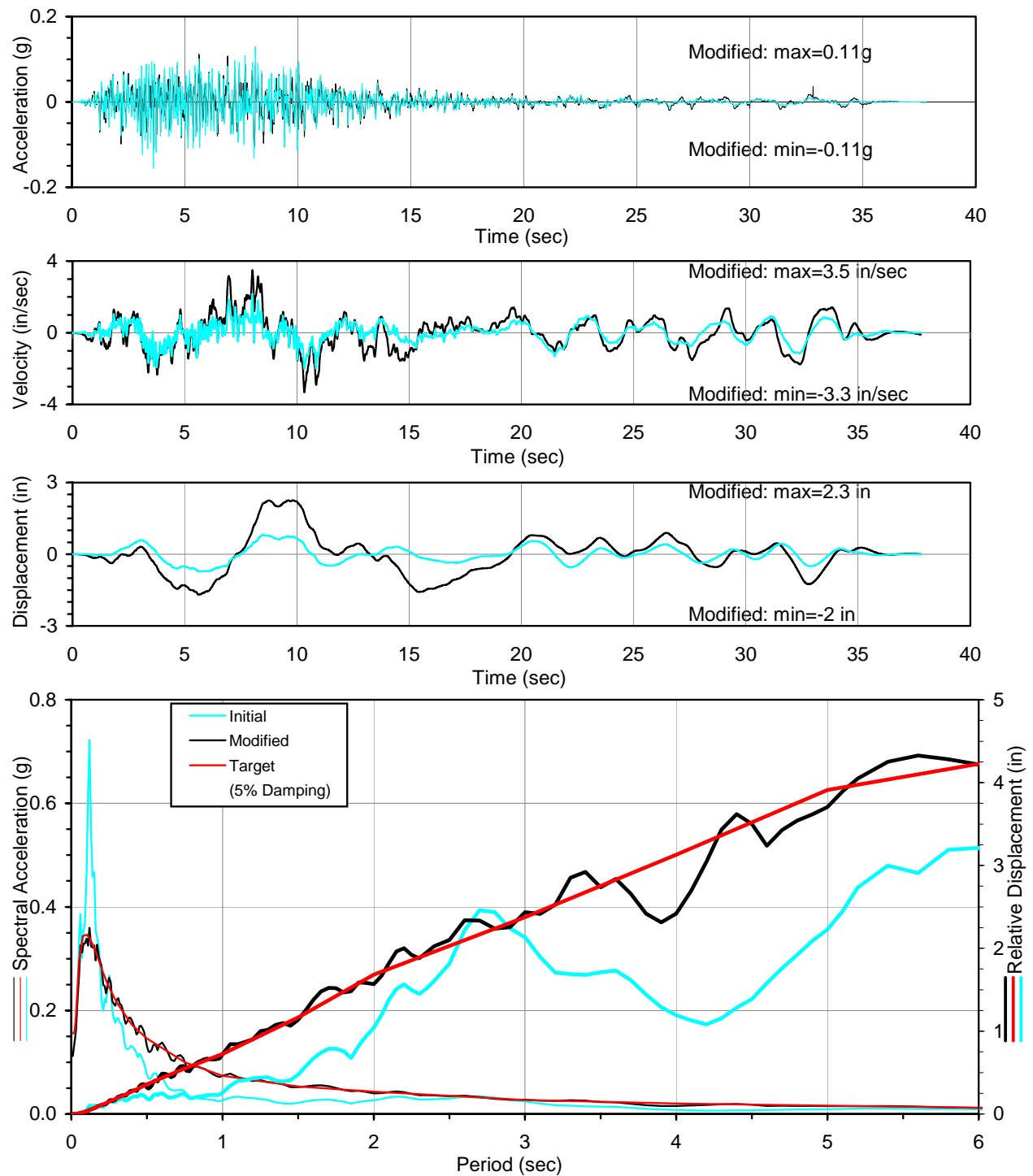
Figure D-12. Firm-Ground Time Histories Compatible to OLE Firm-Ground Spectra, Set 5
(c) FV Component

**Figure D-13. Firm-Ground Time Histories Compatible to OLE Firm-Ground Spectra, Set 6
        (a) FN Component**
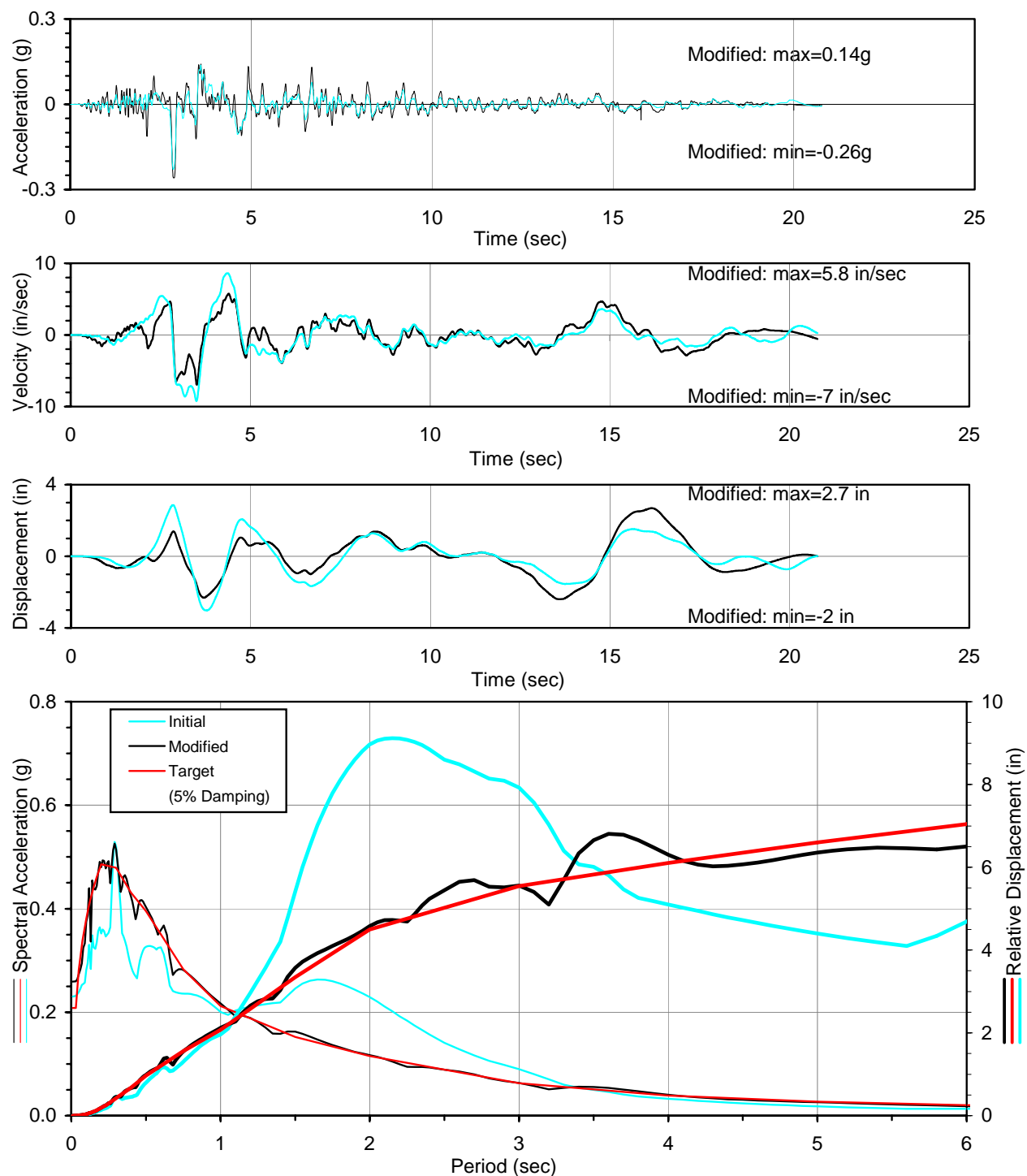
Figure D-13. Firm-Ground Time Histories Compatible to OLE Firm-Ground Spectra, Set 6 (b) FP Component
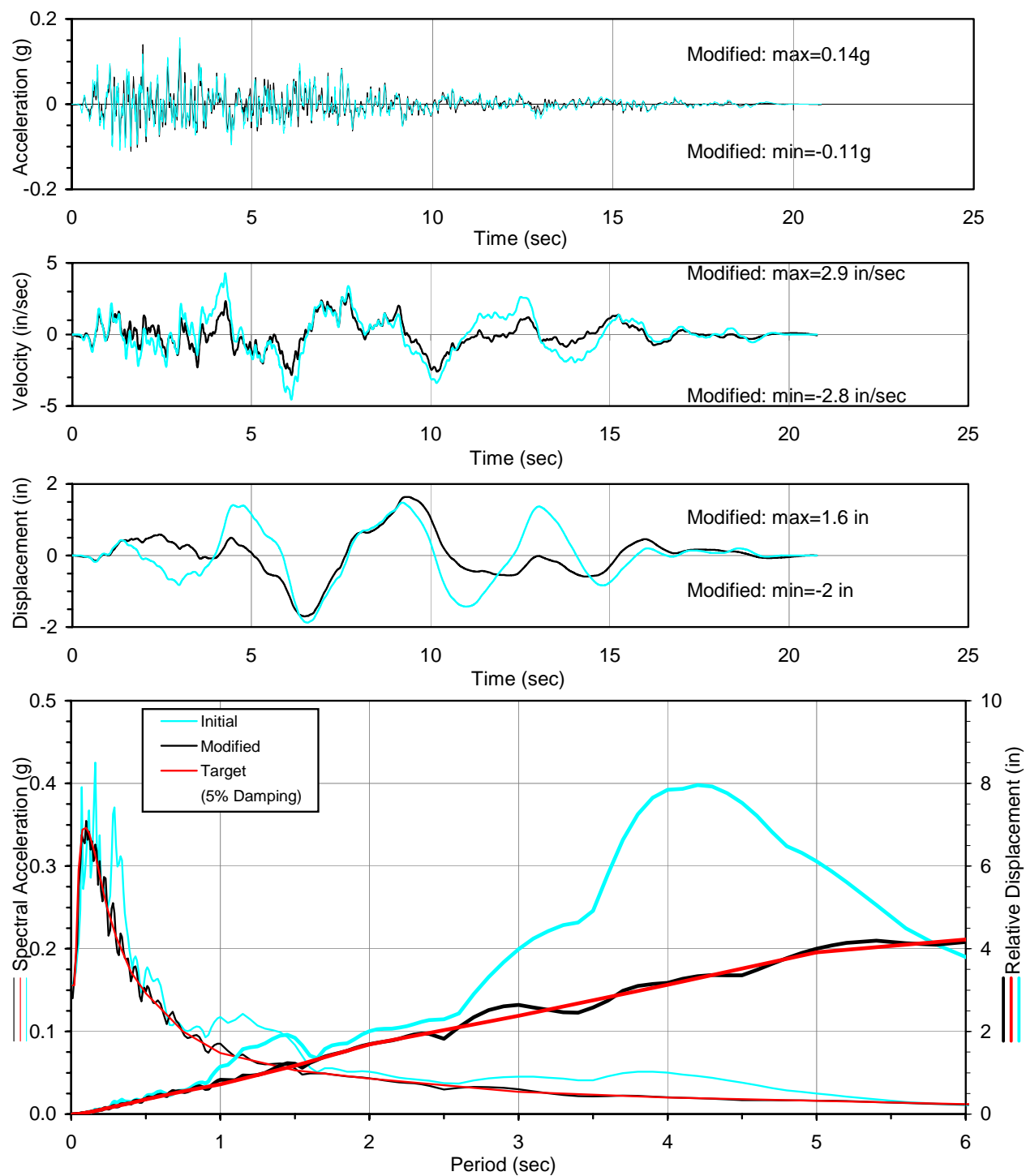
**Figure D-13. Firm-Ground Time Histories Compatible to OLE Firm-Ground Spectra, Set 6
(c) FV Component**

**Figure D-14. Firm-Ground Time Histories Compatible to OLE Firm-Ground Spectra, Set 7
(a) FN Component**
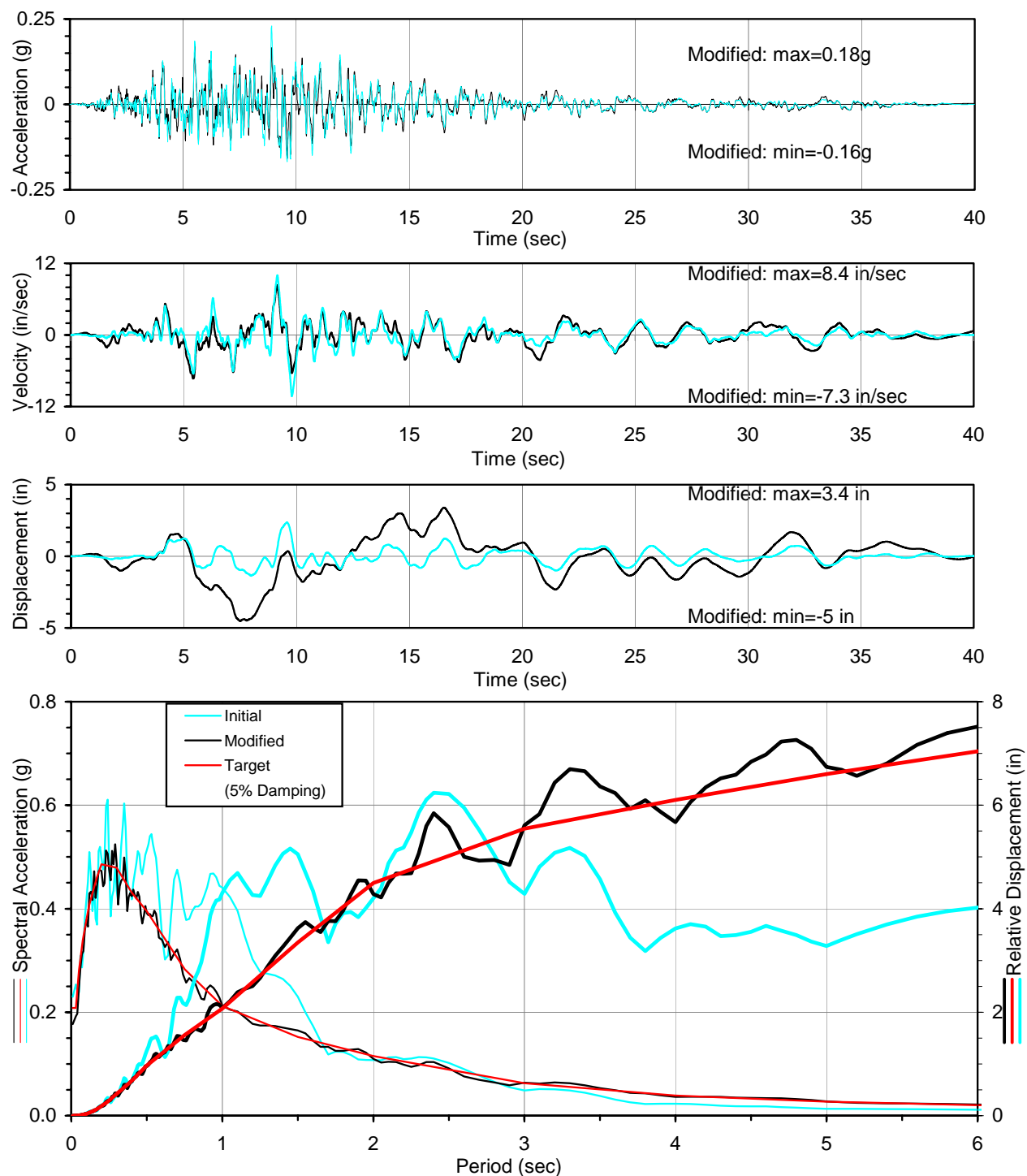
**Figure D-14. Firm-Ground Time Histories Compatible to OLE Firm-Ground Spectra, Set 7
(b) FP Component**
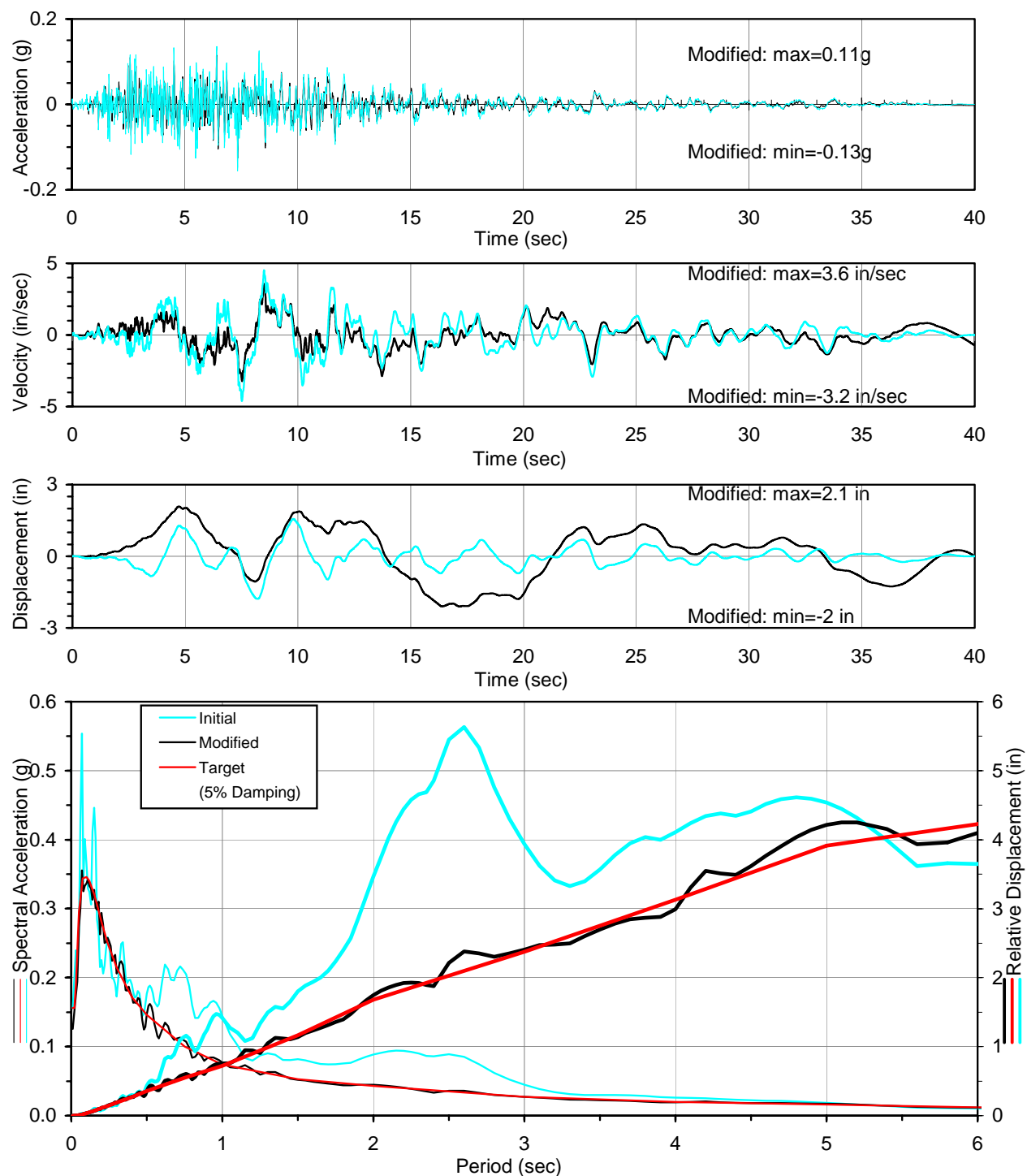
Figure D-14. Firm-Ground Time Histories Compatible to OLE Firm-Ground Spectra, Set 7 (c) FV Component

D.3   DESIGN TIME HISTORIES COMPATIBLE TO CLE DESIGN SPECTRA

Seven (7) sets of 3-component time histories were generated using the seven initial firm-ground motions presented in Section D.1 for the Contingency-Level earthquake event. The resulting ground surface motions were modified to match the CLE target design spectra (Figures 5-7 and 5-8).

For each of the 21 time histories, the following is plotted:

- Initial acceleration, velocity and displacement time histories scaled to PGA,

- Modified (spectrum-matched) ground surface acceleration, velocity and displacement time histories, and

- Comparison of the target CLE design spectrum and the spectrum of the modified time histories.

These plots are shown in Figure D-15 through Figure D-21 for the CLE design time history set number 1 through set number 7 (see Table D-1), respectively.
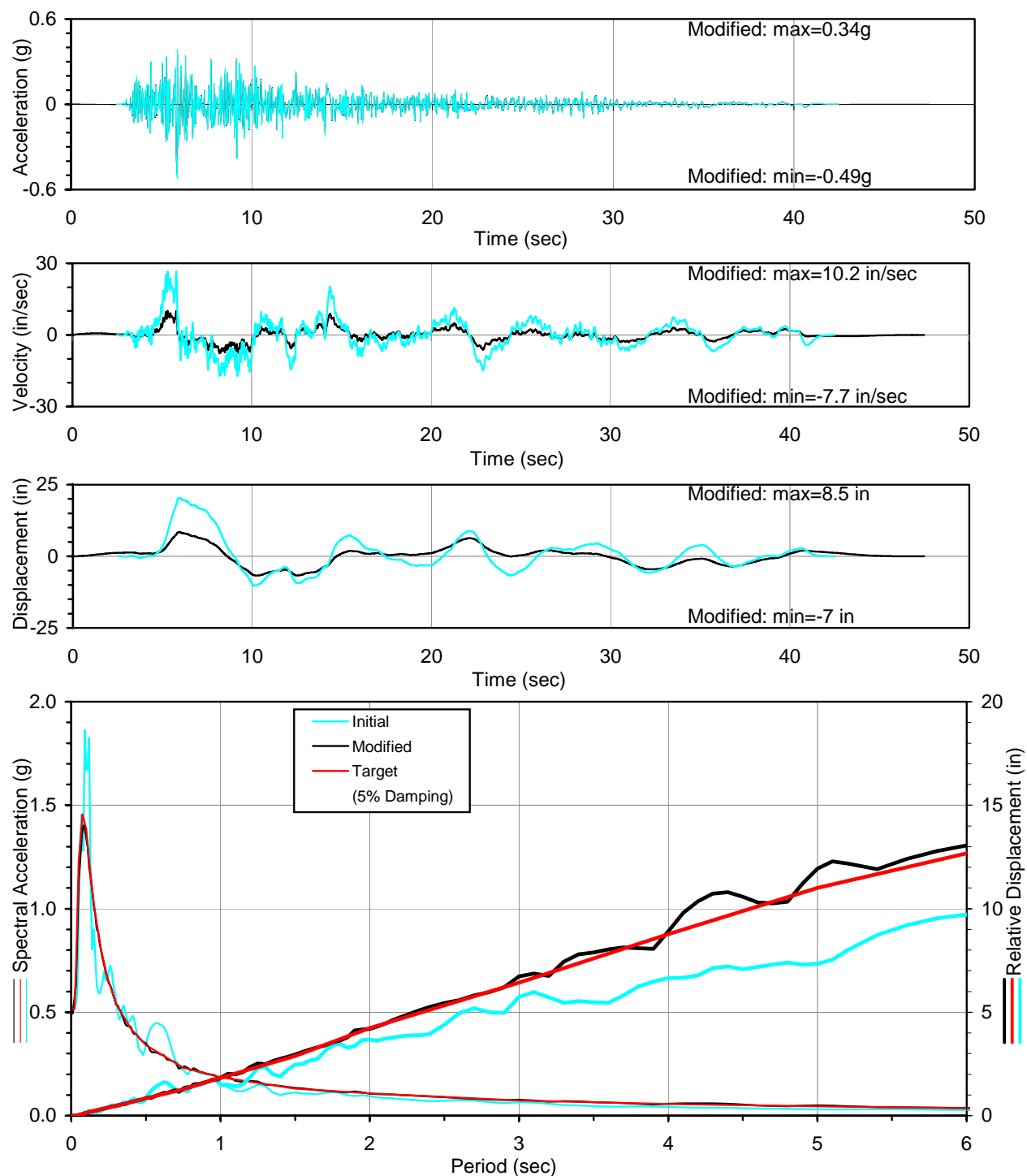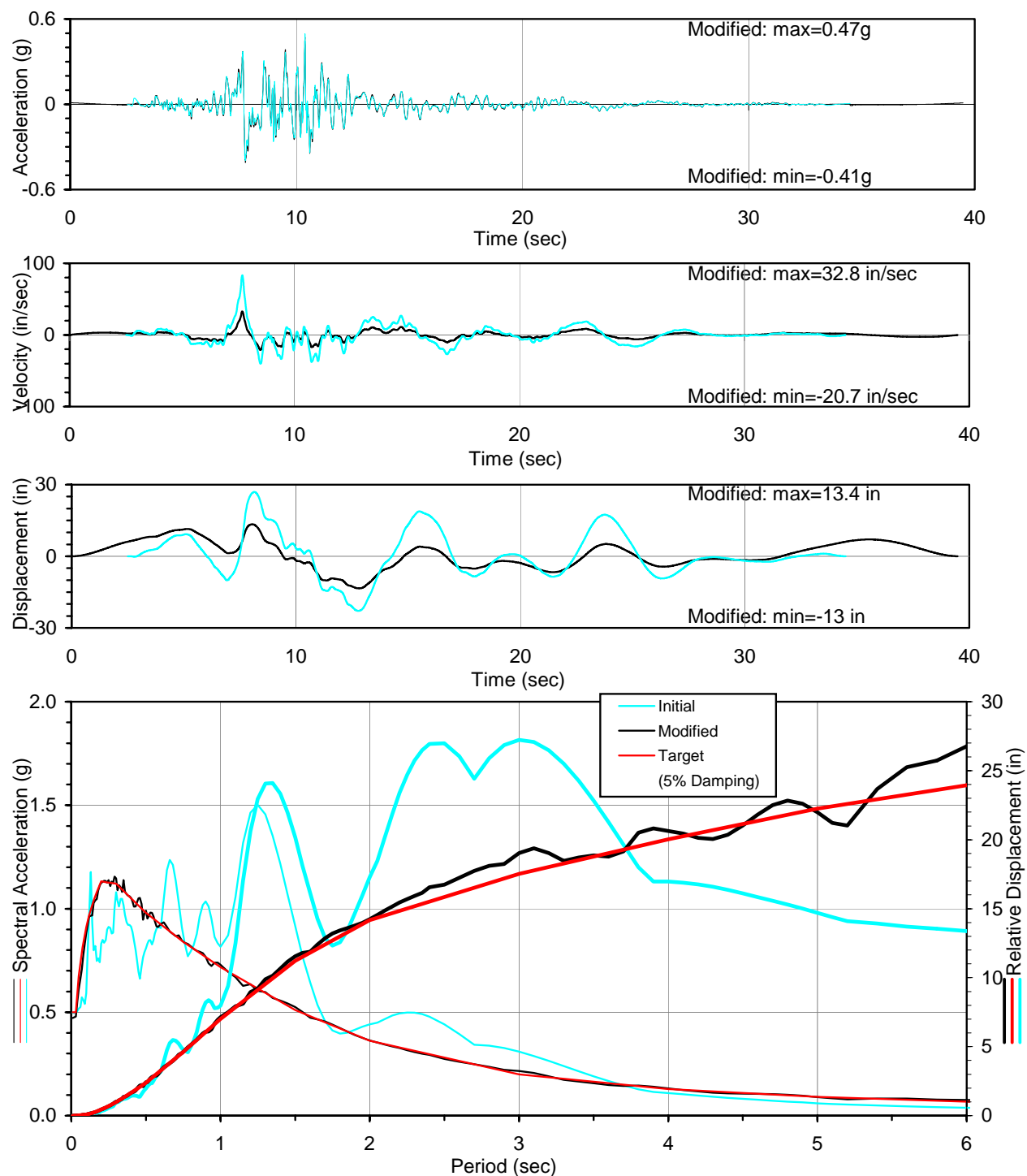
Figure D-15. Design Time Histories Compatible to CLE Design Spectra, Set 1
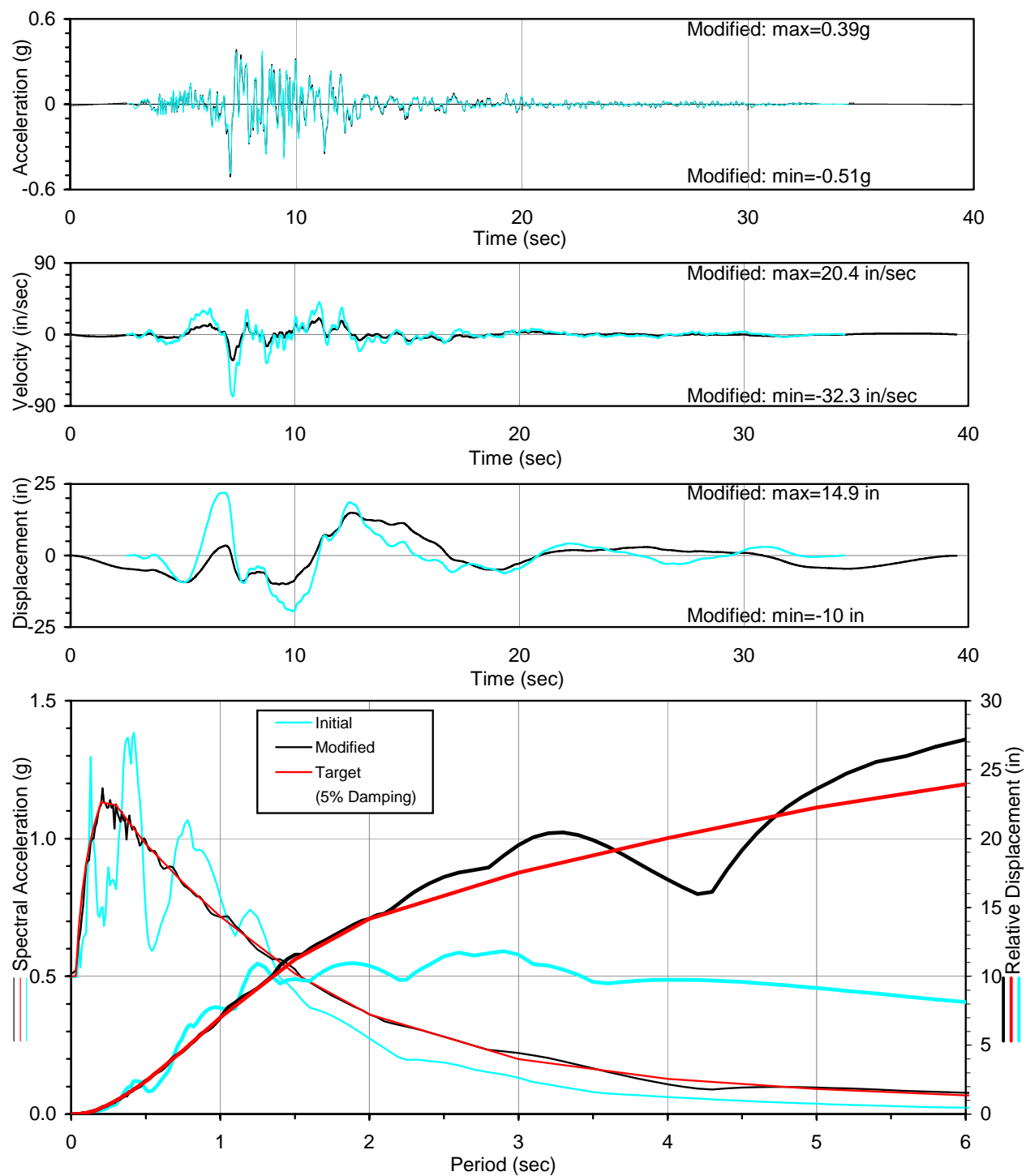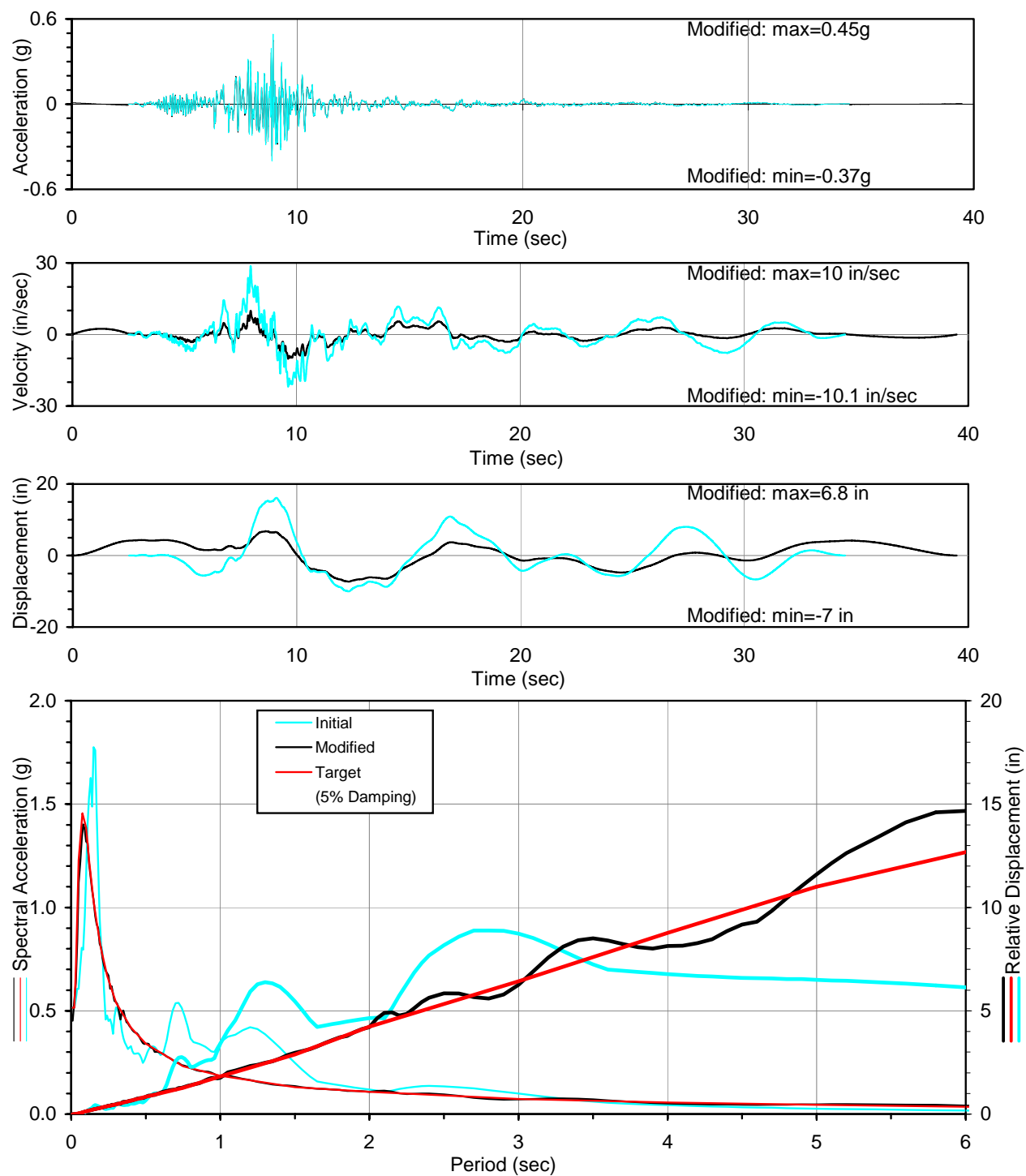   **(a) FN Component**

Figure D-15. Design Time Histories Compatible to CLE Design Spectra, Set 1
      (b) FP Component

Figure D-15. Design Time Histories Compatible to CLE Design Spectra, Set 1
    (c) FV Component

Figure D-16. Design Time Histories Compatible to CLE Design Spectra, Set 2
        (a) FN Component

**Figure D-16. Design Time Histories Compatible to CLE Design Spectra, Set 2
       (b) FP Component**

Figure D-16. Design Time Histories Compatible to CLE Design Spectra, Set 2
    (c) FV Component

Figure D-17. Design Time Histories Compatible to CLE Design Spectra, Set 3
(a) FN Component

**Figure D-17. Design Time Histories Compatible to CLE Design Spectra, Set 3
(b) FP Component**

**Figure D-17. Design Time Histories Compatible to CLE Design Spectra, Set 3
(c) FV Component**

Figure D-18.   Design Time Histories Compatible to CLE Design Spectra, Set 4
(a) FN Component

Figure D-18. Design Time Histories Compatible to CLE Design Spectra, Set 4
            (b) FP Component

Figure D-18. Design Time Histories Compatible to CLE Design Spectra, Set 4
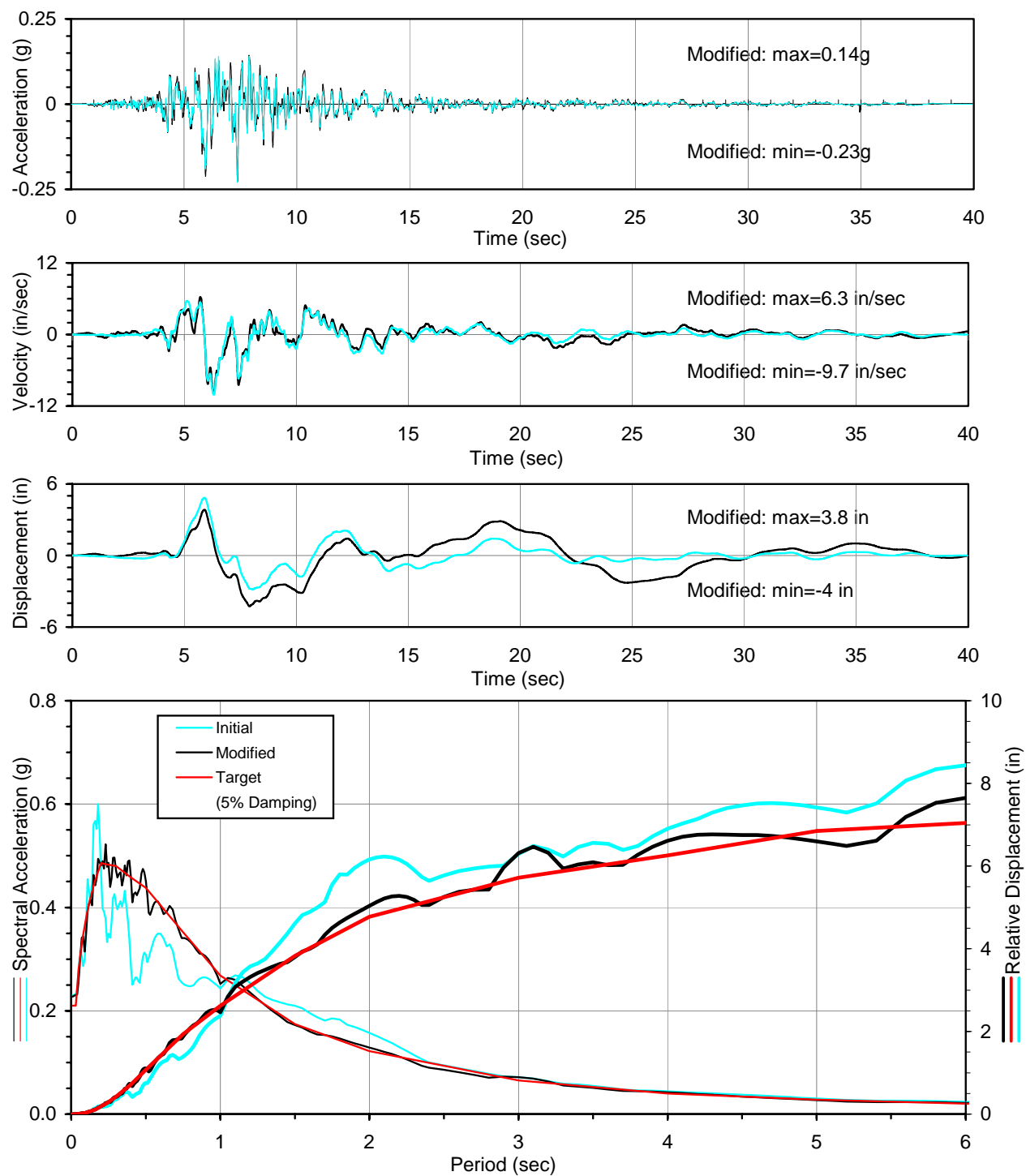**(c) FV Component**

Figure D-19. Design Time Histories Compatible to CLE Design Spectra, Set 5
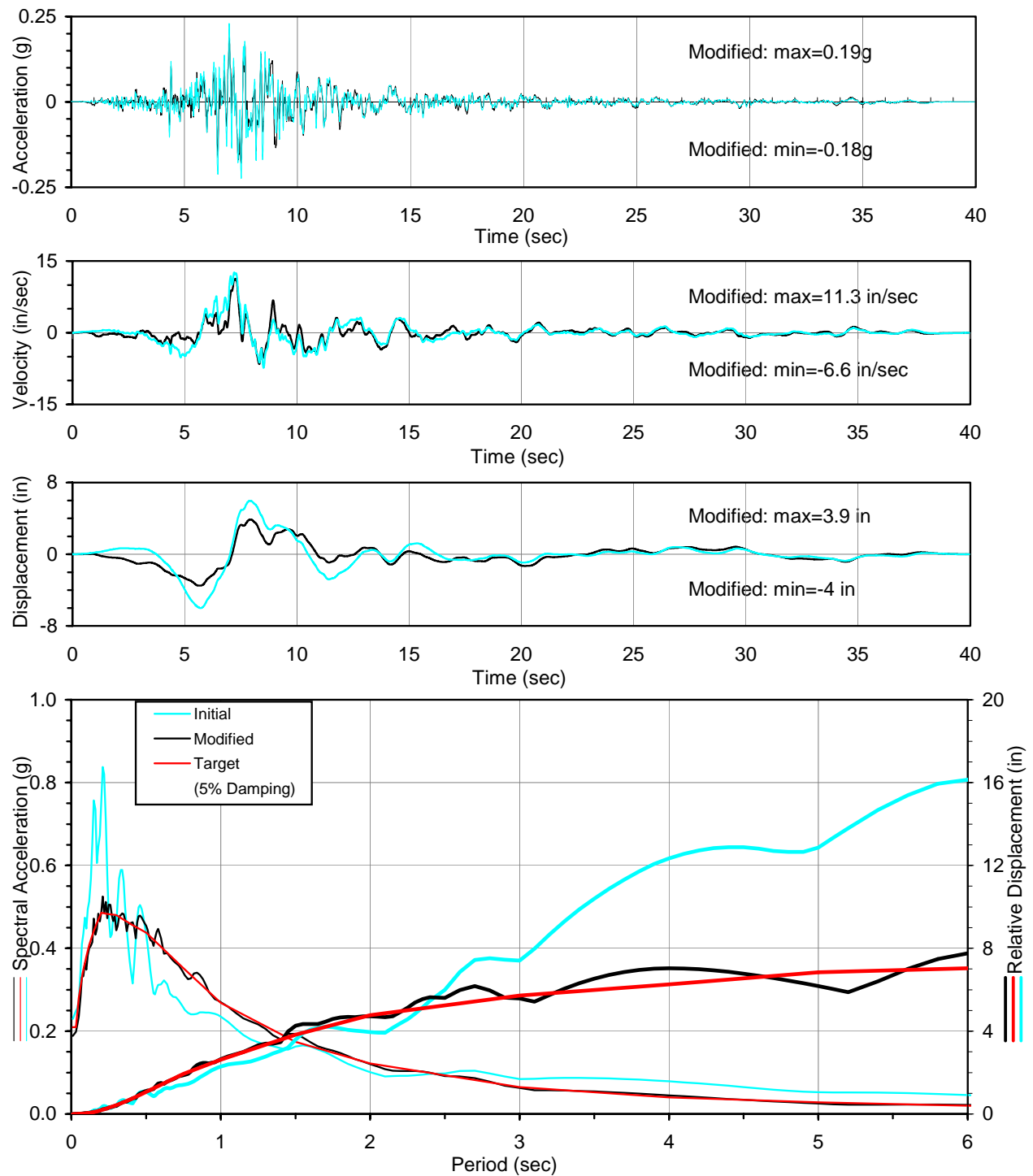   **(a) FN Component**

Figure D-19. Design Time Histories Compatible to CLE Design Spectra, Set 5
(b) FP Component

Figure D-19. Design Time Histories Compatible to CLE Design Spectra, Set 5
(c) FV Component

Figure D-20. Design Time Histories Compatible to CLE Design Spectra, Set 6
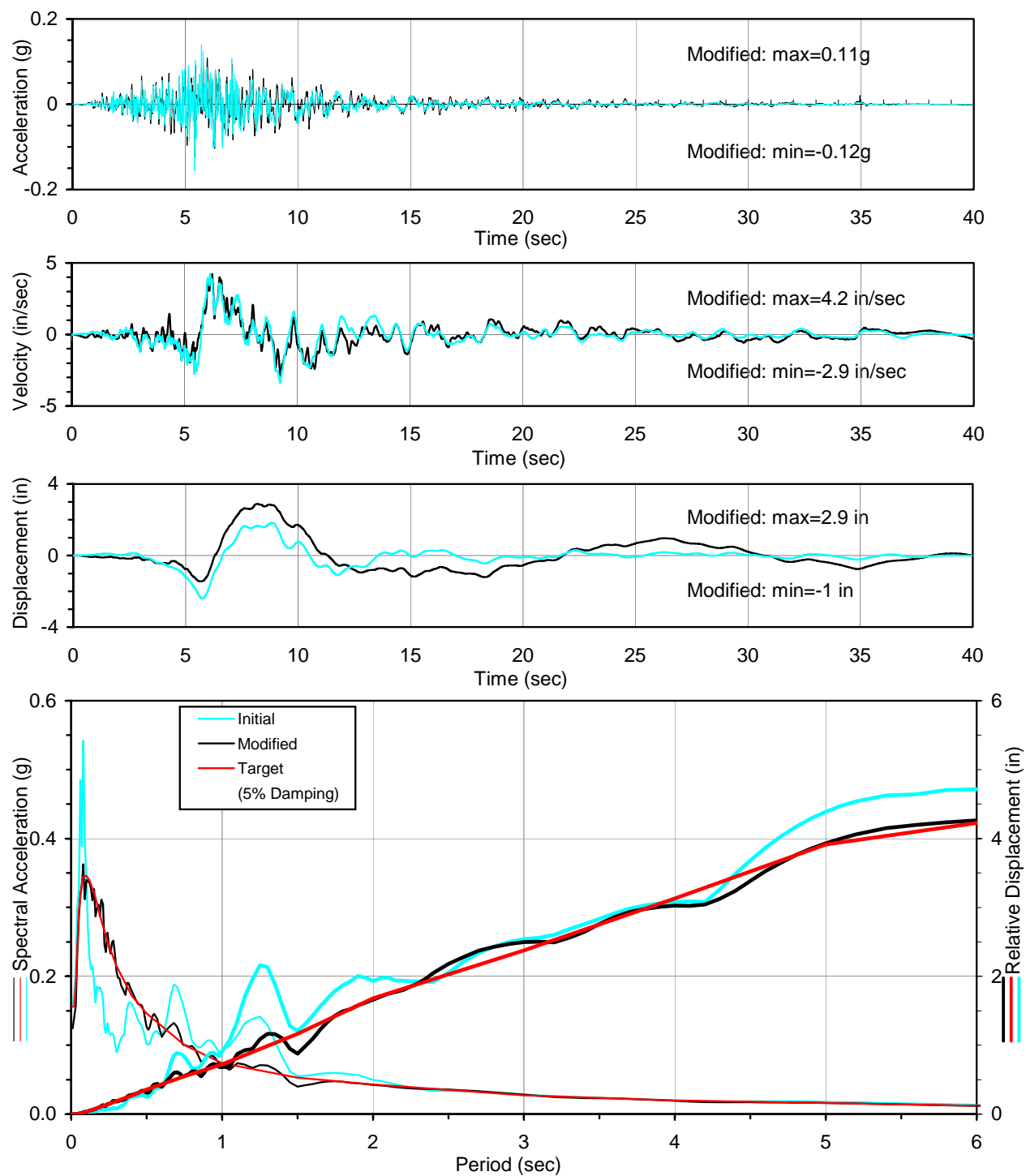   **(a) FN Component**

**Figure D-20. Design Time Histories Compatible to CLE Design Spectra, Set 6
    (b) FP Component**

**Figure D-20. Design Time Histories Compatible to CLE Design Spectra, Set 6
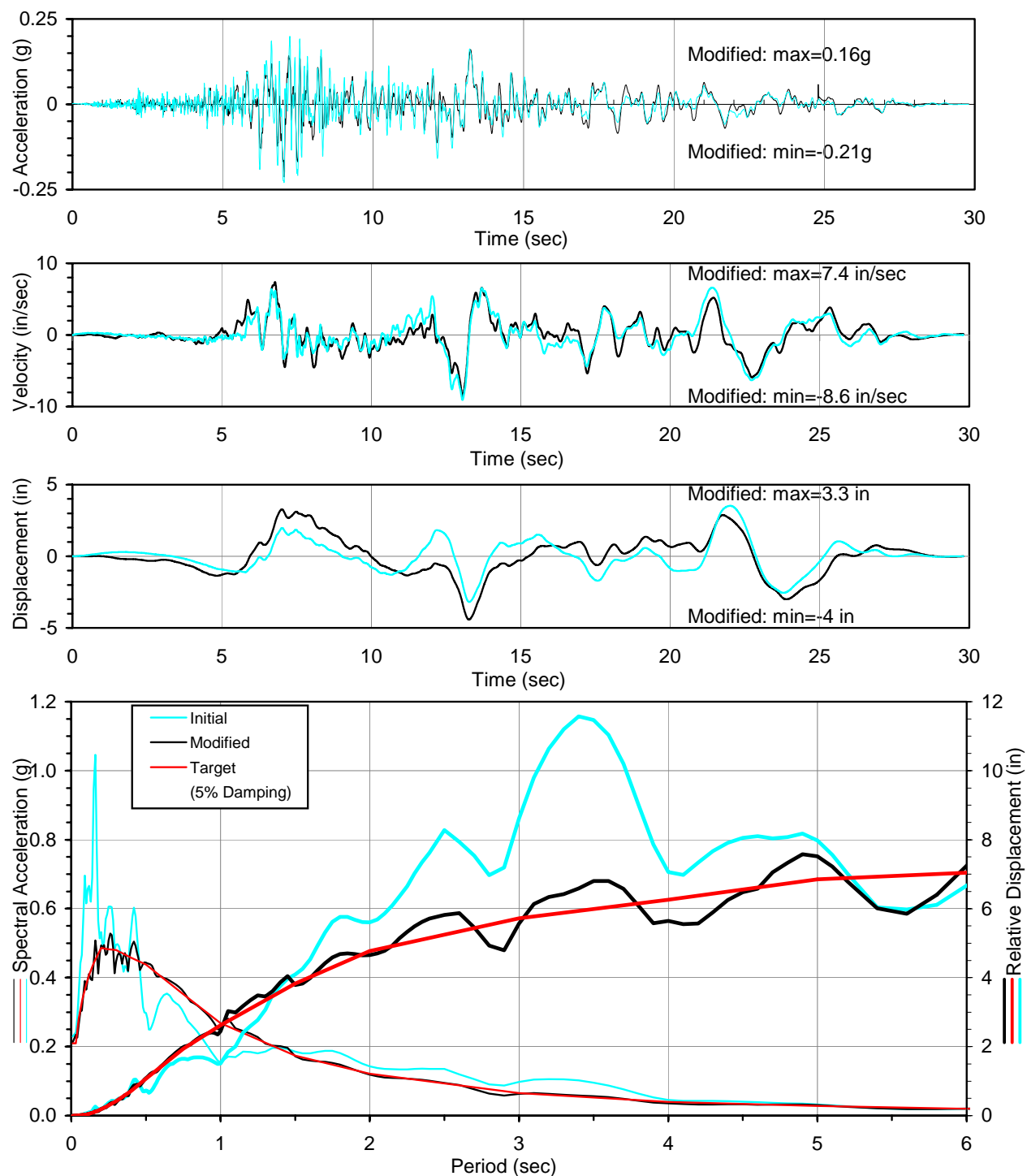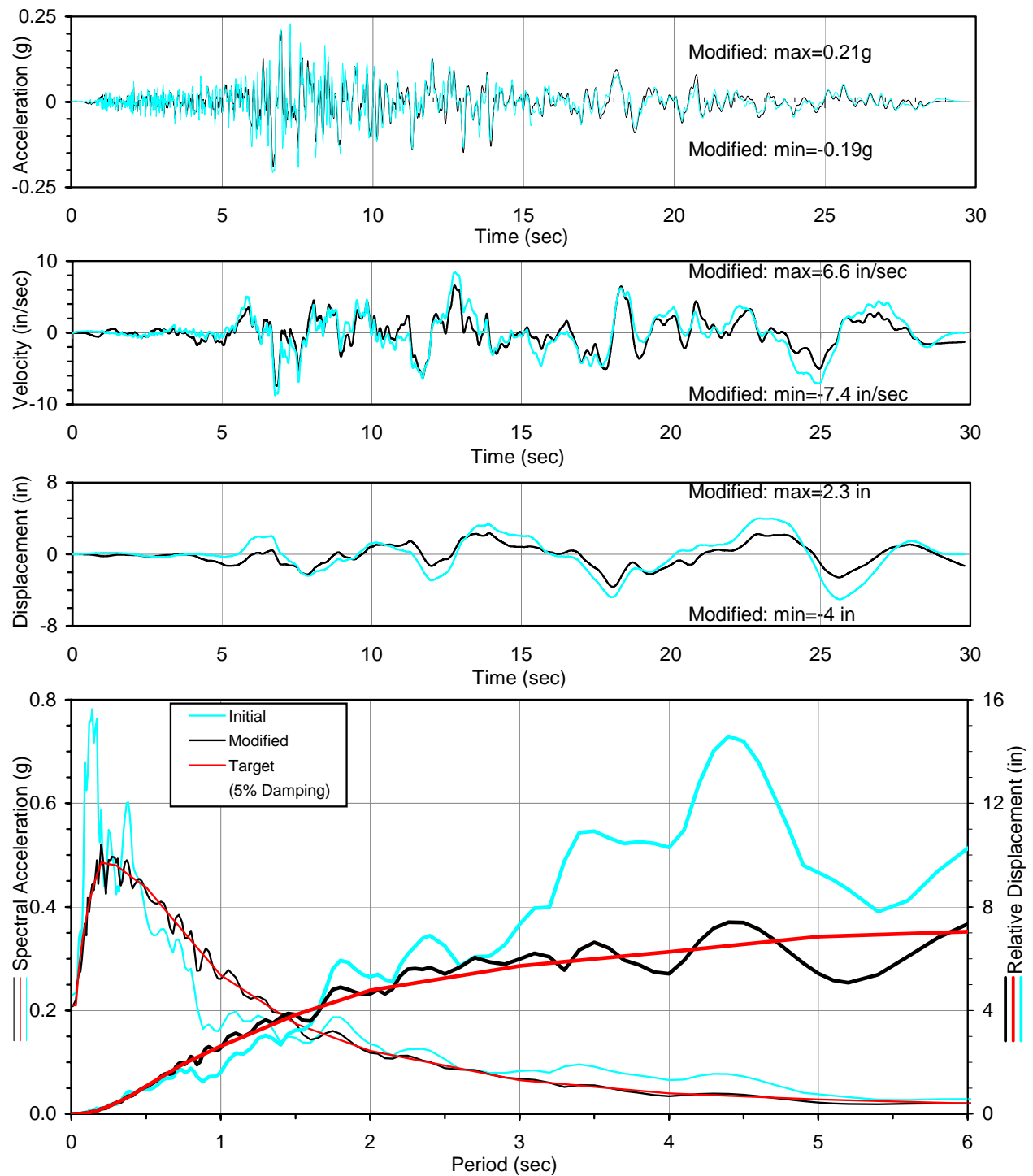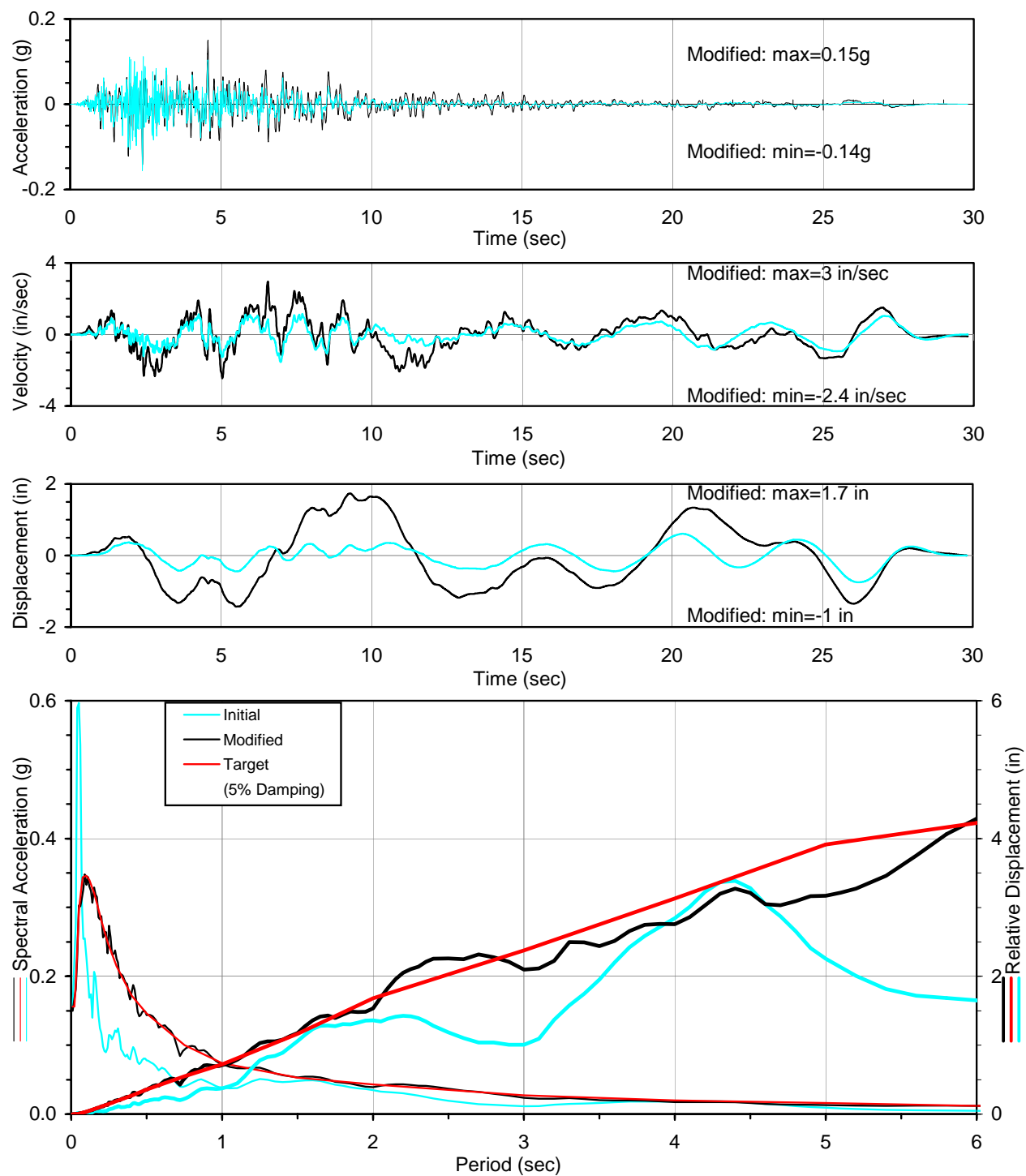   (c) FV Component**

Figure D-21. Design Time Histories Compatible to CLE Design Spectra, Set 7
(a) FN Component

Figure D-21. Design Time Histories Compatible to CLE Design Spectra, Set 7
 (b) FP Component

Figure D-21. Design Time Histories Compatible to CLE Design Spectra, Set 7
(c) FV Component

D.4   DESIGN TIME HISTORIES COMPATIBLE TO OLE DESIGN SPECTRA

Seven (7) sets of 3-component time histories were generated using the initial firm-ground motion presented in Section D.2 to be spectrum-compatible to the design response spectrum adjusted for the site-specific soil conditions for the Operating-Level earthquake event (Figures 5-10 and 5-11).

For each of the 21 time histories, the following is plotted:

- Initial acceleration, velocity and displacement time histories scaled to PGA,

- Modified (spectrum-matched) acceleration, velocity and displacement time histories,

- Comparison of the target CLE design spectrum and the spectrum of the modified time histories.

These plots are shown in Figure D-22 through Figure D-28 for the OLE design time history set number 1 through set number 7 (see Table D-2), respectively.
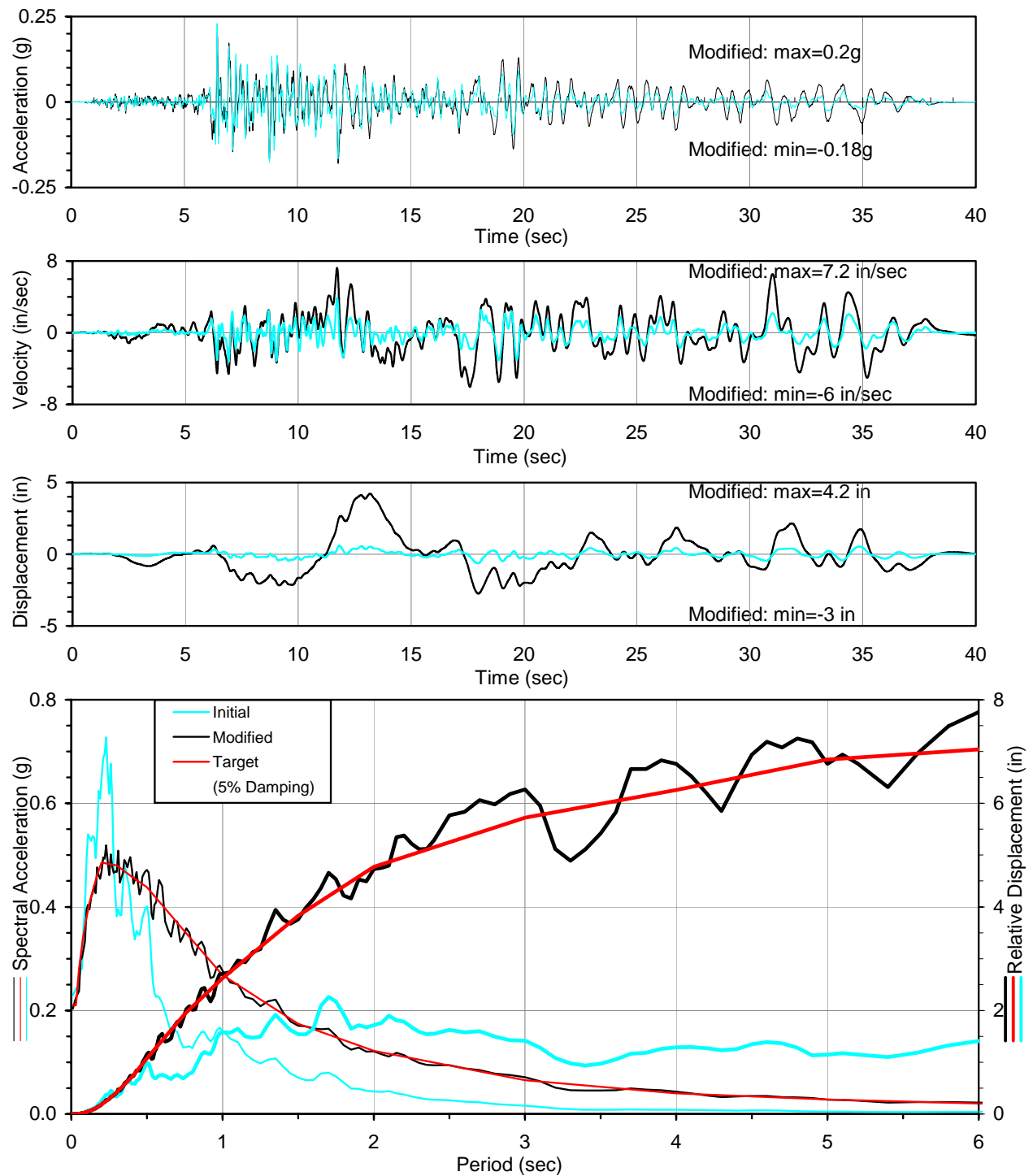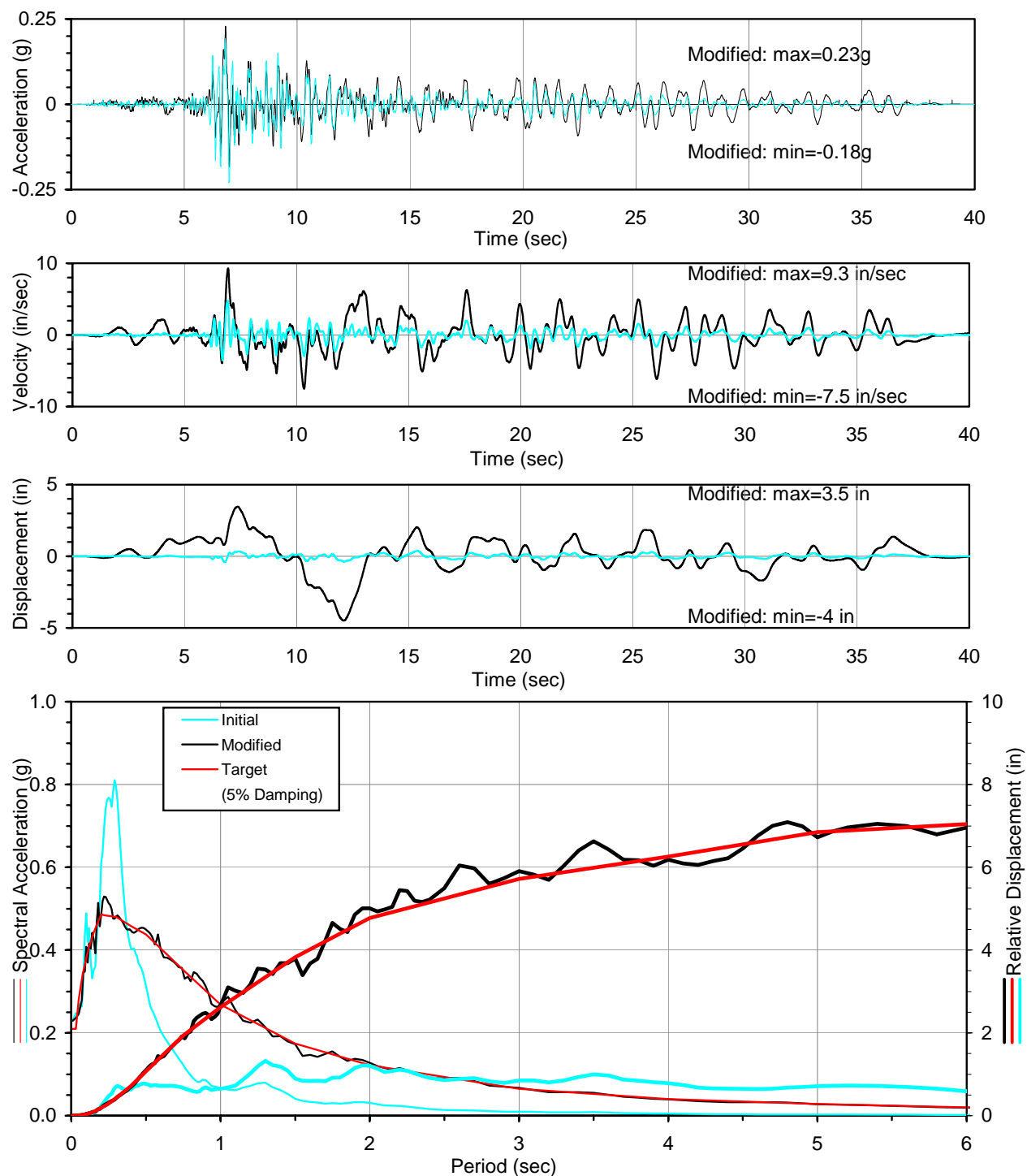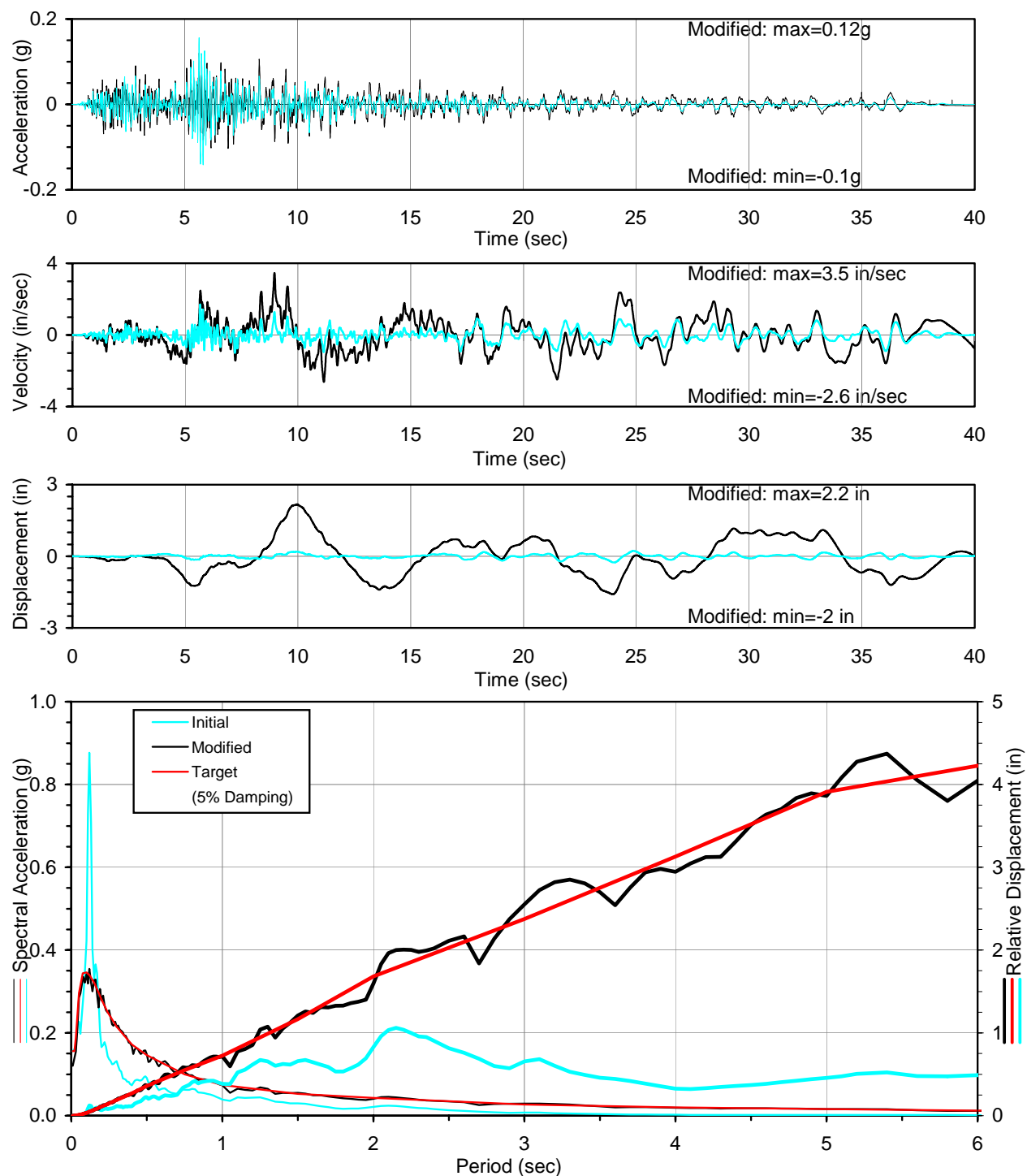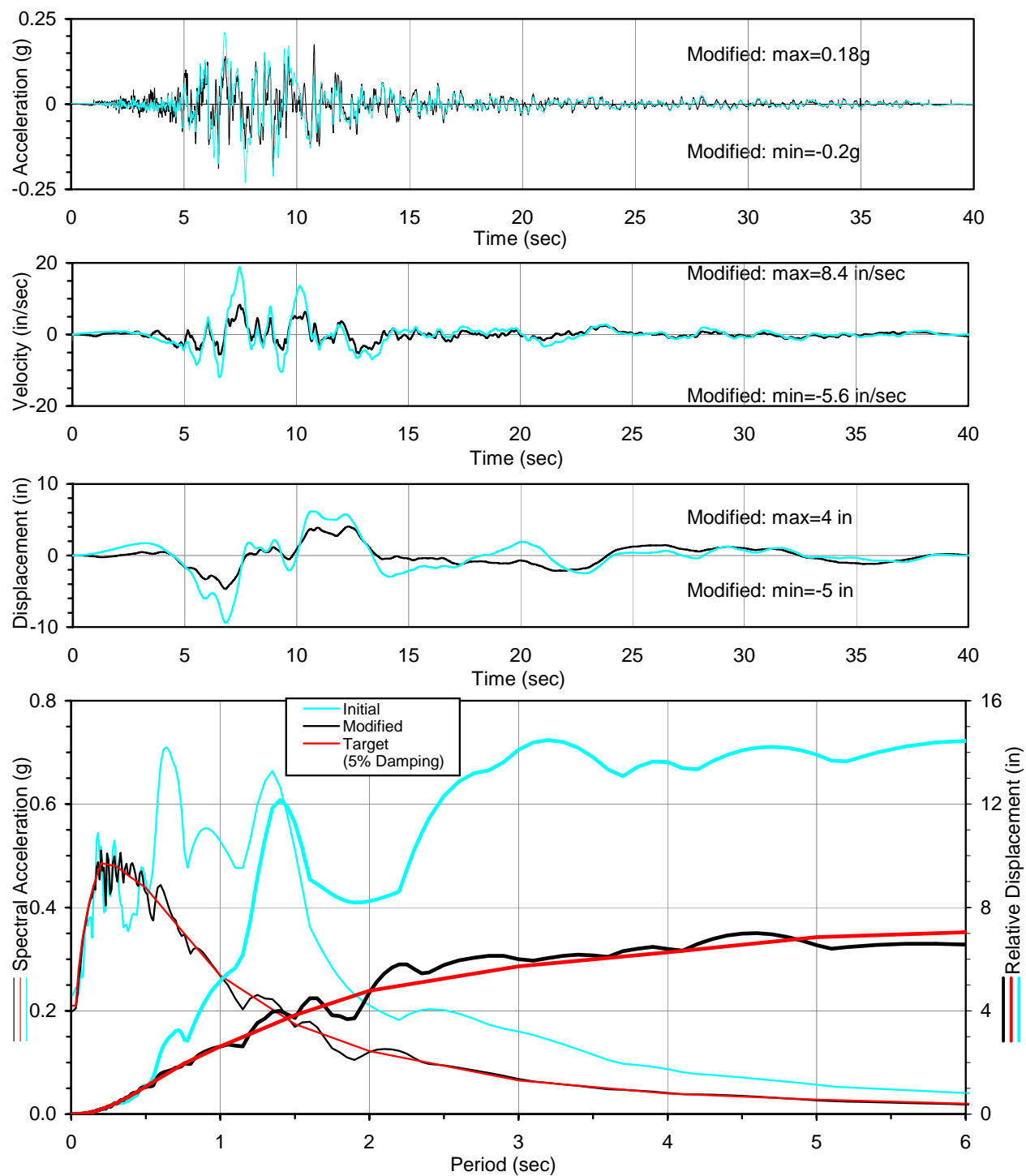
**Figure D-22. Design Time Histories Compatible to OLE Design Spectra, Set 1
(a) FN Component**

Figure D-22   Design Time Histories Compatible to OLE Design Spectra, Set 1
         (b) FP Component

Figure D-22. Design Time Histories Compatible to OLE Design Spectra, Set 1
　　　　(c) FV Component

Figure D-23. Design Time Histories Compatible to OLE Design Spectra, Set 2
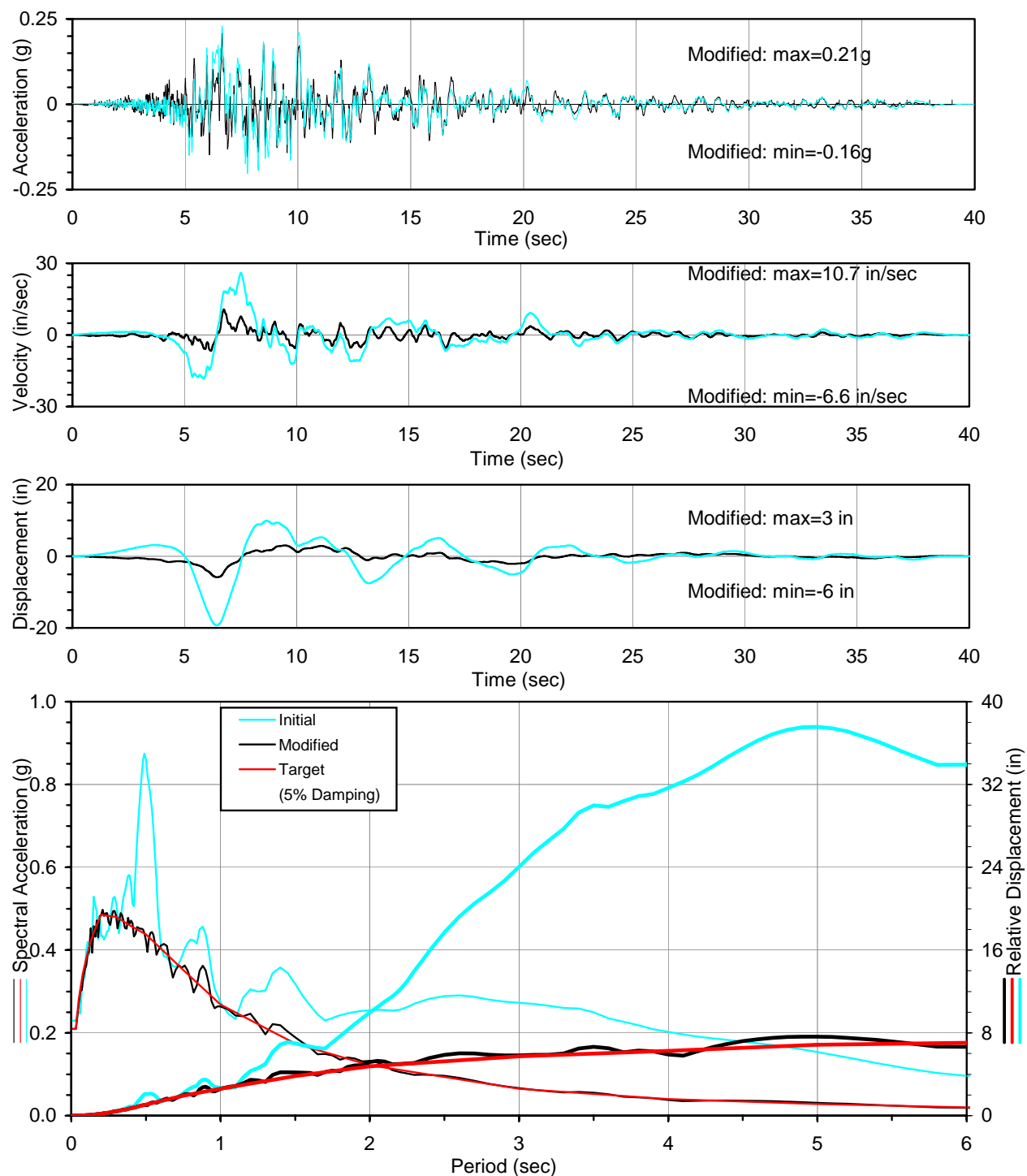**(a) FN Component**

**Figure D-23   Design Time Histories Compatible to OLE Design Spectra, Set 2
(b) FP Component**

Figure D-23.   Design Time Histories Compatible to OLE Design Spectra, Set 2
(c) FV Component

Figure D-24. Design Time Histories Compatible to OLE Design Spectra, Set 3
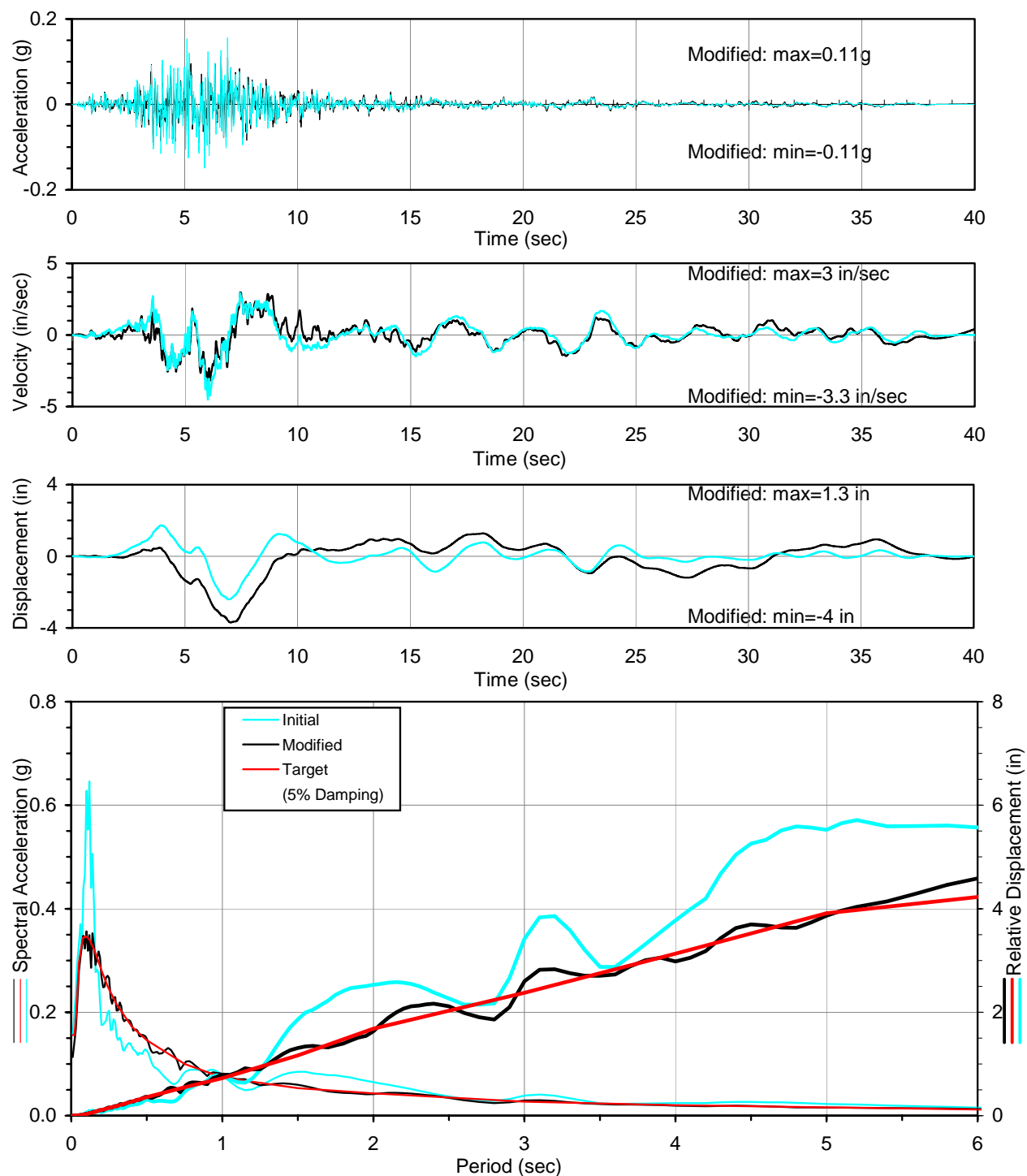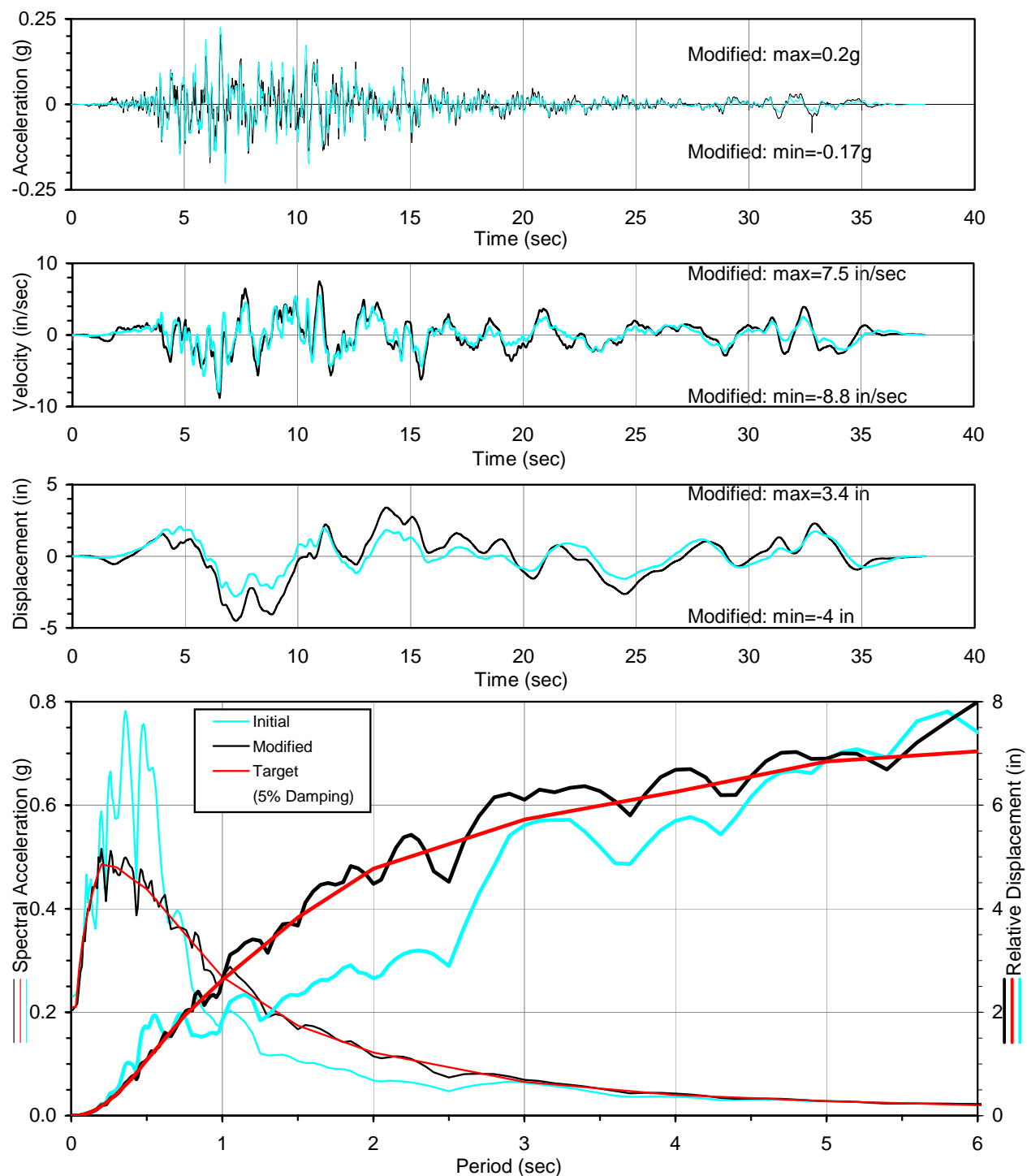   **(a) FN Component**

**Figure D-24. Design Time Histories Compatible to OLE Design Spectra, Set 3
        (b) FP Component**

Figure D-24. Design Time Histories Compatible to OLE Design Spectra, Set 3
         (c) FV Component

Figure D-25. Design Time Histories Compatible to OLE Design Spectra, Set 4
(a) FN Component

Figure D-25. Design Time Histories Compatible to OLE Design Spectra, Set 4
        (b) FP Component

**Figure D-25. Design Time Histories Compatible to OLE Design Spectra, Set 4
(c) FV Component**

Figure D-26. Design Time Histories Compatible to OLE Design Spectra, Set 5
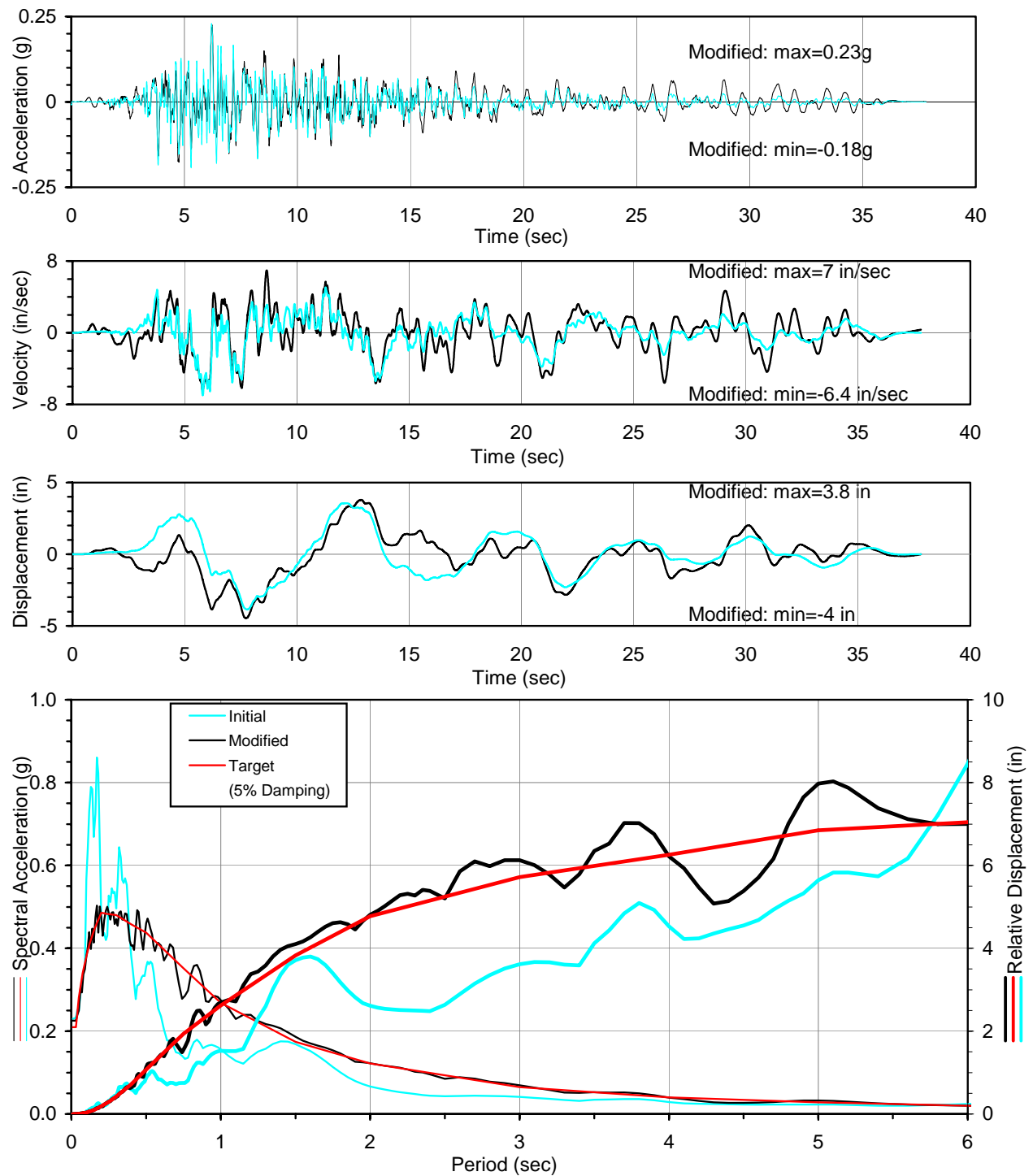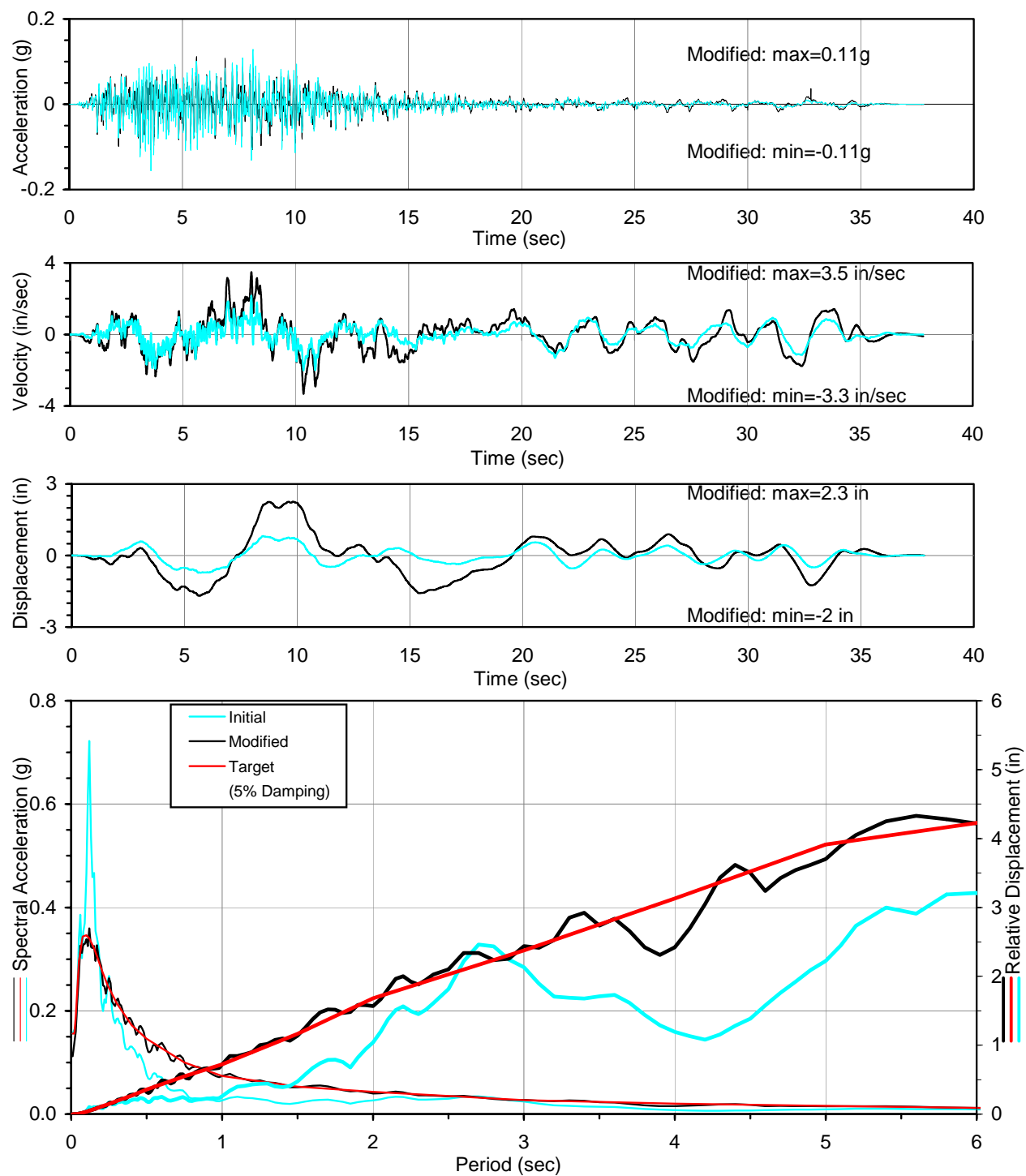**(a) FN Component**

Figure D-26. Design Time Histories Compatible to OLE Design Spectra, Set 5 (b) FP Component

Figure D-26. Design Time Histories Compatible to OLE Design Spectra, Set 5
(c) FV Component

Figure D-27. Design Time Histories Compatible to OLE Design Spectra, Set 6
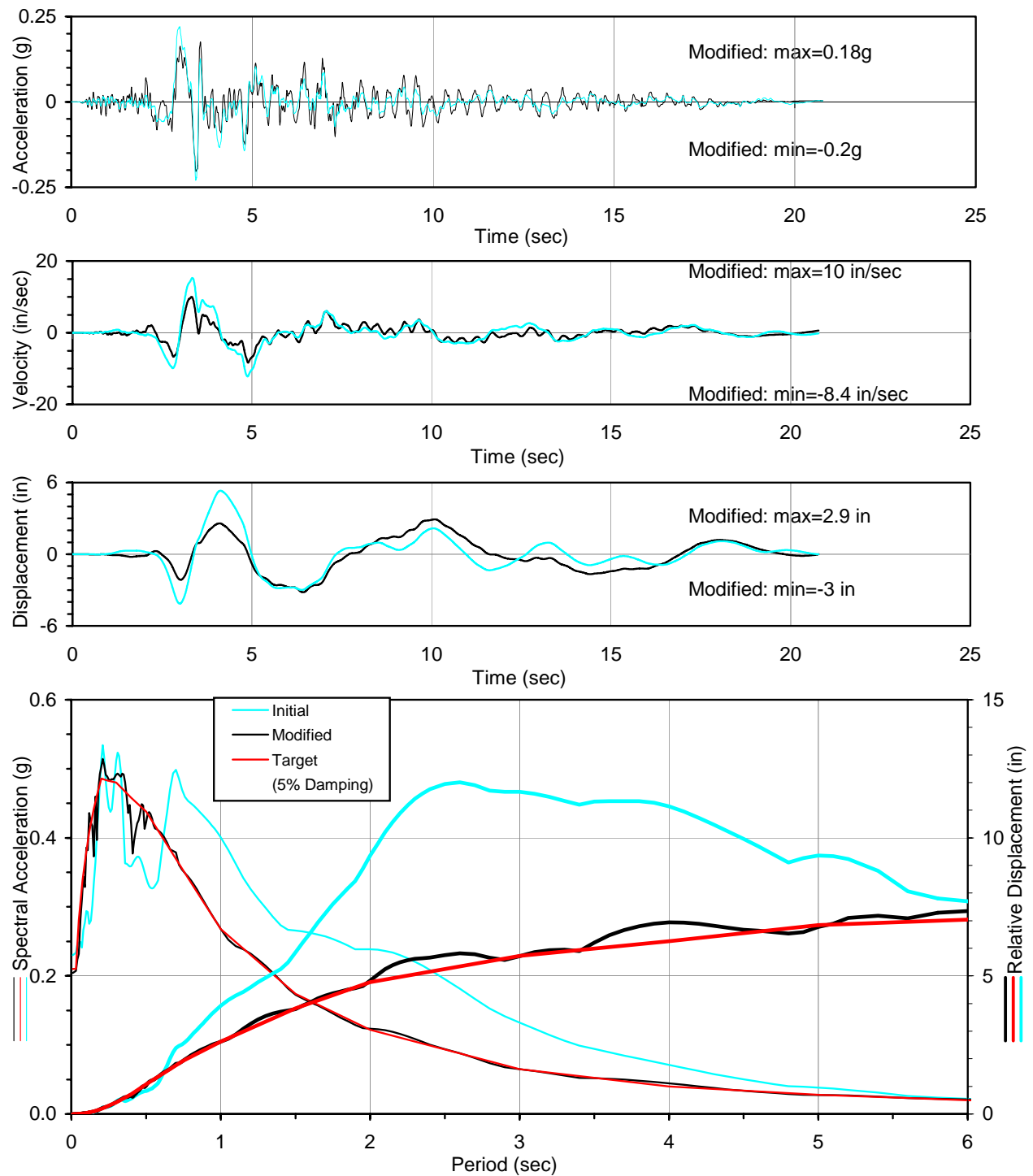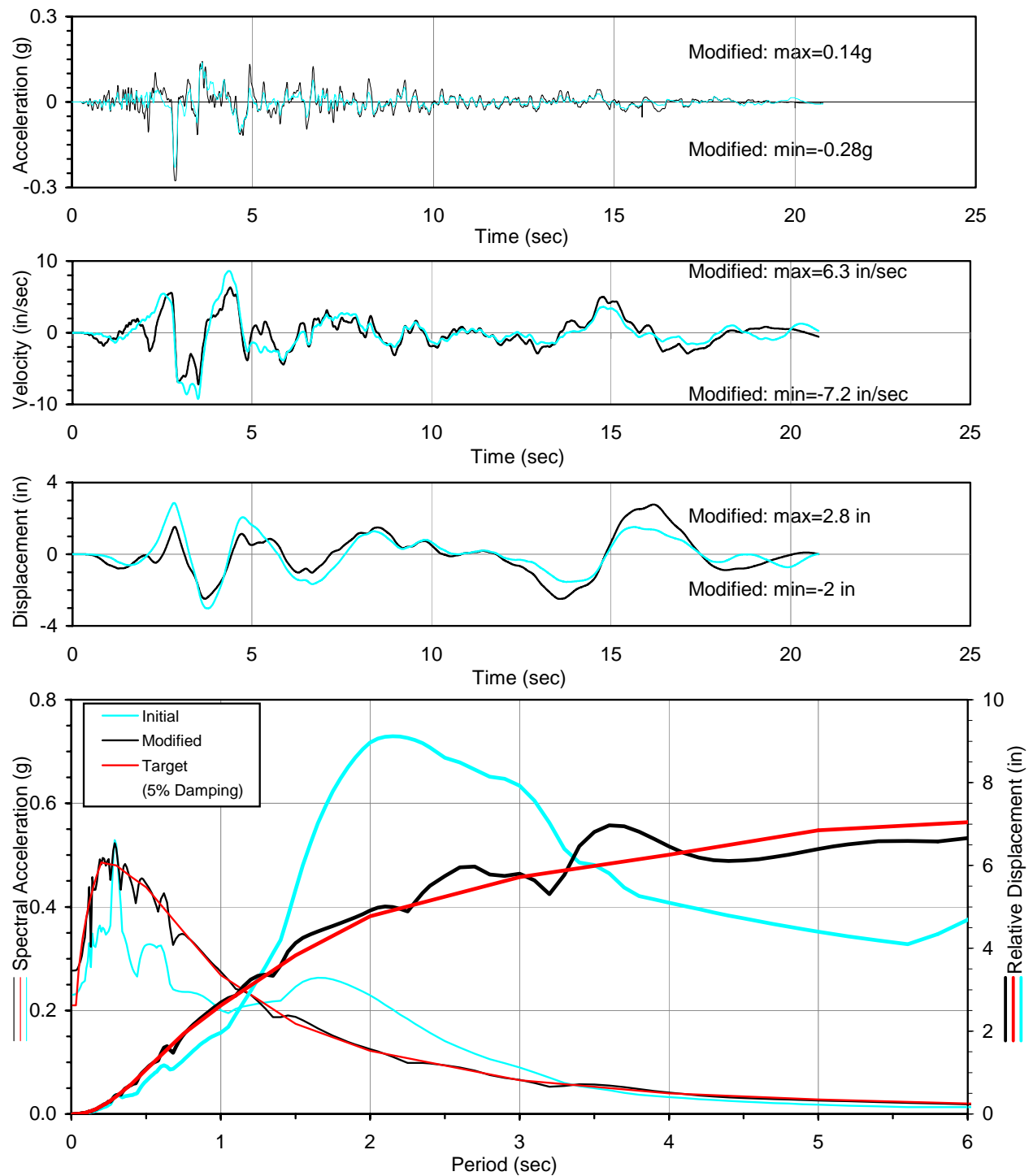 **(a) FN Component**

**Figure D-27. Design Time Histories Compatible to OLE Design Spectra, Set 6
(b) FP Component**

Figure D-27. Design Time Histories Compatible to OLE Design Spectra, Set 6
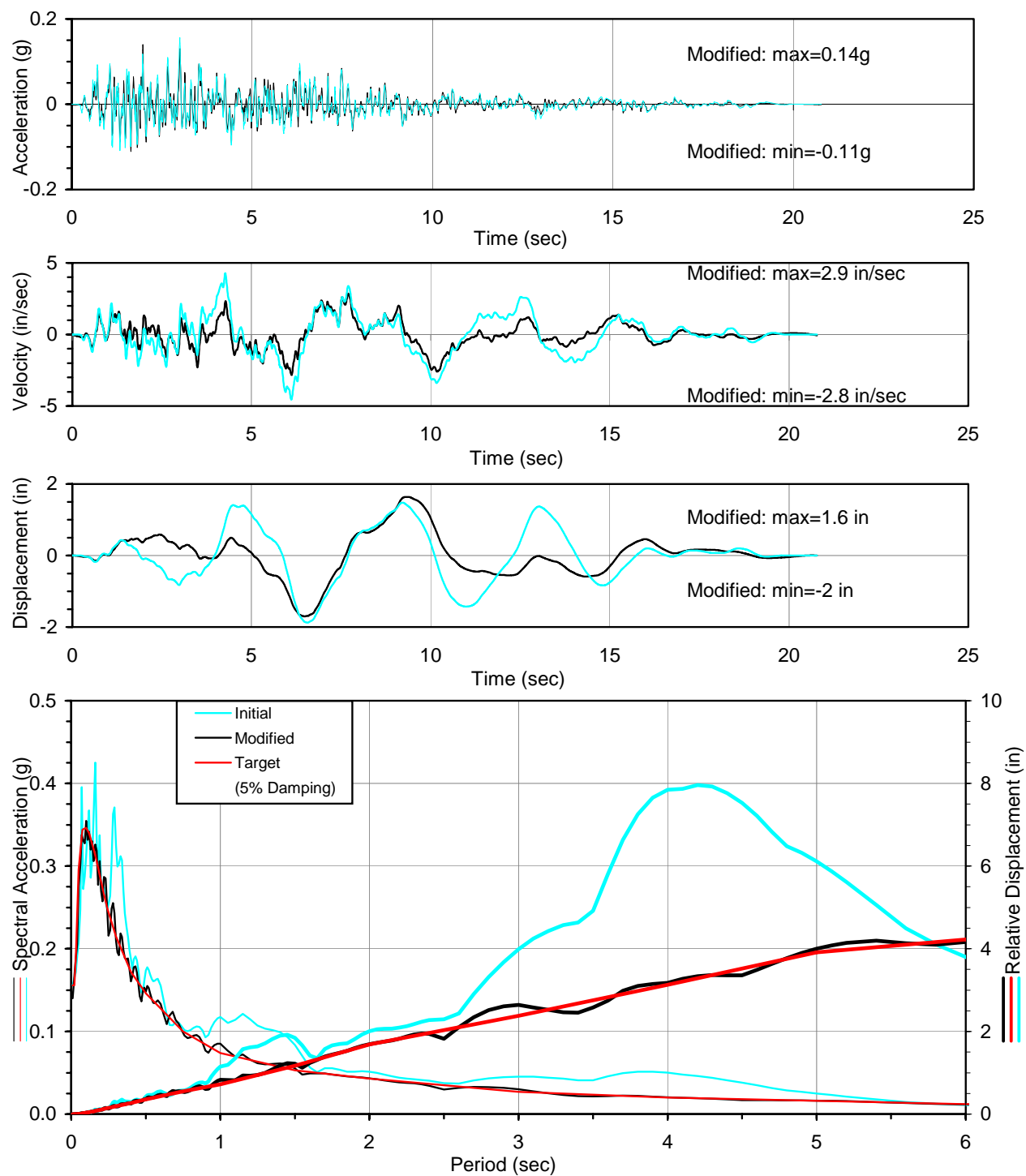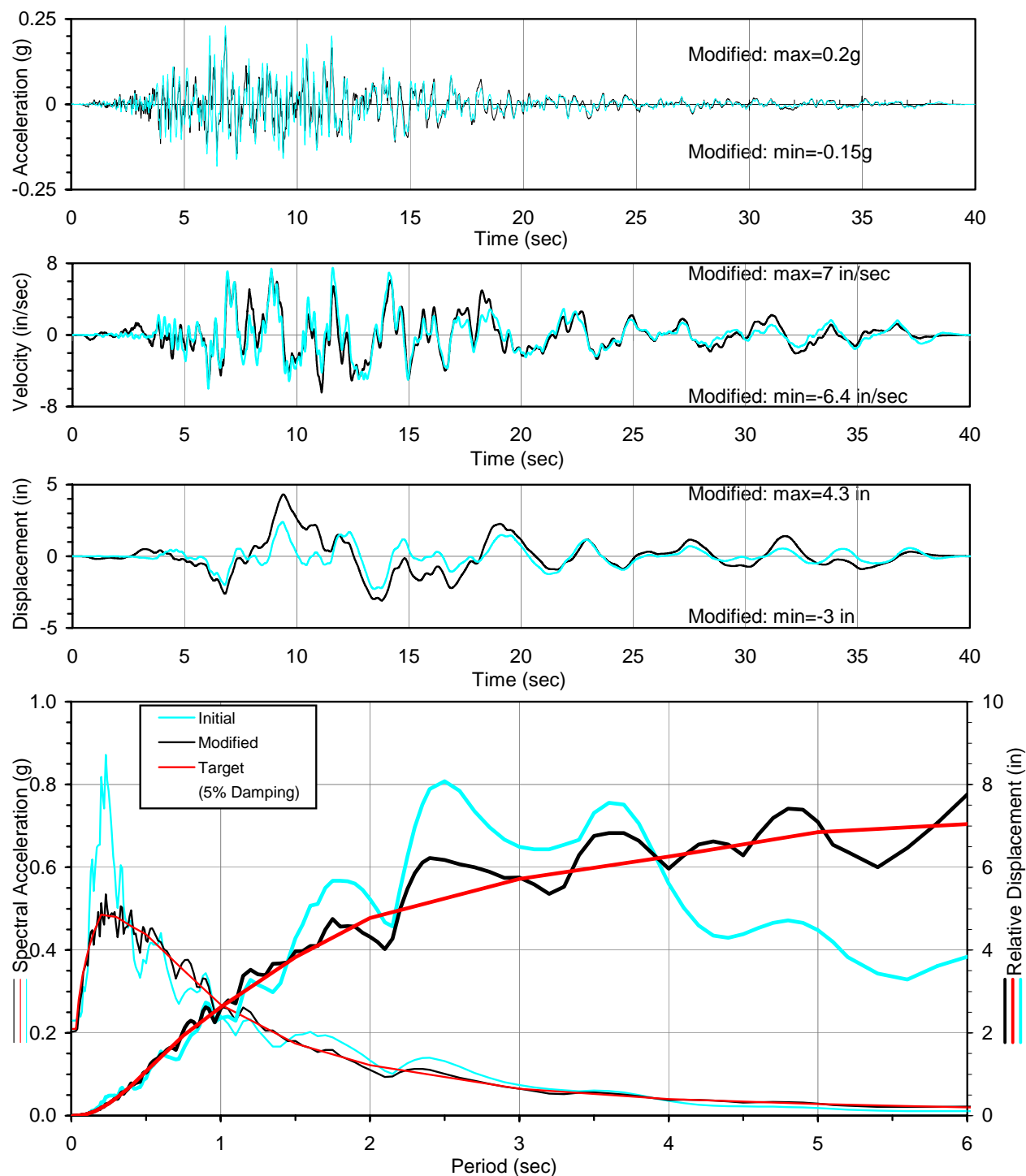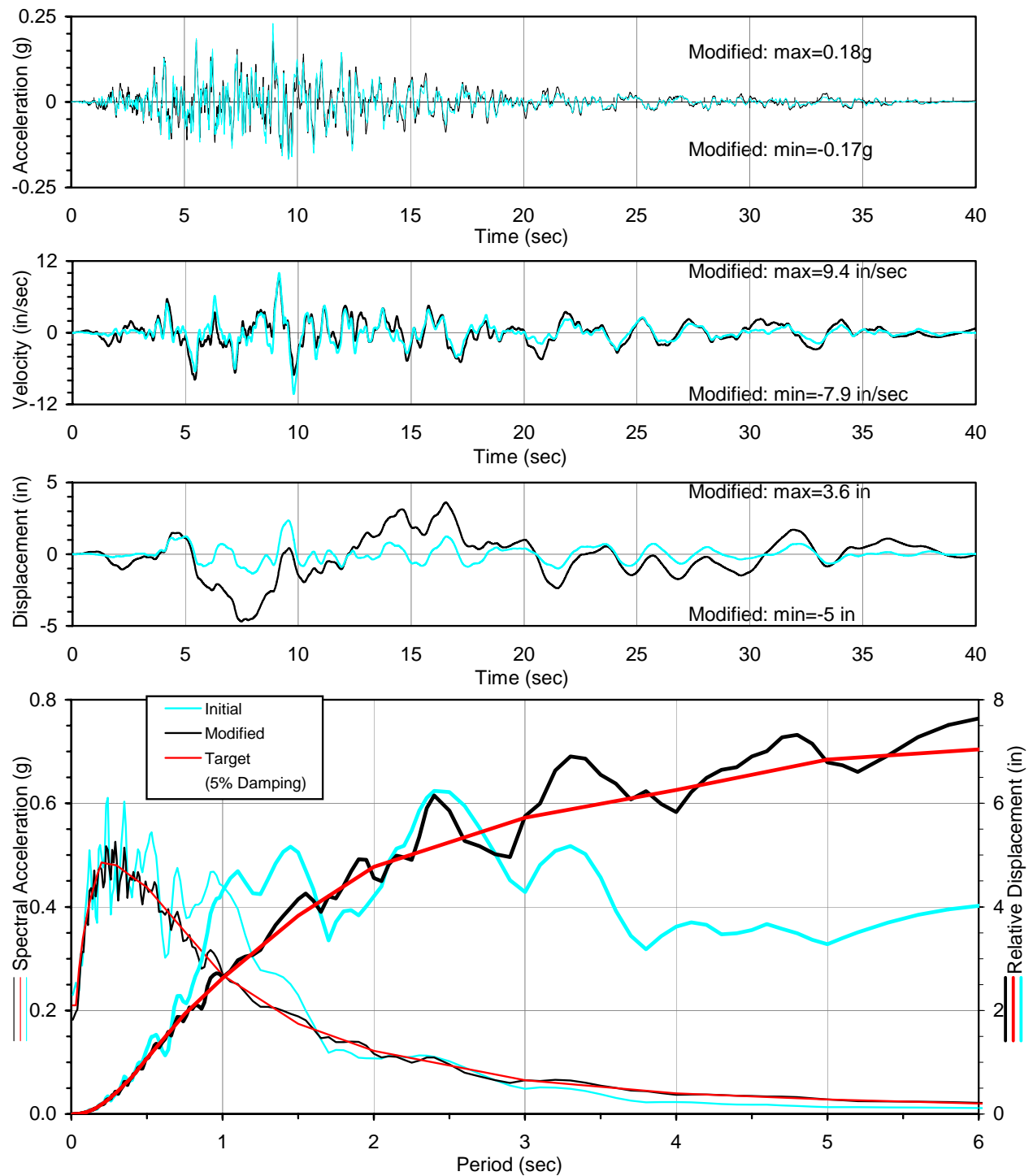 **(c) FV Component**

Figure D-28. Design Time Histories Compatible to OLE Design Spectra, Set 7
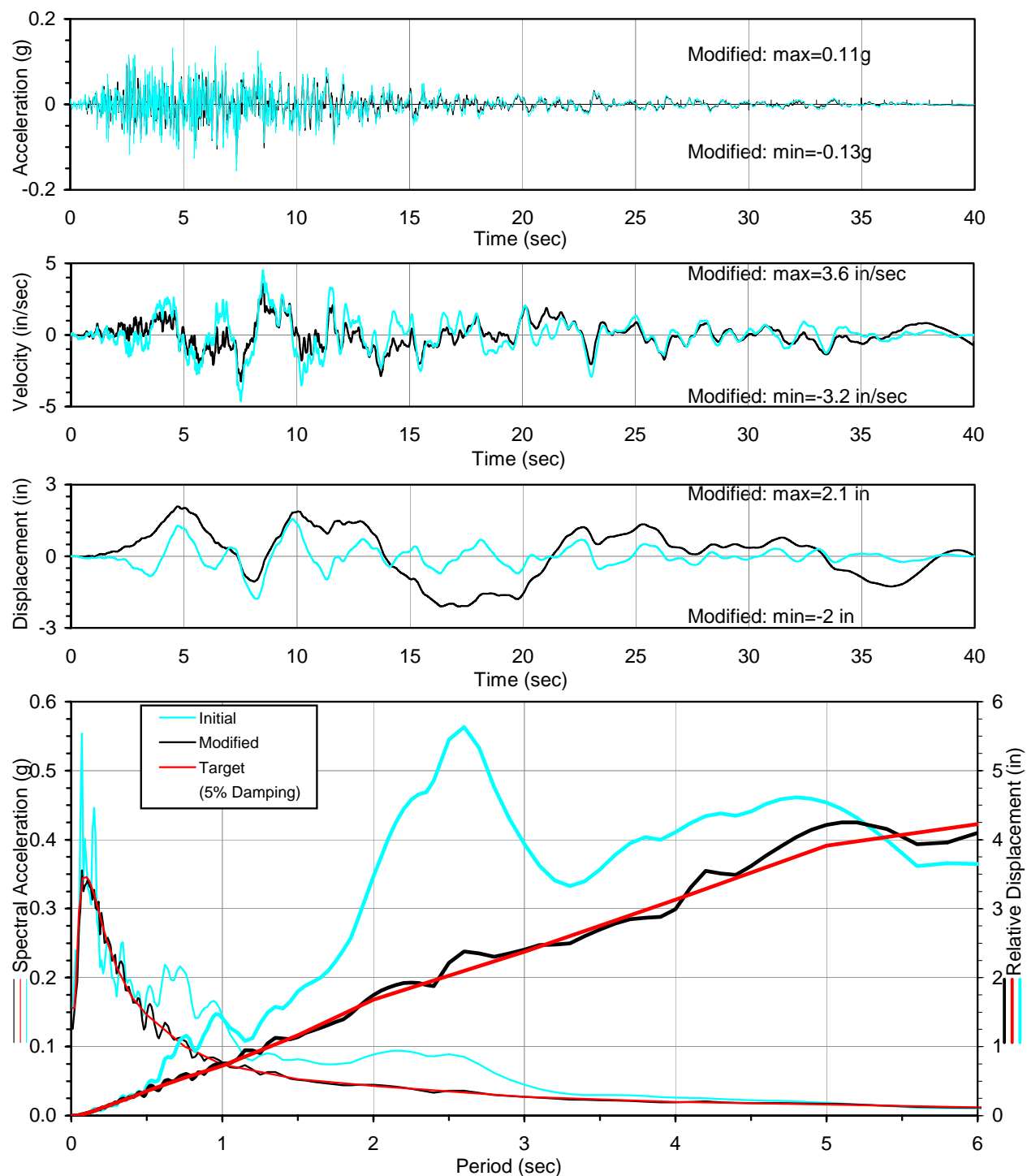**(a) FN Component**

Figure D-28.   Design Time Histories Compatible to OLE Design Spectra, Set 7
(b) FP Component

Figure D-28. Design Time Histories Compatible to OLE Design Spectra, Set 7
(c) FV Component

APPENDIX E

Newmark Displacement Estimates

_____

APPENDIX E
NEWMARK DISPLACEMENT ESTIMATES

TABLE OF CONTENTS

TABLES

FIGURES

APPENDIX E
NEWMARK DISPLACEMENT ESTIMATES

E.1   NEWMARK DISPLACEMENT ESTIMATES FOR CLE

Simplified Newmark sliding block analysis was performed to develop charts of estimated lateral ground displacements as a function of yield acceleration for the CLE (475-year return period) spectral-matched firm-ground motions.

The seven spectral-matched firm-ground horizontal time histories (i.e., horizontal fault-normal and fault-parallel components, a total of 14 time histories) for the CLE events from Appendix D.1 were used in the analyses. The analyses also included all reversed time histories with ground motion acting in the opposite direction. Ground displacement was calculated based on constant yield acceleration levels of 0.03, 0.05, 0.075, 0.1, 0.15, 0.2, 0.25, and 0.3g and down-slope sliding by double-integrating each of the modified time histories. A total of 224 analyses (7 records x 2 components x 2 directions x 8 yield accelerations) were performed.

Figure E-1 shows the resulting lateral displacement versus yield acceleration curves for all 28 (7 records x 2 components x 2 directions) CLE time histories, as well as upper- and lower-bound envelopes of all curves. Since more than seven time histories were used in these evaluations, the average curve is judged to be appropriate for screening evaluations. The use of the average values has been recognized as an acceptable practice when seven of more time histories are considered in the analysis (Bommer et al., 2003; CBC, 2001; IBC, 2000).

Figure E-2 shows the upper- and lower-bound envelopes displacement curves and the recommended design curve. The recommended values are given in Table E-1. The recommended curve may be used as a conservative screening tool to estimate lateral slope displacements during a CLE event.

E.2   NEWMARK DISPLACEMENT ESTIMATES FOR OLE

Simplified Newmark analysis was performed for the OLE spectral-matched firm-ground motions from Appendix D.2 to develop charts of estimated lateral ground displacements as a function of yield acceleration. The same procedure involving a total of 224 analyses as described in Section E.1 was used.

Figure E-3 shows the displacement versus yield acceleration curves for all 28 OLE time histories and the upper- and lower-bound envelopes of all curves. The upper-bound envelope shown is recommended for design and may be used as a conservative screening tool to determine to estimate lateral slope displacements during a OLE event. The recommended values (rounded to the nearest half inch) are given in Table E-1.

Table E-1.　　**Recommended Newmark Displacement Estimates for Site Screening**

Yield Acceleration (g)	Slope Displacement due to OLE (in)	Slope Displacement due to CLE (in)
0.03	10.0	58
0.05	4.0	32
0.075	1.5	18
0.10	1.0	11
0.15	0.5	4.0
0.20	< 0.5	2.0
0.25	< 0.5	1.0
0.30	< 0.5	< 0.5

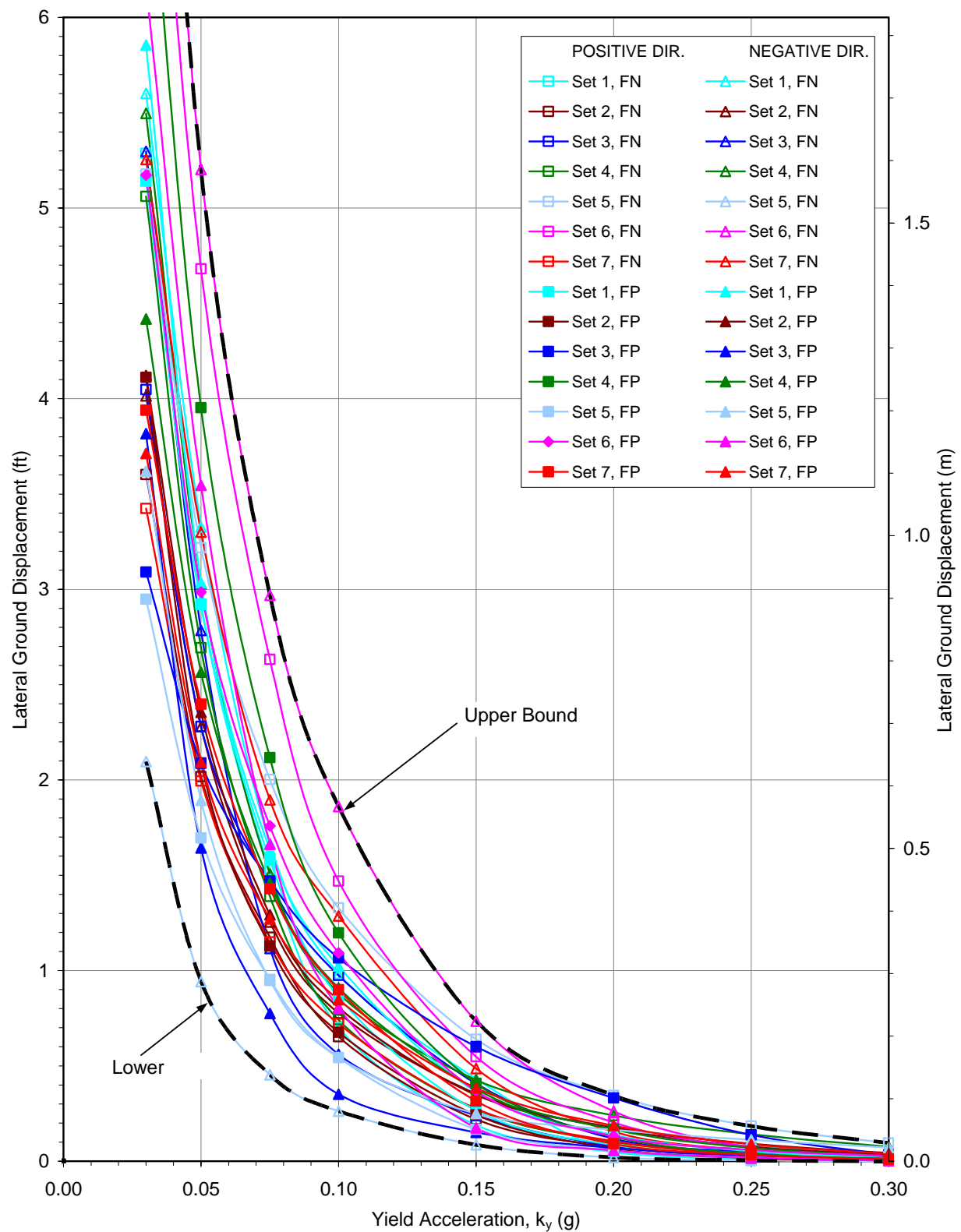**Figure E-1.   Results from Newmark Displacement Analyses for 475-yr Return Period (CLE)**
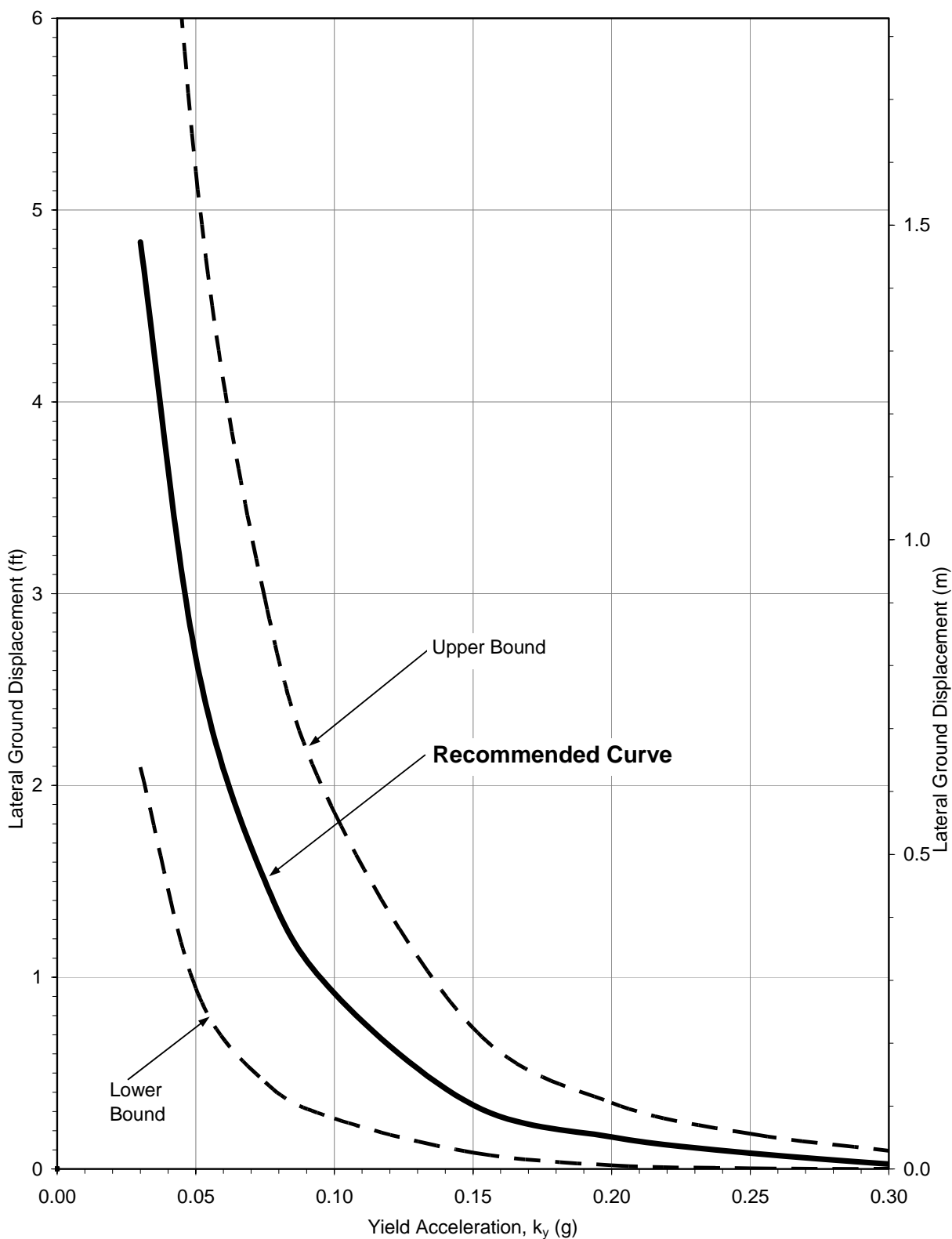
Figure E-2.   Range of Newmark Displacement Estimates and Recommended Screening Curve for Site Screening, 475-yr Return Period (CLE) Event
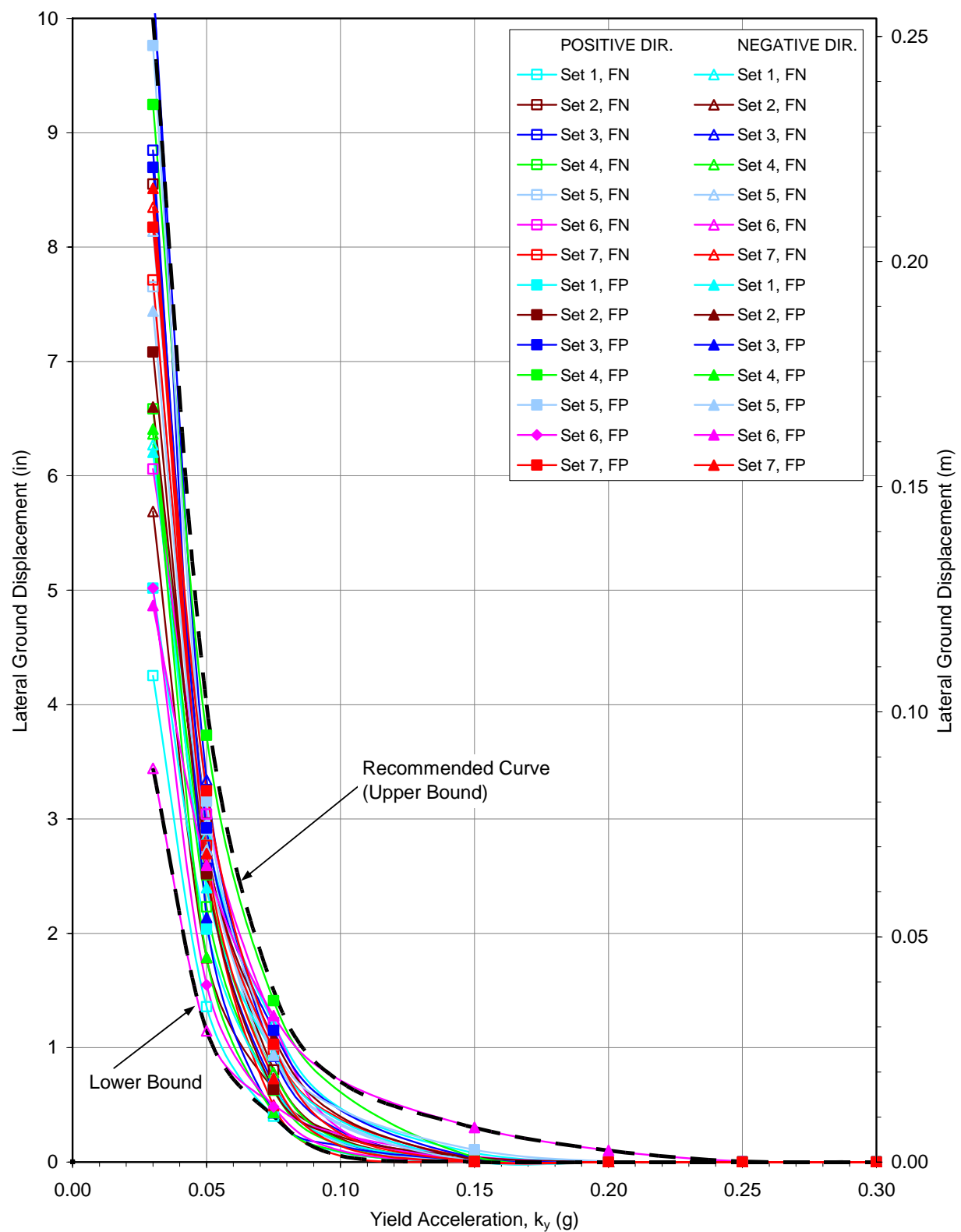
Figure E-3. Results of Newmark Displacement Estimates and Recommended Curve for Site Screening, 72-yr Return Period (OLE) Event

APPENDIX F

ELECTRONIC FILES

APPENDIX F
ELECTRONIC FILES

A Compact Disk is attached containing electronic files of this entire report and the time histories and spectra provided in Appendix D. Table F-1 tabulates all files contained on the disk and provides the file format and descriptions of the file content. Table F-2 lists and describes the contents of the recommended firm-ground and design spectra presented Section 6. Table F-3 provides the contents of the ground motion files presented in Appendix D.

Table F-1.　　Content of Compact Disk

Directory	File name	File Type	Content
(Root)	Readme.doc	Microsoft Word 2002	Description of files
Report	Report.pdf	Adobe Acrobat 6.0	This Report (main text and appendices)
	Binder_Cover.pdf	Adobe Acrobat 6.0	Binder cover
Motion_Files	Spectra.xls	Microsoft Excel 2002	Recommended spectra (see Table F-2)
	FirmGroundCLE.xls	Microsoft Excel 2002	Firm-ground time histories and spectra for CLE given in Appendix D.1 (see Table F-3)
	FirmGroundOLE.xls	Microsoft Excel 2002	Firm-ground time histories and spectra for OLE given in Appendix D.2 (see Table F-3)
	DesignCLE.xls	Microsoft Excel 2002	Firm-ground time histories and spectra for CLE given in Appendix D.3 (see Table F-3)
	DesignOLE.xls	Microsoft Excel 2002	Firm-ground time histories and spectra for OLE given in Appendix D.4 (see Table F-3)

Table F-2.   **Content of Spectra File**

Workbook File Name	Worksheet Name	Content
Spectra.xls	Firm Ground CLE	Spectral acceleration values of firm-ground spectra for CLE for 5% damping (Table 6-2 in main text)
	Firm Ground OLE	Spectral acceleration values of firm-ground spectra for OLE for 5% damping (Table 6-1 in main text)
	Design CLE	Spectral acceleration values of design spectra for CLE for various damping values (Table 6-4 in main text)
	Design OLE	Spectral acceleration values of design spectra for OLE for various damping values (Table 6-3 in main text)

Table F-3.   **Content of Ground Motion Files**

Workbook File Name	Worksheet Name	Content
FirmGroundCLE.xls	Set 1 - FN *Through* Set 7 - FN	Modified and target time histories and spectra of horizontal acceleration, velocity and pseudo relative displacement for Fault Normal component (Fig. D-1b,c through D-7b,c) for CLE Ground Motion Set 1 through 7 (see Table D.1) , respectively
	Set 1 - FP *Through* Set 7 - FP	Modified and target time histories and spectra of horizontal acceleration, velocity and pseudo relative displacement for Fault Parallel component (Fig. D-1b,c through D-7b,c) for CLE Ground Motion Set 1 through 7 (see Table D.1) , respectively
	Set 1 - FV *Through* Set 7 - FV	Modified and target time histories and spectra of horizontal acceleration, velocity and pseudo relative displacement for vertical component (Fig. D-1b,c through D-7b,c) for CLE Ground Motion Set 1 through 7 (see Table D.1) , respectively
FirmGroundOLE.xls	Set 1 - FN *Through* Set 7 - FN	Modified and target time histories and spectra of horizontal acceleration, velocity and pseudo relative displacement for Fault Normal component (Fig. D-8a through D-14a) for OLE Ground Motion Set 1 through 7 (see Table D.2) , respectively
	Set 1 - FP *Through* Set 7 - FP	Modified and target time histories and spectra of horizontal acceleration, velocity and pseudo relative displacement for Fault Parallel component (Fig. D-8b through D-14b) for OLE Ground Motion Set 1 through 7 (see Table D.2) , respectively
	Set 1 - FV *Through* Set 7 - FV	Modified and target time histories and spectra of horizontal acceleration, velocity and pseudo relative displacement for vertical component (Fig. D-8c through D-14c) for OLE Ground Motion Set 1 through 7 (see Table D.2), respectively
DesignCLE.xls	Set 1 - FN *Through* Set 7 - FN	Modified and target time histories and spectra of horizontal acceleration, velocity and pseudo relative displacement for Fault Normal component (Fig. D-15a through D-21a) for CLE Ground Motion Set 1 through 7 (see Table D.1) , respectively
	Set 1 - FP *Through* Set 7 - FP	Modified and target time histories and spectra of horizontal acceleration, velocity and pseudo relative displacement for Fault Parallel component (Fig. D-15b through D-21b) for CLE Ground Motion Set 1 through 7 (see Table D.1) , respectively
	Set 1 - FV *Through* Set 7 - FV	Modified and target time histories and spectra of horizontal acceleration, velocity and pseudo relative displacement for vertical component (Fig. D-15c through D-21c) for CLE Ground Motion Set 1 through 7 (see Table D.1) , respectively
DesignOLE.xls	Set 1 - FN *Through* Set 7 - FN	Modified and target time histories and spectra of horizontal acceleration, velocity and pseudo relative displacement for Fault Normal component (Fig. D-22a through D-28a) for OLE Ground Motion Set 1 through 7 (see Table D.2) , respectively
	Set 1 - FP *Through* Set 7 - FP	Modified and target time histories and spectra of horizontal acceleration, velocity and pseudo relative displacement for Fault Parallel component (Fig. D-22b through D-28b) for OLE Ground Motion Set 1 through 7 (see Table D.2) , respectively
	Set 1 - FV *Through* Set 7 - FV	Modified and target time histories and spectra of horizontal acceleration, velocity and pseudo relative displacement for vertical component (Fig. D-22c through D-28c) for OLE Ground Motion Set 1 through 7 (see Table D.2), respectively